ON THE ENGINEERING GEOLOGY OF GRANITE SAPROLITE AND ITS SIGNIFICANCE TO THE CONSTRUCTION OF INJAKA DAM, SOUTH AFRICA

by

DAVID RODNEY HASKINS

Submitted in fulfilment of the academic requirements for the degree of Doctor of Philosophy in the School of Geological and Computer Sciences, University of KwaZulu-Natal

December 2004

ABSTRACT

The intention of this work is to provide a deeper understanding of the engineering geological behaviour of granite saprolite and how this affects the engineering of such material, with specific reference to the construction of Injaka Dam in the north eastern portion of South Africa. Whilst extensive investigation of weathered granites has been carried out internationally, very little detailed research on the nature of this material is documented locally. The construction of Injaka Dam afforded the opportunity to investigate the saprolite in detail. This study was initially submitted to the Department of Geology and Applied Geology at the University of Natal, Durban (renamed the University of KwaZulu-Natal in 2004) to fulfill the requirement of a Master of Science degree in 2001. Following this submission, and supported by recommendations made by the external examiners and the project supervisor, it was agreed to upgrade the work and submit this thesis for the degree of Doctor of Philosophy.

Intensive chemical weathering of granite at Injaka Dam site has resulted in the formation of thick saprolitic deposits overlying the weathered bedrock. The granite forms part of the 3 075 Ma Nelspruit Suite which has been intersected by the African erosion surface. The extensive, multi-cyclic period of weathering and erosion that formed this surface has resulted in deep (up to 35 m) chemical weathering of the underlying bedrock in this area. The construction of Injaka Dam on this material necessitated a thorough engineering geological investigation to understand the nature of the weathering and the possible influences it exerts on the engineering behaviour of the saprolite. This was accomplished by analysing the weathering of the granite and relating the effects of these weathering processes and changes to the engineering behaviour of the material. By applying various chemical and mineralogical indices to the weathered granite, the intensity of weathering and related changes could be quantified and compared with the engineering behaviour of the material. This was achieved by applying a series of engineering indices to the material and relating these to the quantified weathering changes. In this way tentative extrapolation of the engineering behaviour of the material could be gained and used to predict engineering performance. The resultant effects of the engineering behaviour of the material on the design and construction of the dam are also discussed.

PREFACE

The experimental work described in this dissertation was carried out on a part-time basis at the Council for Geoscience from April 1996 to June 1999 under the joint supervision of Professor F. G. Bell of the School of Geological and Computer Sciences at the University of KwaZulu-Natal, and Doctor A. Schall at the Dams and Underground Unit, Council for Geoscience. Subsequent project supervision fell under Professor R. Maud of Drennan, Maud and Partners.

This study represents original work by the author and has not otherwise been submitted in any form for any degree or diploma to any tertiary institution. Where use has been made of the work by others it is duly acknowledged in the text.

David Rodney Haskins

December 2004

Somerset West

TABLE OF CONTENTS

1. INTRODUCTION 1

2. OVERVIEW OF SITE 4
   - 2.1 Description of Injaka Dam site 4
   - 2.2 Geomorphology of the site 4
   - 2.3 Geology of the site 6

3. CHEMICAL WEATHERING OF GRANITES 11
   - 3.1 Introduction 11
   - 3.2 Processes of chemical weathering 11
   - 3.3 Mineralogical transformations during chemical weathering of granite 13

4. THE DESCRIPTION AND CLASSIFICATION OF WEATHERED GRANITE 16
   - 4.1 Introduction 16
   - 4.2 Review of selected classification systems 16

5. SAMPLING METHODOLOGY AND DESCRIPTION OF SAMPLES 23
   - 5.1 Sampling methodology 23
   - 5.2 Description of materials 28
     - 5.2.1 Granite saprolite with residual soil patches 28
     - 5.2.2 Granite saprolite 30
     - 5.2.3 Highly weathered granite 31
     - 5.2.4 Fresh and slightly weathered granite 31

6. SCANNING ELECTRON MICROSCOPE INVESTIGATION 33
   - 6.1 Introduction 33
   - 6.2 Sample preparation 34
   - 6.3 Equipment and techniques 35
   - 6.4 Nomenclature 36
   - 6.5 Mineral weathering observations 38
     - 6.5.1 Quartz 39
     - 6.5.2 Feldspars 39

6.5.3 Micas 40
6.5.4 Secondary minerals (decomposition products) 44
6.5.5 Intergranular voids and microcracking 46
6.5.6 SEM model of microfabric of weathered granite 50

7. PETROGRAPHIC INVESTIGATIONS 51
7.1 Introduction 51
7.2 Specimen preparation and techniques 51
7.3 Petrographic descriptions 52
7.3.1 Fresh and slightly weathered granite 52
7.3.2 Highly weathered granite 52
7.3.3 Granite Saprolite 54
7.3.4 Granite saprolite with residual soil patches 56
7.4 Characterization of weathering and engineering properties in terms of quantitative micropetrographical indices 58

8. MINERALOGY AND GEOCHEMISTRY 64
8.1. Mineralogy 64
8.1.1 Introduction 64
8.1.2 Equipment and Techniques 64
8.1.3 Fresh to slightly weathered granite 65
8.1.4 Highly weathered granite 65
8.1.5 Granite saprolite 66
8.1.6 Granite saprolite with residual soil patches 66
8.2 Geochemistry 70
8.2.1 Introduction 70
8.2.2 Equipment and Techniques 71
8.2.3 Technique of major elemental analysis 71
8.2.4 Results of elemental analysis 72

9. WEATHERING INDICES 76
9.1 Introduction 76
9.2 Chemical weathering indices 76
9.3 Mineralogical weathering indices 84

10. BASIC ENGINEERING PROPERTIES 91
10.1 Particle size distribution 91
10.1.1 Introduction 91
10.1.2 Evaluation of grading 91
10.2 Consistency limits 95
10.2.1 Introduction 95
10.2.2 Results 96
10.3 Density and void ratio characteristics 97
10.4 Permeability 104
10.4.1 Introduction 104
10.4.2 Permeability tests 104

11. DISPERSIVITY 112
11.1 Introduction 112
11.2 The mechanism of dispersion 112
11.3 Identification of dispersive soils 114
11.3.1 Crumb test 114
11.3.2 Double hydrometer test 116
11.3.3 Pinhole Test 116
11.3.4 ESP-CEC 119
11.4 Discussion 120

12. CONSOLIDATION CHARACTERISTICS OF GRANITE SAPROLITE 122
12.1 Introduction 122
12.2 Consolidation characteristics from double oedometer tests 123
12.2.1 Sample preparation 123
12.2.2 Results from double oedometer tests 123
12.3 Consolidation characteristics from single oedometer collapse potential tests ... 133
12.3.1 Specimen preparation 133
12.3.2 Results from single oedometer collapse potential tests 134
12.4 Collapse potential using the triaxial apparatus with local strain instrumentation . 145
12.4.1 Specimen preparation 145
12.4.2 Results from triaxial collapse settlement tests 146
12.5 Collapse settlement indices 147
12.5.1 Introduction 147

12.5.2 Application of collapse settlement indices 147

13. SHEAR STRENGTH OF UNDISTURBED GRANITE 159
13.1 Introduction 159
13.2 Direct shear tests 160
13.2.1 Introduction 160
13.2.2 Specimen preparation 161
13.2.3 Direct shear tests at natural moisture content 162
13.2.3.1 Explanation of shear strength characteristics 167
13.2.4 Direct shear tests at saturated moisture content 168
13.2.4.1 Explanation of shear strength characteristics 170
13.3 Triaxial tests 170
13.3.1 Introduction 170
13.3.2 Saturated consolidated drained triaxial tests 170
13.3.2.1 Specimen preparation 170
13.3.2.2 Results and discussion 171
13.3.2.3 Explanation of shear strength 175
13.3.3 Shear strength results from triaxial collapse potential tests 176

14 ENGINEERING CHARACTERISTICS OF REMOULDED MATERIAL 178
14.1 Compaction characteristics 178
14.2 Permeability characteristics of remoulded material 180
14.3 Consolidation characteristics of remoulded material 180
14.4 Shear characteristics of remoulded material 184
14.4.1 Direct shear tests on compacted samples at optimum moisture content . 184
14.4.2 Direct shear tests on compacted samples under saturated conditions ... 189
14.4.3 Saturated consolidated drained triaxial tests on compacted samples . 192

15. EFFECT OF GRANITE SAPROLITE ON DESIGN AND CONSTRUCTION OF INJAKA DAM 195
15.1 Introduction 195
15.2 Mitigation against collapse settlement of granite saprolite 195
15.3 Mitigation for moderate permeability and dispersivity of foundation materials .. 198
15.3.1 Alignment of clay core with natural cut-offs 198
15.3.2 Construction of jet grout cut-off 199

15.3.3 Pressure relief wells 204
15.4 Liquefaction potential 205

16. CONCLUSIONS 207

17. REFERENCES 212

APPENDIX 1: COPIES OF RELEVANT SCIENTIFIC PAPERS PUBLISHED BY THE AUTHOR

LIST OF FIGURES

Figure 2.1. Locality of Injaka Dam site in the northeastern portion of South Africa 4

Figure 2.2. Oblique aerial view looking north of completed dam site showing central concrete trough spillway, inlet tower, outlet conduit and rip-rap protected embankment (photo courtesy of Department of Water Affairs and Forestry, 2002) 5

Figure 2.3. Relationship between climate and type of weathering (after Fookes *et al.*, 1971) 6

Figure 2.4a. Regional geology of Injaka Dam site (modified after Chunnett *et al.*, 1991a) showing Post African and African erosion surfaces 7

Figure 2.4b. Geomorphic cross section over Marite River showing position of African and Post African 1 and 2 Surfaces (from Partridge and Maud, 1987) 7

Figure 2.5. Local geology of Injaka Dam site showing positions of sample traverses (see Chapter 5) in relation to the dam foundation footprint 8

Figure 2.6. Geological cross section along dam centreline (post excavation of foundation footprint) 9

Figure 2.7. Typical geological cross-section of the Marite River valley at Injaka Dam site pre-excavation of dam foundation footprint 10

Figure 3.1. Weathering paths of mineral transformations in Hong Kong granites as proposed by Irfan (1996). Paths shown in red indicate mineral transformations of granite weathering at Injaka Dam. 13

Figure 4.1. Weathering classification system of Ruxton and Berry (1957) with grade numbers after Little (1969) 17

Figure 4.2. Idealised diagram of the stages of weathering of rock material (after Dearman, 1974) 20

Figure 4.3. Typical weathering profile encountered at Injaka Dam site. Note the distinct lack of core stones with the very abrupt contact separating granite saprolite from highly weathered granite bedrock 20

Figure 4.4. Classification system used for weathering of granite at Injaka Dam site (modified after Anon, 1995 and Irfan, 1988) 22

Figure 5.1. Sample traverse 1 incorporating right flank samples RF 12 to RF 14 24

Figure 5.2. Sample traverse 2 incorporating right flank samples RF 6 to RF 16 24

Figure 5.3. Sample traverse 3 incorporating left flank samples LF 7 to LF 13 25

Figure 5.4. Sample traverse 4 incorporating left flank samples LF 1 to LF 6 25

Figure 5.5. Sample traverse 5 incorporating left flank samples LF 18 to LF 28 26

Figure 5.6. Sample traverse 6 incorporating right flank samples RF 17 to RF 26 26

Figure 5.7. View of the left flank of Injaka Dam site showing the site geology and positions of sample traverses 3, 4 and 5. Weathering grades for the respective lithologies are also shown. Photograph taken from right flank, looking north 27

Figure 5.8. Granite saprolite (pink) with residual soil patches (red) showing complete loss of fabric structure where irregular patches of highly oxidised red clay aggregations occur (residual soil). Note also loss of fabric around root holes. Locality LF 7 29

Figure 5.9. Close up view of granite saprolite (yellow) with residual soil patches (red brown) showing prevalent concentration of vermiform voids. Note partial disruption to fabric in highly oxidised (red brown) residual soil zones. Locality LF 18 29

Figure 5.10. Variation of granite saprolite typical of mid to upper profile material. Note distribution of vermiform solution voids throughout material and intact relict fabric showing structural interlock of grains. Locality LF 24. 30

Figure 5.11. Variation of granite saprolite typical of material just above bedrock contact. Note retention of fabric. Locality LF 6. 31

Figure 5.12. View looking south of highly weathered granite bedrock showing complete discoloration. Locality RF 25.. 32

Figure 6.1. Example of typical elemental counts per second from the Link ISIS system used to differentiate various minerals under the SEM. 36

Figure 6.2 Possible geometrical arrangements of clay microfabrics after Collins and McGown (1974) 36

Figure 6.3. Intragranular decompositional voids as described by Baynes and Dearman (1978c). 38

Figure 6.4. Goldich's reaction series showing the high susceptibility of plagioclase to weathering 38

Figure 6.5a. Characteristic arcuate etching and pitting on weathered quartz grain surface from granite saprolite with residual soil patches (LF 18). Magnification = 4 590x. 41

Figure 6.5b. Typical smooth and conchoidal fractured surface of an unweathered quartz grain from granite saprolite (LF 10). Magnification = 3 630x. 41

Figure 6.6a. Cupule formation developed on a twinned plagioclase grain in highly weathered granite (RF 2). Magnification = 3 700x 41

Figure 6.6b. Well developed prismatic etch pit formation on a feldspar grain surface in granite saprolite (LF 3). Magnification = 4 500x 41

Figure 6.6c. Magnified view (16 380x) of prismatic etch pits shown in Figure 6.6b. Magnification = 16 380x 41

Figure 6.6d. Structurally controlled prismatic etch trench formation on the surface of a plagioclase grain in granite saprolite (LF 8) - low magnification (603x) 41

Figure 6.6e. Magnified view of Figure 6.6d at 3 500x showing formation of prismatic etch trenches (LF 8) 42

Figure 6.6f. Structurally controlled coalescence of prismatic etch trenches in plagioclase feldspar from granite saprolite (RF 7). Magnification = 4 360x 42

Figure 6.6g. View of Figure 6.6f showing distribution of prismatic etch trenches throughout the grain surface. Magnification = 461x 42

Figure 6.6h. Structurally controlled coalescence of prismatic etch trenches showing sieve-like structure of plagioclase feldspar alongside unweathered quartz in granite saprolite (RF 4). Magnification = 1 720x 42

Figure 6.6i. Enhanced prismatic etch pit formation resulting in a highly porous plagioclase feldspar framework in granite saprolite (LF 13). Magnification = 3 870 42

Figure 6.6j. Another form of the sieve-like feldspar texture developed in plagioclase feldspar from granite saprolite (LF 27). Magnification = 2 200x 42

Figure 6.6k. Highly porous, fragile skeletal plagioclase feldspar framework developed under intense leaching conditions in granite saprolite (LF 27). Magnification = 2 660x 43

Figure 6.6l. Irregular etch crevice formed on the surface of a feldspar grain in highly weathered granite (RF 24). Note the irregular shape of the crevice suggesting no structural control of the feature. Magnification = 3 220x 43

Figure 6.6m. Incongruent weathering of potash feldspar and plagioclase in highly weathered granite (RF 16). Plagioclase (right hand side) shows pitting on the grain surface whilst the potash feldspar (left hand side) exhibits no such features although microcracks are clearly evident. Magnification = 2 000x 43

Figure 6.7. Opening (peeling) of mica cleavage showing feather-edge grain boundary in granite saprolite (LF 12). Magnification 1 250x 43

Figure 6.8a. Platey book-type kaolinite showing extensive formation of clay books in granite saprolite (LF 20). Magnification = 3 920x 47

Figure 6.8b. Platy book-type kaolinite showing large size of books. Magnification = 2 190x 47

Figure 6.8c. Compact version of platy book-type kaolinite showing less well-developed books with more random arrangement (RF 8). Magnification = 4 370x 47

Figure 6.8d. Another form of the compact platy book-type kaolinite (LF 3). Magnification = 2 180x 47

Figure 6.8e. Loose turbostratic arrangement of irregular kaolinite platelets (LF 4) Magnification = 640x. 47

Figure 6.8f. Turbostratic arrangement of irregular kaolinite platelets (RF 10) showing a higher porosity than that in Figure 6.8e. Magnification = 4 030x 47

Figure 6.8g. Pseudomorphic alteration of plagioclase to kaolinite (RF 4). Magnification = 126x. The original shape of the plagioclase grain can still be discerned ... 48

Figure 6.8h. Magnified view (2 060x) of Figure 6.8g showing highly porous pseudomorphic transition from feldspar to kaolinite 48

Figure 6.8i. Formation of kaolinite platelets in skeletal feldspar frame work (LF 26) providing evidence that the argillic transition is a product of solute interaction with the solid phase. Magnification = 16 330x 48

Figure 6.9a Vermiform solution voids showing circular cross-sectional openings formed in kaolinite aggregations (LF 3). Magnification = 100x 48

Figure 6.9b Oblique view into vermiform void formed in massive kaolinite (LF 12). Magnification = 187x 48

Figure 6.9c. Preferential solution void formation alongside quartz grain boundary where relatively higher permeabilities result in solution voids (LF 2). Magnification = 212x 49

Figure 6.9d. Magnified view (864x) of Figure 6.9c showing solution void characteristics . 49

Figure 6.9e. Vermiform void formation alongside a quartz grain (LF 9). The clay bridge shows the tubular nature of the void. Magnification = 174x 49

Figure 6.9f. Clean, open, intergranular microcrack between two feldspar grains. The crack width is 10μm. Magnification = 357x 49

Figure 6.9g. Kaolinite platelets forming within microcracks suggesting direct argillic transition from pore water solutions. Magnification = 1770x 49

Figure 7.1a. Granite showing cloudy and slightly sericitised plagioclase grains alongside cloudy but intact microcline feldspar under plane polarised light (PPL). Magnification = 40x. Grain boundaries are tight with no disruption to microfabric 59

Figure 7.1b. Equivalent micrograph under cross polarised light (CPL), showing commencement of sericite growth in plagioclase grains. Magnification = 40x 59

Figure 7.2a. Clean open microcracks in quartz showing the process of reduction in grain size (RF 14). Decomposed plagioclase occurs on the bottom right with open grain contacts clearly evident (PPL). Magnification = 40x. 59

Figure 7.2b-c. Typical microfabric of highly weathered granite in PPL (b) and CPL (c). Plagioclase grains show increased turbidity with a high degree of sericitisation and numerous microcracks (RF 16). Only minor disruption to the original microfabric is noted. Magnification = 40x 59

Figure 7.2d. Slightly cloudy microcline feldspar (RF 25) with numerous clean microcracks (CPL). Magnification = 40x. 59

Figure 7.2e-f Bleached biotite (RF 16) showing characteristic feather-edged grain boundary and opening of mica cleavage under PPL (e) and CPL (f). Alteration of the edge of the biotite grains to micaceous clay can be observed in the upper right hand portion of the micrograph. Magnification = 40x 60

Figure 7.3a. Broken quartz fragments within a matrix of clay (LF 4). Microcracks traverse the quartz grains and are clay filled with iron oxide staining. This type of microfabric is representative of the most highly weathered granite saprolite samples and approaches that of a residual soil. Disruption to the microfabric can be observed although some grain interlock still occurs (PPL). Magnification = 40x. 60

Figure 7.3b-c. Microfabric of granite saprolite (LF 20) in PPL (b) and CPL (c). The microfabric shows some disruption due to the formation of clay and intense microcracking. A reduction in the grain size compared to that in Figure 7.2 can be observed. Magnification = 40x. 60

Figure 7.3d-e. Formation of clay pseudomorphs (LF 9) derived from complete decomposition of plagioclase grains (note the very turbid nature of the grains). The adjacent microcline grain shows comparatively less alteration in the form of dusty clouding and clay filled microcracks. PPL (d) and CPL (e). Magnification = 40x. 61

Figure 7.3f. Severely microcracked microcline grain under CPL showing characteristic clay infilling along the microcracks (LF 25). Magnification = 40x. 61

Figure 7.3g. Platy, book type kaolinite (LF 20) under CPL within a matrix of fine-grained clay aggregates. Magnification = 40x. 61

Figure 7.3h. Typical appearance of fine-grained clay aggregations under CPL (LF 8). Magnification = 40x. 61

Figure 7.3i. Reticulate pattern of microcracks within the granite saprolite (RF 4) showing the extension of a microcrack propagating into the vermiform void located within the fine-grained clay aggregations (CPL). Magnification = 40x. 61

Figure 7.3j. Characteristic vermiform voids showing clay-lined surfaces with iron-oxide staining (LF 6). The smooth appearance of the voids is typical of solution effects (PPL). Magnification = 40x. 62

Figure 7.3k-l. Structural control on void formation with propagation of the void dictated by the presence of the quartz grain (LF 9). As identified from the SEM investigation, preferred solution along clay-grain contacts is common. PPL (k) and CPL (l). Magnification = 40x. 62

Figure 7.4a. Complete destruction of microfabric with iron-enriched clay and broken quartz grains dominating the microfabric with characteristic reticulate vermiform voids (LF 18). Magnification = 40x. 62

Figure 7.4b. Similar form of reticulate vermiform voids in iron-enriched aggregation of clay (RF 17). Note smooth appearance of void walls showing solution effects. Complete loss of fabric occurs in this particular micrograph. Magnification = 40x. 62

Figure 7.5. Relationship of micropetrographic index (I_p) to dry density (from sand replacement method) of granite weathered granite. 63

Figure 8.1. Typical XRD trace for granite saprolite at Injaka Dam. 68

Figures 8.2a-f. Mineralogical changes as depicted in each sample traverse with depth. 69

Figure 8.3. Increase in clay (kaolinite) with increasing initial void ratio suggesting that solution effects do not preferentially target the kaolinite at the expense of other minerals. 71

Figures 8.4a-h. Variation of volumetric concentration of CaO, Na_2O, K_2O, Fe_2O_3, TiO_2, Al_2O_3, SiO_2 and MgO with dry density. 75

Figures 9.1a-k. Relationship of chemical weathering indices with dry density of weathered granite. 81-82

Figure 9.2. Plot of unaltered feldspar content against I_{mob}. 84

Figure 9.3. Model to illustrate the microfabric consequences of differing degrees of decomposition (Baynes and Dearman, 1978a). White squares are representative of unweathered mineral grains whilst black squares are representative of weathered mineral grains. Assuming all decomposed mineral grains are feldspar then (a) represents 30% weathered mineral grains where $Xd = 0,2$; (b) represents 50% weathered mineral grains where $Xd = 0,5$ and (c) represents 60% weathered mineral grains where $Xd = 0,8$. 86

Figure 9.4. Relationship of Xd_{XRD} with initial voids ratio. 89

Figure 10.1a-c. Grading envelopes (maximum and minimum) for granite saprolite with residual soil patches (a), granite saprolite (b) and highly weathered granite (c) in water and dispersion agent (sodium hexametaphosphate). 92

Figure 10.2. Ternary diagram of saprolite grain size indicating direction of weathering trend. 96

Figure 10.3. A-line plot of granite saprolite including granite saprolite with residual soil patches. 97

Figure 10.4. Plasticity index as a function of clay percentage (calculated from hydrometer analysis using a dispersing agent). 98

Figure 10.5. Potential expansiveness of weathered granite using the method developed by Van Der Merwe (1964). 98

Figure 10.6. Correlations of various density measurement techniques. 101

Figure 10.7. Relationship of dry density and void ratio with depth. 103

Figure 10.8. Electronic data logger well permeameter designed for testing general field permeability (k_{gen}) using principles from the well permeameter as developed by Anon (1968). 105

Figure 10.9. Summary of test parameters for constant head well permeameter tests. 106

Figure 10.10. Constant head permeameter conditions for Traverses 4 and 5. 107

Figure 10.11. Relationship of permeability with depth for Traverses 1 to 6. 110

Figure 10.12. Effect of void ratio on permeability. 109

Figure 10.13a. Lack of correlation between clay (as determined from grading analyses) with permeability. 111

Figures 10.13b. Tentative relationship of permeability with the microfabric index *Xd*. 111

Figure 11.1. Large piping and pervasive runnel erosion developed in granite saprolite foundation excavation. The pipe developed over a period of one year. 115

Figure 11.2. Turbid water exiting from piping erosion on the right excavation flank in granite saprolite. 115

Figure 11.3. ESP vs CEC graph for granite saprolite with residual soil patches and granite saprolite. 119

Figure 12.1a-i. Typical e-log p and e-p curves from double oedometer tests. e-p curves are included to assess the presence of any yield stress using the technique proposed by Vaughan (1985). 126-128

Figure 12.2. Relationship of p_c with depth at Injaka Dam site (shaded area encompasses all samples) and findings by Vargas (1953) showing similar lack of correlation of p_c with overburden pressure. 129

Figure 12.3. Relationship of p_c with depth as determined by Partridge *et al.* (1984) at Zoeknog Dam (shaded area represents p_c envelope for saturated samples). 130

Figure 12.4. Compression index correlations with initial void ratio. 131

Figure 12.5. Relationship of C_{cnmc} and C_{csat} and initial void ratio for granite saprolite at Zoeknog Dam. Shaded area encompasses majority of samples at natural moisture content. 131

Figure 12.6. Typical oedometer curve from collapse potential test showing definition of the collapse potential. 134

Figures 12.7a-f Collapse potential curves for samples from Traverses 1 to 6. 136-138

Figures 12.7g. Collapse potential curves for samples from Traverse 6 (saturation at 381 kPa). 139

Figure 12..8. Relationship of collapse potential and dry density. 140

Figure 12.9. Explanation of one-dimensional collapse potential behaviour for granite saprolite from Injaka Dam (after Haskins *et al.*, 1998). 140

Figure 12.10. Relationship of collapse potential and dry density for Zoeknog Dam granite saprolite 141

Figure 12.11. Collapse potential as a function of degree of saturation (S_r). 142

Figure 12.12. Critical degree of saturation (S_r) found by other studies. 142

Figure 12.13. Collapse potential as a function of degree of saturation (S_r) for granite saprolite at Zoeknog Dam. 143

Figure 12.14. Typical curves of collapse settlement and square root time for granite saprolite. 145

Figure 12.15 Triaxial collapse test apparatus. (After Heymann and Rust, in press). 146

Figure 12.16. Typical e-p curves from triaxial collapse potential tests. 147

Figure 12.17. Relationship of Denisov values with collapse potential (%). 148

Figure 12.18. Stability diagram of Gibbs and Bara (1962) showing data from granite saprolite at Injaka Dam. 150

Figure 12.19. Applicability of Gibbs and Bara's (1962) graphical presentation of metastability (n = number of samples). 151

Figure 12.20. Relationship of collapse index (i_c) and collapse potential (%). 152

Figure 12.21. Relationship of absolute collapse index (i_{ac}) and collapse potential (%). 152

Figures 12.22a-c Construction of Darwell *et al.*'s (1976) graphic method for determination of collapse settlement indices 154

Figure 12.23. Stability chart of granite saprolite at Injaka Dam using Darwell *et al.*'s (1976) graphical method. 154

Figure 12.24. Applicability of Darwell *et al.*'s (1976) graphical method for indexing collapse settlement at Injaka Dam. 155

Figure 12.25. Indexing the collapse potential of granite saprolite using the e/*Xd* chart by Lumb (1962), after Baynes and Dearman (1978a). 156

Figure 12.26. Applicability of Baynes and Dearman's (1978a) method using e/*Xd* for indexing collapse settlement. 156

Figure 12.27a-c Denisov values, i_c and i_{ac} values and collapse potential for Zoeknog Dam granite saprolite. 157

Figure 12.28. Stability diagram of Gibbs and Bara (1962) showing data from granite saprolite at Zoeknog Dam and histogram showing correlation of method with collapse potential. 158

Figure 12.29. Stability chart of granite saprolite at Zoeknog Dam using Darwell *et al.'s* (1976) graphical method and histogram showing correlation of method with collapse potential. 158

Figure 13.1. Characteristic stress-strain behaviour of weathered granite soils after Ebuk *et al.* (1993). 162

Figure 13.2. Stress-strain curves showing volume change in direct shear for right flank undisturbed samples sheared at natural moisture content. 163

Figure 13.3. Stress-strain curves showing volume change in direct shear for left flank undisturbed samples sheared at natural moisture content 164

Figure 13.4. Stress-strain curves showing volume change in direct shear for left flank undisturbed samples sheared under saturated conditions. 169

Figure 13.5. Stress-strain curves for selected granite saprolite samples from saturated consolidated drained triaxial tests. 172

Figure 13.6. Failure type curves for saturated consolidated drained samples 173

Figure 13.7. Results of saturated consolidated drained triaxial tests on granite saprolite at Zoeknog Dam for Partridge *et al.* (1990) 173

Figure 13.8. Effective stress points for maximum deviator stress for consolidated drained triaxial tests on granite saprolite samples. 175

Figure 13.9. Stress-strain curves and pore pressure measurements from undrained triaxial tests. 176

Figure 13.10. Effective stress path for granite saprolite samples. 177

Figure 14.1. Typical compaction curves for granite saprolite with residual soil patches, granite saprolite and highly weathered granite 179

Figure 14.2. Permeability characteristics of remoulded weathered granite materials 180

Figure 14.3. Stress-strain curves showing volume change in direct shear for right flank compacted samples sheared at optimum moisture content. 186

Figure 14.4. Stress-strain curves showing volume change in direct shear for left flank compacted samples sheared at optimum moisture content. 187

Figure 14.5. Relationship of friction angle with Standard Proctor maximum dry density sheared at optimum moisture content. 188

Figure 14.6. Stress-strain curves showing volume change in direct shear for right flank compacted samples sheared under saturated conditions. 190

Figure 14.7. Stress-strain curves showing volume change in direct shear for left flank compacted samples sheared under saturated conditions. 191

Figure 14.8. Relationship of maximum dry density with friction angle for compacted samples sheared saturated. 189

Figure 14.9. Stress strain curves for remoulded granite saprolite compacted to 100% Standard Proctor maximum dry density from saturated consolidated drained triaxial tests. 193

Figure 14.10. Type C failure curve for saturated compacted samples. 194

Figure 14.11. Effective stress points for maximum deviator stress for consolidated drained triaxial tests on compacted granite saprolite. 194

Figure 14.12. Variation of φ' from saturated consolidated drained triaxial tests with maximum dry density. 194

Figure 15.1. Collapse potential as a function of % maximum dry density. 198

Figure 15.2a-b. (a). Test columns for jet grout method in granite saprolite. (b). Good mixing of cementitious grout with saprolite to form homogeneous column.. 201

Figure 15.3. Layout of jet grout curtain and pressure relief wells at Injaka Dam site.. . . . 202

Figure 15.4. Longitudinal section along jet grout curtain showing depth of columns and column layout details... 203

LIST OF TABLES

Table 4.1. Summary of weathering factors taken into account in the Moye (1955) weathering classification with grade numbers from Little (1969) and after Dearman (1995) 17

Table 4.2. Classification of the various stages of the weathering processes on granite (Little 1969) 18

Table 4.3. Key descriptive terms for classifying weathered rock material (after Dearman *et al.*, 1978) 19

Table 4.4. Description of weathering grades of rock mass description used in Figure 4.4. 21

Table 6.1. Nomenclature of scanning electron microscope terminology (modified from Baynes and Dearman, 1978c). 37

Table 7.1. Modal analysis (%) and micropetrographic index (I_p) of fresh and slightly weathered granite. 53

Table 7.2. Modal analysis (%) and micropetrographic index (I_p) of highly weathered granite. 53

Table 7.3. Modal analysis (%) and micropetrographic index (I_p) of granite saprolite. 55

Table 7.4. Modal analysis (%) and micropetrographic index (I_p) of granite saprolite with residual soil patches. 57

Table 8.1. Mineralogical results from XRD analyses for fresh and slightly weathered granite. 65

Table 8.2. Mineralogical results from XRD analyses for highly weathered granite. .. 66

Table 8.3. Mineralogical results from XRD analyses for granite saprolite 67

Table 8.4. Mineralogical results from XRD analyses for granite saprolite with residual soil patches 67

Table 8.5. Major elemental analyses (weight %) from XRF determinations for granite saprolite with residual soil patches. 73

Table 8.6. Major elemental analyses (weight %) from XRF determinations for granite saprolite. 73

Table 8.7. Major elemental analyses (weight %) from XRF determinations for highly weathered granite. 74

Table 9.1. Summary of chemical weathering indices used to measure weathering changes for weathered granite at Injaka Dam. 78

Table 9.2. Summary of chemical weathering indices for Traverses 1-6. 80

Table 9.3. t-Test results for correlation of weathering indices with density 83

Table 9.4. Typical mean values of weathering indices for different weathering grades of granite 84

Table 9.5. Pearson correlation co-efficient (r) for various weathering indices. 85

Table 9.6. Mineralogical weathering indices for sample Traverses 1-6 88

Table 10.1. Particle size parameters for granite saprolite with residual soil patches . . . 93

Table 10.2. Particle size parameters for granite saprolite 94

Table 10.3. Particle size parameters for highly weathered granite 95

Table 10.4. Summary of density and void ratio results for granite saprolite with residual soil patches 99

Table 10.5. Summary of density and void ratio results for granite saprolite 100

Table 10.6. Summary of density and void ratio results for highly weathered granite . 100

Table 10.7. t-Test results for density technique correlations. 102

Table 10.8. Summary of well permeameter results 106

Table 10.9. Summary of permeability test results for granite saprolite with residual soil patches 108

Table 10.10. Summary of permeability test results for granite saprolite 108

Table 10.11. Summary of permeability test results for highly weathered granite 108

Table 10.12. Statistical summary of permeability results 109

Table 11.1. Established methods for determining the dispersivity of soils 114

Table 11.2. Physical and chemical dispersivity test results for granite saprolite with residual soil patches 117

Table 11.3. Physical and chemical dispersivity test results for granite saprolite. 118

Table 12.1. Results from double oedometer tests 124

Table 12.2. Compression indices from double oedometer tests 129

Table 12.3. Comparative values of C_c and p_c for saprolitic soil from granite in Portugal studied by Nouvais-Ferreira and Fonesca (1988) 130

Table 12.4. Percentage collapse as determined from double oedometer tests. 133

Table 12.5. Collapse potential characteristics for granite saprolite from Traverses 1-6 (saturation at 191 kPa and 381 kPa where shown) 135

Table 12.6. Values for coefficients of consolidation and volume compressibility for samples from Traverses 1-6, calculated from collapse potential tests ... 144

Table 12.7. Collapse potential results from triaxial testing 146

Table 12.8. Collapse settlement indices for samples from Traverses 1-6 149

Table 13.1. Shear strength parameters of Grade VI weathered granite from various sources (Deere and Patton, 1971). 160

Table 13.2. Shear strength parameters of Grade V weathered granite from various sources 160

Table 13.3. Summary of direct shear strength parameters for granite saprolite with residual soil patches at natural moisture content 166

Table 13.4. Summary of direct shear strength parameters for granite saprolite at natural moisture content 166

Table 13.5. Summary of saturated direct shear strength parameters for granite saprolite with residual soil patches 168

Table 13.6. Summary of saturated direct shear strength parameters for granite saprolite 168

Table 13.7. Summary of shear strength parameters for saturated consolidated drained triaxial tests on granite saprolite with residual soil patches 174

Table 13.8. Summary of shear strength parameters for saturated consolidated drained triaxial tests on granite saprolite 174

Table 14.1. Average Standard Proctor maximum dry densities and optimum moisture contents 178

Table 14.2. Remoulded engineering properties of granite saprolite with residual soil patches at Injaka Dam 181

Table 14.3. Remoulded engineering properties of granite saprolite at Injaka Dam .. 182

Table 14.4. Remoulded engineering properties of highly weathered granite at Injaka Dam 183

Table 14.5. Summary of consolidation characteristics of remoulded granite saprolite at Injaka Dam (from Chunnett *et al.*, 1991a) 185

Table 15.1. Collapse potential characteristics with % maximum dry density for Traverses 1 to 6 (saturation at 191kPa) 197

Table 15.2. Permeability of granite and diabase saprolite from various methods 198

Table 15.3. Results from jet grout tests in granite saprolite 200

Table 15.4. Falling head and water pressure tests on grout columns 203

Table 15.5. Theoretical and empirical geotechnical limit criteria as determined by Welland (2002) for preliminary liquefaction potential 205

ACKNOWLEDGEMENTS

This part-time study spanned six years of research and compilation and I am indebted to many people that have provided support throughout this time. Firstly, I wish to sincerely thank Professor F.G. Bell and Doctor A. Schall for providing the motivation, guidance and review throughout this project. It has been an enriching experience working under the erudition of two such accomplished members in this profession. The latter part of this research fell under the enthusiastic supervision of Professor R. Maud whose pragmatic advice has been invaluable in providing the scope and direction for the completion of this research and to whom I am greatly indebted.

This research could not have been undertaken without the sound support provided by the Council for Geoscience and Department of Water Affairs and Forestry, and I am deeply grateful to both institutions. In particular, I wish to thank Mrs Wilma Van Der Merwe, Mr Johannes Van Zyl and Mr Andre Van Der Walt.

A small component of research was carried out at the Geology Department, University of Cape Town, and I wish to thank Doctor H. Frimmel for use of their facilities. My thanks are also extended to Melis and Du Plessis Consulting Engineers for providing the facilities and time to produce this dissertation.

Special thanks go to Bruce Springsteen for accompanying my thoughts through the many long nights spent compiling this dissertation.

Finally, I wish to thank my family, and especially Annette, Alexandria, Matthew and James for the unending support that they have provided throughout this rewarding and enriching experience and for all the sacrifices that they have made to make this endeavour possible.

1. INTRODUCTION

The need for understanding the effects of geological processes on soils and rocks and their interaction with the engineered environment is well established. Perhaps the most important of all of these processes is that of weathering. Chemical weathering forms a fundamental component of soil and rock weathering in tropical and sub-tropical environments, whether they be contemporaneous or palaeaoclimatic. As such, chemical weathering exerts a significant influence on the engineering behaviour of these materials (Gidigasu, 1980). By understanding the processes and effects of this weathering it is possible to predict the change in engineering behaviour of such materials as they undergo transition from a fresh to weathered state and this in turn provides a key design solution to engineering on and with such materials.

Weathered granite has been encountered in many civil engineering projects throughout the world, not least of which is at the construction site of Injaka Dam in South Africa. In particular, construction in and with such materials in Australia and the Far East has led to research which has ultimately facilitated a greater understanding of the processes of chemical weathering acting on granites and the effects thereof. However, much of this research has been based on physical, chemical and mineralogical changes of the granite with continuously increasing weathering intensity (the weathering grade spectrum) from fresh bedrock to residual soil, whereas this study concentrates primarily on the granite saprolite phase of weathering (Grade V or completely weathered material - Anon, 1995). In South Africa, whilst much has been written about the engineering properties of residual soils, and granite soils in particular, relatively limited information is available on the physico- and geochemical changes and their effects on the engineering properties of granite saprolite. The catastrophic failure of Zoeknog Dam in 1993, situated some 20km north of Injaka Dam and constructed with similar materials, provided the impetus for detailed investigation of the engineering geological behaviour of the granite saprolite at Injaka Dam.

The term "saprolite" is not commonly used in the South African context, although it forms common terminology internationally. The term was introduced by Becker (1895) in the United States and since that time has received favourable use by pedologists and geologists. Stolt and Baker (1994), define saprolite as crystalline bedrock that has undergone isovolumetric weathering but which still retains the original structure, texture and fabric of the parent rock, whilst essentially behaving geotechnically as a soil. Its engineering weathering grade is equivalent to the commonly used "completely weathered" terminology (ISRM, 1981).

The occurrence of saprolites is widespread and they can be found on every continent (Sowers, 1963), but are particularly common in the tropical and sub-tropical regions of southern Asia, Australia, Africa, southeastern North America, Central America and South America where warm and humid climates occur. In some of the more temperate regions they occur as weathering remnants from tropical and sub-tropical palaeoclimates (as they do in South Africa). The widespread occurrence of these materials means that they often exhibit a variety of characteristics - a reflection of their diverse parent lithologies and variable weathering environments. It is this heterogeneity and complexity that commonly causes these materials to present problems in engineering, or at least exhibit unique engineering behaviour. For instance, saprolites are texturally similar to soils and exhibit the full range of grain sizes as found in sediments; but mineralogically they contain primary rock forming minerals within a complex fabric of alteration and secondary decomposition products, and structurally they retain much of the relict crystalline textures of the parent rock including internal mineral configurations and structural defects. Consequently, the characterisation, sampling, testing and analysis of such soils is complex. In fact, many conventional soil mechanics approaches and relationships developed for transported soils do not readily apply to these soils (Vaughan *et al.*, 1988) and if they do, require careful interpretation. Despite this, the engineering behaviour of many of these soils shows similar characteristics including low density, moderate permeability, generally high shear strengths and metastable behaviour. The granite saprolite at Injaka Dam proved to be no different.

The construction of Injaka Dam began in 1996 and with the dedicated support of the Council for Geoscience and the Department of Water Affairs and Forestry, this research was allowed to flourish. The work represents a three year part-time involvement at Injaka Dam site where the author was commissioned as site geologist. In this role, the author acted in close liaison with the design engineers on all geological aspects of the dam design and construction. The granite saprolite provided a particular area of interest which required further research having been under-studied in South Africa, despite being a characteristically difficult material to engineer.

The objectives of this engineering geological study included analysis of the weathering processes that have acted upon the granite to produce the saprolite and quantification of the engineering geological behaviour of the material. The results from this study were used to guide design engineers during dam construction and enhance the understanding of the engineering behaviour of the saprolite. To achieve these objectives a series of petrographic, electron microscope, chemical and mineralogical techniques were applied to the saprolite to understand the weathering processes and effects. Quantification of the intensity of weathering was achieved by using these techniques to index the changes brought about by weathering. A series of engineering tests were also undertaken to quantify the engineering

characteristics of the material. By indexing the material using these techniques, and comparing the changes in engineering behaviour with weathering, an understanding of the complex effects that weathering has on the engineering behaviour of the material could be gained. This is essentially the hypothesis proposed for this thesis - that the weathering of a granite saprolite can be indexed and that these indices can be used to predict and correlate the engineering behaviour of this material to various degrees of accuracy.

The initial part of this study (Chapters 2 to 9) reviews the many aspects of change that occur in the weathering profile of the granite saprolite and attempts to correlate these changes either mineralogically, geochemically or on a limited scale, structurally through microfabric investigations. The latter part of the study (Chapters 10 to 13) quantifies the engineering behaviour of the material and its relationship to the weathering changes mentioned above. Chapter 14 provides a synopsis of the engineering characteristics of the remoulded granite saprolite which was carried out to assess the material suitability for construction of the earthfill embankment for Injaka Dam. Finally, Chapter 15 reviews the design and construction measures undertaken at Injaka Dam to mitigate against certain problematic engineering characteristics of the granite saprolite.

For comparative purposes, and in an attempt to broaden the application of the results from this study, selected information from the feasibility, design and post-failure investigations undertaken at Zoeknog Dam has been included and discussed in this dissertation together with several comparative data sets for similar material investigated by Falla (1985) in the Johannesburg area of South Africa. It must be appreciated that the level of detail of investigation of these two data sets is not equivalent to that which has been carried out in this study, although the objective of the comparisons is purely to establish the general applicability of selected findings from this research making the results broadly relevant to other sites. Other relevant and comparable data from around the world on similar material is also included to broaden the context of the findings from this study. It is hoped that this research and the results thereof will contribute to an improvement of the understanding of granite saprolite in South Africa and the engineering of such materials, particularly with regard to dam construction.

2. OVERVIEW OF SITE

2.1 Description of Injaka Dam site

Injaka Dam site is situated 10 km south of Bushbuckridge (24° 53' 08" S; 31° 05' 09" E), located in Mpumalanga Province, South Africa (Figure 2.1). The dam is constructed on the eastward-flowing, perennial Marite River which is a major tributary of the Sabie River. The Marite River has its source at the edge of the Drakensberg escarpment (just north of Graskop). The dam comprises a zoned earthfill embankment 550 m long and 53 m high with a central concrete trough spillway and outlet conduit (Figure 2.2). It forms part of the development of the water resources of the Sabie River catchment allowing for expanded water utilization, stabilization of the flow of the Sabie River in the Kruger National Park and transfer of water from the Sabie River sub-catchment to the relatively dry Sand River sub-catchment. Locally, the reservoir will be used to increase the irrigation potential of the surrounding Bushbuckridge Trust Farms.

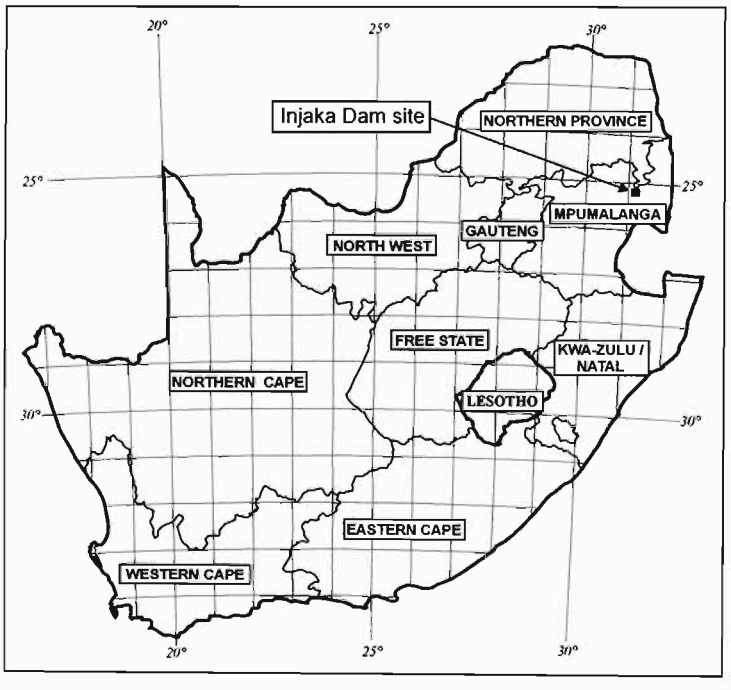

Figure 2.1. Locality of Injaka Dam site in the northeastern portion of South Africa.

2.2 Geomorphology of the Site

Injaka Dam is constructed in a portion of the Marite River valley where the upper valley flanks are formed by two spurs. River bed level at the site occurs at an elevation of approximately 724 m.a.s.l. with the river varying from 10 m to 30 m in width, exhibiting a predominantly dendritic drainage pattern - a feature typical of granitic terrains. Prior to construction, the left flank was

slightly convex with an average gradient of 1V:2H. The less convex right flank exhibited an average gradient of 1V:3H. The lower parts of both valley flanks were somewhat steeper with an average gradient of 1V:1H. Both flanks were heavily vegetated with plantations of *Eucalyptus sp.* on the upper flank shoulders and with natural riverine vegetation (sour lowveld Bushveld type) found on the steeper, lower flank portions. Excavations made during construction of the dam have reduced the valley flanks to straight slopes with significantly increased average gradients. The left flank exhibited an average gradient of 1V:0,75H whilst the right flank was finished to an average gradient of 1V:0,55H.

Figure 2.2. Oblique aerial view looking north of completed dam site showing central concrete trough spillway, inlet tower, outlet conduit and rip-rap protected embankment (photo courtesy of Department of Water Affairs and Forestry, 2002).

The dam site is located in a sub-tropical region with rain falling primarily during the summer period. The maximum average daily summer temperature is 30.1 °C with a minimum average daily winter temperature of 8.9 °C. Annual precipitation is 722 mm, with annual evaporation recorded over 2000 mm (SA Weather Bureau, 1998). This measurement represents 277% of the total annual precipitation. Thornwaite's moisture index of the area is almost zero, suggesting that sub-humid conditions prevail (Schulze, 1958). Using the climatic N-value derived by Weinert (1974), which has been calculated as N=2, and the relationship between climate and type of weathering as shown by Figure 2.3 from Fookes *et al.* (1971), it can be seen that the main weathering mechanism under the current climatic conditions at Injaka Dam site is chemical decomposition.

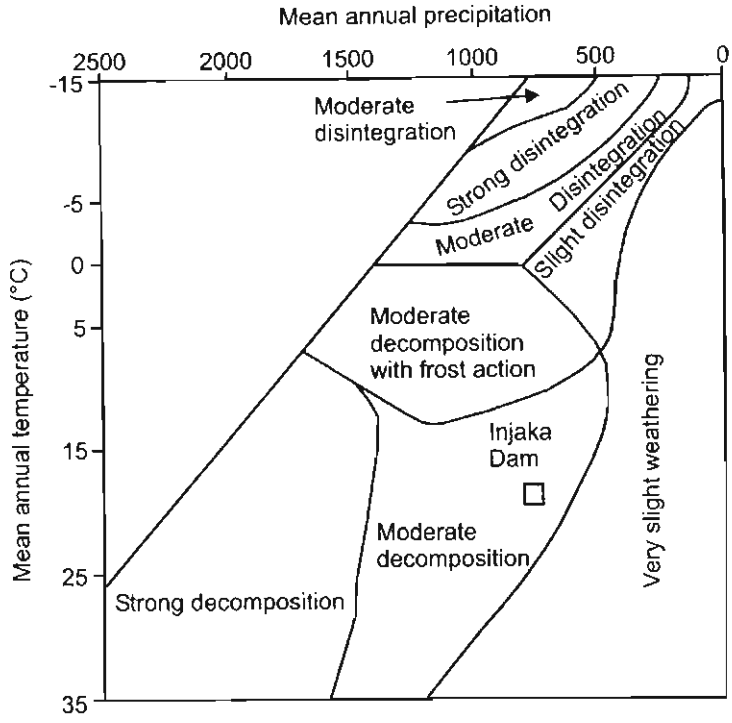

Figure 2.3 Relationship between climate and type of weathering (after Fookes *et al.*, 1971).

2.3 Geology of the Site

The regional geology of the area is depicted in Figure 2.4a with the local geology of the dam site presented in Figure 2.5 and a cross section along the dam centreline shown in Figure 2.6. The majority of the region (including the dam site) is underlain by medium-grained quartz-microcline-plagioclase-biotite migmatite, granite and gneiss. Mafic and ultramafic xenoliths up to 300mm in diameter occur locally, but do not appear to be very common. Towards the western portion of the site, comprising the upper reaches of the reservoir area, white to pale brown, medium to coarse-grained porphyritic biotite granite becomes more predominant. Both lithologies are unnamed, but belong to the 3 075 Ma Nelspruit Suite, SACS (1980). The transition from the more massive granite in the west to the gneissic rocks in the east is gradual with the contact not easily recognised.

Numerous post-Transvaal age diabase dykes (younger than 2 300 Ma) intrude the area, Chunnett *et al.* (1991a). The diabase is generally dark grey, fine-grained and massive. The predominant strike direction of these lineaments is north-northeast with a secondary strike direction for the dykes being approximately east-west. The dykes vary from 10 m to 20 m in thickness and are generally steeply dipping (>70°). A major fault with associated shear zone strikes approximately north-south at the location of the dam site (Figure 2.5). This feature is composed of pegmatite and mylonitic breccia. Detailed geological mapping of the dam site has revealed a complex temporal relationship

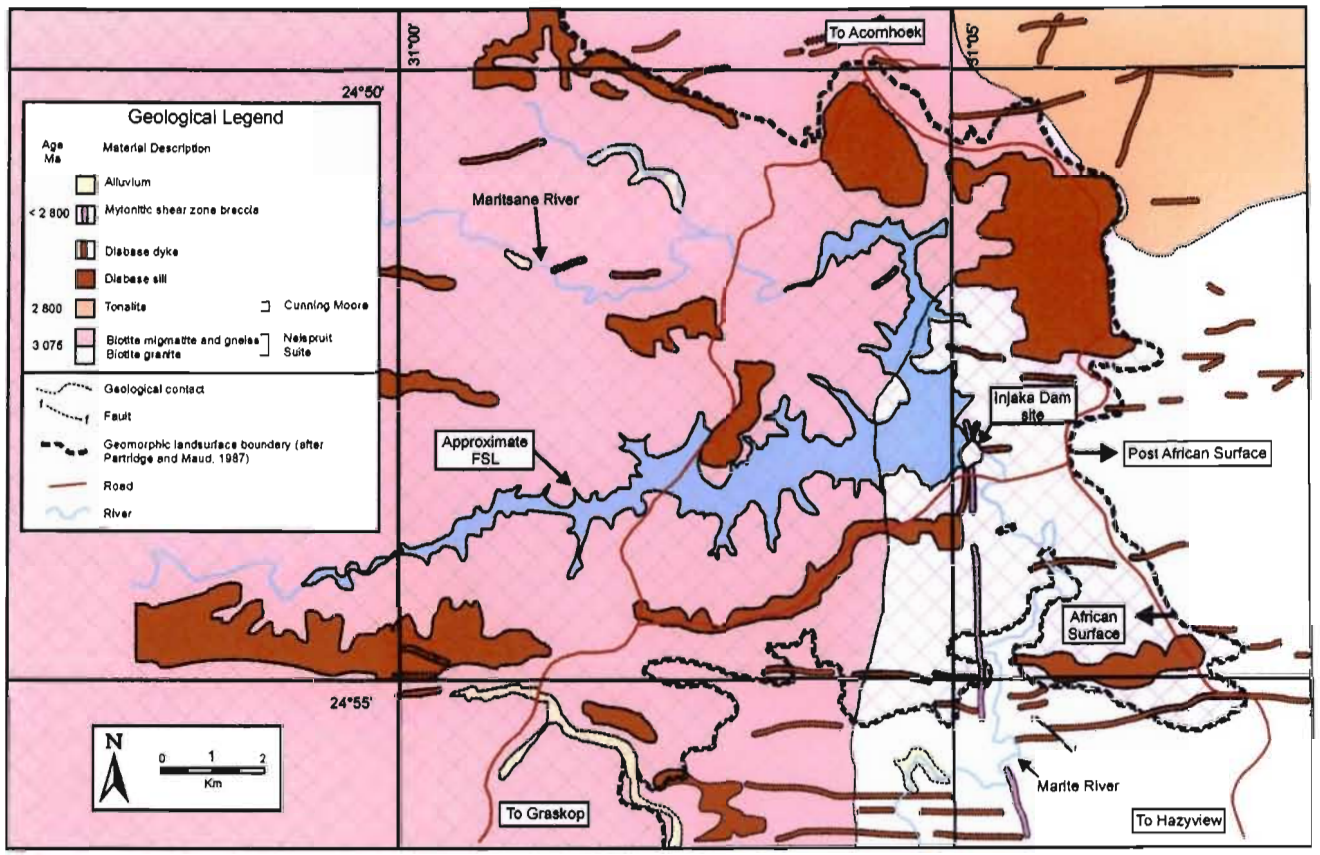

Figure 2.4a. Regional geology of Injaka Dam site (modified after Chunnett *et al.*, 1991a) showing Post African and African erosion surfaces.

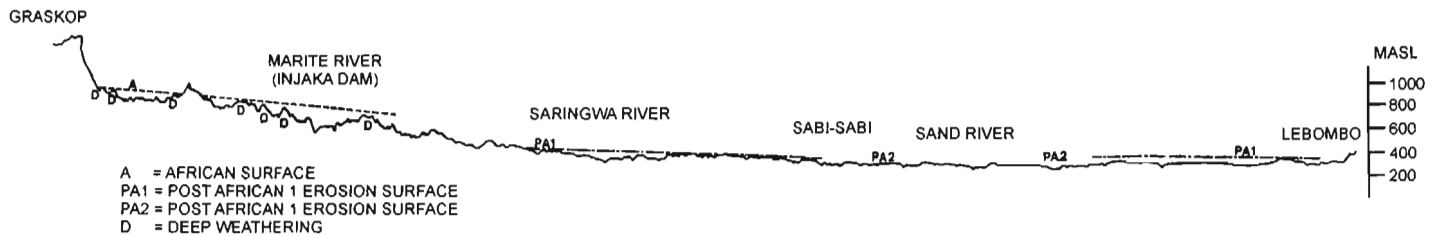

Figure 2.4b. Geomorphic cross section over Marite River showing position of African and Post African 1 and 2 Surfaces (from Patridge and Maud, 1987).

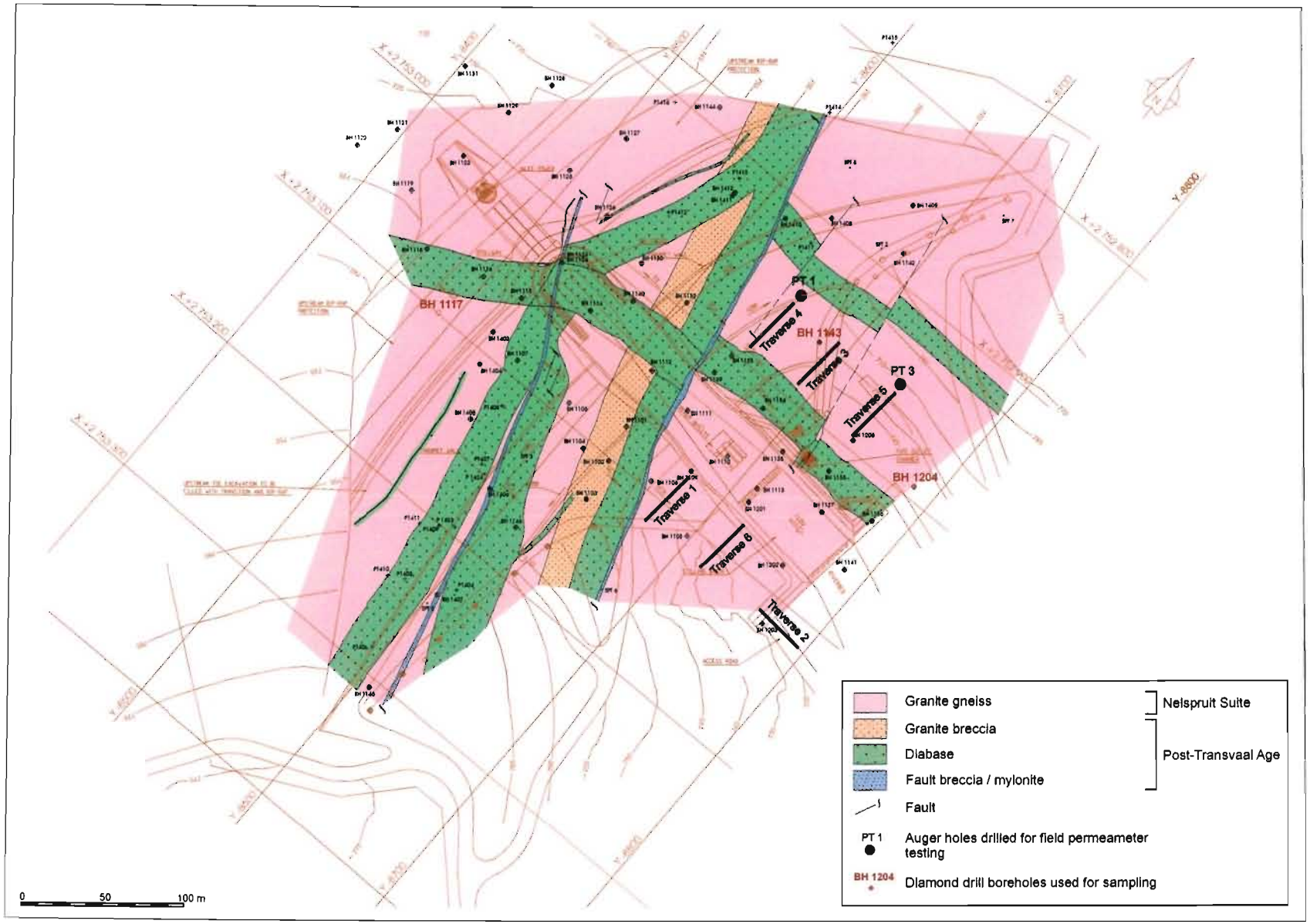

Figure 2.5. Local geology of Injaka Dam site showing positions of sample traverses (see Chapter 5) in relation to dam foundation footprint.

between the faulting and the intrusion of the dykes. A very prominent chlorite schist zone (2 m in width) is associated with post-intrusion emplacement of the linear north-south trending dyke encountered at the site.

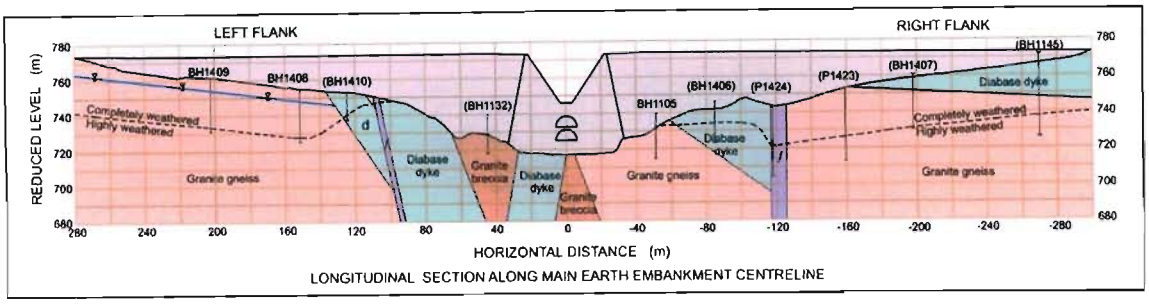

Figure 2.6. Geological cross section along dam centreline (post excavation of foundation footprint).

The major fault zone composed of recemented pegmatite and mylonitic breccia is resistant to erosion and manifests itself as a positive linear ridge clearly observable from aerial photographs and surface inspection. However, the granite and the diabase dykes are very susceptible to chemical weathering forming thick mantles of decomposed material and only outcrop on very steep slopes or in the river channel where erosion and scouring exposes the bedrock (Figure 2.7). This thick weathered mantle has formed from extensive cycles of weathering over geological time.

According to the description of the geomorphic evolution of southern Africa by Partridge and Maud (1987), Injaka Dam site is located below the former position of the African erosion surface as shown in Figures 2.4a and b. This extensive geomorphic surface is representative of enduring, multiple weathering and erosion cycles that started in the Cretaceous and terminated in the Miocene, lasting some 140 million years and that was initiated by a series of continental uplifts. During this period an extensive area of extraordinary smoothness was planated (Brink, 1996). The extreme intensity of the weathering during this period has resulted in the formation of saprolitic soils up to 35 m thick in places typified by extensive kaolinisation of the weathered profile. The current sub-tropical climate of the area has also contributed to the enhanced chemical weathering, although the full extent of this is not known. Subsequent erosion cycles caused by uplift and rejuvenation have intersected the African erosion surface, partially stripping the thick mantle of weathered material. One such surface as shown in Figures 2.4a and b is the Post African 1 surface which was triggered by tectonic uplift in the Miocene and is generally typified by thinner weathered mantles than those observed on the African erosion surface (Falla, 1985).

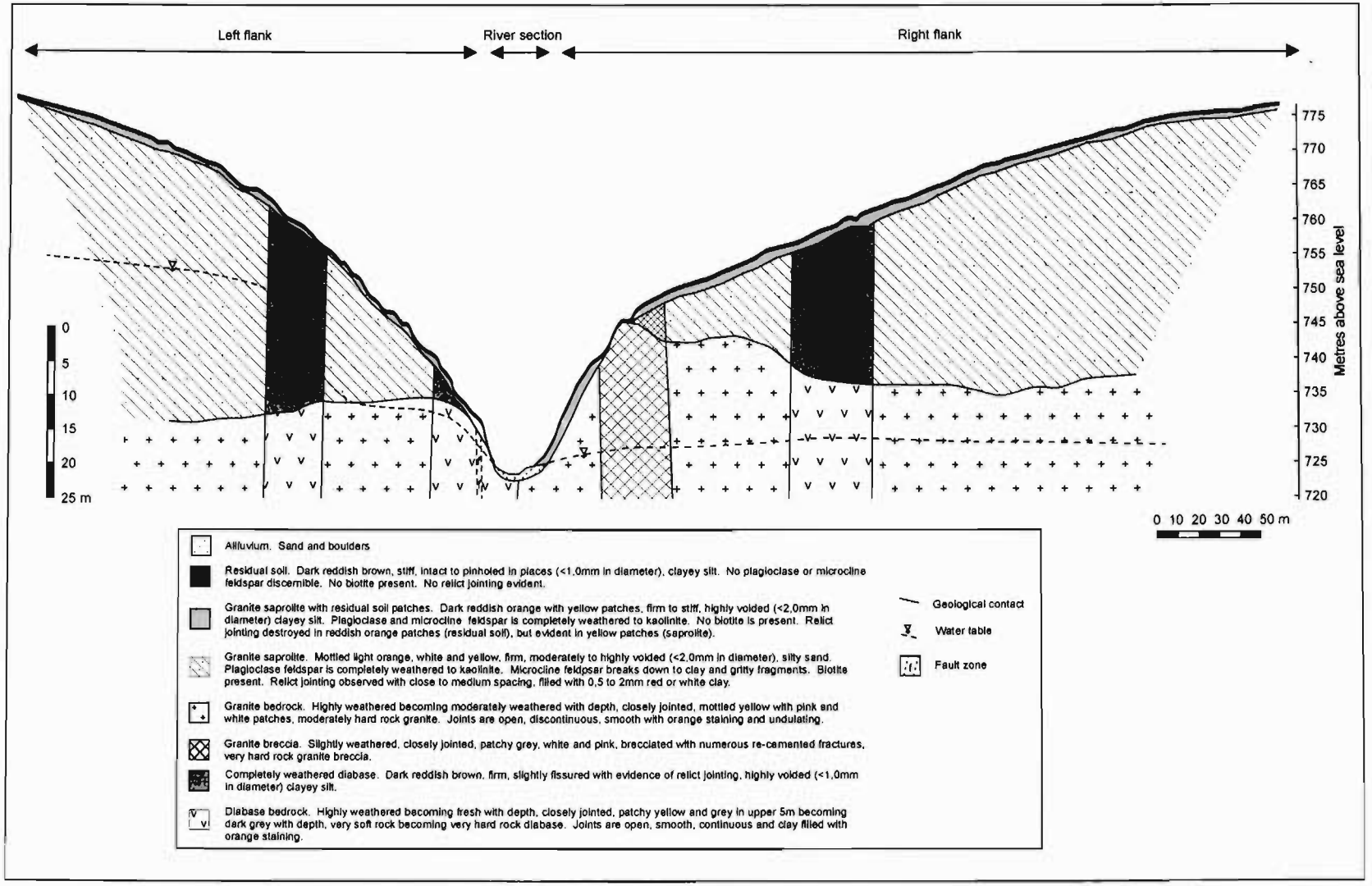

Figure 2.7. Typical geological cross-section of the Marite River valley at Injaka Dam site pre-excavation of dam foundation footprint.

3. CHEMICAL WEATHERING OF GRANITES

3.1 Introduction

Chemical weathering is the disequilibrium reaction of rocks and soils to their surrounding environment. Generally, the nature of this environment is governed by the presence and quantity of water; the availability of oxygen and the formation of carbonic acids. As Velbel (1984) suggests, chemical weathering of rocks and minerals is one of the most important geochemical processes by which chemical elements are fractionated at the earth's surface. The complex interaction of weathering and erosion effects are concentrated in the upper domain of the earth's crust and as all engineering works are carried out at or close to the earth's surface, it is obvious that such activities will be directly influenced by these two processes.

The effects of chemical weathering on the engineering behaviour of rocks and soils are many and varied but generally combine to weaken the material. The most common effect is that of increased porosity due to solution and stress relief (Vaughan and Kwan, 1984). This porosity may be in the form of irregular inter- and intra-granular voids or through the development of inter and intra-granular microfractures which make the material more friable. Through these processes, chemical weathering also results in weakening of mineral grains and a loss or partial loss of bonding between such grains as observed by Nishida and Aoyama (1985) in their study on decomposed granite soil. Sowers (1963) has shown that these effects contribute to an increase in the deformability of the weathered material. In many weathering systems, new minerals are deposited in voids, along grain boundaries and along fractures. In some cases, as in the formation of iron oxide cementation in laterites, these new minerals can strengthen the weathered rock material (Bell, 1999). Alternatively, these new decomposition products can be leached out of the system leaving a more porous structure. These effects can alter the permeability of the material, but this will depend upon the nature of the rock, the presence and type of weathering products and the intensity of the weathering.

3.2 Processes of chemical weathering

Chemical weathering leads to mineral alteration primarily affected by oxidation, reduction, hydration, hydrolysis, carbonation and chelation. Oxidation involves the reaction with oxygen to form oxides, or if water is incorporated, hydroxides. This is considered to be one of the most common chemical weathering reactions and is particularly important in rocks which contain oxidizable substances such as iron. Reduction is the opposite of oxidation and occurs in anaerobic conditions where the availability of oxygen is limited. Hydration is the addition of water to a mineral and is very important in the formation of clay products whilst hydrolysis is the chemical reaction

between the ions of a mineral and the H^+ and OH^- ions of water and occurs whenever a mineral is in contact with water. Carbonation is the reaction of carbonate or bicarbonate ions with minerals. The source of these ions is from dissolved CO_2 in water. Carbonates are not common end products of *in situ* weathering, but the formation of carbonates is an interim step in the weathering of certain minerals, in particular feldspars. Chelation or complexing involves the retention of an ion (usually a metal) within a ring structure of organic origin and is commonly used by plants. Chelation agents allow for the extraction of ions from otherwise insoluble solids, enabling transfer of these ions in chemical environments in which they would normally be precipitated. The most important chemical weathering reactions that occur at Injaka Dam include hydrolysis and hydration leading to the formation of kaolinite end products. During these reactions, solution and leaching play an important part in increasing the porosity of the material.

The rate at which the various weathering processes take place is dictated by three major factors including environmental factors (climate, hydrological, topographical and biological conditions); rock mass properties (homogeneity, nature and spacing of fractures, and secondary permeability) and rock material properties (composition, fabric, texture and primary permeability). These factors control the reaction and equilibrium rates between granite minerals (quartz, alkali feldspars, plagioclase feldspars and micas) and outside reactants, including water, oxygen, carbon dioxide and biological acids to form decomposition products. According to Ollier (1984) the following decomposition products can be considered as diagnostic of chemical weathering of granite :

Clay minerals (kaolinite, illite, gibbsite and smectite)
Insoluble iron oxides and hydroxides
Cations
Silica in solution

The nature and relative abundance of these products is dependent upon the intensity of the chemical weathering, the severity of eluviation processes, the solubility of the elements (order of solubility for common mineral forming elements is Ca>Na>Mg>K>Si>Al>Fe) and the pH of the ambient solutions. According to Loughnan (1969) and Velbel (1984) clay mineralogy in deep weathering profiles is consistent with the aqueous geochemistry of the weathering solutions. Different clay minerals can only develop if the cations integral to their formation are available within the immediate micro-environment or through weathering solutions. If eluviation is not significant, cation-rich clay species such as montmorillonite and illite are formed. Alternatively, intense flushing of the system removing practically all soluble components can result in the formation of kaolinite and eventually gibbsite. Figure 3.1 shows details of the proposed mineral weathering paths for granite in Hong Kong as identified by Irfan (1996). Weathering paths identified for the granite at Injaka Dam are shown in red.

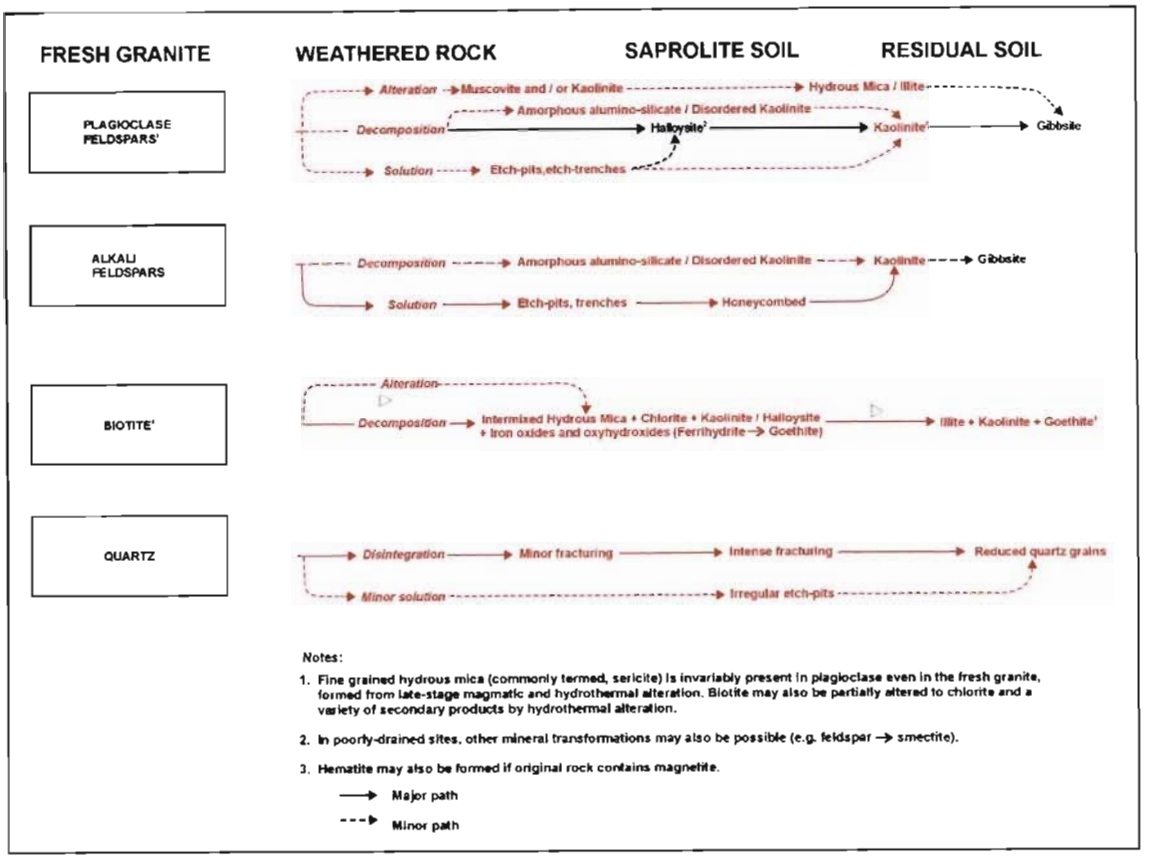

Figure 3.1. Weathering paths of mineral transformations in Hong Kong granites as proposed by Irfan (1996). Paths shown in red indicate mineral transformations of granite weathering at Injaka Dam.

3.3 Mineralogical transformations during chemical weathering of granite

Molecularly the weathering of silica in the form of quartz and silica minerals can be considered to be insignificant. However, the silicate minerals including feldspars and micas are particularly susceptible to chemical weathering. The feldspar minerals can be categorised into two groups: plagioclase and alkali feldspars. The susceptibility of these minerals to chemical weathering is explained by Zhao *et al.* (1994a) who describe the basic unit of silicate minerals, the silica tetrahedron, as being composed of weak Si-O-Si linkages maintained by intricate interactions between geometric and electrostatic factors. During the weathering of silicates the cations are replaced by hydrogen ions as described by the following reaction:

silicate + hydrogen → metal cation + silicon hydroxide (Eqn. 3.3.1)

Eggleton (1986) suggests that the prevelance of defects in the original feldspar mineral governs the rate at which weathering can occur. As plagioclase contains multiple twin boundaries and complex crystallographic textures, it is likely to alter more rapidly than simply twinned sanidine. Microcline containing numerous twin boundaries is also likely to weather rapidly. A summary of the detailed feldspar reactions during weathering is presented below :

Orthoclase (decomposition in acidic solution) (Eqn. 3.3.2)

$$KAlSi_3O_8 + H^+ \rightarrow K^+ + AlSi_3O_8^- + SiO_2 + H_2O$$

Na-plagioclase (decomposition in acidic solution) (Eqn. 3.3.3)

$$NaAlSi_3O_8 + H^+ \rightarrow Na^+ + AlSi_3O_8^- + SiO_2 + H_2O$$

Ca-plagioclase (decomposition in acidic solution) (Eqn. 3.3.4)

$$CaAlSi_3O_8 + H^+ \rightarrow Ca^{2+} + AlSi_3O_8^{2-} + SiO_2 + H_2O$$

The first stages of feldspar weathering can be observed both in optical and scanning electron microscopy. In plane polarised light the development of turbidity and microcracking along cleavage planes in feldspars can be observed. Scanning electron microscopy observations show the development of oriented etch pits, generally in positions related to twin planes (Berner and Holdren, 1979). Etch pits represent sites of crystal dislocations (crystal defects and mismatched bonds) which tend to be preferentially weathered. It is thought that etch pit sites are initially filled with clay formed from *in situ* weathering of the feldspar. Flushing and dissolution of the clay erodes the material, finally resulting in an empty etch pit. The presence of etch pits suggests that the weathering is primarily of a surface-controlled reaction, rather than diffusion-controlled reactions. Montgomery and Brace (1975) suggest that partially annealed cleavages or random fractures developed during early stage cooling of the rock are sites of locally higher porosity (usually twice average rock porosity). This excessive porosity may account for the more rapid decomposition of these sites.

The progressive weathering sequence of feldspar is classically presented as follows, although the formation of either smectite or kaolinite is governed by the drainage conditions during weathering, with smectite forming in poorly drained environments and kaolinite forming under well-drained conditions:

$$\text{Feldspar} \rightarrow \text{smectite} \rightarrow \text{kaolinite} \rightarrow \text{gibbsite} \qquad \text{(Eqn. 3.3.5)}$$

This reaction series can be explained by progressive silication of weathering solutions with reaction progressing as the solutions migrate downwards through the weathering profile.

Micas are 2:1 phyllosilicates with tightly held interlayer cations. Both biotite and muscovite can be found in varying proportions within granite. Goldich (1938), in his classic appraisal of weathering, showed that muscovite is more resistant to weathering attack than biotite. Initial stages of biotite weathering as observed under the optical microscope show orange iron oxide staining along cleavage traces and at grain boundaries. More intense weathering effects result in the formation of orange "halos" encompassing the weathered biotite grain suggesting mobilisation of the metal oxide.

Generally, the classical weathering reaction series for muscovite and biotite are as follows :

Muscovite → vermiculite → beidellite

Biotite → vermiculite-chlorite → vermiculite

Zhao *et al.* (1994a) suggest the following detailed weathering reactions :

Muscovite (decomposition in acidic solution) (Eqn. 3.3.6)

$$KAl_2(Si_3AlO_{10})(OH)_2 + H^+ \rightarrow K^+ + Al^{3+} + AlSi_3O_{10}^{4-} + SiO_2 + H_2O$$

Biotite (decomposition in acidic solution) (Eqn. 3.3.7)

$$K(Mg,Fe)_3(Si_3AlO_{10})(OH)_2 + H^+ \rightarrow K^+ + (Mg^{2+}, Al^{3+}) + AlSi_3O_{10}^{4-} + SiO_2 + H_2O$$

Unlike most other silicates, sheet silicates characteristically dissolve and precipitate during weathering. Dissolution (and precipitation) generally begins on the basal surface (parallel to the layers) and the edge surfaces. As a consequence of the reactivity of the edges of the crystal sheets, sheet silicates tend to dissolve actively from the edge towards the core (Nagy, 1995).

In a similar manner to the rate of weathering of feldspars, the abundance of surface defects on the mica grain surface may also control the susceptibility of the mineral to dissolution effects. Such surface defects include steps, kinks, structural defects, compositional impurities and dislocations. Steps and kinks provide sites of different reactivity because they present different bonding arrangements for dissolution reactions. Structural defects are sites of higher energy, whilst compositional impurities, and particularly dislocations, may be sites of local higher strain energies.

The nature of these weathering reactions encountered at Injaka Dam is presented in the forthcoming Chapters 6 to 9, where petrographic, mineralogical and microfabric studies using a scanning electron microscope are detailed.

4. THE DESCRIPTION AND CLASSIFICATION OF WEATHERED GRANITE

4.1 Introduction

It has been acknowledged by Dearman (1995) that different rock types respond differently to weathering processes - this being a function of their different mineralogy and different macro- and micro-weathering environments. It stands to reason then that no weathering classification system can be devised that is suitable for all rock types. In fact, it has been recognised by Anon (1995) that classification systems can even differ from site to site.

A tremendous amount of literature is available describing the many systems used to classify weathered rock to further understand and predict their engineering behaviour. Many of these systems were developed from studies focussed on granite weathering. It is not the intention of this study to review all these classification systems, however, it is important to illustrate the particular methodology that was used for this study. The need to classify weathering of rock allows for comparable descriptions of zones of rock and soil with particular characteristic qualities to which engineering characteristics can be assigned. For a classification system to be successful it must be able to identify a sequence of recognisable stages in decomposition and/or disintegration of the rock and must show the differences in the progressive changes of the physical and mechanical properties which influence the engineering performance of the weathered material.

4.2 Review of selected classification systems

Moye (1955) was perhaps the first to classify weathered granite into groups using engineering parameters of weathered granitic rock exposed in outcrops, excavations and recovered as drill cores. His classification system provided detailed descriptions of six stages of chemical weathering ranging from fresh granite to granitic soil (Table 4.1). Highly and completely weathered granites classified as engineering soils, whilst fresh to slightly weathered granites classified as rock. The moderately weathered granite proved difficult to classify as the material was often a transition between soil and rock.

Shortly thereafter, Ruxton and Berry (1957) employed a more geologically and pedologically orientated approach to their classification of weathered Hong Kong granite where they made use of identifying the percentage of solid rock within the weathering profile and the characteristics of the residual weathered material ("debris"). They employed a four (I-IV) zone classification, one of which can be sub-divided, as shown in Figure 4.1.

Table 4.1. Summary of weathering factors taken into account in the Moye (1955) weathering classification with grade numbers from Little (1969) and after Dearman (1995).

Degree of weathering	Engineering classification	Recognition factors	Grade number
Granitic soil	Soil	G	VI
Completely weathered	Soil	A B C D E F	V
Highly weathered	Soil	A B C D	IV
Moderately weathered	Rock	A B C	III
Slightly weathered	Rock	A B C	II
Fresh	Rock	A	I

Recognition Factors

A	Joints stained	E	Disintegrates in water
B	Rock and soil material stained	F	Biotite decomposed
C	Feldspars decomposed	G	Original texture absent
D	Strength : NX cores can be broken in the hand		

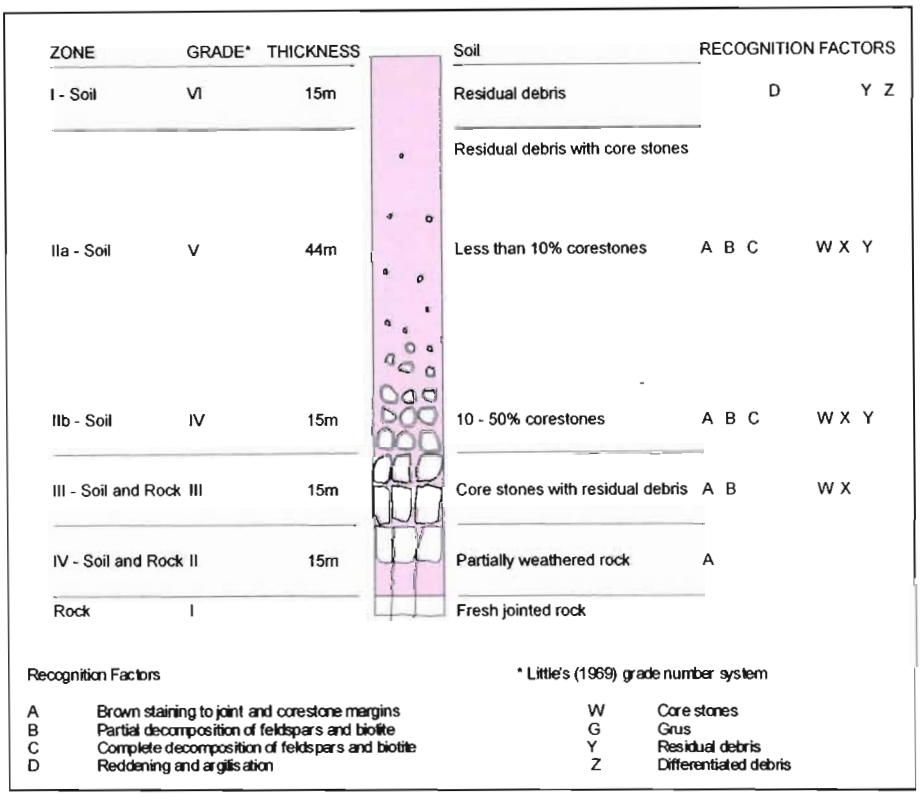

Figure 4.1. Weathering classification system of Ruxton and Berry (1957) with grade numbers after Little (1969).

From the detailed descriptions given by Moye, it is possible to analyse his classification scheme into six classes of "degrees of weathering" in terms of the seven recognition factors A to G given in Table 4.1. In a review of the engineering classification of tropical residual soils, particularly with reference to Hong Kong and Malaysia, Little (1967) developed this idea of six weathering stages each identified by a grade number I-VI. He discerned categorical differences between weathered material using the degree of discolouration, soil:rock ratios and the nature of the relict texture within

the six classes of "degrees of weathering" identified by Moye (1955). This six-fold grading system described the fresh rock as Grade I with the residual soil labelled as Grade VI (Tables 4.1 and 4.2). Little (1969) later updated the concept of rock:soil ratio (previously introduced by Ruxton and Berry, 1957) for the description of weathered granite. His classification is presented in Table 4.2 and is important as it introduces a description of the state of the feldspar grains - which Baynes and Dearman (1978a), Irfan (1988) and Lee and de Freitas (1989) have shown to be so important when assessing the engineering behaviour of the weathered granite.

Table 4.2. Classification of the various stages of the weathering processes on granite (Little, 1969).

Grade	Degree of decomposition	Field recognition	Engineering properties
VI	Soil	No recognisable rock texture; surface layer contains humus and plants	Unsuitable for important foundations. Unsuitable on slopes when cover is destroyed.
V	Completely weathered	Rock is completely decomposed by weathering in place but texture still recognisable. In types of granitic origin, original feldspars completely decomposed to clay minerals. Cannot be recovered as core by ordinary rotary drilling techniques.	Can be excavated by hand or ripping without use of explosives. Unsuitable for foundations of concrete dams or large structures. May be suitable for foundations of earth dams and for fill. Unstable in high cuttings and steep angles. Requires erosion protection.
IV	Highly weathered	Rock so weakened by weathering that fairly large pieces can be broken and crumbled in the hands. Sometimes recovered as core by careful rotary drilling . Stained by limonite. Less than 50% rock.	Similar to Grade V. Unlikely to be suitable for foundations of concrete dams. Erratic presence of boulders make it an unreliable foundation stratum for large structures.
III	Moderately weathered	Considerably weathered throughout. Possessing some strength - large pieces (e.g. NX drill core) cannot be broken by hand. Often limonite stained. %)% to 90% rock.	Excavated with difficulty without use of explosives. Mostly crushes under bulldozers tracks. Suitable for foundations small concrete structures and rockfill dams. May be suitable for semi-pervious fill. Stability in cuttings depends on special features, especially joint attitudes.
II	Slightly weathered	Distinctly weathered through much of the rock fabric with slight limonite staining. Some decomposed feldspar in granites. Strength approaching that of fresh rock. More than 90% rock.	Requires explosives for excavation. Suitable for concrete dam foundations. Highly permeable through open joints. Often more permeable than the zones above or below. Questionable as concrete aggregate.
I	Fresh rock	Fresh rock may have some limonite-stained joints immediately beneath weathered rock.	Staining indicates water percolation along joints; individual pieces may be loosened blasting or stress relief and support may be required in tunnels.

Lee and de Freitas (1989) presented a critical review of the current and past methods used for classifying weathered granite and proposed a new rational approach adopting geological and mechanical information to classify the weathered granite. Their main objection to many of the existing weathering classification schemes was that they lead to difficulties in weathering description and classification because of the imprecise and inadequate nature of the descriptive terms. Martin and Hencher (1986) also found similar fault with the description of weathered rocks in BS 5930 (British Standards Institution, 1981), their criticism directed specifically at this scheme.

Nevertheless, it is clear from the above discussion that the framework of any classification system is driven by the specific needs of the project to classify the weathered material.

The concept of a six-fold classification system has generally found favour with various engineering bodies (Anon, 1981 and 1995) and is also applicable to local igneous rocks in South Africa. The classification system employed for this study used a modification of the prescriptive weathering classification for uniform materials as proposed by Anon (1995). Before presenting this system it is necessary that several of the terms be defined. Any general weathering scheme for granites should include sequences of changes in material properties resulting from both chemical and physical weathering processes acting together or individually (Dearman *et al.*, 1978). The basic description of the weathering grades of rock can be formulated from the key descriptive terms defined in Table 4.3. The use of these terms is flexible and they may be sub-divided using qualifying terms (Lee and de Freitas, 1989). Ultimately, the application of any classification system will require some modification to suit the needs of the particular investigation. A better understanding of the descriptive terms used in Table 4.3 can be gained when seen in the context of the weathering processes as shown by the idealised diagram of weathering of rock material in Figure 4.2. This flow chart shows the effect that disintegration, decomposition and solution processes have on the nature of the rock fabric and mineral grains as weathering proceeds and identifies the different varieties of fabric that can be achieved through these weathering paths.

Table 4.3. Key descriptive terms for classifying weathered rock material (after Dearman *et al.*, 1978).

TERM	DESCRIPTION
Fresh	No visible signs of weathering of rock material.
Discoloured	The colour of the original rock material is changed and is evidence of weathering. The degree of change from the original colour should be indicated. If the colour change is confined to particular mineral constituents this should be mentioned.
Weakened	The rock is weakened to the extent that it is noticeably weakened, however it is not technically a soil.
Decomposed	The rock is weathered to the condition of a soil in which the original material fabric is still intact, but some or all of the mineral grains are decomposed.
Disintegrated	The rock is weathered to a condition of a soil in which the original material fabric is still intact. The rock is friable, but the mineral grains are not decomposed.

As mentioned, the classification of weathered granite at Injaka Dam uses the uniform material classification system prescribed by Anon (1995), and significantly, has been chosen because no corestones occur within the profile (Figure 4.3). Figure 4.4 shows the detail of the classification system, with Table 4.4 addressing the basic definitions of the grade numbers in terms of the weathering of the rock. Figure 4.4 also shows the saprolite as being classed as Grade V material. The material overlying the saprolite, termed granite saprolite with residual soil patches in this study,

straddles the Grades V and VI boundary. Material details for each relevant class are presented in Figure 4.4.

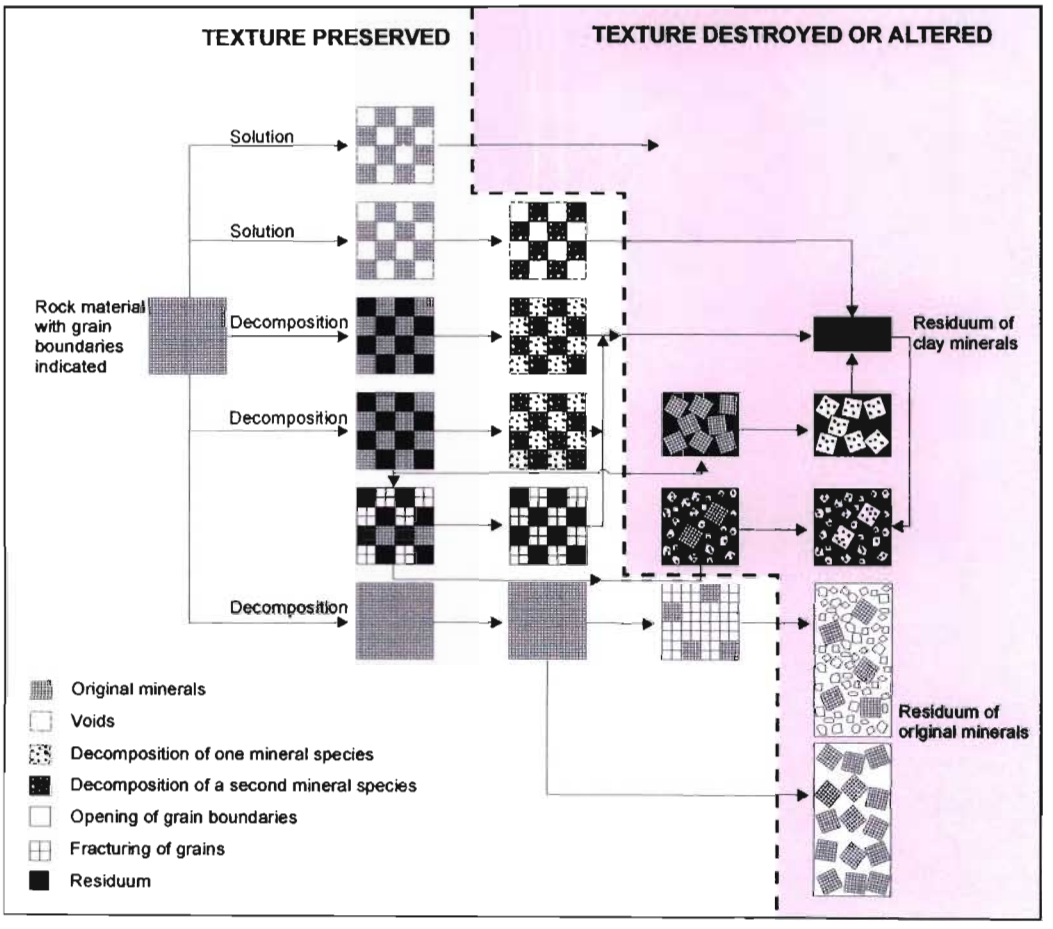

Figure 4.2. Idealised diagram of the stages of weathering of rock material (after Dearman, 1974).

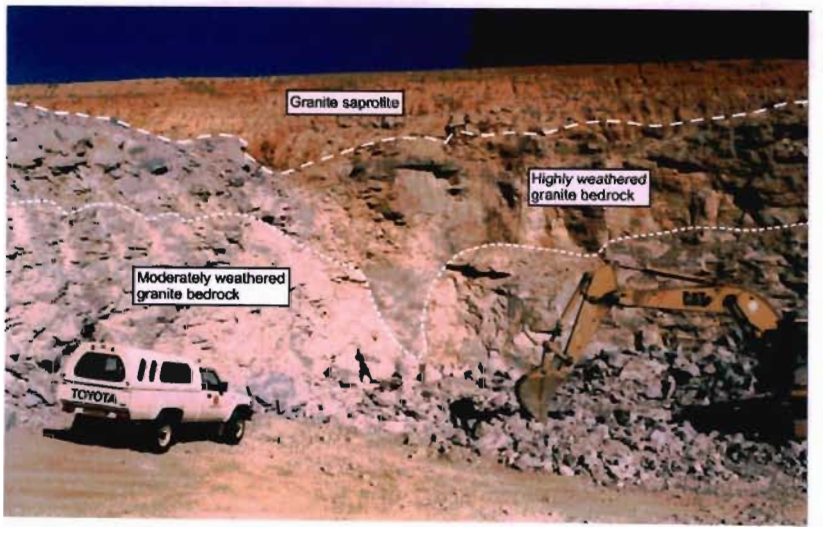

Figure 4.3. Typical weathering profile encountered at Injaka Dam site. Note the distinct lack of core stones with the very abrupt contact separating granite saprolite from highly weathered granite bedrock.

Table 4.4. Description of weathering grades of rock mass description used in Figure 4.4.

Grade	Term	Description
VI	Residual Soil	All rock material is converted to soil. The mass structure and material fabric are destroyed. There is a large change in volume, but the soil has not been significantly transported.
V	Completely weathered	All rock material is decomposed and/or disintegrated to soil. The original mass structure is still largely intact
IV	Highly Weathered	More than half of rock material is decomposed or disintegrated to a soil. Fresh or discoloured rock is present either as a continuous framework or as corestones.
III	Moderately Weathered	Less than half of the rock material is decomposed or disintegrated to soil. Fresh or discoloured rock is present either as a continuous framework or as corestones.
II	Slightly Weathered	Discolouration indicates weathering of rock material and discontinuity surfaces. All rock material may be discoloured by weathering.
I	Fresh	No visible sign of rock material weathering; perhaps slight discolouration on major discontinuity surfaces.

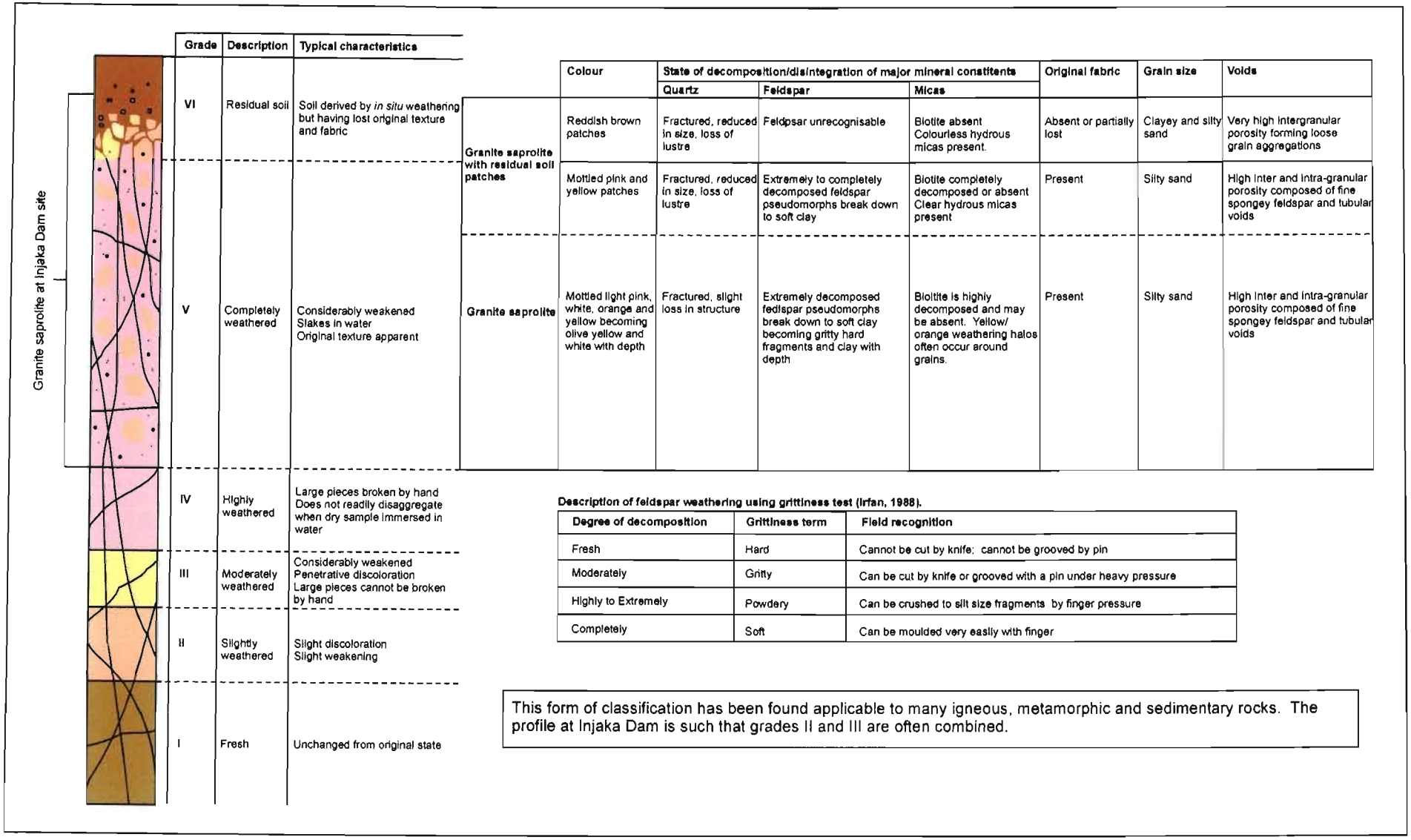

Grade	Description	Typical characteristics
VI	Residual soil	Soil derived by *in situ* weathering but having lost original texture and fabric
V	Completely weathered	Considerably weakened Slakes in water Original texture apparent
IV	Highly weathered	Large pieces broken by hand Does not readily disaggregate when dry sample immersed in water
III	Moderately weathered	Considerably weakened Penetrative discoloration Large pieces cannot be broken by hand
II	Slightly weathered	Slight discoloration Slight weakening
I	Fresh	Unchanged from original state

	Colour	State of decomposition/disintegration of major mineral constituents			Original fabric	Grain size	Voids
		Quartz	Feldspar	Micas			
Granite saprolite with residual soil patches	Reddish brown patches	Fractured, reduced in size, loss of lustre	Feldpsar unrecognisable	Biotite absent Colourless hydrous micas present.	Absent or partially lost	Clayey and silty sand	Very high intergranular porosity forming loose grain aggregations
	Mottled pink and yellow patches	Fractured, reduced in size, loss of lustre	Extremely to completely decomposed feldspar pseudomorphs break down to soft clay	Biotite completely decomposed or absent Clear hydrous micas present	Present	Silty sand	High inter and intra-granular porosity composed of fine spongey feldspar and tubular voids
Granite saprolite	Mottled light pink, white, orange and yellow becoming olive yellow and white with depth	Fractured, slight loss in structure	Extremely decomposed fedlspar pseudomorphs break down to soft clay becoming gritty hard fragments and clay with depth	Biotite is highly decomposed and may be absent. Yellow/ orange weathering halos often occur around grains.	Present	Silty sand	High inter and intra-granular porosity composed of fine spongey feldspar and tubular voids

Description of feldspar weathering using grittiness test (Irfan, 1988).

Degree of decomposition	Grittiness term	Field recognition
Fresh	Hard	Cannot be cut by knife; cannot be grooved by pin
Moderately	Gritty	Can be cut by knife or grooved with a pin under heavy pressure
Highly to Extremely	Powdery	Can be crushed to silt size fragments by finger pressure
Completely	Soft	Can be moulded very easily with finger

This form of classification has been found applicable to many igneous, metamorphic and sedimentary rocks. The profile at Injaka Dam is such that grades II and III are often combined.

Figure 4.4. Classification system used for weathering of granite at Injaka Dam site (modified after Anon, 1995 and Irfan, 1988).

5. SAMPLING METHODOLOGY AND DESCRIPTION OF MATERIALS

5.1 Sampling Methodology

The excavations cut into the left and right valley flanks for the construction of the dam foundation footprint at Injaka Dam site provided ideal exposures from which to cut block samples of the weathered granite material through a vertical profile. This allowed an analysis of the changes in geochemistry, mineralogy, physical structure and engineering behaviour of the weathered granite as a function of depth. By cutting block samples directly from the excavation, disturbance during sampling was minimised. Heymann and Clayton (1999) have shown that block sampling is the preferred option for obtaining undisturbed samples as other methods such as tube and core sampling tend to disrupt the fabric of natural soils.

Undisturbed block samples were carefully hand cut and trimmed from the face of the excavation at vertical intervals of approximately 1 to 2m along six sample traverses (Figures 2.5 and 5.1 - 5.6). These block samples represented a volume of 0,1 to 0,2m^3. After trimming, the samples were immediately brush-covered with molten paraffin wax and then two further alternate layers of mutton cloth and wax until a firm protective layer surrounded the samples minimising any change in moisture content and damage during transit. Heymann (1998) has shown that a combination of cling film and wax proved to be the most effective method for reducing moisture loss from block samples of London Clay. However, the brittle nature of some of the weathered granite block samples from Injaka Dam site required the extra strength afforded by the mutton cloth and wax combination. Furthermore, some of the more delicate samples had to be covered with an integral layer of plaster-of-paris and mutton cloth surrounding the final wax-mutton cloth layer. This provided the extra rigid protection to these samples. The block samples were transported some 450 km to the Department of Water Affairs and Forestry Construction Materials Laboratory in Pretoria on a mattress of moist sawdust and stored in an humidity chamber prior to testing. Loose (disturbed) samples were also collected from the block sample sites, where trimmings from the block samples were collected to obtain representative material for laboratory testing, thus minimising any geochemical, mineralogical and textural differences between the block samples and the loose samples.

The locations of the six sample traverses are shown on Figure 2.5 with specific profile details presented in Figures 5.1 to 5.6. Figure 5.7 shows a photograph of the left flank of the dam foundation excavation during construction with the site geology in relation to the sample traverses on this flank. A total of forty eight samples of weathered granite material were retrieved from the sample traverses. The bulk

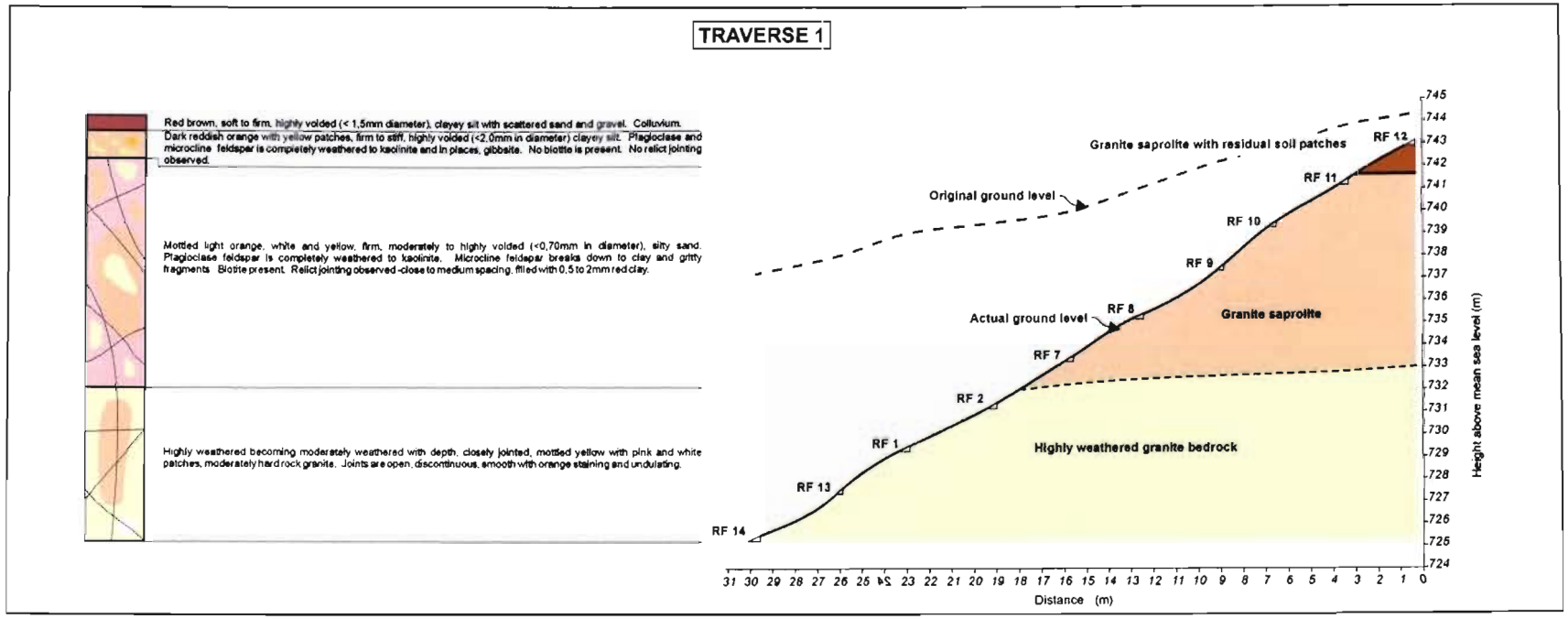

Figure 5.1. Sample traverse 1 incorporating right flank samples RF 12 to RF 14.

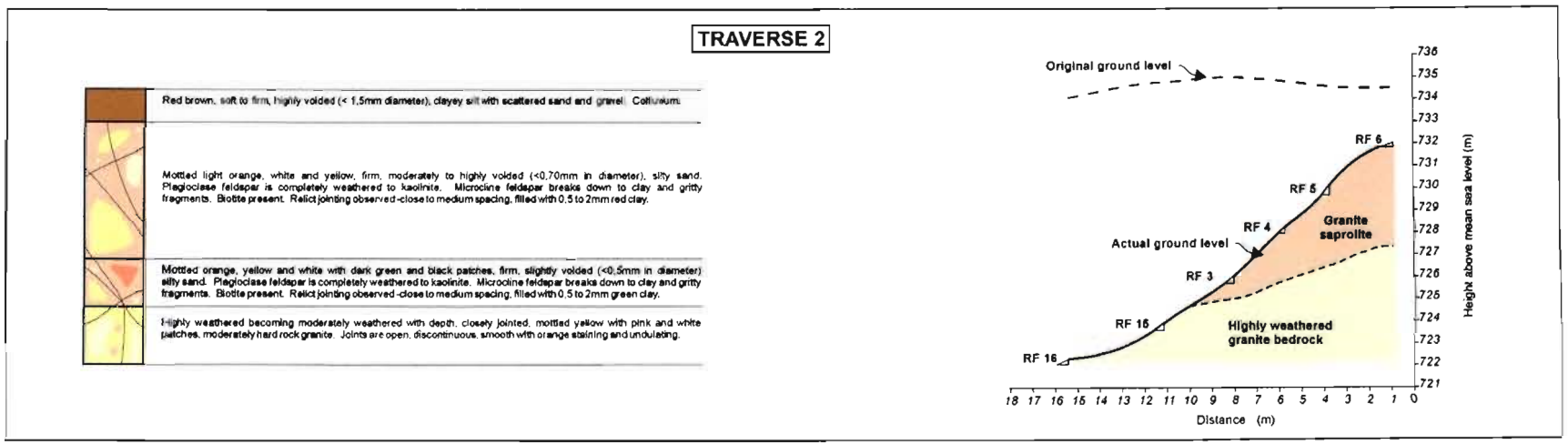

Figure 5.2. Sample traverse 2 incorporating right flank samples RF 6 to RF 16.

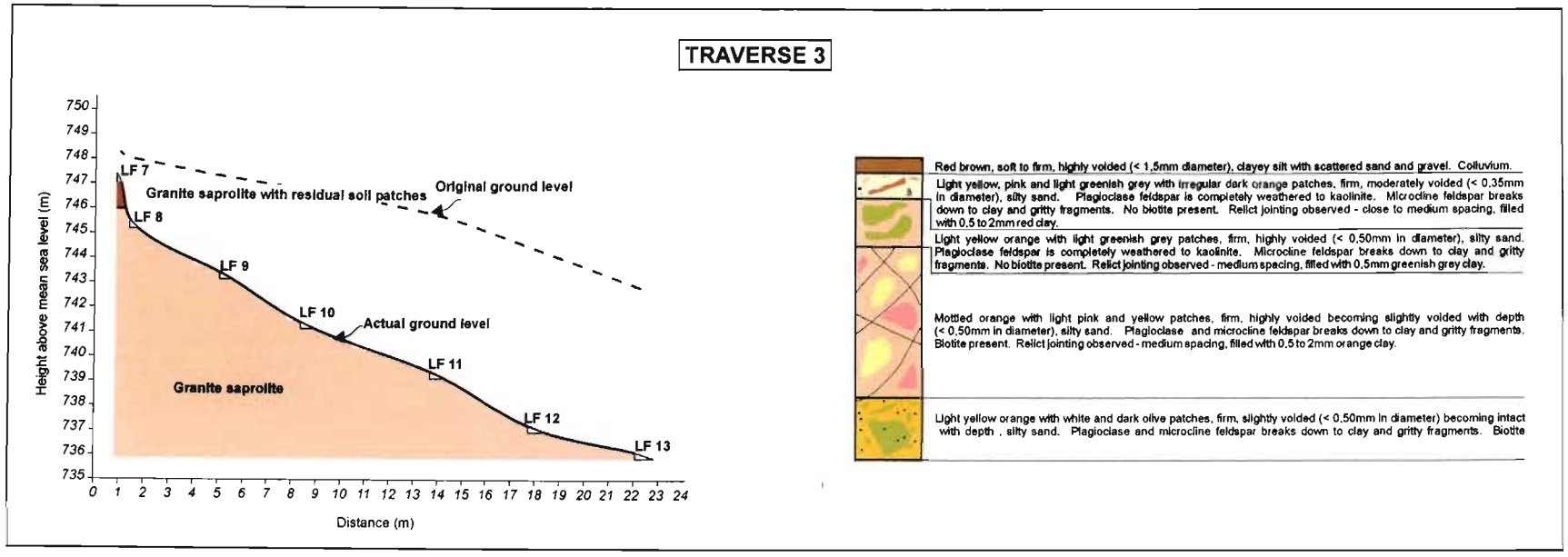

Figure 5.3. Sample traverse 3 incorporating left flank samples LF 7 to LF 13.

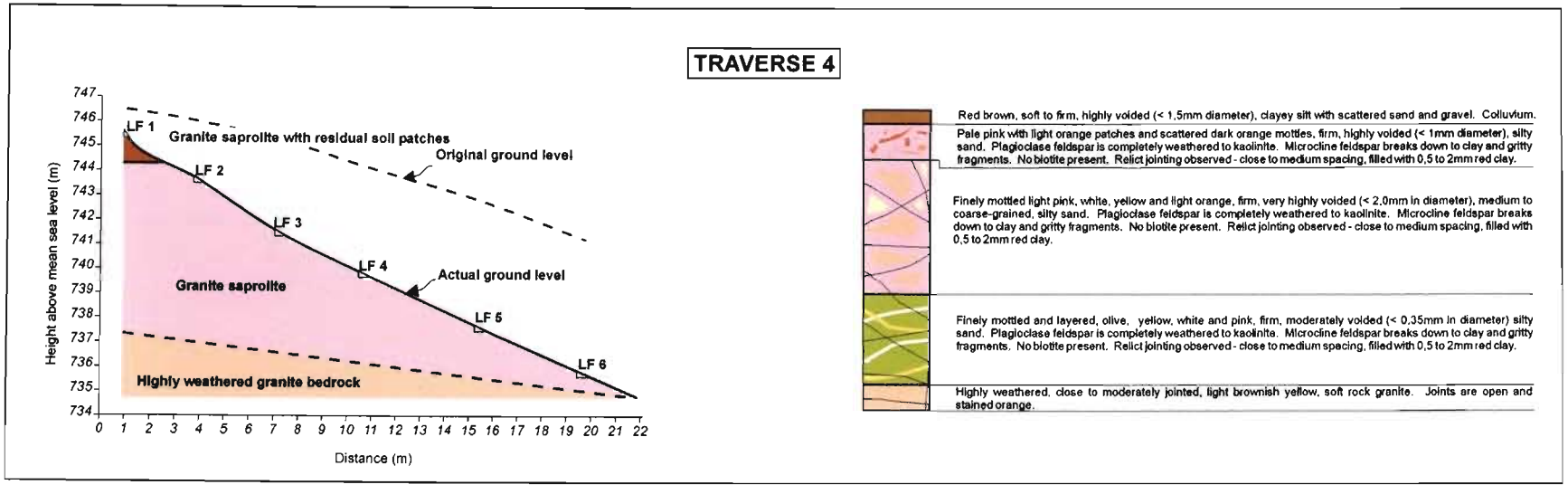

Figure 5.4. Sample traverse 4 incorporating left flank samples LF 1 to LF 6.

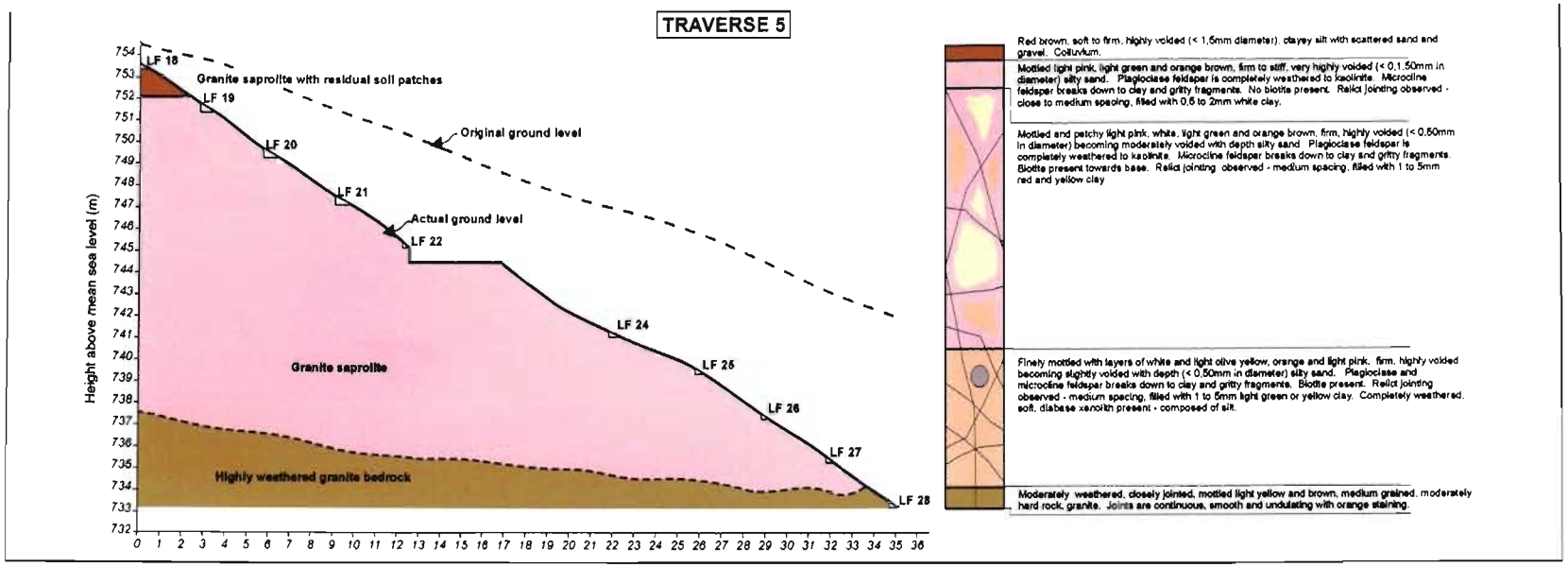

Figure 5.5. Sample traverse 5 incorporating left flank samples LF 18 to LF 28.

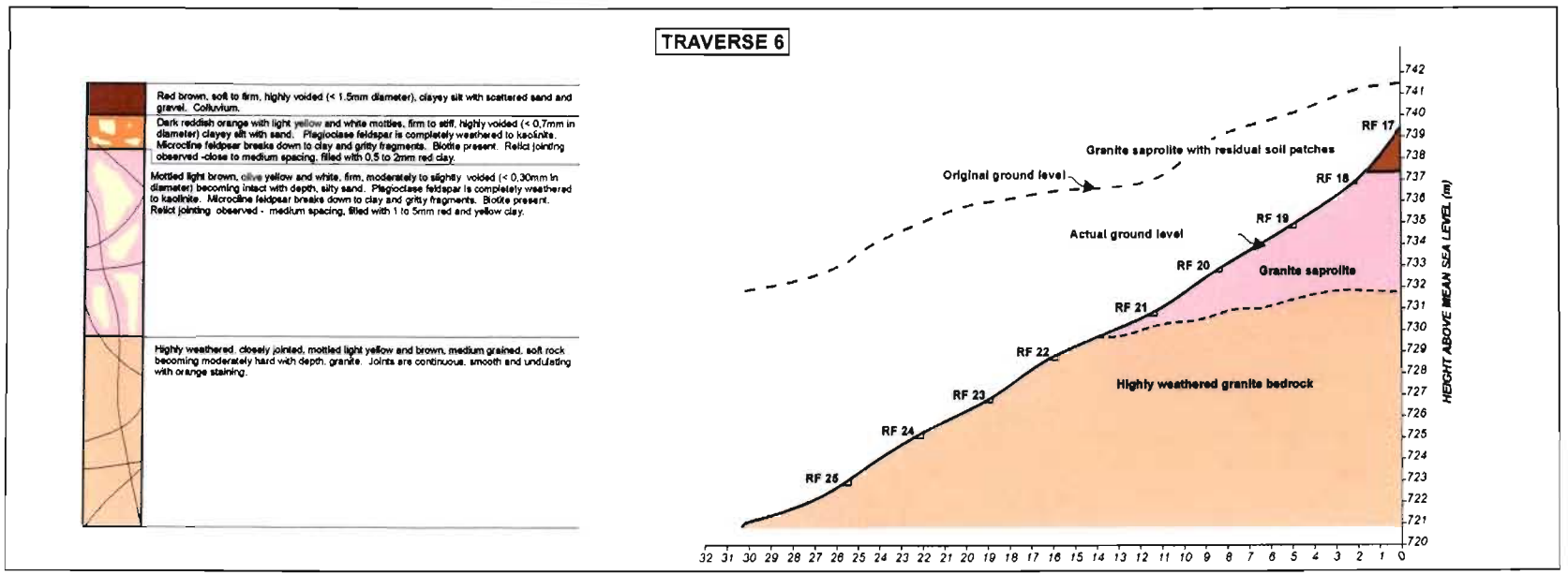

Figure 5.6 Sample traverse 6 incorporating right flank samples RF 17 to RF 26.

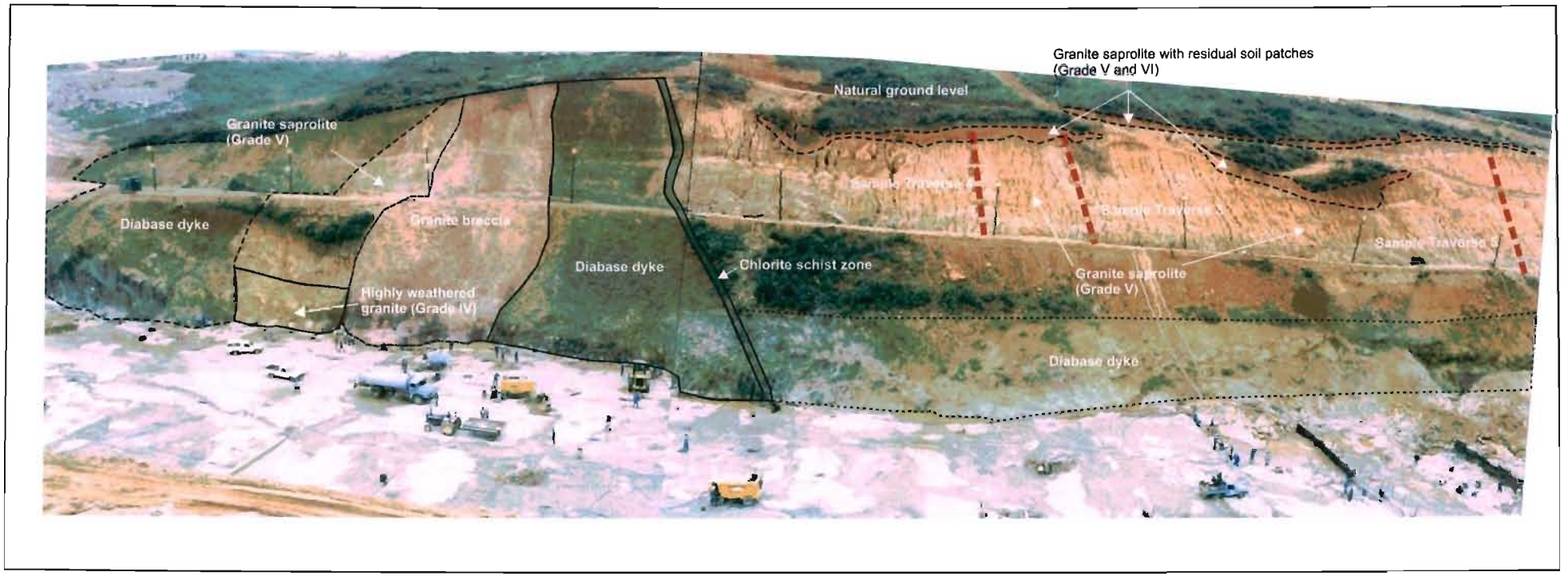

Figure 5.7. View of the left flank of Injaka Dam site showing the site geology and positions of sample traverses 3, 4 and 5. Weathering grades for the respective lithologies are also shown. Photograph taken from right flank, looking north.

of the samples incorporated granite saprolite at varying degrees of weathering intensity with granite saprolite with residual soil patches and weathered granite bedrock sampled for comparative purposes.

5.2 Description of materials

Using the classification system presented in Figure 4.4, detailed macroscopic descriptions of each sample were recorded in the field to compile the profile descriptions at each sample traverse. These are presented in Figures 5.1 to 5.6 depicting the sample traverses in relation to the excavated slope. Samples labelled "RF" were retrieved from the right flank traverses whilst samples labelled "LF" were collected from traverses set out on the left flank. The traverses prove the existence of up to 10m of granite saprolite directly exposed in the excavation flanks (although this thickness increases away from the face of the excavations as shown in Figure 2.7). The samples incorporated granite saprolite with residual soil patches, granite saprolite and weathered granite bedrock.

5.2.1 Granite saprolite with residual soil patches

The granite saprolite with residual soil patches occurs at the top of the profile and is distinguished from the saprolite proper in that it has some loss of relict fabric due to a more advanced weathering state (Figure 5.8). The horizon varies in thickness from 1,0 to 2,0m with a gradational contact with the underlying granite saprolite. This material characteristically features irregular shaped, highly oxidised, reddish brown patches of loose, silt and clay aggregations often having a high porosity. These patches occur irregularly throughout the horizon decreasing in abundance with depth and coalescing towards the surface to grade into the overlying reddish brown colluvial horizon. In some instances these patches coincide with root traces. The remainder of the material comprises a mottling of light pink, pale yellow and white, equigranular, firm, highly voided with void sizes ranging from 177 to 1500μm clayey and silty sand retaining the original fabric of the parent material. The macro-voids exhibit spherical openings and are vermiform (Figure 5.9) whilst the micro-voids can be observed as fine sponge-like accumulations within feldspar pseudomorphs and kaolinite aggregations. The quartz grains are often fractured reduced in size and have a loss of lustre. The plagioclase feldspar grains are extremely decomposed, breaking down to soft clay whilst the microcline feldspar grains break down to clay and occasional gritty fragments when scraped with a knife. Within the reddish brown patches, the feldspars are not recognisable. Biotite is completely absent with clear hydrous micas present.

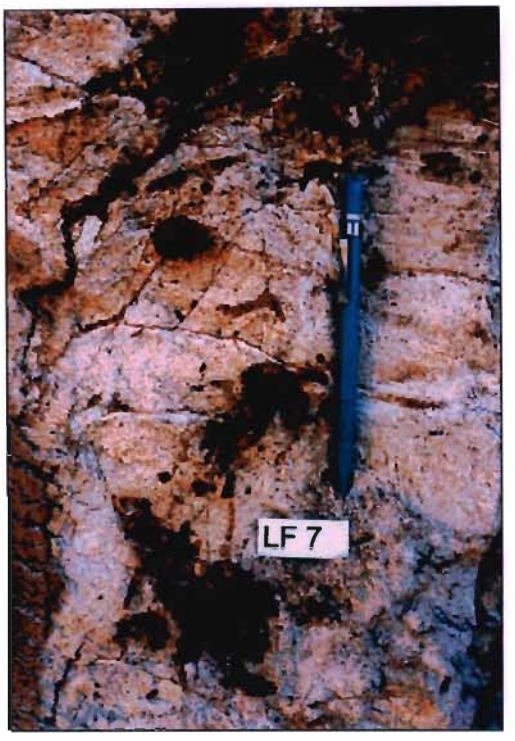

Figure 5.8. Granite saprolite (pink) with residual soil patches (red) showing complete loss of fabric structure where irregular patches of highly oxidised red clay aggregations occur (residual soil). Note also loss of fabric around root holes. Locality LF 7.

Figure 5.9. Close up view of granite saprolite (yellow) with residual soil patches (red brown) showing prevalent concentration of vermiform voids. Note partial disruption to fabric in highly oxidised (red brown) residual soil zones. Locality LF 18.

5.2.2 Granite saprolite

The granite saprolite exhibits a variety of colours and grain sizes which can change over very short distances (0,2m). This heterogeneity is a product of the heterogenous parent material fabric and local differences within the weathering microclimate. The granite saprolite varies from orange with fine yellow and light pink mottles in the upper profile to yellowish white with irregular dark olive patches towards the base of the profile (Figures 5.10 and 5.11).

Figure 5.10. Variation of granite saprolite typical of mid to upper profile material. Note distribution of vermiform solution voids throughout material and intact relict fabric showing structural interlock of grains. Locality LF 24.

The material is equigranular except where localised quartz pegmatite veins occur and is firm in consistency. Typical of this material is the presence of numerous tubular macro-voids (250 to 1000µm in diameter) as shown in Figures 5.10 and 5.11. These voids tend to preferentially form within feldspar-rich and coarser-grained zones. Micro-voids often manifest themselves as a sponge-like texture within feldspar pseudomorphs. The quartz grains are often fractured with a slight loss in lustre. Plagioclase feldspar grains are extremely decomposed forming pseudomorphs which break down to soft clay, whilst the less weathered microcline feldspar is moderately to highly decomposed and breaks down to clay and gritty fragments. Biotite may be absent in the upper reaches, but is highly decomposed lower down, often exhibiting halos of orange staining. The original fabric of the parent material is completely intact.

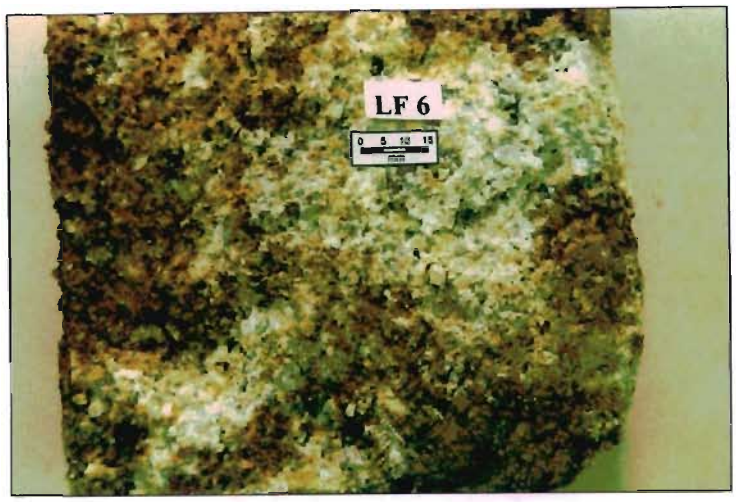

Figure 5.11. Variation of granite saprolite typical of material just above bedrock contact. Note retention of fabric. Locality LF 6.

As shown in Figure 4.3, the contact of the saprolite with the underlying weathered bedrock is abrupt with no formation of corestones. This observation is similar to that described by Zhao *et al.* (1994a) in their study of granite weathering in Singapore. It is not unusual for the saprolite to either directly overly moderately or highly weathered granite, indicating that not all weathering grades are necessarily included in the weathering profile.

5.2.3 Highly weathered granite

The highly weathered bedrock comprises light yellow or olive yellow with white and dark green mottles, close to medium jointed, equigranular (except where quartz pegmatite veins occur) granite (Figure 5.12). No voids are present within the material. Quartz grains are intact without any grain size reduction although they may show signs of fracturing. The plagioclase and microcline feldspars are highly to moderately decomposed breaking down to clay and gritty fragments. Dark green biotite grains are present and ranging from moderately to highly weathered with orange stain halos surrounding the grains.

5.2.4 Fresh and slightly weathered granite

The fresh and slightly weathered granite bedrock is light grey to light greenish grey, medium to coarse-grained with a poorly developed gneissic texture in places. The granite is often characterised by a heterogenic appearance, often caused by pegmatitic zones and darker coloured bands associated with a higher percentage of biotite or amphiboles. The granite is close to medium jointed and equigranular

(except where pegmatite veins occur). In places adjacent to the diabase dykes the granite has been influenced to some extent such that recrystallisation and assimilation has taken place forming granite migmatite. Fracturing also tends to be more intense at these localities. The fresh granite shows no discolouration. Quartz and feldspar grains are hard and intact and dark green biotite grains can be observed.

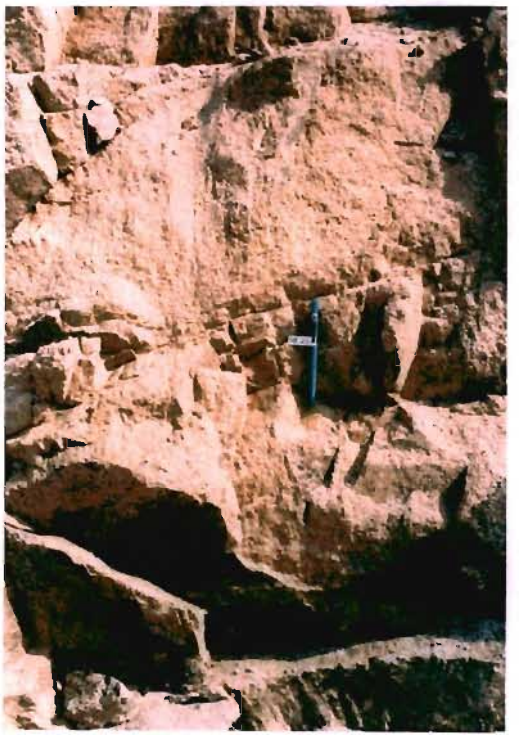

Figure 5.12. View looking south of highly weathered granite bedrock showing complete discolouration. Locality RF 25.

6. SCANNING ELECTRON MICROSCOPE INVESTIGATION

6.1 Introduction

The scanning electron microscope (SEM) has since its inception been used as a tool to assess the microfabric and weathering characteristics of rocks and soils. Baynes and Dearman (1978b) stated that the large range of magnification, advantageous depth of field, ease of sample preparation and analytical capabilities of the SEM greatly surpass the ability of the optical microscope to assess the fine details of weathering and microfabric. Consequently, a greater understanding of these features is gained. In the context of granite weathering, the SEM has been used to describe grain-surface textures of feldspar produced by weathering (Berner and Holdren, 1977), and to assess the nature and origin of some decomposition products (Keller, 1978). Baynes and Dearman (1978c) have also managed to describe the microfabric of weathered granite using this technique.

The objective of this SEM study was to describe qualitatively the weathering characteristics and mineralogical microfabrics of the weathered granite so that these observations can be correlated with the geochemical, mineralogical and engineering characteristic of the material discussed in later chapters. Simply defined, the microfabric of soils and rocks can be considered as the geometry and interaction of the particulate grains with void space which together determine the mechanical (engineering) properties of the material. This relationship is often complex and is affected by molecular bonding (intra-grain forces), mineral bonding (inter-grain forces, either relict or secondary), and volume and distribution of the void space. All these factors are influenced to some degree by the weathering process. The primary microfabric of saprolitic soils is genetically related to the complex crystalline compositions and textures of the parent rock. Secondary, tertiary and even higher orders of microfabric can also be formed by weathering processes as decomposition products form and porosity increases.

In the context of geotechnical engineering, limited work has been conducted on the relationship between microfabric, weathering and engineering behaviour. Vargas (1953), Sowers (1963) and Wallace (1973), suggested various microfabric configurations to explain observed engineering behaviour without observing microfabrics and testing their hypotheses. Collins and McGown (1974) successfully applied their SEM observations to the engineering behaviour of a variety of natural soils, highlighting the importance of the SEM in this area of study. They showed that the sensitivity, collapse and expansiveness of these soils could be described in the context of soil microfabric. Limited work has been carried out on characterising the microfabric of weathered granites through the SEM and its relationship to the engineering properties of the material, with Baynes and Dearman (1978b and c) compiling the most comprehensive discussion on this assessment. They have formulated a model on the microfabric of weathered granite using the

degree of decomposition (Xd) which expresses the extent to which the mineral grains have decomposed to clay and this is discussed in detail in Chapter 9. Collins (1985) has attempted to formulate a three tier framework for microfabric characterisation of tropical lateritic and saprolitic soils using the SEM. He maintained that the microfabric of a saprolite could be broken down into three levels: elementary level - comprising the interaction of elementary particles such as clay platelets and including pore space distributions; assemblage level - comprising the individual particle assemblages formed by various combinations of elementary particle arrangements and including pore space distributions; and a composite microfabric level (comprising a composite of various assemblages in differing proportions based upon the weathering environment and parent rock characteristics). He concluded that there exists a variety of microfabrics in such soils with complex multi-level pore systems. Notably, Collins realised that the link between microstructure characterisation and mechanical behaviour of weathered materials is still at a developmental stage, requiring significant further research and maintained that no single microfabric characterisation could account for a complete explanation of the mechanical behaviour or engineering properties of weathered materials. Furthermore, Baynes and Dearman (1978b) make the point that the size of an SEM sample in relation to the field distribution of particular outcrops and exposures of the weathered material can hardly be considered as representative. However, by observing sequential changes in microfabric features, these features can be related to increasing weathering intensity and in general terms microfabric changes can be reflected with weathering.

With these points in mind, the SEM work for this investigation was undertaken hand-in-hand with a thorough geochemical, mineralogical and petrographical investigation of the weathered granite at Injaka Dam to attempt to quantify the microfabric.

6.2 Sample preparation

The sampling and preparation of samples for SEM analyses is a delicate procedure requiring preservation of the microfabric to prevent the formation of microscopic artifacts. Specimens 250 cm^3 in size were cut from the undisturbed block samples retrieved from the various sample traverses. These specimens were oven dried for 48 hours at 36°C. Although it is suggested by Tovey and Yan (1973) that freeze drying causes the minimum of sample disturbance, this method has been considered technically very difficult by Barden and Sides (1971). Consequently, oven drying was considered the more suitable method for this study.

Smaller specimens ranging from 2 to 4 cm^3 in size, were then carefully separated from the larger cubes. Extreme care was taken during this process not to disturb the observational surface by finger contact or smearing. Generally, the observational surface was 1 to 2 cm^2 in area. Once the required cube size had been trimmed, a thin layer of *Superglue®* was applied to the side and bottom

face of the sample to ensure sample integrity within the SEM. Unlike the peeling methods suggested by Wong and Tovey (1975) and Barden and Sides (1971), it was decided to use delicate air dusting for the cleaning of the observational surface. This procedure removed any disturbed or loose surface detritus and proved successful in preventing the formation of artifacts during cleaning.

In cases where the block samples were considerably heterogeneous in nature, two and sometimes three cube specimens were taken for observation. Once the cube specimens were correctly prepared, they were fixed to a glass slide using carbon glue and then coated with a 300 Å thick layer of carbon. The carbon layer prevented over-charging of the specimen during analysis. In some cases specimens had to be coated twice as the first carbon coating was not thick enough to dissipate the charge.

6.3 Equipment and techniques

A Leica Cambridge Stereoscan 440 scanning electron microscope at the Council for Geoscience, Pretoria, was used for the observational analysis of the cube samples. Analytical determination of the composition of mineral grains and clay aggregates was performed using the Electron Dispersive System Oxford Link ISIS which was fitted to the SEM and operated at 20keV. This system allowed for the determination of the major and minor elements and their ratios to be displayed. The entire system was run off a Pentium 100 MHz computer.

The general observation technique for the SEM was to traverse the sample, identifying the most distinct mineralogical and microfabric features. Observational analysis of these features was carried out at varying magnifications (40 x to 16 000 x) to attempt to discern the properties of these features. Essentially the intention of the SEM investigation was to identify, describe and photograph those features thought to be associated with weathering and microfabric, which in turn are likely to affect the engineering behaviour of the material. These features include microcracking, dissolution and leaching effects, and decomposition products. By characterising these features with the intensity of weathering, a relationship between the microfabric changes and weathering effects could be determined. Whilst this procedure is subjective, it nevertheless still proved to yield very relevant information on the nature of the changes in microfabric with increasing weathering.

Identification of the minerals under the SEM was assisted by petrographic, x-ray diffraction (XRD) and x-ray spectrometry (XRF) investigations as discussed in Chapters 7 and 8. Grain size and particularly crystal form (shape and cleavage) were also employed to discern various minerals. Of particular use was the Link ISIS system which allowed for analytical determination of the composition of the mineral grains or aggregates (Figure 6.1). By focussing a target beam on the particular mineral grain or clay aggregation the ratio of various major and minor elements of that

particular target could be determined and used in identifying the mineral species. Furthermore, by comparing the ratios of elements (particularly Si, Al, Ca, Na, and K) an indication of the degree of weathering and leaching of the various minerals could also be obtained.

6.4 Nomenclature

Prior to discussing the SEM results it is pertinent that the relevant descriptive terms in SEM nomenclature be defined. Table 6.1 provides details of these terms modified from Baynes and Dearman (1978c) with Figure 6.2 showing some of the typical clay particle geometric arrangements and Figure 6.3 showing typical intragranular decompositional voids on feldspar surfaces. Where appropriate, use has been made of this terminology when describing the various features identified in this study.

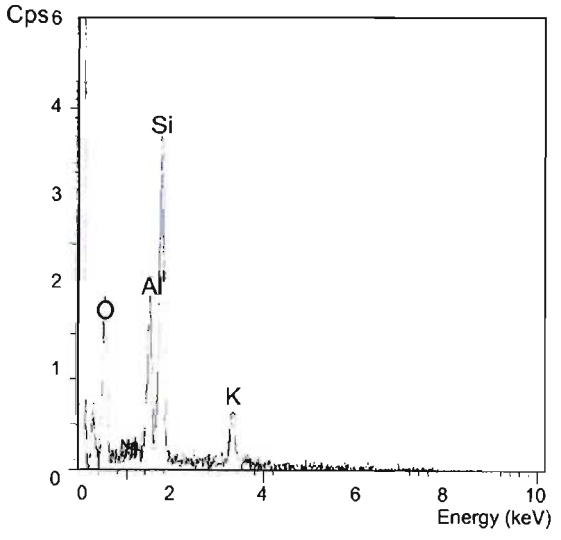

Figure 6.1. Example of typical elemental counts per second from the Link ISIS system used to differentiate various minerals under the SEM.

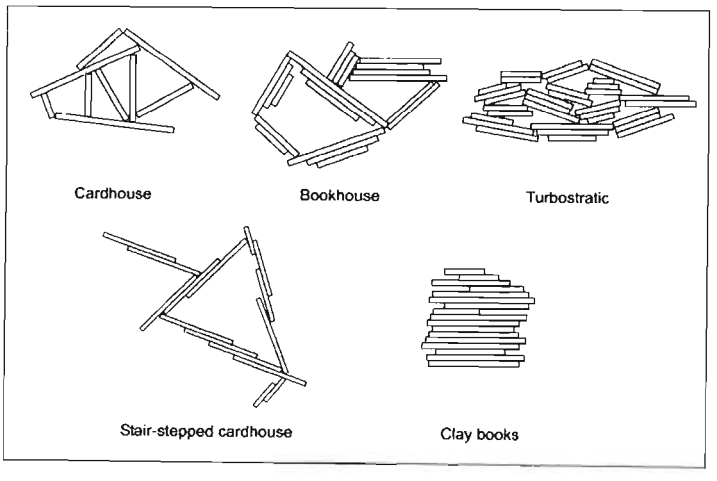

Figure 6.2. Possible geometrical arrangements of clay microfabrics after Collins and McGown (1974).

Table 6.1. Nomenclature of scanning electron microscope terminology (modified from Baynes and Dearman, 1978c).

Terminology	Description
Voids	
Intergranular voids	forming a space between mineral grains.
Intragranular voids	forming a space within mineral grains.
Transgranular voids	forming a space which cuts across a grain boundary.
Prismatic etch pits (PEP's)	roughly equidimensional, structurally controlled, decompositional hollows (see Fig. 6.3). Observations by Berner and Holdren (1977) show such features to be orientated generally in relation to twin planes. PEP's also represent sites of crystal dislocations (crystal defects and mismatched bonds) which tend to have higher crystallographic energies and are preferentially weathered. It is thought that the etch pit sites are initially filled with clay with flushing and dissolution eroding the material resulting in the hollow.
Prismatic etch trenches (PET's)	a structurally controlled decompositional hollow which has a length more than twice its width and forms similarly to PEP's (see Fig. 6.3).
Irregular etch pits (IEP's)	an equidimensional decompositional hollow (see Fig 6.3).
Irregular etch crevasses (IEC's)	a decompositional hollow having a length more than twice its width (see Fig. 6.3).
Clay Microfabrics	
The microfabric of clays can be described at two levels. These include the arrangement of groups of individual clay particles (assemblage level) and the geometrical arrangement of individual clay particles (elementary level). For clay particles that group together and act as units at varying levels of organisation, Yong and Sheeran (1973) presented the following definitions:	
Domain	two or more clay particles acting as a unit.
Cluster	several domains acting as a unit.
Aggregations	large numbers of individual clay particles acting as an internally unordered but coherent group.
The geometrical relationships of individual clay platelets may be described using terms from original conceptual models as proposed by Van Olphen (1963):	
Cardhouse	edge to face (E-F) arrangement (see Fig. 6.2).
Layered	face to face (F-F) arrangement.
Books	face to face (F-F) forming a prismatic stack (see Fig. 6.2). May form interweaving bunches.
Bookhouse	an open structure analogous to the cardhouse in which the individual clay plates are replaced by books (see Fig. 6.2).
Turbostratic	a closed structure consisting of tightly fitting books (see Fig. 6.2).
Stair stepped	face to face (F-F) arrangement in which plates do not cover each other and hence form a stepped tabular structure (see Fig. 6.2). May form interweaving bunches.
Cases may also arise where no clay microfabric is discernable.	

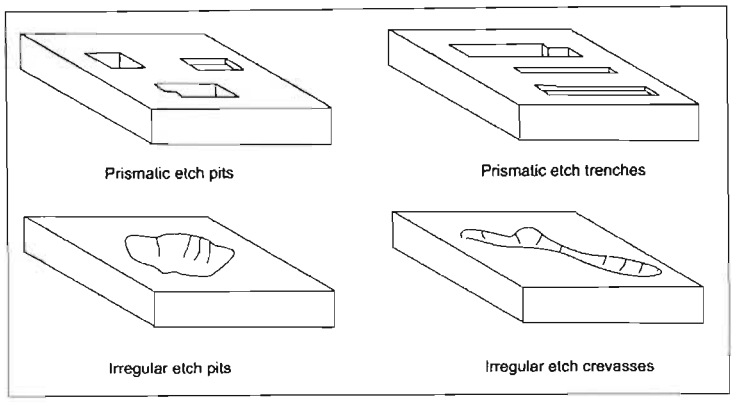

Figure 6.3. Intragranular decompositional voids as described by Baynes and Dearman (1978c).

6.5 Mineral weathering observations

Observations made with the naked eye during field mapping, petrographically and using the SEM clearly indicate that all constituent parent materials do not weather at the same rate. This was highlighted by Goldich (1938) in his double series of differential weathering parent materials, ranging from the most susceptible to least susceptible (Figure 6.4). This weathering series has been refined subsequently and other sequences have been proposed for specific cases. It follows from this that the secondary minerals produced by weathering also appear in a definite order. More recently, Nahon (1991), Anbeek (1992), Anbeek (1993) and Anbeek *et al.* (1994) have provided an insight into the kinetics of dissolution rates of certain major constituent minerals. The following discussion describes the weathering and microfabric characteristics of the various mineralogical components within the granite saprolite in the light of this information.

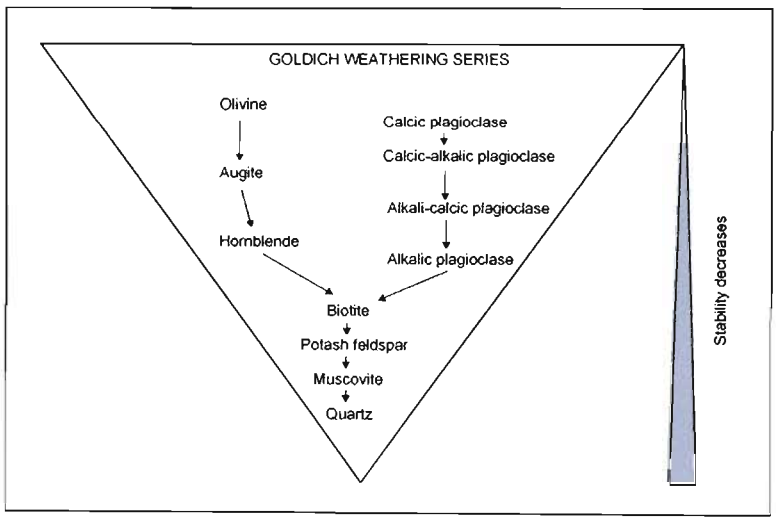

Figure 6.4. Goldich's reaction series showing the high susceptibility of plagioclase to weathering.

6.5.1 Quartz

The stable bonding of the silica tetrahedron structure of quartz molecules means that quartz grains are generally resistant to weathering. Indeed, silica is the major element in water that undergoes the least amount of random variation. Practically then, the weathering effects on quartz can be considered to be almost negligible in comparison to other minerals. However, as observed by Brantley *et al.* (1986), natural etching of quartz through chemical weathering can occur. This is in the form of solution processes (Loughnan, 1969) which form a resistant, coarse-grained residue during the weathering of granites (Lumb, 1962).

Indeed, in several of the samples of granite saprolite with residual soil patches characteristic arcuate etching and pitting as observed by Krinsley and Doornkamp (1973), was observed on the surface of some grains (Figure 6.5a) indicating a locally very high degree of weathering and leaching. Generally, however, the majority of the quartz grains exhibited a smooth or conchoidal fractured surface as shown in Figure 6.5b.

6.5.2 Feldspars

The susceptibility of feldspars to chemical weathering with the plagioclase and potash feldspars tending to undergo incongruent weathering has been described in Chapter 3 and Section 6.5. Observations from this SEM investigation suggest a similar reactivity series for feldspars as that found by Eggleton (1986), that is that the most reactive phase included Ca-plagioclase followed by Na-plagioclase and then microcline. In fact, such was the intensity of the weathering and severity of the leaching of the plagioclase in this weathered granite profile that its absence was conspicuous in the near surface samples (Chapters 7 and 8). Scanning electron microscope observations of feldspar weathering can be correlated with results from the XRD and petrographic analyses (Chapters 7 and 8) where the mobility orders for the alkali and alkali earth metal cations is Ca > Na > Mg > K > Si > Al > Fe > Ti .

The feldspars from this granite saprolite show all classical SEM textures as described by Berner and Holdren (1977 and 1979), Baynes and Dearman (1978c) and Anand *et al.* (1985). The various degrees of etch pitting can be observed from the smallest cupules found in the least weathered feldspars (Figure 6.6a) to the formation of prismatic and irregular etch pits - PEPS (Figures 6.6b and c) in the more highly weathered grains. As weathering proceeds, coalescence of the prismatic etch pits occurs forming prismatic etch trenches (PET's) shown in Figures 6.6d, e, f and g. The PET's tend to develop preferentially along cleavage and twin boundaries as observed in these figures and tend to significantly open up the feldspar structure. This systematic arrangement of etch pits and etch trenches on the feldspar surfaces shows that the crystal structure of feldspar

controls the nature and orientation of these features. Enhanced chemical weathering of the feldspars leads to the coalescence of these etch pits and etch trenches, resulting in skeletal shells of feldspar exhibiting a sieve-like texture as observed in Figures 6.6h, i, j and k.

The formation of the PEP's and PET's occurs on the surface of the feldspar grains but it is not known exactly how deeply these features extend into the mineral grains. Montgomery and Brace (1975) have however, shown by serial sectioning that the shape of these features changes drastically with depth. Obviously with increased weathering, etch pit formation extends deeper into the mineral grain. In fact, as observed by Baynes and Dearman (1978c), feldspar at a highly progressed state of weathering tended to show a sieve-like texture similar to that found in this study.

Anand *et al.* (1985) noted that the feldspars in saprolite material undergo various degrees and styles of alteration when weathered. Similarly, Baynes and Dearman (1978c) noted that not all feldspars decompose in the same way, stating that the formation of irregular etch crevasses (IEC's - irregular, non-parallel sided crevasses evidently formed from a solution origin) on the surface of some feldspars differs from that of the classic etch pit formation. Similar features were observed for the weathered granite at Injaka Dam as shown in Figure 6.6l. These features appear to be less structurally controlled than the etch trenches, having a more irregular shape and more erratic arrangement.

The variability in weathering of the feldspars described above can be a consequence of different weathering regimes where certain weathering mechanisms and decomposition products occur under one environment but not under another. Weathering microenvironments can also differ by distances as small as 200 µm (Anand *et al.*, 1985). The reasons for these differences are not completely understood but they may simply be a consequence of minute differences in permeability within various parts of weathered grain structures or intergranular voids. The spatial arrangement of the minerals, and consequently exchangeable cations, also accounts for microenvironment variations as do the presence of crystallographic flaws within the mineral grain.

The different rates of feldspar weathering can be observed even in the early stages of chemical weathering. Figure 6.6m shows the surface texture of a Na-plagioclase grain alongside a K-feldspar grain located in a sample retrieved from a depth of 11,8 m and classified as highly weathered granite bedrock. The more pitted surface of the Na-plagioclase can clearly be observed.

6.5.3 Micas

Biotite and to a lesser extent muscovite are found in the granite saprolite at various degrees of weathering. Muscovite is the more resistant of the two micas with the absence of biotite in the

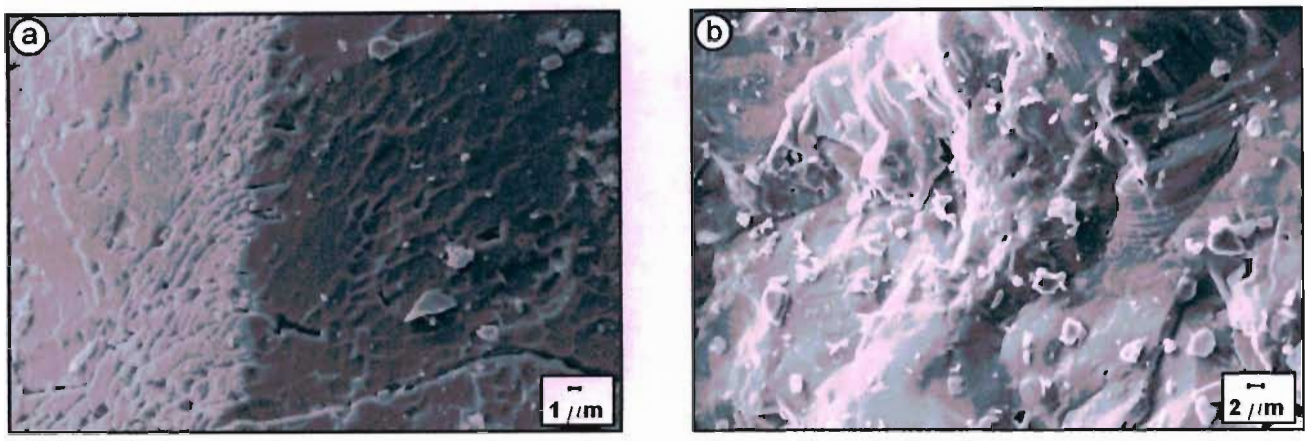

Figure 6.5. (a). Characteristic arcuate etching and pitting on weathered quartz grain surface from granite saprolite with residual soil patches (LF 18). Magnification = 4 590x. (b). Typical smooth and conchoidal fractured surface of an unweathered quartz grain from granite saprolite (LF 10). Magnification = 3 630x.

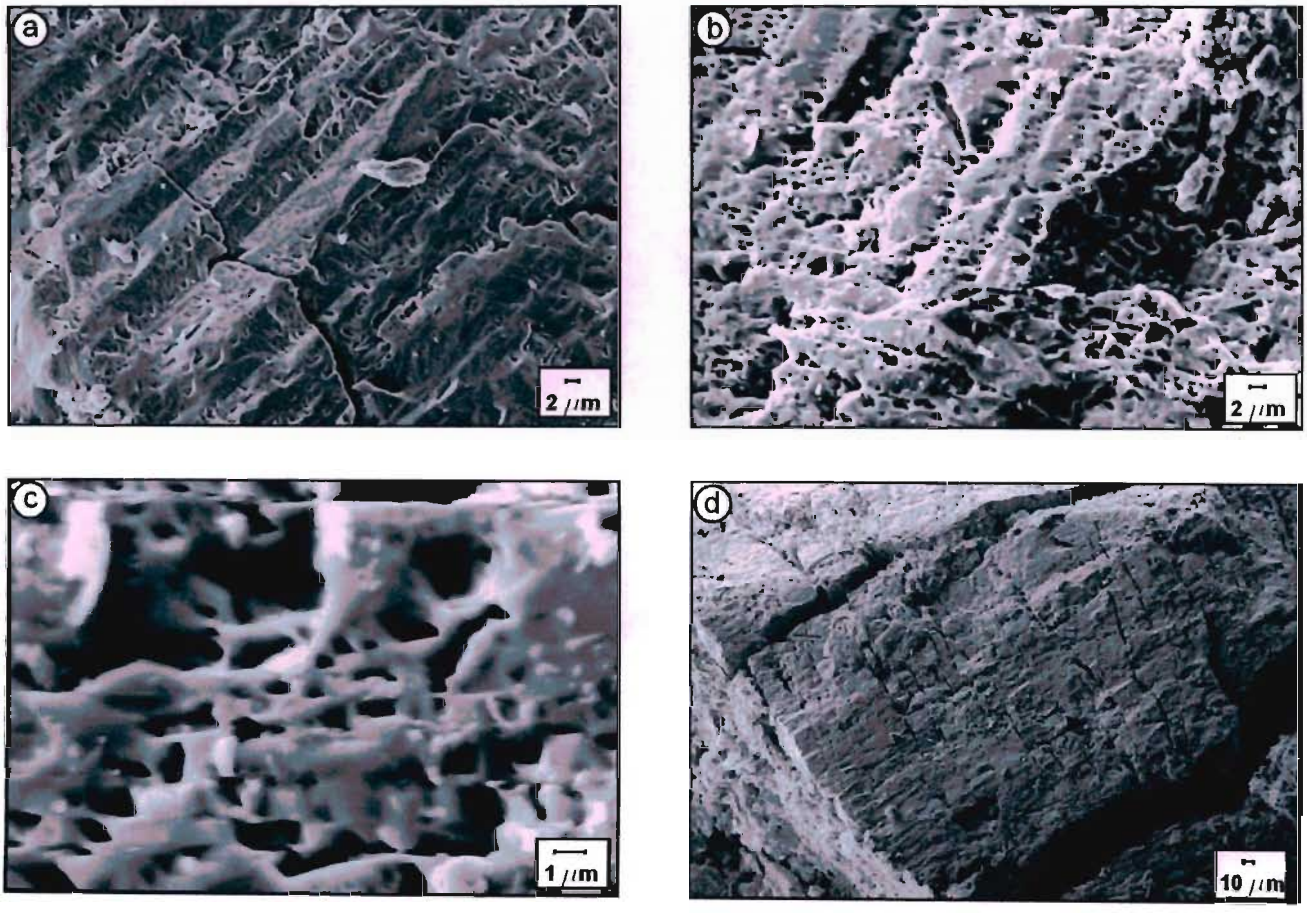

Figure 6.6. (a). Cupule formation developed on a twinned plagioclase grain in highly weathered granite (RF 2). Magnification =3 700x. (b). Well developed prismatic etch pit formation on a feldspar grain surface in granite saprolite (LF 3). Magnification = 4 500x. (c). Magnified view (16 380x) of prismatic etch pits shown in Figure 6.6b. Magnification = 16 380x. (d). Structurally controlled prismatic etch trench formation on the surface of a plagioclase grain in granite saprolite (LF 8) - low magnification (603x).

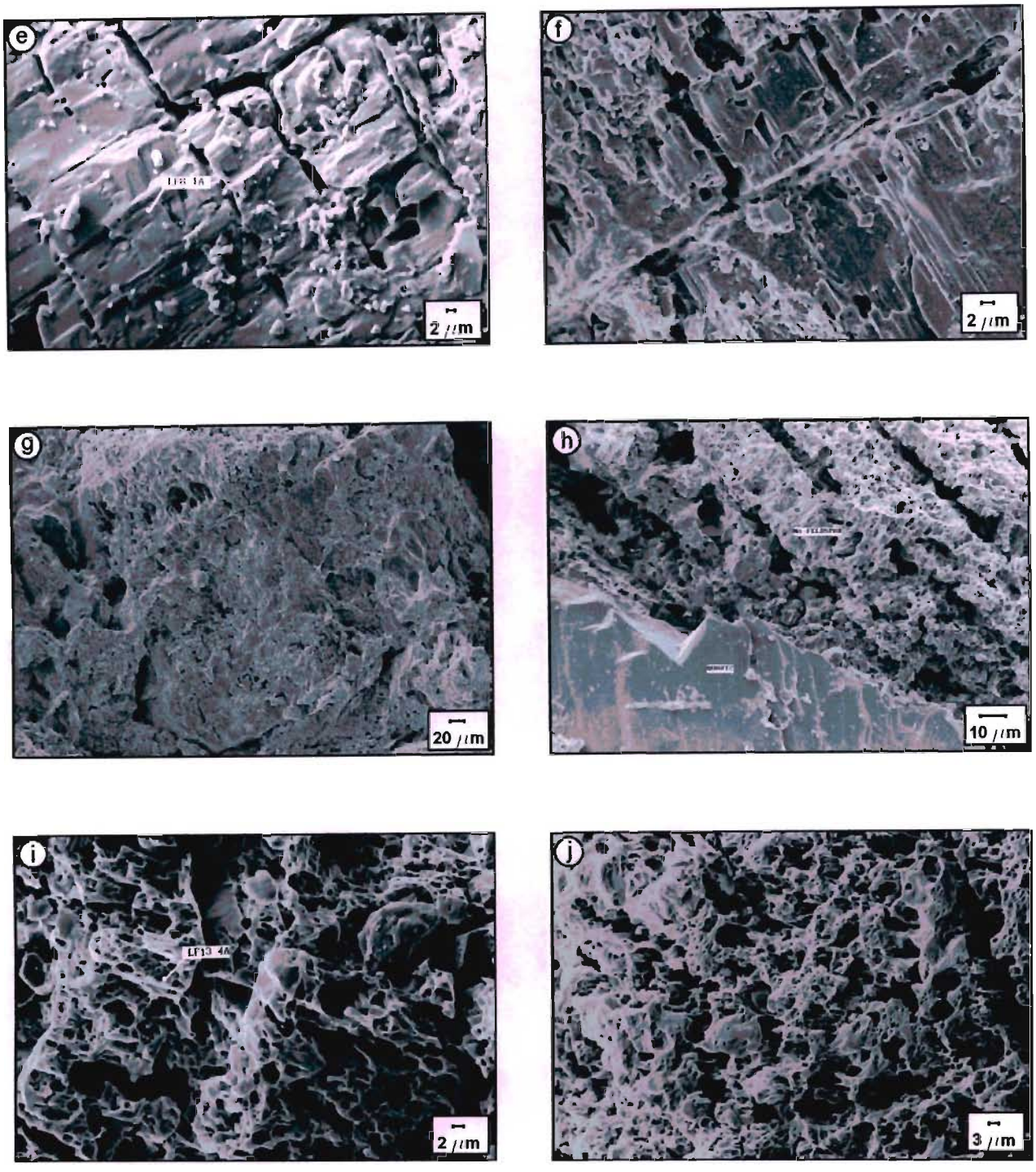

Figure 6.6. (e). Magnified view of Figure 6.6d at 3 500x showing formation of prismatic etch trenches (LF 8). (f). Structurally controlled coalescence of prismatic etch trenches in plagioclase feldspar from granite saprolite (RF 7). Magnification = 4 360x. (g). View of Figure 6.6f showing distribution of prismatic etch trenches throughout the grain surface. Magnification = 461x. (h). Structurally controlled coalescence of prismatic etch trenches showing sieve-like structure of plagioclase feldspar alongside unweathered quartz in granite saprolite (RF 4). Magnification = 1 720x. (i). Enhanced prismatic etch pit formation resulting in a highly porous plagioclase feldspar framework in granite saprolite (LF 13). Magnification = 3 870. (j). Another form of the sieve-like feldspar texture developed in plagioclase feldspar from granite saprolite (LF 27). Magnification = 2200x.

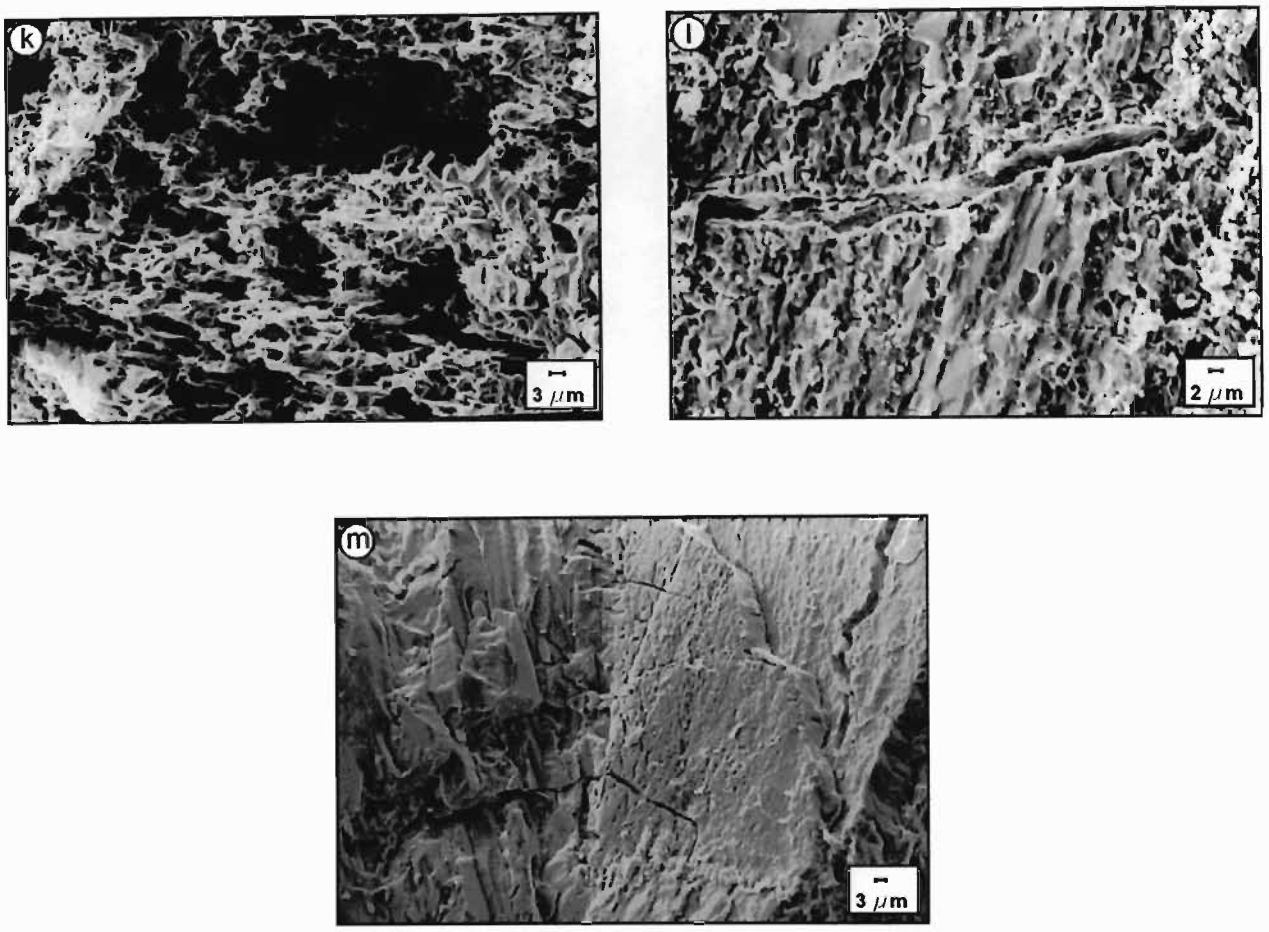

Figure 6.6. (k). Highly porous, fragile skeletal plagioclase feldspar framework developed under intense leaching conditions in granite saprolite (LF 27). Magnification = 2 660x. (l). Irregular etch crevasse formed on the surface of a feldspar grain in highly weathered granite (RF 24). Note the irregular shape of the crevasse suggesting no structural control of the feature. Magnification = 3 220x. (m). Incongruent weathering of potash feldspar and plagioclase in highly weathered granite (RF 16). Plagioclase (right hand side) shows pitting on the grain surface whilst the potash feldspar (left hand side) exhibits no such features although microcracks are clearly evident. Magnification = 2 000x.

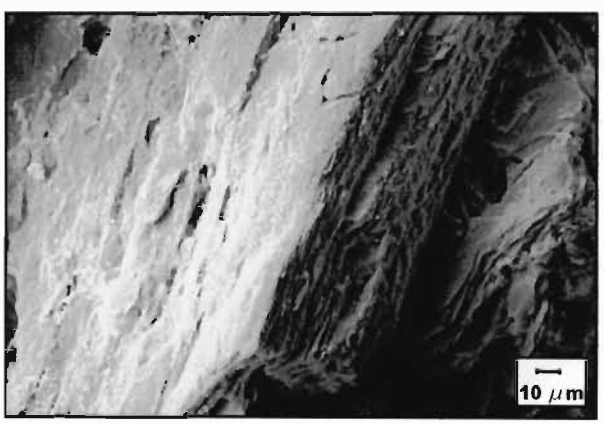

Figure 6.7. Opening (peeling) of mica cleavage showing feather-edge grain boundary in granite saprolite (LF 12). Magnification = 1 250x.

upper profile sections bearing testimony to this. According to Bisdom (1967), Rimsaite (1967), and Sawhney and Voigt (1969), mica crystals undergo three changes that may occur simultaneously during weathering. These include deformation, opening of cleavage and modification of polarizing colours. Gilkes and Suddhiprakarn (1979) also observed the formation of shallow etch pits ("concavities") on the basal surface of biotite. In this investigation only the deformation and opening of cleavage could be identified under the SEM and these features were consistent with those observed in thin sections (Chapter 7). Figure 6.7 shows extensive exfoliation where opened cleavages can be observed. Jackson (1963) stated that the penetration of cleavages by aggressive agencies would allow weathering to proceed whilst maintaining relative crystallographic orientation. The opening of the mica cleavage involves significant volume increase and may cause microfracturing (as observed by Irfan and Dearman, 1978a) and localised disruption of the microfabric.

6.5.4 Secondary minerals (decomposition products)

The major secondary mineral constituents of the granite saprolite include kaolinite with lesser amounts of smectite and in some cases interlayered illite and smectite. With kaolinite being the predominant clay mineral, this implies that continued flushing of the system occurred under well drained conditions. The localised occurrence of the smectite clays can be related to a number of factors, including the close proximity of the weathered diabase dykes and the scattered occurrence of weathered amphibolitic xenoliths, both of which provide a source of smectitic clays when weathered. The occurrence of smectite in the highly weathered granite is most likely attributable to the reduced permeabilities encountered within this material. Hematite forms a minor secondary mineral constituent which is found in highly oxidised, near surface samples of granite saprolite with residual soil patches. The secondary mineral constituents form from a complex series of weathering reactions as outlined in Chapter 4.

The formation of kaolinite as a decomposition product can develop from a variety of sources. The most common is the chemical weathering of feldspar, although Gilkes and Suddhiprakarn (1979) showed that weathered biotite in saprolite materials also formed granular pseudomorphs consisting of kaolinite.

The kaolinization of feldspar may include the formation of a diverse group of kaolinite daughter minerals depending on the weathering environment (Keller, 1978). These tend to occupy extensive pockets within the framework of weathered quartz, feldspars and biotite opened up by void formation. These daughter minerals include the platy, book-type kaolinite and the elongate kaolinite minerals of halloysite-type. Unlike the structurally controlled occurrence of etch pits, no evidence has been found in this study or for that matter by Anand *et al.* (1985), to suggest that the crystal

structure of feldspar controls the nature and orientation of the decomposition products. The most common type of structured kaolinite observed in granite saprolite from Injaka Dam site is that of platy, book-type kaolinite (Figure 6.8a) which is in agreement with similar findings by Keller (1978). No elongate kaolin minerals of halloysite-type were observed. The platy, book-type kaolinite can be further categorised into sheaves, curved books or straight stacks/books. These books are up to 200 μm in length with open face to face contacts as shown in Figure 6.8a. Individual kaolinite platelets can be as large as 8 μm (Figure 6.8b). The random orientation of these plates in relation to feldspar crystallography suggests that the argillic transition was not a solid-state transition or replacement, but that solution in reaction with the solid phases intervened. Platy, book-type kaolinite is postulated to form in systems where geochemical equilibrium is maintained between the groundwater solutions and solid phase parent-daughter minerals over a long period of time. A more compact version of the microfabric mentioned above is shown in Figure 6.8c and 6.8d where the bookhouse arrangement can be clearly observed. Here the clay consists of short (10 to 20 μm) books in a bookhouse arrangement with edge to face contacts. The interstices between the books are filled with irregular kaolinite platelets.

Figures 6.8e and 6.8f show a loose turbostratic arrangement of irregular kaolinite platelets up to 8 μm in size. This loose arrangement between the clay books is responsible for the very open microfabric of the clay where voids as a large as 12 μm were measured. Irregular, elongate voids with smooth rounded internal surfaces often occur and are indicative of a solution origin. These voids can be up to 150 μm in length with openings ranging from circular to elongate. Clearly then, void formation within the clay microfabric occurs at two levels. One type is dictated by the arrangement of the individual clay platelets and books, and the other type is dictated by solution processes. The irregular arrangement of the larger solution voids which are predominant in the turbostratic fabric means that solution occurred after the formation of this fabric.

In some cases pseudomorphic replacement of feldspar by kaolinite occurs. Figure 6.8g shows the outline of an original Na-plagioclase grain. The crystal habit can be clearly observed. Figure 6.8h is a magnified view of Figure 6.8g and shows an open structure of irregular kaolinite platelets with feldspar fragments. Such a structure forms by the progressive alteration of the sieve-like feldspar grain leading to deposition of kaolinite platelets on the open framework of the feldspar grains (Figure 6.8i).

Further evidence for the argillic transition being a product of solution interaction with the solid phase is presented in Figure 6.9g where kaolinite books can be seen developing within a microfracture of K-feldspar. Other parts of the microfracture exhibit irregular edges and are partially filled with irregular kaolinite platelets. It is therefore likely that the microfractures within and adjacent to the feldspars offer suitable microenvironments for the precipitation of kaolinite. This observation can

be extended to field observations which show that many relict joints within the saprolite are filled with fine-grained, white kaolinite.

The micrographs in Figures 6.8a to i show the great diversity of clay microfabrics that can develop within granite saprolite. These microfabrics exhibit great variation in porosity. The widely differing microfabrics were in many cases observed in samples taken very close to one another and in some cases these different microfabrics were observed within the same sample. This variability may reflect the differences in weathering microenvironments, these producing different decomposition products.

6.5.5 Intergranular voids and microcracking

Chemical weathering of granites inevitably involves an increase in porosity. This increase is brought about by the mechanisms discussed above. Inter-, intra- and transgranular porosity all form important components within the granite saprolite. The formation of porosity via etch pitting has been discussed in section 6.5.2, however, a far more important component of porosity involves the formation of large (from 0,3 to 2 mm in diameter), vermiform, intergranular solution voids with circular openings as shown in Figures 6.9a and b. These voids were also studied using the SEM and it was observed that they tend to preferentially accumulate in the bookhouse or turbostratic kaolinite microfabrics and along grain boundaries (Figures 6.9c and d). The formation of these voids along grain boundaries can be attributed to increased permeabilities within these zones resulting in fluids of low saturation within the microenvironment producing more intense solution. Figure 6.9e shows one of these voids alongside a quartz grain. The tubular nature of the void can be observed by the remaining clay bridge. An important observation of the shape of these voids is that they tend to be blind suggesting that the removal of material to form these voids is through solution rather than physical erosion along a series of interconnected channels and flow paths.

Microcracking also forms an important component of weathering effects. Microcracks within the saprolite can be observed at all levels of weathering, but generally increase in abundance, width and continuity with increasing weathering. They vary in width from 7 to 800 μm and can be continuous for more than 50 mm (the length of a petrographic slide). Microcracking affects the entire mineralogy of the saprolite although quartz grains are particularly microcracked. The microcracks can be open as in Figure 6.9f, filled with clay as in Figure 6.9g, or stained with iron oxide.

Interpretation of the precise formation mechanism for these microcracks is complex. Baynes and Dearman (1978c) suggested that a destressing phenomenon may account for a large proportion of microfracturing within weathered granites. They quoted the work by Nur and Simmons (1970) who showed theoretically that the effects of cooling and exhumation may be capable of producing

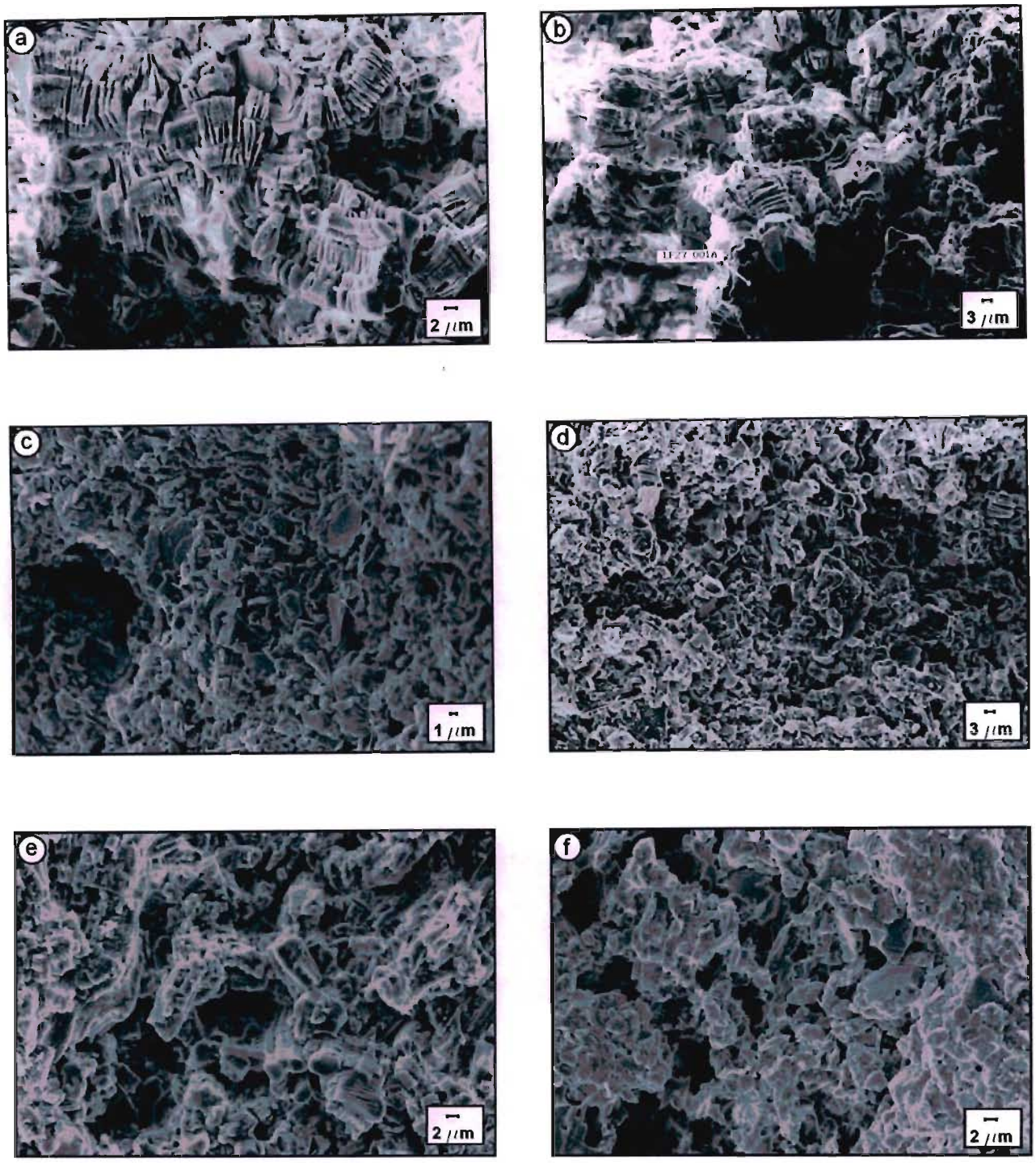

Figure 6.8. (a). Platey book-type kaolinite showing extensive formation of clay books in granite saprolite (LF 20). Magnification = 3 920x. (b). Platy book-type kaolinite showing large size of books. Magnification =2190x. (c). Compact version of platy book-type kaolinite showing less well-developed books with more random arrangement (RF 8). Magnification = 4 370x. (d). Another form of the compact platy book-type kaolinite (LF 3). Magnification = 2 180x. (e). Loose turbostratic arrangement of irregular kaolinite platelets (LF 4). Magnification = 3 640x. (f). Turbostratic arrangement of irregular kaolinite platelets (RF 10) showing a higher porosity than that in Figure 6.8e. Magnification = 4 030x.

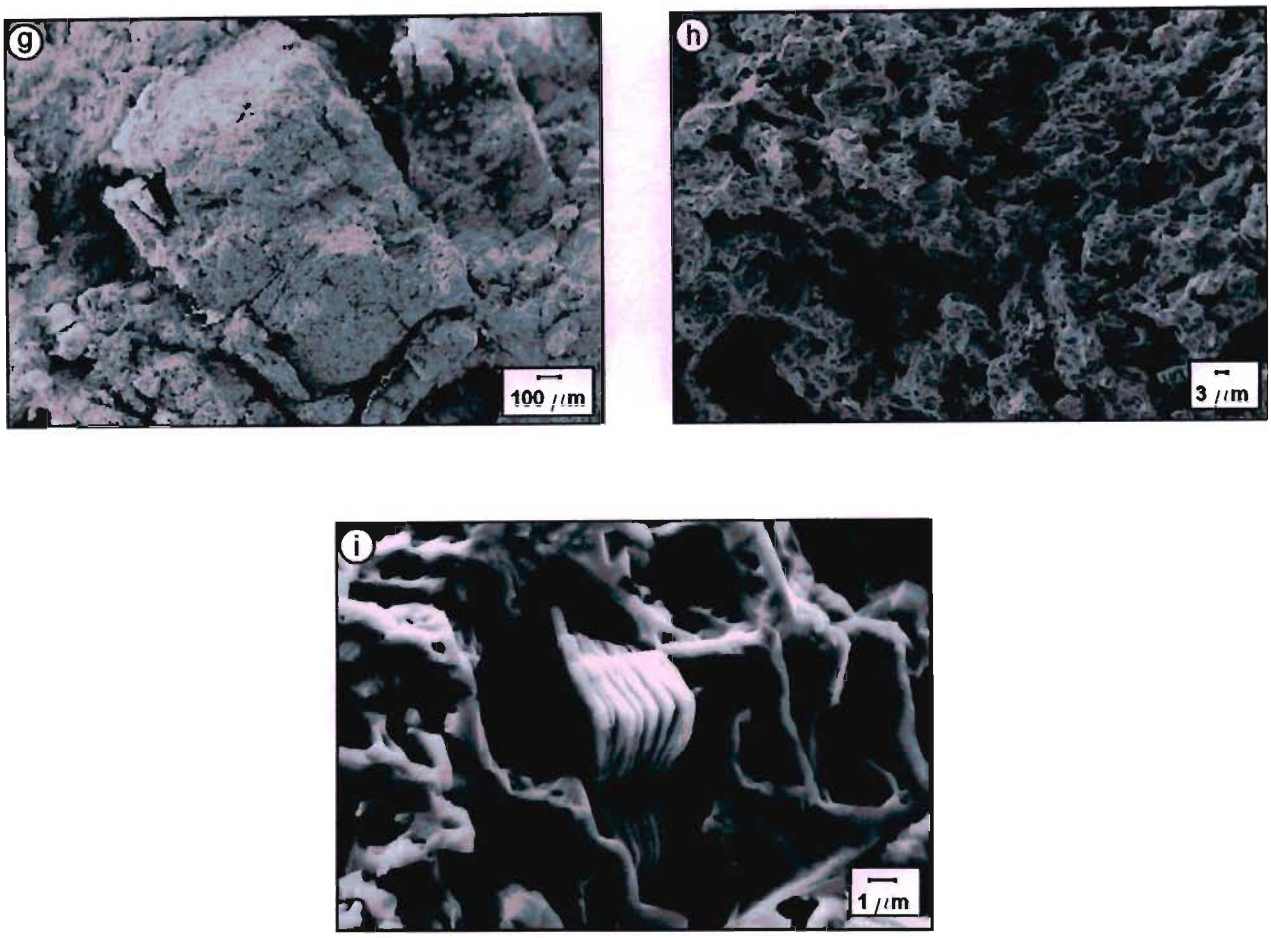

Figure 6.8. (g). Pseudomorphic alteration of plagioclase to kaolinite (RF 4). Magnification = 126x. The original shape of the plagioclase grain can still be discerned. (h). Magnified view (2 060x) of Figure 6.8g showing highly porous pseudomorphic transition from feldspar to kaolinite. (i). Formation of kaolinite platelets in skeletal feldspar framework (LF 26) providing evidence that the argillic transition is a product of solute interaction with the solid phase. Magnification = 16 330x.

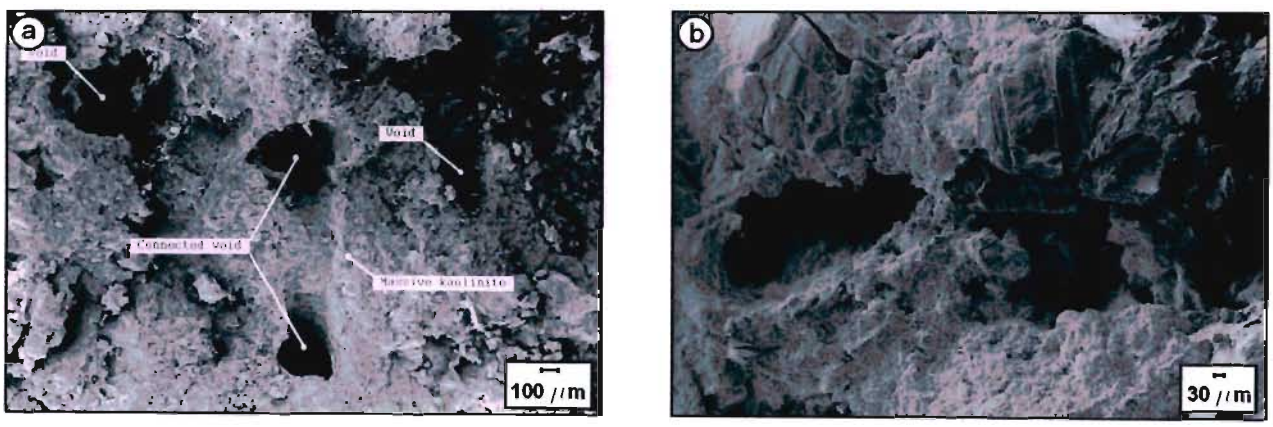

Figure 6.9. (a). Vermiform solution voids showing circular cross-sectional openings formed in kaolinite aggregations (LF 3). Magnification = 100x. (b). Oblique view into vermiform void formed in massive kaolinite (LF 12). Magnification = 187x.

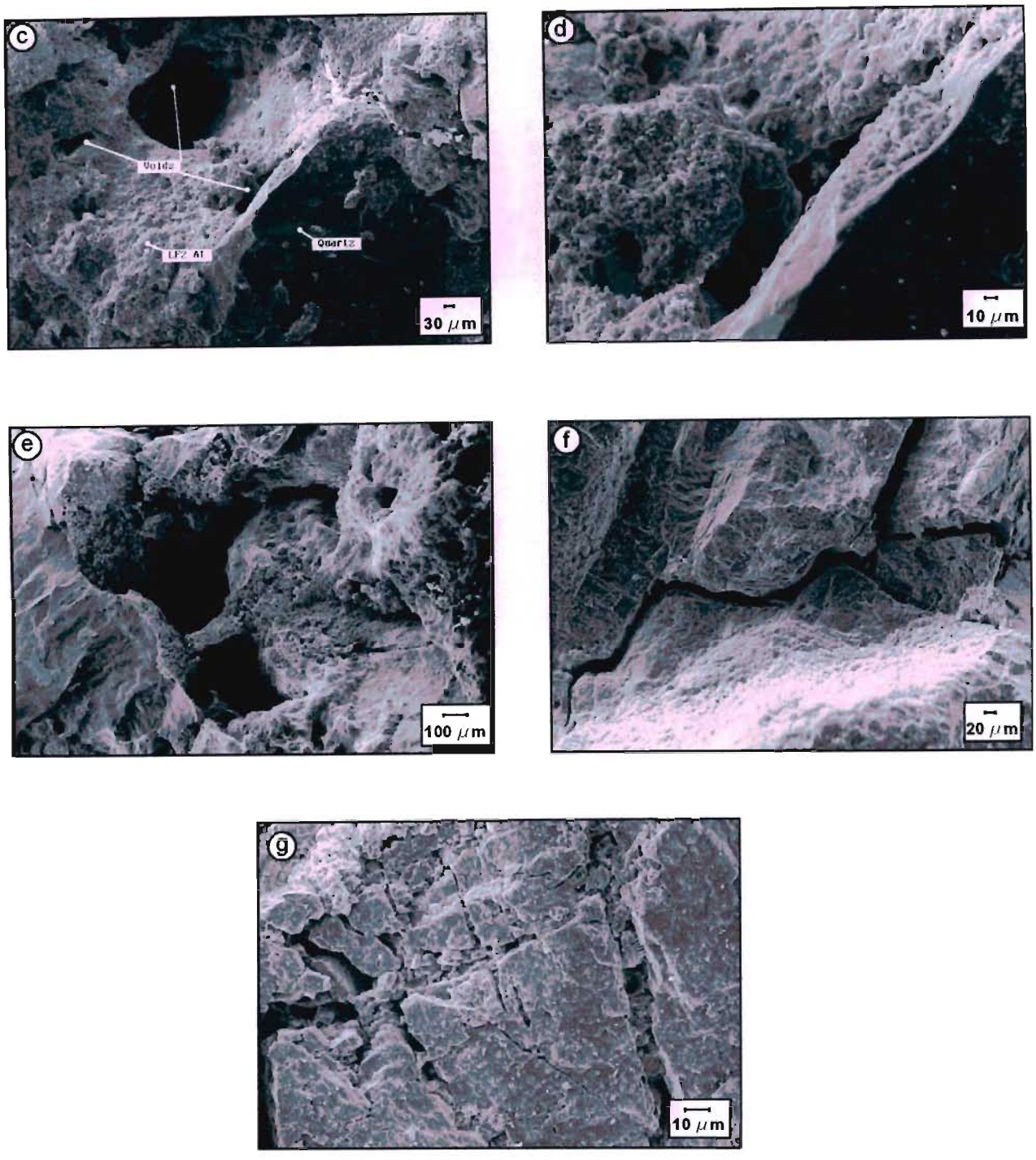

Figure 6.9. (c). Preferential solution void formation alongside quartz grain boundary where relatively higher permeabilities result in solution voids (LF 2). Magnification = 212x. (d). Magnified view (864x) of Figure 6.9c showing solution void characteristics. (e). Vermiform void formation alongside a quartz grain (LF 9). The clay bridge shows the tubular nature of the void. Magnification = 174x. (f). Clean, open, intergranular microcrack between two feldspar grains. The crack width is 10 μm. Magnification = 357x. (g). Kaolinite platelets forming within microcracks suggesting direct argillic transition from pore water solutions. Magnification = 1 770x.

microfractures due to the large difference in thermal expansion and compressibility between quartz and other rock-forming minerals. If some of the stresses that these differences generate are not dispersed, then granites at the earth's surface will be subject to residual stress (Friedman, 1972), where potentially recoverable elastic distortions of the constituent crystals are in internal equilibrium and hence `locked in. Should weathering processes release these stresses allowing locked in strains to relax, microfractures may form. The preferential formation of voids along grain boundaries (as discussed above, observed from petrographic studies in Chapter 7 and noted by Irfan and Dearman (1978a), could allow loosening of the rock texture, releasing the residual stress and accounting for the formation of microfractures. Another likely proposal for the occurrence of these microfractures is the increase in the local stress field by post-emplacement intrusion of the diabase dykes. Stresses during this intrusion process can be high enough to cause such microfracturing as suggested by the closely jointed nature of the granite alongside these intrusions. The difficulties in isolating one or other mechanism for the exact cause of these features is impossible. It is, however, likely that the microfracturing is a consequence of all the above-mentioned processes. These features significantly weaken the material and accelerate the rate of weathering.

6.5.6 SEM model of microfabric of weathered granite

From the above discussions a tentative model of the microfabric development of a weathered granite to granite saprolite can be proposed. In the initial stages of weathering the increase in the porosity of the material is controlled by two processes, that of etch pit and crevasse formation on the surfaces of the feldspar grains, in particular the plagioclase grains. This process occurs in conjunction with microcracking along grain boundaries and the expansion of biotites. Further weathering leads to the continued increase in porosity of feldspar grains (in some cases creating sieve-like textures), but more importantly to the development of clay microfabrics, which as has been observed, are complex and varied in nature. Many of the clay microfabrics themselves exhibit a high porosity due to particle aggregation as well as specific clay particle arrangements. Finally, solution effects play a role in the microfabric formation on a sub-microscopic level in the formation of irregular etch crevasses as well as on a macroscopic level in the formation of vermiform solution voids. All processes identified through this SEM investigation lead to the ultimate increase in porosity of the granite saprolite.

7. PETROGRAPHIC INVESTIGATION

7.1 Introduction

Analysing the petrography of a soil or rock allows for accurate determination of mineralogy and provides a two dimensional insight into the nature of the microfabric of the material. To supplement the SEM observations, qualitative and quantitative petrographic examinations were carried out on the weathered granite samples. Although the many applications of petrology are varied, de Puy (1965), Weinert (1964) and Irfan and Dearman (1978a) have attempted to correlate the petrography of certain materials (including weathered granite) with their engineering properties. They found that the petrographic properties which influence this engineering behaviour include mineral composition (primary and secondary) and texture (including grain size, grain boundary relationships, microcracks and voids). By studying these parameters, an improved understanding of the engineering behaviour of a material can be gained, particularly when the relevant parameters are quantitatively defined.

7.2 Specimen preparation and techniques

Petrographic thin sections of granite saprolite with residual soil patches, granite saprolite, weathered granite bedrock and fresh bedrock were prepared. Thin sections were cut directly from the fresh rock samples, whilst the procedure for the granite saprolite with residual soil patches, granite saprolite and weathered granite bedrock samples involved air drying at 30°C followed by epoxy impregnation by soaking with Araldite® resin. Initial attempts at vacuum impregnation were unsuccessful as this resulted in the formation of numerous air bubbles forming within the resin. The resin was coloured blue with an organic dye (dispersed phalocyanine blue) to distinguish any inherent voids and microcracks within the samples as opposed to those formed by the sectioning process. Thin sections 40 by 20 mm in size were cut from the hardened, resin-impregnated samples.

The thin sections were qualitatively examined and quantitatively assessed to ascertain differences in their petrographic nature in response to weathering. The modal analysis was determined using the standard point count technique (Chayes, 1956) using a petrological microscope and a Swift Automatic Point Counter (Model F) with 12 reset counters, electromechanical stage unit and intermediate interval changing unit controlling a mechanical stage holding the thin section. A horizontal and vertical grid spacing of 0,4 mm between each point was selected with a total point count of 800 being used as representative of the sample and complying with similar procedures as used by Irfan and Dearman (1978a).

7.3 Petrographic descriptions

7.3.1 Fresh and slightly weathered granite

In order to obtain an indication of the petrographic nature of the parent rock, several thin sections were made from borehole cores drilled in close proximity to the sample traverses (Figure 2.5). This material revealed the "freshest" granite state, although some indications of alteration were already noticeable on a microscopic scale.

The major mineral constituents of the fresh and slightly weathered granite are presented in Table 7.1 and include quartz (59%), microcline (12%) and plagioclase feldspar (17%) with minor amounts of chlorite (4%) and mica including biotite (4%) and muscovite (1%). The texture is generally equigranular and medium grained (with an average grain size between 1 and 4 mm) with some feldspars occasionally exceeding 10 mm in size. The anhedral quartz grains are fresh, occasionally exhibiting tight, transgranular hairline microcracks. Although the feldspars are hard and sound in hand specimen, dusky clouding is already commonplace within the centre of most plagioclase grains (Figures 7.1a and b). Most of the anhedral to euhedral plagioclase grains also show a small amount of micaceous mineral growth (sericite - 2%) along cleavage planes and concentrated within the centre of the grains (Figure 7.1b). Scanning electron microscope observations have already shown the formation of prismatic etch pits on the surface of the plagioclase grains at the onset of weathering. These contribute to the cloudy appearance of the grains as observed under the microscope. Microcracking is also present although not as common as within the quartz grains. The anhedral microcline grains are generally fresh and exhibit characteristic cross-hatch twinning as shown in Figure 7.1b. Intra-granular microcracks occur but are limited. Biotite may exhibit iron oxide stain halos, although the grains still show characteristic distinctive pleochroism with no opening of mica cleavage observable.

The microfabric is essentially intact without any disruption to grain interlock and tight grain contacts occur.

7.3.2 Highly weathered granite

Table 7.2 presents a summary of the modal analysis for these samples. The anhedral quartz grains (32%) are 3,0 to 0,3 mm in size and often exhibit undulatory extinction with further weathering opening the transgranular microcracks The microcracks range in width from 30 to 50 μm and are occasionally filled with clay, otherwise remaining open as shown in Figure 7.2a. It is interesting to note the large discrepancy between the quartz content in the highly weathered granite (average = 32,2%) and the fresh granite (average = 59,4%). This difference cannot be explained by any loss

Table 7.1. Modal analysis (%) and micropetrographic index (I_p) of fresh and slightly weathered granite.

Sample	Depth (m)	Quartz	Microcline	Plagioclase	K-Feldspar	Biotite	Muscovite	Chlorite	Sericite	Amorphous kaolinite	Kaolinite books	Hematite	Microcracks	Voids	Illite /smectite	Dry density ($kg.m^{-3}$)	I_p
BH 1143	23,7	67,2	8,4	14,4	0	2,0	1,0	5,0	1,0	0	0	0	1,0	0	0	2673	13,3
BH 1143	28,5	59,0	11,5	17,5	0	4,3	1,0	3,7	2,0	0	0	0	1,0	0	0	2618	13,9
BH 1117	18,9	60,0	13,4	14,7	0	3,2	1,0	3,6	3,1	0	0	0	1,0	0	0	2599	23,4
BH 1117	21,0	62,7	10,2	13,1	0	3,2	1,0	6,8	2,0	0	0	0	1,0	0	0	2684	32,3
BH 1204	25,2	48,1	15,7	22,6	0	5,1	1,0	2,6	2,0	0	0	0	3,0	0	0	2644	19,0
Average		59,4	11,8	16,5	0	3,6	1,0	4,3	2,0	0	0	0	1,6	0	0	2643	20,4

Table 7.2. Modal analysis (%) and micropetrographic index (I_p) of highly weathered granite.

Sample	Depth (m)	Quartz	Microcline	Plagioclase	K-Feldspar	Biotite	Muscovite	Sericite	Kaolinite amorphous	Kaolinite books	Hematite	Microcracks	Voids	Illite/ smectite	Dry density ($kg.m^{-3}$)	I_p
RF 2	8,2	29,3	13,8	20,2	0	0,6	4,6	8,7	6,5	1,6	0	13,0	1,3	0	1779	2,2
RF 1	9,6	24,7	16,2	17,0	0	0	1,8	9,2	9,1	4,8	0,6	9,2	2,8	0	1823	1,7
RF 14	11,8	33,6	23,3	18,8	1,3	1,8	1,1	5,2	4,8	0,6	0,1	6,8	2,0	0	2159	4,1
RF 15	10,9	27,6	3,0	21,8	1,1	1,8	0,2	10,1	3,6	15,8	0	10,0	1,7	0	2087	1,3
RF 16	11,8	36,1	20,0	29,1	4,7	2,6	0,6	4,6	0	0	0	2,1	0	0	2480	13,9
RF 22	7,7	32,3	9,2	36,5	5,5	3,0	0,6	8,2	0,1	0	0	4,2	0	0	2350	7,0
RF 23	9,1	39,1	14,2	28,4	6,6	2,1	0,9	6,3	0,1	0	0	0,9	0,6	0	2210	11,6
RF 24	9,8	31,6	13,5	31,3	5,5	1,4	1,7	7,4	3,5	0	0	3,5	0	0	2250	5,9
RF 25	10,2	30,3	14,6	30,4	4,6	3,8	0,8	6,5	4,0	0	0	4,5	0	0	2437	5,6
Average		32,2	13,5	25,7	5,46	1,8	1,0	6,6	3,3	2,2	0,1	5,8	0,8	0	2242	7,3

of quartz through weathering, but rather shows the heterogenic nature of the granite mass. Plagioclase grains (26%) show a dirty grey, turbid appearance with this form of alteration often disseminated consistently throughout the grain with Figures 7.2b and c illustrating this. The grains range in size from 0,08 to 3,2 mm in size. Sericitization (7%) along cleavage planes is commonplace increasing as weathering increases. Scanning electron microscope observations show the occurrence of prismatic etch pits and in some cases skeletal plagioclase feldspar frameworks at this stage of weathering. The plagioclase grains are commonly microcracked, the cracks being clay-filled or open (Figure 7.2c). Microcline feldspar (14%) is clear with tight, transgranular microcracking as shown in Figure 7.2d. Turbidity can be observed spreading from the centre of some grains. The anhedral grains are 0,9 to 2,7 mm in size. Biotite (2%) is olive brown in colour with occasional iron oxide staining around the edge of the grains and segregation occurs along cleavage planes (Figure 7.2e). Feather-edge grain boundaries occur as part of the onset of alteration as seen in Figure 7.2f. The grains are generally between 0,2 and 1 mm in size.

Inter-granular microcracks often exhibit a reticulate pattern and most are filled with clay minerals and sericite. Orange staining along the surfaces of the microcracks is commonplace enhancing the brown discoloration of the samples. A plausible explanation for the formation of these microcracks can be attributed to de-stressing of the quartz and feldspar grains during weathering. This can occur as residual stress is released when grain boundaries are opened up and increased porosity occurs when solution effects become prominent (Dobereiner and Porto, 1993). The microcracking related to different values of mineral thermal expansion on cooling of the rock (as highlighted by Nur and Simmons, 1970), should be more related to intra-granular features since the large inter-particle microcracks were not observed in the fresh rock.

No significant disruption to the microfabric has taken place although localised loosening along grain boundaries does occur.

7.3.3 Granite saprolite

A distinct petrographical change in texture occurs with a wide range of petrographic fabrics and mineralogy observable in the saprolite (Table 7.3). These fabrics depend upon the degree of alteration and leaching which are affected by the weathering microenvironment. Microcracking of quartz grains (21%) increases from narrow open microcracks to complete fragmentation of the quartz grains with individual grains separated by clay aggregates or voids with iron oxide staining on the grain boundaries (Figures 7.3a, b and c). The intensity of the microcracking reduces the grain size of the quartz. Plagioclase grains (4%) show moderate to often complete alteration. The alteration occurs throughout the grain and along cleavage and twinning planes (Figures 7.3d and e). Sericitization (2%) is still common within the moderately altered grains whilst the completely altered

Table 7.3. Modal analysis (%) and micropetrographic index (I_p) of granite saprolite.

Sample	Depth (m)	Quartz	Microcline	Plagioclase	K-Feldspar	Biotite	Muscovite	Sericite	Kaolinite amorphous	Kaolinite books	Hematite	Microcracks	Voids	Illite/ smectite?	Dry density ($kg.m^{-3}$)	I_p
RF 10	3,5	20,7	7,8	4,5	0	0,2	0,3	5,3	11,1	18,5	9,7?	5,1	16,3	0	1330	0,5
RF 9	4,9	22,2	12,5	8,5	0	0,2	1,6	4,8	8,5	32,1	0,1	3,5	5,6	0	1375	0,8
RF 8	5,7	34,6	18,0	1,8	0	0,1	3,7	4,3	7,3	11,7	0,5	4,7	3,2	0	1482	1,4
RF 7	6,6	23,5	16,5	11,7	0	0,6	3,8	3,3	4,6	6,5	0	8,2	5,0	0	1855	1,4
RF 6	2,5	22,8	4,4	0	0	0	0,9	0	11	49,0	2,6?	4,6	4,3	0	1458	0,4
RF 5	4,8	23,7	32,1	2,2	0	0	2,0	0	4,1	21,4	0,1	11,7	2,3	0	1763	1,5
RF 4	6,9	23,2	3,8	7,8	0	0,2	0	0,2	8	40,7	0,3	8,5	6,8	0	1457	0,5
RF 3	9,2	22,8	3,1	7,8	0,5	0,1	0,3	1,1	1,4	51,8	0	6,3	3,9	0	1683	0,5
RF 18	3,8	19,7	5,6	0	3,0	0,1	0	0,1	41,7	13,0	0	2,7	13,8	0	1383	0,4
RF 19	5,2	29,9	13,7	14,2	4,6	2,5	0,3	1,6	20,0	3,2	0	6,2	3,9	0	1696	1,9
RF 20	6,1	18,3	4,1	17,0	2,2	3,0	0,3	9,5	17,7	7,0	0	9,9	10,5	0	1479	0,8
RF 21	6,2	17,5	5,6	14,5	6,3	3,0	0,2	9,7	15,5	9,2	0	10,7	7,5	0	1663	0,9
LF 2	2,4	6,6	4,5	0	1,6	0	0,2	0	25,2	35,2	4,5?	7,3	14,6	0,2	1400	0,2
LF 3	3,8	18,8	20,6	0	7,0	0	0,1	0	0,6	32,2	2,7?	6,6	9,8	1,2	1416	0,9
LF 4	4,5	24,2	9,7	0	0	0	0,8	0	0,2	49,4	1,7	3,1	9,6	0,8	1523	0,5
LF 5	5,2	23,7	8,1	0	0	0	0,9	0	2,2	55,3	1,9?	2,3	1,7	1,9	1610	0,5
LF 6	7,4	2,5	0	0	1,4	0,2	0	0	37,3	27,4	0,8	0,8	0		1433	0,5
LF 8	2,8	21,9	11,7	0	0	0	0	0	16,5	27,1	2,2?	6,6	12,9	0	1434	0,5
LF 9	4,0	23,6	9,8	0	0	0	0,1	0	23,4	22,4	2,4?	6,5	11,3	0	1429	0,5
LF 10	5,5	13,0	13,9	0	0	0	0,1	0,1	19,2	35,9	2,5?	2,5	10,8	0	1431	0,4
LF 11	6,5	19,5	20,4	0	0	0	0	0	12,8	35,2	0,7	7,2	3,5	0	1362	0,7
LF 12	7,3	4,4	1,3	1,3	0	0,2	0,8	0	6,6	62,3	1,1	2,7	12,1	0	1226	0,1
LF 13	7,7	14,5	5,7	15,8	0	0,7	0	5,3	12,2	35,3	0,2	1,2	5,6	0	1625	0,6
LF 19	2,3	23,5	3,2	0	4,6	0	0,1	0	20,5	31,8	0,2	3,3	12,0	0,5	1535	0,5
LF 20	3,2	24,3	3,8	0	3,3	0	0,1	0	32,2	20,7	0,5	3,0	12,1	0	1307	0,5
LF 21	4,0	19,7	3,0	0	3,5	0	0,2	0	43,0	5,2	8,1?	1,3	9,2	6,5	1386	0,4
LF 22	5,1	19,7	8,0	0	4,5	0	0,1	0	43,2	3,5	5,5?	0,6	11,2	3,5	1409	0,5
LF 24	5,7	20,7	3,2	0	9,6	0,7	0,1	0,1	26,4	22,3	0	5,4	10,9	0	1398	0,5
LF 25	6,2	31,4	1,1	0,5	8,7	0,9	0	0	24,5	19,1	0	5,1	8,3	0	1533	0,7
LF 26	7,2	14,6	5,0	7,0	6,5	2,4	0,3	12,3	19,2	16,2	0	6,2	9,1	0	1522	0,6
LF 27	7,8	30,0	5,4	18,4	4,1	3,3	0,4	7,7	11,6	3,4	0	8	7,3	0	1797	1,6
Average		20,5	8,6	4,3	2,3	0,6	0,6	2,1	17,0	25,9	1,5	5,2	8,2	0,5	1457	0,7

grains are composed of clay aggregates forming clay pseudomorphs (Figures 7.3d and e). Microcline (8,6%) exhibits slight cloudiness with intense microcracking (Figure 7.3f), with SEM observations suggesting a porous structure. The microcracks may be tight or open and filled with clay, with partial alteration occurring along microcracks and cleavage. The open microcracking has resulted in disaggregation of the grains effectively reducing grain size. The majority of the biotite (0,5%) has been highly altered, although few remnant grains do exist. Where these occur, the mineral experiences a loss in pleochroism associated with iron loss. Opening of cleavage is visible causing disruption of the biotite structure, whilst grain boundaries become feather-edged. Where alteration is more intense, the biotite alters to a variety of fine-grained secondary micaceous and kaolinite minerals. The occurrence of kaolinite is common in this stage of weathering. It occurs as a platy variety (26%) in Figure 7.3g and as disseminated fine-grained aggregates (17%) in Figure 7.3h. A small amount of iron-oxide minerals also occur with localised dissemination. They predominantly occur within microcracks and as coatings on the void walls. X-ray diffraction results show the iron oxide to be hematite.

Void formation includes open, inter-granular microcracks and vermiform voids. The microcracks form a reticulate pattern (Figure 7.3i) throughout the microfabric causing a degree of disruption to the fabric. They tend to be open or filled with clay and/or stained with iron oxide. The width of the cracks decreases systematically with a reduction in weathering intensity. The voids tend to be irregular, although maintaining smooth edges typical of solution voids (Figure 7.3j). The vermiform voids range in diameter from 0,02 to 2mm and their free surfaces are often clay-lined with iron oxide staining. The voids tend to be preferentially situated within amorphous clay aggregations (Figure 7.3j) but, as observed from the SEM investigation, also develop preferentially along the grain boundaries of the more competent grains (Figures 7.3k and l). The majority of grain boundaries are open and are responsible for the significant difference in strength and density observed between the granite saprolite and underlying highly weathered granite.

7.3.4 Granite saprolite with residual soil patches

The nature of this material approaches that of a true residual soil where the material comprises irregular, fine, iron-enriched clay aggregations within an incipient fabric similar to the granite saprolite (as described above). Within the clay aggregations complete destruction of any original fabric has occurred (Figure 7.4a) where essentially the only primary mineral grains include broken quartz (20%) with subordinate microcline fragments (4%). The grains are much reduced in size due to enhanced weathering. Plagioclase is distinctly absent (Table 7.4), with the advanced stage of weathering having completely decomposed the grains to kaolinite which forms the predominant mineralogy (55%).

Table 7.4. Modal analysis (%) and micropetrographic index (I_p) of granite saprolite with residual soil patches.

Sample	Depth (m)	Quartz	Microcline	Plagioclase	K-Feldspar	Biotite	Muscovite	Sericite	Kaolinite amorphous	Kaolinite books	Hematite	Microcracks	Voids	Illite/ smectite?	Dry density ($kg.m^{-3}$)	I_p
RF 12	1.	21,8	6,1	0,8	0	0,1	0,3	0,2	50,0	4,5	1,6	6,8	7,3	0	1511	0,4
RF 17	2,2	20,5	5,4	0	0	0	0,1	0,1	42,1	14,9	0,5	2,5	13,9	0	1389	0,3
LF 1	0,9	12,2	6,5	0	1,8	0	2,7	0	48,6	1,2	6,2	2,7	17,7	0	1478	0,3
LF 7	1,1	23,8	13,3	0	0	0	1	0	32,2	13,2	0,7	7,3	8,3		1444	0,6
LF 18	1,1	19,6	0,5	0	0,8	0	0,1	0	22,0	25,5	10,3	5,0	15,3	0,6	1535	0,3
Average		19,6	6,4	0,2	0,5	0	4,2	0,1	39,0	11,9	3,9	4,9	12,5	1,8	1471	0,4

Void formation is well-developed in the iron-enriched clay aggregations and is represented by a concentration of vermiform voids (Figure 7.4b).

7.4 Characterization of weathering and engineering properties in terms of quantitative micropetrographical indices

Irfan and Dearman (1978a) have advocated the application of standard petrographic techniques to evaluate the successive mineralogical and textural changes that occur during the weathering process. There study on weathered granite in England proved this to be an applicable technique. They maintained that petrographically relevant properties which can be expected to influence the engineering behaviour of the weathered granite include primary mineral composition, secondary alteration products, grain structure, texture and porosity (in the form of voids and microcracks). The micropetrographic index (I_p) suggested by them provides a means of quantifying these properties and is defined as follows:

$$I_p = \frac{\%\ sound\ constituents}{\%\ unsound\ constituents} \qquad \text{(Eqn. 7.4.1)}$$

where sound constituents include quartz, plagioclase, potash feldspar, biotite, muscovite and accessory minerals such as magnetite and unsound constituents include sericite, kaolinite, gibbsite, chlorite, secondary muscovite, iron oxides, microcracks and voids. The percentage composition of the various constituents is obtained from modal analysis. Results for I_p values for the different grades of granite weathering are presented in Tables 7.1 to 7.4 and show that I_p decreases with increasing weathering.

The values of I_p are similar to those obtained by Irfan (1988) where I_p measured between 0,39 to 0,87 for similar material and Gupta and Rao (2001) where I_p measured an average of 0,8. The values are also in agreement with qualitative observations of mineralogy and microfabric (Chapter 8) suggesting that this index can be used to characterise the microfabric of the granite saprolite. The association can be extended to correlations with certain engineering characteristics of the material. A clear relationship is noted when plotting I_p against the dry density of the weathered granite (Figure 7.5). The scatter of results is attributed to the small area of the thin section that may not be entirely representative of the sample. The inherent variability within the parent material may compound this.

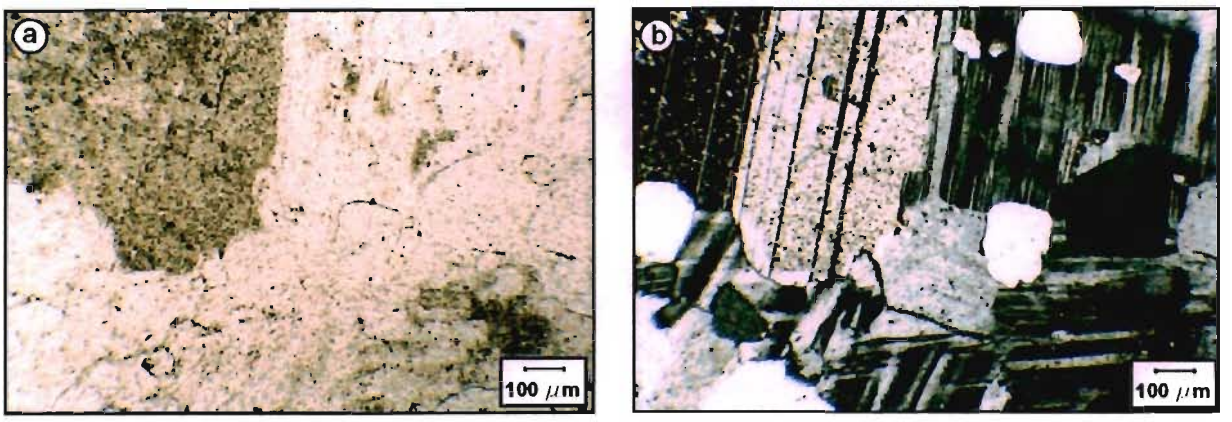

Figure 7.1. Photomicrographs of fresh and slightly weathered granite (BH 1143). (a). Granite showing cloudy and slightly sericitised plagioclase grains alongside cloudy but intact microcline feldspar under plane polarised light (PPL). Magnification = 40x. Grain boundaries are tight with no disruption to microfabric. (b). Equivalent micrograph under cross polarised light (CPL), showing commencement of sericite growth in plagioclase grains. Magnification = 40x.

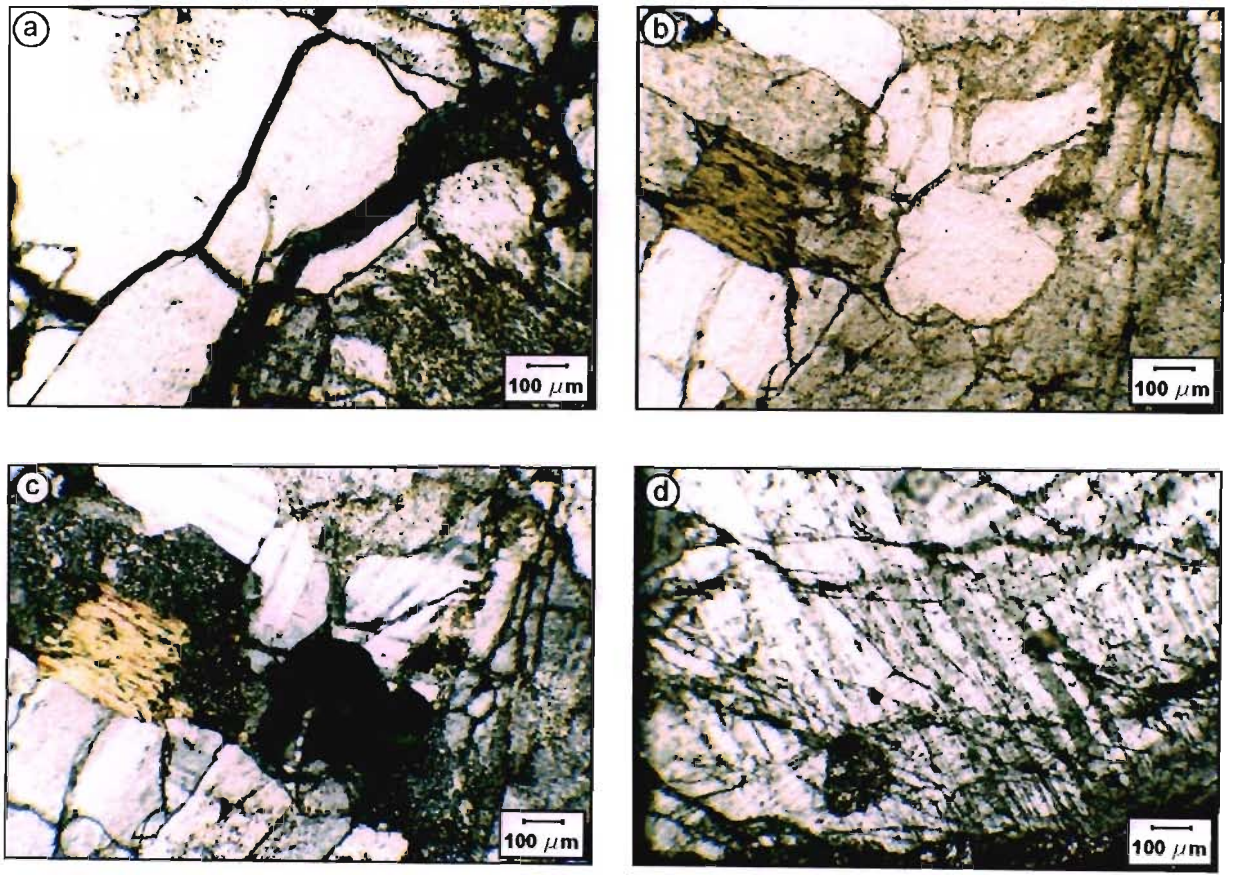

Figure 7.2. Photomicrographs of highly weathered granite. (a). Clean open microcracks in quartz showing the process of reduction in grain size (RF 14). Decomposed plagioclase occurs on bottom right with open grain contacts clearly evident (PPL). Magnification = 40x. (b) and (c). Typical microfabric of highly weathered granite in PPL (b) and CPL (c). Plagioclase grains show increased turbidity with a high degree of sericitisation and numerous microcracks (RF 16). Only minor disruption to original microfabric is noted. Magnification = 40x. (d). Slightly cloudy microcline feldspar (RF 25) with numerous clean microcracks (CPL). Magnification = 40x.

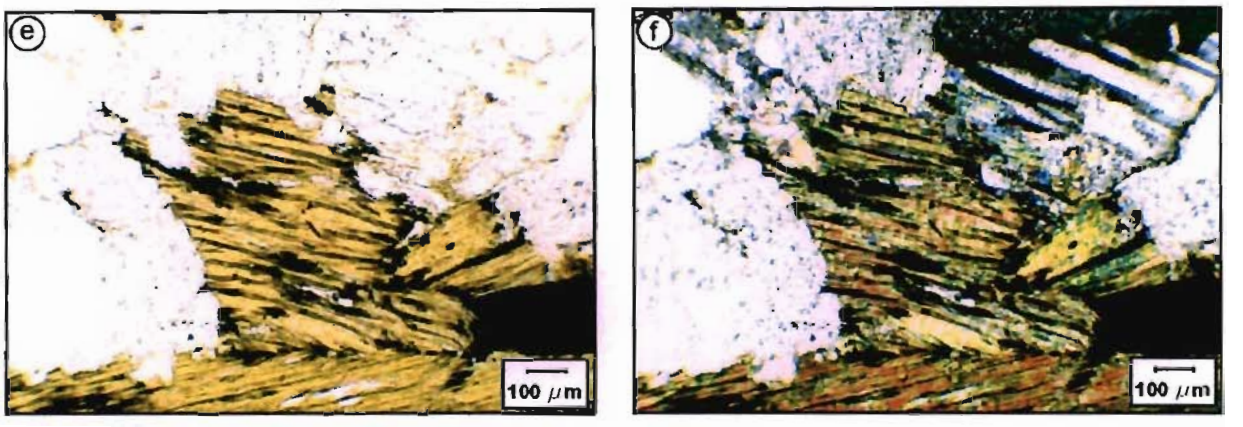

Figure 7.2 (continued). Photomicrographs of highly weathered granite. (e) and (f). Bleached biotite (RF 16) showing characteristic feather-edged grain boundary and opening of mica cleavage under PPL (e) and CPL (f). Alteration of the edge of the biotite grains to micaceous clay can be observed in the upper right hand portion of the micrograph. Magnification = 40x.

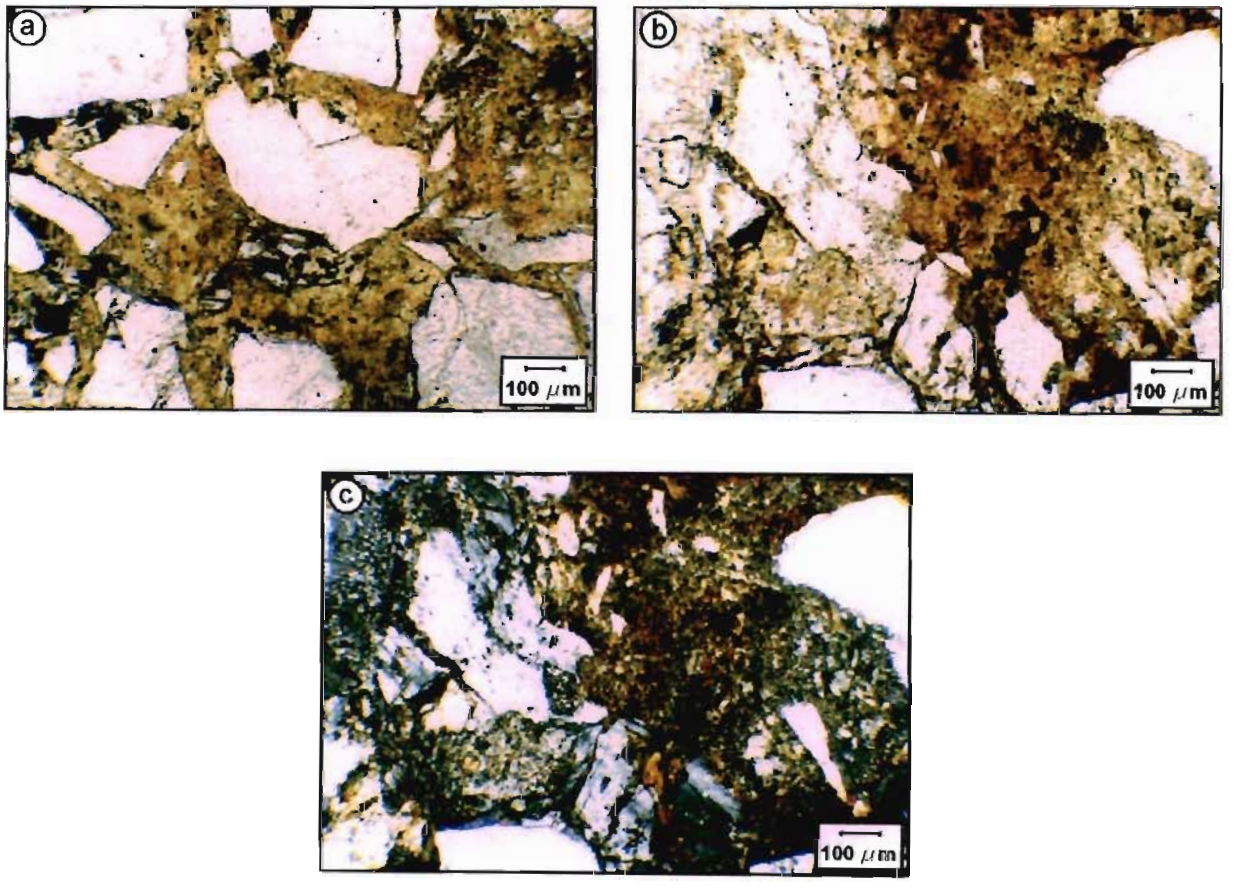

Figure 7.3. Photomicrographs of various microfabrics encountered within the granite saprolite. (a). Broken quartz fragments within a matrix of clay (LF 4). Microcracks traverse the quartz grains and are clay filled with iron oxide staining. This type of microfabric is representative of the most highly weathered granite saprolite samples and approaches that of a residual soil. Disruption to the microfabric can be observed although some grain interlock still occurs (PPL). Magnification = 40x. (b) and (c). Microfabric of granite saprolite (LF 20)in PPL (b) and CPL (c). The microfabric shows some disruption due to the formation of clay and intense microcracking. A reduction in the grain size compared to that in Figure 7.2 can be observed. Magnification = 40x.

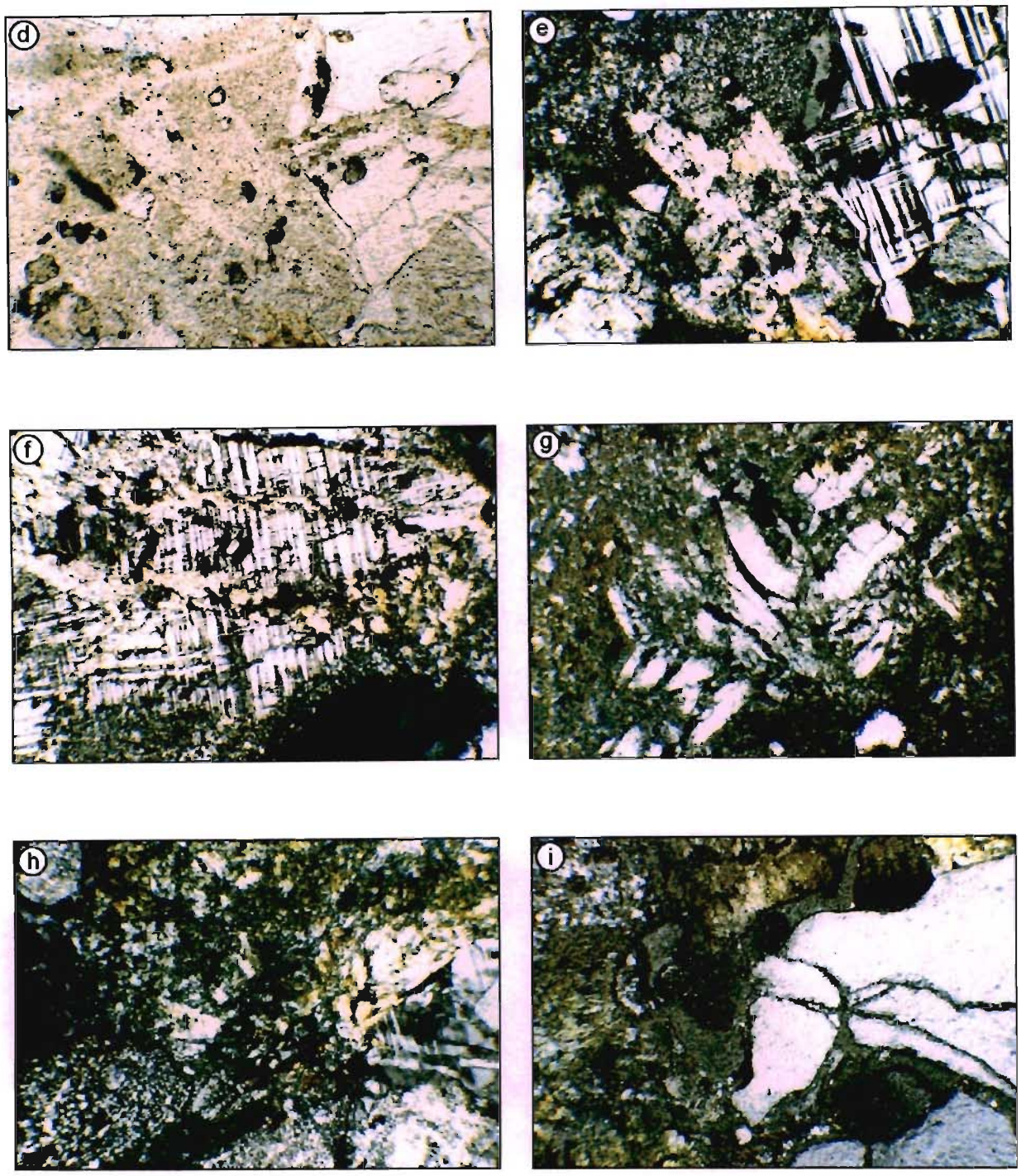

Figure 7.3 (continued). Photomicrographs of various microfabrics encountered within the granite saprolite. (d) and (e). Formation of clay pseudomorphs (LF 9) derived from complete decomposition of plagioclase grains (note the very turbid nature of the grains). The adjacent microcline grain shows comparatively less alteration in the form of dusty clouding and clay filled microcracks. PPL (d) and CPL (e). Magnification = 40x. (f). Severely microcracked microcline grain under CPL showing characteristic clay infilling along the microcracks (LF 25). Magnification = 40x. (g). Platy, book-type kaolinite (LF 20) under CPL within a matrixof fine-grained clay aggregates. Magnification = 40x. (h). Typical appearance of fine-grained clay aggregations under CPL (LF 8). Magnification = 40x. (i). Reticulate pattern of microcracks within the granite saprolite (RF 4) showing the extension of a microcrack propagating into the vermiform void located within the fine-grained clay aggregations (CPL). Magnification = 40x.

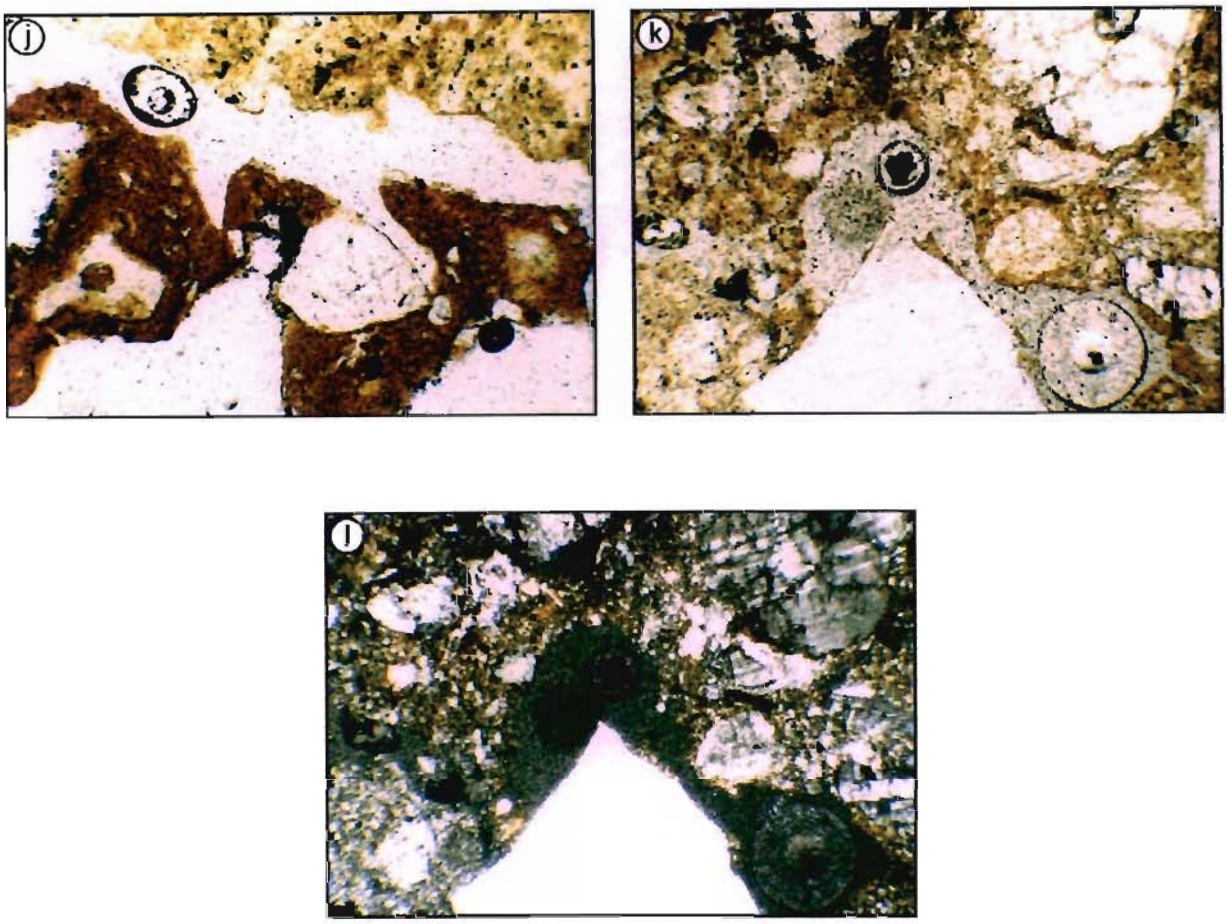

Figure 7.3 (continued). Photomicrographs of various microfabrics encountered within the granite saprolite. (j). Characteristic vermiform voids showing clay-lined surfaces with iron-oxide staining (LF 6). The smooth appearance of the voids is typical of solution effects (PPL). Magnification = 40x. (k) and (l). Structural control on void formation with propagation of the void dictated by the presence of the quartz grain (LF 9). As identified from the SEM investigation, preferred solution along clay-grain contacts is common. PPL (k) and CPL (l). Magnification = 40x.

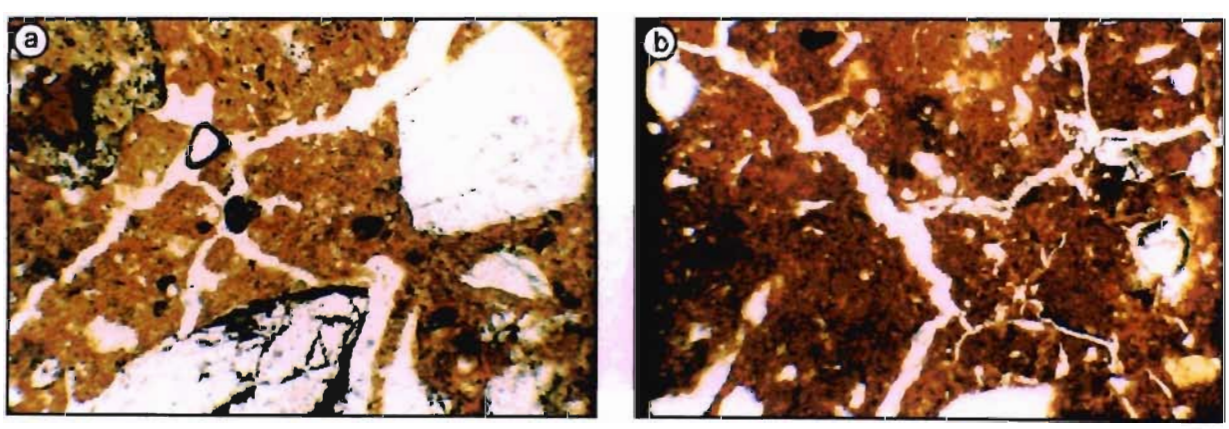

Figure 7.4. Photomicrographs of granite saprolite with residual soil patches. (a) Complete destruction of microfabric with iron-enriched clay and broken quartz grains dominating the microfabric with characteristic reticulate vermiform voids (LF 18). Magnification = 40x. (b). Similar form of reticulate vermiform voids in iron-enriched aggregation of clay (RF 17). Note smooth appearance of void walls showing solution effects. Complete loss of fabric occurs in this particular micrograph. Magnification = 40x.

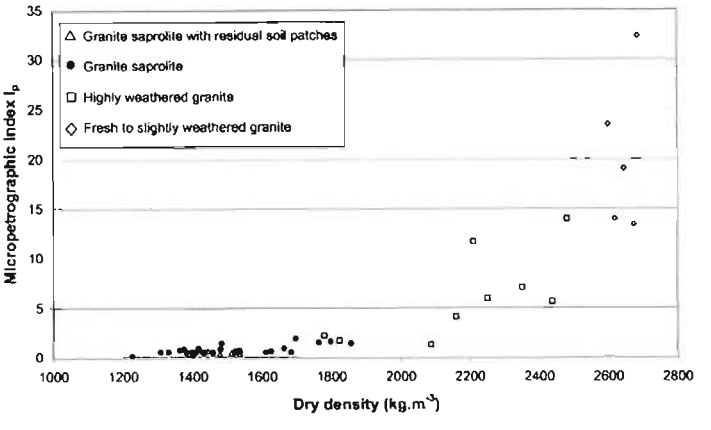

Figure 7.5. Relationship of micropetrographic index (I_p) and dry density (from sand replacement method) of weathered granite.

The petrographic investigation also revealed the important effect that microcracks have on the microfabric. However, the interpretation of the quantification or indexing of these features is somewhat more complex and should be carried out with care. Irfan and Dearman (1978a) suggest the use of a microfracture index (I_f) which is quantified by counting the number of microcracks in a 10 mm traverse of the thin section and differentiating these cracks according to their filling. This procedure is successful with highly weathered granites which only show a slight disruption to their original microfabric. However, with granite saprolite the microcracks often become widened and filled with clay such that apparently fewer microcracks will be observed over any particular 10 mm traverse, giving the impression that microcracking decreases with increasing weathering. It is therefore recommended that I_p provides a more appropriate index for the granite saprolite and in fact has been demonstrated to successfully quantify mineralogical and fabric changes that have occurred throughout the various defined weathering grades.

8. MINERALOGY AND GEOCHEMISTRY

8.1 Mineralogy

8.1.1 Introduction

A study of granite weathering is not complete without a review of its mineralogy. For this purpose, samples of the weathered granite were analysed for whole rock composition using a Siemens D500 X-ray diffractometer. Although many previous studies on weathered granite have utilised petrographic techniques to determine the mineralogical composition of these materials, X-ray diffraction (XRD) techniques have perhaps not been used as often as expected. Apart from being semi-quantitative, the advantages of this technique are that it is able to provide a good indication of broad mineralogical changes that occur throughout the weathering spectrum and allows for the determination of the very fine-grained products which are difficult to identify in thin section. A summary of the XRD results for each weathering grade of the granite is presented in Tables 8.1 to 8.4. The mineralogical results confirm the nature of chemical weathering and its effects on the granite as identified in the SEM and petrographic studies and these are discussed below.

8.1.2 Equipment and Techniques

A Siemens D5000 X-ray system at the Council for Geoscience, Pretoria, was used for the semi-quantitative XRD analysis. This system is equipped with a 2,2kW Cu long fine focus tube, variable slit secondary graphite monochromator sample spinner and 40 position automated sample changer. Bulk samples for whole rock analysis in random powder preparation were scanned from 2° to 65° 2θ $Cu_{K\alpha}$ radiation at a speed of 0,02° 2θ step size per second with generator settings of 35kV and 25mA.

Representative samples of the saprolite or weathered rock were air dried, crushed, milled and homogenised to a fine powder (approximately 10μm in size). A sub sample of this powder was then pressed into a shallow aluminium sample holder against a rough filter paper in order to ensure random orientation of the sample material. No specific sample treatments were undertaken using foramide, hydrazine or ethylene glycol, for example.

Mineral phase concentrations were determined as semi-quantitative estimates using relative peak height/area proportions according to Brime (1985). Detection limits range from 0,5% to approximately 5% depending upon the sample composition and origin. Mineral phase identification was based upon

the SIEMENS DIFFRAC^{Plus} - EVA evaluation programme with checking and final analysis of the XRD traces carried out by the machine operator at the Council for Geoscience.

8.1.3 Fresh to slightly weathered granite

The fresh to slightly weathered granite can be seen to consist primarily of quartz, microcline and plagioclase with minor chlorite and mica (Table 8.1). The percentage composition of the major minerals is somewhat variable with the quartz content varying from 42% to 71 % and plagioclase ranging between 14% and 27%. Microcline generally occurs in lower proportions but also with a notable variability ranging from 5% to 18%. The mica content varies from 2% to 8% whilst chlorite ranges from 1% to 7%.

Table 8.1. Mineralogical results from XRD analyses for fresh and slightly weathered granite.

Sample	Microcline	Plagioclase	Quartz	Kaolinite	Mica	Smectite	Interstratified Illite and Smectite	Hematite	Calcite	Chlorite
BH1143 (23.7m)	5	14	71	0	3	0	0	0	0	7
BH 1143 (28.5m)	18	16	52	0	2	0	0	0	0	1
BH 1117 (18.9m)	16	18	53	0	8	0	0	0	0	5
BH 1117 (21.0m)	9	14	65	0	7	0	0	0	0	5
BH 1204 (25.2m)	17	27	42	0	8	0	0	0	0	6
Average	13	18	57	0	6	0	0	0	0	5

8.1.4 Highly weathered granite

The highly weathered granite is also composed primarily of quartz, microcline, plagioclase and mica, with variable kaolinite content (Table 8.2). The quartz content varies from 22% to 75 % with plagioclase in lower proportions ranging from 10% to 33 %. Microcline varies from 9% to 17%. The occurrence of kaolinite suggests the onset of the decomposition of the plagioclase feldspars with kaolinite varying between 0% and 13%. The changing proportion of plagioclase and secondary clay (kaolinite) reveals the inverse relationship between these two minerals. Mica contents are low, varying from 5% to 14%, but still remain higher than in the fresh to slightly weathered granite, this probably being due to the increased formation of illite. The mineralogical analyses also revealed the presence of minor smectite. As explained in Chapter 7, this is probably due to the relatively poor drainage conditions (supported by permeability results as found by Chunnett *et al.*, 1991a) within the rock mass at this grade of weathering, where the effects of leaching are not significant.

Table 8.2. Mineralogical results from XRD analyses for highly weathered granite.

Sample	Microcline	Plagioclase	Quartz	Kaolinite	Mica	Smectite	Interstratified Illite and Smectite	Hematite	Calcite	Chlorite
RF 2	13	17	51	3	9	3	0	0	3	0
RF 1	17	12	48	13	8	0	0	0	2	0
RF 13	11	33	46	4	6	0	0	0	0	0
RF 14	17	22	54	0	5	0	0	0	2	0
RF 15	9	27	22	10	10	21	0	0	0	0
RF 16	18	23	50	0	5	2	0	0	2	0
RF 22	9	23	54	0	6	8	0	0	0	0
RF 23	13	10	75	0	2	0	0	0	0	0
RF 24	6	20	68	0	2	4	0	0	0	0
RF 25	7	25	50	0	14	4	0	0	0	0
LF 28	13	23	54	2	8	0	0	0	0	0
Average	12	21	52	3	7	4	0	0	1	0

8.1.5 Granite saprolite

The granite saprolite can be seen to consist primarily of quartz, kaolinite and feldspar (Table 8.3). The quartz content varies from 17% to 65%, whilst kaolinite can be as high as 69% with a low of 7% - this being reflective of the degree of weathering. No halloysite-type minerals were identified from the XRD analysis. The feldspar component varies according to the intensity of weathering, with plagioclase being very sensitive to weathering (0% to 34 %). The more resistant microcline occurs in variable proportions ranging from 0% to 22% but is on average higher than plagioclase. Mica is also present in significant concentrations (5 to 22%) and apparently increases with increasing weathering (this being a function of increased secondary muscovite and illite formation). Small accumulations of smectitic clays may be the product of localised poor drainage conditions within the material or could be derived from amphibolitic xenoliths or the nearby weathered diabase dykes. A typical XRD trace for the granite saprolite is presented in Figure 8.1.

8.1.6 Granite saprolite with residual soil patches

Mineralogical analysis shows the granite saprolite with residual soil patches to be composed essentially of quartz, microcline, kaolinite and mica (Table 8.4). The quartz content varies from 20% to 49%, with microcline between 0% and 11%. As expected, the clay content is very high, with kaolinite forming between 30% and 53% of the material. As with the granite saprolite, no halloysite-type minerals were identified. There is significant variation of the mica content (from 5% to 33%) within the granite saprolite with residual soil patches. The presence of smectite in most of these samples suggests poor drainage conditions within the material allowing for the formation of such clays. Hematite was only found in two of the samples and its presence suggests the beginning of laterisation within these samples.

Table 8.3. Mineralogical results from XRD analyses for granite saprolite.

Sample	Microcline	Plagioclase	Quartz	Kaolinite	Mica	Smectte	Interstratified illite and smectite	Hematite	Calcite	Chlorite
RF 10	8	10	61	14	7	0	0	0	0	0
RF 9	9	14	39	30	8	0	0	0	0	0
RF 8	2	3	41	46	9	0	0	0	0	0
RF 7	3	17	44	29	6	0	0	0	0	0
RF 6	6	0	33	48	14	0	0	0	0	0
RF 5	14	0	43	25	18	0	0	0	0	0
RF 4	0	4	30	46	20	0	0	0	0	0
RF 3	22	17	29	16	16	0	0	0	0	0
RF 18	7	0	17	69	9	3	0	0	0	0
RF 19	5	22	51	12	6	2	0	0	0	0
RF 20	3	17	41	17	22	0	0	0	0	0
RF 21	5	34	34	14	8	5	0	0	0	0
LF 2	8	0	38	45	6	0	3	0	0	0
LF 3	12	0	38	39	7	0	3	0	0	0
LF 4	13	0	36	39	12	0	0	0	0	0
LF 5	10	3	45	27	11	4	0	0	0	0
LF 6	6	0	38	40	11	0	6	0	0	0
LF 8	8	0	33	40	19	0	0	0	0	0
LF 9	21	7	30	34	8	0	0	0	0	0
LF 10	3	0	42	42	13	0	0	0	0	0
LF 11	15	0	25	50	10	0	0	0	0	0
LF 12	5	2	51	34	4	0	4	0	0	0
LF 13	13	17	30	27	8	0	5	0	0	0
LF 19	0	0	65	20	12	4	0	0	0	0
LF 20	5	0	41	39	12	3	0	0	0	0
LF 21	14	0	21	52	10	3	0	0	0	0
LF 22	12	0	29	51	5	3	0	0	0	0
LF 24	6	0	51	36	7	0	0	0	0	0
LF 25	4	0	57	31	8	0	0	0	0	0
LF 26	12	25	38	20	5	0	0	0	0	0
LF 27	7	21	39	17	15	0	0	0	0	0
Average	8	7	39	34	11	1	1	0	0	0

Table 8.4. Mineralogical results from XRD analyses for granite saprolite with residual soil patches.

Sample	Microcline	Plagioclase	Quartz	Kaolinite	Mica	Smectte	Interstratified illite and smectite	Hematite	Calcite	Chlorite
RF 12	3	2	49	33	5	4	0	5	0	0
RF 17	5	0	20	53	16	3	0	3	0	0
LF 1	5	0	43	32	17	2	0	0	0	0
LF 7	11	0	48	30	12	0	0	0	0	0
LF 18	0	0	36	31	33	0	0	0	0	0
Average	5	0	39	36	17	2	0	2	0	0

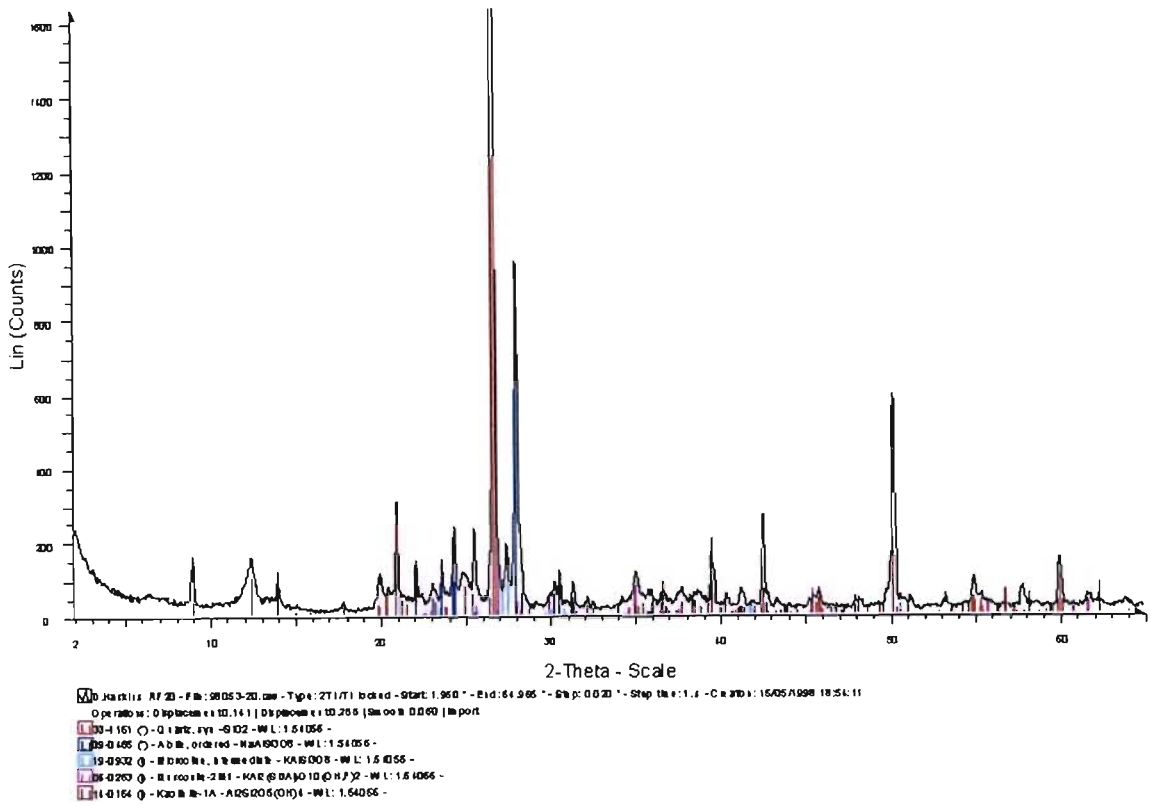

Figure 8.1. Typical XRD trace for granite saprolite at Injaka Dam.

Figures 8.2a to 8.2f show the relationship of mineralogical composition with depth for each of the six sample traverses. The most striking feature of these figures is the very high degree of variability within the mineralogical profiles. However, certain systematic relationships can be observed with the most significant being the increase in kaolinite and corresponding decrease in plagioclase towards the surface. A general decrease in microcline with increasing weathering occurs, although this is only noticeable above 5 m depth. The variation of quartz can be considered to be dictated by its variation within the parent material. Although the mica content appears neither to increase or decrease it must be realised that the XRD mica analysis includes primary and secondary forms of mica and consequently, the alteration of biotite is off-set by the formation of illite.

Figure 8.3 shows the simple relationship of initial void ratio (e_0) with kaolinite (%) determined from XRD analysis. In order to validate these correlations, the r value was tested for significance using the Student's t-Test, where:

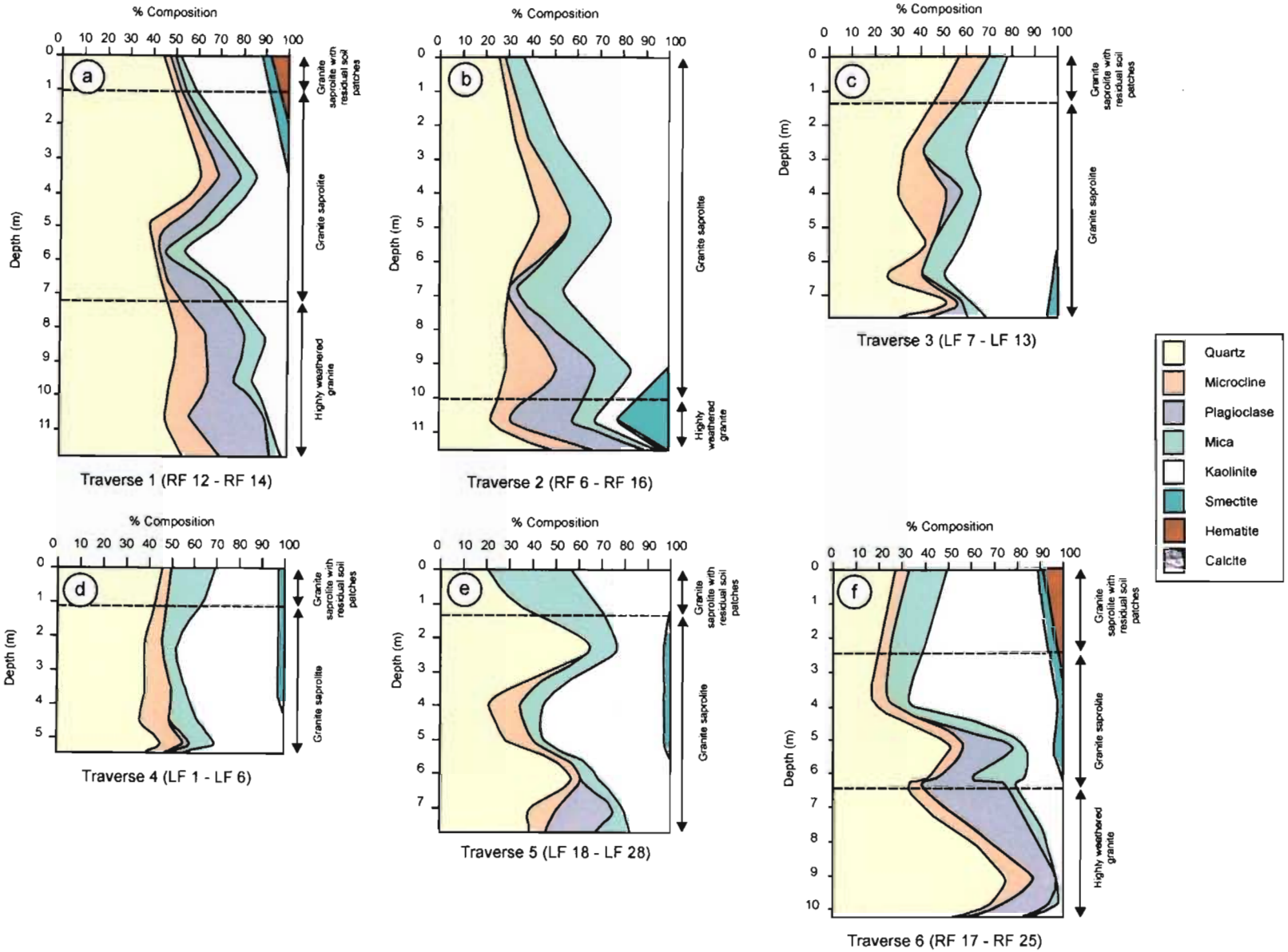

Figures 8.2a to 8.2f. Mineralogical changes as depicted in each sample traverse with depth.

$$t = r\sqrt{\frac{N-2}{1-r^2}} \qquad \text{(Eqn. 8.1.1)}$$

N-2 = degrees of freedom r = correlation coefficient = 0,79 t = t sampling distribution α = 0,05 = level of significance

Values from the Student's t-test suggest that the results are acceptable within the 95% confidence interval ($t_{critical} = 2,021$ and $t_{obtained} = 4,108$). Figure 8.3 shows that increased porosity corresponds to increased kaolinite formation. The importance of this relationship is that it shows that clay formation is equivalent to the rate of pore formation (through leaching). There are two possible explanations for this, both supported by observations from electron microscopy. The first is that leaching does not necessarily preferentially target clay minerals, but occurs through direct solution of the feldspars at a crystallographic level. The second possible reason is that pore formation eventually results in vermiform macrovoids. Such voids give rise to very high porosities, with a free draining system present. The large diameters of these pores causes them to act as channels, preferentially draining water away from smaller solution systems. Thus, in effect, the volume of the soil system exposed to dissolution by water is decreased. The standing time for solutions to react is also very much reduced due to higher flow rates through the system and this retards the solution reactions.

8.2 Geochemistry

8.2.1 Introduction

An analysis of the geochemistry of weathered granites provides an insight into the weathering processes acting on the weathered rock and enhances our understanding of the mineralogical and chemical changes that occur throughout the weathered profile and that affect the engineering behaviour of the material. Accordingly, major element analysis was conducted on most of the weathered granite samples.

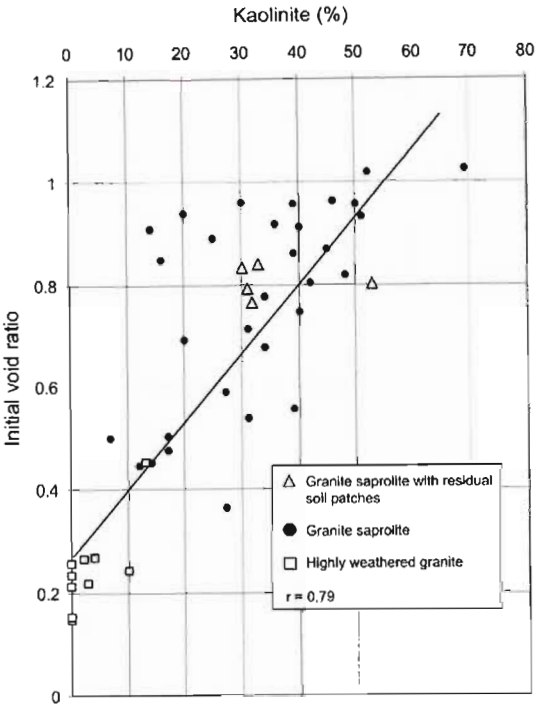

Figure 8.3. Increase in clay (kaolinite) with increasing initial void ratio suggesting that solution effects do not preferentially target the kaolinite at the expense of other minerals.

8.2.2 Equipment and Techniques

After appropriate splitting, crushing and milling, each sample of weathered granite was analysed for Si, Ti, Al, Fe, Mn, Mg, Ca, Na, K, P and Cr. The samples were initially dried at 110°C and roasted at 1000°C. Two grams of the roasted sample was weighed off with 8g of 12:22 flux (35.29 % lithium tetraborate and 64.71% lithium metaborate) and fused at 1050°C to form a glass bead. The fused beads were analysed with a Philips PW1480 wavelength sequential X-ray spectrometer containing Rh/Sc side window tube.

8.2.3 Technique of major elemental analysis

The interpretation of the geochemistry of weathering profiles is often based on a reference frame which formulates a comparison of the element concentrations (in weight %) in the soils to those of the parent rock, the so-called immobile element approach (Goldich, 1938 and Kronberg *et al.*, 1987). In this manner the absolute amounts of element removal or addition are usually based on comparisons with an element (usually Ti or Al) assumed to be immobile during weathering (Middelburg *et al.*, 1988).

However, as pointed out by Gardner (1980), and confirmed by this study, the assumption of Ti and Al immobility is questionable. Alternatively, it has been shown by Millot and Bonifas (1955), that the isovolumetric technique can be very useful when assessing element mobility throughout the weathered profile. The isovolumetric technique allows for the identification of element mobility within empirically defined reaction progress diagrams that can be explained by certain stochiometric equations. The reaction progress diagrams were first introduced by Helgeson *et al.* (1969) and are essentially plots of element volumetric concentration (weight % multiplied by dry density) against dry density. In this way the relationship of the element mobility with weathering (and hence a change in density) can be identified. Certain conditions apply, including the assumption that no deposition has occurred from outside the weathered profile and no volume change (expansion or compression) has taken place. As Middelburg *et al.* (1988) state, the assumption of constant volume is unequivocal and SEM and petrographic investigations (Chapters 6 and 7) have shown this to be essentially true for the granite saprolite and highly weathered granite bedrock at Injaka Dam.

8.2.4 Results of elemental analysis

The weight based concentration data and sample dry densities are presented for the various weathering grades in Tables 8.5 to 8.7. The empirical reaction progress diagrams are shown in Figures 8.4a to 8.4h. These diagrams exhibit similar trends to those presented by Irfan (1996). Distinct trends in the weathering of the granite can be observed from these diagrams with the early stages of weathering characterised by a rapid removal of CaO and Na_2O from the weathered profile, whilst K_2O gradually declines until a dry density of 1600 $kg.m^{-3}$ is reached. This relationship can be explained by the preferential weathering of plagioclase in comparison with the potash feldspars. Middelburg *et al.* (1988) have shown plagioclase to alter three times faster than the potash feldspars. The decrease in CaO and Na_2O to zero signifies the completion of plagioclase weathering at around 1400 $kg.m^{-3}$. The acceleration in the loss of K_2O from 1600 $kg.m^{-3}$ is due to the increase in the rate of weathering of the K-feldspars, although significantly, the decrease never reaches zero as microcline is still present even within the granite saprolite with residual soil patches (Chapter 7 and Section 8.1.5).

Table 8.5. Major element analyses (weight %) from XRF determinations for granite saprolite with residual soil patches.

Sample	SiO_2	TiO_2	Al_2O_3	Fe_2O_3	FeO*	MnO	MgO	CaO	Na_2O	K_2O	P_2O_5	Cr_2O_3	H_2O^+	CO_2	S	Total	H_2O^-
RF 12	56,82	0,58	22,20	6,94	0,10	0,04	0,31	0,09	0,04	1,87	0,04	0,04	9,45	1,42	0,001	99,78	1,08
RF 17	63,83	0,49	20,82	3,37	0,19	0,03	0,36	0,09	0,07	2,67	0,04	0,02	7,14	0,24	0,001	99,29	0,96
LF 1	69,99	0,24	17,45	2,22	0,40	0,02	0,24	0,09	0,04	3,17	0,02	0,04	5,62	0,41	0,001	99,88	0,09
LF 7	69,63	0,12	18,64	1,22	0,15	0,02	0,14	0,09	0,05	3,48	0,02	0,04	5,79	0,35	0,001	99,67	0,44
LF 18	66,53	0,44	19,71	2,39	0,40	0,02	0,59	0,10	0	2,93	0,03	0,01	5,90	0,14	0,001	99,19	0,43
Average	65,36	0,37	19,76	3,23	0,25	0,03	0,33	0,09	0,04	2,82	0,03	0,03	6,78	0,51	0,001		0,60

* determined through analysis

Table 8.6. Major element analyses (weight %) from XRF determinations for granite saprolite.

Sample	SiO_2	TiO_2	Al_2O_3	Fe_2O_3	FeO*	MnO	MgO	CaO	Na_2O	K_2O	P_2O_5	Cr_2O_3	H_2O^+	CO_2	S	Total	H_2O^-
RF 10	69,50	0,26	17,72	2,03	0,19	0,03	0,35	0,16	1,46	3,35	0,02	0,02	4,18	0,10	0,001	99,38	0,05
RF 9	68,55	0,25	18,09	1,95	0,14	0,03	0,40	0,15	1,77	3,07	0,02	0,02	4,35	0,08	0,001	98,84	0,43
RF 8	64,45	0,61	18,09	5,27	0,19	0,05	0,74	0,36	0,64	2,50	0,04	0,03	6,68	0,17	0,001	99,8	0,05
RF 7	69,18	0,30	16,10	2,35	0,10	0,04	0,60	0,56	4,56	2,87	0,04	0,02	1,87	0,05	0,001	98,49	0,56
RF 6	63,96	0,35	20,92	3,08	0,15	0,02	0,33	0,08	0	2,03	0,03	0,02	8,17	0,65	0,001	99,8	1,07
RF 5	73,70	0,07	15,49	0,76	0,20	0,02	0,27	0,12	0,04	5,57	0	0	3,50	0,05	0,001	99,76	0,30
RF 4	68,51	0,30	18,75	2,25	0,10	0,04	0,38	0,12	0,60	2,98	0,03	0	5,82	0,06	0,001	99,92	0,62
RF 3	73,36	0,18	15,08	1,07	0,20	0,03	0,27	0,22	2,70	4,75	0,02	0	1,85	0,05	0,001	99,73	0,22
RF 18	66,35	0,47	19,23	2,88	0,19	0,03	0,47	0,18	0,61	3,02	0,02	0,02	5,88	0,08	0,001	99,42	0,76
RF 19	72,04	0,17	16,02	1,32	0,10	0,02	0,26	0,22	3,02	3,54	0,02	0,02	2,34	0,05	0,001	98,97	0,29
LF 2	64,43	0,48	20,08	4,03	0,20	0,02	0,21	0,24	0,05	2,53	0,07	0,04	7,28	0,24	0,001	99,84	0,67
LF 3	67,87	0,27	18,89	2,19	0,10	0,02	0,15	0,10	0,06	4,17	0,04	0,04	5,81	0,13	0,001	99,75	0,51
LF 4	68,29	0,37	17,71	2,64	0,30	0,04	0,38	0,10	0,16	4,99	0,06	0,04	4,74	0,05	0,001	99,74	0,07
LF 5	68,96	0,39	17,17	2,70	0,20	0,04	0,44	0,14	0,72	4,63	0,06	0,04	4,28	0,05	0,001	99,77	0,48
LF 6	64,01	0,73	18,80	5,60	0,20	0,07	0,84	0,11	0,18	2,21	0,11	0,04	6,99	0,05	0,001	99,84	0,97
LF 8	68,96	0,21	18,67	1,75	0,30	0,02	0,32	0,11	0,04	3,91	0,02	0,04	5,33	0,13	0,001	99,75	0,31
LF 9	69,26	0,24	17,72	1,45	0,10	0,02	0,13	0,13	0,10	6,64	0,03	0,04	3,85	0,09	0,001	99,70	0,07
LF 10	63,61	0,73	19,81	5,23	0,20	0,04	0,48	0,08	0,04	2,14	0,08	0,04	7,30	0,06	0,001	99,77	0,19
LF 11	68,67	0,37	17,46	2,97	0,29	0,05	0,39	0,10	0,28	4,47	0,06	0,04	4,71	0,05	0,001	99,77	0,48
LF 12	64,52	0,89	17,49	6,42	1,11	0,07	0,69	0,20	0,28	1,34	0,12	0,04	6,58	0,05	0,001	99,75	0,42
LF 13	67,23	0,44	16,77	3,10	0,28	0,06	0,69	0,24	2,47	3,72	0,06	0,04	3,29	0,07	0,001	98,42	0,28
LF 19	69,65	0,19	18,64	1,20	0,30	0,01	0,36	0,10	0	2,44	0,01	0	6,10	0,12	0,001	99,13	0,28
LF 20	67,93	0,31	18,96	2,45	0,20	0,02	0,27	0,09	0	2,76	0,03	0	6,55	0,07	0,001	99,64	0,42
LF 21	67,27	0,34	18,65	2,49	0,15	0,01	0,18	0,10	0	4,03	0,04	0	5,85	0,05	0,001	99,12	0,47
LF 22	68,82	0,23	17,68	1,64	0,10	0,02	0,14	0,09	0	4,61	0,02	0	5,17	0,06	0,001	99,60	0,36
LF 24	69,26	0,21	17,75	1,67	0,20	0,02	0,23	0,10	0,01	4,07	0,02	0	5,60	0,09	0,001	99,25	0,40
LF 25	68,66	0,42	15,63	5,92	0,10	0,03	0,48	0,16	0,19	2,27	0,10	0,03	5,80	0,16	0,001	99,95	0,79
LF 26	74,16	0,13	15,53	0,98	0,10	0,03	0,26	0,16	1,25	4,40	0,02	0,01	2,15	0,05	0,001	99,18	0,16
LF 27	70,98	0,25	16,31	1,02	0,2	0,03	0,42	0,22	2,45	4,41	0,03	0,01	2,20	0,05	0,001	98,54	0,27
Average	68,60	0,34	17,66	2,70	0,21	0,03	0,39	0,19	0,95	3,46	0,04	0,02	5,0	0,1	0,001	99,471	0,87

* determined through analysis

Table 8.7. Major element analyses (weight %) from XRF determinations for highly weathered granite.

Sample	SiO_2	TiO_2	Al_2O_3	Fe_2O_3	FeO*	MnO	MgO	CaO	Na_2O	K_2O	P_2O_5	Cr_2O_3	H_2O^+	CO_2	S	Total	H_2O^-
RF 2	78,23	0,08	12,21			0,1	0,02	0,19	2,83	4,4	0,02	0,01				99,67	
RF 1	72,42	0,16	16,22			0,03	0,06	0,09	1,33	4,55	0,02	0,01				99,95	
RF 13	74,42	0,10	14,45	0,90	0,1	0,02	0,19	0,34	3,58	4,13	0,02	0,02	0,86	0,05	0,001	99,05	0,05
RF 14	74,83	0,17	13,37	1,44		0,03	0,40	0,31	2,97	4,73	0,01					99,42	0,28
RF 15	71,8	0,22	15,41	1,81	0,19	0,05	0,64	0,62	4,51	2,33	0,03	0,02	1,45	0,05	0,001	99,08	0,05
RF 16	77,23	0,1	11,92	0,72		0,1	0,27	0,37	3,2	4,61	0,02	0,01				99,32	0,11
RF 22	75,99	0,10	13,11			0,02	0,18	0,51	3,87	3,80	0,02	0,02				99,11	0,24
RF 23	74,65	0,10	14,16			0,02	0,15	0,90	4,33	3,88	0,04	0,02				99,50	0,18
RF 24	74,69	0,10	14,07			0,02	0,2	0,61	3,96	3,99	0,02	0,02				99,29	0,29
RF 25	71,86	0,22	15,38			0,03	0,45	0,37	4,24	4,33	0,03	0,02				99,59	0,44
Average	74,61	0,14	14,03			0,26	0,43	3,48	4,08	0,02	0,02	1,2				99,40	0,21

* determined through analysis

The characteristic curved relationship of Fe_2O_3 is similar to that described by Gardner *et al.*(1978). A gradual loss is experienced at the onset of weathering, with progressive weathering causing a steady increase as dry density reduces. TiO_2 exhibits a similar relationship but with a scatter of results. The relationship shows that the mobilisation of Ti is more active in the advanced weathering stages. Al_2O_3 shows a clear trend decreasing with decreasing dry density. These two observations substantiate the findings by Gardner (1980) that mobilisation of Al and Ti during weathering may be more common than is generally assumed. SiO_2 decreases linearly in all cases with the least amount of scatter. The relationship of MgO is slightly more complex. In the less weathered granite, the bulk of the element is located in biotite which alters rapidly during progressive weathering. Thus one would expect a constant decrease in MgO with decreasing dry density. However, the formation of illite and secondary micas during weathering counteracts this loss. This accounts for the characteristic curved relationship and is supported by XRD results.

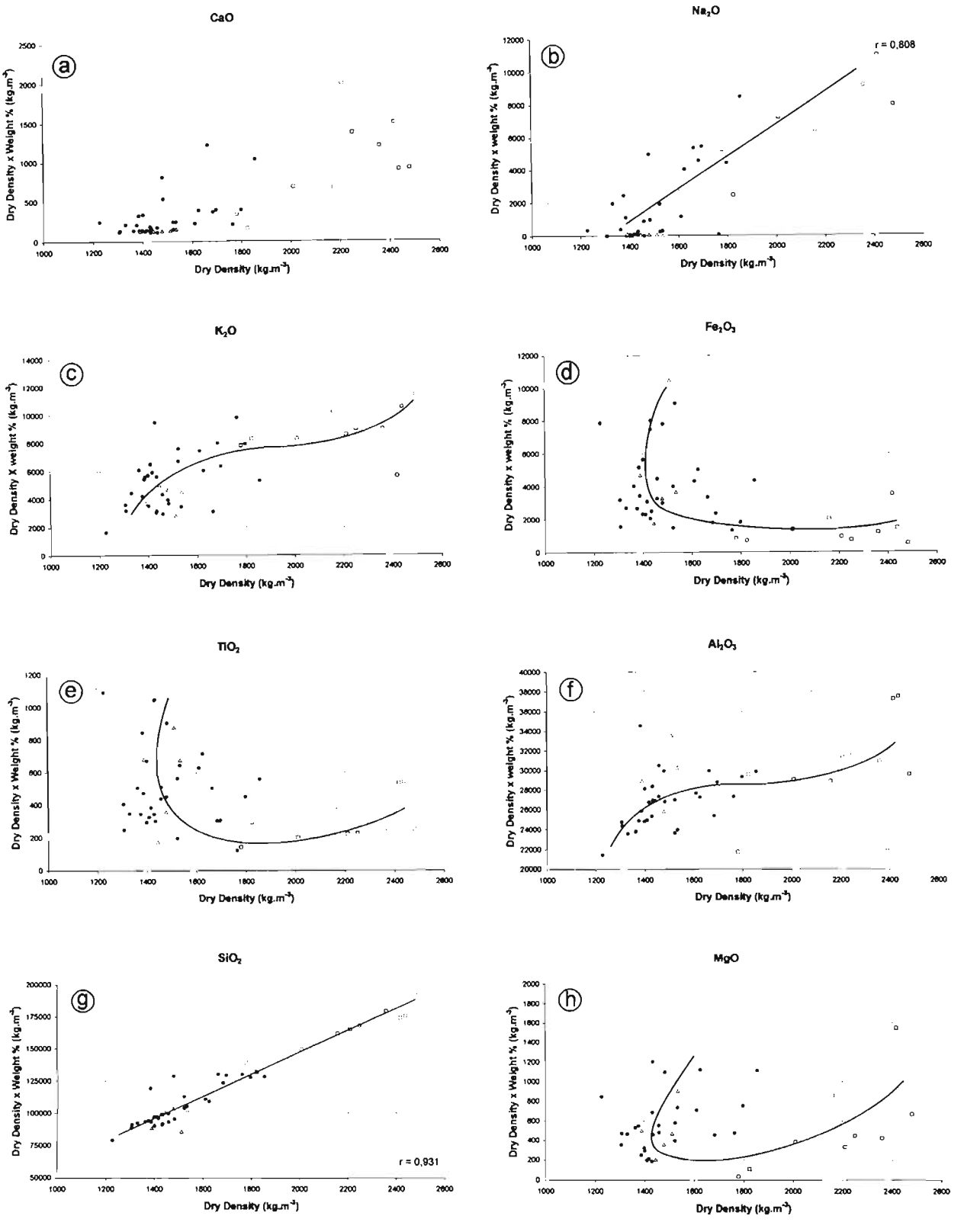

Figures 8.4a to h. Variation of volumetric concentration of CaO, Na2O, K2O, Fe2O3, TiO2, Al2O3, SiO2 and MgO with dry density. □ = Highly weathered granite, • = granite saprolite and △ = granite saprolite with residual soil patches.

9. WEATHERING INDICES

9.1 Introduction

Chapters 6 to 8 have demonstrated how the changes in microfabric of the chemically weathered granite saprolite at Injaka Dam are conceptually reflected in the geochemical and mineralogical trends or signatures of the material. The corollary to this is that the degree of weathering (and its implied changes to the physical and engineering behaviour of the weathered material) can be scaled quantitatively according to these mineralogical and geochemical changes. This can be achieved by the use of chemical and mineralogical weathering indices. According to Aydin and Duzgoren-Aydin (2002) over 30 such chemical weathering indices have been proposed. Many were not originally designed for engineering geological purposes but have subsequently become popular in the last ten years due to their successful application, particularly on the weathering of basalts and granites as shown by Irfan (1996), Tugrul and Gurpinar (1997), Arel and Tugrul (2001), Gupta and Rao (2001), Ng *et al.* (2001) and Kim and Park (2003).

9.2 Chemical weathering indices

The role of chemical weathering indices is essentially to quantify the degree of depletion of mobile components relative to immobile components during weathering (Harnois, 1988). These indices can then be applied to standard weathering grades of material set up by specific weathering classifications systems which in turn are correlated to engineering behaviour. For the successful application of chemical weathering indices four important factors should be noted :

1. Only those elements which have consistent geochemical behaviour during weathering should be used. There is some discrepancy in the literature with regard to the consistency of certain elements, particularly Al and Ti (Gardner, 1980), but generally Ca, Na, Mg, K, Si and Fe can be considered to assess weathering trends. This study has included results using Al and Ti.
2. The indices should be independent of the degree of oxidation of the weathered material.
3. Only those chemical elements commonly reported in analyses should be utilised. This means that such indices can be calculated and routinely applied from standard analyses.
4. Chemical indices should be relatively easy to use and simple to apply.

Furthermore, Duzgoren-Aydin *et al.* (2002) have shown that the behaviour of different chemical elements is complex due to the redistribution and type of the weather products and they concluded that chemical weathering indices should be selected according to site specific behaviour.

Several chemical weathering indices have been proposed and refined since the inception of Reiche's (1943), Weathering Potential Index (WPI - Eqn. 9.2.1). These indices range from a ratio of many variables to simple binomial ratios. The common elemental oxides repeatedly used in many of the indices include K_2O, Na_2O, CaO, MgO, Al_2O_3, SiO_2, Fe_2O_3, FeO, TiO_2 and H_2O^+. These have been selected because of their respective mobility or resistance to leaching. Na, Ca, Mg and Si can be considered to be leached during the weathering of granite, although the behaviour of silica is often irregular and the total proportion lost is ordinarily very small (Parker, 1970). Al and Ti can be considered to remain essentially within the weathering system (although some loss does occur with increased weathering), whilst Fe and K exhibit more complicated behaviour dependent upon the redox conditions and chemistry of ambient fluids, respectively. H_2O^+ can be defined as the amount of water within the internal structure of minerals (hydroxyl water) and it increases with increasing weathering (increasing clay formation).

The selected chemical indices shown in Table 9.1 have been applied to the weathered granite at Injaka Dam site to assess its degree of weathering and to attempt to relate these indices to the density of the material which in turn has bearing on its engineering performance. All of these indices were derived using molecular weight percentages. It can be seen from Table 9.1 that a decrease in WPI reflects a loss in the mobile cations from the weathering system, and similarly a decreasing Product Index (PI - Eqn. 9.2.2) suggests a decreasing silica content which occurs with the onset of weathering. The Silica-Alumina Ratio (Eqn. 9.2.3) formulated by Ruxton (1968) provides a measure of the total element loss (he assumed silica loss to equate to total element loss) as a ratio of the alumina content. He considered the ratio of SiO_2 to Al_2O_3 to indicate the degree of weathering and found this to be applicable to free draining, acidic weathering environments in humid climates on acidic rocks. The Parker Index (W_p - Eqn. 9.2.4) derived by Parker (1970) is based upon the proportions of the major alkaline metals and their bond strength with oxygen used as a weighting factor. Gupta and Rao (2001) considered this index to be applicable to acid, intermediate and basic rocks where hydrolysis is the main process of silicate weathering. The Vogt Ratio (VR - Eqn. 9.2.5) derived by Vogt (1927) and advocated by Roaldset (1972) attempted (incorrectly) to determine the ratio of immobile to mobile cations, but assumed that potassium remained stable within the weathering system. Vogel (1975) modified Reiche's WPI in his assessment of the weathering of acid metavolcanics whereby the H_2O^+ and oxidation state of iron were omitted from the original WPI equation to form the Modified Weathering Potential Index (MWPI - Eqn. 9.2.6). Nesbitt and Young (1982), understanding that feldspars are the most abundant reactive minerals in the earth's upper crust, realised that calcium, sodium and potassium are generally removed from the feldspars during weathering by aggressive soil solutions. They proposed that during weathering the proportion of alumina to alkalis would typically increase in the weathered product and that a good measure of the degree of weathering could be obtained by the Chemical Index of Alteration (CIA - Eqn. 9.2.7). Harnois (1988) in his discussion suggesting that

Table 9.1. Summary of chemical weathering indices used to measure weathering changes for weathered granite at Injaka Dam.

Chemical Weathering Index	Formula	Reference	Equation	Weathering grade applied in past studies
Weathering potential index (WPI)	$WPI = \frac{(CaO + Na_2O + MgO + K_2O - H_2O^+) \cdot 100}{(SiO_2 + Al_2O_3 + Fe_2O_3 + FeO + TiO_2 + CaO + MgO + Na_2O + K_2O)}$	Reiche (1943)	9.2.1	I-VI?
Product index (PI)	$PI = \frac{(SiO_2 \cdot 100)}{(SiO_2 + TiO_2 + Fe_2O_3 + FeO + Al_2O_3)}$	Reiche (1943)	9.2.2	I-VI?
Silica-Alumina Ratio	$Silica - Alumina\ Ratio \quad \frac{SiO_2}{Al_2O_3}$	Ruxton (1968)	9.2.3	I-VI?
Parker Index (W_p)	$W_p = [\frac{2Na_2O}{0.35} + \frac{MgO}{0.9} + \frac{2K_2O}{0.25} + \frac{CaO}{0.7}] \cdot 100$	Parker (1970)	9.2.4	I-VI
Vogt Ratio (VR)	$VR \quad \frac{Al_2O_3 + K_2O}{MgO + CaO + Na_2O}$	Vogt (1927) and Roaldset (1972)	9.2.5	I-VI
Modified Weathering Potential Index* (MWPI)	$MWPI \quad \frac{(Na_2O + K_2O + CaO + MgO) \cdot 100}{(Na_2O + K_2O + CaO + MgO + SiO_2 + Al_2O_3 + Fe_2O_3)}$	Vogel (1975)	9.2.6	I-III?
Chemical Index of Alteration (CIA)	$CIA \quad \frac{Al_2O_3 \cdot 100}{Al_2O_3 + Cao + Na_2O + K_2O}$	Nesbitt and Young (1982)	9.2.7	I-VI?
Chemical Index of Weathering (CIW)	$CIW = \frac{Al_2O_3 + K_2O}{Al_2O_3 + CaO + Na_2O} \times 100$	Harnois (1988)	9.2.8	I-VI
Ignition (H_2O^+) loss	H_2O^+	Sueoka et al. (1985), Jayawardena (1993)	9.2.9	I-VI
Si-Ti Index	$\frac{\frac{SiO_2}{TiO_2}}{\frac{SiO_2}{TiO_2} - \frac{SiO_2}{Al_2O_3} \cdot \frac{Al_2O_3}{TiO_2}}$	Jayawardena and Izawa (1994)	9.2.10	I-VI
Mobiles Index	$I_{mob} = \frac{(K_2O + Na_2O + CaO)\ FRESH\ ROCK - (K_2O + Na_2O + CaO)\ WEATHERED\ ROCK}{(K_2O + Na_2O + CaO)\ FRESH\ ROCK}$	Irfan (1996)	9.2.11	I-V

potassium cations, whilst been leached during weathering can in fact be adsorbed on other clays in the weathered profile through ion exchange, and may consequently disrupt geochemical trends of K^+. He therefore proposed the Chemical Index of Weathering (CIW - Eqn. 9.2.8), devoid of K_2O, as an improved measure of degree of weathering to that of the WPI, W_p VR, MWPI and CIA. The Ignition Loss Index or H_2O^+ as proposed by Sueoka *et al.* (1985) and used by Jayawardena (1993) represents the amount of crystalline water within the weathered material. An increasing H_2O^+ (Eqn. 9.2.9) content is caused by hydration and clay formation during weathering. Jayawardena and Izawa (1994) determined through their analyses of metamorphic rocks in Sri Lanka that possible relationships exist between Al_2O_3, SiO_2 and TiO_2 and proposed the silica-titania index for chemical weathering (Eqn. 9.2.10). Irfan (1996) in his comprehensive review of weathered granite in Hong Kong proposed the Mobiles Index (I_{mob} - Eqn 9.2.11) which compared the different behaviour of "mobile" and "immobile" elements during weathering using the fresh rock as a comparative component for the index derivative.

The applicability of the various weathering indices to different material types and weathering conditions has long been a source of debate. Parker (1970) stated that the Silica-Alumina Ratio was restricted as to its use because the amount of sesquioxides must remain approximately constant during weathering and there must preferably be no formation of smectites or vermiculites as initial weathering products. Harnois (1988), maintained that the use of K_2O as a mobile component in the CIA, WPI and MWPI limits their application to soils in which potassium has been leached as potassium, through its high exchange capacity can be adsorbed onto other clays in the weathering profile, thus masking its mobility. The Vogt Ratio uses K_2O as an immobile component which contradicts the evidence that potassium is commonly leached. The common point made by all of these authors is that for chemical weathering indices to be effective, an understanding of the geochemical composition and nature of geochemical processes and trends of the particular material of interest is required for the successful application of any weathering index.

Table 9.2 provides a summary of the above-mentioned chemical weathering index values obtained for samples from each sample traverse. From this table it can be seen that a relationship exists between the weathering indices, density and grade of weathering (Figures 9.1a to k). Density has been chosen as the comparative index property because the petrographic and SEM studies have shown that weathering effects manifest themselves most significantly through a change in the material porosity, and consequently density. Chapters 10, 12, 13 and 14 also discuss the significance of this basic index property and how it can be used as an index to the engineering behaviour of the weathered granite, particularly with regard to consolidation characteristics. In general, the values of WPI, PI, Si-Al, W_p and MWPI decrease as the weathering grade or density increases. This is in accordance with findings from Jayawardena and Izawa (1994) and Gupta and Rao (2001). Decreasing values of WPI, MWPI and W_p indicate decreasing mobile cations and increasing

Table 9.2. Summary of chemical weathering indices for Traverses 1-6.

SAMPLE	DEPTH (m)	DENSITY ($kg.m^{-3}$)	WPI	PI	Si-Al	W_p	VR	MWPI	CIA	CIW	H_2O^+	I_{mob}	Si-Ti
Traverse 1													
RF 12*	1	1511	-39,77	77,80	4,34	17,33	23,91	2,41	90,78	98,98	9,45	0,80	70,58
RF 10	3,5	1330	-11,38	85,74	6,66	43,28	5,97	5,00	73,72	86,81	4,18	0,45	78,76
RF 9	4,9	1375	-11,92	85,42	6,43	43,87	5,10	5,25	73,55	85,04	4,35	0,43	78,26
RF 8	5,7	1482	-22,84	82,93	6,05	30,09	5,81	4,58	80,39	91,38	6,68	0,61	76,08
RF 7	6,6	1855	1,71	86,62	7,29	69,48	1,91	8,87	58,07	65,40	1,87	-0,02	79,91
RF 2#	8,2	1779	6,34	91,51	10,87	63,99	3,36	6,34	55,57	70,95		0,14	86,01
RF 1#	9,6	1823	5,06	88,21	7,58	51,29	8,45	5,07	69,03	87,34		0,36	81,05
RF 13#	10,6	2010	4,30	89,20	8,74	69,46	2,71	7,50	56,83	69,00	0,86	0,04	83,26
RF 14#	11,8	2159	7,57	89,75	9,50	69,44	2,86	7,58	55,85	71,05		0,07	83,34
Traverse 2													
RF 6	2,5	1458	-31,87	82,17	5,19	18,35	23,59	2,36	89,93	99,31	8,17	0,79	74,42
RF 5	4,8	1763	-8,65	88,44	8,07	48,72	22,26	4,73	71,05	98,20	3,5	0,45	82,33
RF 4	6,9	1457	-19,37	84,88	6,20	32,19	10,15	3,80	80,89	93,96	5,82	0,61	77,54
RF 3	9,2	1683	0,12	88,44	8,25	66,53	3,66	7,07	60,17	75,70	1,85	0,12	82,14
RF 15#	10,9	2417	2,95	87,68	7,91	64,70	1,76	8,40	58,20	64,33	1,45	0,03	81,37
RF 16#	11,8	2480	7,48	91,29	10,99	70,33	2,56	7,49	52,18	66,76		0,04	86,00
Traverse 3													
LF 7*	1,1	1444	-19,98	85,66	6,34	30,63	37,35	3,08	82,29	98,70	5,79	0,65	78,48
LF 8	2,8	1434	-17,43	85,10	6,27	34,74	21,30	3,73	80,59	98,60	5,33	0,61	78,00
LF 9	4,0	1429	-9,61	86,02	6,63	58,00	34,14	5,49	70,02	97,79	3,85	0,33	78,78
LF 10	5,5	1431	-27,65	81,58	5,45		15,53	2,77	88,68	98,94	7,3	0,79	74,17
LF 11	6,5	1362	-14,11	85,20	6,67	41,87	13,69	4,54	76,11	96,45	4,71	0,52	78,40
LF 12	7,3	1226	-24,13	81,84	6,26	16,37	7,37	2,98	88,49	95,50	6,58	0,80	75,64
LF 13	7,7	1625	-5,81	85,27	6,80	56,87	3,33	7,18	66,30	78,85	3,29	0,25	78,39
Traverse 4													
LF 1*	0,9	1478	-19,31	85,75	6,81	28,18	24,97	3,01	82,66	98,70	5,62	0,68	79,17
LF 2	2,4	1400	-27,40	82,28	5,44	23,14	21,74	2,79	86,04	97,48	7,28	0,71	74,87
LF 3	3,8	1416	-19,66	84,72	6,10	36,64	35,47	3,68	79,76	98,54	5,81	0,58	77,36
LF 4	4,5	1523	-14,02	85,10	6,54	45,15	16,44	4,79	75,18	97,55	4,74	0,49	78,11
LF 5	5,2	1610	-11,56	85,61	6,81	47,53	8,69	5,27	72,69	92,27	4,28	0,43	78,63
LF 6	5,5	1433	-25,20	82,16	5,78	23,02	8,09	3,69	86,68	97,43	6,99	0,75	75,04
Traverse 5													
LF 18*	1,1	1535	-20,40	83,46	5,73	26,76	13,67	3,49	85,46	99,09	5,9	0,71	75,84
LF 19	2,3	1307	-21,71	85,48	6,34	21,97	19,49	2,64	86,85	99,03	6,1	0,75	78,26
LF 20	3,2	1305	-23,71	84,46	6,08	24,41	25,93	2,75	85,75	99,14	6,55	0,72	77,19
LF 21	4,0	1386	-20,09	84,53	6,12	34,98	36,13	3,59	80,41	99,03	5,85	0,60	77,19
LF 22	5,1	1409	-16,81	85,90	6,60		43,79	3,91	77,43	99,08	5,17	0,55	78,75
LF 24	5,7	1398	-18,68	85,85	6,62	35,54	28,41	3,66	79,41	98,90	5,6	0,60	78,86
LF 25	6,2	1533	-20,29	85,29	7,45	22,76	9,95	3,05	83,63	96,28	5,8	0,73	79,71
LF 26	7,2	1522	-2,94	88,43	8,10	50,01	6,76	5,19	68,60	86,87	2,15	0,38	82,12
LF 27	7,8	1797	-1,48	87,27	7,38	61,75	3,84	6,95	63,93	78,64	2,20	0,19	80,31
Traverse 6													
RF 17*	2,2	1389	-26,69	81,94	5,20	24,54	19,94	3,01	86,79	98,68	7,14	0,72	74,09
RF 18	3,8	1383	-19,61	83,69	5,85	33,02	8,93	4,15	80,70	93,53	5,88	0,60	76,09
RF 19	5,2	1696	-2,28	87,65	7,63	59,17	3,30	6,62	63,53	74,91	2,34	0,19	81,10
RF 20	6,1	1479	5,98	87,76	7,31	46,45	2,96	5,99	68,30	75,73		0,32	80,18
RF 21	6,2	1663	6,12	88,52	7,89	45,04	2,43	6,14	66,08	71,81		0,30	80,22
RF 22#	7,7	2350	7,70	90,69	9,84	69,74	2,22	7,71	53,48	64,26		0,00	84,73
RF 23#	9,1	2210	8,64	89,86	8,95	75,57	2,01	8,65	52,22	61,79		-0,14	83,56
RF 24#	9,8	2250	8,11	89,93	9,01	72,49	2,26	8,12	54,09	64,86		-0,04	83,65
RF 25#	10,2	2437	8,92	88,62	7,93	78,03	2,28	8,93	55,50	66,80		-0,08	81,41

Note: * Granite saprolite with residual soil patches # Highly weathered granite
H_2O^+ expressed as weight percentage

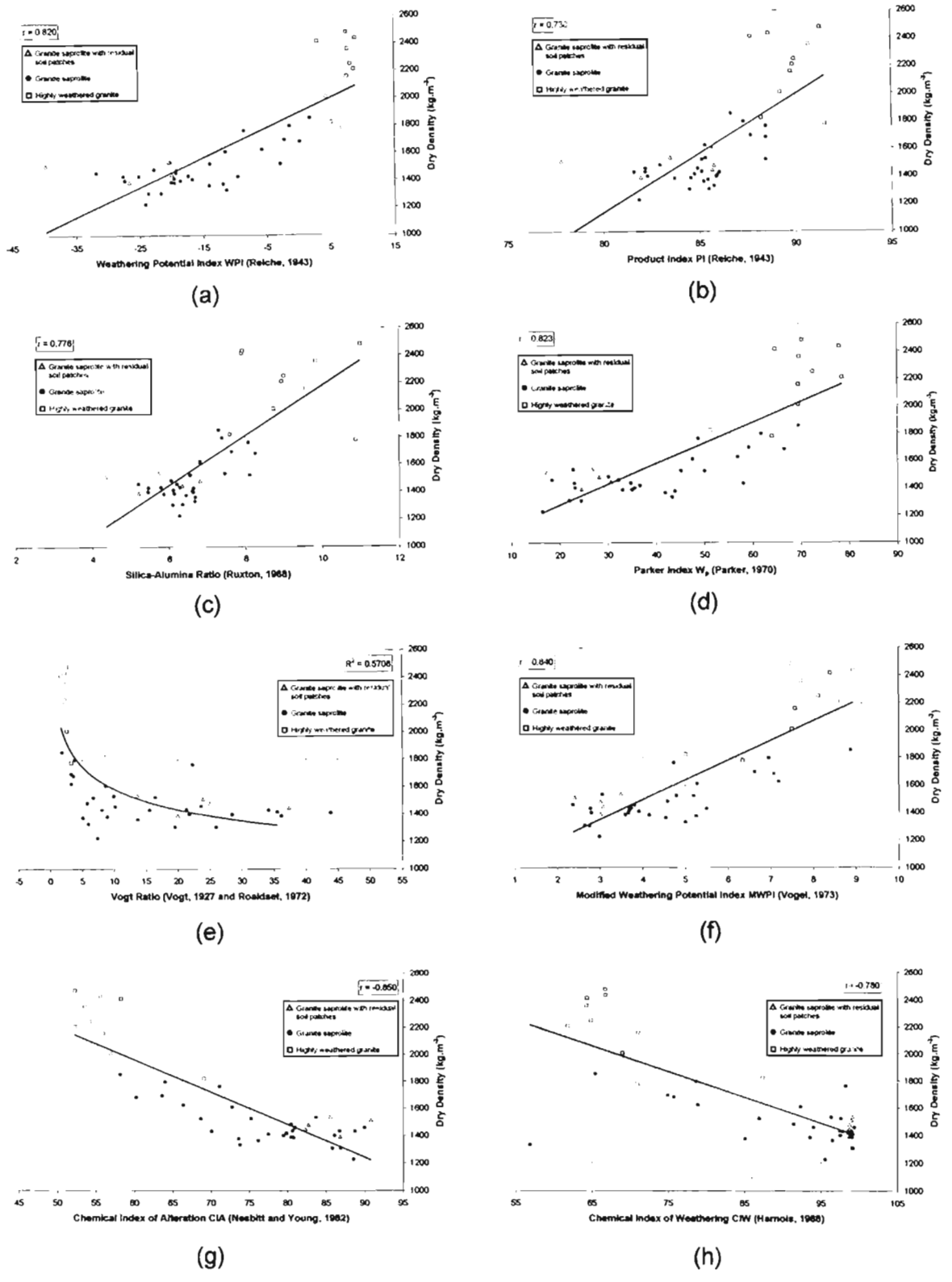

Figures 9.1a to h. Relationship of chemical weathering indices and dry density of weathered granite.

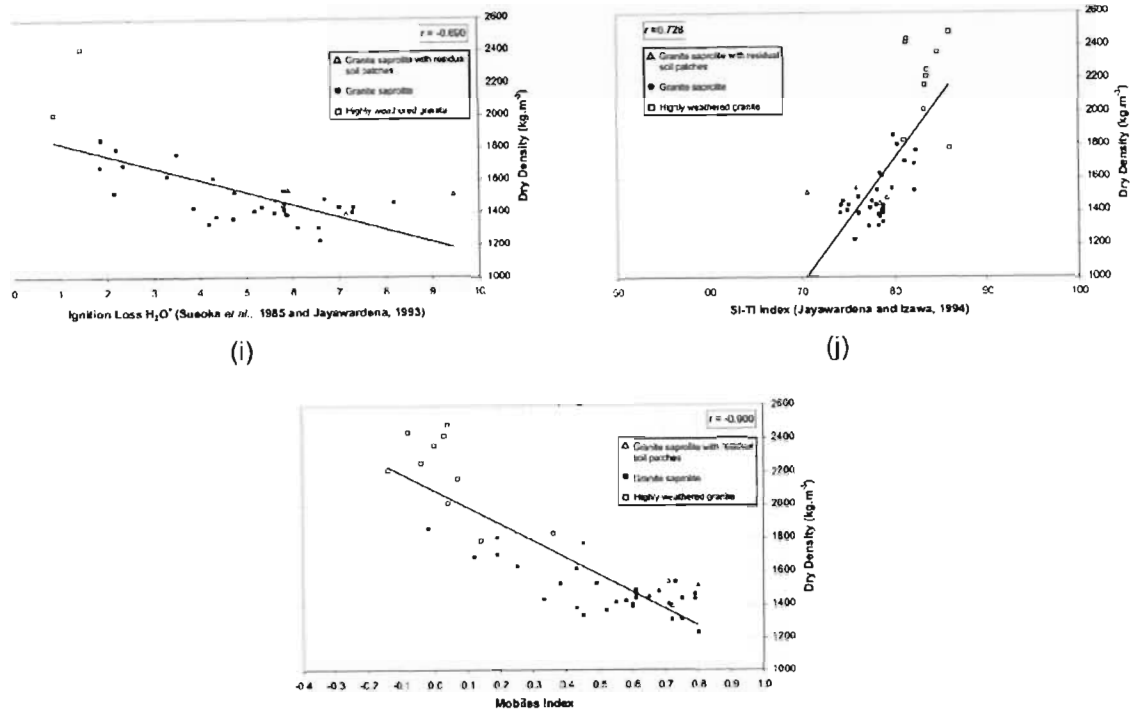

Figure 9.1i to k (continued). Relationship of chemical weathering indices and dry density of weathered granite.

hydroxyl water with increasing weathering. Decreasing PI, Si-Al and Si-Ti values are indicative of a decreasing silica content. It can be seen that in all graphic relationships that there is a sharp decrease in the weathering indices from the highly weathered granite to granite saprolite state and this confirms the field observations of the abrupt change between the weathered rock and saprolite as shown in Chapters 4 and 5. Alternatively, CIA, CIW, H_2O^+ and I_{mob} show a continuous increase with increasing degree of weathering. This can also be attributed to the loss of mobile cations and alteration of the crystal structure - hence the increase in hydroxyl water.

When the relationship between dry density and weathering index value is plotted for the granite saprolite, acceptable correlations can be observed for all weathering indices (Figures 9.1a to 9.1k) with the exception of VR. In order to validate these correlations, the r value was tested for significance using the Student's t-Test and the results from this assessment show that all the correlations are significant at the 95% confidence limit (Table 9.3). The poor correlation shown by VR is due to the incorrect use of K_2O as an immobile component for the determination of VR. Findings presented in Chapters 7 and 8 have proven that potassium is extensively leached from the weathering system at Injaka Dam.

Although an acceptable correlation was obtained using the Si-Al index value, it should also be noted that it is subject to a number of restrictions as to its reliability (Parker, 1970). The sesquioxides content must remain approximately constant during weathering, and there must preferably be no formation of smectite or vermiculite as initial weathering products. Mineralogical analyses (Chapter 8) have shown that some smectite formation can occur in the early stages of weathering of the granite at Injaka Dam where free-draining conditions do not occur and this should be borne in mind when assessing this index under such weathering conditions.

Table 9.3. t-Test results for correlation of weathering indices with density.

Weathering index	N	r	$t_{critical}$ $\alpha = 0,05$	$t_{obtained}$
WPI	44	0,820	2,015	9,28
PI	44	0,730	2,015	6,92
Si-Al	44	0,776	2,015	7,97
W_p	42	0,823	2,015	9,16
VR	44	-0,570	2,015	-4,50
MWPI	44	0,840	2,015	10,03
CIA	44	-0,85	2,015	-10,46
CIW	44	-0,780	2,015	-8,08
H_2O^+	36	-0,690	2,015	-5,56
Si-Ti	44	0,728	2,015	6,92
I_{mob}	44	-0,900	2,015	-13,38

The mobiles index (I_{mob}) was developed by Irfan (1996) to measure the relative removal of the mobile cations from the rock with weathering. Consequently, it serves as an index for the degree of decomposition of feldspars, particularly under highly leached conditions such as those encountered within the granite saprolite at Injaka Dam. A plot of I_{mob} against the amount of unaltered feldspar content is given in Figure 9.2 and shows a near linear relationship confirming this. Once again, the t-Test was applied to validate the results and it was found that the correlation is significant at the 95% confidence limits ($t_{obtained}$ = 18,742; $t_{critical}$ = 1,683). Irfan (1996) also demonstrated a similar relationship with his study on Hong Kong granites.

A summary of the weathering index values with respect to the weathering grade of the granite is presented in Table 9.4 which is effectively a compilation of Table 9.2. This table shows that these indices can be tentatively used to rationally classify the weathered granite according to its degree of weathering (and density). Jayawardena and Izawa (1994) were also able to demonstrate this in their study of weathered granite gneiss from Sri Lanka.

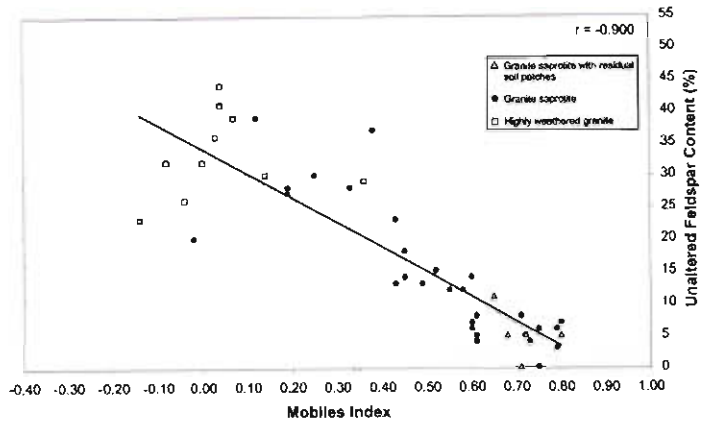

Figure 9.2. Plot of unaltered feldspar content and I_{mob}.

Table 9.4. Typical mean values of weathering indices for different weathering grades of granite.

	Mean of weathering index		
Weathering index	Highly weathered granite	Granite saprolite	Granite saprolite with residual soil
WPI	6,71	-15,46	-25,23
PI	89,67	85,11	82,92
Si-Al	9,13	6,59	5,68
W_p	68,80	39,98	25,49
VR	3,05	15,54	23,97
MWPI	7,57	4,52	3,00
CIA	56,30	76,85	85,60
CIW	68,71	91,06	98,83
H_2O^+	1,16	4,97	6,78
Si-Ti	83,44	78,20	75,63
I_{mob}	0,04	0,52	0,71

Table 9.5 details the Pearson correlation co-efficient values (r) for the various weathering indices and shows that all indices excluding the Vogt ratio show good correlation against one another. Kim and Park (2003) showed similar results in their study of weathered granites around Seoul, South Korea. Chemical weathering indices are only useful in engineering characterisation of material if they can be related to some measurable physical or mechanical properties (Irfan, 1996). It can be concluded that the application of a number of chemical weathering indices to the granite saprolite at Injaka Dam has proven that these indices can be successfully used to assess the degree of weathering of this material and can in fact provide an indication of their engineering behaviour based upon dry density relationships.

Table 9.5. Pearson correlation coefficient (r) for various weathering indices.

	PI	SI-Al	Wp	VR	MWPI	CIA	CIW	H2O+	IMOB	Si-Ti
WPI	0.931	0.890	0.959	-0.613	0.923	-0.973	-0.838	-0.998	-0.955	0.916
PI		0.942	0.857	-0.433	0.768	-0.893	-0.707	-0.902	-0.841	0.990
Si-Ti			0.811	-0.536	0.753	-0.883	-0.736	-0.914	-0.815	0.965
Wp				-0.588	0.967	-0.987	-0.841	-0.946	-0.990	0.837
VR					-0.675	0.606	0.738	0.477	0.606	-0.449
MWPI						-0.962	-0.891	-0.905	-0.983	0.757
CIA							0.876	0.966	0.989	-0.887
CIW								0.743	0.888	-0.708
H2O+									0.940	-0.899
IMOB										-0.828

9.3 Mineralogical weathering indices

In a similar manner to chemical weathering indices, mineralogical indices, using suitable ratios of specific minerals can be applied to assess the weathering of rocks. As feldspars undergo significant changes during weathering, and quartz is relatively resistant, these two minerals can be used to assess weathering trends. When microfracturing and decomposition have reduced granite to an engineering soil it consists of an interlocking granular aggregate in which a certain proportion of the grains has decomposed (Baynes and Dearman, 1978b). Lumb (1962) proposed a quantitative mineralogical measure of this degree of decomposition which he called *Xd*. This can be defined as follows :

$$Xd = \frac{(Nq - Nq_0)}{(1 - Nq_0)} \qquad \text{(Eqn. 9.3.1)}$$

where

$$Nq = \frac{(Weight\ Quartz)}{(Weight\ Quartz + Weight\ Feldspar)}\ SOIL \qquad \text{(Eqn. 9.3.2)}$$

and

$$Nq_0 = \frac{(Weight\ Quartz)}{(Weight\ Quartz + Weight\ Feldspar)}\ ORIGINAL\ ROCK \qquad \text{(Eqn. 9.3.3)}$$

It follows that if $Xd = 1$, then weathering and leaching has reduced the feldspar content to zero, and the soil can be considered to be in a state of advanced weathering. Baynes and Dearman (1978b), provided a visual impression of variations for *Xd* (Figure 9.3) using a grid of blocks representing unweathered and weathered remnant granite minerals.

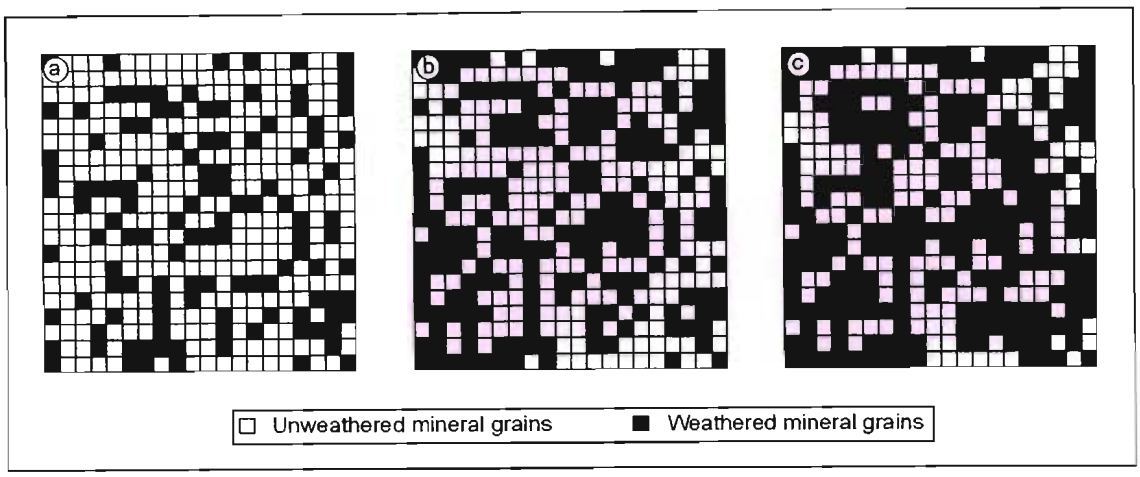

Figure 9.3. Model to illustrate the microfabric consequences of differing degrees of decomposition, (Baynes and Dearman, 1978a). White squares are representative of unweathered mineral grains whilst black squares are representative of weathered mineral grains. Assuming all decomposed mineral grains are feldspar then (a) represents 30% weathered mineral grains where $Xd = 0{,}2$; (b) represents 50% weathered mineral grains where $Xd = 0{,}5$ and (c) represents 60% weathered mineral grains where $Xd = 0{,}8$.

This shows that when Xd is less than 0,5 the microfabric consists of an interlocking granular aggregate enclosing isolated decomposed minerals (granular-framework). As Xd approaches 0,5 so the microfabric develops into a framework of original granitic minerals containing decomposition products. When Xd is greater than 0,5 the microfabric is dominated by the decomposition products which enclose remnant original granite minerals (clay-matrix microfabric). Nq has traditionally been determined by physically separating the quartz and feldspar grains from a disaggregated specimen of weathered granite. This was accomplished by Lumb (1962) using a binocular microscope. Due to the difficulty in manipulating the very fine grains only the fraction retained on the BS 100 sieve was examined by Lumb. As this method was considered to be time consuming, cumbersome and possibly inaccurate due to exclusion of material finer than that retained on BSS 100, it was decided to use the same weight ratio equation but with semi-quantitative mineralogical results derived from the XRD analyses to produce Xd_{XRD}:

$$Xd_{XRD} = \frac{(Nq - Nq_0)}{(1 - Nq_0)} \qquad \text{(Eqn. 9.3.4)}$$

where

$$Nq_{0_{XRD}} = \frac{(\%\ Quartz)}{(\%\ Quartz + \%\ Feldspar)}\ ORIGINAL\ ROCK \qquad \text{(Eqn. 9.3.5)}$$

and

$$Nq_{XRD} = \frac{(\%\ Quartz)}{(\%\ Quartz\ +\ \%\ Feldspar)}\ SOIL \qquad \text{(Eqn.9.3.6)}$$

Although the average value of Nq_0 for granite at Injaka Dam site is 0,648 (calculated from XRD analyses), this value was normalised to 0,333 such that the results from Lumb 1962 could be made comparable with results from this investigation.

Table 9.6 provides a summary of the results obtained for the samples from Traverse 1 to 6. The granite saprolite with residual soil patches shows advanced weathering with values of Xd_{XRD} ranging from 0,70 to 1,00. The granite saprolite shows a much higher variability with Xd values ranging from 0,14 to 1,00. It follows then, that the granite saprolite exhibits a broad range of weathering intensities with the high average Xd_{XRD} value suggesting that the majority of the samples are in a state of intense weathering. Xd values for the highly weathered granite bedrock are significantly lower, ranging from 0,07 to 0,65 and are indicative of a significantly lower weathering intensity.

Mineralogical indices are also only useful if they can be applied to assessing the engineering behaviour of a material. The void ratio (and density) of a soil is an important component of the soil fabric exerting significant influence on the engineering behaviour of the material. For saprolitic soils it can be expected that the void ratio increases away from the fresh rock, although local variations of this trend will occur. The relationship between void ratio and weathering can be expressed using Xd_{XRD} and is shown in Figure 9.4. There is a considerable scatter of points as is to be expected from the crudeness of the measure of Xd_{XRD} and the variations in original rock composition. Lumb (1962) constructed two simplified boundary conditions for the relationship of Xd and void ratio, expressing "full leaching" conditions and "no leaching" conditions, respectively. The "no leaching" boundary can be defined as no leaching apart from the loss of colloids removed during feldspar alteration. Alternatively, the "full leaching" boundary is defined as the complete loss of colloids with no loss of quartz. Neither of these two conditions is entirely correct and both simplify actual conditions. However, the "no leaching" boundary condition represents the early stages of weathering, whilst the "full leaching" condition can be applied to advanced stages of weathering. These boundary conditions can be defined according to the void ratio as follows:

"No leaching" condition :

$$e_0 = \frac{1 - N_k}{N_k + \dfrac{N_{qo}}{Xd.(1 - N_{qo})}} \qquad \text{(Eqn. 9.3.7)}$$

Table 9.6. Mineralogical weathering indices for sample Traverses 1-6.

Sample	Depth (m)	Dry density (kg.m^{-3})	Nq_{XRD}	$Nq_{e\,XRD}$	Xd_{XRD}	Kaolinite	Plagioclase	Microcline
Traverse 1								
RF 12*	1	1511	0,91	0,33	0,86	33	2	3
RF 10	3,5	1330	0,77	0,33	0,66	14	10	8
RF 9	4,9	1375	0,63	0,33	0,45	30	14	9
RF 8	5,7	1482	0,89	0,33	0,84	31	3	2
RF 7	6,6	1855	0,69	0,33	0,53	7	17	3
RF 2#	8,2	1779	0,63	0,33	0,45	3	17	13
RF 1#	9,6	1823	0,62	0,33	0,44	13	12	17
RF 13#	10,6	2010	0,51	0,33	0,27	4	33	11
RF 14#	11,8	2159	0,58	0,33	0,37	0	22	17
Traverse 2								
RF 6	2,5	1458	0,846	0,33	0,77	48	0	6
RF 5	4,8	1763	0,754	0,33	0,63	25	0	14
RF 4	6,9	1457	0,882	0,33	0,82	46	4	0
RF 3	9,2	1683	0,426	0,33	0,14	16	17	22
RF 15#	10,9	2417	0,379	0,33	0,07	10	27	9
RF 16#	11,8	2480	0,549	0,33	0,33	0	23	18
Traverse 3								
LF 7*	1,1	1444	0,81	0,33	0,72	30	0	11
LF 8	2,8	1434	0,81	0,33	0,71	40	0	8
LF 9	4,0	1429	0,52	0,33	0,30	34	7	21
LF 10	5,5	1431	0,93	0,33	0,90	42	0	3
LF 11	6,5	1362	0,63	0,33	0,44	50	0	15
LF 12	7,3	1226	0,88	0,33	0,82	34	2	5
LF 13	7,7	1625	0,50	0,33	0,25	27	17	13
Traverse 4								
LF 1*	0,9	1478	0,90	0,33	0,85	32	0	5
LF 2	2,4	1400	0,83	0,33	0,74	45	0	8
LF 3	3,8	1416	0,76	0,33	0,64	39	0	12
LF 4	4,5	1523	0,74	0,33	0,60	39	0	13
LF 5	5,2	1610	0,78	0,33	0,67	27	3	10
LF 6	5,5	1433	0,86	0,33	0,80	40	0	6
Traverse 5								
LF 18*	1,1	1535	1,00	0,33	1,00	31	0	0
LF 19	2,3	1307	1,00	0,33	1,00	20	0	0
LF 20	3,2	1305	0,89	0,33	0,84	39	0	5
LF 21	4,0	1386	0,60	0,33	0,40	52	0	14
LF 22	5,1	1409	0,71	0,33	0,56	51	0	12
LF 24	5,7	1398	0,90	0,33	0,84	36	0	6
LF 25	6,2	1533	0,93	0,33	0,90	31	0	4
LF 26	7,2	1522	0,51	0,33	0,26	20	25	12
LF 27	7,8	1797	0,58	0,33	0,38	17	21	7
Traverse 6								
RF 17*	2,2	1389	0,80	0,33	0,70	53	0	5
RF 18	3,8	1383	0,71	0,33	0,57	69	0	7
RF 19	5,2	1696	0,65	0,33	0,48	12	22	5
RF 20	6,1	1479	0,67	0,33	0,51	17	17	3
RF 21	6,2	1663	0,47	0,33	0,20	14	34	5
RF 22#	7,7	2350	0,63	0,33	0,45	0	23	9
RF 23#	9,1	2210	0,77	0,33	0,65	0	10	13
RF 24#	9,8	2250	0,72	0,33	0,59	0	20	6
RF 25#	10,2	2437	0,61	0,33	0,42	0	25	7

Note: * Granite saprolite with residual soil patches # Highly weathered granite

"Full leaching" condition :

$$e_0 = \frac{1 - N_{qo}}{N_{qo}} . Xd \qquad \text{(Eqn. 9.3.8)}$$

where : N_k = weight of kaolinite produced from unit weight of feldspar = 0,5.
N_{qo} = 0,333

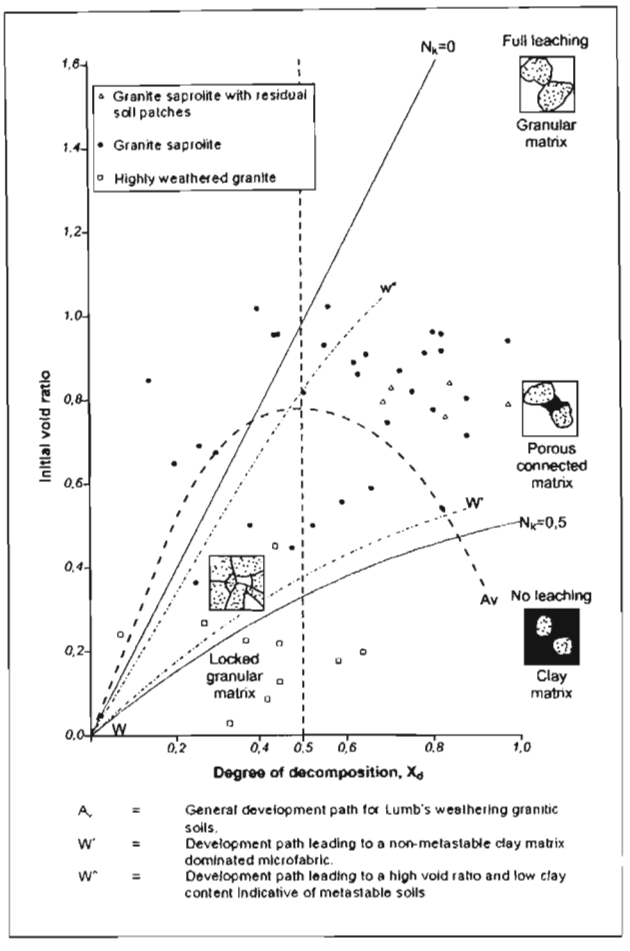

Figure 9.4. Relationship of Xd_{XRD} with initial voids ratio.

Baynes and Dearman (1978a) have shown that when $Xd < 0,5$ a granular microfabric is present with interlocking grains and minimal leaching conditions. When $Xd > 0,5$ they have shown that a variety of microfabrics can occur including poorly leached, but highly decomposed microfabric ("no leaching, clay matrix"); porous interconnected granular and clay microfabric ("porous connected matrix") and full leaching conditions resulting in a granular matrix with minimal clay ("full leaching -

granular matrix"). The plot of Lumb's average trend for weathered granites in Hong Kong (line A_v) shows an increase in porosity up to $Xd = 0,5$ where after collapse of the microfabric occurs producing a poorly leached, more dense microfabric (which approaches that of a residual soil proper). The results from this study show a much different relationship with increasing *Xd* suggesting increasing porosity and very little densification of the material at high *Xd* values. This is in agreement with the field observations which show only a poorly developed, thin veneer of material exhibiting a true residual soil structure. The difference between these observations and Lumb's results can probably be related to the much higher rainfall encountered in Hong Kong and consequently more advanced weathering of Lumb's materials. The trend shown by the weathered granites at Injaka Dam shows that the microfabric comprises predominantly of a porous connected matrix. This has been substantiated by SEM and petrographic investigations.

10. BASIC ENGINEERING PROPERTIES

10.1 Particle size distribution

10.1.1 Introduction

It is well known that the analysis of grain size of saprolitic soils is sensitive to the test procedures used (Sandroni, 1985) and is also influenced by variability in the initial grain size and mineral composition of the parent rock. This sensitivity is caused by the effects of weathering where aggregation of clay particles (as seen in the SEM investigation in Chapter 6) cause the clay to behave as a coarser fraction. Only significant disaggregation energy will allow the "correct" grading of this material. The grain size composition of the fragile and honeycombed weathered feldspars is also susceptible to the amount of applied disaggregation energy where hand crushing will reduce these grains to a clay and silt sized fraction when in fact they exist as a much coarser component *in situ*. It is reasonable to assume then that different grading characteristics can be produced for the same material depending upon the approach used. However, whilst grading interpretations are realized within the context of the test method employed, useful interpretation of this index test can be gained.

10.1.2 Evaluation of grading

Grading determination according to ASTM D 422-63 (1986) was used to analyze the particle size distribution. The procedure involved gentle crushing of the saprolite clods in a mortar with rubber covered pestle after which the sample was sieved and tested using an hydrometer. It can be assumed that modest disaggregation energy was applied to the material. Two grading procedures were carried out on each sample - one involving the use of water and the other using a dispersion agent (sodium hexametaphosphate). This was necessary to assess the dispersivity of the material (details of which are presented in a Chapter 11).

The particle size distribution curves for the various grades of weathered granite are shown in Figures 10.1a, b and c. In order to quantify the analysis of these curves, specific geometric values known as grading characteristics can be defined and used to categorise the grading. One such grading characteristic is the Uniformity co-efficient (C_u) which represents the ratio of the 60^{th} percentile to the 10th percentile on the logarithmic grading curve. The granite saprolite with residual soil patches is well-graded as shown by its high C_u values varying from 87,50 to 220,00 (Table 10.1). The clay content averages at 16% and the samples can be identified according to the Unified Soil Classification System (USCS) as clayey or silty sands (SC and SM).

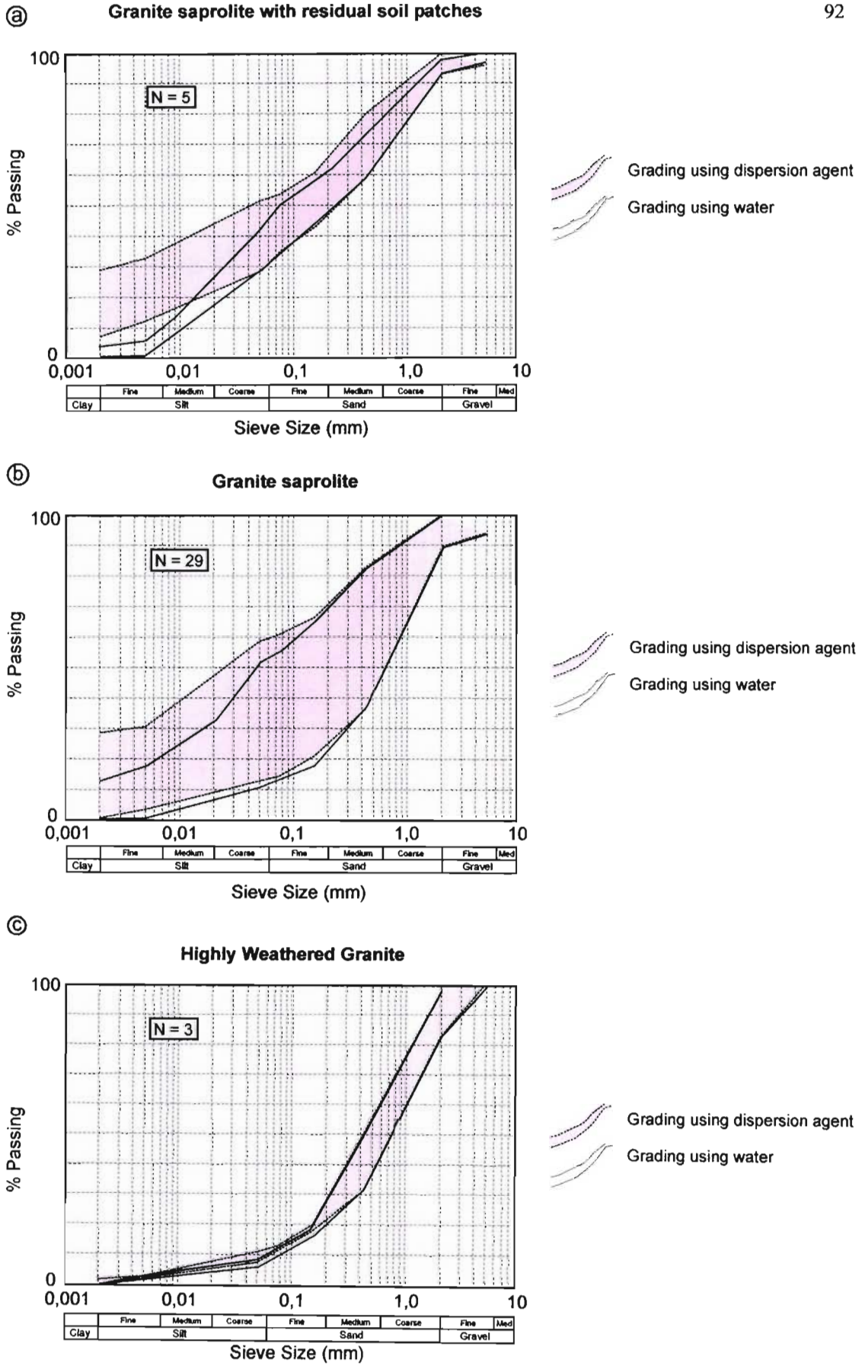

Figures 10.1a, b and c. Grading envelopes (maximum and minimum) for granite saprolite with resdiual soil patches (a), granite saprolite (b) and highly weathered granite (c) in water and dispersion agent (sodium hexametaphosphate).

Table 10.1. Particle size parameters for granite saprolite with residual soil patches.

Sample	Percent passing (mm)								Median	Mean	S_o	S_k	C_u	LL	PL	PI	LS
	4.750	2.000	0.425	0.150	0.075	0.050	0.005	0.002	(mm)	(mm)				(%)	(%)		(%)
RF 12	98	95	72	59	54	54	33	31	0,031	0,261	17,49	0	133,33	44,0	26,4	17,6	8,7
LF 1	97	93	59	45	39	31	16	11	0,220	0,461	6,547	0,390	220,00	23,3	18,7	4,6	2,0
LF 7	100	97	62	43	35	29	12	8	0,208	0,384	5,235	0,462	124,590	26,0	18,6	7,5	3,7
LF 18	100	98	69	59	52	42	20	11	0,069	0,299	8,142	1,103	87,50	31,7	25,4	6,3	3,3
RF 17	100	100	80	61	52	44	26	18	0,069	0,183	8,000	0,336	92,86	34,2	22,6	11,6	6,7

S_o = Sorting coefficient S_k = Skewness C_u = Uniformity coefficient LL = Liquid limit

PL = Plastic limit PI = Plasticity index LS = Linear shrinkage

Grading curves for the granite saprolite show the material to be very well-graded with high C_u values and a significant degree of variability (Table 10.2). The curves are all skew with a wider range of fine material than coarse with this relationship being comparable to findings by Lumb (1962). Lumb also noted a bimodal grading distribution due to the quartz fraction remaining relatively unchanged throughout weathering whilst the feldspar became progressively finer, resulting in two fractions of widely differing modes. This relationship is not easily observable from these results, this being due to the decrease in quartz grain size with increased weathering, identified in the SEM and petrographic studies for the Injaka Dam samples. The granite saprolite showed lower clay contents (average = 7%) than the granite saprolite with residual soil patches and this is indicative of a less advanced degree of weathering (Table 10.2). According to the USCS, the majority of the samples classified as silty sands (SM) with the most weathered samples classifying as clayey sands (SC).

In their geotechnical investigations carried out for Zoeknog Dam site situated some 25km north of Injaka Dam, Partridge *et al.* (1984 and 1990) also studied the engineering properties of the weathered granite encountered at this site on the Mutlumuvi River. The Zoeknog Dam site has many similarities to that of Injaka being underlain by granite-gneiss of the Nelspruit Suite Granite and situated below the African erosion surface on a 30m thick, deeply weathered, intensely leached mantle of granite saprolite. The 38m high homogeneous earth embankment dam with centrally located morning glory spillway and conduit became infamous following its breaching in January 1993, three months after completion and following the start of impoundment. Grading indicators from the saprolite at Zoeknog Dam site show somewhat higher clay contents than that identified at Injaka, averaging 15,6% although the material also classifies as silty sand (SM) and occasionally clayey sand (ML) or silt and very fine sand (ML).

Falla (1985), in his comparative synopsis of weathered crystalline rocks on various erosion surfaces in the greater Johannesburg area, has reported similar grading characteristics for granite saprolite under the African erosion surface. According to Falla (1985), the granitic rock types in this study belong to the Basement Complex (~3 100 to ~3 300 Ma) and comprise a complex suite of migmatites, gneisses, porphyritic granodiorites with felsic dykes, veins of aplite and coarse-grained

pegmatite in places. The mesocratic granite gneisses consist of hornblende (partly altered to chlorite), biotite, sodic-plagioclase, quartz and microcline with the leucocratic variety comprising abundant quartz and biotite with sodic-plagioclase altered to sericite and variable amounts of muscovite, microcline and chlorite. Part of Falla's analysis comprised an investigation of the upper 2m and 5m of the saprolite profile. His findings on the grading of the material are similar to that encountered at Injaka Dam with clay contents reported to average between 16% and 22% for the upper 2m with the lower 3m of the saprolite profile exhibiting average clay contents varying from 9% to 18% - the resultant decrease in clay with depth representative of reduced weathering as found at Injaka Dam site.

Table 10.2. Particle size parameters for granite saprolite.

Sample	Percent passing (mm)								Median	Mean	S_o	S_k	C_u	LL	PL	PI	LS
	4.750	2,000	0.425	0.150	0.075	0.050	0.005	0.002	(mm)	(mm)				(%)	(%)		(%)
RF 10	100	100	78	60	53	51	23	21	0,044	0,133	6,583	0806	100	37,1	24,6	12,6	5,3
RF 9	100	100	68	49	41	30	12	4	0,140	0,311	5,222	0,673	62,500	33,2	25,0	8,2	4,0
RF 8	100	99	68	52	47	44	20	16	0,150	0,304	0,8554	0,219	160	36,1	25,6	10,5	5,0
RF 7	100	100	48	22	14	13	4	2	0,440	0,540	2,490	0,721	22,727				
RF 6	100	100	83	67	61	61	31	29	0,021	0,116	11,63		42,86	41,2	28,5	12,7	7,0
RF 5	100	99	70	38	30	26	8	6	0,220	0,287	3,471	0,482	55,357				
RF 4	100	100	68	47	39	39	10	9	0,160	0,308	6,325	0,352	54,000	37,6	30,9	6,7	2,7
RF 3	100	93	46	25	18	18	5	4	0,460	0,595	2,739	0,695	55,00				
LF 2	99	92	61	48	38	31	13	8	0,160	0,426	6,142	0,713	133,333	34,6	25,7	8,9	3,0
LF 3	100	96	55	45	38	28	11	6	0,230	0,466	5,388	0,527	126,250	32,4	20,9	11,5	3,7
LF 4	100	98	55	41	33	24	8	2	0,300	0,470	4,726	0,403	75,756	36,6	26,0	10,6	4,0
LF 6	100	98	71	53	40	31	10	4	0,120	0,278	4,515	0,957	44,00	40,2	33,2	7,0	2,7
LF 8	94	90	61	49	43	35	20	11	0,130	0,455	9,487	0,533	192,50	36,0	26,6	9,8	4,7
LF 9	97	89	50	36	29	24	8	4	0,410	0,554	4,255	0,362	92,424	30,0	23,1	6,9	2,7
LF 10	100	99	72	60	53	44	18	8	0,065	0,255	7,454	1,065	68,085	39,9	28,2	11,7	4,7
LF 11	100	89	48	37	30	26	7	2	0,450	0,556	5,109	0,217	96,429	35,8	29,4	6,4	2,7
LF 12	100	96	59	43	33	28	8	3	0,205	0,417	4,924	0,628	70,724	42,9	33,3	9,6	4,7
LF 19	100	98	71	59	54	40	18	6	0,064	0,273	7,314	1,306	61,818	32,5	27,1	5,4	2,7
LF 20	100	99	71	58	49	40	15	6	0,008	0,266	6,876	0,894	60,000	34,0	26,7	7,3	3,0
LF 21	100	97	58	43	36	26	9	3	0,220	0,426	5,143	0,525	79,310	31,6	25,8	5,8	2,3
LF 22	100	100	73	44	34	25	9	5	0,150	0,275	3,162	1,111	40,351	23,5	19,4	4,1	2,0
LF 24	100	99	55	42	35	29	11	5	0,270	0,440	5,323	0,350	121,951	31,7	25,7	6,0	2,3
LF 25	100	98	66	51	40	37	2	2	0,130	0,341	5,606	0,820	77,143	33,6	26,3	7,3	3,0
LF 26	100	93	44	31	24	19	6	3	0,500	0,593	3,576	0,378	70,000	35,4	29,7	5,7	2,2
LF 27	99	91	37	21	15	13	4	1	0,610	0,695	2,513	0,613	39,048	24,4	19,8	4,6	1,7
RF 18	100	100	75	54	41	34	12	5	0,120	0,215	4,528	0,569	50,000	30,8	24,6	6,2	2,7
RF 19	100	99	54	30	19	17	5	2	0,340	0,505	2,860	0,856	42,500				
RF 20	100	100	65	43	30	23	6	2	0,20	0,351	2,860	0,86	38,75				
RF 21	100	100	61	37	25	19	5	2	0,27	0,407	2,86	0,86	38,10				

S_o = Sorting coefficient S_k = Skewness C_u = Uniformity coefficient LL = Liquid limit
PL = Plastic limit PI = Plasticity index LS = Linear shrinkage

The highly weathered granite at Injaka Dam shows a poor grading consisting predominantly of sand (Table 10.3). The curves are low in clay (averaging 2%) and the grading typifies the extent of the limited alteration of these samples, with many of the feldspars behaving as granular fragments.

Table 10.3. Particle size parameters for highly weathered granite.

Sample	Percent passing (mm)								Median	Mean	S_o	S_k	C_u	LL	PL	PI	LS
	4.750	2,000	0.425	0.150	0.075	0.05	0.005	0.002	(mm)	(mm)				(%)	(%)		(%)
RF 2	100	99	49	22	15	14	5	3						-	-	-	-
RF 1	99	83	32	18	13	11	3	1	0,730	0,870	2,50	0,676	25,000	-	-	-	-
RF 13	100	98	50	20	12	8	3	2	0,410	0,563	2,330	0,999	10,000	-	-	-	-

S_o = Sorting coefficient S_k = Skewness C_u = Uniformity coefficient LL = Liquid limit

PL = Plastic limit PI = Plasticity index LS = Linear shrinkage

A comparison of the XRD mineralogical results (Chapter 8) with the grading results discussed above shows that the two cannot be reconciled with regard to the fine (clay) fraction. Mineralogical determination of clay content (kaolinite) is significantly higher than that gained from mechanical grading methods. This perceived discrepancy can be explained by the fact that the disaggregation was probably not complete and by the unique texture and microfabric of the weathered granites where many clay minerals are "locked" within the partially weathered feldspars, forming an integral component of the weathered feldspar structure. Disaggregation during mechanical grading methods is not sufficient to free these clay particles. The rigorous mechanical breakdown (during milling of the XRD samples) allows the clays to be released from the feldspars, consequently resulting in higher compositional determinations. Furthermore, SEM observations in Chapter 6 have shown that the kaolinite platelets can be silt sized (between 3 and 6 μm) and consequently will not behave mechanically as a clay during hydrometer settlement measurements. Aggregation of the clay platelets is also common compounding this effect.

Another way of illustrating the textural changes that occur during weathering of granite is shown by the ternary diagram in Figure 10.2. The weathering of the primary mineral grains to finer decomposition products is shown by the increase in silt and clay contents for increasing weathering. This relationship can also be identified when comparing the sorting coefficient (S_o) with depth. The sorting co-efficient measures the square root of the ratio of the 75th percentile to the 25th percentile (from the logarithmic grading curve). The clear reduction in S_o with increasing depth (Tables 10.1, 10.2 and 10.3) shows a continual coarsening of the grain size as weathering decreases. Analysis of the grading data presented by Partridge *et al.* (1990) shows a similar trend for S_o.

10.2 Consistency limits

10.2.1 Introduction

As the science of soil mechanics was largely developed in relation to transported and often fine-grained soils found in temperate latitudes, reproducible results from some standard tests may be difficult to obtain when studying residual tropical soils. This was experienced when carrying out indicator tests on the weathered granite material. In some cases the coarser granite saprolites and highly weathered granite samples could not be tested due to their lack of plasticity.

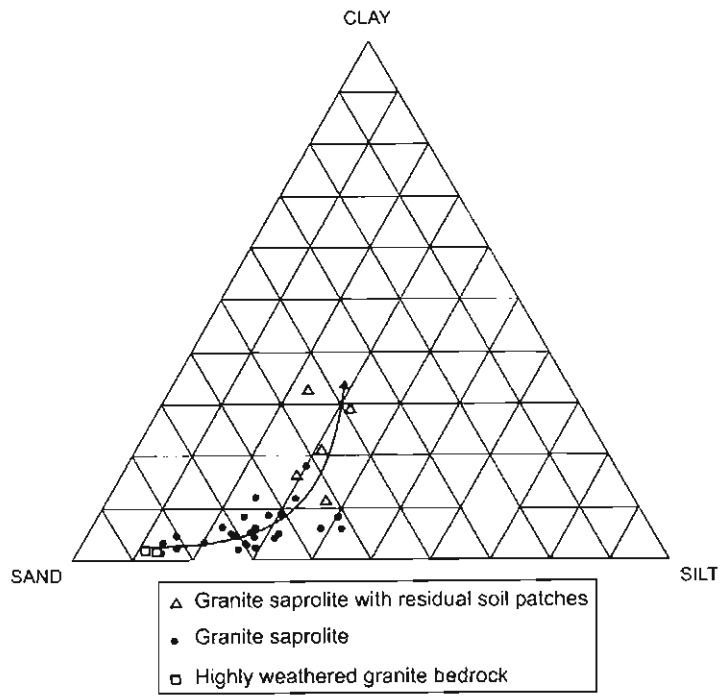

Figure 10.2. Ternary diagram of weathered granite grain size indicating direction of weathering trend.

10.2.2 Results

Standard test methods were carried out for the liquid limit and plastic limit (ASTM D4318-84, 1986), and linear shrinkage (TMH1 1996, Method A4). The results of these tests are shown in Tables 10.1 to 10.3 and Figure 10.3. According to Anon (1979), the granite saprolite with residual soil patches exhibits slightly plastic to moderately plastic behaviour with an average PI of 9,5. Similar behaviour is shown by the granite saprolite, although the average PI is slightly lower at 8,1. The studies undertaken by Partridge *et al.* (1984 and 1990) show slightly higher indicator characteristics for the material at Zoeknog Dam site where average PI was measured at 13,3%. This corresponds to the higher clay contents reported for this material. Falla's (1985) PI measurements for granite saprolite in Johannesburg are also slightly higher for the first 2m of the saprolite profile, recorded as being an average varying from 12% to 18% with the deeper profile (up to 5m below the start of the saprolite horizon) measuring between 11% and 21% - once again reflective of the higher clay contents for these materials in comparison to that encountered at Injaka Dam. No consistency limits could be obtained for the friable, highly weathered granite samples.

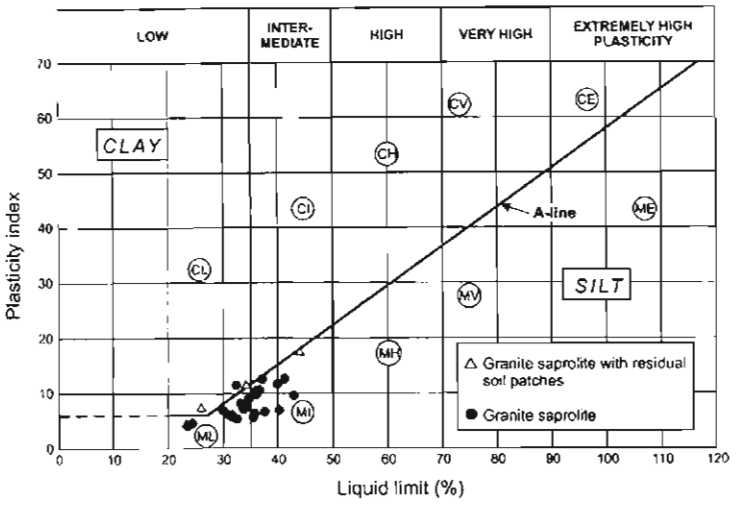

Figure 10.3. A-line plot of granite saprolite including granite saprolite with residual soil patches.

In broad terms, the plasticity index reflects the ratio of clay mineral to silt and fine sand in a soil, that is the proportion of clay minerals in the fines (Carter and Bentley, 1994). This relationship is clearly illustrated in the activity chart presented in Figure 10.4, where the plasticity index is plotted against percentage clay. Using the t-Test, the linear relationship in Figure 10.4 was validated where this test proved the correlation of r = 0,75 to be acceptable within the 95% confidence limits ($t_{critical}$ = 1,703; $t_{obtained}$ = 5,670). Consequently, it can be assumed that with increased weathering and clay formation, the plasticity of the saprolite increases.

As expected with soils containing kaolinite (which exhibits an activity between 0,3 to 0,5 in the pure form), the linear shrinkage of both the granite saprolite with residual soil patches and granite saprolite was low, between (1,7 and 8,7%) and the saprolite can be considered to exhibit low expansiveness as shown by the method developed by Van der Merwe (1964) in Figure 10.5. Findings at Zoeknog Dam site (Partridge *et al.*, 1984 and 1990) and on the Basement Complex in Johannesburg (Falla, 1985) are similar.

10.3 Density and void ratio characteristics

It is well known in basic soil mechanics applications that soil density is one of the most important parameters affecting the engineering behaviour of a soil (Lambe and Whitman, 1969 and Irfan and Dearman, 1978b). Density is the measure of the state of packing of the soil which is inherently dictated by the microfabric and mineralogy - two features which have shown important implications during the weathering process. An increase in packing is accompanied by an increase in strength, a decrease in compressibility and a decrease in permeability. Consequently, it is essential that the density of a soil is well-determined prior to relating it to other forms of engineering behaviour. With

respect to saprolitic materials, the use of density is most often in index tests directed to assess the degree of weathering and leaching.

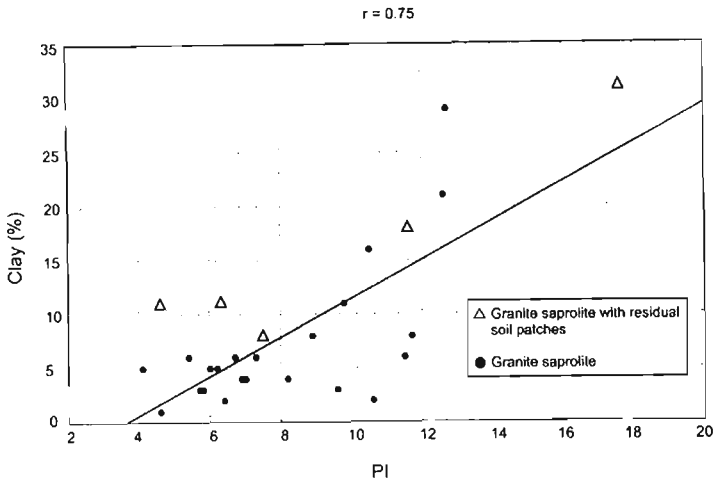

Figure 10.4. Plasticity index as a function of clay percentage (calculated from hydrometer analysis using a dispersing agent).

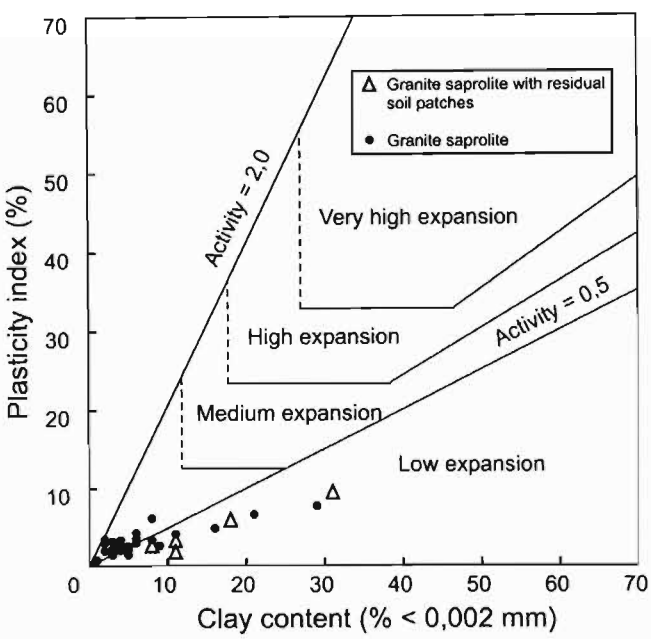

Figure 10.5. Potential expansiveness of weathered granite using the method developed by Van der Merwe (1964).

The density of the weathered granite was determined from laboratory methods (BS 1377:1975 Test 15A) and field techniques including the sand replacement (TMH1 Method A10(a), 1986) and nuclear probe methods (TMH1 A10(b), 1986). As all of the samples were extracted from the side of the foundation excavation over a period of time spanning seasonal change, the bulk densities (ρ_b) of the samples cannot be considered for analysis *per se* as these values are dependent upon the

seasonal (and consequently rainfall) conditions at the time of sampling. A comparison of dry density values (ρ_d) provides considerably more insight into understanding the nature of the weathering effects.

Laboratory density tests were conducted on undisturbed block samples, whilst the sand replacement and nuclear methods were both carried out immediately adjacent to the site from which the blocks were extracted. Results for the various test procedures are presented in Tables 10.4, 10.5 and 10.6. Results from the laboratory tests show a higher degree of scatter than the field results. In fact, correlations between the different types of testing show the sand replacement and nuclear methods to be the most complementary with high r-values obtained during data regression of the dry density values (Figure 10.6). Once again, the t-Test was employed to assess the correlations and this test found all of these results to be significant within the 95% confidence limits (Table 10.7).

These results corroborate the deductions made by Shai and Livneh (1983), that the repeatability in nuclear testing is high and justifies its practical use. However, Wates (1987) does suggest the use of the sand replacement method as the most definitive technique for determining density values of soils. The lack of precision with regard to laboratory densities can be attributed to the test utilising smaller, and thus less representative samples for analysis, in comparison to the field methods. Accordingly, density results obtained from the sand replacement tests have been used for indexing the material properties.

From Tables 10.4 to 10.5, it can be seen that a significant degree of density variability occurs, even within material of a similar weathering class. Haskins *et al.* (1998a) have mentioned a density difference of up to 15% for material from the same block sample of granite saprolite at Injaka Dam site. This characteristic has been identified throughout the literature concerning the weathering of granite (Matsuo *et al.*, 1968; Baynes and Dearman, 1978a; Irfan and Powell, 1985 and Zhao *et al.* 1994b) and can be attributed to the compositional variability of the granite parent bedrock and to differing degrees of weathering intensity which have locally variable distribution.

Table 10.4. Summary of density and void ratio results for granite saprolite with residual soil patches.

Sample	Dept	Bulk Density	Dry Density (kg.m^{-3})			e	G_s	m	S_r
	(m)	(kg.m^{-3})	Laboratory	Sand	Nuclear			(%)	(%)
RF 12	1,0	1873	1463	1511	1461	0,839	2,7	22,6	72,5
LF 1	0,9	1610	1478			0,759	2,5	5,6	19,2
LF 7	1,1	1659	1444			0,828	2,6	12,7	40,5
LF 18	1,1	1656	1516	1535	1480	0,788	2,6	15,3	52,0
RF 17	2,2	1712	1487	1389	1350	0,796	2,6	15,1	50,7

e = initial void ratio G_s = specific gravity m = natural moisture content S_r = degree of saturation

Table 10.5. Summary of density and void ratio results for granite saprolite.

Sample	Dept	Bulk Density	Dry Density (kg.m^{-3})			e	G_s	m	S_r
	(m)	(kg.m^{-3})	Laboratory	Sand	Nuclear			(%)	(%)
RF 10	3,5	1642	1369	1330	1297	0,907	2,6	15,5	44,6
RF 9	4,9	1639	1349	1375	1377	0,957	2,6	15,3	42,2
RF 8	5,7	1892	1715	1482	1492	0,539	2,6	7,9	36,7
RF 7	6,6	1998	1747	1855	1597	0,500	2,6	11,1	58,2
RF 6	2,5	1795	1469	1458	1466	0,818	2,6	18,1	59,1
RF 5	4,8	1649	1388	1763	1630	0,888	2,6	16,3	48,1
RF 4	6,9	1534	1342	1457	1434	0,960	2,6	12,5	34,3
RF 3	9,2	1694	1744	1683	1648	0,848	2,6	14,4	45,0
LF 2	2,4	1654	1419	1400	1338	0,868	2,6	12,9	39,4
LF 3	3,8	1695	1430	1416	1402	0,860	2,6	14,9	46,1
LF 4	4,5	2087	1708	1523	1297	0,556	2,6	17,5	83,8
LF 5	5,2	1989	1680	1610	1553	0,589	2,6	15,3	69,3
LF 6	5,5	1773	1399	1433	1676	0,909	2,6	22,4	65,8
LF 8	2,8	1768	1419	1434	1375	0.745	2,6	13,6	48,3
LF 9	4,0	1760	1557	1429	1419	0,676	2,6	10,7	41,3
LF 10	5,5	1835	1460	1431	1373	0,801	2,6	21	68,9
LF 11	6,5	1674	1371	1362	1337	0,955	2,6	20,5	57,5
LF 12	7,3	1826	1487	1226	1209	0,775	2,6	19,1	65,0
LF 13	7,7	2089	1927	1625	1631	0,365	2,6	4,8	34,6
LF 19	2,3	1627	1394	1307	1314	0,937	2,6	19,5	54,7
LF 20	3,2	1535	1366	1305	1319	0,955	2,6	16,9	49,5
LF 21	4,0	1591	1313	1386	1410	1,018	2,6	21,2	55,1
LF 22	5,1	1569	1373	1409	1415	0,930	2,6	14,2	40,5
LF 24	5,7	1667	1379	1398	1424	0,914	2,6	20,9	60,3
LF 25	6,2	1676	1541	1533	1539	0,713	2,6	8,7	32,3
LF 26	7,2	1689	1554	1522	1512	0,692	2,5	13,2	47,1
LF 27	7,8	1878	1756	1797	1767	0,501	2,6	6,4	33,8
RF 18	3,8	1551	1336	1383	1318	1,022	2,7	15,3	40,7
RF 19	5,2	1949	1818	1696	1515	0,447	2,6	7,2	42,4
RF 20	6,1	1722	1453	1479	1447	0,817	2,6	18,5	59,8
RF 21	6,2	1607	1394	1663	1541	0,650	2,6	15,3	62,1

e = initial void ratio G_s = specific gravity m = natural moisture content S_r = degree of saturation

Table 10.6. Summary of density and void ratio results for highly weathered granite.

Sample	Dept	Bulk Density	Dry Density (kg.m^{-3})			e	G_s	m	S_r
	(m)	(kg.m^{-3})	Laboratory	Sand	Nuclear			(%)	(%)
RF 2	8,2	2299	2191	1779		0,219	2,6	2,6	31,8
RF 1	9,6	1942	1826	1823		0,451	2,6	2,5	14,7
RF 13	10,6	2277	2080	2010		0,269	2,6	4,1	40,2
RF 14	11,8	2209	2159			0,227	2,6	2,3	26,8
RF 15	10,9	2258	2087			0,242	2,6	3,0	32,8
RF 16	11,8	2532	2480			0,034	2,6	0.3	22,9
RF 22	7,7	2392	2350			0,128	2,6	1,8	37,4
RF 23	9,1	2259	2210			0,199	2,6	2,2	29,3
RF 24	9,8	2286	2250			0,178	2,6	1,6	23,9
RF 25	10,2	2466	2437			0,087	2,6	1,2	36,4
LF 28	8,7	2256	2221			0,202	2,6	1,6	21,1

e = initial void ratio G_s = specific gravity m = natural moisture content S_r = degree of saturation

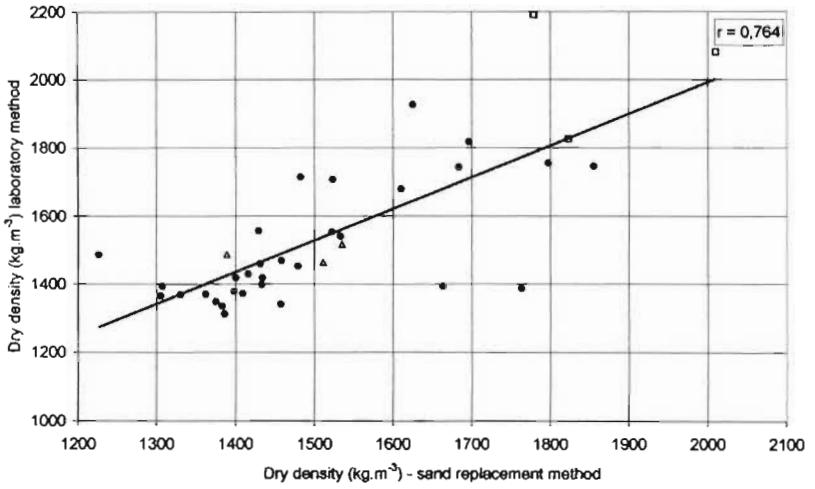

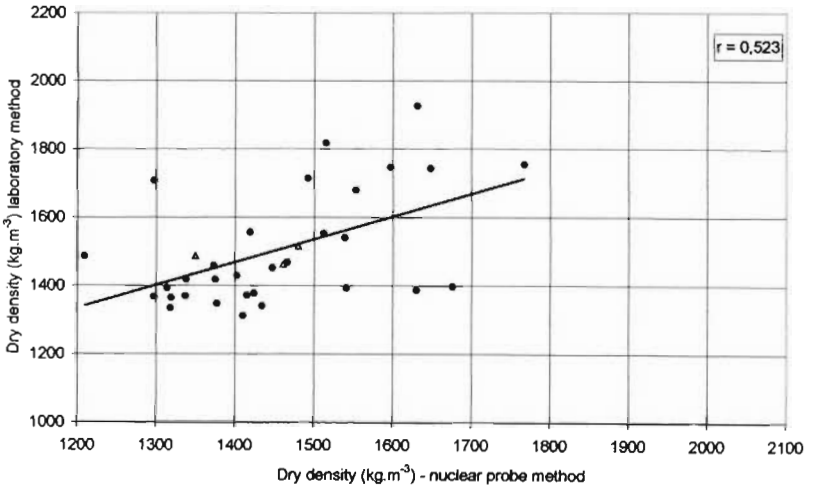

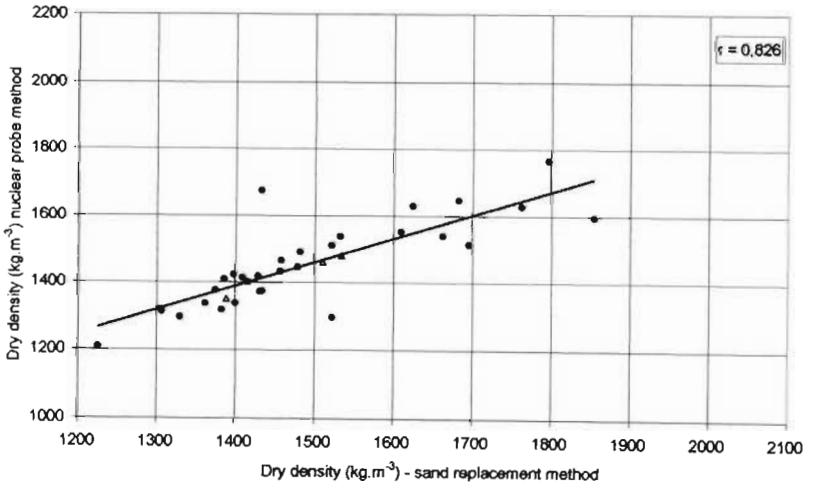

Figure 10.6. Correlations of various density measurement techniques.

Table 10.7. t-Test results for density technique correlations.

Correlation	N	r	$t_{critical}$ $\alpha = 0,05$	$t_{obtained}$
Nuclear method with sand replacement technique	35	0,826	2,042	8,418
Laboratory method with sand replacement technique	36	0,764	2,042	6,904
Laboratory method with nuclear method	35	0,523	2,042	3,525

The increase in density with a reduction in weathering and increasing depth is clearly shown in Figure 10.7. An interesting observation from this figure is the fact that the granite saprolite with residual soil patches exhibits a slightly higher or equivalent density to the granite saprolite that directly underlies it. As leaching intensifies towards the surface (confirmation of which was obtained from the SEM and geochemical investigations), the saprolite becomes increasingly metastable, where at a point, it can no longer support its own weight and collapses into a denser form. Colluvial processes (reworking) including percolating water often enhance this densification. Individual results show that the granite saprolite may exhibit ρ_d values as low as 1200 kg.m^{-3} with the higher ρ_d values in the order of 1600 kg.m^{-3}. The density of the saprolite is directly related to the intensity of leaching of the material where higher void ratios are indicative of the presence of more pronounced eluvial processes. Leaching does not occur homogeneously throughout the weathering system but instead is concentrated in areas of preferential flow thus accounting for the scatter of density data shown in Figure 10.7.

A marked increase can be observed in density between the granite saprolite and highly weathered granite bedrock. This complies with field observations which show a very abrupt change between the material types with a transition zone of approximately only 0,5-1 m (Figure 4.3). This abrupt change has also been identified in other regions (Zhao *et al.*, 1994a). The highly weathered granites show significantly higher dry densities ranging from 1826 to 2524 kg.m^{-3} with much lower moisture contents which can be attributed to their lower porosity. Figure 10.7 also shows the characteristic decrease in void ratio with depth. Scanning electron microscopy, petrography and mineralogical results show this to be a function of decreasing leaching within the weathering system, where the porosity of the feldspars, clay aggregations and intra- and inter-granular voids decrease.

At Zoeknog Dam site, tests by Partridge *et al.* (1990) showed the granite saprolite to exhibit similar dry densities to those measured at Injaka Dam. The granite saprolite at Zoeknog Dam varied from 1319 to 1741 kg.m^{-3} between a depth range of 5 to 10,5m with equivalent initial void ratios ranging from 0,520 to 0,972 and these results compare favourably to those encountered at Injaka Dam. Falla's (1985) study on granite saprolite showed dry density results varying from an average of 1354 to 1495 kg.m^{-3} for the upper 2m of the saprolite profile with equivalent average initial void ratios in the order of 0,755 to 0,972. From 3 to 5m depth in the saprolite profile he identified average dry densities between 1327 and 1511 kg.m^{-3} with corresponding average initial void ratios between

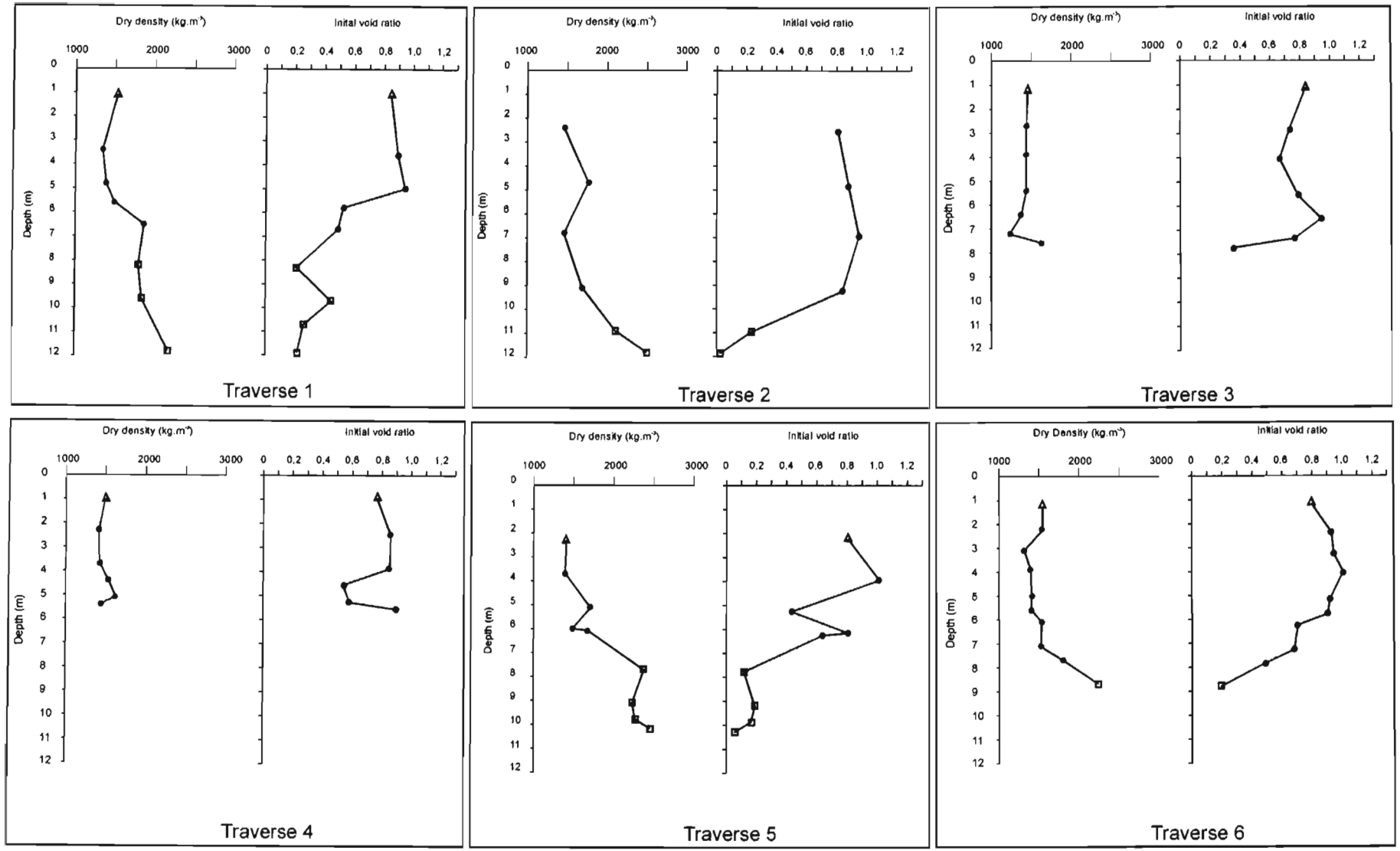

Figure 10.7. Relationship of dry density and void ratio with depth. All values of dry density are from the sand replacement method except for highly weathered granite samples, values of which were derived from laboratory results.

0,761 and 1,050. The range of these values is all well within that determined for the granite saprolite at Injaka Dam.

A further comparison of the dry density and void ratio results with similar granitic materials from Hong Kong as described by Lumb (1962) and Irfan (1988) shows that the granite saprolite at Injaka Dam exhibits higher dry densities and lower void ratios than the Hong Kong material. The weathered Hong Kong granite described by Irfan exhibits dry densities between 1200 and 1300 $kg.m^{-3}$ with initial void ratios generally above unity. This suggests a more intense leaching of the Hong Kong granite than that encountered in this investigation and may be explained by the higher rainfall experienced in Hong Kong.

10.4 Permeability

10.4.1 Introduction

The *in situ* permeability of saprolitic soils is typically high due to the aggregation of clay minerals and other microstructural features causing high porosities. These features have been observed from SEM observations in Chapter 6 and from the large discrepancy between grading parameters and mineralogical analyses. Unlike true sedimentary soils, permeability of saprolites may not necessarily correlate with the grain size of the saprolite. This was found by Lumb (1962) where permeability results were applied to various grading parameters without much success. This suggests that using the permeability of these soils as an index may be difficult. It has further been suggested by Sridharan (1988) and Costa Filho *et al.* (1989) that the results of permeability in saprolitic soils are difficult to determine and may be inconsistent due to the microfabric heterogeneity. As a consequence of these observations a suite of permeability tests were undertaken to quantify this engineering parameter of the material.

10.4.2 Permeability tests

In order to define the permeability of the granite saprolite three complementary permeability test methods were applied, including a laboratory falling head test, field falling head test and a field constant head test. The laboratory falling head test (k_{lab}) was conducted in a similar manner to that described by Head (1982), where the test was carried out in an oedometer consolidation ring with an applied vertical load of 3,18 kg. The field falling head test (k_{field}) employed the method prescribed by Lambe and Whitman (1969), and was conducted at the locality from which the block samples were cut. The test requires a standpipe to be inserted into the soil and filled with water. A check was conducted to determine the rate at which the water level drops within the standpipe. At saturation, this rate of drop is constant and the permeability of the soaked material can be determined. The equation used to determine the permeability is described as follows:

$$k_m = \frac{\pi \cdot D}{11 \cdot (t_2 - t_1)} \cdot \ln\frac{H_1}{H_2} \qquad \text{(Eqn. 10.4.1)}$$

where : k_m = mean coefficient of permeability ($cm.s^{-1}$)
D = diameter pipe (cm)
H_1 = piezometric head (cm) for time = t_1 (s)
H_2 = piezometric head for time = t_2 (s)

The field constant head test (k_{gen}) followed a similar procedure to that proposed by Anon (1968). This procedure uses a traditional mechanical apparatus, although an electronic data logging system using the same principles was developed by the author for this investigation (Figure 10.8). This comprised a computer controlled electronic level switch attached to a solenoid valve, flow meter and data logger. The general permeability of the hole (k_{gen}) was determined by augering two boreholes at the top of Traverses 4 and 5, respectively. The intention of the procedure was to correlate k_{gen} with the average value of k_{field} for each traverse. Prior to testing, washed and weighed 19 mm aggregate was carefully poured into the percussion holes up to the level required for testing. The function of the aggregate was to prevent collapse of the hole during saturation and also allowed for a check of the hole volume. The test procedure determines the permeability over the entire hole length and does not account for vertical changes in permeability. Figure 10.9 provides a summary of the test parameters with Figure 10.10 showing the conditions applying to each hole. The results are presented in Table 10.8 with average k_{field} values for the respective traverses shown for comparative purposes.

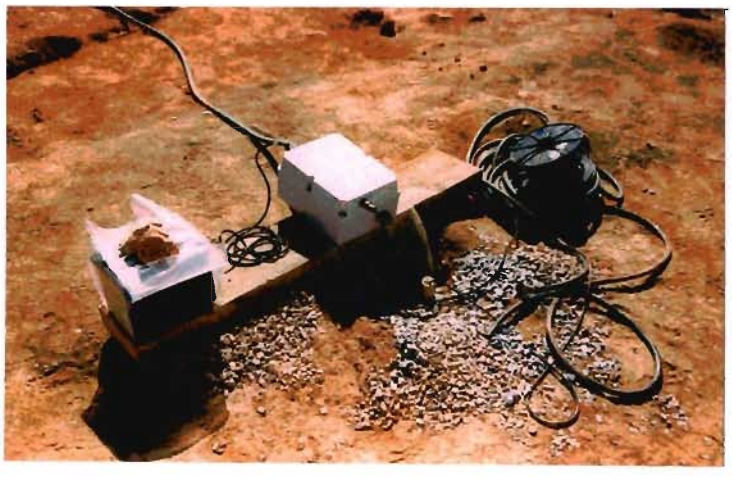

Figure 10.8. Electronic data logger well permeameter designed for testing general field permeability (k_{gen}) using principles from the well permeameter as developed by Anon (1968).

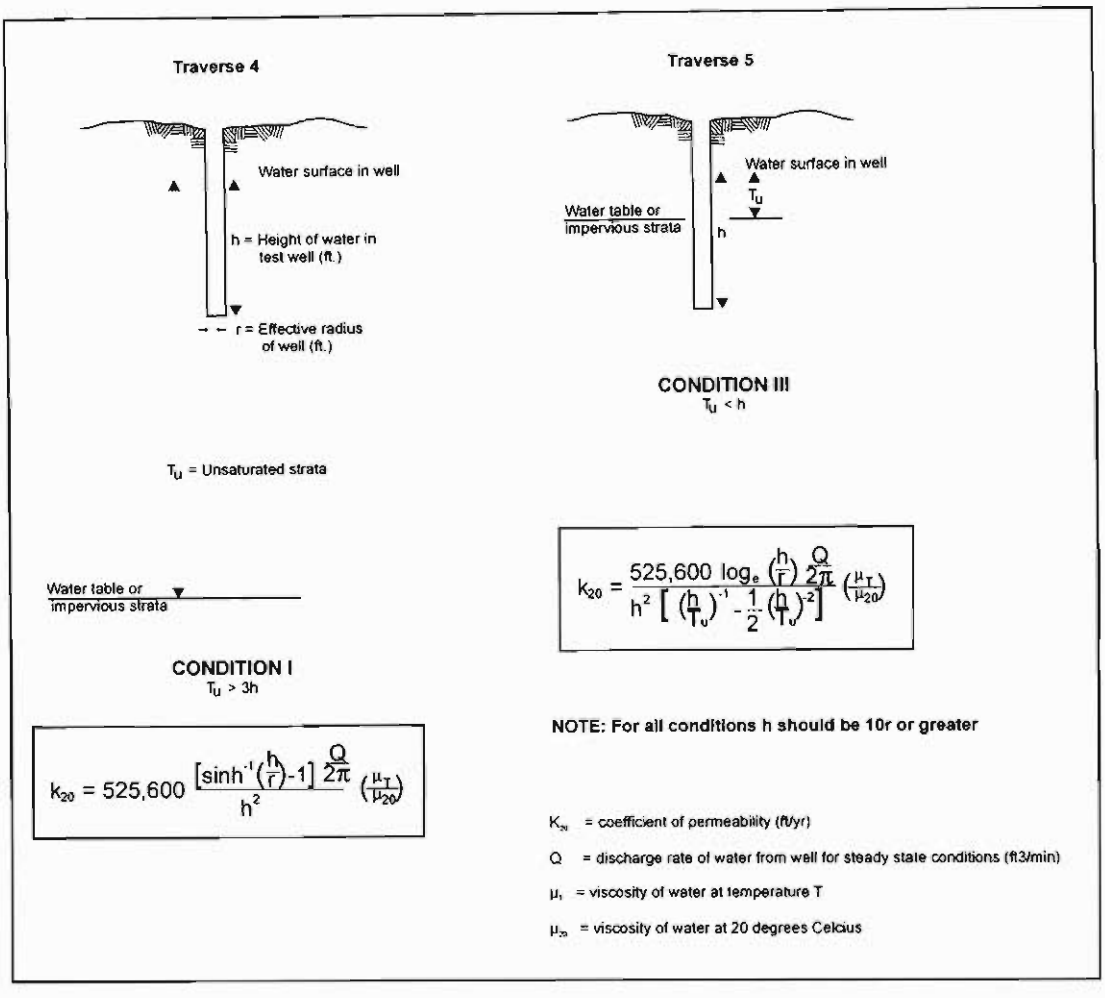

Figure 10.9. Summary of test parameters for constant head well permeameter tests.

Table 10.8. Summary of well permeameter test results.

Traverse	Drilled Depth (m)	Drilled Ø (m)	Calculated Diameter Ø (m)	T_u (m)	Q ($l.hr^{-1}$)	k_{gen} ($cm.s^{-1}$)	Average k_{field}
k_{gen} Traverse 4	8,72	0,100	0,104	28,96	47	$1,7 \times 10^{-5}$	$4,7 \times 10^{-5}$
k_{gen} Traverse 5	13,93	0,110	0,110	13,50	73	$1,8 \times 10^{-5}$	$7,9 \times 10^{-5}$

for an explanation of symbols see Figure 10.9

Plots of water volume intake against time (Figure 10.10) show that the saprolite became saturated after 25 hours. Smearing of the holes during augering may account for the slightly lower values of k_{gen} in comparison to the average k_{field} for the respective traverses. The permeability results for the field and laboratory falling head tests are presented in Tables 10.9 to 10.11.

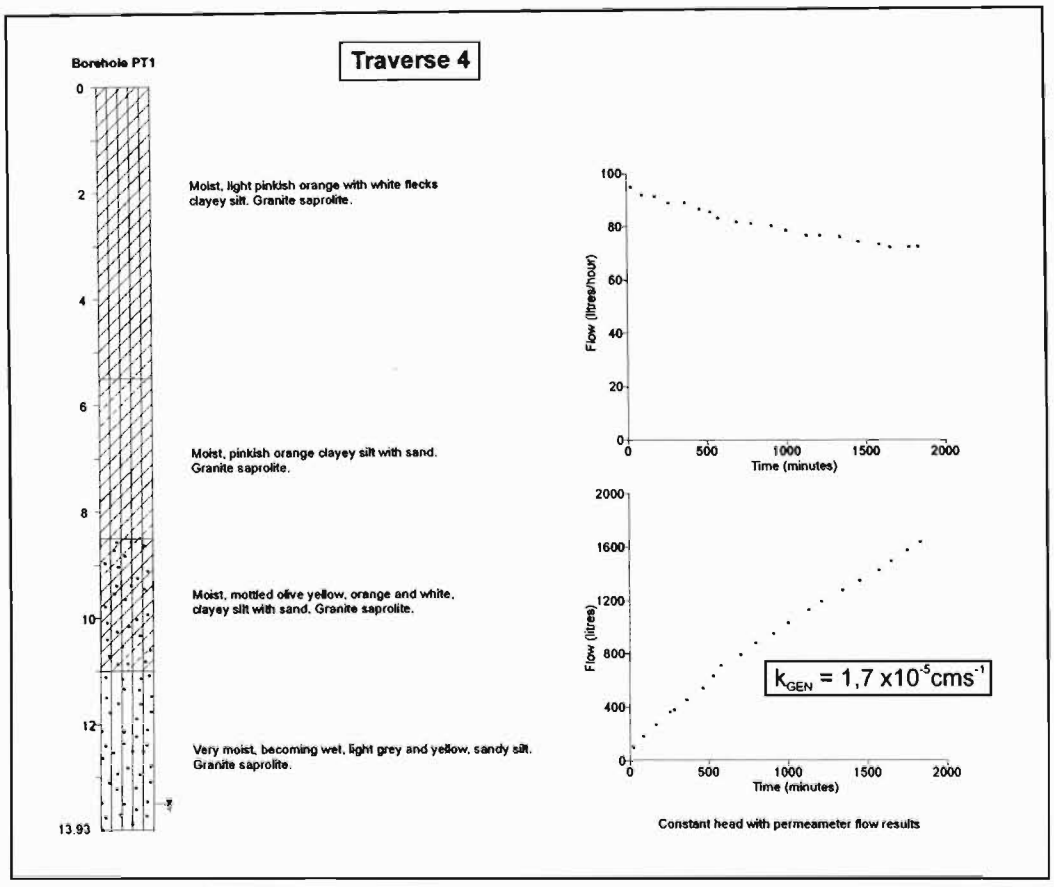

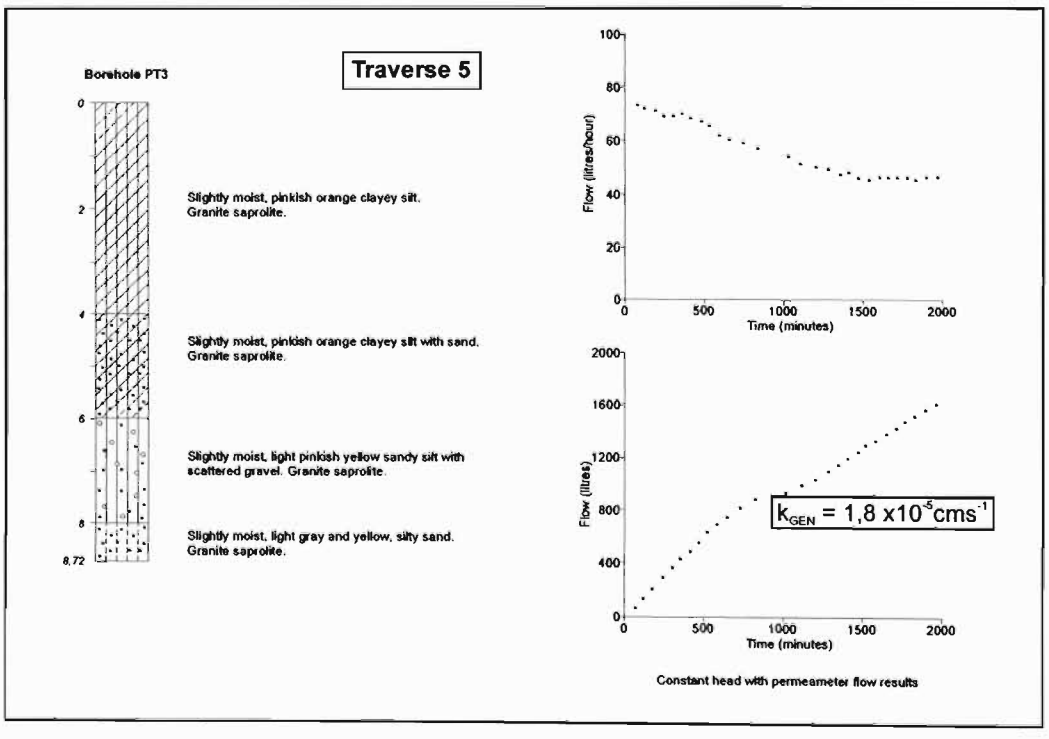

Figure 10.10. Constant head permeameter conditions for Traverses 4 and 5.

Table 10.9. Summary of permeability test results for granite saprolite with residual soil patches.

Sample	Field Falling Head Test	Laboratory Falling Head Test
	k_{field} (cm.s^{-1})	k_{lab} (cm.s^{-1})
RF 12	5,3 x 10^{-5}	6,5 x 10^{-5}
LF 7		1,2 x 10^{-4}
LF 18	1,3 x 10^{-4}	5,0 x 10^{-4}
RF 17	6,8 x 10^{-5}	4,1 x 10^{-5}

Table 10.10. Summary of test results for granite saprolite.

Sample	Field Falling Head Test	Laboratory Falling Head Test
	k_{field} (cm.s^{-1})	k_{lab} (cm.s^{-1})
RF 10	1,2 x 10^{-4}	8,4 x 10^{-5}
RF 9	9,6 x 10^{-5}	2,0 x 10^{-4}
RF 8	4,7 x 10^{-5}	9,3 x 10^{-5}
RF 7	5,1 x 10^{-5}	2,9 x 10^{-4}
RF 6	6,3 x 10^{-5}	8,1 x 10^{-4}
RF 5	1,4 x 10^{-4}	3,1 x 10^{-5}
RF 4	1,4 x 10^{-4}	1,7 x 10^{-4}
RF 3	8,3 x 10^{-5}	7,9 x 10^{-5}
LF 2	4,5 x 10^{-5}	1,9 x 10^{-4}
LF 3	4,6 x 10^{-5}	1,1 x 10^{-4}
LF 4	5,3 x 10^{-5}	1,2 x 10^{-4}
LF 5	6,1 x 10^{-5}	2,3 x 10^{-4}
LF 6	3,1 x 10^{-5}	3,3 x 10^{-4}
LF 8	1,4 x 10^{-4}	9,5 x 10^{-4}
LF 9	8,0 x 10^{-5}	
LF 10	3,8 x 10^{-5}	1,6 x 10^{-4}
LF 11	5,3 x 10^{-5}	6,2 x 10^{-4}
LF 12	1,0 x 10^{-4}	
LF 13	6,1 x 10^{-5}	2,3 x 10^{-5}
LF 19	3,1 x 10^{-5}	3,1 x 10^{-5}
LF 20	8,6 x 10^{-5}	8,6 x 10^{-4}
LF 21	8,0 x 10^{-5}	8,0 x 10^{-4}
LF 22	4,0 x 10^{-5}	4,0 x 10^{-4}
LF 24	8,7 x 10^{-5}	8,7 x 10^{-5}
LF 25	4,7 x 10^{-5}	4,7 x 10^{-5}
LF 26	5,6 x 10^{-5}	5,6 x 10^{-5}
LF 27	3,2 x 10^{-5}	3,2 x 10^{-5}
RF 18	1,3 x 10^{-5}	5,5 x 10^{-7}
RF 19	5,5 x 10^{-5}	7,3 x 10^{-5}
RF 20	8,3 x 10^{-5}	1,7 x 10^{-4}
RF 21	1,0 x 10^{-5}	

Table 10.11. Summary of permeability results for highly weathered granite.

Sample	Field Falling Head Test	Laboratory Falling Head Test
	k_{field} (cm.s^{-1})	k_{lab} (cm.s^{-1})
RF 2	7,0 x 10^{-5}	
RF 1	3,9 x 10^{-5}	2,1 x 10^{-4}
RF 15	2,2 x 10^{-5}	4,6 x 10^{-4}

Figure 10.11 shows the relationship of k_{field} and k_{lab} values with depth. A striking feature of the values is the high degree of scatter, particularly with regard to k_{lab}. In fact, k_{lab} values may not be considered useful as the standard deviation for these values exceeds the mean of these values (Table 10.12). This highlights the difficulties with regard to laboratory testing of saprolitic soils where sample disturbance during trimming and flow bypass along sample-oedometer ring contacts is difficult to control. Furthermore, samples used for the determination of k_{lab} are small and consequently not likely to homogenise the effects of the inherent parent material variability.

Table 10.12. Statistical summary of permeability results.

Test Type	Permeability ($cm.s^{-1}$)			
	Mean	Median	N	Standard deviation
Laboratory Falling Head Test	$1,6 \times 10^{-4}$	$9,3 \times 10^{-5}$	33	$2,0 \times 10^{-4}$
Field Falling Head Test	$6,5 \times 10^{-5}$	$5,6 \times 10^{-5}$	38	$3,5 \times 10^{-5}$
Field Constant Head Test	$1,8 \times 10^{-5}$	———	2	———

With the exception of Traverse 1, all granite saprolite with residual soil patches samples showed lower k_{field} values than the granite saprolite. This relationship agrees with the more dense nature of the granite saprolite with residual soil patches and supports the notion of densification by collapse once a critical, advanced state of weathering has been achieved. It is difficult to comment on the relationship of the granite saprolite permeability with respect to depth as no particular correlation is expressed in Figure 10.11. However, values for k_{field} prove the saprolite to have a medium permeability (1×10^{-5} to $1,4 \times 10^{-4}$ $cm.s^{-1}$), suggesting that the material is free draining and indicating good seepage conditions - a factor which is discussed in Chapter 14. A comparison of k_{field} with void ratio (Figure 10.12) shows a general increase in permeability with increasing void ratio. This implies that increased leaching leads to a more free-draining material, as would be expected.

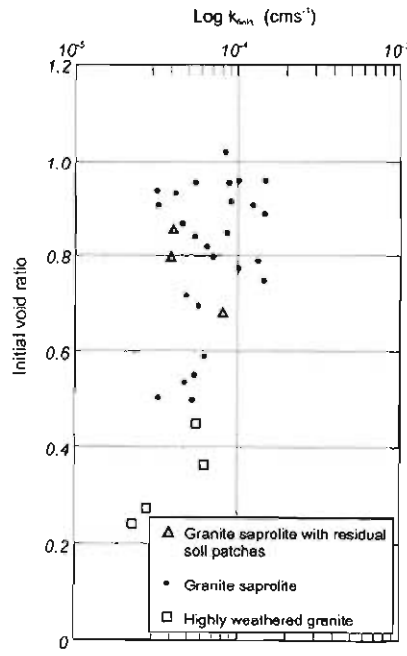

Figure 10.12. Effect of void ratio on permeability.

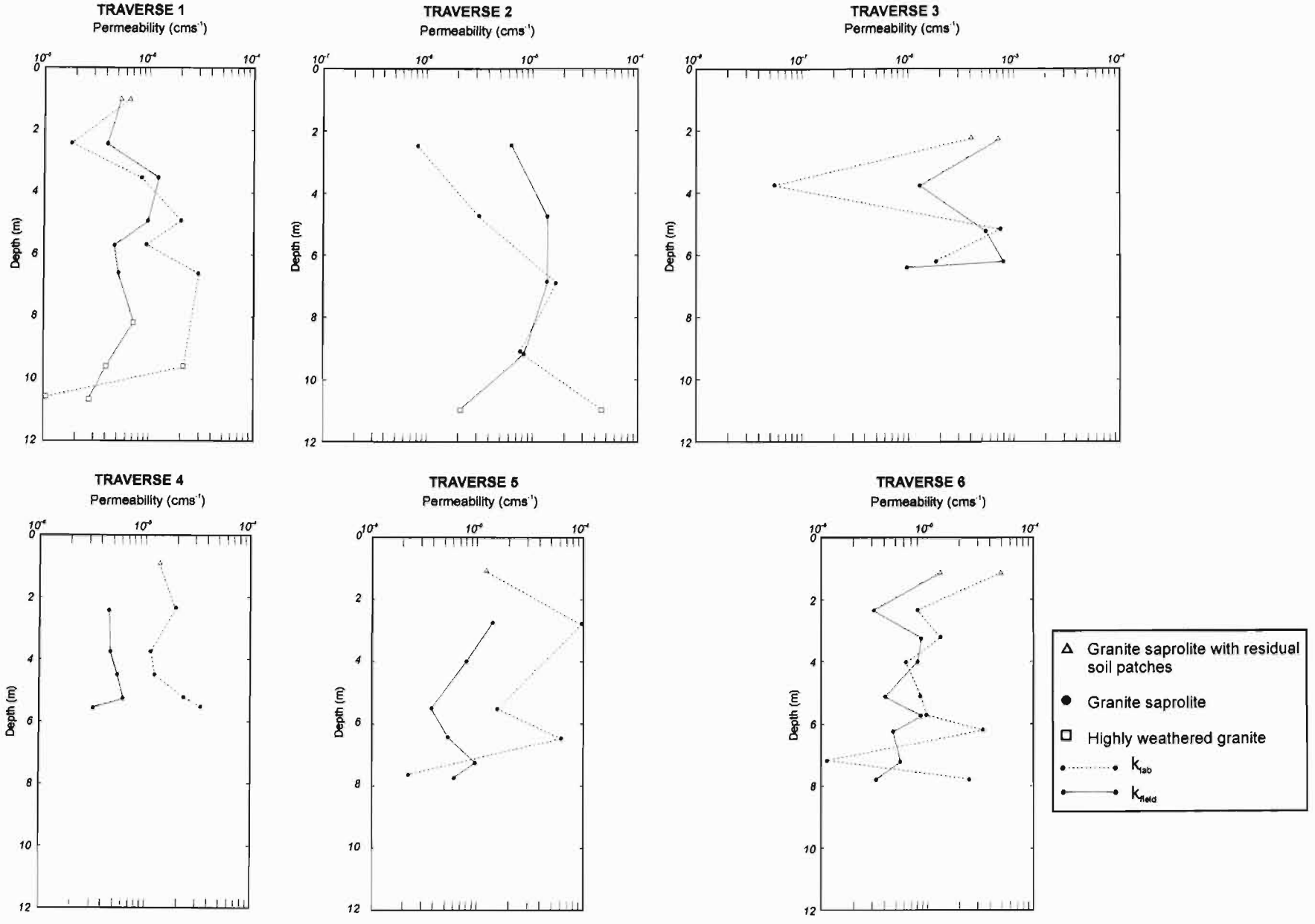

Figure 10.11. Relationship of permeability with depth for Traverses 1 to 6.

The poor correlation of grading (clay content) with permeability is shown in Figure 10.13a, where the lack of any relationship suggests that permeability is not only a function of grading but is affected by the texture and structure of the material. This supports the findings of Lumb (1962) and Sridharan (1988). With this in mind, a comparison of *Xd* with permeability (Figure 10.13b) was made. This shows a general increase in permeability with increasing *Xd*. As weathering advances (an increase in *Xd*) so leaching causes porosity to become a prominent microfabric feature thus increasing permeability (hence the positive relationship observed).

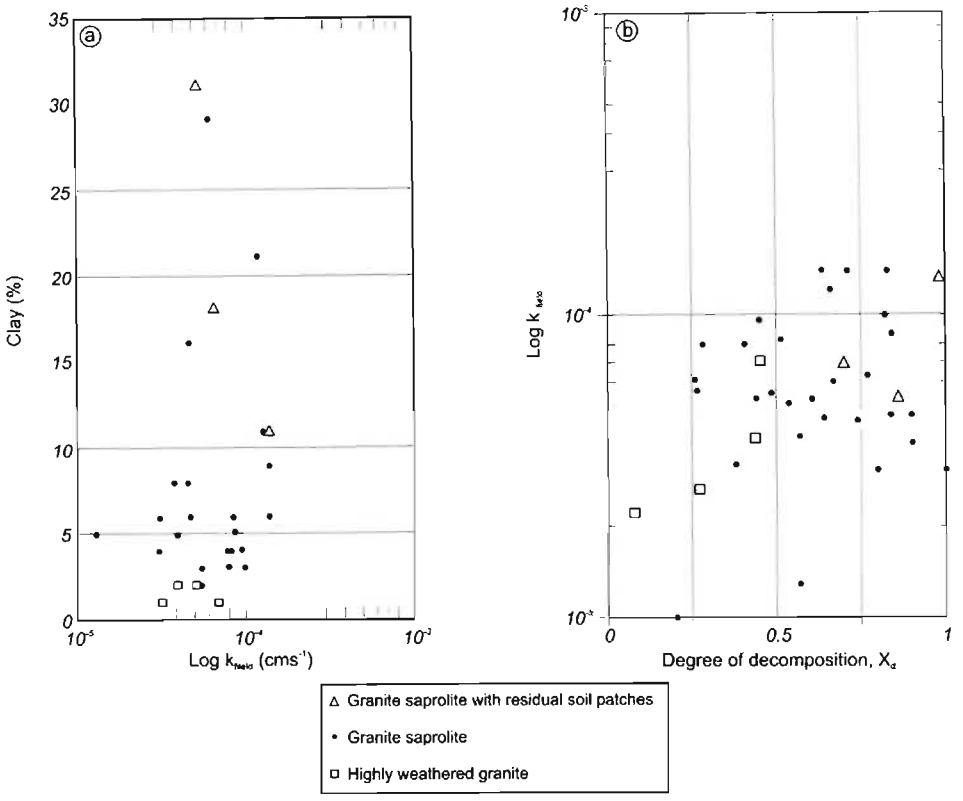

Figure 10.13. (a). Lack of correlation between clay (as determined from grading analyses) with permeability. (b). Tentative relationship of permeability with the microfabric index *Xd*

Permeabilities determined for granite saprolite at Zoeknog Dam by Partridge *et al.* (1984 and 1990) show similar values to those determined in this study at Injaka Dam. For depths ranging from 1,2m to 12,25m values of k for the granite saprolite as determined by falling head permeability tests on block samples ranged from 2,4 x 10^{-4}cm.s^{-1} to 5,2 x 10^{-7} cm.s^{-1}. Partridge *et al.* (1984 and 1990), found that there was a general trend for the permeability to increase with depth and whilst they could not explain this relationship, a broad comparison of these results with the clay content of the material shows that the highest permeabilities correspond to the lowest clay contents, in effect suggesting that flow through microcracks and fissures not clogged by clay aggregations may be the predominant seepage mechanism. This observation differs to those findings from Injaka Dam as discussed above.

11. DISPERSIVITY

11.1 Introduction

Dispersive soils are highly erodible due to deflocculation of clay particles in the presence of relatively pure water to form colloidal suspensions that are removed from the soil through natural permeability. According to Sherard *et al.* (1976a), the nature of these soils was first identified in the American agricultural industry in the 1930's where significant problems with regard to erosion of structures and arable land were encountered. These soils were first identified in South Africa in the mid-1960's as a result of the failure of a number of small earth dams in the Free State and Northern Cape Provinces (Donaldson, 1975). Since that time, work characterising the nature, behaviour and identification of these soils used in local embankment dams has been carried out culminating in a review of the topic by Elges (1985) and Gerber (1986). A synopsis of this literature reveals that no absolute methods for identifying dispersive soils have been developed - this being the result of dispersivity being dependent upon the complex interaction of a number of physico-chemical properties of the soil and soil water, respectively.

The occurrence of dispersive soils in South Africa is generally restricted to old pediment surfaces with gentle rolling topography of low relief and smooth flat slopes (Bell and Maud, 1994). However, dispersion can also be associated with flood plain deposits, colluvial sediments, lake bed deposits and residual soils. It has been acknowledged that climate also plays a major role in the occurrence of these soils with their association common, but not exclusive to regions which experience Weinerts's (1980) climatic N-values ranging between 2 and 10.

11.2 The mechanism of dispersion

The mechanism of dispersion in soils is brought about when the repulsive forces between the clay particles in water exceed the attractive forces resulting in deflocculation of these particles. This has important implications for erodibility when considering the movement of water through the soil. In non-dispersive soils the clay particles adhere to one another and are only eroded by water flowing above a definite threshold velocity. In dispersive soils the clay particles readily deflocculate and go into suspension even in quiet water. This makes the erodibility of these soils critical, as even the smallest hydraulic gradients can remove significant amounts of colloidal material from a soil system.

The process of dispersion is complex, being affected by a number of intrinsic geochemical and physical parameters of the soil, including clay content, percentage dissolved sodium, pH, cation exchange capacity and total dissolved solids (considered as the total content of calcium, magnesium,

sodium and potassium in milliequivalents per litre). In many instances, the complex interrelationship of these parameters is not fully understood and prevents identification of any single absolute parameter that can be used to singularly identify such soils. According to Elges (1985), the dispersion phenomenum is caused by a high percentage of exchangeable sodium on the surface of the clay particles. Sodium is loosely held on the clay surface and imparts a negative charge to it. The adjacent negatively charged particles tend to repel one another, and if the forces of repulsion are great enough to overcome the forces of attraction, the clay particles deflocculate and can be carried away. The percentage dissolved sodium content can be defined as the quantity of sodium from a sample of pore water divided by the total dissolved solids (TDS) - in this case defined by the summation of the quantities of the four main alkali and alkaline earth cations in solution (calcium, magnesium, sodium and potassium). Dispersive soils contain a percentage dissolved sodium content higher than ordinary soils, being up to 12 %. The presence of exchangeable sodium is the main chemical factor contributing towards dispersive behaviour and is expressed in terms of the exchangeable sodium percentage :

$$ESP = \frac{Exchangeable\ Sodium\ Concentration}{Cation\ Exchange\ Capacity} \times 100 \qquad \text{(Eqn. 11.2.1)}$$

where the units are given in meq/100 g of dry soil. A threshold value of 10% has been recommended above which soils that have their free salts leached by seepage of relatively pure water are prone to dispersion (Elges, 1985). Gerber and Harmse (1987), have shown that soils with ESP values above 15% are highly dispersive whilst those with low cation exchange capacities of (15 meq/100g clay) have been found to be completely non-dispersive at ESP values of 6% or below. The cation exchange capacity (CEC, expressed in meq/100g clay) can also be routinely applied to the identification of dispersive soils, with high CEC's indicative of soils readily able to exchange cations with the ambient solutions.

For deflocculation to occur, a certain proportion of clay is required within the soil. Dispersive soils often contain a high to moderate proportion of clay, although no significant differences in the clay fractions of dispersive and non-dispersive soils have been ascertained. Sherard *et al.* (1976a) have suggested that soils with less than 10% clay particles may not have enough colloids to support dispersive piping.

The typical pH range for dispersive soils is between 6 and 8, whilst highly dispersive soils have been found to have pH values above 8. Another important property claimed to govern the susceptibility of clayey soils to dispersion is the total content of dissolved solids (TDS) within the water (Sherard *et al.* 1976a). The lower the content of dissolved salts the greater is the susceptibility of sodium saturated clays for dispersion.

11.3 Identification of dispersive soils

The identification of dispersive soils cannot be conducted using routine soil mechanics testing such as natural moisture content, particle size distribution and Atterberg limits. For this reason, a number of specialised physical and chemical tests have been developed to recognise dispersive soils (Table 11.1). However, no single test can be relied upon to absolutely identify these soils as the boundary between deflocculated and flocculated states varies considerably. Hence, it is often necessary to conduct a suite of tests to satisfactorily determine the dispersivity of the soils. The physical tests show the erodibility of the soil or its direct reaction to exposure in water, whilst the chemical tests show the cause of the dispersivity by measuring the presence of sodium on the clay surface.

Table 11.1. Established methods for determining the dispersivity of soils.

Test Type	Reference
Physical Tests	
Crumb Test	Emerson (1964)
Double Hydrometer Test (SCS Test)	Volk (1937) and Kinney (1979)
Pinhole Test	Sherard *et al.* (1976b)
Chemical Tests	
Total Dissolved Solids and Percentage Sodium	Sherard *et al.* (1976a)
ESP	Gerber & Harmse (1987)
ESP-CEC	Gerber & Harmse (1987)

Substantial piping erosion and "runnel erosion" (Figure 11.1) has occurred on the flanks of the dam foundation excavation over a relatively short period of one year (one rainfall season). These features are characteristic of highly dispersive soils. Furthermore, during erosion of the flanks, the runoff water remains highly turbid even throughout long durations of rainfall (Figure 11.2). Consequently, research was initiated to quantify the dispersivity of the weathered granite. In order to accomplish this, a number of dispersivity tests were undertaken, including the physical tests (crumb test, double hydrometer and pinhole tests) and chemical tests (ESP, CEC and pH). Although the Atterberg limits do not provide a means of directly identifying potentially dispersive soils (Resendiz, 1977 and Tandanier and Ingles, 1985), it is generally accepted that the higher the values of the plastic limit, liquid limit and plasticity index, the higher is the resistance to dispersion.

11.3.1 Crumb test

The crumb test was first described by Emerson (1964) and is the simplest of all dispersivity tests measuring the reaction of hydration of a soil clod ("crumb") when placed in distilled water. The tendency for the colloidal sized particles to deflocculate is observed over a ten minute period and this reaction is graded accordingly. According to Elges (1985), the crumb test generally gives a good indication of the potential erodibility of clay soils although soils containing kaolinite with known

field dispersion problems have shown non-dispersive reactions. This was not the case in this study, where the crumb test showed all samples to be dispersive, a characteristic noticed from field observations.

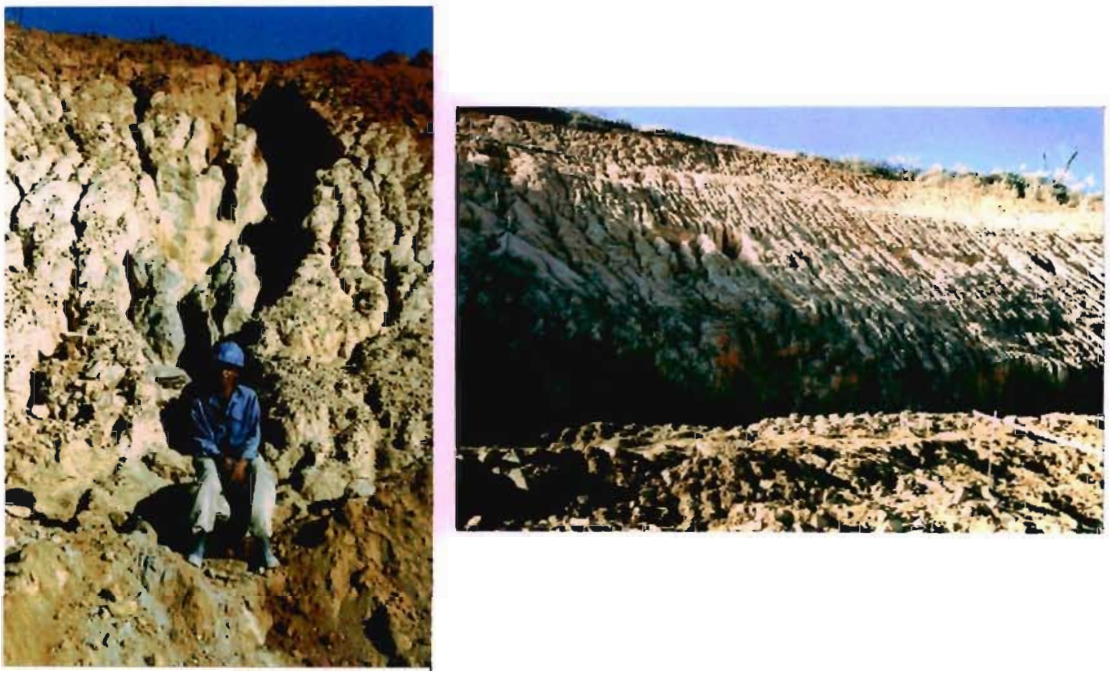

Figure 11.1. Large piping and pervasive runnel erosion developed in granite saprolite foundation excavation. The pipe developed over a period of one year.

Figure 11.2. Turbid water exiting from piping erosion on the right excavation flank in granite saprolite.

All samples of granite saprolite with residual soil patches tested positively as dispersive soils exhibiting Grade 3 and one Grade 4 reaction (Table 11.2). The granite saprolite was also susceptible to the crumb test with an overall more vigorous reaction as suggested by the Grade 4 results in Table 11.3.

11.3.2 Double hydrometer test

The double hydrometer test has been developed from the initial method proposed by Volk (1937) and described later by Kinney (1979). This test was one of the first methods developed for soil dispersivity and describes the tendency of the clay particles to naturally go into suspension. The test measures the content of the five micron size particles in a standard hydrometer test with a parallel test being conducted in which no chemical dispersant is used The amount of <5μm soil particles that goes into suspension naturally is expressed as a percentage of that in the standard test. Bell and Maud (1994) have defined certain broad classifications into which the double hydrometer test identifies the dispersivity of South African soils. They maintain that values less than 15% suggest non-dispersive behaviour; between 15% and 30% defines slightly dispersive characteristics; between 30% and 50% includes soils that are dispersive and greater than 50% includes soils that can be considered to be highly dispersive.

Table 11.2 shows 60 % of the samples of granite saprolite with residual soil patches to classify as non-dispersive, whilst 40 % classify as slightly dispersive. The granite saprolite shows a much wider range of dispersivity classifications (Table 11.3) with 26 % indicating non-dispersive characteristics; 19 % showing slight dispersivity; 16 % exhibiting moderate dispersivity and 39 % showing a susceptibility to be highly dispersive.

11.3.3 Pinhole test

In the pinhole test a cylinder of soil is compacted at moisture content equal to its plastic limit using a miniature compacter. A 1 mm pinhole is punched through the soil specimen and water is percolated through the pinhole under constant head ranging from 50 to 380 mm. The flow rate, effluent turbidity and pinhole size are used to assess the disposition of the soil to disperse. This test is widely considered to be the most reliable physical dispersivity test and was first developed by Sherard *et al.* (1976b). Jermy and Walker (1999) have advanced the qualitative assessment of this test by using a spectrophotometer to quantitatively assess the turbidity of the effluent emanating from the pinhole. Results from this investigation show that the samples of granite saprolite with residual soil patches classify as non-dispersive (Table 11.2). The majority (94 %) of the granite saprolite samples also showed non-dispersive tendencies from this test, whilst only 6 % showed moderate dispersivity (Table 11.3).

Table 11.2. Physical and chemical dispersivity test results for granite saprolite with residual soil patches.

Sample	Clay (%)	W_L	I_P	A	LS	pH	K	Ca	Mg	Na	TDS	ESP-CEC Graph			EC	Crumb Test		Double Hydrometer		Pinhole Test	
												ESP	CEC	Dispersivity		Grade	Dispersivity	(%)	Dispersivity	Classification	Dispersivity
RF 12	31	44,0	17,6	0,6	8,7											Gr 3	D	18,2	SD	ND 1	ND
RF 17	18	34,2	11,6	0,6	6,7											Gr 3	D	11,5	ND	ND 1	ND
LF 1	11	23,3	4,6	0,4	2,0	5,9	0,8	<1,0	<1,0	6,0	39,0				5,0	Gr 3	D	6,3	ND	ND 1	ND
LF 7	8	26,0	7,5	0,9	3,7	5,9	1,9	<1,0	<1,0	6,0	37				5,4	Gr 3	D	25,0	SD	ND 2	ND
LF 18	11	31,7	6,3	0,6	3,3	6,7	1,2	1,0	<1,0	4,0	32,0	3,45	41,04	MD	4,1	Gr 4	D	10,0	ND	ND 1	ND

Table 11.3. Physical and chemical dispersivity test results for granite saprolite.

Sample	Clay (%)	W_L	I_P	A	LS	pH	K	Ca	Mg	Na	TDS	ESP-CEC Graph			EC	Crumb Test		Double Hydrometer		Pinhole Test	
												ESP	CEC	Dispersivity		Grade	Dispersivity	(%)	Dispersivity	Classification	Dispersivity
RF 10	21	37,1	12,6	0,6	5,3											Gr 4	D	47,8	MD	ND 1	ND
RF 9	4	33,2	8,2	2,0	4,0											Gr 4	D	75,0	HD	ND 1	ND
RF 8	16	36,1	10,5	0,7	5,0											Gr 4	D	90,0	HD	ND 3	MD
RF 7	2		Too sandy													Gr 4	D	100,0	HD	ND 2	ND
RF 6	29	41,2	12,7	0,4	7,0											Gr 3	D	16,1	SD	ND 1	ND
RF 5	8		Too sandy													Gr 4	D	100,0	HD	ND 1	ND
RF 4	10	37,6	6,7	0,7	2,7											Gr 4	D	100,0	HD	ND 1	ND
RF 3	5		Too sandy													Gr 4	D	80,0	HD	ND 1	ND
RF 18	5	30,8	6,2	1,2	2,7											Gr 4	D	50,0	ND	ND 1	ND
RF 19	2		Too sandy													Gr 4	D	80,0	HD	ND 1	ND
RF 20	2		Too sandy													Gr 4	D	100,0	HD	ND 1	ND
RF 21	2		Too sandy													Gr 4	D	80,0	HD	ND 1	ND
LF 2	8	34,6	8,9	1,1	3,0	5,1	0,3	<1,0	<1,0	3,0	21,0				2,4	Gr 3	D	12,5	ND	ND 1	ND
LF 3	6	32,4	11,5	1,9	3,7	5,2	0,5	<1,0	<1,0	3,0	21,0				2,1	Gr 4	D	16,7	SD	ND 1	ND
LF 4	2	36,6	10,6	5,3	4,0	7,0	0,8	4,0	<1,0	3,0	36,0				4,9	Gr 4	D	50,0	MD	ND 3	MD
LF 5	3	29,1	8,4	2,8	2,7	6,3	1,0	<1,0	<1,0	3,0	28,0				3,0	Gr 4	D	60,0	HD	ND 2	ND
LF 6	4	40,2	7,0	1,8	2,7	6,4	0,6	1,0	<1,0	3,0	30,0				3,1	Gr 4	D	50,0	MD	ND 1	ND
LF 8	11	36,0	9,8	0,9	4,7	5,9	1,3	<1,0	<1,0	3,0	27,0				3,5	Gr 4	D	5,0	ND	ND 1	ND
LF 9	4	30,0	6,9	1,7	2,7	6,4	0,7	<1,0	<1,0	3,0	19,0				2,1	Gr 4	D	12,5	ND	ND 1	ND
LF 10	8	39,9	11,7	1,5	4,7	6,1	0,9	<1,0	<1,0	2,0	25,0				2,2	Gr 4	D	16,7	SD	ND 1	ND
LF 11	2	35,8	6,4	3,2	2,7	6,5	0,7	<1,0	<1,0	2,0	21,0				2,0	Gr 4	D	14,3	ND	ND 1	ND
LF 12	3	42,9	9,6	3,2	4,7	6,6	0,8	<1,0	<1,0	3,0	25,0				2,3	Gr 4	D	37,5	MD	ND 1	ND
LF 13	4	36,8	9,2	2,3	4,3	6,7	0,7	1,0	<1,0	3,0	27,0				2,7	Gr 4	D	55,0	HD	ND 1	ND
LF 19	6	32,5	5,4	0,9	2,7	6,4	1,0	1,0	<1,0	3,0	24,0	3,69	48,58	MD	3,4	Gr 3	D	11,1	ND	ND 1	ND
LF 20	6	34,0	7,3	1,2	3,0	6,5	0,9	1,0	<1,0	3,0	27,0	2,99	34,93	ND	3,4	Gr 4	D	20,0	SD	ND 1	ND
LF 21	3	31,6	5,8	1,9	2,3	5,4	0,4	<1,0	<1,0	2,0	19,0	2,43	42,99	ND	2,1	Gr 4	D	11,1	ND	ND 1	ND
LF 22	5	23,5	4,1	0,8	2,0	6,2	0,6	<1,0	<1,0	3,0	24,0	8,95	14,18	MD	2,4	Gr 4	D	22,2	SD	ND 1	ND
LF 24	5	31,7	8,0	1,2	2,3	6,2	1,6	<1,0	1,0	6,0	43,0	3,77	23,73	ND	6,2	Gr 4	D	9,1	ND	ND 1	ND
LF 25	6	33,6	7,3	1,2	3,0	6,5	0,6	<1,0	<1,0	4,0	25,0	7,96	21,57	MD	2,9	Gr 4	D	16,7	SD	ND 1	ND
LF 26	3	35,4	5,7	1,9	2,7	6,3	0,7	<1,0	<1,0	4,0	27,0	3,05	31,79	ND	3,1	Gr 4	D	100,0	HD	ND 2	ND
LF 27	1	24,4	4,6	4,6	1,7	6,4	0,5	<1,0	<1,0	3,0	27,0	6,58	36,27	D	2,4	Gr 4	D	50,0	MD	ND 1	ND

11.3.4 ESP vs CEC

The introduction to this chapter highlighted the presence of exchangeable sodium as the main chemical factor contributing towards dispersive behaviour. However, some difference of opinion exists as to the value of ESP above which a soil can be considered to be dispersive. Sherard *et al.* (1976a), considered soils with an ESP value between 7 and 10 as being moderately dispersive, whilst Harmse (1980) suggested that dispersive soils are characterised by an ESP value greater than 5. Gerber (1983) integrated the relationship of ESP with the cation exchange capacity (CEC) of soil which is dependent upon its clay mineralogy. He devised a chart defining specific degrees of dispersivity depending upon the relationship of these two parameters (Figure 11.3).

As a result of cost implications, relatively few samples were submitted for this test in this research and consequently only samples from Traverse 5 were tested. The single sample of granite saprolite with residual soil patches classified as non- or marginally dispersive, whilst the granite saprolite showed a range of dispersivity characteristics extending from non-dispersive to dispersive (Figure 11.3). Results from Chunnett *et al.* (1991a) conducted on similar material from the same site show a higher indication of dispersivity for these samples using this test, although the reason for this is not known.

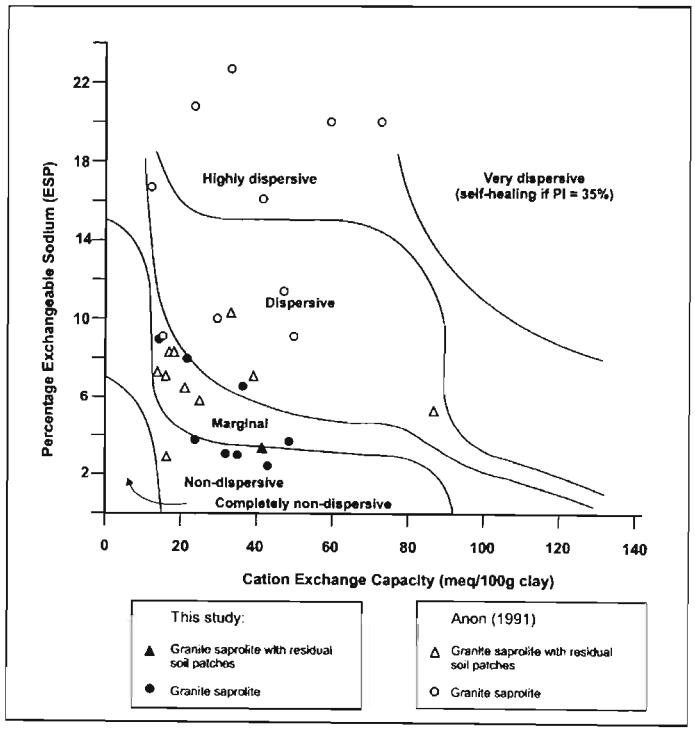

Figure 11.3. ESP vs CEC graph for granite saprolite with residual soil patches and granite saprolite.

11.4 Discussion

The various tests conducted on the granite saprolite with residual soil patches show this material to be non-dispersive or only marginally dispersive. This is confirmed by field observations which show a much less pronounced runnel formation within this material in comparison to the granite saprolite. This can probably be related to the low exchangeable sodium within these samples as a result of extensive leaching.

The boundary between flocculated and deflocculated states for the granite saprolite is considerably less well-defined so that the transition between non-dispersive and dispersive soils is wide. Consequently, as Bell and Maud (1994) recommend, several different tests have been conducted to determine the dispersive nature of the material. They have proposed a tentative rating system for the different test methods from their study on selected South African soils. Subsequently, Bell and Walker (2000), have modified this rating system using their sample population derived from soils in KwaZulu-Natal. Both of these systems incorporated a variety of soil types from a variety of origins but essentially determined the ESP vs CEC method as being most significant in assessing dispersive soils.

The limited data from the various dispersivity tests carried out on samples from Injaka Dam produced disparate results. The crumb test and double hydrometer test proved the granite saprolite to be dispersive and are in accordance with the field observations of the effects of dispersivity. Consequently, these tests are recommended as suitable measures for quantifying the dispersivity of the granite saprolite. The limited data from the ESP vs CEC test showed 50% of the samples to be dispersive and the applicability of this test on granite saprolite at Injaka Dam is questionable. Results from the pinhole test proved not to correlate with field observations and other dispersivity tests and can be considered to be unsuitable when assessing this material for dispersivity.

Partridge *et al.* (1984) carried out a similar suite of tests on the granite saprolite at Zoeknog Dam and found the saprolite to be non-dispersive as determined by the pinhole test, double hydrometer and ESP tests. Subsequent to the breaching of Zoeknog Dam, several investigations were undertaken on the embankment materials constructed from granite saprolite. The investigation by Partridge *et al.* (1993) undertook further ESP tests, double hydrometer and pinhole tests to validate the results from earlier investigations. These subsequent tests show the material to have low ESP values, generally less than 1% which is indicative of non-dispersive soils. Partridge *et al.* (1993) make the notable point that particularly with ESP testing, it is necessary that the soil water is in equilibrium with the soil and Elges (1985) maintains that this is not always the case when sampling from the breach of recently failed dams. Partridge *et al.*(1993), conclude that in the light of the highly leached nature of the granite saprolite at Zoeknog Dam with low soil pH, the retention of

sodium cations necessary for dispersion to occur can be precluded. They consequently maintain that for the double hydrometer and pinhole tests which showed intermediate dispersivity characteristics for the saprolite, this was considered a reflection of the erodability rather than dispersivity of the soil.

Keller *et al.* (1994) in their post failure investigations at Zoeknog Dam confirmed that the pinhole and crumb tests showed the granite saprolite to be non-dispersive whilst the double hydrometer showed the material to exhibit marginal dispersive characteristics.

It is quite apparent from the above that owing to the poorly defined flocculated and deflocculated states for the granite saprolite, the transition between the dispersive and non-dispersive state is wide, resulting in the ambiguous results as determined from the laboratory testing. It is pertinent to note, however, that the granite saprolite is considered by the above references and the author to be highly erodible.

12. CONSOLIDATION CHARACTERISTICS OF GRANITE SAPROLITE

12.1 Introduction

When subjected to vertical pressure with lateral confinement, differences in terms of the consolidation stress paths have been noted between saprolitic soils formed *in situ* and those soils derived from sedimentary processes. Indeed, it has been shown by Vaughan *et al.* (1988), that the consolidation of residual soils and saprolite is significantly governed by its texture, in particular its void ratio, density and bonding (or "structural interlock") which often impart a characteristic yield stress observed on void ratio-pressure (e-p) curves. Further to this, it is well known that saprolitic soils are prone to collapse settlement because of their metastable structure (Dudley, 1970) - a result normally of the intense leaching and clay-bridged microfabric of the material. This chapter describes the one-dimensional consolidation characteristics of the granite saprolite with particular emphasis on collapse settlement behaviour.

Throughout the literature on the consolidation of saprolitc soils, the preconsolidation pressure (p_c) is regarded as one of the most important soil characteristics although its relationship to the weathering in such soils has been the source of much debate. Chang (1988) describes the p_c of a soil as one of the most important factors which influences soil engineering behaviour stating that p_c separates small strain and predominantly elastic behaviour from a large strain and predominantly plastic behaviour of a soil. The p_c of saprolitic soils has been ascribed to the interlocking grain texture of saprolites as well as to the effects of dessication forming cementitious bonds which create a "yield stress" when consolidating such soils. The early studies of saprolitic soils by Vargas (1953), noted that these soils exhibited a "virtual preconsolidation pressure". A review of this work shows that this was probably attributable to desiccation of the material or grain interlock, as Vargas found that p_c tended to decrease with increasing depth (Figure 12.2). Findings by Sowers (1963) also noted that residual soil derived from crystalline rock exhibited a preconsolidation pressure, but one which is highly variable, has no correlation with the current overburden load and generally increases with depth. He noted that p_c is probably related to the residual mineral bonds (interlock) of the parent rock, substantiating this hypothesis by the observation that the "least weathered soils" (soils closest to bedrock) tend to have the highest preconsolidation loads. Vaughan (1985) has concluded that there is general agreement that "quasi preconsolidation pressure" is due to the weathering (resulting in secondary bonding) and structure of these soils rather than their stress history.

To analyse the consolidation characteristics of the weathered granite at Injaka Dam, a series of oedometer tests were undertaken. Nine double oedometer tests (Knight, 1961) and forty one single oedometer collapse potential tests (Jennings and Knight, 1975) were carried out on selected undisturbed samples and the results of these tests are discussed below.

12.2 Consolidation characteristics from double oedometer tests

Nine double oedometer tests were carried out on selected undisturbed samples of the granite saprolite to compare their consolidation characteristics at natural moisture content with those under saturated conditions and thereby obtain an indication of their consolidation characteristics and metastability. Cost and time considerations limited the volume of this component of testing to only the nine samples described below.

12.2.1 Sample preparation

In the double oedometer test, two specimens were tested in the normal manner of consolidometer testing with both samples taken as close together as possible from the same block sample. One specimen was tested at natural moisture content whilst the other was tested under saturated conditions. The specimens were 76 mm in diameter with an initial height of 25 mm. For all tests, a floating ring oedometer was used with a porous stone provided at the top and bottom of the specimens. The following load increments were applied: 25, 89, 191, 381, 762 kPa, with unloading allowing rebound to 191 and 25 kPa, respectively.

12.2.2 Results from double oedometer tests

The results from the double oedometer tests carried out on weathered granite are presented in Table 12.1 and reflect the variation in the granite saprolite showing that the initial void ratios from specimens cut from the same undisturbed sample block are significantly different. This observation is in agreement with previous studies of saprolitic soils reviewed by Vaughan (1985). The shape of the oedometer curves for natural and saturated moisture conditions also varies significantly. Typical sets of double oedometer e-log p and e-p curves for the granite saprolite are shown in Figures 12.1a to i. These curves are similar to those of Massey *et al.* (1988) in that they do not display a clearly defined yield stress as described by Vaughan *et al.* (1988). This observation is confirmed by the construction of linear e-p plots (Figures 12.1a to i) prescribed by Vaughan (1985) as being necessary for identifying this type of consolidation behaviour. Massey *et al.* suggested that this lack of clearly defined yield

Table 12.1. Results from double oedometer tests.

Sample	LF 18*	LF 18*	LF 19	LF 19	LF 20	LF 20	LF 21	LF 21	LF 22	LF 22	LF 25	LF 25	RF 10	RF 10	RF 6	RF 6	RF 4	RF 4
Moisture condition	NMC	SAT	NMC	SAT	NMC	SAT	NMC	SAT	NMC	SAT	NMC	SAT	NMC	SAT	NMC	SAT	NMC	SAT
Pressure (kPa)	0	0	0	0	0	0	0	0	0	0	0	0	0	0	0	0	0	0
Void ratio	1,350	0,911	1,487	1,026	1,015	1,149	1,133	1,188	1,103	1,079	1,058	0,990	1,504	1,042	1,114	0,812	1,505	1,086
Pressure (kPa)	25	25	25	25	25	25	25	25	25	25	25	25	25	25	25	25	25	25
Void ratio	1,341	0,905	1,477	1,007	0,995	1,098	1,087	1,100	1,075	1,029	1,046	0,935	1,5	1,034	1,103	0,771	1,483	1,033
M_v	0,141	0,121	0,165	0,354	0,386	0,965	0,863	1,6411	0,535	1,130	0,228	1,120	0,067	0,1567	0,217	0,9221	0,352	1,022
C_v	1,030	6,052	151,92	8,411	147,350	148,150	149,300	146,700	156,460	155,160	157,27	148,530	67,776	157,960	150,93	149,08	156,78	155,570
Pressure (kPa)	89	89	89	89	89	89	89	89	89	89	89	89	89	89	89	89	89	89
Void ratio	1,306	0,853	1,435	0,937	0,967	0,938	1,022	0,994	1,035	0,925	1,013	0,754	1,452	0,982	1,091	0,747	1,440	0,969
M_v	0,240	0,441	0,268	0,576	0,228	1,300	0,502	0,838	0,308	0,782	0,264	1,614	0,312	0,415	0,086	0,213	0,274	0,507
C_v	36,388	36,686	66,114	64,350	63,931	59,446	35,397	33,434	37,844	15,964	38,444	58,304	37,324	38,328	66,346	15,967	35,933	34,556
Pressure (kPa)	191	191	191	191	191	191	191	191	191	191	191	191	191	191	191	191	191	191
Void ratio	1,270	0,785	1,378	0,853	0,928	0,823	0,931	0,920	0,985	0,852	0,969	0,678	1,377	0,909	1,080	0,691	1,391	0,885
M_v	0,157	0,372	0,235	0,445	0,20	0,618	0,467	0,381	0,243	0,386	0,218	0,440	0,308	0,374	0,053	0,327	0,203	0,436
C_v	35,287	61,136	63,491	59,399	61,770	29,041	32,754	30,552	36,216	32,900	65,753	28,394	35,492	63,963	36,915	61,000	65,353	34,0533
Pressure (kPa)	381	381	381	381	381	381	381	381	381	381	381	381	381	381	381	381	381	381
Void ratio	1,203	0,711	1,27	0,753	0,866	0,728	0,841	0,855	0,958	0,782	0,812	0,608	1,260	0,838	1,049	0,608	0,608	1,2920,7
M_v	0,105	0,148	0,163	0,194	0,113	0,190	0,167	0,118	0,047	0,133	0,294	0,148	0,178	0,132	0,052	0,177	0,146	0,195
C_v	59,928	42,353	59,214	53,786	21,099	16,568	29,815	50,536	61,96	54,142	33,353	46,297	32,727	33,373	64,293	31,588	34,540	54,823
Pressure (kPa)	763	763	763	763	763	763	763	763	767	767	763	763	763	763	763	763	767	767
Void ratio	1,169	0,630	1,23	0,657	0,754	0,636	0,738	0,780	0,893	0,715	0,738	0,536	1,101	0,763	1,003	0,527	1,192	0,682
M_v	0,041	0,130	0,053	0,152	0,167	0,147	0,155	0,111	0,090	0,102	0,112	0,123	0,199	0,112	0,060	0,139	0,119	0,157
C_v	7,155	51,580	31,155	27,062	30,023	23,227	26,849	46,872	33,240	50,137	52,267	42,372	28,938	54,782	32,780	28,529	10,133	17,604
Pressure (kPa)	191	191	191	191	191	191	191	191	191	191	191	191	191	191	191	191	191	191
Void ratio	1,176	0,641	1,228	0,669	0,766	0,645	0,758	0,786	0,898	0,712	0,742	0,543	1,087	0,755	0,991	0,516	1,179	0,674
Pressure (kPa)	25	25	25	25	25	25	25	25	25	25	25	25	25	25	25	25	25	25
Void ratio	1,186	0,679	1,237	0,707	0,783	0,676	0,756	0,806	0,908	0,746	0,752	0,566	1,080					

NMC =- natural moisture content SAT = saturated conditions

c_v = coefficient of consolidation m_v = coefficient of volume change

* Granite saprolite with residual soil patches

$$m_v = \frac{\Delta e}{\Delta p}\left(\frac{1}{1+e}\right) \qquad c_v = \frac{\kappa}{m_v}$$

stress may be due to three factors, namely specimen disturbance, small specimen thickness in relation to maximum particle size or to bedding error in the measurement of vertical displacement. The yield point for the material may also be so low that it is not detected by the test due to the magnitude of the first load increment (25 kPa).

The consolidation curves for the saturated samples generally show a complete loss of strength even at the lowest pressure application of 25 kPa. The settlement curves for these samples tend to be much steeper than those of the samples tested at natural moisture content with the samples showing loss of strength under saturation. This is confirmed by a comparison of the compression indices (Table 12.2). It is suggested that this is due to the softening of the clay particles, aggregations and pseudomorphs as well as the dispersive nature of the soil which causes slight fabric disruption during saturation of the sample within the oedometer ring. This effect is discussed in more detail when analysing the single oedometer results.

The granite saprolite exhibited a p_c at natural moisture content (p_{cNMC}) that varied from 90 to 210 kPa, reducing to a value ranging from 35 to 110 kPa in the saturated state (p_{cSAT}). These results are summarised in Table 12.2 and are in agreement with similar values quoted by Nouvais-Ferreira and Fonesca (1988) for saprolitic soil derived from granite in Portugal (Table 12.3). In all cases p_{cNMC} was much greater than the current overburden pressure (p_0) which is also shown in Table 12.2 and Figure 12.2. In this respect, the compressibility characteristics of all samples excluding LF 21 and RF 4 are similar to those of over-consolidated soils. It can also be seen, as observed by Vargas (1953), that above a certain depth preconsolidation appears to be independent of the overburden pressure, and as the clay decomposition products form *in situ*, this does not reflect the loading history of the soil. No correlation could be ascertained between p_c and density on the one hand, or degree of decomposition on the other hand. Consequently, the explanation offered by Sowers (1963) for the presence of a preconsolidation pressure cannot be substantiated using results from this study. Partridge *et al.* (1984) have found a similar relationship in their assessment of the granite saprolite at Zoeknog Dam (Figure 12.3) where they noted that p_{cNMC} was considerably higher than the overburden line and ascribed this to the possibility of relict "cementation" between particles. They also noted a sharp reduction in p_{cSAT} and attributed this to the possibility of loss of structure and debonding due to saturation, as observed with the Injaka Dam samples.

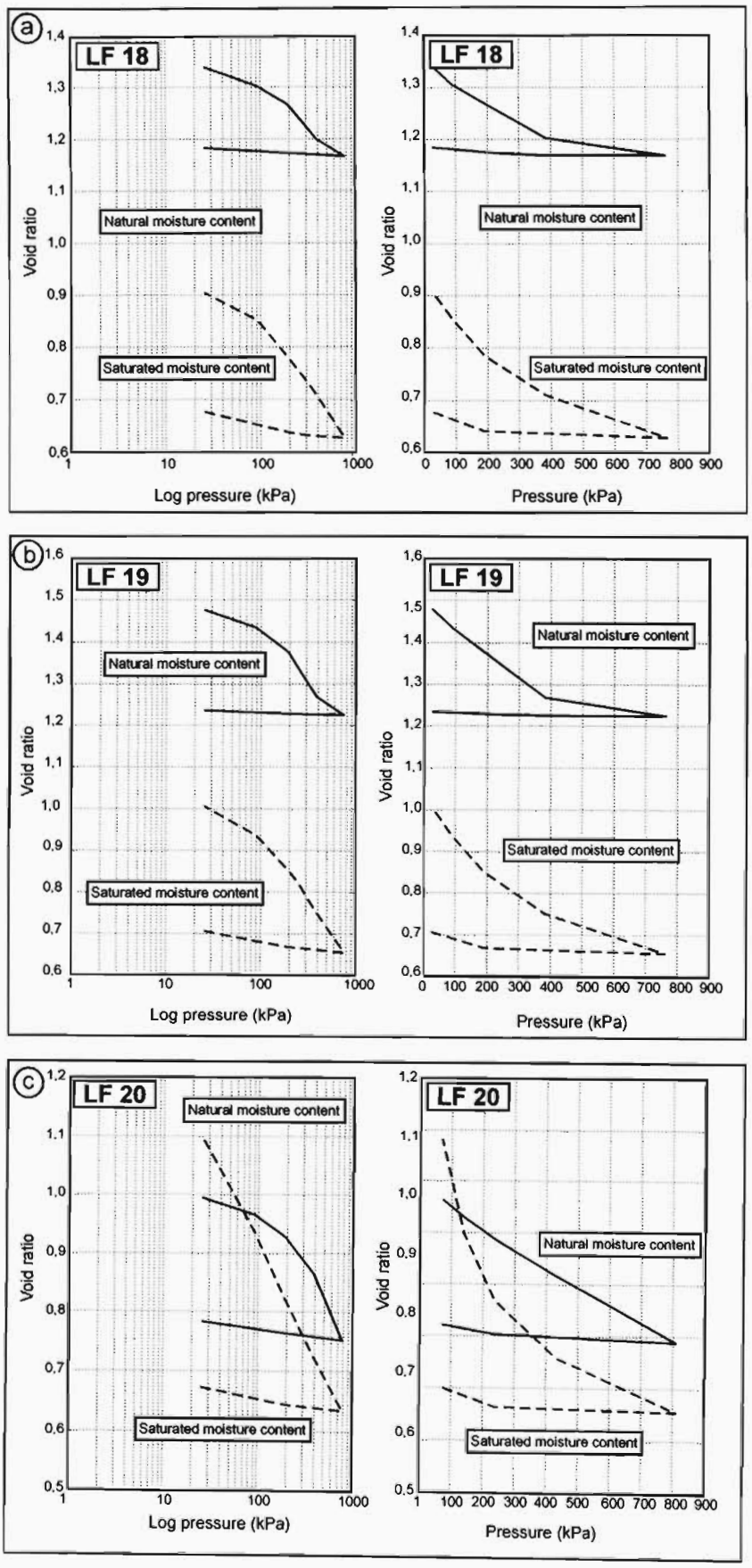

Figure 12.1a, b and c. Typical e-log p and e-p curves from double oedometer tests. e-p curves are included to assess the presence of any yield stress using the technique proposed by Vaughan (1985).

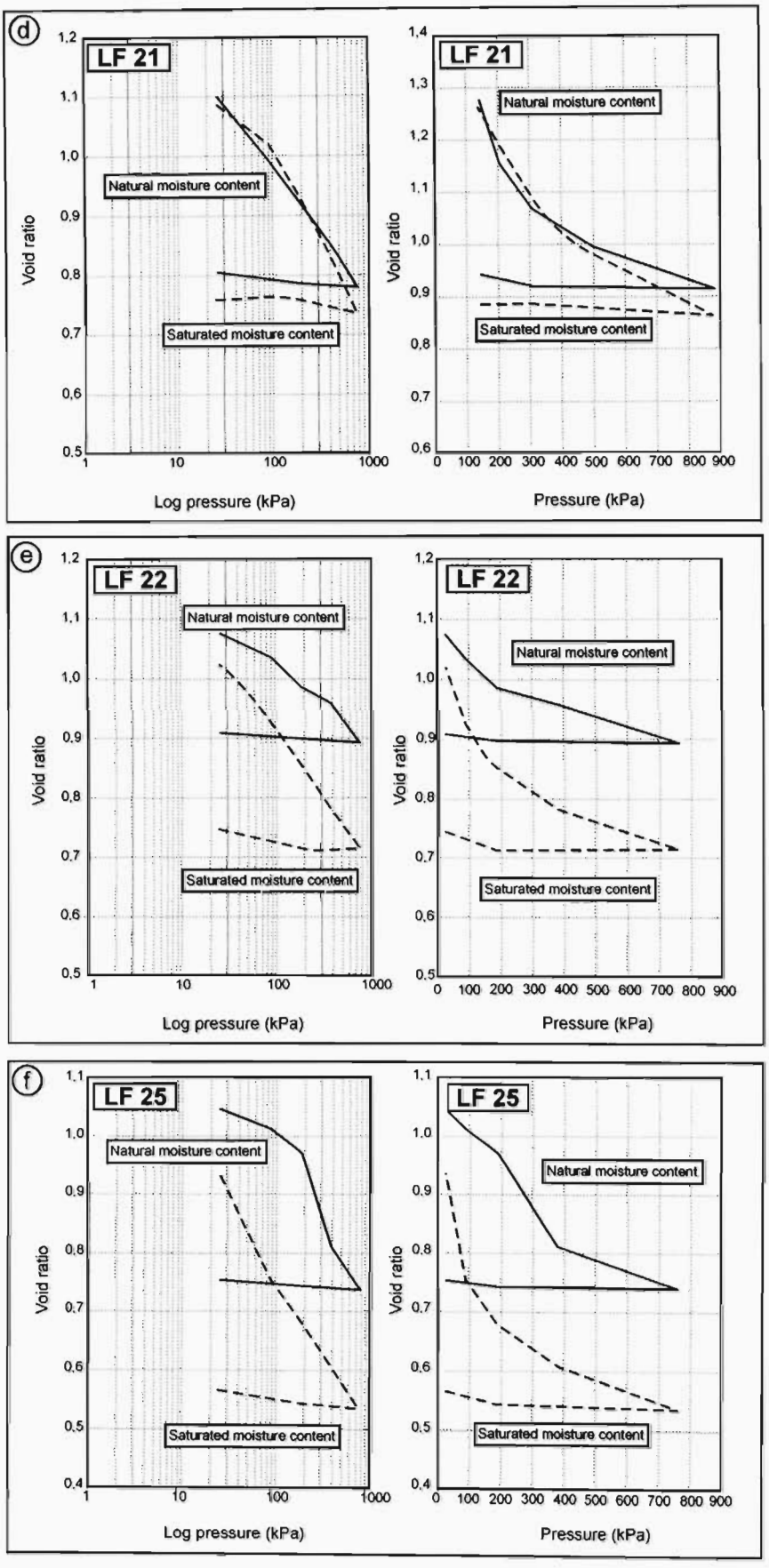

Figure 12.1d, e and f. Typical e-log p and e-p curves from double oedometer tests. e-p curves are included to assess the presence of any yield stress using the technique proposed by Vaughan (1985).

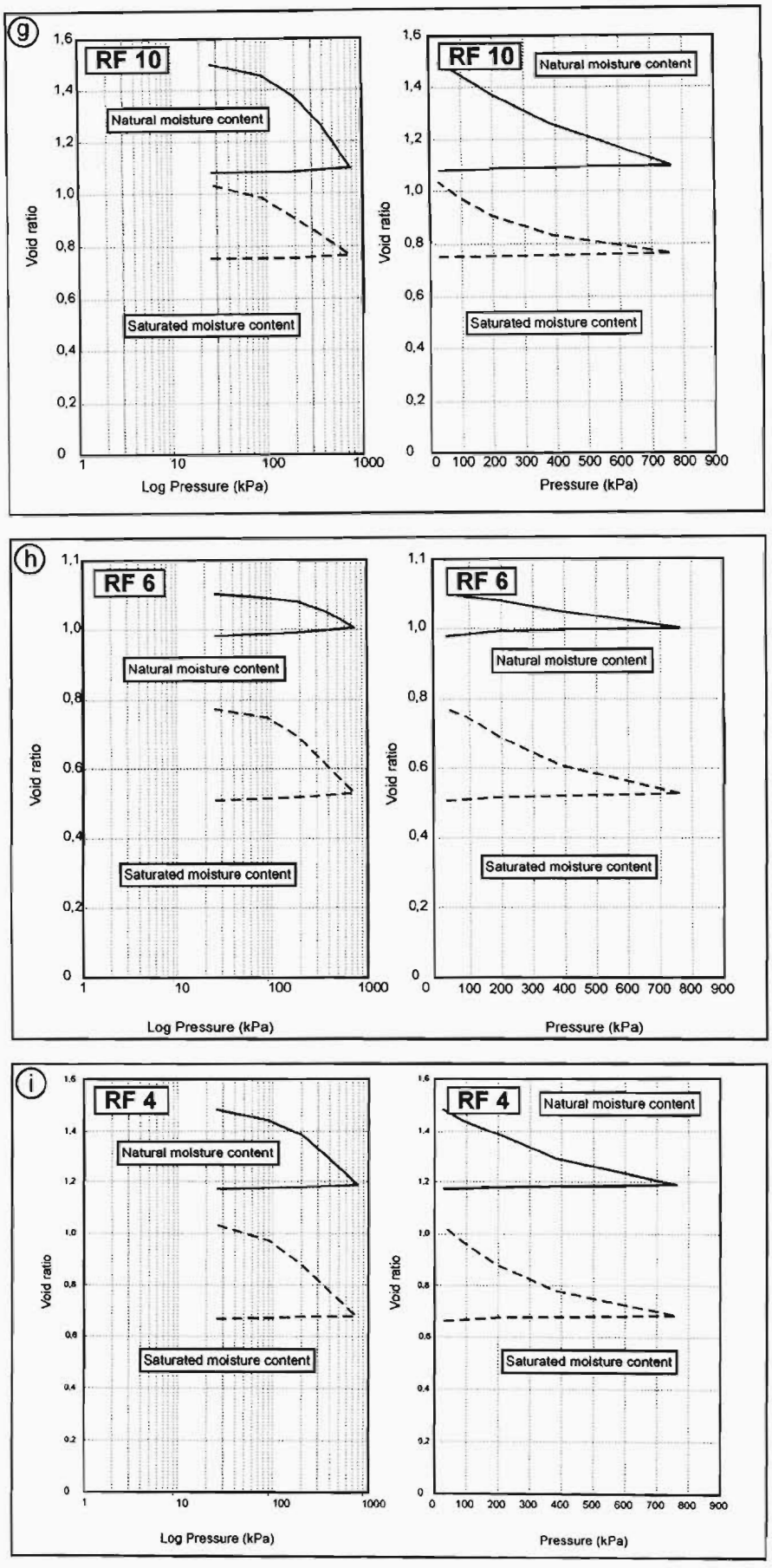

Figure 12.g, h and i. Typical e-log p and e-p curves from double oedometer tests. e-p curves are included to assess the presence of any yield stress using the technique proposed by Vaughan (1985).

Table 12.2. Compression indices from double oedometer tests.

Sample	Depth (m)	p_{cNMC} (kPa)	p_{cSAT} (kPa)	p_0 (kPa)	$C_{c\ nat}$	$C_{r\ nat}$	$C_{c\ sat}$	$C_{r\ sat}$	*Xd*	ρ_d (kg.m^{-3})	OCR
LF 18*	1,1	110	80	18	0,17	0,01	0,26	0,03	1,00	1535	6,1
LF 19	2,3	120	92	37	0,25	0,01	0,33	0,03	1,00	1307	3,2
LF 20	3,2	200	35	51	0,37	0,02	0,31	0,04	0,84	1305	3,9
LF 21	4,0	90	80	63	0,32	0,01	0,24	0,02	0,40	1386	1,4
LF 22	5,1	130	40	80	0,22	0,01	0,23	0,02	0,56	1409	1,6
LF 25	6,2	150		98	0,42	0,01	0,24	0,02	0,90	1533	1,5
RF 10	3,5	190	85	58	0,53		0,25		0,66	1330	3,3
RF 6	2,5	210	110	41	0,30		0,23		0,77	1458	5,1
RF 4	6,9	160	105	113	0,30		0,34		0,82	1457	1,4

p_{cNMC} = preconsolidation pressure at natural moisture content
p_{cSAT} = preconsolidation pressure at saturated moisture content
p_0 = overburden pressure
C_{cNMC} = compression index at natural moisture content
LF 18* = granite saprolite with residual soil patches

C_{cSAT} = compression index at saturated moisture content
Xd = degree of decomposition (after Lumb, 1962)
ρ_d = dry density
OCR = over consolidation ratio (p_{cNMC}/p_0)

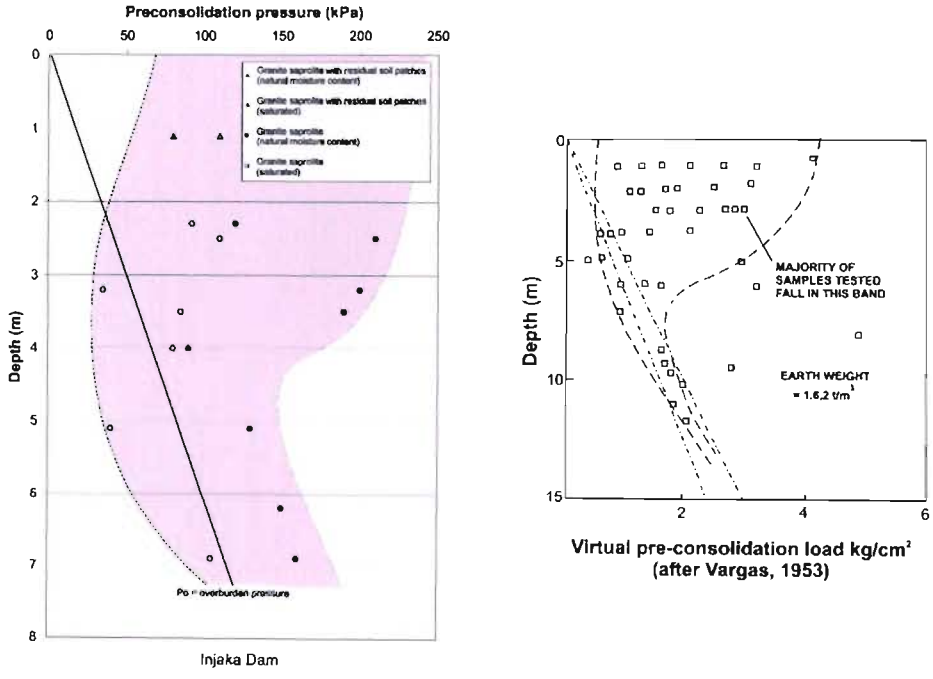

Figure 12.2. Relationship of p_c with depth at Injaka Dam site (shaded area encompasses all samples) and findings by Vargas (1953) showing similar lack of correlation of p_c with overburden pressure.

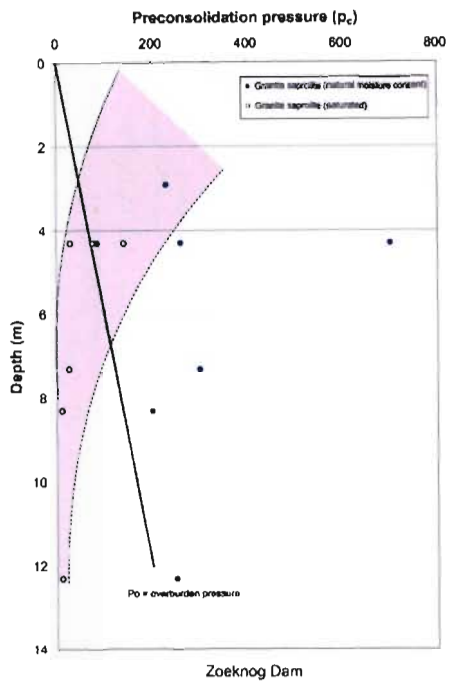

Figure 12.3. Relationship of p_c with depth as determined by Partridge *et al.* (1984) at Zoeknog Dam (shaded area represents p_c envelope for saturated samples).

The compression index (C_c) was calculated from the e-log p curves (refer to Table 12.2 and Figures 12.1a to i) with the value of C_{cNMC} ranging from 0,17 to 0,53 which is typical of silty material. Lower values were obtained for C_{cSAT} showing the softening of the material under saturation. These results are similar to those found by Nouvais-Ferreira and Fonesca (1988) in their study of granite saprolite in Portugal (Table 12.3). Partridge *et al.* (1984), in their study of the granite saprolite at Zoeknog Dam also found similar values of C_{cNMC} ranging from 0,13 to 0,38 and C_{cSAT} ranging from 0,18 to 0,33. Although Brummer (1980), Wallace (1973), Sowers (1963) and Partridge *et al.* (1984) managed to define tentative relationships between C_c and initial void ratio (Figures 12.4 and 12.5), no such relationship could be established for the weathered granite from this study.

Table 12.3. Comparative values of C_c and p_c for saprolitic soil from granite in Portugal studied by Nouvais-Ferreira and Fonesca (1988).

Stress path values	C_c	p_c (kPa)
< 100 kPa	0,024 - 0,037	
> 316,8 kPa	0,080 - 0,232	100 - 150

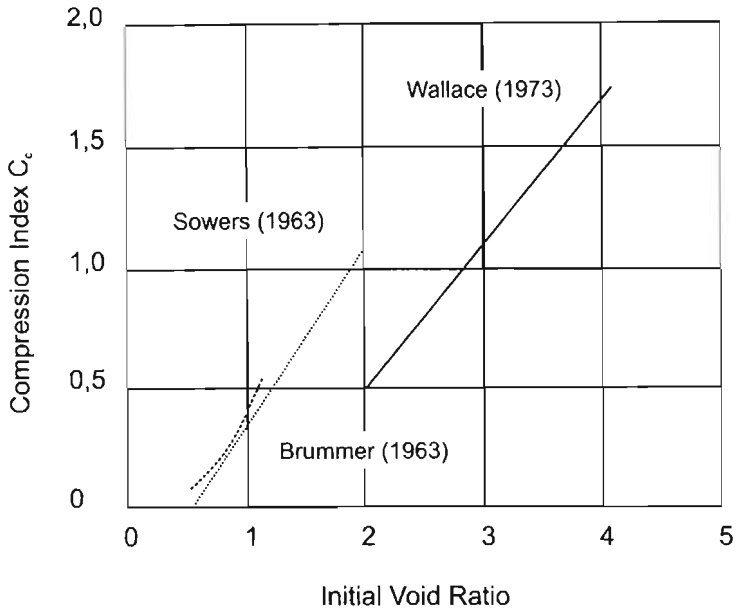

Figure 12.4. Compression index correlations with initial void ratio.

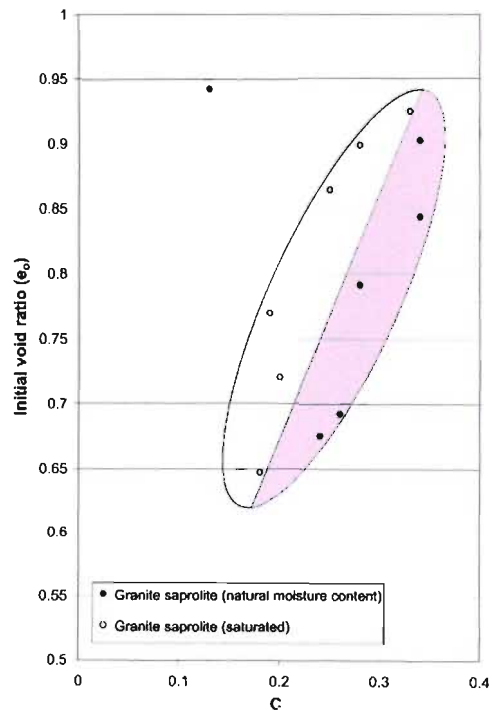

Figure 12.5. Relationship of C_{cnmc} and C_{csat} and initial void ratio for granite saprolite at Zoeknog Dam. Shaded area encompasses majority of samples at natural moisture content.

Of particular concern with regard to the compressibility of saprolitic soils is the fact that they often exhibit a metastable structure leading to collapsible behaviour under consolidation. This mechanism of soil collapse is well understood and according to Schwartz (1985), a collapsible soil may be defined as that which can withstand a relatively large imposed stress with small settlements at low *in situ* moisture content, but which exhibits a decrease in volume and associated notable settlement with no increase in applied stress upon saturation. This decrease in volume is associated with collapse of the soil structure where the changes in compression characteristics are brought about by a decrease in the negative pore pressure (capillary tension) resulting from partial saturation (Jennings and Knight, 1975, Day, 1996 and Dudley, 1970) and collapse or breaking of the respective soil elements.

The collapse phenomenum of weathered granites in South Africa was first documented in the 1950's by Jennings and Knight (1956, 1957). Since this time, engineers have been aware of the settlement problems that can arise due to the collapse of completely weathered granite material. The granite saprolite at Injaka Dam is no exception and exhibits a significant degree of metastability.

The main variables that govern the amount of one dimensional collapse are the soil type, moisture content, dry density and applied vertical pressure. However, a number of criteria are required for a soil to exhibit collapse potential :

- The soil must have a high porosity and some degree of strength i.e. a collapsible fabric.

- The soil must be in a condition of partial saturation as collapse settlement does not occur in soils below the water table. Jennings and Knight (1975) suggested a critical degree of saturation above which collapse will not occur. This depends upon the grain size distribution and the following guidelines were presented :

  Grain size 1-6 mm (fine gravels): S_r = 6-10%
  Grain size 150-2μm (fine silty sands): S_r = 50-60%
  Grain size 150-0,2μm (clayey silts) : S_r = 90-95%

  Errera (1977) also demonstrated that for residual granite this value appears to be 52%. Schwartz (1985) has also shown that some relationship exists between collapse behaviour and the particle size distribution.

- There must be an increase in moisture content which serves as the triggering mechanism for collapse settlement to occur. The rate of collapse is dependent upon the rate of saturation.

- The soil needs to be subjected to an imposed pressure greater than overburden pressure before collapse will take place.

Using the method proposed by Jennings and Knight (1957), the percentage collapse at an applied pressure of 200 kPa was determined from the double oedometer tests and is summarised in Table 12.4. These results are comparable with the collapse potential values achieved using the single oedometer collapse potential test (Table 12.5).

Table 12.4. Percentage collapse as determined from double oedometer tests.

Sample	Material type	Collapse at applied pressure = 200 kPa
LF 18	Granite saprolite with residual soil patches	2,4%
LF 19	Granite saprolite	2,6%
LF 20	Granite saprolite	7,6%
LF 21	Granite saprolite	0,5%
LF 22	Granite saprolite	3,0%
LF 25	Granite saprolite	1,8%
RF 10	Granite saprolite	4,0%
RF 6	Granite saprolite	3,3%
RF 4	Granite saprolite	2,0%

12.3 Consolidation characteristics from single oedometer collapse potential tests

Single oedometer collapse potential tests as described by Jennings and Knight (1975) were also carried out to determine the collapse potential characteristics of the weathered granite. This test involves loading an undisturbed specimen at natural moisture content in the oedometer up to a given load. At this point the specimen is flooded and the resulting collapse strain is recorded. The specimen is then subjected to further loading. The resulting typical oedometer curve is shown in Figure 12.6 where the collapse potential is defined. The collapse potential of five samples of granite saprolite with residual soil patches and twenty-nine granite saprolite samples from the six sample traverses were tested.

12.3.1 Specimen preparation

Specimens measuring 76 mm in diameter with an initial height of 25 mm were cut from the block samples. For all tests, a floating ring oedometer was used with a porous stone provided at the top and bottom of the specimens. The following load increments were applied to the specimens 25, 89, 191,

381 and 762 kPa, with flooding carried out at 191 kPa. Subsequent tests were conducted on selected samples with flooding at a higher applied stress of 381 kPa. Hence, the degree of collapse has to be qualified in terms of the level of loading at which flooding takes place.

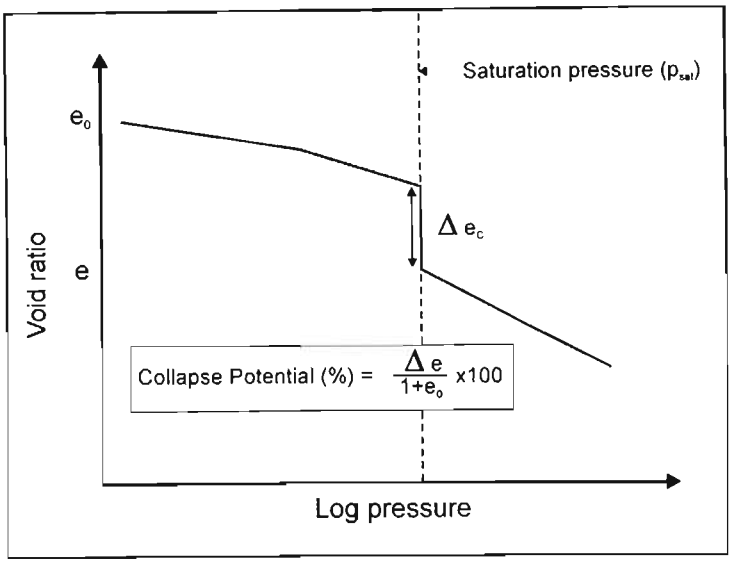

Figure 12.6. Typical oedometer curve from collapse potential test showing definition of the collapse potential.

12.3.2 Results from single oedometer collapse potential tests

Table 12.5 and Figures 12.7a to f illustrate the collapse potential values using an applied saturation pressure of 191 kPa (and 381 kPa for samples from Traverse 5 - Figure 12.7g). The collapse potential (CP) varied both laterally and with depth, with a general decrease in collapse with increasing depth and increasing dry density (Figure 12.8), despite some inherent variability. The granite saprolite with residual soil patches exhibited a variable CP at 191 kPa, ranging from 0,61% to 5,69%, whilst the granite saprolite exhibited values between 0,14% and 5,83%. No samples of highly weathered granite could be tested in the oedometers as they were too brittle to be cut into an oedometer ring. Figure 12.8 also shows the criteria as suggested by Brink (1996) indicating the maximum possible dry density at which collapse of weathered granite soils ("residual granite") is likely to occur. It can be seen that for a dry density above 1600 kg.m^{-3}, CP can be expected to be less than 1% for this material.

Although only seven samples were tested at the higher saturation pressure of 381 kPa, a distinct increase in collapse can be observed with the granite saprolite with residual soil patches increasing from 2,45% to 7,96%. The granite saprolite also showed a substantial increase in collapse with values

Table 12.5. Collapse potential characteristics for granite saprolite from Traverses 1 to 6 (saturation at 191 kPa and 381 kPa where shown).

SAMPLE	DEPTH (m)	SPECIFIC GRAVITY	S_R (%)	W (%)	ρ_b (kg.m^{-3})	ρ_d (kg.m^{-3})	C.P. (%) 191 kPa	C.P. (%) 381 kPa
Traverse 1								
RF 12*	1,0	2,71	71,9	22,6	1873	1463	0,61	-
RF 10	3,5	2,61	44,6	15,5	1642	1369	3,91	-
RF 9	4,9	2,64	42,2	15,3	1639	1349	5,83	-
RF 8	5,7	2,64	38,7	7,9	1892	1715	0,32	-
RF 7	6,6	2,62	58,2	11,1	1998	1747	3,01	-
Traverse 2								
RF 6	2,5	2,67	59,1	18,1	1795	1469	0,86	-
RF 5	4,8	2,62	48,1	16,3	1649	1388	0,07	-
RF 4	6,9	2,63	34,3	12,5	1534	1342	0,14	-
RF 3	9,2	2,65	45,0	14,4	1694	1434	1,47	-
Traverse 3								
LF 7*	1,1	2,64	40,5	12,7	1659	1444	5,69	-
LF 8	2,8	2,65	48,3	13,6	1768	1518	3,27	-
LF 9	4,0	2,61	41,3	10,7	1760	1557	2,26	-
LF 10	5,5	2,63	68,9	21	1835	1460	1,14	-
LF 11	6,5	2,68	57,5	20,5	1674	1371	1,42	-
LF 12	7,3	2,64	65,0	19,1	1826	1487	2,24	-
LF 13	7,7	2,63	34,6	4,8	2089	1927	0,75	-
Traverse 4								
LF 1*	0,9	2,58	39,4	5,6	1610	1478	3,38	-
LF 2	2,4	2,65	39,4	12,9	1654	1419	2,89	-
LF 3	3,8	2,66	46,1	14,9	1695	1430	3,11	-
LF 4	4,5	2,66	60,2	16,9	1780	1523	0,82	-
LF 5	5,2	2,63	71,2	15,3	1989	1680	0,55	-
LF 6	5,5	2,67	65,8	22,4	1773	1399	0,61	-
Traverse 5								
LF 18*	1,1	2,68	46,8	15,3	1656	1436	2,45	7,96
LF 19	2,3	2,65	53,6	19,5	1627	1361	3,79	6,41
LF 20	3,2	2,62	43,6	16,9	1535	1313	3,62	-
LF 21	4,0	2,62	55,1	21,2	1591	1313	1,66	2,62
LF 22	5,1	2,61	40,6	14,2	1569	1373	5,14	5,04
LF 24	5,7	2,62	60,3	20,9	1667	1379	0,04	3,11
LF 25	6,2	2,67	32,3	8,7	1676	1541	1,44	3,62
LF 26	7,2	2,58	45,4	13,2	1689	1492	1,22	2,02
Traverse 6								
RF 17*	2,2	2,66	50,9	15,1	1712	1487	0,92	-
RF 18	3,8	2,72	40,7	15,3	1551	1345	4,05	-
RF 20	5,2	2,61	54,8	18,5	1644	1387	0,16	-
RF 21	6,1	2,60	46,0	15,3	1607	1394	0,10	-

* Granite saprolite with residual soil patches.

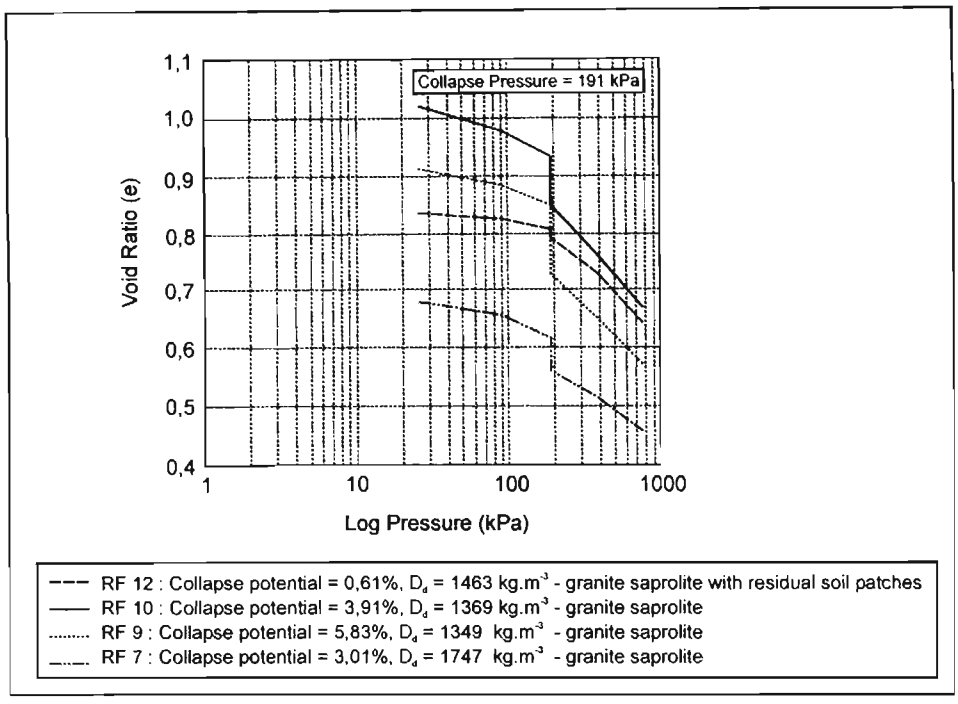

Figure 12.7a. Collapse potential curves for samples from Traverse 1.

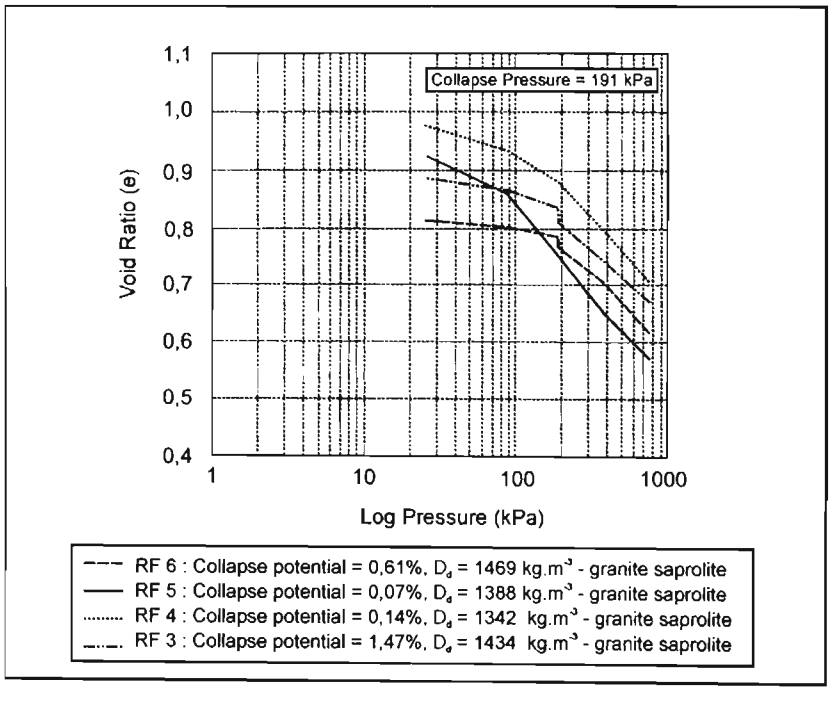

Figure 12.7b. Collapse potential curves for samples from Traverse 2.

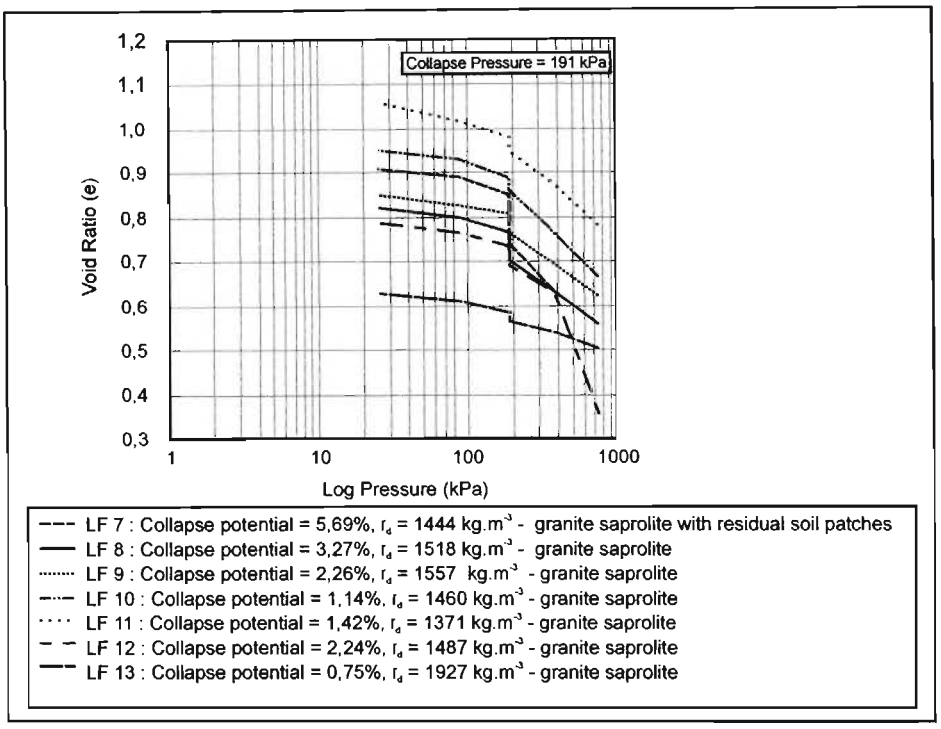

Figure 12.7c. Collapse potential curves for samples from Traverse 3.

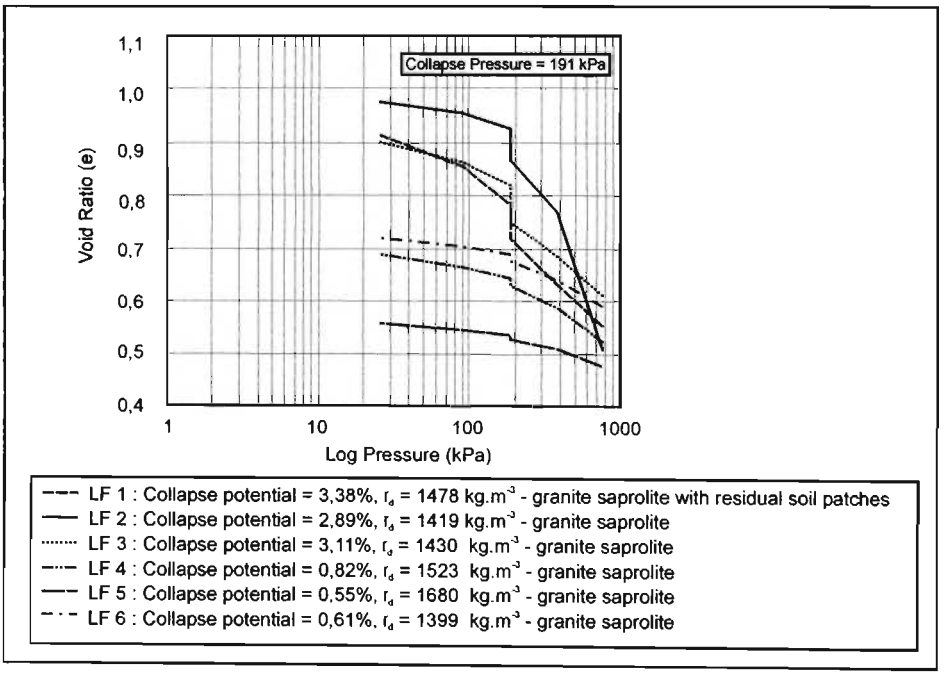

Figure 12.7d. Collapse potential curves for samples from Traverse 4.

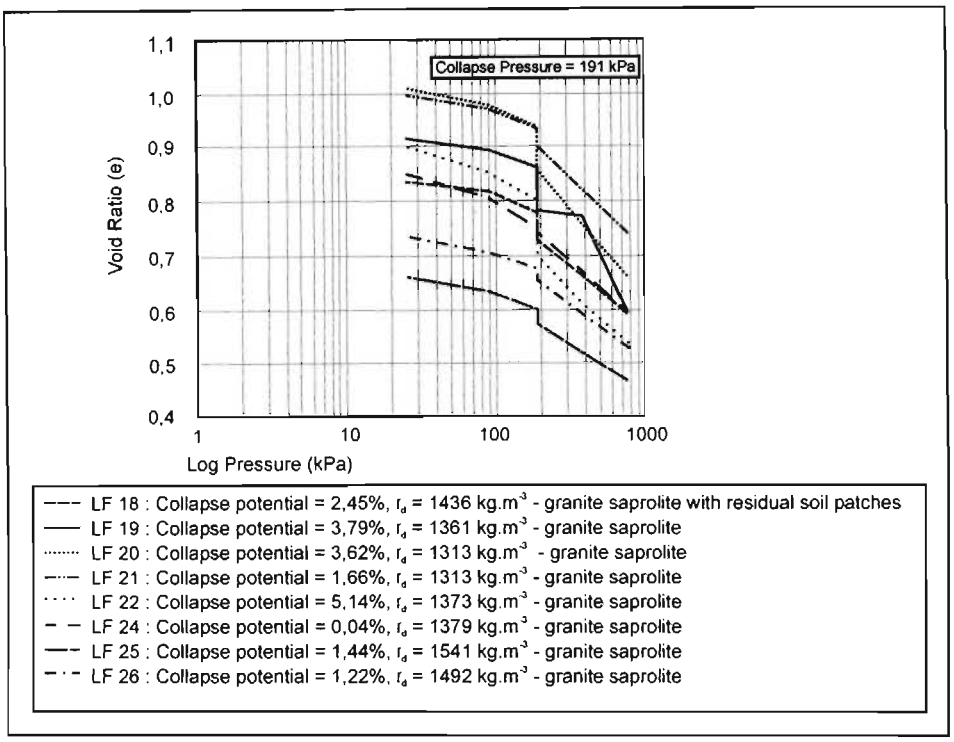

Figure 12.7e. Collapse potential curves for samples from Traverse 5.

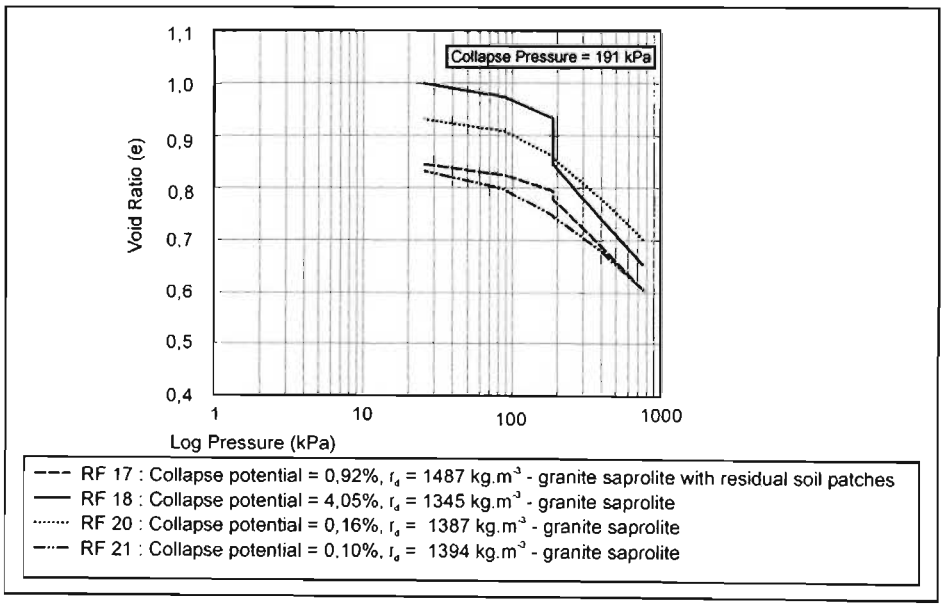

Figure 12.7f. Collapse potential curves for samples from Traverse 6.

generally increasing by 150 to 250%. The very much higher value for LF 24 and lower value for LF 22 can probably be attributed to the heterogeneity of the material or limitations with regard to the test method which include sample disturbance, small specimen thickness in relation to maximum particle size or to bedding errors in the measurement of vertical displacement.

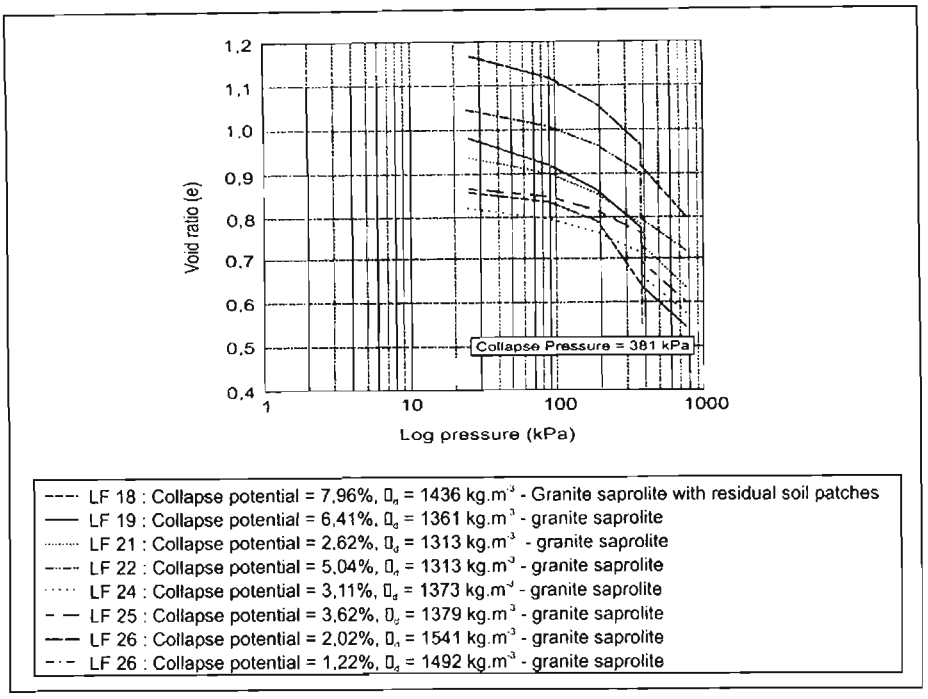

Figure 12.7g. Collapse potential curves for samples from Traverse 6 (saturation at 381 kPa).

From Figures 12.7a to f it can be seen that all specimens exhibit an initial stiffness which generally increases with decreasing void ratio (as shown by the much flatter portions of the curves at the start of loading for the samples with lower void ratios). The collapse potential of the saprolite can be attributed to three components, namely, fabric, permeability and dispersivity. Haskins *et al.* (1998b) presented a summary of the following description of the collapse process shown in Figure 12.9. During flooding of the oedometer specimens, saturation occurred almost instantaneously. The high porosity and moderate permeability (1.4 x 10^{-4} to 3.1 x 10^{-5} cm.s^{-1} - calculated from falling head tests) of the samples enabled this to occur. During saturation the clay particles and aggregates undergo softening. It is also thought that the dispersivity of the soil partially disrupts or loosens the interlocking fabric as the clays undergo deflocculation. The softened and disrupted fabric enhances the movement of water through the specimen resulting in accelerated saturation. The initial stiffness of the soil can be attributed to the relict interlocking fabric of the granite and the fact that the skeletal feldspar grains may account for some component of strength under partially saturated conditions. Once saturated, the deflocculation

of the clays partially disrupts the relict fabric, simultaneously reducing the strength component of the interlock and effectively increasing the load on the skeletal grains resulting in their collapse. This can clearly be seen when comparing the oedometer curves of the same specimens but with saturation at different applied stresses (compare Figures 12.7e and g). Even when the sample is loaded to 381 kPa under natural moisture conditions, the material still exhibits a reasonable stiffness. This is only lost once flooding occurs.

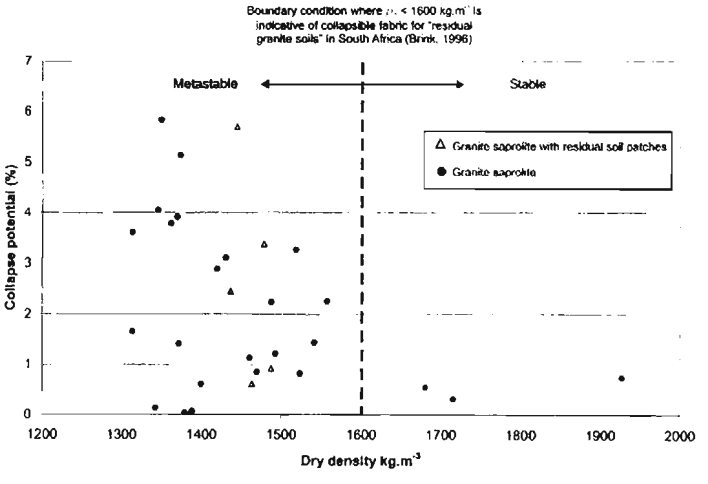

Figure 12.8. Relationship of collapse potential and dry density.

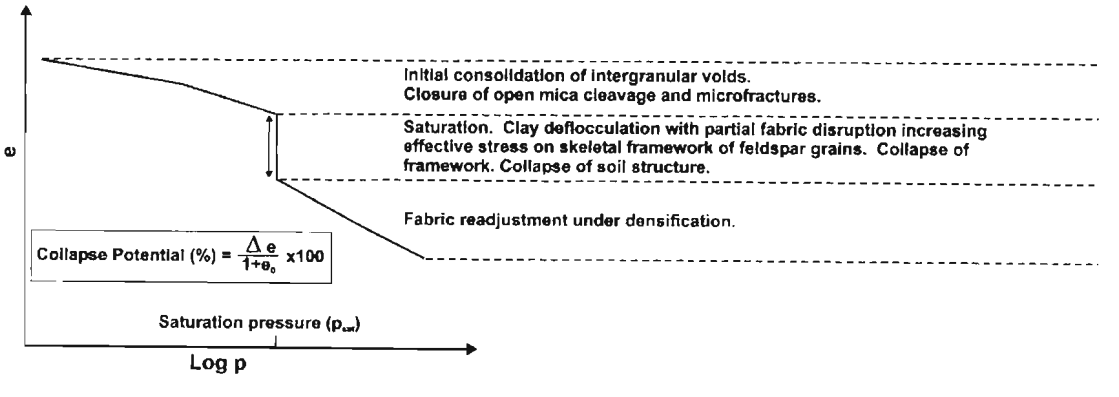

Figure 12.9. Explanation of one dimensional collapse potential behaviour for granite saprolite from Injaka Dam (after Haskins *et al.*, 1998b).

Partridge *et al.* (1984 and 1990) showed similar collapse potential results for the granite saprolite at Zoeknog Dam where values ranging from 0 to 11,8% (average = 3,82%) were measured for saturation pressures of 200kPa. They also noticed a distinct increase in collapse potential at a higher saturation pressure of 400kPa where values ranged from 4,57 to 12,10% (average = 8,01%) and a tentative relationship of decreasing collapse potential with increasing dry density (Figure 12.10). They also found

that despite the significant variation of collapse potential, dry density values in excess of 1600kg.m^{-3} showed collapse potentials less than 1%.

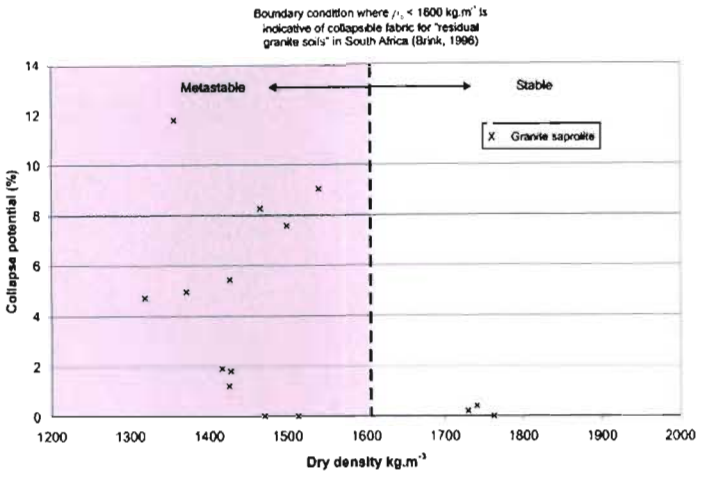

Figure 12.10. Relationship of collapse potential and dry density for Zoeknog Dam granite saprolite.

Falla (1985), was able to determine a range of collapse potential values for granite saprolite residing on or below the African surface in the Johannesburg area. His summary results are broadly comparable to that found at Injaka Dam with collapse potential results averaging between 2 and 5% but ranging from 0 to as high as 17%.

In accordance with the findings of Jennings and Knight (1957) and in order to determine the effect of moisture content variation on collapse settlement, a plot of collapse potential against the degree of saturation (S_r) is shown in Figure 12.11. Although there is some variation, this shows that the granite saprolite undergoes a significant increase in collapse settlement when S_r is less than 60%. This value is very similar to the critical degree of saturation value proposed by Jennings and Brink (1975) for "residual granite" (Figure 12.12). As shown by this figure, a good relationship exists between the particle size distribution and collapse settlement of various other soils with coarser-grained soils showing a lower critical degree of saturation.

Partridge *et al.* (1984 and 1990) found a similar relationship for the granite saprolite at Zoeknog dam, however with considerably more variation. Nevertheless, a general trend can be observed in Figure 12.13 which shows that where S_r is less than 70% a considerable increase in collapse settlement may be expected.

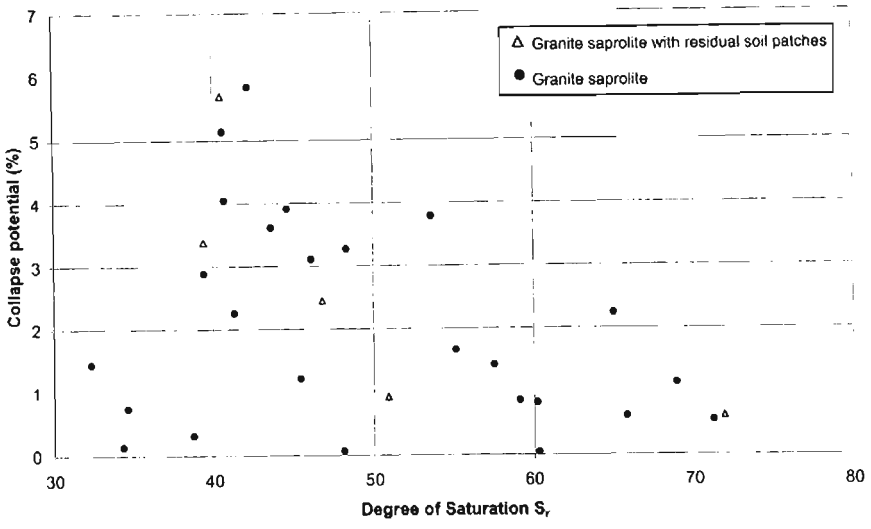

Figure 12.11. Collapse potential as a function of degree of saturation (S_r).

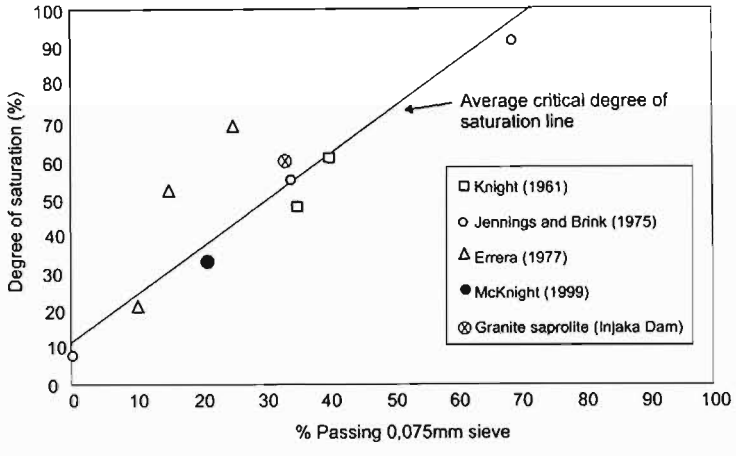

Figure 12.12. Critical degree of saturation (S_r) found by other studies.

An analysis of the coefficients of consolidation (c_v) and volume compressibility (m_v) during the collapse potential testing of the samples provides insight into the consolidation behaviour of the saprolite. Values for c_v and m_v at the specific load increments are presented in Table 12.6 and this shows that the value of the coefficient of volume compressibility (m_v) generally decreases with increased loading. After saturation however, there is often an increase in the value of m_v which again decreases at higher loading. According to Northmore *et al.* (1996), this increase suggests a loosening of the soil structure as it becomes more plastic. For a loading between 381 and 763 kPa, m_v ranges from 0,0935 to 0,2813 $m^2.MN^{-1}$.

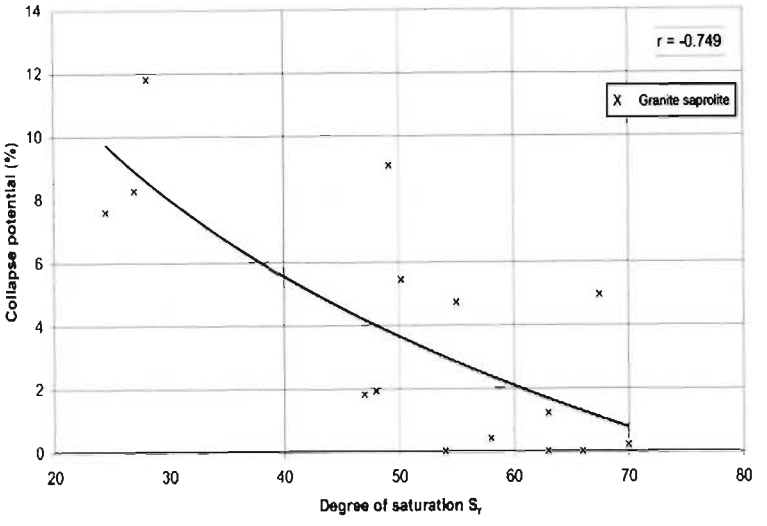

Figure 12.13. Collapse potential as a function of degree of saturation (S_r) for granite saprolite at Zoeknog Dam.

The high values for the coefficients of consolidation (c_v) for the saprolites suggests that consolidation occurs rapidly. In fact, in many instances, primary consolidation occurs within the first four minutes of loading. For a loading between 381 kPa and 763 kPa, c_v values range from 26,3 to 45,6$m^2.year^{-1}$ for all samples. Upon flooding in the oedometer, specimens of granite saprolite become saturated almost instantaneously. Figure 12.14 shows a plot of collapse settlement versus square root time for typical samples of granite saprolite. Note that in this figure the majority of collapse settlement occurs within four minutes of loading. Day (1996), referred to this portion of the consolidation curve as primary collapse. The remaining portion of the consolidation curve is termed secondary collapse. Figure 12.14 also shows how the time for 90% collapse is greatly extended when collapse is numerically small. Booth (1975) found similar results in his investigation of collapse of compacted fill and suggested that the clay bridges carried a portion of stress under these circumstances. With regard to the saprolite, slower consolidation rates for smaller collapse settlements can be attributed to a similar process where the fabric of the samples exhibiting low collapse settlements contain lower clay contents and thus a stronger interlocking fabric, and the saprolite also possesses a lower void ratio reducing the permeability and hence movement of water through the sample.

Table 12.6. Values for coefficients of consolidation and volume compressibility for samples from Traverses 1 to 6, calculated from collapse potential tests (* granite saprolite with residual soil patches).

Sample	Depth	Specimen load range	0-25kPa	25-89 kPa	89-191kPa	191kPa	191-382kPa	382-763kPa	Collapse potential (%)
Traverse 1									
RF 12*	1,0	m_v	1,1504	0,1038	0,0825	0,0631	0,1910	0,1364	0,614
		c_v	38,4	1,3	7,1	1,9	9,9	10,5	
RF 10	3,5	m_v	0,7834	0,3188	0,2456	0,4281	0,2617	0,1469	3,912
		c_v	14,3	16,4	4,7	4,4	5,1	7,5	
RF 9	4,9	m_v	1,1457	0,2307	0,1873	0,6507	0,2464	0,1333	5,834
		c_v	47,3	13,8	19,3	6,3	9,4	4,5	
RF 8	5,7	m_v	0,7726	0,1241	0,1141	0,0325	0,0857	0,0650	0,317
		c_v	84,4	10,5	14,0	1,9	19,5	18,7	
RF 7	6,6	m_v	0,3380	0,2098	0,2265	0,3198	0,1908	0,1017	3,013
		c_v	9,5	2,7	4,2	2,3	4,5	4,1	
Traverse 2									
RF 6	2,5	m_v	1,0733	0,1188	0,0974	0,0891	0,1866	0,1448	0,859
		c_v	21,0	1,7	3,8	4,9	18,7	17,1	
RF 5	4,8	m_v	1,4115	0,5471	0,5916	0,0076	0,3006	0,1372	0,069
		c_v	33,5	5,0	28,5		20,0	6,5	
RF 4	6,9	m_v	0,4550	0,3557	0,2807	0,0146	0,2372	0,1366	0,140
		c_v	21,3	5,7	10,0		12,9	16,5	
RF 3	9,2	m_v	0,3473	0,2103	0,1484	0,1522	0,1959	0,1090	1,469
		c_v	21,2	9,2	7,0	1,5	3,2	1,4	
Traverse 3									
LF 1*	0,9	m_v	1,4978	0,4683	0,3935	0,3821	0,2722	0,1299	3,381
LF 2	2,4	m_v	0,4152	0,1603	0,1461	0,3032	0,2896	0,4577	2,888
LF 3	3,8	m_v	1,2530	0,3184	0,2512	0,3415	0,2224	0,1107	3,110
LF 4	4,5	m_v	0,8475	0,2477	0,1249	0,0858	0,1517	0,1089	0,823
LF 5	5,2	m_v	0,1920	0,1312	0,0680	0,0550	0,0747	0,0513	0,548
LF 6	5,5	m_v	1,0988	0,1488	0,1001	0,0636	0,1132	0,0853	0,613
Traverse 4									
LF 7*	1,1	m_v	0,1923	0,1741	0,2133	0,6171	0,3385	0,1284	5,690
		c_v	0,4	21,1	5,1	1,7	0,7	4,6	
LF 8	2,8	m_v	1,0628	0,2137	0,1788	0,3512	0,2368	0,1214	3,270
		c_v	15,4	2,0	4,2	5,3	3,0	2,2	
LF 9	4,0	m_v	0,5868	0,2044	0,1090	0,2362	0,2128	0,1220	2,257
		c_v	2,5	7,8	19,7	6,3	8,1	2,4	
LF 10	5,5	m_v	1,1345	0,2002	0,2288	0,1205	0,2947	0,1550	1,136
		c_v	14,9	2,7	19,3	2,7	10,2	3,9	
LF 11	6,5	m_v	0,1920	0,3050	0,2012	0,1472	0,2103	0,1380	1,418
		c_v	1,4	21,7	0,9	0,2	1,2	10,3	
LF 12	7,3	m_v	1,1281	0,2082	0,1943	0,2399	0,1891	0,5324	2,241
		c_v	-	-	-	-	-	-	
LF 13	7,7	m_v	1,1457	0,1851	0,1457	0,0783	0,1108	0,0630	0,748
		c_v	-	-	-	-	-	-	
Traverse 5									
LF 18*	1,1	m_v	1,0875	0,19	0,191	0,2619	0,2195	0,177	2,447
		c_v	95,5	91,8	50,1	30,6	44,7	26,3	
LF 19	2,3	m_v	1,433	0,1639	0,1707	0,4114	0,042	0,2813	3,788
		c_v	224,1	213,8	33,3	21,8	28,9	41,9	
LF 20	3,2	m_v	0,4475	0,2472	0,1977	0,3851	0,321	0,1482	3,615
		c_v	230,1	35,8	96,0	32,6	20,5	26,4	
LF 21	4,0	m_v	0,4203	0,2081	0,1814	0,1723	0,223	0,1259	1,681
		c_v	231,4	56,5	24,3	33,8	31,9	45,6	
LF 22	5,1	m_v	0,5895	0,4036	0,2874	0,5729	0,2938	0,1256	5,14
		c_v	222,0	53,3	16,5	46,4	26,8	37,5	
LF 24	5,7	m_v	1,4055	0,3682	0,3264	0,0047	0,2285	0,1319	0,043
		c_v	213,2	50,3	47,6		44,1	40,2	
LF 25	6,2	m_v	1,249	0,2701	0,2276	0,1547	0,1832	0,0935	1,442
		c_v	96,7	51,8	49,8	30,7	29,2	42,5	
LF 26	7,2	m_v	0,6732	0,2432	0,1894	0,127	0,201	0,1126	1,218
		c_v	230,0	55,7	53,6	52,1	31,7	29,2	
Traverse 6									
RF 17*	2,2	m_v	0,5232	0,1616	0,1608	0,0953	0,2468	0,1486	0,922
		c_v	-	-	-	-	-	-	
RF 18	3,8	m_v	0,6992	0,2211	0,2124	0,4389	0,2968	0,1505	4,053
		c_v	-	-	-	-	-	-	
RF 20	5,2	m_v	0,7877	0,2246	0,2425	0,0163	0,2157	0,1298	0,156
		c_v	221,0	94,9	51,4	-	48,0	28,1	
RF 21	6,1	m_v	1,2391	0,307	0,304	0,011	0,1845	0,1302	0,103
		c_v	214,1	135,7	129,1	-	80,5	74,1	

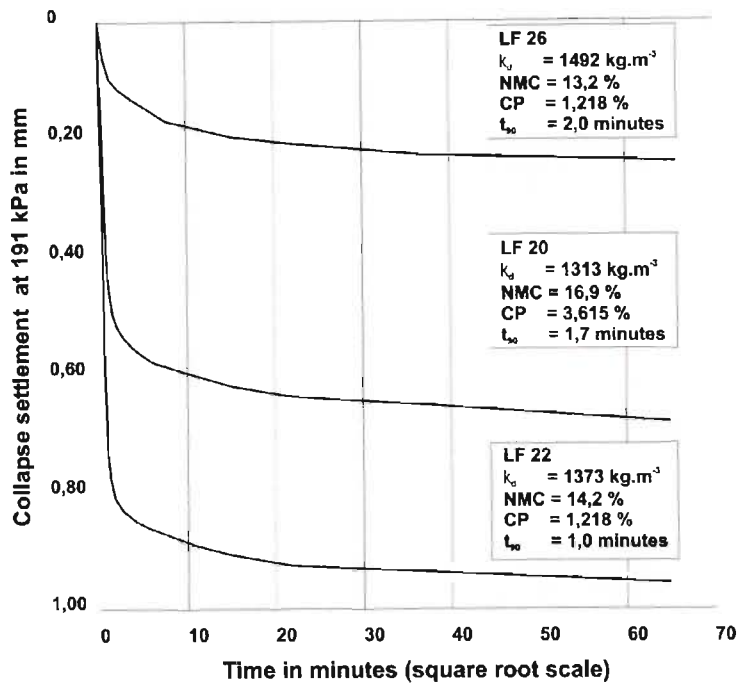

Figure 12.14. Typical curves of collapse settlement and square root time for granite saprolite.

12.4 Collapse potential using the triaxial apparatus with local strain instrumentation

For comparison with the double and single oedometer test results, two collapse potential tests were conducted in the triaxial apparatus using local strain instrumentation. Cost implications limited the number of tests to only two samples. These two undisturbed samples were retrieved after excavation of the dam foundation footprint on the left flank at a depth of 6m in the granite saprolite (Table 12.7).

12.4.1 Specimen preparation

The samples were placed in the triaxial cell at natural moisture content and the cell pressure was increased in increments up to 200 kPa before wetting the sample by flushing it with de-aired water at atmospheric back pressure. Full saturation was ensured by using sufficient back pressure to achieve high B-values. Linear variable differential transformers (LVDT's) were fitted to the middle of the specimen over a gauge length of 55mm. This technique avoids bedding errors which occur at the interface between the specimen and the ridged specimen ends in the cell. In this way the collapse

potential is measured with significantly more accuracy compared with conventional collapse potential tests using the oedometer. A layout of the apparatus used in shown in Figure 12.15.

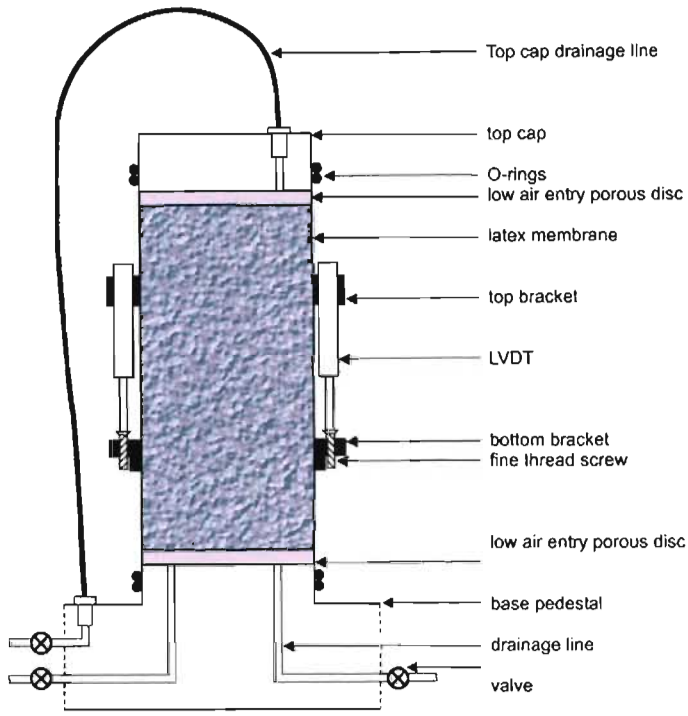

Figure 12.15. Triaxial collapse test apparatus (after Heymann and Rust, in press).

12.4.2 Results from triaxial collapse settlement tests

The results from these tests show a much lower collapse settlement than those observed from the single and double oedometer tests (Table 12.7). This can be explained by the much higher degree of saturation of these samples which as shown by Figure 12.11 implies lower collapse potential values. As with the double and single oedometer tests, the triaxial collapse potential tests also showed the granite saprolite to display no significant yield stress. This is shown in Figure 12.16 where a plot of effective stress against axial strain is illustrated for the two samples with neither curve showing an obvious yield point.

Table 12.7. Collapse potential results from triaxial testing.

Sample	Depth (m)	Dry Density (kg.m^{-3})	S_r (%)	Collapse Potential at 200 kPa (%)
CH 150,79	6,5	1444	80,0	0,30
CH 150,79	6,5	1461	76,5	0,04

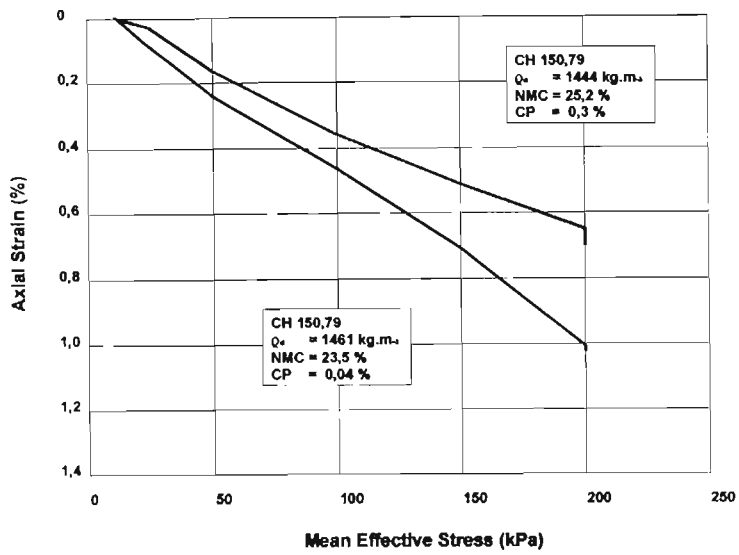

Figure 12.16. Typical e-p curves from triaxial collapse potential tests.

12.5 Collapse Settlement Indices

12.5.1 Introduction

A considerable amount of work has been conducted on quantifying parameters that qualify settlements associated with collapse. These include the previously discussed double oedometer test (Jennings & Knight, 1956), triaxial tests (Grigorian, 1967) and shear tests (Milovic, 1969). The main disadvantage of these tests is that they are specialised and time consuming and may in many cases be uneconomical to conduct in certain geotechnical investigations, as was the case for this study. Consequently, a number of collapse potential indices or criteria have been proposed. The applicability of these indices has been met with varied success depending upon the material type to which they have been applied and the majority of work done has concentrated on loess or loess-like materials due to their prevalent metastable characteristics.

12.5.2 Application of collapse settlement indices

Denisov (1951) was amongst the first to recognise that metastability of soils is determined to some extent by their natural porosity and based his criterion on an evaluation of the voids ratio at the natural moisture content and the liquid limit. He suggested that a soil may be metastable if it is capable of

absorbing enough water to take it up to or beyond the liquid limit and proposed that a soil may be metastable if :

$$\frac{e_L}{e_o} < 1 \qquad \text{(Eqn. 12.5.1)}$$

where e_L = void ratio at W_L
and e_o = void ratio at natural moisture content

Table 12.8 presents a summary of the results of various collapse settlement indices including the values obtained from Denisov's (1951) equation. A plot of the Denisov values against collapse potential suggests that granite saprolite with a Denisov value of less than 1 generally exhibits more than 3% collapse potential (Figure 12.17).

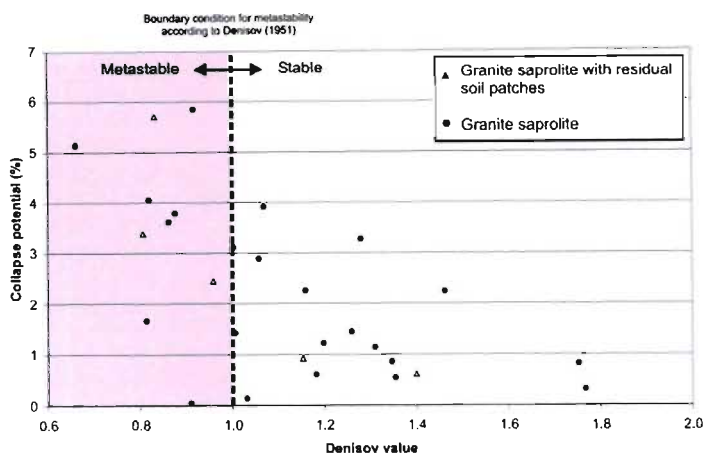

Figure 12.17. Relationship of Denisov values with collapse potential (%).

Gibbs & Bara (1962) presented Denisov's (1951) criterion in a graphical form (Figure 12.18), suggesting that a soil with high enough void space to retain its liquid limit moisture content at saturation is susceptible to collapse on wetting. Their method only applies if the soil is uncemented and the liquid limit is above 20%. As seen from the SEM and petrographic investigations the granite saprolite from Injaka Dam is uncemented and Section 10.2 shows the liquid limit to fall within this requirement. The Gibbs and Bara (1962) chart is divided into two regions by lines drawn at 100% S_r for soils with specific densities of 2,60 and 2,70. Soils which plot above the line of saturation are potentially metastable, whilst those which plot below the line behave as stable or heaving soils. This graphical criterion has been

Table 12.8. Collapse settlement indices for samples from Traverses 1 to 6.

Sample	Depth (m)	Denisov Value (Denisov, 1951)	Collapse index (i_c) (Feda, 1988)	Absolute collapse index(i_{ac}) (Feda, 1988)	Liquidity Index (LI) (Gibbs and Bara, 1962 & Handy, 1973)	Xd_{XRD}	Collapse potential (%)
Traverse 1							
RF12*	1,0	1,503	0,287	5,05	-0,216	0,86	0,614
RF10	3,5	1,006	0,804	10,13	-0,728	0,66	3,912
RF9	4,9	0,952	1,372	11,25	-1,183	0,45	5,834
RF8	5,7	1,220	-0,492	-5,17	-1,686	0,84	0,317
Traverse 2							
RF 6	2,5	1,32	0,17	2,12	-0,82	0,77	0,859
RF 5	4,8	1,11				0,63	0,069
RF 4	6,9	1,23	0,84	5,59	-2,75	0,82	0,140
Traverse 3							
LF 1*	0,9	0,81	2,22	10,20	-2,85	0,85	3,381
LF 2	2,4	1,03	0,80	7,04	-1,44	074	2,888
LF 3	3,8	0,98	0,99	11,44	-0,52	0,64	3,110
LF 4	4,5	1,30	-0,48	5,11	-0,80	0,60	0,823
LF 5	5,2	1,21	0,10	0,80	-0,64	0,67	0,548
LF 6	5,5	1,24	0,12	0,83	-1,54	0,80	0,613
Traverse 4							
LF 7*	1,1	0,83	1,70	12,77	-0,79	0,72	5,690
LF 8	2,8	1,13	0,16	1,54	-1,38	0,71	3,270
LF 9	4,0	0,95	0,41	2,81	-1,80	0,30	2,257
LF 10	5,5	1,25	0,19	2,27	-0,62	0,90	1,136
LF 11	6,5	0,99	1,00	6,23	-1,39	0,44	1,418
LF 12	7,3	0,98	-0,41	-3,93	-1,48	0,82	2,241
LF 13	7,7	1,56	-1,49	-13,73	-2,48	0,25	0,748
Traverse 5							
LF 18*	1,1	1,14	1,16	7,29	-1,60	1,00	2,447
LF 19	2,3	0,84	1,72	9,28	-1,41	1,00	3,788
LF 20	3,2	0,88	1,65	12,06	-1,34	0,84	3,615
LF 21	4,0	0,93	2,19	12,68	-0,79	0,40	1,661
LF 22	5,1	0,72	3,80	15,58	-1,27	0,56	5,140
LF 24	5,7	0,95	1,49	8,96	-0,8	0,84	0,043
LF 25	6,2	1,21	0,09	0,64	-2,41	0,90	1,442
LF 26	7,2	1,31	-0,11	-0,63	-2,89	0,26	1,218
Traverse 6							
RF17*	2,2	0,99	0,61	7,06	-0,65	0,70	0,922
RF 18	3,8	0,87	2,09	12,99	-1,5	0,57	4,053

* granite saprolite with residual soil patches

successfully applied to predicting subsidence at a number of dam and canal sites (Clemence & Finbarr, 1981).

The metastability as determined by the collapse potential values of the granite saprolite was analysed using this chart and a good relationship was obtained (Figure 12.19). In general, the chart showed that samples exhibiting a collapse potential greater than 3% are potentially metastable, whilst material exhibiting a collapse potential between 2 and 3% can be considered to be marginal in terms of its metastability. Material with a collapse potential of less than or equal to 1 can be considered to be potentially stable according to this method.

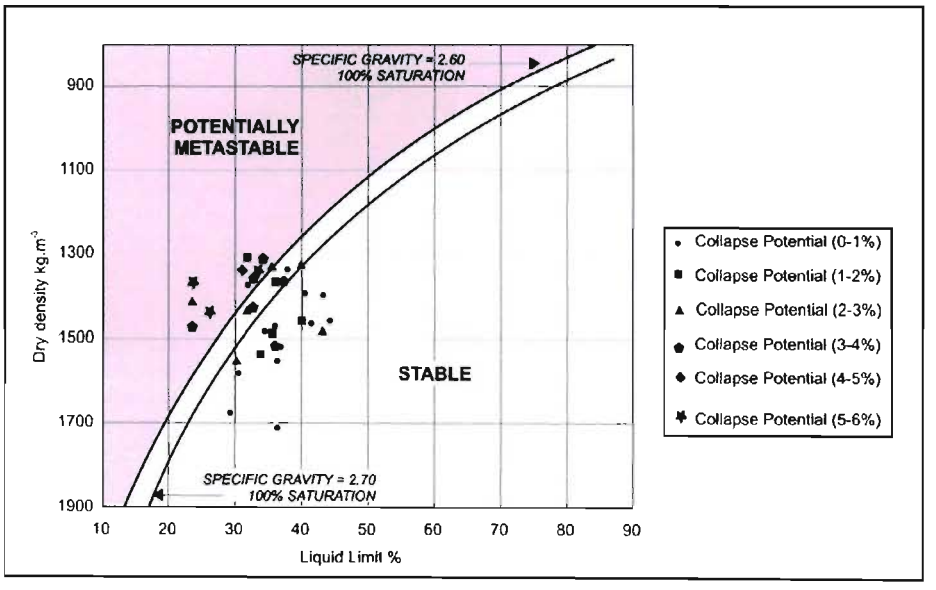

Figure 12.18. Stability diagram of Gibbs and Bara (1962) showing data from granite saprolite at Injaka Dam.

Feda (1966 and 1988), has arguably produced the most comprehensive work on collapse indices on his studies of loess. He proposes the collapse index i_c, (previously known as the subsidence index - K_L):

$$i_c = \frac{\frac{m}{S_r} - PL}{PI} \qquad \text{(Eqn. 12.5.2)}$$

where m = natural moisture content S_r = degree of saturation PL = plastic limit PI = plasticity index

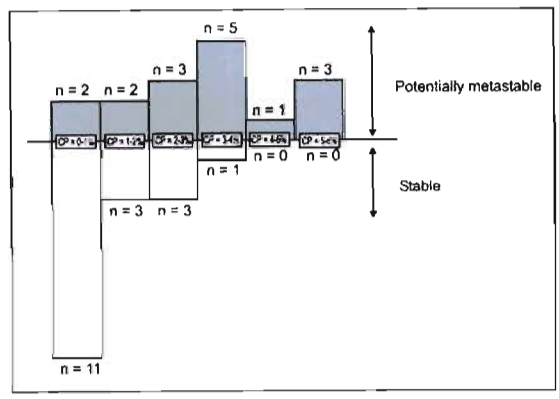

Figure 12.19. Applicability of Gibbs and Bara's (1962) graphical presentation of metastability (n = number of samples).

Feda stipulated that in order to use this criterion the soil must have a critical porosity greater than or equal to 40%. This requirement is satisfied by the granite saprolite from Injaka Dam site. Feda also proposed that the absolute collapse index, i_{ac}, could be used for collapse prediction where,

$$i_{ac} = \frac{m}{S_r} - PL \qquad \text{(Eqn 12.5.3)}$$

Collapse index (i_c) and absolute collapse index (i_{ac}) values for all of the samples are shown in Table 12.8. Feda suggested that if i_c was greater than 0,85 this was indicative of a metastable soil. A plot of i_c against percentage collapse potential shows a reasonable relationship (Figure 12.20) suggesting that when i_c is greater than 0,2 a collapse potential greater than 1% can be assumed. If Feda's criterion of 0,85 is used, collapse potential greater than 3% can be expected for this material. Figure 12.21 shows the relationship of i_{ac} with collapse potential and suggests that where i_{ac} is greater than 0, a collapse potential larger than 1% can be expected.

Gibbs and Bara (1962) and Handy (1973) have shown that when the saturation moisture content exceeds the liquid limit, collapse of the soil structure (in loess) from an increase in load is possible. They express this instability criterion in terms of the liquidity index defined as:

$$LI = \frac{w - PL}{L\,L - PL} \qquad \text{(Eqn. 12.5.4)}$$

where LI = liquidity index w = natural moisture content PL = plastic limit LL = liquid limit

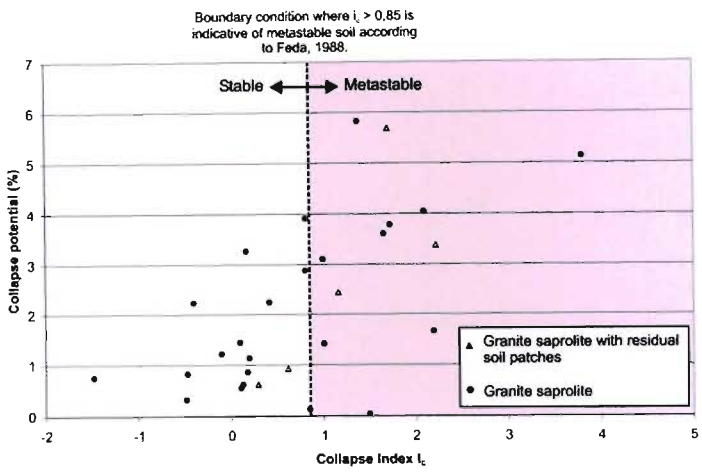

Figure 12.20. Relationship of collapse index (i_c) and collapse potential (%).

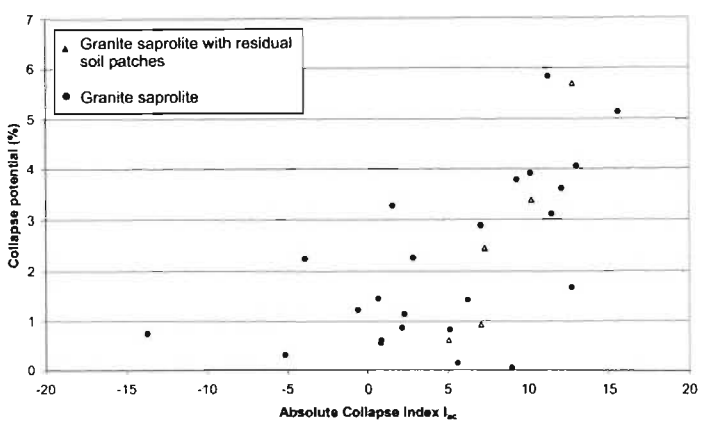

Figure 12.21. Relationship of absolute collapse index (i_{ac}) and collapse potential (%).

When the liquidity index approaches or exceeds a value of unity, experience has shown that collapse may occur. However, the liquidity index values for the granite saprolite correlate poorly with the actual

values of collapse potential (Table 12.8) and consequently it is considered a poor criterion for indexing the collapse settlement of this material.

Darwell *et al.* (1976), have developed a relationship between plastic limit, liquid limit and dry density which can be used to assess the possibility of metastability. They adapted Feda's collapse index i_c and rearranged this equation to include values for natural dry density and specific gravity:

$$LL + \frac{3}{17}PL < \frac{1}{0,85}\left[\frac{\rho_w}{\rho_d} - \frac{1}{G_s}\right] \qquad \text{(Eqn. 12.5.5)}$$

where ρ_w = bulk density ρ_d = dry density G_s = specific gravity LL = liquid limit PL = plastic limitt

This expression can be written as a series of parallel lines of liquid limit against plastic limit with each line being given a unique combination of natural dry density. One particular line is shown in Figure 12.22a. This line runs from the upper boundary line where LL = PL to the liquid limit axis where PL = 0. The area shaded in Figure 12.22a between the three line represents the inequality presented in Equation 12.5.5. Consequently, all points in this shaded region represent cases where the liquid and plastic limits are such that collapse index is greater than 0,85 for given values of dry density and specific gravity and thus any soil with indices located in this region would be metastable. To allow for the prediction of soils with a wide range of dry density and specific gravity values, a series of lines is drawn for these different values. Examples of these lines are shown in Figure 12.22b. The central line is the case in which G_s= 2,65 whilst the outer two lines represent G_s= 2,55 and G_s= 2,75 for the same dry density. Any specific gravity can be interpolated between these three lines or extrapolating outside of them if necessary. By varying the dry density, a series of these lines can be created as shown in Figure 12.22c.

To evaluate the metastability of a soil the following procedure is used. If a point given by the liquid and plastic limits of the soil lies to the left of the line corresponding to its dry density, then metastability is likely as the criteria of i_c being greater than 0,85 is met. In Figure 12.23, values for the granite saprolite at Injaka Dam are plotted as points whilst the trend for weathered granite derived from data given by Lumb (1962), Lamb (1962) and Little (1967) is plotted as a stippled area. It can be seen that for this stippled zone, metastability is possibly where the dry density is less than 1600 kg.m^{-3}. This corresponds to Brink's (1996) statement that collapsible soils characteristically have dry densities less than 1600 kg.m^{-3} and is confirmed by Figure 12.8.

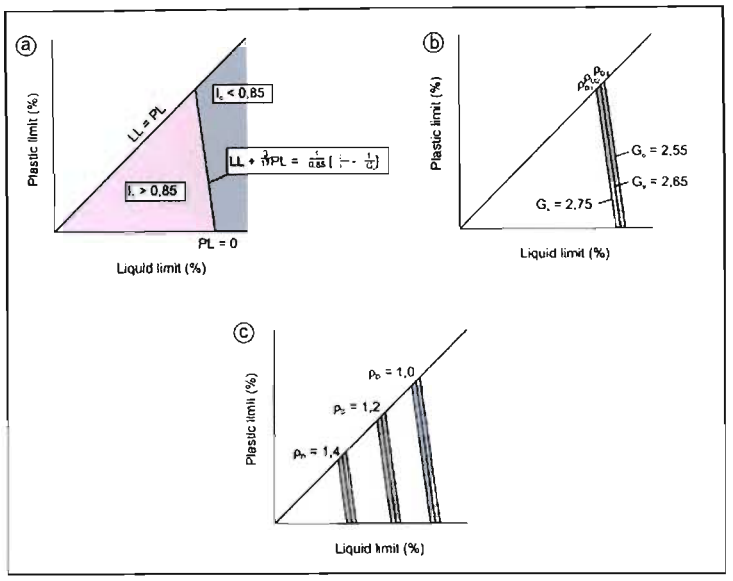

Figure 12.22a to c. Construction of Darwell *et al. 's* (1976) graphic method for determination of collapse settlement indices.

Each sample point for the granite saprolite at Injaka Dam was plotted to assess the likelihood of metastability. A good relationship between Darwell *et al. 's* (1976) chart and actual collapse potential values was obtained (Figure 12.24). It can be seen from this figure that Darwell *et al. 's* (1976) method shows the granite saprolite to be potentially metastable when exhibiting a collapse potential greater than 2%. Consequently, it can be seen that the application of the chart proposed by Darwell *et al.* (1976) can serve as a useful indicator for metastability of the granite saprolite at Injaka Dam.

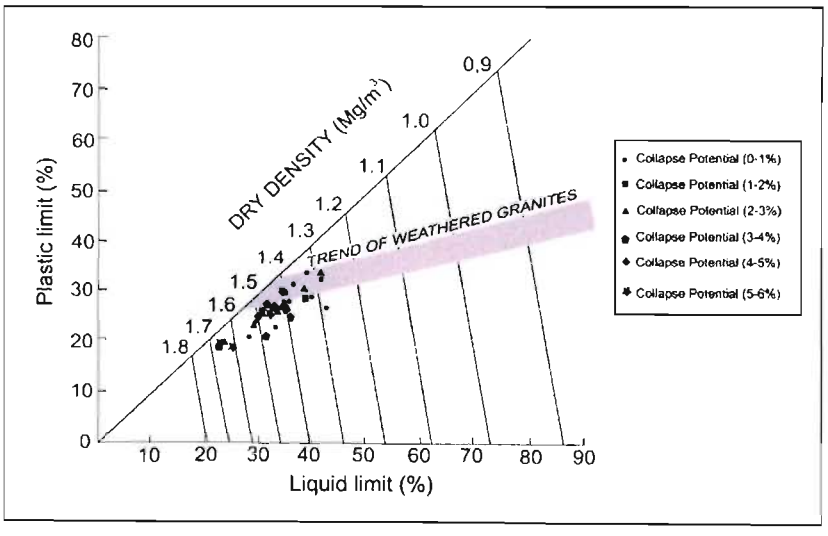

Figure 12.23. Stability chart of granite saprolite at Injaka Dam using Darwell *et al. 's* (1976) graphical method.

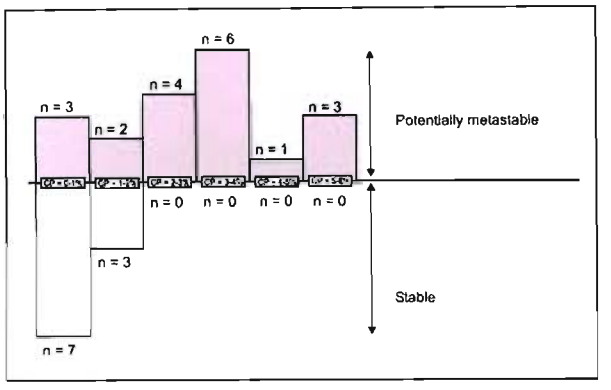

Figure 12.24. Applicability of Darwell *et al. 's* (1976) graphical method for indexing collapse settlement at Injaka Dam.

Baynes & Dearman (1978a) attempted to use the graphic form of Lumb's (1962) degree of decomposition (*Xd*) with void ratio as a metastability index. They used Darwell *et al. 's* (1976) suggestion that any material with a density below 1600 kg.m^{-3} can be considered to exhibit potential metastability. This criteria is represented in terms of void ratio on Figure 12.25 and is shown by the shaded area. Any material that falls within this shaded area in terms of its microfabric can be considered to be metastable. The results of collapse potential tests from this study have been plotted on this chart to determine its suitability as an indicator of metastability. Figure 12.26 shows the applicability of this chart to indexing the collapse potential of the granite saprolite at Injaka Dam. The relationship shows that this method categorises almost all samples as metastable and is unable to differentiate between the metastability of the saprolite. Thus this method cannot successfully be used to differentiate and index the collapse potential of granite saprolite.

In order to evaluate the collapse settlement indices for the granite saprolite at Zoeknog Dam a similar exercise was carried out for the limited number of samples that were tested by Partridge *et al.* (1984 and 1990). The findings from this exercise for the Denisov value, i_c and i_{ac} are presented in Figures 12.27a, b and c. It can be seen from these figures that a collapse potential of greater than 1,5% can be expected for a Denisov value of less than 1,6. A Denisov value of less than 1 generally does not show the material at Zoeknog Dam to exhibit any collapse potential and Denisov's (1951) criterion of a value less than unity for metastable conditions does not apply. Figures 12.27 b and c show a general increase in collapse potential with increasing i_c and i_{ac}, although the criterion for $i_c > 0,85$ for metastable conditions appears to be too high for this material.

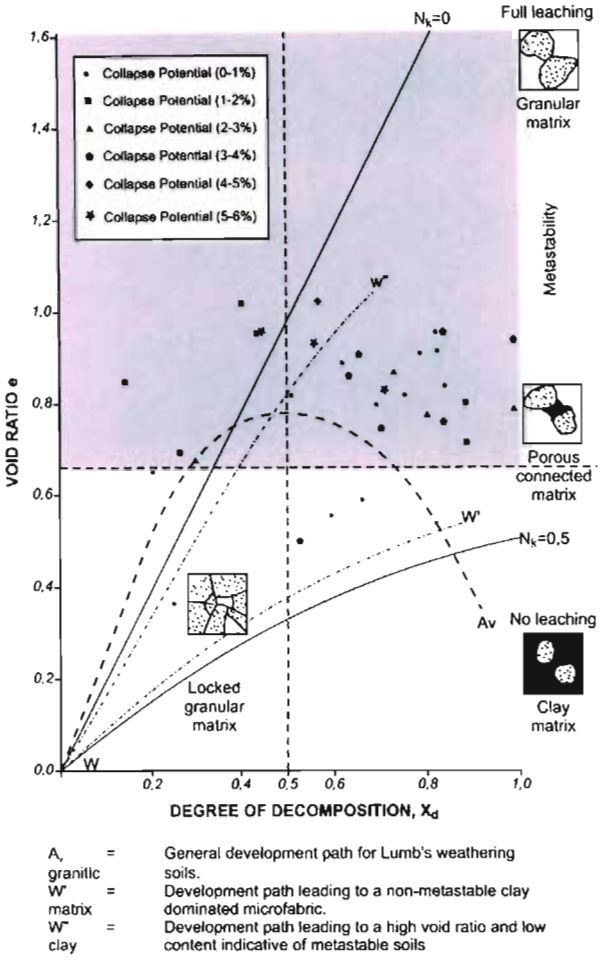

Figure 12.25. Indexing the collapse potential of granite saprolite using the e/*Xd* chart by Lumb (1962), after Baynes and Dearman (1978a).

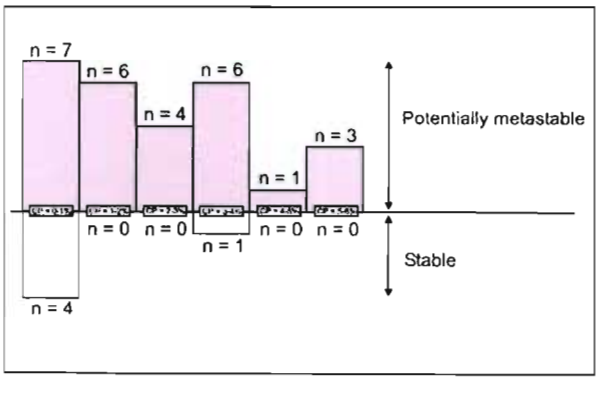

Figure 12.26. Applicability of Baynes and Dearman's (1978a) method of using e/*Xd* for indexing collapse settlement.

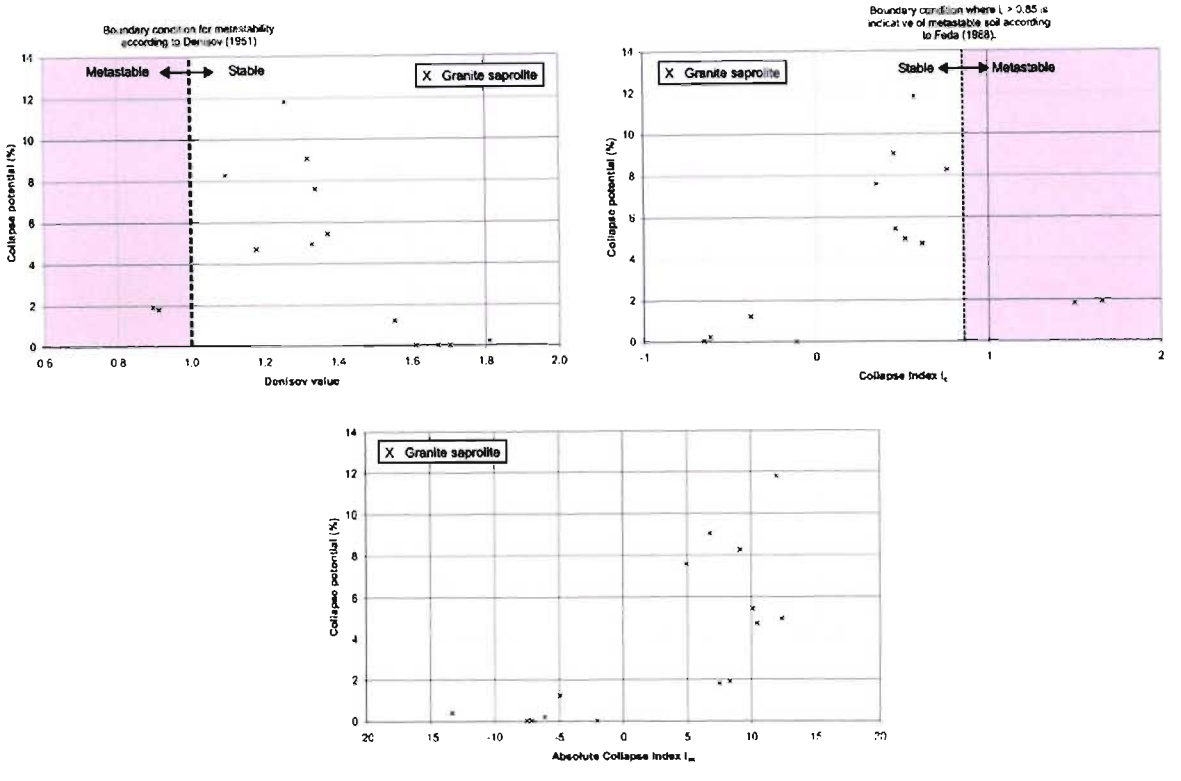

Figures 12.27a, b and c. Denisov values, i_c and i_{ac} values and collapse potential for Zoeknog Dam granite saprolite.

Figures 12.28 and 12.29 show the application of the Gibbs and Bara (1962) and Darwell *et al.* (1976) method respectively, for the Zoeknog Dam granite saprolite. It can be seen from these figures that these graphical methods are not considered suitable for the granite saprolite at Zoeknog Dam. The likely reason for this is that these samples have slightly higher liquid and plastic limits for equivalent density material as would be found at Injaka Dam. Chapter 10 has noted that the Zoeknog Dam samples have slightly higher clay contents which could account for such behaviour. It is to be noted in conclusion then, that such collapse potential indices should be treated with care when being applied to particular materials and general relationships should be established before employing such indices.

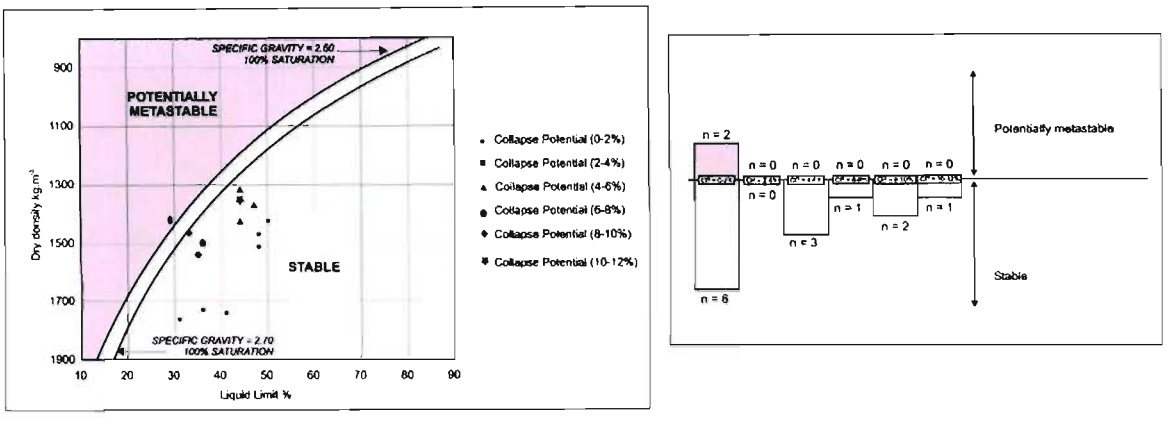

Figure 12.28. Stability diagram of Gibbs and Bara (1962) showing data from granite saprolite at Zoeknog Dam and histogram showing correlation of method with collapse potential.

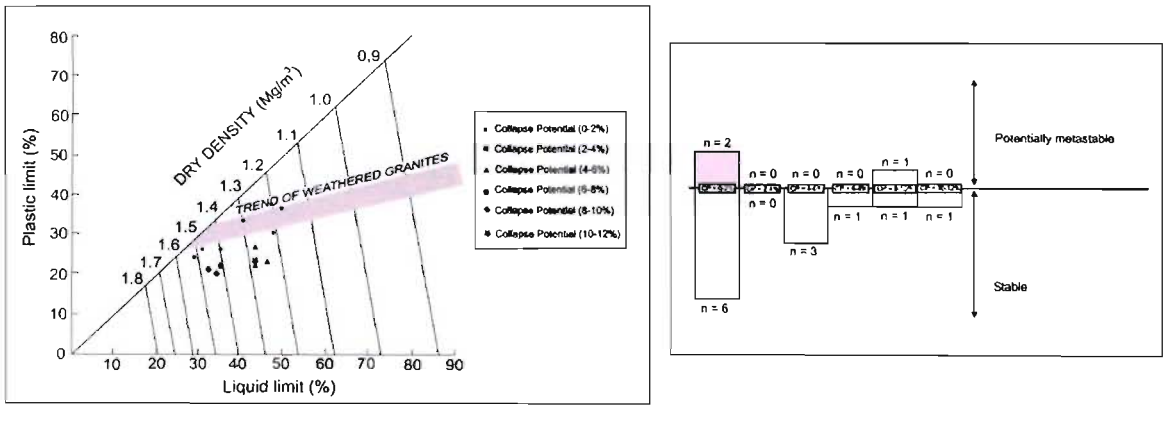

Figure 12.29. Stability chart of granite saprolite at Zoeknog Dam using Darwell *et al.'s* (1976) graphical method and histogram showing correlation of method with collapse potential.

13. SHEAR STRENGTH OF UNDISTURBED GRANITE SAPROLITE

13.1. Introduction

The shear strength of a soil is its maximum resistance which it can offer to shear stress. Once this maximum has been achieved (the peak shear strength), the soil is considered to have failed with failure occurring along a single plane or shear zone (the residual shear strength). The shear strength value determined experimentally is not a unique constant of the material, but varies according to the method of determination and the stresses imposed on the soil element.

Unweathered granite has a large cohesion (c ≈ 15 000 kPa) and high angle of friction ($\varphi \approx 59°$) due to the strength of intergranular bonds and the interlocking texture. When granite is weathered to produce a friable highly weathered rock, cohesion is significantly reduced by opening of grain boundaries and microfracturing. The angle of friction is reduced by the action of weathering due to mineralogical changes and internal weakening of grains. As the granite becomes more intensely weathered, developing into saprolite, the grains become separated and/or altered to clay. This results in a reduction of cohesion to zero when totally saturated (Lumb, 1962). The friction angle also reduces significantly, although generally remains higher than the value attributable to basic mineral friction alone, which is approximately 30° for granite minerals and somewhat less for their weathering products (Coulson, 1971). A summary of the shear strength parameters of grade VI and V weathered granite is presented in Tables 13.1 and 13.2, respectively. The tremendous range displayed by the shear characteristics is according to Dearman *et al.* (1978), because of the wide variety of microfabrics encountered within this material.

According to Ebuk *et al.* (1993), the presence of relict structure in weathered granite soils makes the engineering behaviour of these soils different from those of temperate soils exhibiting similar grading. As widely documented in the literature (Vargas, 1953; Wallace, 1973; Brink and Kantey, 1961 and Sowers, 1963), this structure is generally responsible for the residual bonding within these soils and accounts for the cohesion intercept on the strength envelope even when the soil is porous and contracts during shear (Leroueil and Vaughan, 1990). This bonding can be attributed to relict crystalline structure and the clay microfabric. The influence of moisture content is variable, but generally as the clay microfabric becomes more dominant, so the moisture content plays a more significant role.

Table 13.1. Shear strength parameters of Grade VI weathered granite from various sources (Deere and Patton, 1971) .

Material Description	Locality	Type of Test	Strength Parameters		Remarks	Source
			c	φ		
Decomposed granite	Hong Kong	Triaxial test	c' = 0-200 kPa	φ' =20-40°	Medium soil. c' approaches 0 when fully saturated	Lumb (1962)
Decomposed granite	Hong Kong	Drained triaxial test	c' = 0-225 kPa	φ' = 25-35°		Lumb (1962)
Decomposed granite	Hong Kong	Undrained triaxial test	c' = 0 kPa	φ' = 35-41,5°	Pore pressure measurements	Lamb (1962)
Slightly laterised decomposed granite		Triaxial test	c' = 0 kPa	φ' = 31°	Fully saturated	Vargas (1953)

Table 13.2. Shear strength parameters of Grade V weathered granite from various sources.

Material Description	Locality	Type of Test	Strength Parameters		Remarks	Source
			c	φ		
Decomposed granitic soil and altered granitic soil . Hong Kong	Hong Kong	Direct shear test	c = 0 kPa	φ = 39°	Average shear strength envelope with dilatant behaviour	Cheung *et al.* (1988)
Residual granite soil	Portugal	Saturated, undrained triaxial test	c' = 59 kPa	φ' = 26°	Post envelope inflection	Novais-Ferreira & Viana Da Fonesca (1988)
Residual granitic soil	Portugal	Direct shear test	c = 26,5 kPa	φ = 34°	Sample consolidated under 200 kPa before testing	Novais-Ferreira & Viana Da Fonesca (1988)
Granite saprolite	Egypt	Direct shear test	c = 0-15 kPa	φ = 40-45°	Partially saturated	Radwan (1988)
Highly weathered granite	Egypt	Direct shear test	c =22-38 kPa	φ = 40-48°	Partially saturated	Radwan (1988)
Completely decomposed granite	Hong Kong	Saturated, consolidated drained and undrained triaxial tests	c' = 7,5 kPa	φ' = 31°	Average parameters for drained and undrained conditions	Massey *et al.* (1989)
Completely decomposed granite	Hong Kong	Saturated, consolidated drained and undrained triaxial tests	c' = 10-20 kPa	φ' = 32-39°	Average parameters for drained and undrained conditions	Massey *et al.* (1989)
Decomposed Granite	Hong Kong	Direct shear test	c = 0 kPa	φ =35-40°	Saturated. Coarse Soil	Lumb (1962)
Decomposed Granite	Hong Kong	Direct shear test	c = 0-200 kPa	φ =35-40°	Medium soil. C' approaches 0 when fully saturated	Lumb (1962)
Decomposed Granite	Hong Kong	Drained triaxial test	c = 0-75 kPa	φ =33-40°		Lumb (1962)
Decomposed granite	Hong Kong	Consolidated, undrained triaxial test	c' = 0 kPa	φ' =35-41,5°	Pore pressures measured	Lamb (1962)
Decomposed granite		Triaxial test	c' = 50-70 kPa	φ' =33,5-41,5°	Dependent upon weathering index *i*, varying between 15 and 30	Hamrol (1961)
Decomposed granite	Australia	Direct Shear	c = 25-30 kPa	φ =26-29°	55% saturated	Hosking (1960)
Decomposed Granite	Hong Kong	Drained shear test	c' = 0-2,3 kPa	φ' =25-38°	Unsaturated	Lumb (1962)
Grade V weathered granite	England	Consolidated, undrained triaxial test	c' = 0 kPa	φ' =39,5°		Baynes and Dearman (1978a)

13.2 Direct shear tests

13.2.1 Introduction

Direct shear tests were conducted on undisturbed samples of the granite saprolite to assess the shear strength of the material. Although this test is limited in its application as no pore water pressures can be measured and the failure plane is predetermined, Cheung *et al.* (1988) stated that

it offers some advantages over the triaxial test, and in fact they found that the test could be used satisfactorily for the routine measurement of shear strength of saprolitic soils. The direct shear test is a much simpler and quicker test to perform than the triaxial test with both the shear and normal stresses on the plane of failure being measured directly. Furthermore, saturation of the soil by soaking can be simulated more easily in the direct shear test as drainage paths are short and excess pore pressures can dissipate rapidly, particularly with coarse-grained material.

13.2.2 Specimen preparation

Direct shear specimens were trimmed from the larger block samples by carefully using a knife, hacksaw blade and sample mitre. Extreme care was taken during this procedure not to disturb or unduly stress the sample, although difficulties were encountered with coarser grained material where large quartz grains at or near the boundary of the specimen disaggregated the sample during trimming. In such instances the sample was trimmed by abrading with sand paper. Unfortunately, the disruption of the microfabric during sample preparation can severely affect shear strength results as shown by Gidigasu (1980). Irfan (1988) has also suggested that partial destruction of bonds in completely decomposed materials may occur as a result of stress relief during sampling, disturbance during trimming and the application of normal stress in the higher stress range.

Direct shear tests were performed on 60 mm square by 20 mm thick specimens in a Wykenham Farrance model shear machine. Although Bishop (1948) and Hennes (1952) concluded that there is no significant scale effect in direct shear testing of cohesionless soils due to the size of the shear box itself, particle size has been found to be important in relation to the shear box size. This is supported by results from the investigation by Cheung *et al.* (1988) who observed that shear strengths were over-estimated when using smaller shear box sizes. ASTM (1985) prescribes that the specimen thickness be greater than or equal to six times the maximum grain diameter of the soil, with the specimen diameter (or width) being equivalent to or greater than twice the specimen thickness. Investigations in China as quoted by Cheung *et al.* (1988) suggest that the specimen thickness should be between four and eight times the maximum grain diameter and the specimen diameter should be between eight and twelve times the maximum grain diameter.

Although the granite saprolite can have a maximum grain size of 8 mm or more, these very coarse grained samples could not be tested using the shear box as they disintegrated during sample preparation. The majority of the samples that were tested exhibited a maximum grain size between 4,75 and 2,0 mm. Consequently, the size of the shear box used in this investigation can be expected to provide acceptable results.

The rate of shear applied to the specimen will affect the pore pressure distribution within the sample, particularly under saturated conditions for soils with low permeability. However, Cheung *et al.* (1988) found very little significant difference in shear strength between different shear rates applied to weathered Hong Kong granites. This can probably be attributed to the free-draining nature of the material. Samples from the investigation at Injaka Dam were subjected to a rapid shear rate of 1,2 mm/minute.

The specimens were tested at natural moisture content and under saturated conditions. The specimens were allowed to saturate overnight (16 hours) as this was considered the most practically efficient method for the schedule of testing. Each sample was subjected to direct shear testing at four normal stress intervals of 60, 120, 175 and 220 kPa.

13.2.3 Direct shear tests at natural moisture content

In their study investigating the effects of strain rate, moisture content, normal loading, sample size and box types on the shear strength and shear mechanisms of Grade IV and V weathered granite, Ebuk *et al.* (1993), recognised seven different categories of shear failure type (Figure 13.1). Each of these shear failure types defined a particular microfabric with respect to crystalline and/or clay bonding depending on the degree of weathering of the granite. This investigation showed several similar types of characteristic failure curves for the material from Injaka Dam. Figures 13.2 and 13.3 show the stress-strain curves and displacement-strain curves for samples derived from the right flank and left flank of the dam site, respectively. They have been separated according to each flank to allow the characteristics of the curves to be observed.

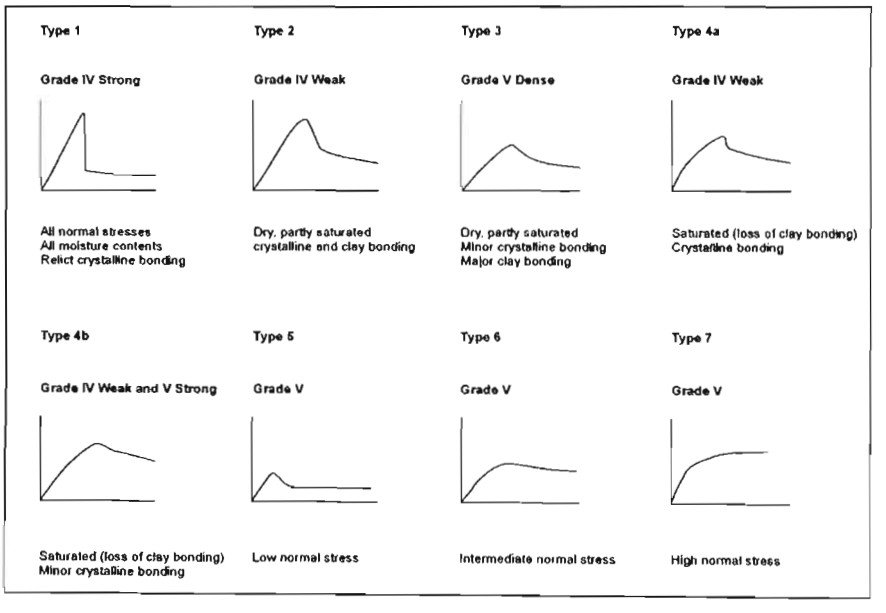

Figure 13.1. Characteristic stress-strain behaviour of weathered granite soils after Ebuk *et al.* (1993).

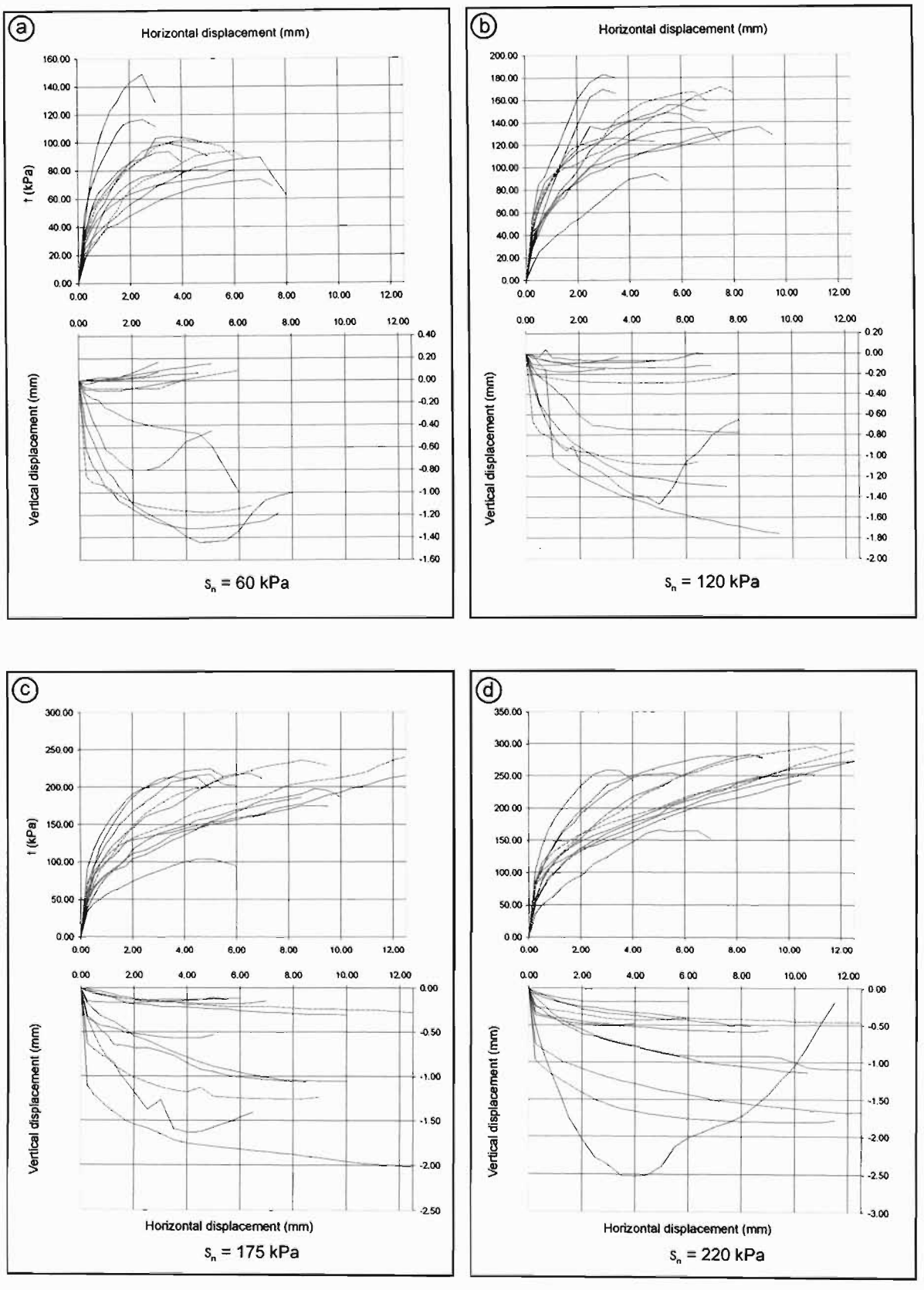

Figure 13.2. Stress-strain curves showing volume change in direct shear for right flank undisturbed samples sheared at natural moisture content. --- = granite saprolite with residual soil patches; — = granite saprolite.

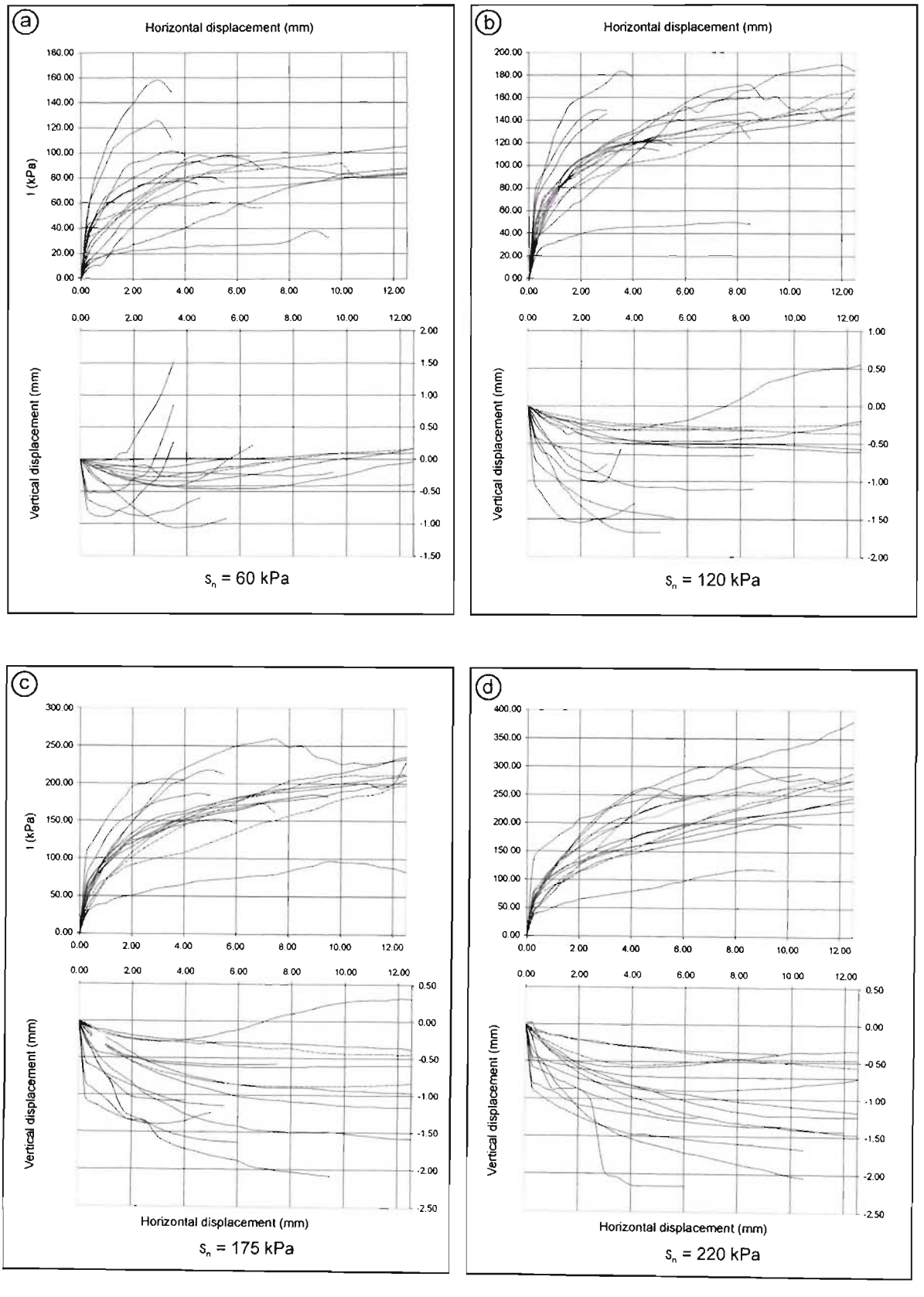

Figure 13.3. Stress-strain curves showing volume change in direct shear for left flank undisturbed samples sheared at natural moisture content. --- = granite saprolite with residual soil patches; — = granite saprolite.

The stress-strain relationship for the granite saprolite with residual soil patches is characterised by Type 7 curves over the entire applied normal pressure range. The gentle shape of these curves with no clearly defined peak shear stress can be explained by the disrupted microfabric characteristic of these samples (Chapter 7). The volume change behaviour is dominated by contraction, even at low applied normal stresses and is due to compression of the clay dominated microfabric.

With regard to the shear behaviour of the granite saprolite, a distinction could be made between the behaviour of the samples from the left and right flank, respectively. Generally, the material from the right flank displays a Type 3 and 4b failure curve (Figure 13.1) at low (60 kPa) to intermediate (120 kPa) normal stress. In these curves a broad peak is reached between 4 and 8% strain with a gradual reduction in shear stress as failure continues - the distinction made between Type 3 and Type 4b depending upon the rate of reduction in shear stress. Type 3 failure was often accompanied with dilatancy, particularly at the lowest normal stress (60 kPa), whilst Type 4b failure showed compressive behaviour throughout. This compressive behaviour does not correlate with results presented by Massey *et al.* (1988) where direct shear tests conducted by them on granite saprolite showed distinct dilation at low normal stresses. The discrepancy can probably be explained by the minimum normal load of 60 kPa in this investigation exceeding the "critical normal stress" identified by Massey *et al.*, below which dilation occurs. They found this critical normal stress to be 40 kPa. As the normal stress increases from 120 to 220 kPa, so the shear type failure curves progress to Type 7, where there is no clearly defined peak strength even at high strains of 21%. This is in agreement with the findings of Ebuk *et al.* (1993) who identified a peak shear strength that either remains constant or shows small increase with increasing strain. The volume change is associated exclusively with compression - this being a function of the higher normal stresses (Figures 13.2a, b, c and d).

The samples retrieved from the left flank showed Type 7 shear behaviour (Figures 13.3a, b, c and d), even at low normal stresses. Interestingly, dilatant behaviour was observed for several of the samples at low (60 kPa) to intermediate (120 kPa) normal stresses and low strains (<8%). The high porosity, normal grain size and moderate to low density characteristics of these samples (Chapter 10) cannot account for their dilatant behaviour with respect to the other samples and their behaviour can only be considered extraordinary. Over higher strains, several of the samples exhibited gradual dilation. At higher normal stresses almost all the samples exhibited compressive behaviour.

A summary of the shear strength parameters determined from the direct shear tests is presented in Tables 13.3 and 13.4. As with Baynes and Dearman (1978a), a similarly large scatter of results is shown but these are nevertheless comparable to the partially saturated samples presented in Table 13.2. The right flank samples show φ varying from 33,0° to 57,0° with an average of 41,7°.

The left flank samples exhibit lower parameters, a feature associated with their higher clay contents and generally higher moisture contents. Phi values vary from 26,1° to 50,3° with an average of 37,6°in this case. Cohesion is highly variable for both left and right flank samples. Right flank samples exhibited c values ranging from 6,9 to 85,8 kPa with an average of 41,4 kPa, whilst left flank samples showed an average of 52,3 kPa, ranging from 7,5 to 129 kPa.

Table 13.3. Summary of direct shear strength parameters for granite saprolite with residual soil patches at natural moisture content.

Sample	Depth (m)	Dry density ($kg.m^{-3}$)	Moisture (%)	e	I_p	*Xd*	φ (°)	c (kPa)
RF 12	1,0	1511	22,6	0,839	0,413	0,862	44,3	42,2
LF 7	1,1	1444	12,7	0,828	0,618	0,722	45,2	7,5
LF 18	1,1	1535	15,1	0,788	0,267	1,000	40,5	39,3
RF 17	2,2	1389	15,1	0,796		0,701	41,4	52,1

Table 13.4. Summary of direct shear strength parameters for granite saprolite at natural moisture content.

Sample	Depth (m)	Dry density ($kg.m^{-3}$)	Moisture (%)	e	I_p	*Xd*	φ (°)	c (kPa)
RF 10	3,5	1330	15,5	0,907	0,508	0,660	43,4	15,8
RF 9	4,9	1375	15,3	0,957	0,824	0,446	35,7	51,9
RF 8	5,7	1482	7,9	0,539	1,409	0,838	36,4	85,8
RF 7	6,6	1855	11,1	0,500	1,417	0,534	43,3	44,9
RF 6	2,5	1458	18,1	0,818	0,393	0,770	33,0	54,7
RF 5	4,8	1763	16,3	0,888	1,515	0,633	57,0	6,9
RF 4	6,9	1457	12,5	0,960	0,543	0,824	37,6	43,0
RF 3	9,2	1683	14,4	0,848	0,536	0,144	44,4	35,5
LF 2	2,4	1400	16,9	0,868	0148	0,740	42,6	17,2
LF 3	3,8	1416	14,9	0,860	0,876	0,642	41,8	43,3
LF 4	4,5	1523	17,5	0,556	0,535	0,604	26,1	129,0
LF 5	5,2	1610	15,3	0,589	0,501	0,665	39,0	97,5
LF 6	5,5	1433	22,4	0,909	0,463	0,796	35,1	79,5
LF 8	2,8	1434	13,6	0,746	0,515	0,709	40,8	48,3
LF 10	5,5	1431	21,0	0,801	0,380	0,900	33,2	56,2
LF 11	6,5	1362	20,5	0,955	0,671	0,440	30,6	45,2
LF 19	2,3	1307	19,0	0,937	0,460	1,000	31,9	58,3
LF 20	3,2	1305	17,7	0,955		0,838	41,4	25,2
LF 26	7,2	1522	12,4	0,692	0,568	0,264	27,6	72,1
LF 27	7,8	1797	6,4	0,501	1,621	0,376	50,3	13,9
RF 18	3,8	1383	15,3	1,022	0,398	0,565	41,9	22,1

13.2.3.1 Explanation of shear strength characteristics

The nature of granite saprolite as defined by its complex microfabrics has been used by Lumb (1962), Baynes and Dearman (1978a), Irfan (1988) and more recently Ebuk *et al.* (1993) to explain, in part, the shear behaviour of this material. Although the shear strength of a material is a function of many parameters including grain size, grain shape, particle packing, dry density, moisture content and stress regime, the use of microfabric indices often incorporates many of these parameters and may be used to identify a crude relationship with shear strength.

Lumb (1962) was the first to apply a definitive index (*Xd*) to explain microfabric in weathered granite and successfully applied it to changes in degree of weathering and grain size. He recognised a great variety of microfabrics as indicated by the range of *Xd* values, but could not reconcile these with the consistently high φ values for the weathered granite. Baynes and Dearman, and Irfan found a similar lack of correlation between *Xd* and φ. The fact that *Xd* only considers the quartz and feldspar variations within the material, means that it excludes any structural components of microfabric such as cracks and voids - features which have significant effect on the shear resistance of a material. In addition, the decomposition state of other minerals which can influence the strength behaviour are not accounted for in the *Xd* determination. The micropetrographic index (I_p) has achieved more success in characterising shear behaviour (Irfan, 1988) and this can be attributed to this index incorporating changing mineralogical and microcrack regimes within the weathered material. Consequently an element of the structural characteristic of the microfabric is included in I_p. Although no clear relationship could be observed between *Xd*, I_p and φ for this study, broad observations of the microfabric variability can tentatively explain certain relationships. The Type 7 failure curves exhibited by the granite saprolite with residual soil patches over the complete range of normal stresses are indicative of the greater clay dominated microfabrics of these samples which show a distinct loss of structure. This prevents any definite peak shear from being achieved as the softer clay matrix along the failure plane resists readjustment of the more competent quartz grains as shearing continues. The clay dominated microfabric reduces the interparticle contact of the more competent grains with each other, thus resulting in characteristic compressive behaviour during shear.

The Type 3 and 4b failure curves from the right flank granite saprolite samples are characteristic of material which shows less fabric disruption to the original fabric. These curves exhibit higher shear stresses with a defined peak shear stress at low horizontal displacement (increased stiffness). This relationship can be explained by the existence of relict crystalline structure and bonding (with a lesser component of clay microfabric) which resists shearing. At a given point (4 to 8% strain) the structure is broken resulting in a rapid reduction of shear stress. This type of failure may be associated with some dilatancy at low normal stress where the less prominent clay microfabric allows the more competent quartz and broken feldspar grains into contact with each other causing

overriding and possibly rotation within the fabric formed along the shear plane. At higher normal stresses the Type 3 failure curves change to Type 7 curves where the increased normal stress compresses the soil fabric breaking up relict bonding and structure with subsequent gradual collapse of the porous honeycombed feldspars as shearing progresses. This results in the compressive behaviour observed with very poorly defined peak shear stress curves.

For both the left and right flank samples, the irregular nature of some of the stress-strain curves can be attributed to particle crushing of the feldspar grains and reorientation within the confines of the shear box.

13.2.4 Direct shear tests at saturated moisture content

Direct shear tests were also carried out on saturated material. Cost and time implications prevented all samples from being tested. As can be seen from Figure 13.4, the effect of saturation on the samples is clearly shown by their characteristic Type 7 failure curves, with contraction predominating throughout the shear process. This observation is common to both the granite saprolite with residual soil patches and granite saprolite, respectively. No defined peak shear stress was achieved with shear stress increasing negligibly with strain.

As with the samples tested at natural moisture content, the saturated shear strength parameters exhibit some variation (Tables 13.5 and 6). A distinct reduction in cohesion is noted for the granite saprolite (between 0 and 55,2 kPa), probably as a result of softening and deflocculation of the clay within the sample, whilst the values of φ are comparable with the samples tested at natural moisture content (between 32,4° and 45,8°).

Table 13.5. Summary of saturated direct shear strength parameters for granite saprolite with residual soil patches.

Sample	Depth (m)	e	I_p	*Xd*	φ (°)	c (kPa)
LF 7	1,1	0,828	0,618	0,722	38,7	22

Table 13.6. Summary of saturated direct shear strength parameters for granite saprolite.

Sample	Depth (m)	e	I_p	*Xd*	φ (°)	c (kPa)
LF 3	3,8	0,860	0,876	0,642	37,5	25,0
LF 4	4,5	0,556	0,535	0,604	39,8	25,0
LF 5	5,2	0,589	0,501	0,665	37,5	38,7
LF 6	5,5	0,909	0,463	0,796	32,4	55,2
LF 8	2,8	0,746	0,515	0,709	43,4	34,3
LF 10	5,5	0,801	0,38	0,900	40,5	3,0
LF 11	6,5	0,955	0,671	0,440	45,8	0

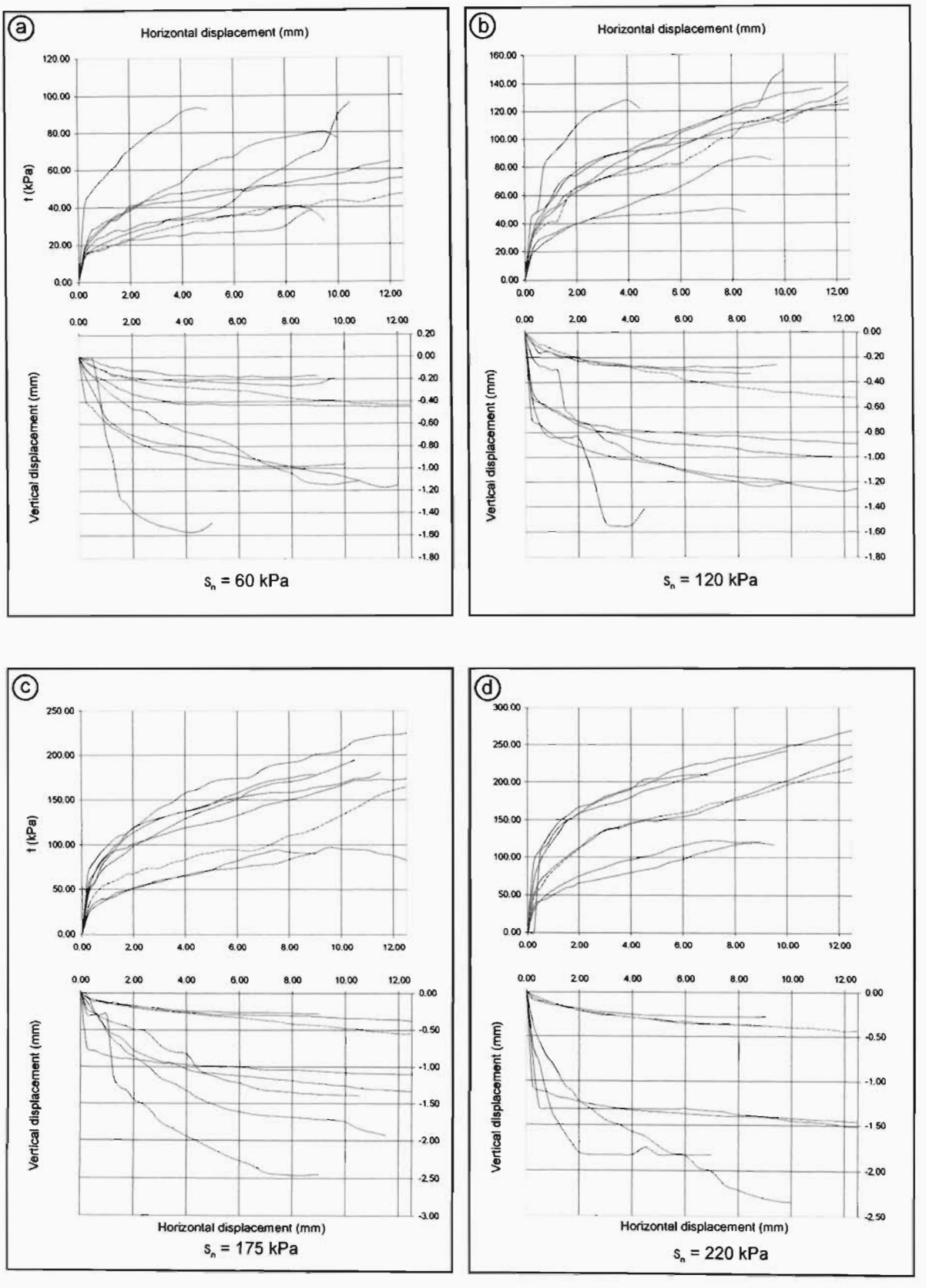

Figure 13.4. Stress-strain curves showing volume change in direct shear for left flank undisturbed samples sheared under saturated conditions. --- = granite saprolite with residual soil patches; — = granite saprolite.

13.2.4.1 Explanation of shear strength characteristics

The Type 7 failure curves can be explained by softening of kaolinite during saturation, forming a medium in which the more competent quartz grains and broken feldspar fragments are constantly readjusted in position through "ploughing" and to a lesser extent rotation. The resultant densification of the material prevents peak shear strength from being achieved, even at 21 % strain. The volume reduction throughout shear can also be associated with the metastable nature of the saprolite and the clay dominated microfabric which accommodates compression. The stress-strain curves are generally smoother in comparison to the natural moisture content curves suggesting that saturation softens the material facilitating particle crushing of the skeletal feldspar grains and reorientation of the more competent quartz grains. This accounts for the absence of any significant stiffness in the early part of displacement.

13.3 Triaxial tests

13.3.1 Introduction

As the direct shear test predetermines the failure plane of the sample, Sowers (1963) suggested that unduly high shear strength results can be achieved from this test method, particularly if the material exhibits any form of fabric. By not predetermining a failure plane within the sample, triaxial tests allow failure to occur "naturally" through the soil structure. In contrast to the findings of Cheung *et al.* (1988), Sowers suggested that the triaxial shear test is the only suitable method of testing the strength of "residual" soils and even then, numerous tests are required to obtain an accurate indication of the shear strength parameters of these soils.

Saturated consolidated drained triaxial tests were conducted on the undisturbed block samples of the granite saprolite. The objective of these tests was to establish typical values of drained shear strength parameters of the weathered granite. Although direct shear testing has provided an indication of the shear strength of the granite saprolite, the method of triaxial testing means that effective shear strength parameters can be obtained. Shear strength results forming part of the triaxial collapse potential tests (discussed in Section 12.4) are also presented here.

13.3.2 Saturated consolidated drained triaxial tests

13.3.2.1 Specimen preparation

The sample preparation for triaxial testing requires a significantly sensitive approach, particularly where the specimens are brittle. The nature of trimming the cylindrical specimens can give rise to difficulties, particularly with regard to the coarser grained samples where large quartz grains at or

near the boundary of the specimen can disaggregate the sample during trimming. Cylindrical samples 38 mm in diameter and 76 mm in length were used for the test procedure.

After installation in the triaxial cell, a back pressure and cell pressure of 200 kPa were gradually applied to the specimen. The back pressure was applied until Skempton's B value was close to unity, implying total saturation. In most cases B values very close to unity could be achieved overnight. The back pressure value of 200 kPa was chosen to simulate a head of water 20 m in height, thus representative of the pore pressure increase due to reservoir loading on the foundations. With these values of pressure, similar levels of the appropriate field pressures are operative throughout the test. The application of the cell pressure allowed for the increase in the pore pressure within the specimen so that air as a separate phase in the void spaces is eliminated, allowing for saturation of the sample. After saturation, cell pressures of 275, 350 and 500 kPa were applied respectively to each specimen to obtain the shear strength envelope. It should be noted that these confining pressures are significantly higher than the normal pressures used in the direct shear box tests. As a result subtle differences between the two shear tests, particularly within the lower stress intervals may occur. A rate of strain of 0,0457 mm.minute^{-1} was used, correlating to a strain of 3,6 % per hour. This rate of strain was considered suitable as no excess pore pressure was observed during testing.

13.3.2.2 Results and discussion

Consolidated drained and undrained triaxial tests were conducted by Massey *et al.* (1988) on granitic saprolite soils using lower confining pressures ranging from 10 to 300 kPa. The objective of these tests was to determine the effect of microfabric on the shear strength characteristics of the material. Massey *et al.* were able to identify a region in the stress paths where a "critical effective confining pressure" existed, below which the material derives additional strength from dilation and possibly also from shearing of weaker bonds. The much higher cell pressures used in this investigation prevented any identification of this relationship for these materials.

A typical set of stress-strain curves for the granite saprolite are shown in Figure 13.5. As with the direct shear tests, two anomalous failure type curves can be identified when plotting deviator stress against strain. These include Type A and Type B curves (Figure 13.6) similar to the Type 3 and Type 6 curves identified in Section 13.2. The Type A curves are characteristic of the least weathered samples at low (275 kPa) and intermediate (350 kPa) confining pressures. The failure curves show a distinct stiffness at low strain with an abrupt increase to a defined peak shear stress at around 2,5 to 3% strain followed by a very gradual reduction in shear stress. The Type B failure curves are similar to the Type 6 curves in Figure 13.1 and are characterised by more weathered samples. The curves exhibit a gradual increase in shear stress with a poorly defined peak shear at extended strain of up to 10 to 15%. In accordance with observations from the direct shear tests,

it was found that as the confining pressure increased so the Type 3 curves changed to Type 7, indicative of disruption of the microfabric interlock at these high confining pressures.

A summary of the shear strength parameters derived from the triaxial testing is shown in Tables 13.7 and 8 and once again shows the variation of the strength of the granite saprolite. The wide scatter of results is not unusual with Brummer (1980), Jaros (1978) and Gidigasu (1980) finding similar relationships. Partridge *et al.* (1990) also found similar strength characteristics at Zoeknog Dam as shown in Figure 13.7.

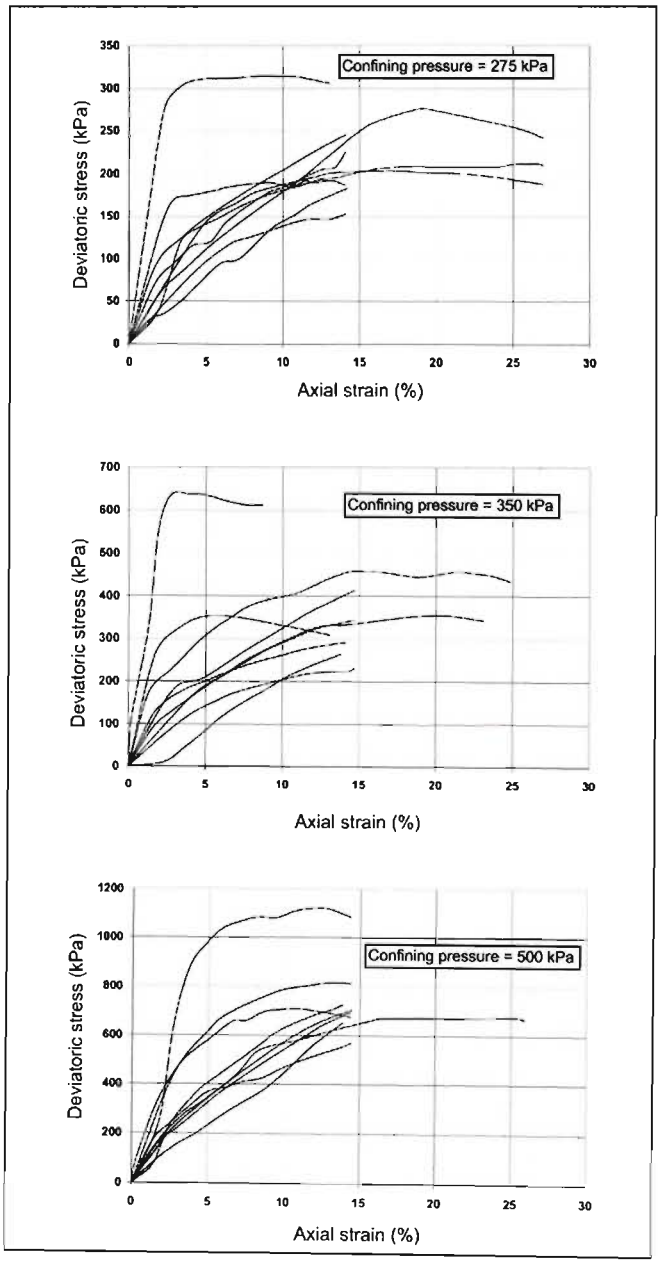

Figure 13.5. Stress-strain curves for selected granite saprolite samples from saturated consolidated drained triaxial tests. σ_3 = 275, 300 and 500 kPa, respectively.

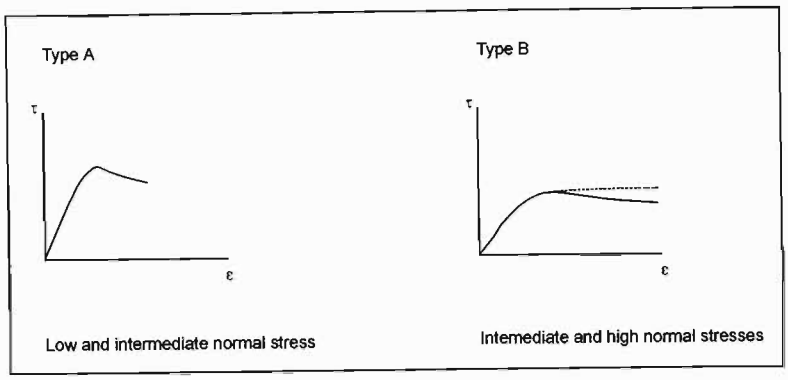

Figure 13.6. Failure type curves for saturated consolidated drained samples.

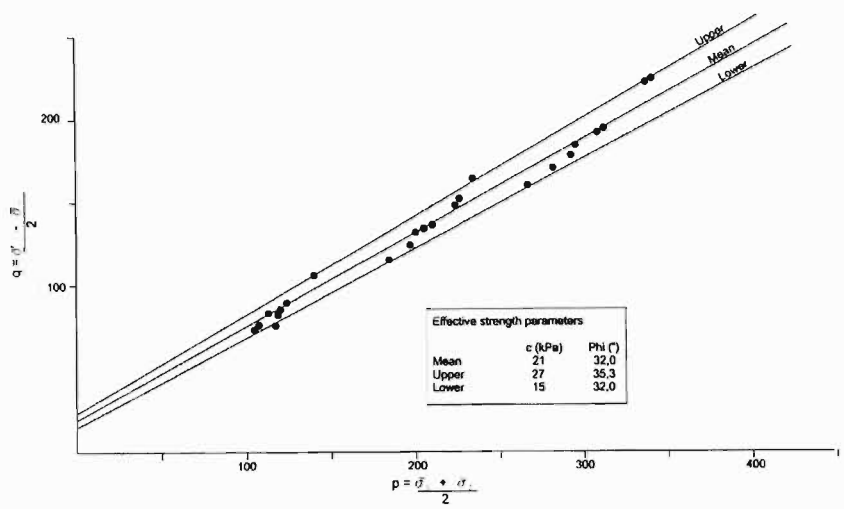

Figure 13.7. Results of saturated consolidated drained triaxial tests on granite saprolite at Zoeknog Dam from Partridge *et al.* (1990).

Fell *et al.* (1992) have shown that when a number of triaxial tests have been conducted on a soil, it is recommended that the design shear strength parameters are obtained from the MIT stress path plot of the test results rather than by averaging the individual φ' and c' values from each test, or plotting all Mohr circles from the test results on a diagram. This method of construction to determine the shear strength parameters is superior as it eliminates errors of judgement in choosing the best common tangent to the Mohr circles; avoids ignoring the weakest specimens in the test series and allows for the continual monitoring of $(\sigma_1' + \sigma_3')/2$ and $(\sigma_1' - \sigma_3')/2$ values during shear to give a stress path of the successive states of stress within a sample as it approaches failure (Vickers, 1978). Effective stress points for the maximum deviator stress are shown in Figure 13.8 The data represents points s' and t' as defined by Atkinson and Bransby (1978) for the MIT stress path concept. It is possible to determine 'α and d', the stress path counterparts for φ' and c' from this data. Linear regression through these points shows that d = 0,35 kPa and α'=28,6°with

calculation of the shear strength parameters giving the average results for the granite saprolite as $\varphi' = 33{,}0°$ and $c' = 0$ kPa.

Table 13.7. Summary of shear strength parameters for saturated consolidated drained triaxial tests on granite saprolite with residual soil patches.

Sample	Depth (m)	Dry density (kg.m^{-3})	e	I_p	*Xd*	φ' (°)	c' (kPa)
RF 12	1,0	1511	0,839	0,413	0,862	33,0	11,3
RF 17	2,2	1389	0,796	0,500	0,701	32,4	15,9
LF 7	1,1	1444	0,829	0,618	0,722	36,0	17,5
LF 18	1,1	1535	0,788	0,267	1,000	30,0	25,7

Table 13.8. Summary of shear strength parameters for saturated consolidated drained triaxial tests on granite saprolite.

Sample	Depth (m)	Dry density (kg.m^{-3})	e	I_p	*Xd*	φ' (°)	c' (kPa)
RF 10	3,5	1330	0,907	0,508	0,660	28,2	12,3
RF 9	4,9	1375	0,957	0,824	0,446	31,0	90,0
RF 8	5,7	1482	0,539	1,409	0,838	20,3	36,4
RF 7	6,6	1855	0,500	1,417	0,534	38,0	95,0
RF 6	2,5	1458	0,818	0,393	0,770	24,7	25,0
RF 5	4,8	1763	0,888	1,515	0,633	39,0	69,0
RF 4	6,9	1457	0,960	0,543	0,824	29,2	29,0
RF 3	9,2	1683	0,848	0,536	0,144	34,2	15,0
RF 18	3,8	1383	1,022	0,398	0,565	32,1	18,0
RF 20	6,1	1479	0,971	0,822	0,511	30,2	29,3
RF 21	6,2	1663	0,828	0,895	0,203	27,8	38,0
LF 2	2,4	1400	0,868	0,148	0,740	29,7	90,0
LF 3	3,8	1416	0,860	0,876	0,642	28,0	9,8
LF 4	4,5	1523	0,556	0,535	0,604	30,4	4,0
LF 5	5,2	1610	0,589	0,501	0,665	27,8	13,6
LF 6	5,5	1433	0,909	0,463	0,796	34,3	2,5
LF 8	2,8	1434	0,746	0,515	0,709	35,7	8,0
LF 9	4,0	1429	0,676	0,508	0,279	35,7	2,8
LF 10	5,5	1431	0,801	0,380	0,900	32,3	4,2
LF 11	6,5	1362	0,955	0,671	0,440	27,7	14,8
LF 13	7,7	1625	0,365	0,584	0,254	31,4	8,4
LF 19	2,3	1307	0,937	0,460	1,000	31,1	3,3
LF 20	3,2	1305	0,955	0,500	0,838	29,0	16,8
LF 24	5,7	1398	0,914	0,527	0,843	30,0	15,0
LF 25	6,2	1533	0,713	0,747	0,902	30,9	13,4
LF 26	7,2	1522	0,692	0,568	0,264	31,5	24,4
LF 27	7,8	1797	0,501	1,621	0,376	40,0	16,9

The granite saprolite exhibits a characteristic zero cohesion when totally saturated due to the loss of capillary forces (Lumb, 1962). The value of 33,0° for φ' is still higher than the value attributable

to basic mineral friction alone (which is 30° for granite minerals and less for their weathering products (Kanji, 1970; and Coulson, 1971). The fact that φ' is higher is probably related to the surface roughness of the mineral grains induced by weathering, rather than the angularity and interlocking texture, as samples tend to consolidate and produce positive pore-water pressures during shear (Baynes and Dearman, 1978a). The value of φ' still lies between 30° and 35° which encompasses the results from other authors summarised in Table 13.2.

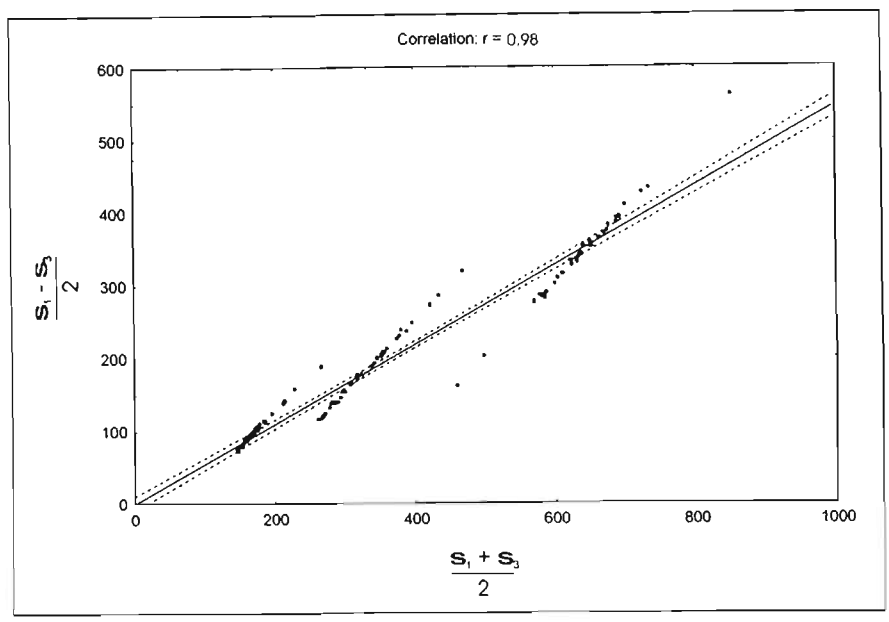

Figure 13.8. Effective stress points for maximum deviator stress for consolidated drained triaxial tests on granite saprolite samples.

13.3.2.3 Explanation of shear strength

The weathering effects on the granite saprolite reduce the interlock effect that the mineral grains have with surrounding grains. The shear strength parameters φ' and c' have traditionally been defined in terms of interparticle obstruction forces and particle attraction, respectively. Consequently, it can be expected that with increased weathering φ' and c' will decrease as interparticle bonding is reduced. The Type A curves are characteristic of material with lower clay microfabrics. The microfabric comprises significant relict bonding and structure (interlock) with lesser clay and decomposition products. Microcracking is also not as intensely developed. It is this interlocking fabric that accounts for the stiffness observed in these specimens at low to intermediate confining pressures. At failure, the interlocking fabric is broken, with the competent quartz and broken feldspar fragments interacting with the lesser clay microfabric to allow only a small reduction in shear stress. The Type B curves show a more plastic failure mode with a poorly defined peak shear stress even over significant strain. The saturation of these samples results in softening of the specimens due to their higher clay content and this accounts for the characteristic failure curves typical of Type B. The more competent quartz and broken feldspar fragments are

constantly readjusted within the clay microfabric along the plane of failure. The resulting densification causes the gradual increase in shear stress.

13.3.3 Shear strength results from triaxial collapse potential tests

During the triaxial collapse potential tests discussed in Section 12.4, the undrained shear behaviour of these two samples was also determined. Figure 13.9 shows the stress-strain curves and pore pressure measurements for the undrained compression tests. The shear strength parameters measured from these tests show these samples of granite saprolite to exhibit a φ' of 24° and a c' of 22 kPa. The internal angle of friction value is somewhat lower than that determined from the saturated consolidated drained triaxial tests, but this discrepancy is within the range of material variability. From Figure 13.10 it can be seen that the granite saprolite showed brittle behaviour accompanied by strain softening at low initial mean effective stresses, with peak deviatoric stresses at low initial effective stresses typically reached at axial strains between 2,0 and 2,5%. At higher initial mean effective stresses, the behaviour becomes more ductile. This behaviour is typical of soils with significant levels of "bonding" or structure. Figure 13.10 confirms this as the stress paths showed post-peak compressive behaviour. This occurs when the load is shed from the saprolite skeleton to the pore water as restructuring takes place for shear past the peak stress.

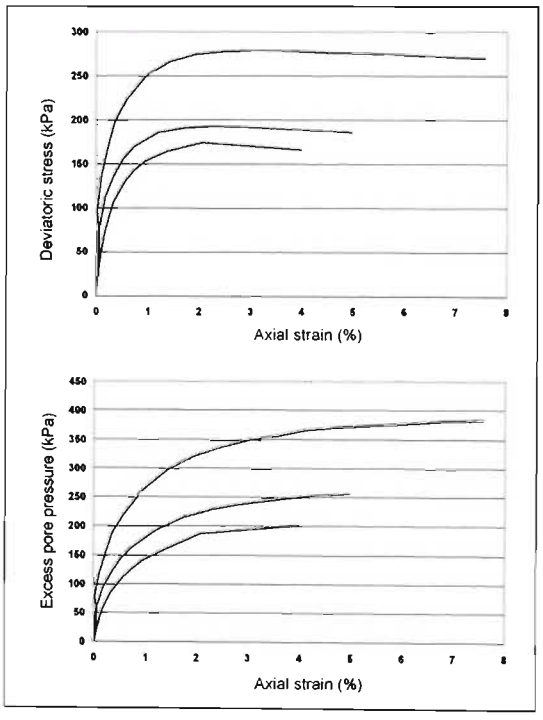

Figure 13.9. Stress-strain curves and pore pressure measurements from undrained triaxial tests.

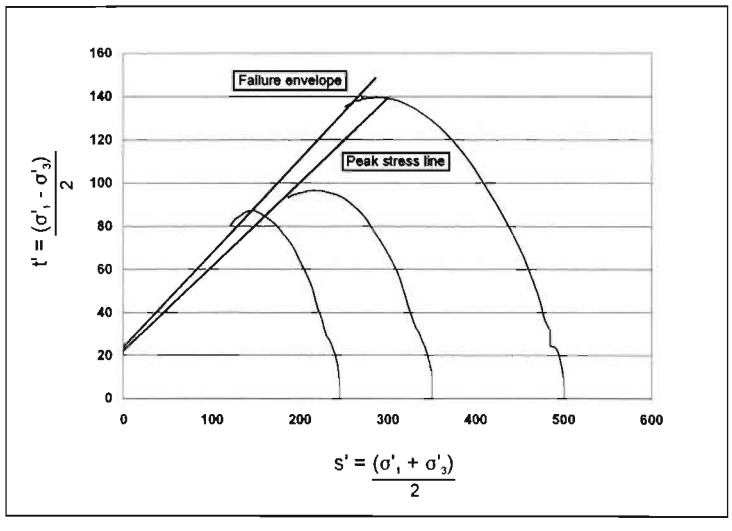

Figure 13.10. Effective stress path for granite saprolite samples.

14. ENGINEERING CHARACTERISTICS OF REMOULDED MATERIAL

The bulk of this research has comprised an engineering geological assessment of the *in situ* granite saprolite at Injaka Dam. To complete the study, this chapter includes an analysis of the engineering behaviour of the remoulded material. To determine the suitability of the weathered granite for use in the embankment fill material, Standard Proctor compaction tests were performed on selected samples extracted from each of the traverses shown in Figure 2.5. This chapter describes the results of various engineering properties of the remoulded materials and compares them to that of the *in situ* conditions.

14.1 Compaction characteristics

Typical compaction curves of the various weathered granite materials are shown in Figure 14.1. The compaction curves identify a spread of results for the various materials and this is confirmed by Partridge *et al.* (1990) who observed similar characteristics for weathered granite at Zoeknog Dam. Whilst the range of Standard Proctor maximum dry densities can be observed in Figure 14.1, the average results for the various materials is presented in Table 14.1. Summary results of granite saprolite from Zoeknog Dam as investigated by Partridge *et al.* (1984) are also shown and are comparable.

Table 14.1. Average Standard Proctor maximum dry densities and optimum moisture contents.

Material type	This study		Partridge *et al.*, (1990)	
	Maximum dry density ($kg.m^{-3}$)	Optimum moisture content (%)	Maximum dry density ($kg.m^{-3}$)	Optimum moisture content (%)
Granite saprolite with residual soil	1702	18	1708	16.9
Granite saprolite	1704	17		
Highly weathered granite	1683	16	-	-

It can be seen from this table that the optimum moisture content decreases slightly but steadily from the granite saprolite with residual soil patches to the highly weathered material. The maximum dry density values follow a similar relationship although very little difference is observed between the granite saprolite and the granite saprolite with residual soil patches. The compaction curves for both of these material types fall along or close to the 5% air voids line as shown in Figure 14.1. The lower maximum dry density and optimum moisture content for the highly weathered granite is attributable to the poor grading and low clay content respectively of the material (Chapter 10). Figure 14.1 also shows the compaction curves to follow the zone between the 5% and 10% air voids line.

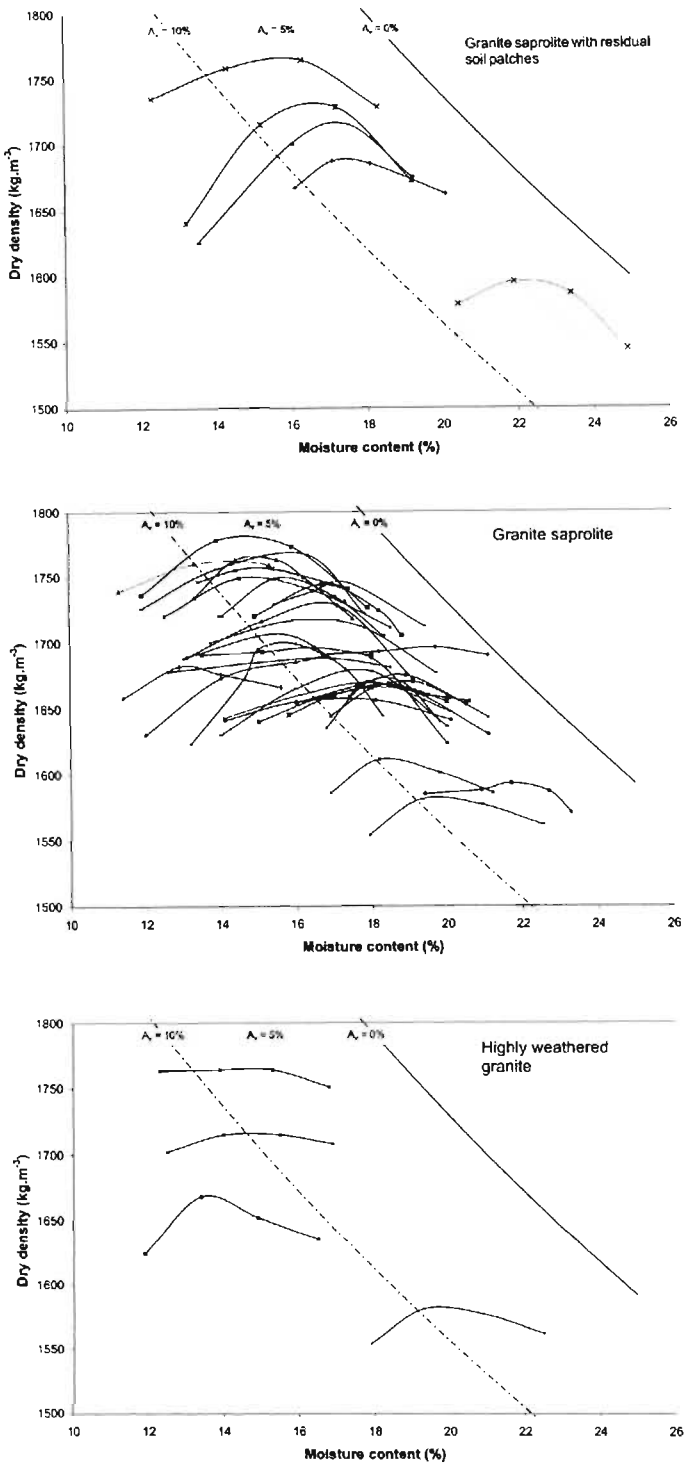

Figure 14.1. Typical compaction curves for granite saprolite with residual soil patches, granite saprolite and highly weathered granite.

14.2 Permeability characteristics of remoulded material

Permeability tests were performed on remoulded samples compacted at approximately optimum moisture content to 95% of Standard Proctor maximum dry density and using the falling head permeameter. The results shown in Figure 14.2 and Tables 14.2 to 14.4 show some degree of scatter with permeability generally varying between 1 x 10^{-4} and 1 x 10^{-7} cm.s^{-1} for the granite saprolite with an average of 1,7 x 10^{-5} cm.s^{-1}. This represents only a small reduction in permeability in comparison to the *in situ* materials (Table 10.10). The highest value of permeability in Figure 14.2 (4,5 x 10^{-4} cm.s^{-1}) is represented by a sample of highly weathered granite and is indicative of the poor compaction effort achievable for this material type. The granite saprolite with residual soil patches exhibits similar permeability characteristics to that of the granite saprolite.

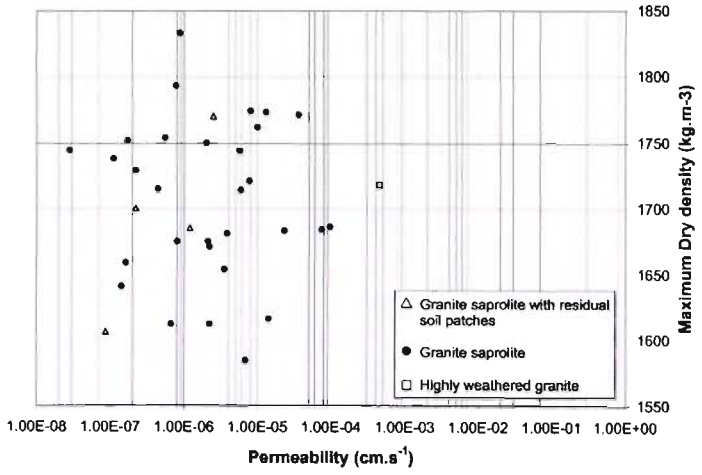

Figure 14.2. Permeability characteristics of remoulded weathered granite materials.

These results are higher than those reported by Partridge *et al.* (1990), who found constant head permeability results between 1,7 x 10^{-6} and 6,7 x 10^{-7} cm.s^{-1} on remoulded granite saprolite at Zoeknog Dam. The lower permeabilities experienced at Zoeknog dam are likely to be due to the higher clay contents of this material.

14.3 Consolidation characteristics of remoulded material

For this particular study no consolidation tests were carried out on the remoulded compacted granite saprolite. However, Chunnett *et al.*(1991b) have analysed the consolidation behaviour of both the remoulded granite saprolite and granite saprolite with residual soil patches at Injaka Dam site. This

Table 14.2. Remoulded engineering properties of granite saprolite with residual soil patches at Injaka Dam.

Sample	Depth (m)	Maximum dry density ($kg.m^{-3}$)	Optimum moisture content (%)	e_{max}	Permeability ($cm.s^{-1}$)	Direct shear at optimum moisture content		Direct shear at saturated moisture content		Saurated consolidated drained triaxial	
						φ(°)	c (kPa)	φ(°)	c (kPa)	φ(°)	c (kPa)
RF 12	1,0	1606	21,8	0,675	$8,6 \times 10^{-8}$	34,9	67,3	30,6	9,4	31,8	3,6
LF 1	0,9	1750	15,9	0,486	1.6×10^{-8}					39,6	2,9
LF 7	1,1	1685	16,7	0,567	$1,2 \times 10^{-8}$	41,3	68,3	37,8	14,8	35,1	4,6
LF 18	1,1	1770	16,7	0,531	$2,5 \times 10^{-8}$	43,6	67,4	33,4	13,5	30,1	25,7
RF 17	2,2	1700	17,8	0,571	$2,2 \times 10^{-7}$	51,5	173,8	36,9	9,0	25,0	24,2

Table 14.3. Remoulded engineering properties of granite saprolite at Injaka Dam.

Sample	Depth (m)	Maximum dry density ($kg.m^{-3}$)	Optimum moisture content (%)	e_{max}	Permeability ($cm.s^{-1}$)	Direct shear at optimum moisture content		Direct shear at saturated moisture content		Saurated consolidated drained triaxial	
						φ(°)	c (kPa)	φ(°)	c (kPa)	φ(°)	c (kPa)
RF 10	3,5	1612	18,5	0,619	$6,6 \times 10^{-7}$	47,1	56,7	32,5	20,2	30,5	17,5
RF 9	4,9	1654	18,9	0,596	$3,5 \times 10^{-6}$	24,1	93,9	31,4	31,8	37,4	0,7
RF 8	5,7	1715	18,8	0,575	$4,4 \times 10^{-7}$	35,2	60,7			32,2	11,3
RF 7	6,6	1683	13,0	0,557	$2,3 \times 10^{-5}$	55,3	3,7	36,5	19,9	34,7	17,7
RF 6	2,5	1584	19,9	0,686	$6,8 \times 10^{-6}$	37,8	86,2	26,9	32,5	26,0	23,9
RF 5	4,8	1752	16,0	0,495	$1,7 \times 10^{-7}$	43,1	14,7	47,2	45,5	36,4	1,1
RF 4	6,9	1616	19,2	0,627	$1,4 \times 10^{-5}$	45,0	48,5	33,0	16,2	31,5	7,7
RF 3	9,2	1744	15,4	0,519	$5,7 \times 10^{-6}$	49,3	37,3	39,1	5,2	35,5	5,0
LF 2	2,4	1671	18,2	0,586	$2,2 \times 10^{-6}$	37,6	67,9	44,4	5,4	34,5	5,8
LF 3	3,8	1681	16,5	0,582	$3,8 \times 10^{-6}$	43,5	69,8	42,1	0	33,6	6,5
LF 4	4,5	1721	16,9	0,547	$7,7 \times 10^{-6}$	41,4	58,4	38,9	8,8	33,6	2,5
LF 5	5,2	1774	15,5	0,505	$8,0 \times 10^{-6}$	49,7	42,7	25,9	28,6	30,8	4,4
LF 6	5,5	1659	17,0	0,609	$1,6 \times 10^{-7}$	33,0	84,0	44,6	14,3	28,1	10,6
LF 8	2,8	1750	17,4	0,554	$2,0 \times 10^{-6}$	43,0	61,3	19,9	27,9	36,5	1,7
LF 9	4,0	1773	15,7	0,472	$1,3 \times 10^{-6}$	47,8	56,8	36,4	9,7	34,1	15,2
LF 10	5,5	1612	20,8	0,631	$2,2 \times 10^{-6}$	39,5	112,3	33,9	26,4	31,4	4,4
LF 11	6,5	1641	17,7	0,633	$1,4 \times 10^{-7}$	36,7	70,5	45,8	1,8	30,6	9,7
LF 12	7,3	1729	17,0	0,527	$2,2 \times 10^{-7}$	34,9	81,3	32,3	6,0	35,2	0
LF 13	7,7	1714	17,8	0,534	$5,9 \times 10^{-6}$	35,7	66,9	26,7	34,2	36,6	9,4
LF 19	2,3	1745	17,1	0,547	$2,8 \times 10^{-6}$	44,9	61,0	30,1	16,1	31,1	3,3
LF 20	3,2	1675	17,5	0,594	$2,1 \times 10^{-6}$	43,6	68,8	27,0	17,7	29	16,8
LF 21	4,0	1738	16,2		$1,1 \times 10^{-7}$					39,8	0,3
LF 22	5,1	1793	14,5		$7,7 \times 10^{-7}$					33,0	16,1
LF 24	5,7	1771	14,0		$3,6 \times 10^{-5}$					35,2	15
LF 25	6,2	1762	14,8		$9,9 \times 10^{-6}$					35	15,2
LF 26	7,2	1754	15,0	0,499	$5,5 \times 10^{-7}$	43,7	90,9	33,2	20,7	34	23,9
LF 27	7,8	1833	14,5	0,446	$8,7 \times 10^{-7}$	47,7	59,7			35,4	42,8
RF 18	3,8	1675	18,3	0,624	$8,0 \times 10^{-7}$	36,2	37,8	30,6	9,9	27,0	5,5
RF 19	5,2	1709	15,4	0,539		49,0	20,0	45,0	0	26,1	33,5
RF 20	6,1	1684	17,4		$7,4 \times 10^{-5}$	40,7	92,1			39,1	10,2
RF 21	6,2	1686	17,8		$9,6 \times 10^{-5}$	43,5	52,8			36,1	28,9

Table 14.4. Remoulded engineering properties of highly weathered granite at Injaka Dam.

Sample	Depth (m)	Maximum dry density ($kg.m^{-3}$)	Optimum moisture content (%)	e_{max}	Permeability ($cm.s^{-1}$)	Direct shear at optimum moisture content		Direct shear at saturated moisture content		Saurated consolidated drained triaxial	
						φ(°)	c (kPa)	φ(°)	c (kPa)	φ(°)	c (kPa)
RF 2	8,2	1718	14,7	0,554		50,3	34,0	27,3	32,2	33,9	20,4
RF 13	10,6	1765	15,0	0,496	$1,0 \times 10^{-5}$	48,1	24,3	50,6	13,0	36,3	14,9
RF 15	10,9	1668	13,4	0,589	$4,6 \times 10^{-4}$	37,6	32,5	36,0	5,0	32,7	32,7

information is accordingly presented in Table 14.5. Double oedometer consolidation tests performed at optimum moisture content and at saturation were carried out on samples of granites saprolite and granite saprolite with residual soil patches compacted to 100% Standard Proctor maximum dry density. The compression of the granite saprolite with residual soil patches under a pressure of 500 kPa varies between 3,0 and 4,6% at optimum moisture content and between 5,4 and 6,4% when saturated. The saturation collapse at a pressure of 500 kPa varies between 0 and 2,5%. The compression of the granite saprolite under a pressure of 500 kPa varies between 2,5 and 4,0% at optimum moisture content and between 4,0 and 6,3% when saturated. The saturation collapse at a pressure of 500 kPa varies between 0 and 1%.

These results are summarised in Table 14.5 and it is evident that the granite saprolite and granite saprolite with residual soil patches are not highly compressible after being compacted at optimum moisture content to 100% Standard Proctor maximum dry density. This is the case even for the saturated condition. The C_v values suggest that consolidation settlement will also take place fairly slowly.

14.4 Shear characteristics of remoulded material

Direct shear testing was carried out on Standard Proctor compacted samples for comparative analysis with shear strength results obtained from the undisturbed material as outlined in Chapter 13. The shear tests were conducted at optimum moisture content and under saturated conditions. Saturated consolidated drained triaxial tests were also undertaken on the remoulded material.

14.4.1 Direct shear tests on compacted samples at optimum moisture content

Figures 14.3 and 14.4 show the stress-strain and vertical displacement-strain curves for the right and left flank samples, respectively tested in direct shear at optimum moisture content (the left and right flank samples have been separated for ease of observation of the curves). In general, the samples of granite saprolite and granite saprolite with residual soil patches all behaved similarly, exhibiting Type 3 failure curves (Figure 13.1) at low and intermediate normal stresses but developing Type 7 curves (Figure 13.1) at intermediate and high normal stresses. At low normal stresses the curves show a rapid increase in shear stress with failure occurring at low displacements (4-5 % strain). A clearly defined peak shear stress is achieved. At higher normal stresses the peak shear stress becomes less obvious and occurs at greater strains (between 5 and 12,5%). The slightly irregular curve shapes on Figures 14.3 and 14.4 can be attributed to readjustment of the more competent quartz grains and broken

Table 14.5. Summary of consolidation characteristics of remoulded granite saprolite at Injaka Dam (from Chunnett *et al.*, 1991a)

Material type	Depth (m)	Maximum dry density ($kg.m^{-3}$)	Specific gravity	Moisture condition (%)	Compression to (%)		Saturation collapse at (%)		Coefficient of volume change, m_v (m^2/kN)		Coefficient of consolidation, C_v (m^2/yr)	Permeability ($cm.s^{-1}$)
					500 kPa	1000 kPa	200-500 kPa	500 - 1000 kPa	200 - 500 kPa	500 - 1000 kPa		
Granite saprolite with residual soil patches	3,5	1687	2,66	OMC 16,3 SMC 23,1	3,154	4,082	0	2,3	0,0000246 0,0000732	0,0000178 0,0000606	592	$9,5 \times 10^{-7}$
Granite saprolite with residual soil patches	3,5	1701	2,64	OMC 15,9 SMC 21,8	3,064	4,392	2,5	4,3	0,0000360 0,0000268	0,0000983 0,0000598	548	$4,7 \times 10^{-7}$
Granite saprolite with residual soil patches	5,0	1765	2,63	OMC 17,9 SMC 20,1	4,663	6,680	0	0	0,0000553 0,0000687	0,0000403 0,0000372	753	$1,4 \times 10^{-7}$
Granite saprolite	4,0	1772	2,66	OMC 14,7 SMC 19,3	4,040	5,353	0	4,0	0,0000275 0,0000497	0,0000291 0,0000275	493	$2,0 \times 10^{-6}$
Granite saprolite	6,5	1878	2,69	OMC 11,1 SMC 17,7	2,563	3,579	9,0	1,6	0,0000330 0,0000661	0,0000200 0,0000328	751	$5,1 \times 10^{-7}$
Granite saprolite	4,4	1455	2,80	OMC 30,3 SMC 33,6	3,839	5,668	0	1,3	0,0000748 0,0000609	0,0000366 0,0000619	780	$2,6 \times 10^{-7}$

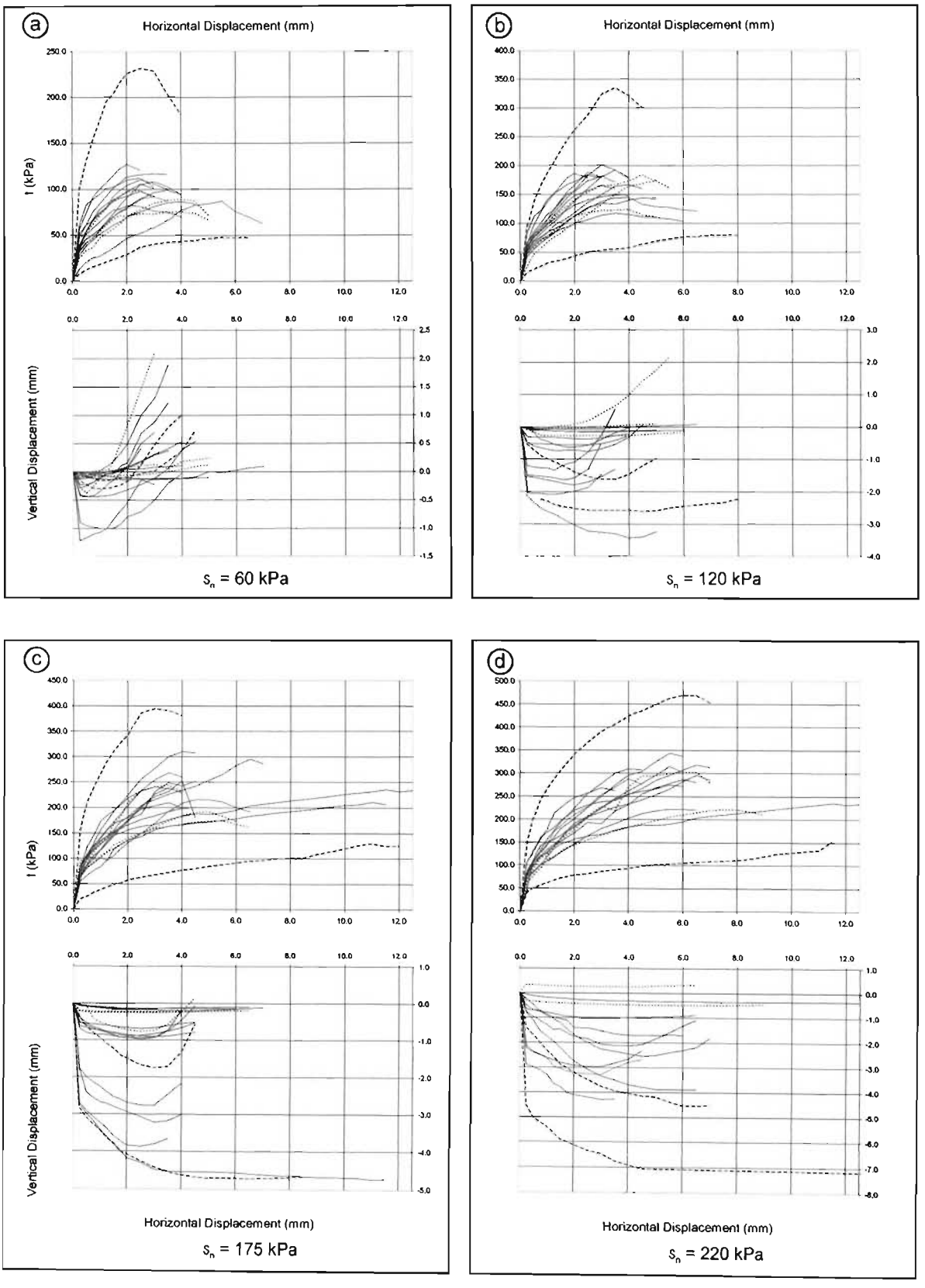

Figure 14.3. Stress-strain curves showing volume change in direct shear for right flank compacted samples sheared at optimum moisture content.

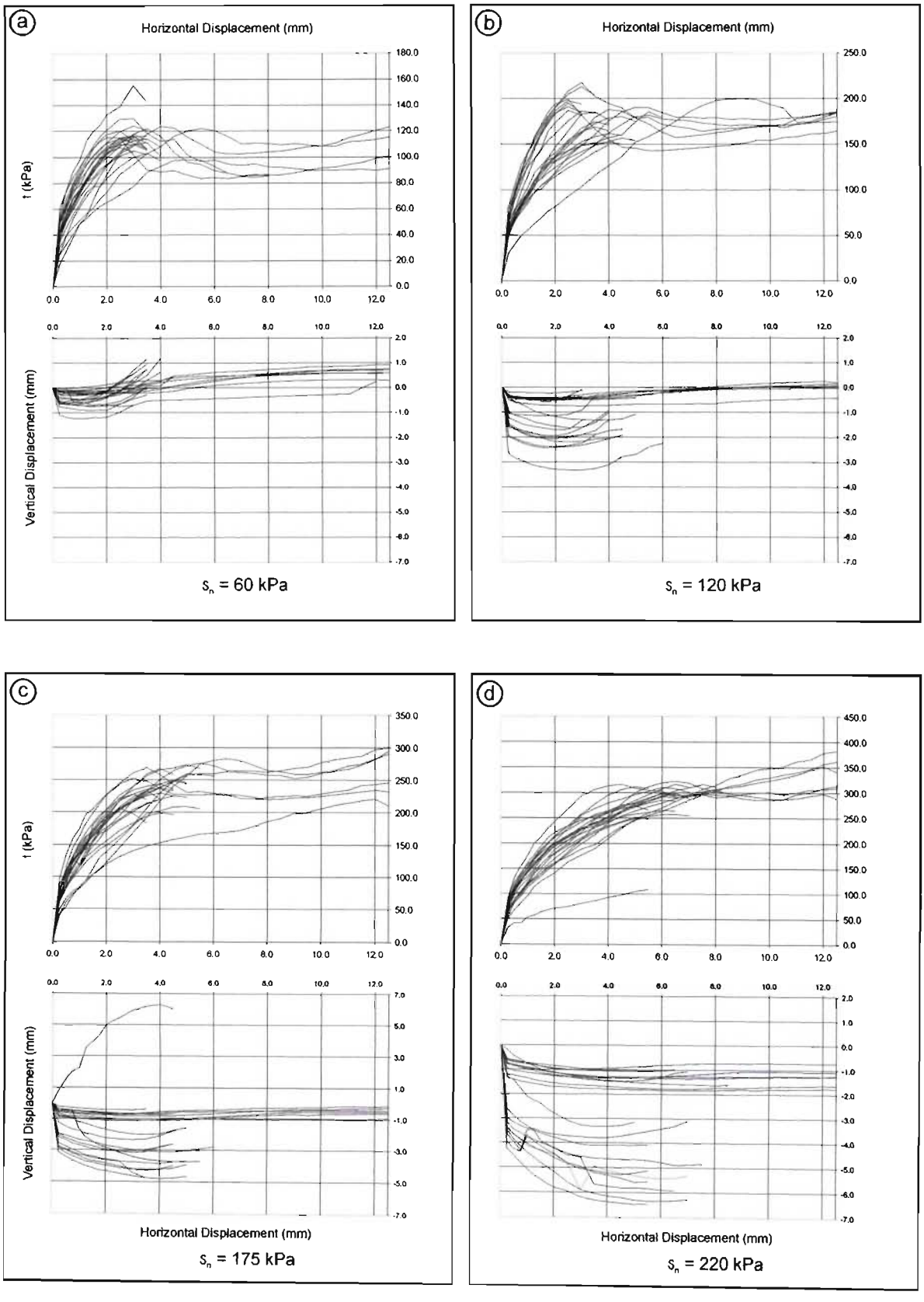

Figure 14.4. Stress-strain curves showing volume change in direct shear for left flank compacted samples sheared at optimum moisture content.

microcline feldspar grains along the failure surface. In all cases (with the exception of one sample - LF 9 at 175 kPa normal stress) the initial shearing of the sample is associated with contraction. Subsequent shearing results in a decrease in the rate of contraction. Thereafter, at low and intermediate normal stresses rapid dilation occurs as the dense matrix, quartz and unaltered feldspars undergo reorientation and overriding during shear. At higher normal stresses the dilation is less pronounced and in some cases very little volume change can be observed. Generally however, as shearing continues, so dilation commences with the peak shear strength very broadly related to the commencement of dilation. The shear strength curves for the remoulded highly weathered granite were similar, although they showed higher dilation at low to intermediate stresses due to the more competent grain component resident within these less weathered samples.

Although Carter and Bentley (1994) and others show that a relationship exists between φ' and density, Figure 14.5 illustrates that this relationship is complex, although a general increase in the friction angle can be related to increasing maximum dry density.

Only a slight increase in the shear strength parameters is noted for the compacted samples at optimum moisture content in comparison to the undisturbed samples (compare Tables 14.2 and 4 with Tables 13.3 and 4). φ for the compacted material at optimum moisture content varies from 34,9 to 55,3° with an average of 42,9° whilst cohesion increases significantly, having an average of 55,1kPa.

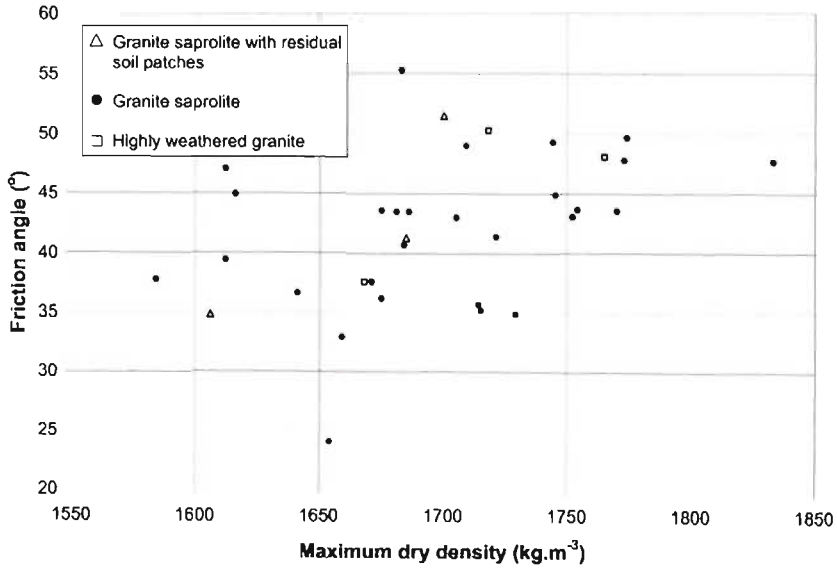

Figure 14.5. Relationship of friction angle with Standard Proctor maximum dry density sheared at optimum moisture content.

14.4.2 Direct shear tests on compacted samples under saturated conditions

Figures 14.6 and 14.7 show the stress-strain and vertical displacement-strain curves for the right and left flank saturated compacted samples, respectively. The results show a striking reduction in the shear strength upon saturation indicating that moisture content plays a significant role in the shear strength of the remoulded material. A broader and generally much lower peak strength is achieved as softening of the material occurs. The majority of the samples of granite saprolite and granite saprolite with residual soil patches are characterised by a Type 7 failure curve at all ranges of normal stress. Generally, the initial shearing of the sample is associated with contraction with subsequent shearing resulting in a decrease in the rate of contraction until, in many cases, very little volume change can be observed. The shear strength curves for the remoulded highly weathered granite were generally very similar, with the higher moisture contents of this material resulting in the smoother Type 7 curves. A poor relationship exists between the shear strength and density for these samples (Figure 14.8).

Saturation of the compacted samples shows a decrease in the shear strength parameters as compared to those obtained at optimum moisture content with φ' averaging 36,1 ° and cohesion averaging at 16,3kPa. Importantly, these values are less than the strength parameters of the undisturbed samples under saturated conditions and provides good evidence of the strength that the microfabric affords to the material in its undisturbed state.

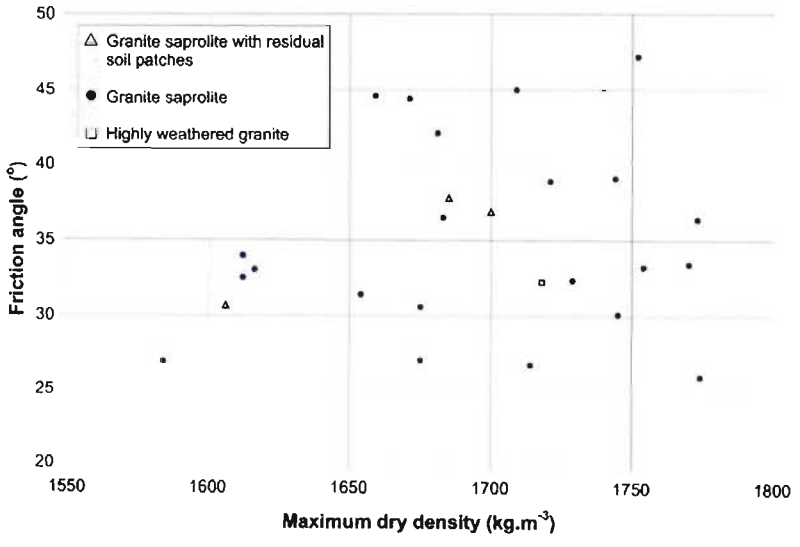

Figure 14.8. Relationship of maximum dry density with friction angle for compacted samples sheared saturated.

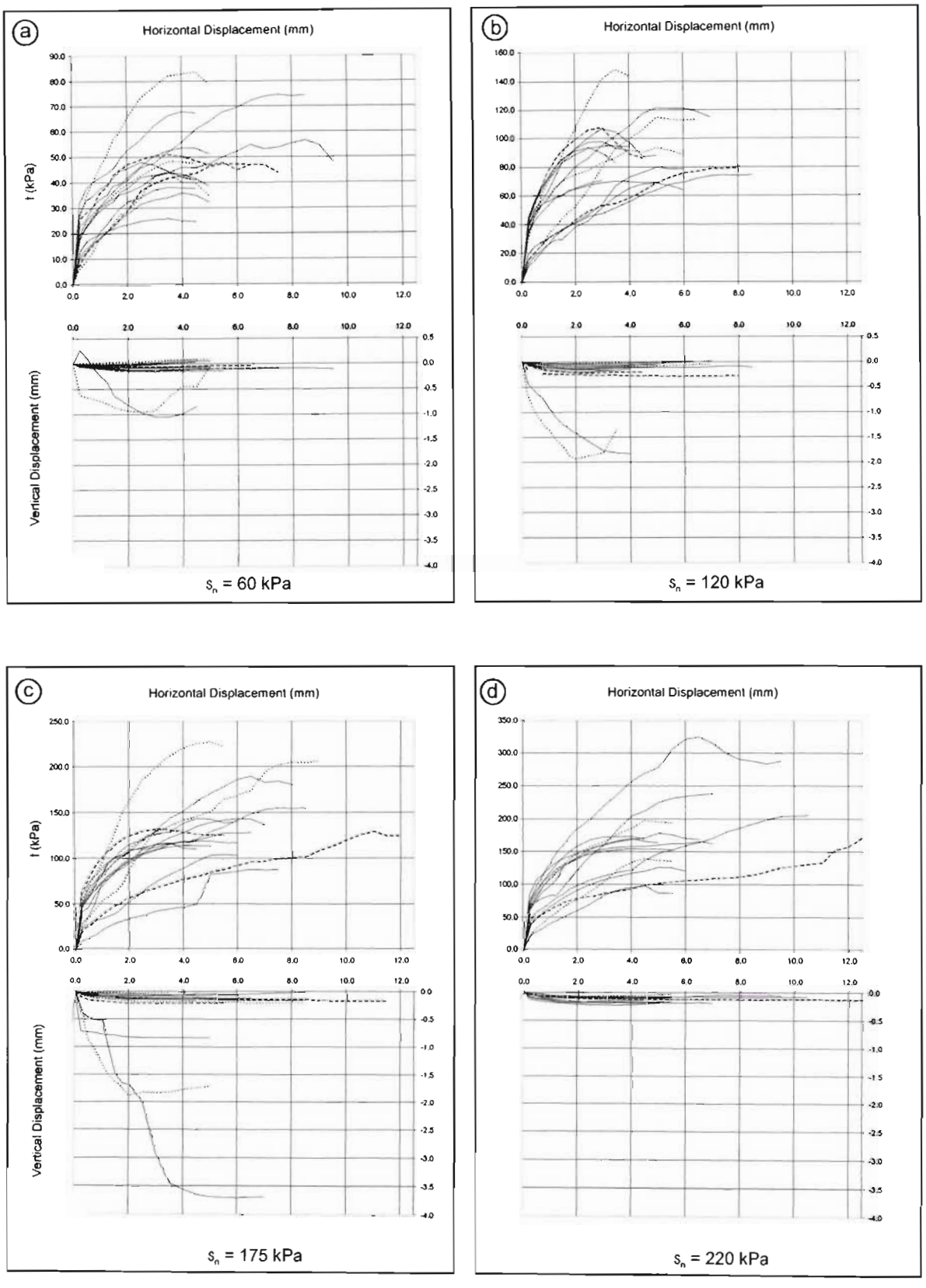

Figure 14.6. Stress-strain curves showing volume change in direct shear for right flank compacted samples sheared under saturated conditions.

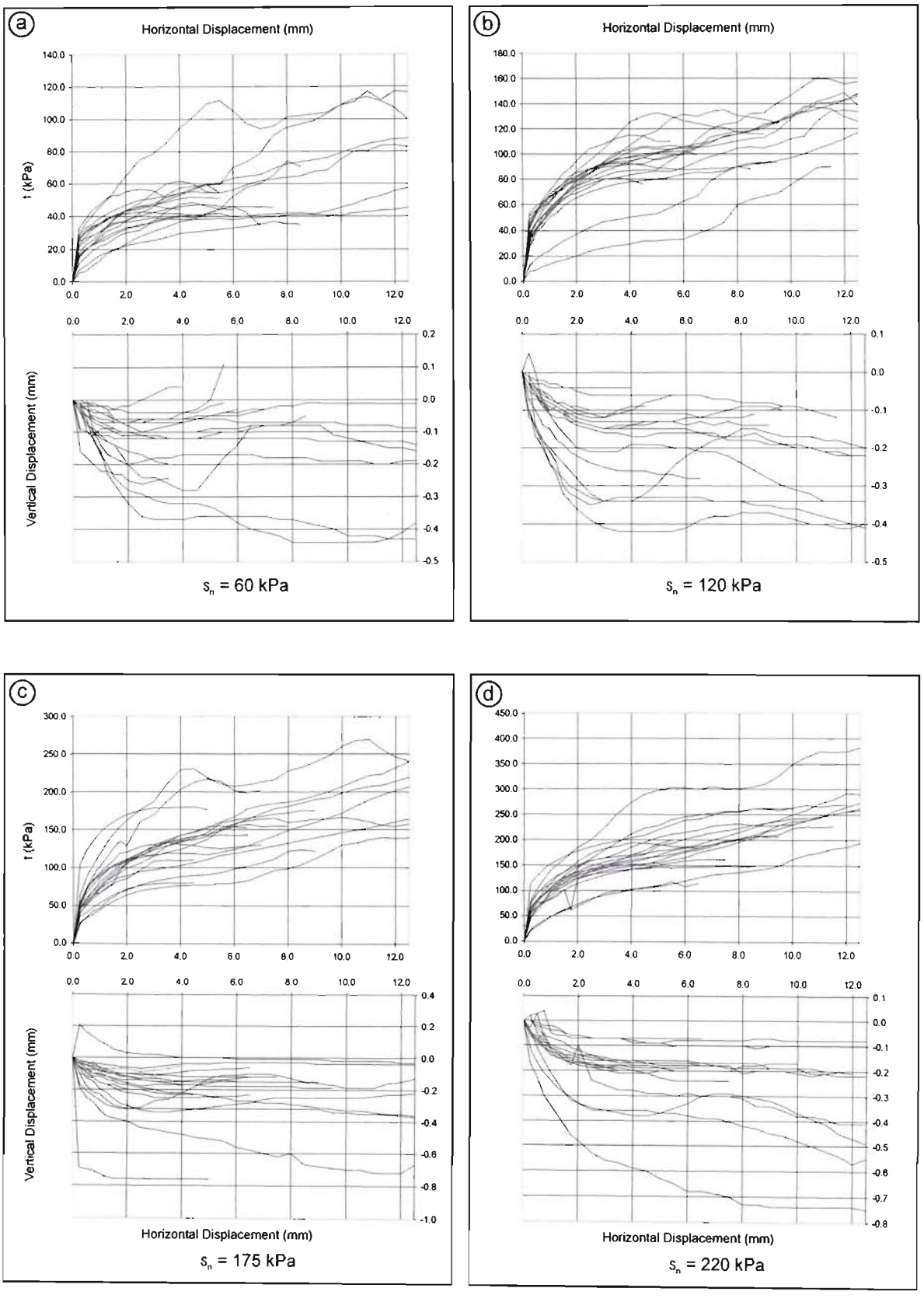

Figure 14.7. Stress-strain curves showing volume change in direct shear for left flank compacted samples sheared under saturated conditions.

14.4.3 Saturated consolidated drained triaxial tests on compacted samples

Saturated consolidated drained triaxial tests were conducted on samples of the weathered granite compacted to maximum dry density (Standard Proctor). Figure 14.9 shows the stress-strain curves for various selected samples at different cell pressures. The curves show a dramatic increase in stiffness in comparison to the tests conducted on the undisturbed samples (Figure 13.5) with much higher maximum shear stresses being achieved as is most likely due to the extra strength afforded by the consolidation process. As with the undisturbed samples two failure type curves can be identified, namely Type B (Figure 13.6) and Type C (Figure 14.10). Type C curves show a marked increase in stiffness in comparison to Type A, with only slight reduction in the shear stress being achieved post failure. These curves are characteristic of lower and intermediate confining pressures. As the confining pressure increases so the curves change to Type C, exhibiting a lower stiffness with a poorly defined peak shear stress.

A summary of the shear strength parameters for the compacted samples is shown in Tables 14.2 to 14.4. Effective stress points for the maximum deviator stress are shown in Figure 14.11. The data represents points s' and t' as defined by Atkinson and Bransby (1978) for the MIT stress path concept. It is possible to determine 'α and d', the stress path counterparts for φ' and c' from this data. Linear regression through these points shows that d' = 0,23 kPa and α'=30,1 °with calculation of the shear strength parameters giving the average results for the granite saprolite as $\varphi' = 35{,}4°$ and $c' = 0$ kPa. This represents only a 7 % increase in the effective angle of internal friction in comparison to the undisturbed samples. Averaging the shear strength parameters in Tables 14.2 to 14.4 gives values of $\varphi' = 33{,}4°$ and c' = 9,05.

The relationship of effective shear strength parameters from these triaxial tests shows a very general increase in the effective friction angle with increasing maximum dry density as shown in Figures 14.12.

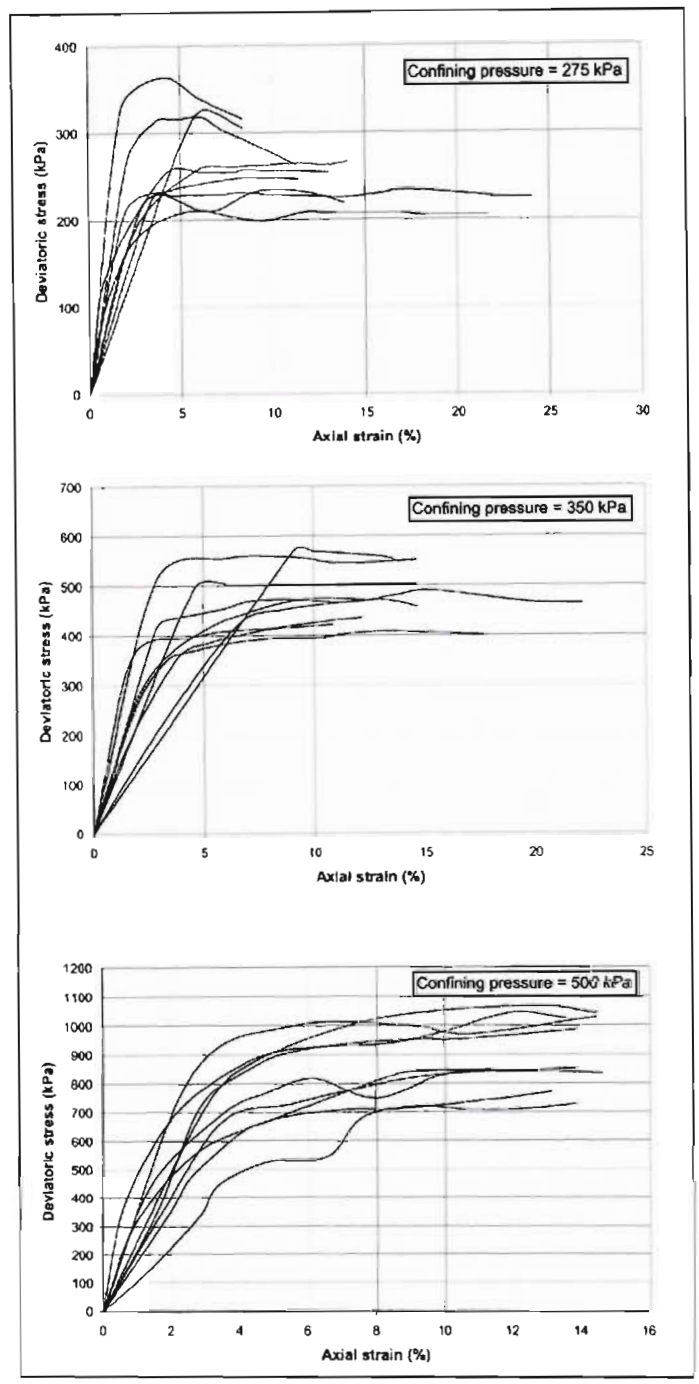

Figure 14.9. Stress strain curves for remoulded granite saprolite compacted to 100% Standard Proctor maximum dry density from saturated consolidated drained triaxial tests.

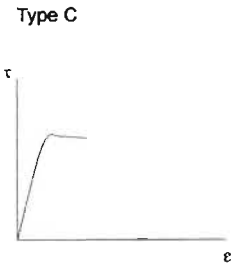

Figure 14.10. Type C failure curve for saturated compacted samples.

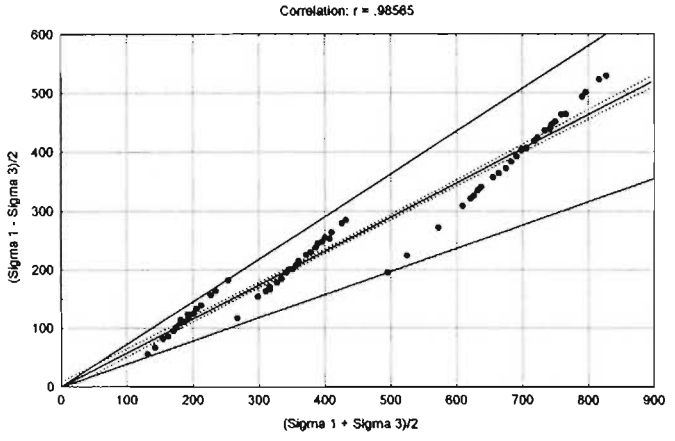

Figure 14.11. Effective stress points for maximum deviator stress for consolidated drained triaxial tests on compacted granite saprolite.

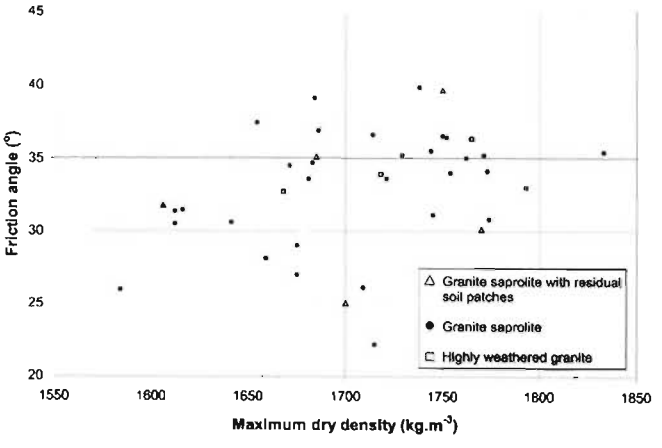

Figure 14.12. Variation of φ' from saturated consolidated drained triaxial tests with maximum dry density.

15. EFFECT OF GRANITE SAPROLITE ON DESIGN AND CONSTRUCTION OF INJAKA DAM

15.1 Introduction

The preceding chapters have described in detail the weathering of the granite saprolite at Injaka Dam and the geochemical, mineralogical, petrographical and engineering characteristics associated with the weathering of this material. This chapter serves to discuss the engineering measures undertaken at Injaka Dam to mitigate against certain problematic characteristics of the granite saprolite with particular emphasis on the treatment of the dam foundations.

It must be appreciated that due to the complex nature of the dam foundation geology as shown in Figure 2.5 the design solution for Injaka Dam was not based entirely upon the engineering performance of the granite saprolite alone, but also included the intimate inter-relationship of this material with the weathered diabase dykes that intersect the foundation. Nevertheless, this chapter deals primarily with the effects of the weathered granite and the following characteristics of the founding material (granite saprolite) for the earthfill embankment were considered as critical during the design and construction of Injaka Dam and required some form of engineering remediation:

- deep weathering profile resulting in thick saprolite deposits overlying bedrock with intense leaching forming low density, high porosity material susceptible to collapse settlement and consolidation,
- high porosities leading to moderate permeabilities of the granite saprolite and permeability differentials between diabase and granite saprolite,
- dispersive nature of the granite saprolite

15.2 Mitigation against collapse settlement of granite saprolite

The intensely leached nature of the granite saprolite with its open soil micro-structure makes the material susceptible to collapse settlement upon saturation (Chapter 12). The effect of this on the settlement of the dam foundation and embankment during construction and impoundment was cause for concern by the design engineers. There exist a number of methods for reducing the collapse settlement in dam foundations. These include removal of the problematic horizon; removal, backfill and re-compaction; pre-wetting and loading; and *in situ* compaction of the horizon. Choudry (1988), described various measures adopted in the construction of the Guri embankment dams in Venezuela

which were constructed upon thick granite-gneiss saprolites which exhibited low dry densities and low degrees of saturation. Choudry's description of the measures adopted included the removal of a certain amount of the collapsible material, several changes in alignments of the dams and pre-wetting of the foundations using canals and drainage holes. Similarly, measures employed at Zoeknog Dam included the stripping of the highly collapsible granite saprolite to depths and densities that correlated to approximately 1600kg.m^{-3} - the suggested dry density limit of collapse settlement soils as proposed by Brink (1996).

At Injaka Dam, the initial design calculations based upon early geotechnical investigations suggested that by removing the upper 5m of the granite saprolite, a significant reduction in the collapse settlement could be achieved as the density of the granite saprolite was thought to improve considerably beyond this depth. During construction of the dam and opening of the foundation footprint, the results as shown in Chapter 12 and published by Haskins and Bell (2002) suggested differently. They showed the granite saprolite to exhibit a maximum collapse potential of 6% at 191kPa saturation pressure (extending to 8% at 381kPa saturation) and that even at 7,5m depth a collapse potential of 2% could be measured. Their conclusions demonstrated that the initial design assumption for the final excavation level of the foundation footprint was inadequate They determined this by assessing the relationship of the dry density and depth with the collapse potential. This relationship is shown in Figure 12.8 and illustrates the reduction in collapse potential beyond a dry density of 1600kg.m^{-3}.

During the excavation of the dam foundation footprint numerous compaction tests were carried out on the granite saprolite to assess its suitability for embankment construction. Results for samples collected from Traverses 1 to 6 for this research have been discussed in Chapter 14. When a comparison of the collapse potential with the ratio of dry density to maximum dry density (as determined by Standard Proctor compaction) i.e. a measure of the metastable state, is carried out it can be seen that at 90% maximum dry density/dry density ratio, the collapse potential is generally below 1% (Table 15.1 and Figure 15.1).

The final design measures required an excavation level for the foundation footprint that met either of the above two requirements: $\rho_d \geq 1600kg.m^{-3}$ or %mdd $\geq$ 90%. This ultimately translated to a maximum excavation depth of 13m below original ground level at the deepest point in the foundation, becoming shallower towards the edges of the embankment. On average, an 8m excavation depth was required over the foundation footprint.

Table 15.1. Collapse potential characteristics with % maximum dry density for Traverses 1 to 6 (saturation at 191 kPa).

Sample	Depth (m)	ρ_d (kg.m^{-3})	Maximum dry density (kg.m^{-3})	Optimum moisture content (%)		Collapse potential (%)
Traverse 1						
RF 12*	1,0	1463	1606	21,8	94	0,61
RF 10	3,5	1369	1612	18,5	83	3,91
RF 9	4,9	1349	1654	18,9	83	5,83
RF 8	5,7	1715	1715	18,8	88	0,32
RF 7	6,6	1747	1683	13,0	100	3,01
Traverse 2						
RF 6	2,5	1469	1584	19,9	92	0,86
RF 5	4,8	1388	1752	16,0	100	0,07
RF 4	6,9	1342	1616	19,2	90	0,14
RF 3	9,2	1434	1744	15,4	97	1,47
Traverse 3						
LF 7*	1,1	1444	1685	16,7	86	5,69
LF 8	2,8	1518	1750	17,4	85	3,27
LF 9	4,0	1557	1773	15,7	81	2,26
LF 10	5,5	1460	1612	20,8	89	1,14
LF 11	6,5	1371	1641	17,7	83	1,42
LF 12	7,3	1487	1729	17,0	71	2,24
LF 13	7,7	1927	1714	17,8	95	0,75
Traverse 4						
LF 1*	0,9	1478	1750	15,9	84	3,38
LF 2	2,4	1419	1671	18,2	84	2,89
LF 3	3,8	1430	1681	16,5	84	3,11
LF 4	4,5	1523	1721	16,9	88	0,82
LF 5	5,2	1680	1774	15,5	91	0,55
LF 6	5,5	1399	1659	17,0	86	0,61
Traverse 5						
LF 18*	1,1	1436	1770	16,7	87	2,45
LF 19	2,3	1361	1745	17,1	75	3,79
LF 20	3,2	1313	1675	17,5	78	3,62
LF 21	4,0	1313	1738	16,2	80	1,67
LF 22	5,1	1373	1793	14,5	79	5,14
LF 24	5,7	1379	1771	14,0	79	0,04
LF 25	6,2	1541	1762	14,8	87	1,44
LF 26	7,2	1492	1754	15,0	87	1,22
Traverse 6						
RF 17*	2,2	1487	1700	17,8	82	0,92
RF 18	3,8	1345	1675	18,3	83	4,05
RF 20	5,2	1387	1684	17,4	88	0,16
RF 21	6,1	1394	1686	17,8	98	0,10

* Granite saprolite with residual soil patches.

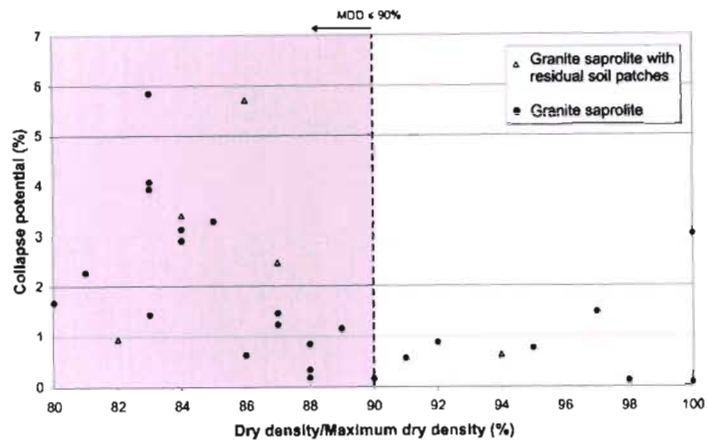

Figure 15.1. Collapse potential as a function of % maximum dry density.

15.3 Mitigation for moderate permeability and dispersivity of foundation materials

15.3.1 Alignment of clay core with natural cut-offs

The granite saprolite has been shown to have a variable, but moderate permeability (Chapter 10) and compounding this, the material classifies as being dispersive (Chapter 11) and highly erodible. These characteristics require special attention in dam design. In light of the very deeply weathered and intensely leached foundation material, it was realised during the early design phase of the dam that seepage would occur beneath the dam wall through the weathered granite saprolite. It was also realised that the finer-grained diabase dykes and their weathering products would act as natural cutoffs across the foundation An extensive testing programme was thus undertaken to quantify the permeability of these weathered materials and the results of the weathered granite are presented and discussed in Chapter 10 and summarised with the weathered diabase results in Table 15.2.

Table 15.2 Permeability of granite and diabase saprolite from various methods.

Test type	Material	k_{mean} (cm.s^{-1})	N
Laboratory falling head test (Head, 1982)	Granite saprolite	1,6 x 10^{-4}	33
	Diabase saprolite	1,0 x 10^{-5}	2
Field falling head test (Lambe and Whitman, 1969)	Granite saprolite	6,5 x 10^{-5}	38
	Diabase saprolite	5,0 x 10^{-5}	4
Field constant head test (Anon, 1968)	Granite saprolite	1,8 x 10^{-5}	2
	Diabase saprolite	1,5 x 10^{-5}	5

Table 15.2 shows that the granite saprolite exhibits a slightly higher permeability in comparison to the diabase. This, together with the fact that the weathered diabase was determined to be less dispersive and erodible than the granite saprolite, meant that the diabase provided a superior flow resistance to water moving through the foundation with less chance of piping failure developing through this material. The favourable position of the diabase dykes (generally coincidental with the clay core of the dam centerline (Figure 2.5) meant that the majority of the length of the clay core with some minor alignment readjustments could be tied into the dykes to provide a natural, extended cut-off.

15.3.2 Construction of jet grout cut-off

Notwithstanding this design option of tying in the clay core into the weathered diabase, Figure 2.5 shows that on the upper left flank of the dam foundation the alignment of the clay core does not coincide with any of the dykes intersecting the foundation and no natural cut-off was available in this area. This essentially exposed a 120m long section of 20m deep, intensely leached granite saprolite through which seepage could occur.

Initial considerations to use permeation grouting as a method of reducing the permeability of the granite saprolite were investigated. Permeation grouting is the application where grout, generally under low pressure, permeates through the interstices between the soil grains without deforming the grain structure of the *in situ* formation. Parry-Davies (1991) confirms that this is the ideal solution for soils to render them less permeable to the passage of water. The efficacy of such a method is determined primarily by the grain size of the soil and its permeability. An extensive grout testing programme was undertaken to determine the success of permeation and tube-a-manchette grouting techniques using super fine cementitious products and chemical grouts to permeate the granite saprolite. The results from this programme proved that neither method nor grout type were suitable for successfully grouting up the saprolite. Consequently, in the area beneath the clay core where no diabase dykes were present, an alternate solution had to be found. This incorporated the design and construction of a jet grout curtain as discussed by Haskins and Van Zyl (2002), to minimise seepage through the foundation and thus prevent the possible formation of piping failure beneath the dam wall. Heinz and Segatto (1999) consider this grouting method to be extremely effective in reducing seepage in deeply weathered dam foundations that are considered to be dispersive.

According to Parry-Davies (1991), jet grouting is a relatively new form of grouting that was originally developed around 1960. The method consists of mixing a cement with the *in situ* soil using a rotating lance and essentially improves the consolidation and cementation of the host material. By doing this,

the permeability of the material is also reduced. The basis of the system is the high pressure injection of grout into a soil through a rotating drilling rod forming mixed soil and grout columns as the rod is withdrawn from the drilled pilot hole. By interlocking the columns so formed an impervious barrier can be created.

To test the efficacy of the jet grout method in the granite saprolite, a number of secant test columns were constructed to determine the various factors that affect column diameter and mixing within the columns. The diameter and mixing are critical when creating a cut-off wall as the interlock between columns is determined by the column spacing (dictated by column diameter) whilst the mixing should produce an homogeneous mixture of cementitious product and soil to reduce the permeability of the material within the columns. The factors that affect the diameter and mixing include withdrawal and rotation rate of the cement water jet, the pressure at which the jet is operated and the strength of the material being treated. Following the test jet grouting programme, the columns were exposed within the dam foundation and Table 15.3 presents a summary of the results.

Table 15.3. Results from jet grout tests in granite saprolite.

Column	Depth of jetting	Jetting pressure	Withdrawal rate	Diameter of	Water: cement	Cement
1	5-3	400	9	±750	1:1	±500
1	3-1	400	7	±725	1:1	±500
2	5-1	400	6	±600	1:1	±300
3	22-1	400	6	±600	1:1	±300

The test jet grout programme showed that by slightly increasing the withdrawal rate of the jet nozzle from 9 to 6 seconds per 75mm, only 150mm reduction in the column diameter was evident (from 750mm to 600mm). However, a significant reduction in the cement consumption could be won by increasing this rate, with a saving of approximately 200kg of cement per metre length using the faster withdrawal rate. Figures 15.2a and b show the interlocking test columns and the satisfactory mixing achieved within the columns by the jet grout process.

From this information the jet grout curtain was designed with columns chosen to be 600mm in diameter with a centre-to-centre spacing of 450mm, resulting in a 150mm interlock between adjacent columns. The layout of the jet grout cut-off was positioned along the centerline of the dam and tied into the diabase dykes (Figure 15.3). Although the majority of the 129m long cut-off wall comprised only a single row of interlocking columns, a double row of columns was constructed where the diabase dyke intersects the granite along the line of the cut-off (Figures 15.3 and 4). This double row was necessary

to provide an effective cut-off over this geological contact that was considered to be a preferential seepage pathway.

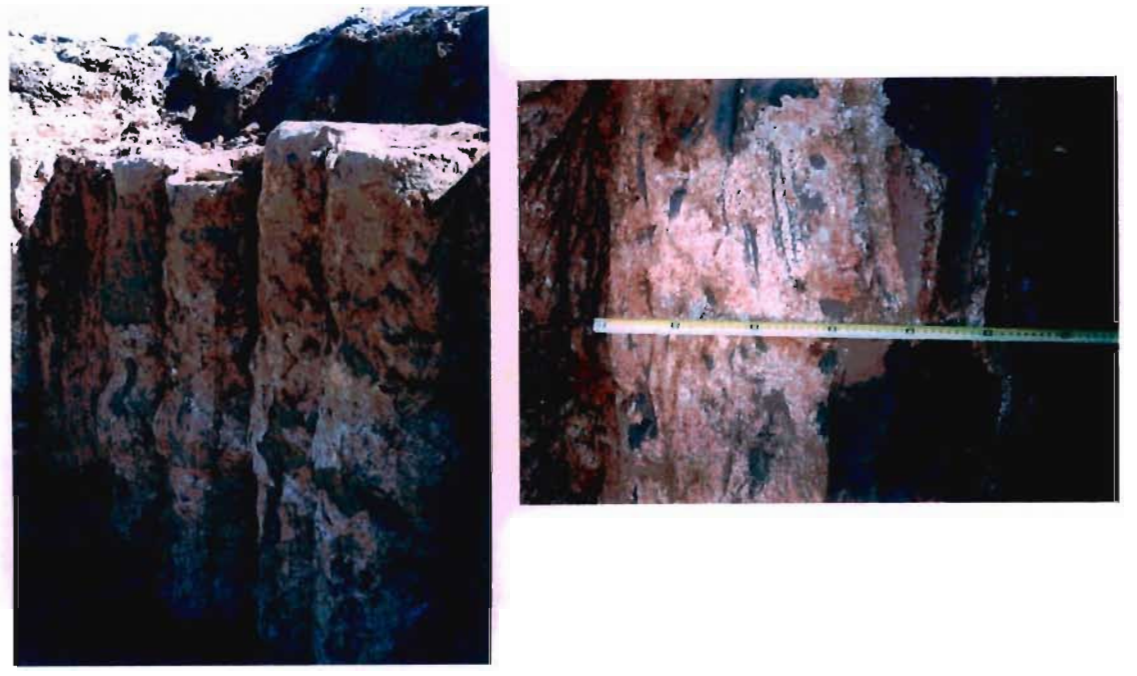

Figures 15.2a and b. (a) Test columns for jet grout method in granite saprolite. (b) Good mixing of cementitious grout with saprolite to form homogeneous column.

The deepest column in the cut-off extended to 26m below foundation invert level in the granite saprolite whilst those in the diabase averaged to a depth of 13m. All columns were jetted to 2m below ground level (final excavation level for the foundation footprint), whilst the base of the columns was determined by refusal or near refusal of the tricone bit used to drill the pilot hole.

As the columns were designed to reduce the saprolite permeability and not serve a structural function the grout mix was changed from that used in the initial tests and consisted of water and cementitious product, with the cementitious product consisting of Pulverised Fly Ash (PFA) and Ordinary Portland Cement (OPC) in an original mass ratio of 50:50 at a water:cementitious product ratio of 1. This was later changed when the PFA and OPC was used in a mass ratio of 67:33 at a water:cementitious product ratio of 0,82. The mix was injected at a pressure of 40 MPa and average strengths for the jet grout mixture was determined to be 7,5 MPa. There were a number of advantages in using the OPC-PFA mix in the jet grout columns and these included:

- PFA as a pozzolan reacts with the by-products of the hydration process of the OPC contributing to the long-term strength increase in the columns.
- The shape of the PFA particles provides higher workability of the grout and the water/cement ratio could therefore be reduced without loss of workability.
- PFA bulking significantly reduced the cost of the columns.
- PFA produces a cementitious product which is less permeable than that which is made up of only OPC.

In order to check the integrity of the jet grout columns a number of core holes were drilled through the columns. These were either drilled vertically to obtain an indication of the mixing within the column or were inclined at 30° to check the condition of the column interlocks. Permeability testing using falling head tests and water pressure testing using packer tests was carried out in these holes. The results from these tests are shown in Table 15.4 and indicate that an acceptable cut-off was achieved using the jet grout columns.

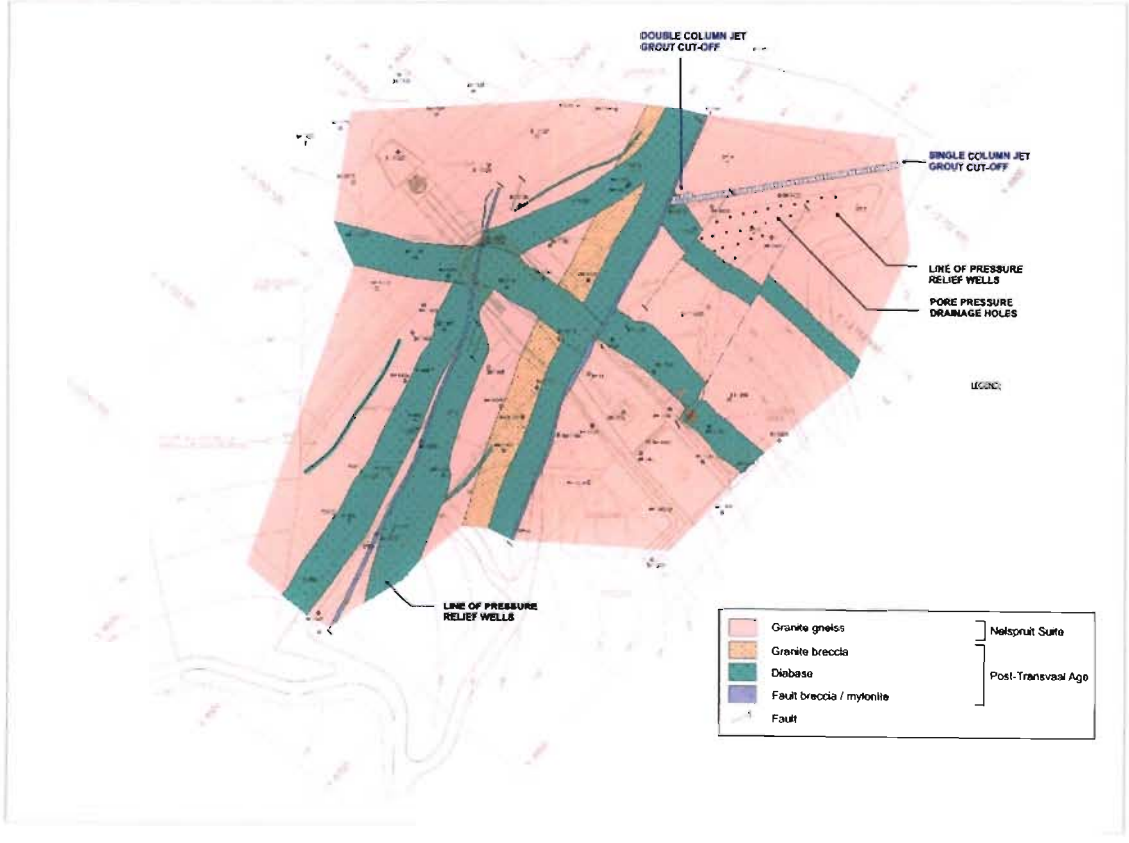

Figure 15.3. Layout of jet grout curtain and pressure relief wells at Injaka dam.

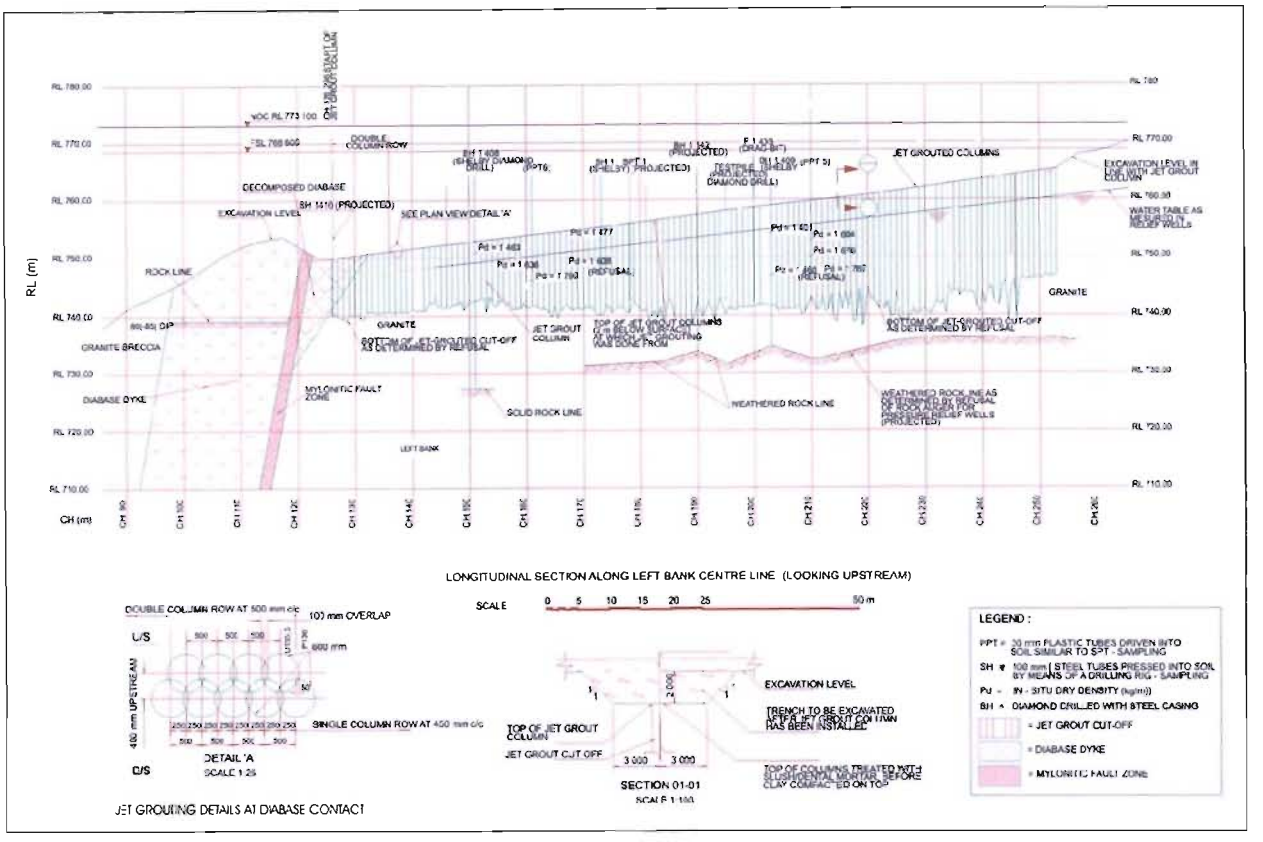

Figure 15.4. Longitudinal section along jet grout curtain showing depth of columns and column layout details.

Table 15.4. Falling head and water pressure tests on grout columns.

	Falling head tests			Water pressure tests			
Hole No.	Time (mins)	Water level drop (mm)	Depth (m)	Pressure (kPa)	Time (mins)	Flow (l)	Depth (m)
C1	5	43	0-18,4	100	5	0	8-18,4
C2	5	20	0-35,5	50	5	0,4	8-35,3
C3	5	25	0-27,34	100			
C4	5	17	0-15,0	100	5	0,9	8-28,5
C5	5	12	0-14,16	100	5	0	8-29,5
C6	5	85	0-23,5	100	5	0	0-23,5

As a consequence of the expected differential settlement between the jet grout columns and the in situ saprolitic material, with the associated risk of cracks developing through the clay core, a 2m thick flexible clay capping (placed wet of optimum moisture content) was constructed over the jet grout

columns (Figure 15.4). The flexible clay capping was designed to allow for plastic deformation around the top of the columns.

15.3.3 Pressure relief wells

In order to prevent any uncontrolled seepage through the weathered granite foundation that may lead to piping, a line of 23 pressure relief wells, varying in diameter from 1 200mm to 600mm was constructed along the toe of the dam on both the right and left flanks. The wells were auger drilled to depths varying between 9m and 34m and refused on highly weathered granite or weathered diabase, depending upon their location. Although the drilling of the wells was carried out easily on the right flank where no water table was measured, the shallow water table conditions encountered on the upper left flank (Figure 15.4) proved to be problematic. The shallow water table (between 3,5m and 5,5m below the final excavation level) occurred as a result of the confining nature of the diabase dyke which strikes perpendicular to the slope of the valley (Figures 15.3 and 15.4).

Initial attempts at augering the large diameter holes with casing support proved to be unsuccessful below the water table. The large diameter casing could not be advanced continuously with the auger drill resulting in short sections (0,5m to 1,0m) of the holes being unsupported at times during the drilling operation. Severe caving and collapse of the sidewalls as a result of the softened saprolite material in these areas prevented any further advance of the holes and in fact two of the original pressure relief wells had to be abandoned because of this. With the realisation that conventional auger drill and casing techniques would not be successful for such deep, large diameter drilling in the granite saprolite, a new form of hole support was identified for the drilling operations. This incorporated the use of the organic drilling mud, PAC-R. This product is an organic cellulose gum derived from the linter of cotton. Although other types of cheaper drilling muds could have been chosen, PAC-R was identified because it could also fulfil the requirements necessary for drilling the pressure relief wells. These include the requirement that the drilling mud should not permanently seal the sides of the hole and that the mud must maintain the hole open for a period of 3 to 4 days (thus ensuring support of the hole even in the event of plant break down).

Despite the fact that the PAC-R temporarily seals the sides of the hole during use, the product is biodegradable after 20 days and washes out. The polymer can also be promptly destroyed by the addition of chlorine should this be required. A further advantage of this product was the fact that it could be recycled and used for multiple holes. During filling of the pressure relief well holes with filter sand, the excess drilling mud was pumped back into the mixing hopper for re-use.

15.4 Liquefaction potential

Whilst not forming the direct brief of this research, it was felt appropriate to include a section on the liquefaction potential of the granite saprolite to complete the analysis of the engineering geological behaviour of this material. This problem also formed a component of the concerns addressed by the design engineers, although the results of this investigation were presented by Welland (2002).

Liquefaction can be considered to be the transformation of a granular material from a solid to a liquefied state as a consequence of increased pore water and reduced effective stress (Marcuson, 1978). As liquefaction occurs it allows large cyclic deformations to take place caused by softening of the soil, which may be accompanied by loss of shear strength that may lead to flow failure (Youd and Idriss, 2001) and possible catastrophic consequences in respect of dam construction.

Welland (2002), has proposed a methodology for estimating the liquefaction potential using theoretical and empirical methods and has carried out an analysis of the Injaka Dam site (pre-construction and post-impoundment) using these methods. He proposes a generalised relationship of liquefaction potential with a suite of geotechnical limit characteristics as shown in Table 15.5 and concludes that the average soil parameters of the in situ granite saprolite at Injaka Dam site (pre-construction) are such that they it is able to withstand moderate earthquake intensities of V and peak ground accelerations of 0,1*g*. This he considers to be due directly to the reasonably high average in situ relative density of the saprolite and indirectly to the fairly deep water table at 15 m, which places the potentially liquefiable layer at a safe enough depth to pre-empt liquefaction.

Table 15.5. Theoretical and empirical geotechnical limit criteria as determined by Welland (2002) for preliminary liquefaction potential.

Parameter	Liquefaction potential		
	Very likely	Marginal	Very unlikely
Dr (%)	< 33	33 -54	> 54
Corrected SPT 'N'	< 10	10 - 25	> 25
Consistency	Very loose	Loose	> Medium
Bulk density (kg.m^{-3})	1700 - 1800	1800 - 1900	> 1900
Dry density (kg.m^{-3})	1300 - 1400	1400 - 1500	> 1500
Friction angle (°)	< 35	35 - 38	> 38
Suitability No. S_n	< 20	20 - 50	> 50
Silt and clay (%)	< 10	10 - 15	> 15
D_{60}(mm)	0,2 - 1,0		<0,2 or > 1,0
D_{10}(mm)	0,05 - 0,1	0,01 - 0,05 or 0,1 - 0,25	< 0,01 or > 0,25
$Cu = D_{60}/D_{10}$	2 - 4	4 - 5	< 2 or > 5

For the post-impoundment case the probability of liquefaction increases until a "Class 2" (liquefaction unlikely) is attained with a head of 10 m. He maintains that the analysis shows that only after considering a ground acceleration of 0,2*g* that a Class 4 (liquefaction very likely) is realised under the post-impoundment conditions. This is considered to be an unlikely scenario based upon the seismicity of the Injaka Dam area.

16. CONCLUSIONS

The weathering of granite at Injaka Dam site has taken place over an extensive period (140 million years) where intense leaching of the weathered profile has resulted in a very porous weathered mantle overlying the bedrock. This comprises a thick sequence (over 36m) of granite saprolite overlying weathered bedrock, and underlying a thin veneer (1m) of granite saprolite with residual soil patches.

The nature of weathered granites, and granite saprolite in particular, is complex with the heterogeneity of the material presenting problems in its characterisation and testing. This research has managed to classify the weathering of granite at Injaka Dam, with specific emphasis on the Grade V and VI material and has related this (where possible) to the engineering behaviour of the material.

Scanning electron microscope (SEM), petrographical, mineralogical and geochemical techniques were used to study the nature of the weathering. The SEM research proved invaluable in investigating and understanding the complex nature of the microfabric of the weathered granite - a feature which is critical in assessing the engineering behaviour of this material. Although the technique is only qualitative, the results from these observations could be reconciled with petrographic studies and changes in mineralogy and geochemistry. The results showed that progressive weathering led to a significant increase in porosity through solution effects and microcracking. In particular, a high sub-microscopic porosity was achieved through solution of the feldspar grains (particularly plagioclase) where intense etching of these grains can reduce them to skeletal fragments. Macroporosity in the form of vermiform solution voids and open microcracks also contributed to an increase in the porosity of the granite as weathering intensified. The transformation of the granite bedrock to granite saprolite involved the formation of significant amounts of kaolinite primarily from the decomposition of plagioclase feldspars with chemical weathering of microcline and biotite (to a lesser extent) also producing clay. Importantly, the formation of this clay occurred without significant disruption to the original microfabric of the parent rock, resulting in the characteristic relict fabric retained by the saprolite.

The petrographic research supported the results from the SEM studies, showing the increase in porosity in the form of microcracking, solution voids and etching with advancing weathering. The advantage of the petrographic studies was that the microfabric could be quantified using the micropetrographic index (I_p). This index showed a very clear relationship with the density of the weathered material.

Aside from semi-quantitatively characterising the mineralogy of the weathered granite, XRD results corroborated the findings from the SEM and petrographic studies, showing that leaching and decomposition played a significant role in the formation of this granite saprolite. The semi-quantitative nature of the XRD studies allowed for general mineralogical weathering trends to be identified as weathering advances from the highly weathered bedrock at depth, to the granite saprolite with residual soil patches at the surface. A very prominent inverse relationship between the plagioclase feldspars and the formation of kaolinite could be identified.

An analysis of the geochemistry augmented the understanding of the weathering processes and the effects thereof. The leaching relationships of specific elements, in particular Ca, Na and K can be reconciled with observations from the SEM study and mineralogical and petrographical studies and in fact can be related to the change in density of the material as weathering advances. The mineralogical and geochemical analysis also allowed specific geochemical and mineralogical weathering indices to be formulated. These were compared to changes in the density of the weathered granite and acceptable relationships between these indices and material density could be derived. In this way, the weathering grade of the granite and its associated microfabric could be indexed.

The typical engineering relationships which have been developed for transported soils, which relate the results of soil classification tests to engineering properties appear to be more complex for saprolitic soils. It has been shown from this research that the determination of a meaningful grain size for the saprolite is difficult. The clay content of the material using standard sieve and hydrometer techniques was appreciably lower than that obtained from XRD analysis and has proven that the clay mineralogy acts as a coarser fraction within the material and may in fact be "locked" within primary minerals. This behaviour means that the classification of these soils may be affected. Generally, however, the weathered profile progresses from a coarser to finer grained structure with the granite saprolite classifying as a sandy silt whilst the finer-grained ,overlying granite saprolite with residual soil patches tends to plot closer to the A-line.

The density of the weathered granite proved to be an important criteria in the indexing of weathering, and generally increased with depth. Localised variations in density were noted and are attributed to inherent mineralogical variations within the parent rock and local variations of the weathering environment (macro- and micro-scale). The dry density of the granite saprolite with residual soil patches varied from 1444 to 1516 kgm^{-3}, whilst the granite saprolite ranged from a low of 1226 to a high of 1855 kgm^{-3}. The underlying highly weathered granite bedrock exhibited significantly higher densities ranging from 2080 to 2480 kgm^{-3} and is indicative of the characteristically abrupt transition in the weathered profile from granite saprolite to weathered bedrock.

Permeability tests were also conducted on the material and showed the granite saprolite with residual soil patches to exhibit values of permeability between $6,8 \times 10^{-5}$ and $1,3 \times 10^{-4}$ cms^{-1}. The saprolite showed similar permeability values ranging from $1,4 \times 10^{-4}$ to $1,0 \times 10^{-5}$ cms^{-1}, indicative of good drainage conditions. The high degree of scatter of the permeability results made it very difficult to apply index values to this parameter, although a tentative relationship with Xd has been shown.

Anomalous runnel and piping formation on certain excavations within the weathered granite profile have shown this material to be dispersive and erodible. In order to quantify this dispersivity, a suite of tests was undertaken on the material. Typically, and as found by previous studies and research on this subject, poor correlation was achieved between the tests, although the crumb test and double hydrometer test proved to be the most suitable in characterising the dispersive behaviour of the weathered granite. It is consequently recommended that these two tests be used when assessing the dispersivity of this material.

The relatively low densities and high void ratios produced by the intense leaching conditions has meant that the granite saprolite is particularly prone to collapse settlement - this being exacerbated by the enigmatic nature of the "porous-connected" microfabric typical of this material. A series of consolidation tests including double oedometer and single oedometer collapse potential tests were undertaken. A number of observations were made including the fact that the samples which consolidated under saturated conditions exhibited a significant loss in strength and stiffness. It is postulated that this may be due to the dispersive nature of the material as well as softening during saturation which results in localised disruption of the microfabric.

The collapse potential tests proved the weathered granite to exhibit metastability with collapse potential values at 200 kPa saturation ranging from 0,6 to 5,7% for the granite saprolite with residual soil patches and from 0,1 to 6,4% for the granite saprolite. Typically higher values were noted when the saturation pressure was increased. The results from this research also showed the granite saprolite to exhibit a critical degree of saturation of 60%, with any value below this suggesting a propensity for collapse potential above 1% to occur upon saturation and under load of 200 kPa. To augment these results a new technique assessing collapse potential using local strain instrumentation in the triaxial apparatus was used. Limited results from this technique were presented in this study.

The development of collapse settlement indices is useful in that they may predict the metastability behaviour of a material and therefore reduce the need for many expensive and time-consuming laboratory tests. A variety of such indices developed by previous authors were applied to the material to assess their suitability. Generally, all of the indices, with the exception of Xd, proved to

satisfactorily differentiate metastability within the weathering profile, although it is to be noted that such indexing must be calibrated to specific material or site conditions.

A series of dry and saturated quick shear tests as well as saturated consolidated drained triaxial tests were carried out to determine the shear strength parameters of the weathered granite. Results from the direct shear tests at natural moisture content showed $\varphi \approx 40°$ with a variable cohesion intercept. Under saturated conditions a distinct reduction in cohesion was noted with φ values remaining comparable to results from the natural moisture state. Saturated consolidated drained triaxial tests showed effective shear strength parameters of $c' \approx 0$ kPa and $\varphi' \approx 33°$. The nature of the shear failure was tentatively explained in this research using broad observations of microfabric. Limited stress path tests determined from the triaxial tests were useful in assessing the significance of the relict structure in contributing to the nature of shear failure.

Engineering characterisation of the remoulded, compacted weathered granite was carried out to assess the suitability of the material for use in the earthfill embankment. Standard Proctor compaction tests showed the granite saprolite with residual soil patches and the granite saprolite to exhibit similar compaction behaviour having a maximum dry density of 1700 $kg.m^{-3}$ with an optimum moisture content of around 17 or 18%. The highly weathered granite exhibited a lower maximum dry density of 1683$kg.m^{-3}$ with an optimum moisture content of 16%. Permeability tests carried out on the remoulded samples showed the granite saprolite to exhibit an average permeability of 1,7 x 10-5 $cm.s^{-1}$ whilst the lower compaction effort achieved by the highly weathered granite resulted in its higher permeability of 4,5 x 10^{-4} $cm.s^{-1}$. Consolidation characteristics on the remoulded granite saprolite showed it to exhibit a low compression and reasonably low collapse settlement at various defined saturation pressures. A suite of shear tests was carried out on the various grades of remoulded weathered granite. The nature of the shear failure curves and their differences with regard to the shear failure curves recorded for the undisturbed material was tentatively explained. Generally, only a slight increase in the shear strength of the compacted material was noted against that of the undisturbed material.

A number of engineering solutions were required to construct Injaka Dam in the granite saprolite. These were guided by findings from this study. Some of these solutions including excavation and recompaction of the foundation material to minimise collapse settlement and the installation of pressure relief wells, are generally considered standard practice for dam construction under such conditions. However, the jet grouting cut-off solution provided to be a unique and successful method for increasing the seepage paths through the granite saprolite foundation material and may be considered for other dams constructed on similar material.

This research has proven that any detailed engineering geological study of weathered profiles requires a thorough understanding of the nature and processes of weathering and the application of indexing this weathering and applying these indices to the engineering behaviour. In this way the engineering performance of the material can be predicted and used to guide design and construction solutions.

17. REFERENCES

Anand, R.R., Gilkes, R.J., Armitage, T.M. and Hillyer, J.W. (1985). Feldspar weathering in lateritic saprolite. *Clays and Clay Minerals*, **33**, No. 1, 31-43.

Anbeek, C. (1992). The dependance of dissolution rates on grain size of some fresh and weathered feldspars. *Geochimica et Cosmochimica Acta,* **56**, 3957-3970.

Anbeek, C. (1993). The effect of natural weathering on dissolution rates. *Geochimica et Cosmochimica Acta*, **57**, 4963-4975.

Anbeek, C., van Breemen, N, Meijer, E.L. and van der Plas, L. (1994). The dissolution of naturally weathered feldspar and quartz. *Geochimica et Cosmochimica Acta,* **58**, No. 21, 4601-4613.

Anon (1968). *Earth Manual.* United States Department of the Interior, Bureau of Reclamation. US Government Printing Office. 783pp.

Anon, (1979). Classification of rocks and soils for engineering geological mapping. Part I: Rock and soil materials. *Bulletin of the International Association of Engineering Geology,* **19**, 364-371.

Anon, (1981). Basic geotechnical description of rock masses. (ISRM Commission on classification on rocks and rock masses). *International Journal of Rock Mechanics and Mining Science,* **18,** 85-110.

Anon (1995). The description and classification of weathered rocks for engineering purposes. Geological Society Working Party Report. *Quarterly Journal of Engineering Geology,* **23**, 207-242.

Arel, E. and Tugrul, A. (2001). Weathering and its relation to geomechanical properties of Cavusbasi granitic rocks in northwestern Turkey. *Bulletin of Engineering Geology and the Environment*, **60**, 123-133.

ASTM (1985). Standard method for direct shear test of soils under consolidated drained conditions. *1985 Annual Book of ASTM Standards,* Test D3080-72, American Society for Testing and Materials, Philadelphia, 514-518.

ASTM D422-63 (1986). Standard method for the particle size analysis of soils. *1986 Annual Book of ASTM Standards,* American Society for Testing and Materials, Philadelphia, 116-126.

ASTM D4318-84 (1986). Standard test method for liquid limit, plastic limit and plasticity index of soils. *1986 Annual Book of ASTM Standards,* American Society for Testing and Materials, Philadelphia, 769-784.

Atkinson, J.H. and Bransby, P.L. (1978). *The Mechanics of Soil - An Introduction to Critical State Soil Mechanics*. McGraw-Hill, Netherlands.

Aydin, A. and Duzgoren-Aydin, N. (2002). Indices for scaling and Predicting Weathering-Induced Changes in Rock Properties. *Environmental and Engineering Geoscience,* **VIII,** 2, 121-135.

Barden, L. and Sides, G.R. (1971). Sample disturbance in the investigation of clay structures. *Geotechnique,* **21**, 211-222.

Baynes, F.J. and Dearman, W.R. (1978a). The relationship between the microfabric and the engineering properties of weathered granite. *Bulletin of the International Association of Engineering Geology,* **18**, 191-197.

Baynes, F.J. and Dearman, W.R. (1978b). Scanning electron microscope studies of weathered rocks: a review of nomenclature and methods. *Bulletin of the International Association of Engineering Geology,* **18**, 199-204.

Baynes, F.J. and Dearman, W.R. (1978c). The microfabric of a chemically weathered granite. *Bulletin of the International Association of Engineering Geology,* **18**, 91-100.

Becker, G.F. (1895). A reconnaissance of the goldfields of the Southern Appalachians. *16th Annual Report U.S. Geological Survey,* Washington DC, **3**, 251-331.

Bell, F.G. (1999). *Engineering Properties of Soils and Rocks*. Fourth Edition. Blackwell Scientific Publications, Oxford. 485pp.

Bell, F.G. and Maud, R.R. (1994). Dispersive Soils : a review from a South African perspective. *Quarterly Journal of Engineering Geology,* **27,** 195-210.

Bell, F.G. and Walker, D.J.H. (2000). Further studies of dispersive soils in Natal, South Africa. *Quarterly Journal of Engineering Geology and Hydrology,* **33**, 187-200.

Berner, R.A. and Holdren, G.R. (1977). Mechanism of feldspar weathering : some observational evidence. *Geology*, **5**, 369-372.

Berner, R.A. and Holdren, G.R. (1979). Mechanism of feldspar weathering - II. Observations of feldspars from soils. *Geochimica et Cosmochimica Acta,* **43**, 1173-1186.

Bisdom, E.B.A. (1967). The role of microcrack systems in the spheroidal weathering of an intrusive granite in Galicia (NW Spain). *Geologie en Mynbow,* **46**, 333-340.

Bishop, A.W. (1948). A large shear box for testing sands and gravels. *Proceedings of the 2nd International Conference on Soil Mechanics and Foundation Engineering, Rotterdam,* 207-211.

Booth, A.R. (1975) The factors influencing collapse settlement in compacted soils. *6th Regional Conference for Africa on Soil Mechanics and Foundation Engineering, Durban, South Africa,* 54-63.

Brantley, S.L., Crane, S.R., Crerar, D.A. Hellman, R. and Stallard, R. (1986). Dissolution at dislocation etch pits in quartz. *Geochimica et Cosmochimica Acta,* **50**, 2349-2361.

Brime, C. (1985). The accuracy of X-ray diffraction method for determining mineral mixtures. *Min. Mag.,* **49**, 531-538

Brink, A.B.A. (1996). *Engineering Geology of Southern Africa.* Fontein Publishing Company, South Africa. 319pp.

Brink, A.B.A and Kantey, B.A. (1961). Collapsible grain structure in residual soils in Southern Africa. *Proceedings of the 5th International Conference on Soil Mechanics and Found. Engineering., Paris,* **I**, 611-614.

British Standards Institution (1981). BS 5930:1981. *Code of Practice for Site Investigations.* British Standards Institution, London. 147pp.

Brummer, R.K. (1980). The engineering properties of deep highly weathered residual soil profiles. Unpublished M.Sc. Thesis. University of Witwatersrand. 71pp.

BS 1377 (1975) Test 15A. Methods of tests for soils for civil engineering purposes. British Standards Institution, London.

Carter, M and Bentley, S.P. (1994). *Correlations of Soil Properties.* Pentech Ltd, London. 130pp.

Chang, M.F. (1988). Written discussion: preconsolidation of residual soils. *Proceedings of the 2nd International Conference on Geomechanics in Tropical Soils, Singapore.* A.A. Balkema, Rotterdam, 25-35.

Chayes, F. (1956). *Petrographical Modal Analysis.* Wiley, New York. 113pp.

Cheung, C.K., Greenway, D.R. and Massey, J.B. (1988). Direct shear testing of a completely decomposed granite. *Proceedings of the 2nd International Conference on Geomechanics and Tropical Soils, Singapore,* 109-118.

Choudry, T. (1988). Prevention of collapse in residual foundation soils of Guri embankment dams. *Proceedings of the 2nd International Conference on Geomechanics in Tropical Soils, Singapore.* A.A. Balkema, Rotterdam, 363-368.

Chunnett, Fourie and Partners (1991a). *Sabie River Catchment Development: Sabie-Sand First Phase Feasibility Study. Report on the Engineering Geological and Geotechnical Investigations of the Injaka Dam Site on the Marite River.* **1.** Unpublished report. 51pp.

Chunnett, Fourie and Partners (1991b). *Sabie River Catchment Development: Sabie-Sand First Phase Feasibility Study. Report on Construction Materials for the Sabie Sand First Phase Feasibility Study.* **1.** Unpublished report. 27pp.

Clemence, S.P. and Finbarr, A.O. (1981). Design considerations for collapsing soils. *Journal of the Geotechnical Engineering Division, ASCE,* **107**, 305-317.

Collins, K. (1985). Towards characterisation of tropical soil microstructure. *TropicaLS'85,* 85-96.

Collins, K. and McGown, A. (1974). The form and function of microfabric features in a variety of natural soils. *Geotechnique*, **24**, No. 2, 223-254.

Costa Filho, L.M., Dobereiner, L., De Campos, T.M.P. and Vargas, E. (1989). Fabric and engineering properties of saprolites and laterites. *Proceedings of the Twelfth International Conference on Soil Mechanics and Foundation Engineering, Rio De Janerio,* **4**, 2763-2476.

Coulson, J.H. (1971). Shear strength of flat surfaces in rock. Stability of rock slopes. *Proceedings 13th Symposium Rock Mechanics, Urbana, Illinois.* Cording, E.J. (Ed). American Society of Civil Engineers, New York, 77-105.

Darwell, J.L., Denness, B. and Conway, B.W. (1976). Prediction of metastable soil collapse. *International Association of Hydrological Sciences, Proceedings of Anaheim Symposium.* Publication No. 121, 544-552.

Day, R. (1996). Compression and collapse behaviour of fill. *Environmental & Engineering Geoscience,* **II**, No. 3. Technical notes, 407-414.

Dearman, W.R. (1974). Weathering classification in the characterisation of rock for engineering purposes in British practice. *Bulletin of the International Association of Engineering Geology*, **9**, 33-42.

Dearman, W.R. (1995). Description and classification of weathered rocks for engineering purposes: the background to the BS5930:1981 proposals. *Quarterly Journal of Engineering Geology,* **28**, 267-276.

Dearman, W.R., Baynes, F.J. and Irfan, T.Y. (1978). Engineering grading of weathered granite. *Engineering Geology,* **12**, 345-374.

Deere, D.U. and Patton, E.D. (1971). Slope stability in residual soils. *4th PanAmerican Conference on Soil Mechanics and Foundation Engineering, San Juan, Puerto Rico, American Society of Civil Engineers*, 87-170.

Denisov, N. Ya. (1951). *The Engineering Properties of Loess and Loess Like Soils* (in Russian). Gosstroiizdat. 133p.

Department of Water Affairs and Forestry (2002). Oblique aerial view looking north of completed dam site showing central concrete trough spillway, inlet tower, outlet conduit and rip-rap protected embankment. Unpublished photographs, Civil Design Directorate.

de Puy, G.W. (1965). Petrographic investigations of rock durability and comparisons of various test procedures. *Bulletin of the American Association of Engineering Geologists,* **2**, 31-46.

Dobereiner, L. and Porto, C.G. (1993). Consideration on the weathering of gneissic rocks. In: *The Engineering Geology of Weak Rock.* Cripps *et al. (*eds.), Balkema, Rotterdam, 193-205.

Donaldson, G.W. (1975). The occurrence of dispersive soil piping in central South Africa. *Proceedings 6th Regional Conference for Africa on Soil Mechanics and Foundation Engineering, Durban,* 229-235.

Dudley, J.H. (1970). Review of collapsing soils. *Journal of the Soil Mechanics and Foundations Division, ASCE,* **96**, No. SM3, 925-947.

Duzgoren-Aydin, N.S., Aydin, A. and Malpas, J. (2002). Reassessment of chemical weathering indices: Case study on pyroclastic rocks of Hong Kong. *Engineering Geology*, **63**, 99-119.

Ebuk, E.K., Hencher, S.R. and Lumsden, A.C. (1993). The influence of structure on the shearing mechanism of weakly bonded soils derived from granites. In: *The Engineering Geology of Weak Rock.* Cripps *et al.* (eds.), Balkema, Rotterdam, 207-215.

Eggleton, R.A. (1986). The relations between crystal structure and silicate weathering rates. In : *Rates of Chemical Weathering of Rocks and Minerals.* Colman, S.M. and Dethier, D.P. (eds.), Academic Press, London. 603pp.

Elges, H.K.W. (1985). Dispersive Soils. *The Civil Engineer in South Africa,* **27**, 347-355.

Emerson, W.W. (1964). The slaking of soil crumbs as influenced by clay mineral composition. *Australian Journal of Soil Research,* **2**, 211-217.

Errera, L.A. (1977). Stress paths and collapsing soils. Unpublished M.Sc. Thesis. Department of Civil Engineering, University of Cape Town. Various pagings.

Falla, W.J. (1985). On the Significance of Climate and Morphology in Predicting Geotechnical Characteristics of Residual Soils Developed on Igneous Rocks. Unpublished PhD Thesis. University of the Witwatersrand. 376pp.

Feda, J. (1966). Structural stability of subsident loess soils from Praha-Dejvice. *Engineering Geology,* **1**, 201-219.

Feda, J. (1988). Collapse of loess upon wetting. *Engineering Geology,* **25**, 263-269.

Fell, R., MacGregor, P. and Stapledon, D. (1992). *Geotechnical Engineering of Embankment Dams.* Balkema, Rotterdam. 675pp.

Fookes, P.G, Dearman, W.R. and Franklin, J.H. (1971). Some engineering aspects of weathering with field examples from Dartmoor and elsewhere. *Quarterly Journal of Engineering Geology,* **3**, 1-24.

Friedman, M. (1972). Residual elastic strain in rocks. *Tectonophysics,* **15**, 297-330.

Gardner, L.R. (1980). Mobilization of Al and Ti during weathering - isovolumetric geochemical evidence. *Chemical Geology,* **30**, 151-165.

Gardner, L.R., Kheoruenromne, I. And Chen, H.S (1978). Isovolumetric geochemical investigation of a buried granite saprolite near Columbia, S.C., USA. *Geochimica et Cosmochimica Acta,* **42**, 417-424.

Gerber, F.A. (1983). *'n Evaluering van die Fisies-chemiese Eienskappe van Dispersiewe Grond en die Metodes vir Identifiseering van Dispersiewe Grond.* Unpublished M.Sc. Thesis. PU for CHE. 127pp.

Gerber, F.A. (1986). *'n Evaluering van die Fisies-chemiese Eienskappe van Dispersiewe Grond en die Metodes vir Identifiseering van Dispersiewe Grond.* Tegniese Verslag TR 123, Department van Waterwese, Suid Afrika. 137pp.

Gerber, F.A. and Harmse, H.J. von M. (1987). Proposed procedure for identification of dispersive soils by chemical testing. *The Civil Engineer in South Africa,* **29**, 397-399.

Gibbs, H.J. and Bara, J.P. (1962). Predicting surface subsidence from basic soils tests. American Society for Testing and Materials Special Technical Publication, 231-246.

Gidigasu, M.D. (1980). Some contributions to tropical soils engineering in Ghana. *7th regional Congress for Africa on Soil Mechanics and Foundation Engineering, Accra, June 1980,* 509-626.

Gilkes, R.J. and Suddhiprakarn, A. (1979). Biotite alteration in deeply weathered granite. I. Morphological, mineralogical, and chemical properties. *Clays and Clay Minerals*, **27**, No. 5, 349-367.

Goldich, S.S. (1938). A study of rock weathering. *Journal of Geology,* **46**, 17-58.

Grigorian, A.A. (1967). Prediction of deformation of loess soils under building and structure foundations. *Proceedings of the 3rd Asian Regional Conference on Soil Mechanics and Foundation Engineering,* **1/3**, 9-12.

Gupta, A.S and Rao, K.S. (2001). Weathering indices and their applicability for crystalline rocks. *Bulletin of Engineering Geology and the Environment,* **60**, 201-221.

Hamrol, A. (1961). A quantitative classification of the weathering and weatherability of rocks. *Proceedings of the 5th International Conference on Soil Mechanics and Foundation Engineering*, Paris, **2**, 269-274.

Handy, L. (1973). Collapsible loess in Iowa. *Soil Science Society of America Proceedings,* **37**, 281-284.

Haskins, D.R. and Bell, F.G. (2002). Indexing the collapse behaviour of granite saprolite at Injaka Dam, South Africa. In: van Rooy, J.L. and Jermy, C.A. (eds.) *Proceedings of the 9th Congress of the International Association of Engineering Geology and the Environment, Durban,* 526-536.

Haskins, D.R., Schall, A. and Bell, F.G. (1998a). The evaluation of granite saprolite as a founding medium at Injaka Dam, South Africa. *8th International Association of Engineering Geology and the Environment Congress, Vancouver, Canada,* 3035-3041.

Haskins, D.R., Schall, A. and Bell, F.G. (1998b). The scanning electron microscope: A tool for improving the understanding of the weathering and engineering behaviour of a granite saprolite in South Africa. *8th International Association of Engineering Geology and the Environment Congress, Vancouver, Canada,* 3035-3041.

Haskins, D.R. and Van Zyl, J.P. (2002). Injaka Dam: Mitigative measures for difficult foundation conditions. In: van Rooy, J.L. and Jermy, C.A. (eds.) *Proceedings of the 9th Congress of the International Association of Engineering Geology and the Environment, Durban,* 1978-1986.

Harmse, H.J. von M. (1980). Dispersiewe grond, hul ontstaan, identifikasie en stabilasie. *Grond Profile,* **20**, 10-31.

Harnois, L. (1988). The CIW index : a new chemical index of weathering. *Sedimentary Geology,* **55**, 319-355.

Head, K.H. (1982). *Manual of Soil Laboratory Testing Volume 2 Permeability, Shear Strength and Compressibility Tests.* Pentech Press, London, 449-458.

Heinz, W.F. and Segatto, P.I. (1999). Grouting of dispersive dam foundations. In: *Proceedings of the 12th Regional Conference for Africa on Soil Mechanics and Geotechnical Engineering, Durban,* 539-550.

Helgeson, H.C., Garrels, R.M. and McKenzie, F.T. (1969). Evaluation of irreversible reactions in geochemical processes involving minerals and aqueous solutions, II. Applications. *Geochimica et Cosmochimica Acta,* **33**, 455-481.

Hennes, R.G. (1952). The strength of gravel in direct shear. *American Society for Testing and Materials, STP, 131,* 51-62.

Heymann, G. and Clayton, C.R.I (1999). Block sampling of soil: some practical considerations. In: *Geotechnics for Developing Africa,* Wardle, G.R., Blight, G.E. and Fourie, A.B. (eds.), Balkema, Rotterdam, 331-339.

Heymann, G. (1998). The stiffness of soils and weak rocks at very small strains. PhD Thesis, University of Surrey, UK. 405pp.

Heymann, G. and Rust, E. (in press). The measurement of soil collapse in the triaxial apparatus. Submitted to ASTM Geotechnical Testing Journal.

Hosking, A.D. (1960). Slope stability studies in the valley of the Geehi River. *3rd Australia New Zealand Conference on Soil Mechanics and Foundation Engineering,* 169-176.

Irfan, T.Y. (1988). Fabric variability and index testing of a granite saprolite. *Proceedings of the 2nd International Conference on Geomechanics in Tropical Soils, Singapore.* A.A. Balkema, Rotterdam, 25-35.

Irfan, T.Y. (1996). Mineralogy, fabric properties and classification of weathered granites in Hong Kong. *Quarterly Journal of Engineering Geology,* **29**, 5-35.

Irfan, T.Y. and Dearman, W.R. (1978a). The engineering petrography of a weathered granite in Cornwall, England. *Quarterly Journal of Engineering Geology,* **11**, 233-244.

Irfan, T.Y. and Dearman, W.R. (1978b). Engineering classification and index properties of a weathered granite. *Bulletin of the International Association of Engineering Geology*, **17**, 79-90.

Irfan, T.Y. and Powell, G.E. (1985). Engineering geological investigations for pile foundations on a deeply weathered granite rock in Hong Kong. *Bulletin of the International Association of Engineering Geology*, **32**, 67-80.

ISRM (1981). *Rock Characterisation and Monitoring.* Brown, E.T. (ed), Pergamon Press, Oxford. 211pp.

Jackson, M.L. (1963). Interlayering of expansible layer silicates in soils by chemical weathering. *Clays and Clay Minerals Monograph No. 13. Earth Science Series Proceedings of the 11th National Conference.* Ingerson, E. (ed), Pergamon Press.

Jaros, M.B. (1978). The settlement of two multi-storey buildings on residual Ventersdorp Lava. *Seminar on Soil Structure Interaction, Sixth Quinquennial Convention of SAICE, Durban.*

Jayawardena, U. De S. (1993). Use of H_2O^+ for classification of residual soils. In : *Geotechnical Engineering of Hard Soils - Soft Rocks.* Anagnostopoulos *et al.* (eds.), Balkema, Rotterdam, 169-171.

Jayawardena, U. de S. and Izawa, E. (1994). Application of present indices of chemical weathering for *Precambrian* metamorphic rocks in Sri Lanka. *Bulletin International Association of Engineering Geology*, **49**, 55-61.

Jennings, J.E. and Knight, K. (1956). Recent experiences with the consolidation test as a means of identifying conditions of heaving or collapse of foundations on partially saturated soils. *Transactions of the South African Institute of Civil Engineers*, **6**, No. 8, 255-256.

Jennings, J.E. and Knight, K. (1957). The additional settlement of foundations due to collapse structure of sandy subsoils on wetting. *Proceedings of the 4th International Conference on Soils Mechanics and Foundation Engineering*, London, **1**, 316-319.

Jennings, J.E. and Knight, K. (1975). A guide to construction on or with materials exhibiting additional settlement due to "collapse" of grain structure. *5th Regional Conference for Africa on Soil Mechanics & Foundation Engineering, Durban, South Africa*, 99-105.

Jermy, C.A. and Walker, D.J.H. (1999). Assessing the dispersivity of soils. *Geotechnics for Developing Africa.* Wardle, Blight and Fourie. Balkema, Rotterdam, 341-346.

Kanji, M.A. (1970). Shear strength of soil-rock interfaces. M.Sc. Thesis, Department of Geology, University of Illinois, Urbana. 69pp.

Keller, H., Grimsehl, H.W. and van Schalkwyk, A. (1994). *Investigation concerning the failure of Zoeknog Dam: Pertinent Information.* Unpublished report to the Lebowa Government, Department of Agriculture and Environmental Conservation Branch: Water Affairs. 61pp.

Keller, W.D. (1978). Kaolinization of feldspar as displayed in scanning electron micrographs. *Geology,* **6**, 184-188.

Kim, S. and Park, H. (2003). The relationship between physical and chemical weathering indices of granites around Seoul, Korea. *Bulletin of Engineering Geology and the Environment,* **62**, 207-212.

Kinney, J.L. (1979). *Laboratory Procedures for Determining the Dispersivity of Clayey Soils.* Report No. REC-ERC-79-10. Bureau of Reclamation, Denver.

Knight, K. (1961). The collapse structure of sandy sub-soils on wetting. Unpublished PhD Thesis. Department of Civil Engineering, University of Witwatersrand.

Krinsley, D.H. and Doornkamp, J.C. (1973). *Atlas of Quartz Sand Surface Textures.* Cambridge Earth Science Series, Cambridge University Press. 91pp.

Kronberg, B.I., Nesbitt, H.W. and Fyfe, W.S. (1987). Mobilities of alkalis, alkaline earths and halogens during weathering. *Chemical Geology,* **60**, 41-49.

Lamb, D.W. (1962). Decomposed granite as fill material with particular reference to earth dam construction. *Symposium on Hong Kong Soils, Hong Kong Joint Group.* 57pp.

Lambe, T.W. and Whitman, R.V. (1969). *Soil Mechanics.* Wiley, New York. 553pp.

Lee, S.G. and de Freitas, M.H. (1989). A revision of the description and classification of weathered granite and its application to granites in Korea. *Quarterly Journal of Engineering Geology,* **22**, 31-48.

Leroueil, S. and Vaughan, P.R. (1990). The general and congruent effects of structure in natural soils and weak rocks. *Geotechnique,* **40**, No. 3, 467-488.

Little, A.L. (1967). Laterites. *Proceedings of the 3rd Asian Conference on Soil Mechanics and Foundation Engineering, Haifi,* **2**, 299-308.

Little, A.L. (1969). Engineering classification of residual tropical soils. *Proceedings of the 7th International Conference on Soil Mechanics and Foundation Engineering, Mexico,* **1**, 1-10.

Loughnan, F.C. (1969). *Chemical Weathering of the Silicate Minerals.* Elsevier, New York. 154pp.

Lumb, P. (1962). The properties of decomposed granite. *Geotechnique,* **12**, 226-243.

Marcuson, W.F. (1978). Definition of terms related to liquefaction. *Journal of Geotechnical Engineering Division, ASCE,* **104 (9)**, 1197-1200.

Massey, J.B., Irfan, T.Y. and Cipullo, A. (1988). The characterisation of granitic saprolitic soils. *Proceedings of the 12th International Conference on Soil Mechanics and Foundation Engineering, Rio De Jainero,* **1**, 533-542.

Matsuo, S., Nishida, K. and Yamashita, S. (1968). Weathering of granite soils and its influence on the stability of slope. *Memoirs of the Faculty of Engineering Kyoto University,* **30**, Part 2, 85-93.

Martin, R.P. and Hencher, S.R. (1986). Principles for description and classification of weathered rock for engineering purposes. In: *Site Investigation Practice : Assessing BS 5390, Engineering Geology Special Publication No. 2.* Hawkins, A.B. (ed), Geological Society of London, 299-307.

McKnight, C.L. (1999). The stratigraphy and engineering geological characteristics of collapsible residual soils on the Southern Mozambique coastal plain. In: *Proceedings of the 12th Regional Conference for Africa on Soil Mechanics and Geotechnical Engineering, Durban,* 539-550.

Middelburg, J.J., Van Der Weijden, C. and Woittiez, J.R.W. (1988). Chemical processes affecting the mobility of major, minor and trace elements during weathering of granitic rocks. *Chemical Geology,* **68**, 253-273.

Millot, G. and Bonifas, M. (1955). Transformations isovolumétriques dans les phénomènes de lateritisation et de bauxitisation. *Bulletin Serve Carte Géologe, Alsace Lorraine,* **8**, 3-20.

Milovic, D.M. (1967). On some comparative studies of land loess and swamp loess. *Proceedings of the 3rd Asian Conference on Soil Mechanics and Foundation Engineering, Haifi,* **2**, 25-28.

Montgomery, C.W. and Brace, W.F. (1975). Micropores in plagioclase. *Contributions to Mineralogy and Petrography,* **52**, 17-28.

Moye, D.G. (1955). Engineering geology of the Snowy Mountains scheme. *Journal of the Institution of Engineers of Australia,* **27**, 281-299.

Nagy, K.L. (1995). Dissolution and precipitation kinetics of sheet silicates. In : *Reviews in Mineralogy Chemical Weathering Rates of Silicate Minerals Volume 31.* White, A.F. and Brantley, S.L. (eds.), BookCrafters Inc., Chelsea, Michigan.

Nahon, D.B. (1991). *Introduction to Petrology of Soils and Chemical Weathering.* Wiley-Interscience Publications, New York. 313pp.

Nesbitt, H.W. and Young, G.M. (1982). Early Proterozoic climates and plate motions inferred from major element chemistry of Lutites. *Nature,* **299**, 715-717.

Ng, C.W.W., Guan, P. and Shang, Y.J. (2001). Weathering mechanisms and indices of the igneous rocks of Hong Kong. *Quarterly Journal of Engineering Geology and Hydrogeology,* **34**, 133-151.

Nishida, K. and Aoyama, C. (1985). Physical properties and shear strength of decomposed granite soil. *Tropical Soils '85,* 371-382.

Northmore, K.J., Bell, F.G. and Culshaw, M.G. (1996). The engineering properties of the brickearth of south Essex. *Quarterly Journal of Engineering Geology*, **29**, 147-161.

Nouvais-Ferrira, H. and Fonesca, A. Viana da. (1988). Engineering properties of a saprolite soil from granite. *Geomechanics in Tropical Soils,* **1**. Publications Committee of 2 ICOTS (eds.), Balkema, Rotterdam, 181-188.

Nur, A. and Simmons, G. (1970). The origin of small cracks in igneous rocks. *International Journal of Rock Mechanics and Mining Science,* 7, 307-314.

Ollier, C.D. (1984). *Weathering.* Second Edition. Longman, London. 270pp.

Parker, A. (1970). An index of weathering for silicate rocks. *Geological Magazine,* **103**, 501-504.

Parry-Davies, R. (1991). Grouting in Southern Africa. Unpublished PhD Thesis, University of Pretoria. Various pagings.

Partridge, De Villiers & Associates. (1984). *Report on an Engineering Geological Investigation for the Proposed Zoeknog Dam.* Unpublished Report. 40pp.

Partridge, Maud & Associates. (1990). *Report on Additional Engineering Geological Investigations for the Proposed Zoeknog Dam.* Unpublished Report. 32pp.

Partridge, Maud & Associates. (1993). *Zoeknog Dam Failure Report on Samples Taken from Within the Breached Area and Comments on Possible Failure Mechanisms.* Unpublished report. 16pp.

Partridge, T.C. and Maud, R.R. (1987). Geomorphic evolution of southern Africa since the Mesozoic. *South African Journal of Geology,* **90** (2), 179-208.

Radwan, A.M. (1988). Properties of granitic soil in Aswan, Egypt. *Geomechanics in Tropical Soils,* **1**. Publications Committee of 2 ICOTS (eds.), Balkema, Rotterdam, 203-210.

Resendiz, D. (1977). Relevance of Atterberg limits in evaluating piping and breaching potential. *In:* Sherard, J.L. and Decker, R.S.(eds.), *Proceedings Symposium on Dispersive Clays, Related Piping and Erosion in Geotechnical Projects, Philadelphia.* American Society for Testing and Materials Special Publication 623, 341-353.

Reiche, P. (1943). Graphic presentation of chemical weathering. *Journal of Sedimentary Petrology,* **13**, No. 2, 58-68.

Rimsaite, J.H.Y. (1967). Studies of rock forming minerals. *Bulletin of the Geological Survey of Canada,* **149**, 82.

Roaldset, E. (1972). Mineralogy and geochemistry of Quaternary Clays in Numedal Area, Southern Norway. *Narsk. Geol. Tidsskr,* **52**, 335-369.

Ruxton,B.P. (1968). Measures of the degree of chemical weathering of rocks. *Journal of Geology,* **76**, 518-527.

Ruxton, B. P. And Berry, L. (1957). Weathering of granite and associated erosional features in Hong Kong. *Bulletin of the Geological Society of America,* **68**, 1263-1292.

SA Weather Bureau. (1998). Climate of South Africa, WB 42, climate statistics 1961-1990. Bosbokrand, Station Number 0595195. Faxed data sheets.

Sandroni, S.S. (1985). Sampling and testing of residual soils in Brazil. In: *Sampling and Testing of Residual Soils : A Review of International Practice.* Brand, E.W. and Phillipson, H.B (eds.), Scorpion Press, Hong Kong, 290-296.

Sawhney, B.L. and Voigt, G.K. (1969). Chemical and biological weathering in vermiculite from Transvaal. *Soil Science Society of America Proceedings,* **33**, 625-629.

Schulze, B.R. (1958). The climate of South Africa according to Thornwaite's rational classification. *South African Geographical Journal,* **40**, 31-53.

Schwartz, K. (1985). Collapsible soils. *The Civil Engineer in South Africa,* **27**, no. 7, 379-393.

Shai, I. and Livneh, M. (1983). Comparative accuracy of in-situ nuclear density testing. *Geochemical Engineering,* **14**, 1-21.

Sherard, J., Dunnigan, L.P. and Decker, R.S. (1976a). Identification and nature of dispersive soils. *Proceedings American Society Civil Engineers, Journal of Geotechnical Engineering Division,* **102**, 287-301.

Sherard, J., Dunnigan, L.P., Decker, R.S and Steele, E.F. (1976b). Pinhole tests for identifying dispersive soils. *Proceedings American Society Civil Engineers, Journal of Geotechnical Engineering Division,* **102**, 69-85.

SACS (1980). South African Committee for Stratigraphy. *Lithostratigraphy of the Republic of South Africa, South West Africa, Namibia and the Republics of Bophuthatswana, Transkei and Venda.* Handbook Geological Survey of South Africa, **8**, Part 1. 690pp.

Sowers, G.F. (1963). Engineering properties of residual soils derived from igneous and metamorphic rocks. In: Kindo, A. (ed) *2nd PanAmerican Conference on Soil. Mechanics and Foundation Engineering. Budapest, Hungary,* Hungarian Acad. Sci., Budapest, 39-62.

Sridharan, A. (1988). Engineering properties of tropical soils. In *Proceedings of the 2nd International Conference on Geomechanics in Tropical Soils, Singapore.* A.A. Balkema, Rotterdam, 527-540.

Stolt, M.H. and Baker, J.C. (1994). Strategies for Studying Saprolite and Saprolite Genesis. In : *Whole Regolith Petrology. Soil Science Society of America Special Publication* Number 34. 136pp.

Sueoka, T., Lee, I.K., Huramatsu, M. and Imamura, S. (1985). Geomechanical properties and engineering classification for decomposed granite soils in Kaduna district, Nigeria. *Proceedings of the First international Conference on Geomechanics in Tropical Lateritic and Saprolitic Soils, Brasil,* **1**, 175-186.

Tandanier, R. And Ingles, O.G. (1985). Soil security test for water retaining structures. *Proceedings American Society Civil Engineers, Journal of Geotechnical Engineering Division, 111, 289-301.*

TMH1 Method A4. (1986) The determination of the linear shrinkage of soil. *Standard Methods of Testing Road Construction Materials. Technical Methods for Highways,* 15-16.

TMH1 Method A10(a), (1986). The determination of the in-place dry density of soil or gravel by the sand replacement method. *Standard Methods of Testing Road Construction Materials. Technical Methods for Highways,* 49-54.

TMH1 Method A10(b), (1986). The determination of the in-place dry density of soil or gravel by the nuclear method. *Standard Methods of Testing Road Construction Materials. Technical Methods for Highways,* 55-62.

Tovey, N.K. and Yan, W.K. (1973). The preparation of soils and other geological materials for the S.E.M. *International Symposium on Soil Structure,* Gothenburg, Swedish Geotechnical Society, Stockholm, 60-68.

Tugrul, A. and Gurpinar, O. (1997). The effects of chemical weathering on the engineering properties of Eocene basalts in northeastern Turkey. *Environmental & Engineering Geoscience,* **3**, 225-234.

Van Der Merwe, D.H. (1964). The prediction of heave from the Plasticity Index and percentage clay fraction. *Transactions South African Institute of Civil Engineers,* **6**, 103-107.

Vargas, M. (1953). Correlation between angle of internal friction and angle of shearing resistance in consolidated quick triaxial compression tests on residual clays. *Proceedings of the 3rd International Conference on Soil Mechanics and Foundation Engineering, Zurich,* 1-64.

Vaughan, P.R. (1985). Mechanical and hydraulic properties of tropical lateritic soils, particularly as related to their structure and mineral components. *General Report, Session 2, First International Conference on Geomechanics in Tropical Lateritic and Saprolitic Soils,* Brasilia, **3**, 231-263.

Vaughan, P.R., Maccarini, M and Mokhtar, S.M. (1988). Indexing the engineering properties of residual soil. *Quarterly Journal of Engineering Geology,* **21**, 69-84.

Vaughan, P.R. and Kwan, C.W., (1984). Weathering, structure and in situ stress in residual soils. *Geotechnique,* **34**, No. 1, 43-59.

Velbel, M. A. (1984). Weathering processes of rock forming minerals. In: *Short Course in Environmental Geochemiistry, London, May 1994.* Fleet, M.E. (ed). Mineralogical Association of Canada. 306pp.

Vickers, (1978). *Laboratory Work in Soil Mechanics*. Granada, London. 169pp.

Volk, G.M. (1937). Method of determination of degree of dispersion of the clay fraction of soils. *Proceedings of the Soil Science Society of America,* **2**, 561-567.

Vogel, D.E. (1975). Precambrian weathering in acid metavolcanic rocks for the Superior Province, Villebond Township, South-central Quebec. *Canadian Journal of Earth Science,* **12**, 2080-2085.

Vogt, T. (1927). Sulitjelmefeltets Geologi og Petrografi. *Nor. Geol. Unders,* **121**, 1-560.

Wallace, K.B. (1973). Structural behaviour of the continually wet Highlands of Papua New Guinea. *Geotechnique,* **23**, 203-218.

Wates, J. A. (1987). Comparisons between nuclear gauges and conventional density measurements. *The Civil Engineer in South Africa,* 482-488.

Weinert, H.H. (1964). Basic igneous rocks in road foundations. *CSIR Inf. 218. Bulletin of the National Institute of Road Res., Pretoria,* **5**. 47pp.

Weinert, H.H. (1974). A climatic index of weathering and its application in road construction. *Geotechnique*, **24**, No.4. 475-488.

Weinert, H.H. (1980). *The Natural Road Construction Materials of South Africa.* Academa, Cape Town. 298pp.

Welland, N. (2002). Estimation of liquefaction potential of soils by empirical and theoretical methods with special reference to Injaka Dam, South Africa. In: van Rooy, J.L. and Jermy, C.A. (eds.) *Proceedings of the 9th Congress of the International Association of Engineering Geology and the Environment, Durban,* 2380-2390.

Wong, K.Y. and Tovey, N.K. (1975). A new specimen preparation for the electron microscope. *Geotechnique,* **25**, 142-145.

Youd, T.L.and Idriss, I.M. (2001). Liquefaction resistance of soils: summary report from 1996 NCEER and 1998 NCEER/NSF workshop on evaluation of liquefaction resistance of soils. *Journal of Geotechnical and Geoenvironmental Engineering, April 2001,* 297-313.

Zhao, J., Broms, B.B., Zhou, Y. and Choa, V. (1994a). A study of the weathering of the Bukit Timah Granite Part A: review, field observations and geophysical survey. *Bulletin of the International Association of Engineering Geology,* **49**, 97-106.

Zhao, J., Broms, B.B., Zhou, Y. and Choa, V. (1994b). A study of the weathering of the Bukit Timah Granite Part B: field and laboratory investigations. *Bulletin of the International Association of Engineering Geology,* **50**, 105-111.

APPENDIX 1

This appendix contains copies of the following relevant papers published by the author as part of this research:

Haskins, D.R., Schall, A. and Bell, F.G. (1998a). The evaluation of granite saprolite as a founding medium at Injaka Dam, South Africa. *8th International Association of Engineering Geology and the Environment Congress, Vancouver, Canada,* 3035-3041.

Haskins, D.R., Schall, A. and Bell, F.G. (1998b). The scanning electron microscope: A tool for improving the understanding of the weathering and engineering behaviour of a granite saprolite in South Africa. *8th International Association of Engineering Geology and the Environment Congress, Vancouver, Canada,* 3035-3041.

Haskins, D.R. and Bell, F.G. (2002). Indexing the collapse behaviour of granite saprolite at Injaka Dam, South Africa. In: van Rooy, J.L. and Jermy, C.A. (eds.) *Proceedings of the 9th Congress of the International Association of Engineering Geology and the Environment, Durban,* 526-536.

Haskins, D.R. and Van Zyl, J.P. (2002). Injaka Dam: Mitigative measures for difficult foundation conditions. In: van Rooy, J.L. and Jermy, C.A. (eds.) *Proceedings of the 9th Congress of the International Association of Engineering Geology and the Environment, Durban,* 1978-1986.

8th International IAEG Congress/8ème Congrès International de AIGI © 1998 Balkema, Rotterdam, ISBN 90 5410 990 4

The evaluation of granite saprolite as a founding medium at Injaka Dam, South Africa

D.R. Haskins & A. Schall
Environmental, Engineering and Marine Geoscience Division, Council for Geoscience, Pretoria, South Africa
F.G. Bell
Department of Geology and Applied Geology, University of Natal, Durban, South Africa

ABSTRACT: Injaka Dam site is underlain by weathered granite and granite-gneiss of the Nelspruit Suite (3 075 Ma.), which has subsequently been intruded by several post-Transvaal age diabase dykes. Intensive chemical weathering and leaching of this part of the 30 million year old African erosion surface has resulted in the formation of low density saprolitic soils up to 35m thick. This paper presents the results of a series of geotechnical tests conducted on the granite saprolite to assess the suitability of the material as a founding medium for the dam. Field density tests proved to be the most accurate "quick" index test with acceptable correlations with dry density, collapse potential and shear strength respectively. At the feasibility stage, excavation depth for the dam foundation was considered to be 5m. However, results from subsequent investigation indicated that this was too shallow and consequently an excavation depth of 8m was recommended for design purposes.

RESUME: Le site de construction du barrage d'Injaka Dam repose sur les granites et granites-gneiss altérés de la "Nelspruite Suite" (3075 Ma) qui, par la suite, ont été pénétrés par de nombreux dykes doléritiques d'âge post-Transvaal. L'intense altération et lessivage chimiques de la surface d'érosion vieille de 30 millions d'années ("African Erosion surface") est à l'origine de la formation de sols saprolitiques de faible densité et d'épaisseur pouvant atteindre 35 mètres. Cet article présente les résultats d'une série de tests géotechniques effectués sur la saprolite granitique afin d'estimer l'à-propos de ce matériel en tant que milieu de foundation pour le barrage. Les tests de densité obtenus sur le terrain se sont montrés les plus précis des tests "rapides", avec des corrélations acceptables avec, respectivement, la densité sèche, le potentiel d'effondrement et la force de cisaillement. Au stade de faisabilité, la profondeur d'excavation pour la fondation du barrage était estimée à 5 mètres. Cependant les résultats d'investigation ultérieure ont indiqué que cette épaisseur était trop mince et, conséquemment, une profondeur d'excavation de 8 mètres a été recommandée pour la conception de l'ouvrage.

1 INTRODUCTION

According to Stolt and Baker (1994), the term saprolite is used to describe completely weathered bedrock that retains the original structure and fabric of the parent rock but behaves essentially geotechnically as a soil. As a consequence of their mode of formation, saprolitic soils are uniquely different in structure and engineering behaviour from transported sedimentary soils. In fact, as Irfan (1988) has pointed out, their basic soil mechanics parameters are difficult to determine because of the variability of grain size; the variability of void size and void distribution; the occurrence and behaviour of decomposition products; the influence of weak bonding, and the nature of macro- and microfabric associations within the material. Furthermore, interpretation of these parameters may not necessarily provide for the correct analytical deductions.

Injaka Dam is located on the Marite River in Mpumalanga Province, South Africa. This zoned earthfill dam will be 53 m high and 550 m long when completed and will have a central concrete trough spillway. The construction of the dam forms part of

the development of the water resources of the Sabie River Catchment, allowing for greater water utilization and flow stabilisation of the Sabie River through the Kruger National Park. Locally, the reservoir will satisfy the increasing domestic and irrigation needs of the surrounding Bushbuckridge settlement.

2 GEOGRAPHY AND GEOLOGY OF THE DAM SITE

The dam site is located in a sub-tropical region, with rain falling primarily during the summer period. The maximum average daily summer temperature is 30.1°C with a minimum average daily winter temperature of 8.9°C. Annual precipitation is 722 mm, with annual evaporation recorded at 147 mm. This measurement represents 20% of the total annual precipitation. Thornwaite's moisture index for the area is roughly zero, suggesting that sub-humid conditions prevail, (Schulze, 1958). Weinert's (1974) climatic N-value is 2 which indicates that chemical weathering is the major type of rock weathering.

The geology of the dam site is shown in Figure 1. The majority of the site is underlain by medium-grained quartz-microcline-plagioclase-biotite granite migmatite and gneiss. Towards the western portion of the site, white to pale brown, medium- to coarse-grained porphyritic biotite granite becomes more predominant. Both lithologies are unnamed, but belong to the Nelspruit Suite (3 075 Ma). Numerous post-Transvaal age diabase dykes intrude the area. The predominant strike direction of the dykes is north-northwest with a secondary strike direction of east-west. The dykes vary from 10 m to 20 m in thickness and are generally steeply dipping (>70°).

A major fault, with associated shear zone, strikes approximately north-northwest. In places, this feature contains pegmatites and mylonitic breccia. Another fault with a mylonitic shear zone is located adjacent to the downstream, north-northwest trending diabase dyke. This 2m wide shear zone consists of soft chlorite schist.

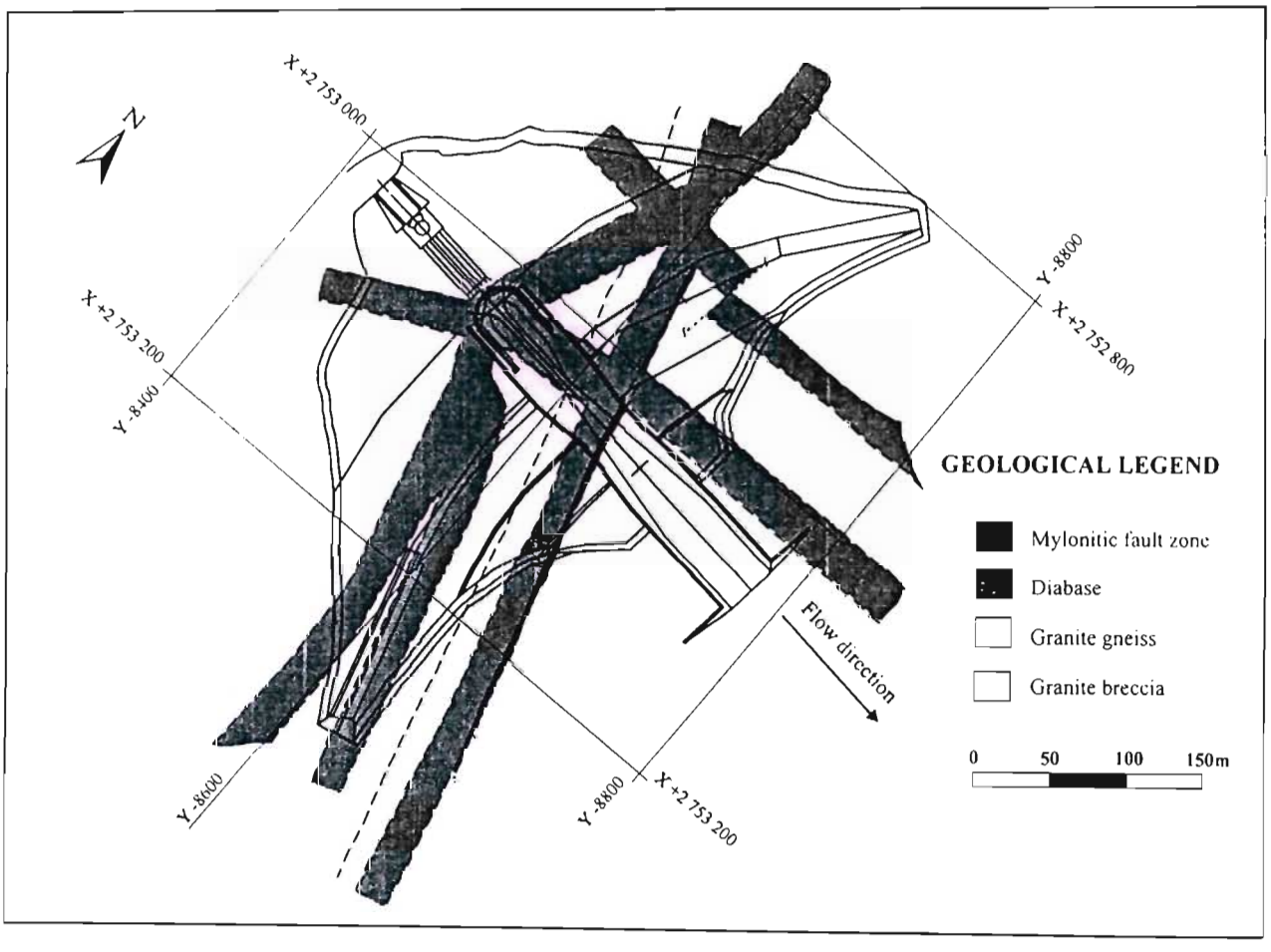

Figure 1. Geology of dam site

The geological lithologies excluding the resistant pegmatite and mylonitic breccia, show evidence of intense chemical weathering and leaching. According to Partridge and Maud (1983), Injaka Dam site is located on the African erosion surface. This surface was formed by a cycle of erosion that lasted 30 million years planating an extensive area. The extreme intensity of the weathering during this period resulted in the formation of saprolitic soils up to 50m thick in places. Consequently, intensely leached mantles of thick saprolite overlie the granites, migmatite and diabase at the dam site. Generally, the thickness of the saprolite increases towards the flanks from 6m near the river up to 30 and 35m on the upper left and right flanks, respectively. The focus of this investigation was to evaluate the engineering properties of the granite saprolite to a depth of 10m. A typical lower flank profile encountered at the site is illustrated in Figure 2. This profile clearly highlights the very porous nature of saprolite, demonstrating the important role that leaching has played in the formation of this material. The transition from saprolite to highly weathered bedrock is generally sharp although some areas do show a gradational change. Corestones are absent and this can be attributed to the closely jointed nature of the granite.

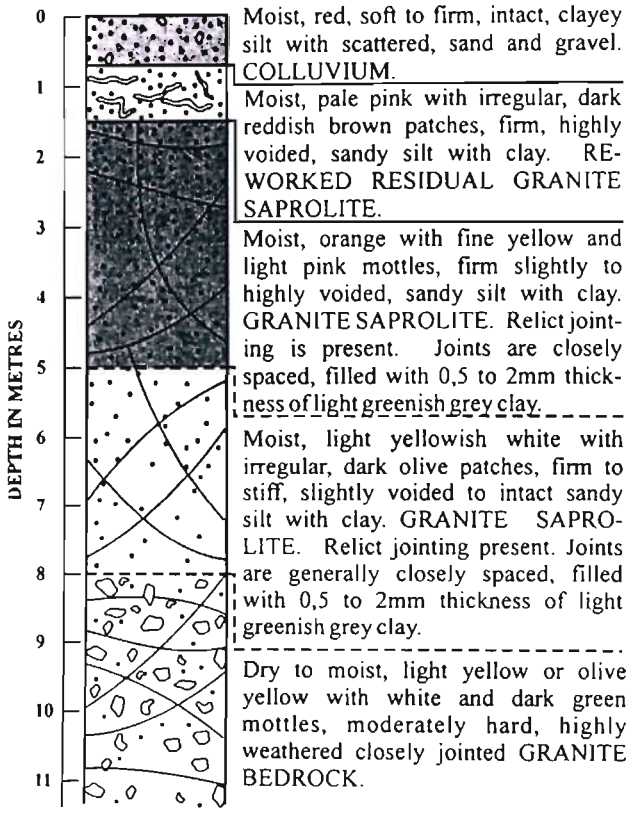

Figure 2. A typical lower flank granite saprolite profile.

Five sample traverses were excavated in the lower left and right valley flanks of the dam excavation in order to retrieve representative block samples of the granite saprolite for laboratory testing. These samples occupied a volume of $0.1m^3$. *In situ* density and permeability tests were also conducted at the sample localities.

3 THE CHEMICAL WEATHERING OF GRANITE

Baynes and Dearman (1978a) describe the chemical weathering of granite as a series of aggressive chemical reactions that occur between the atmospheric agencies (including, water, oxygen and carbon dioxide) and the granite mineral constituents (predominantly quartz, alkali feldspars, plagioclase feldspars and micas). The degree of leaching that occurs during these chemical reactions governs the type of residual minerals which form. If only small amounts of cations are flushed out the system, montmorillonite or illite can form. However, should extensive eluviation processes occur, resulting in significant loss of soluble material, then kaolinite and finally gibbsite are produced. The investigation at Injaka Dam has shown that the granite saprolite developed under intense chemical weathering that occurred under well drained conditions.

4 MINERALOGY

Samples of the granite saprolite were analysed for whole rock composition using a Siemens D5000 X-ray diffractometer. Figure 3 shows the major mineral constituents as a function of increasing depth. Gibbsite and goethite only occur at the top of the profile where the most intense chemical weathering is present. With increasing depth the percentage of kaolinite decreases with a corresponding increase in the plagioclase (oligoclase) and potash feldspar content. The mica content increases towards the surface with chlorite becoming a predominant mineralogical component.

5 ENGINEERING PROPERTIES

The granite saprolite had a natural moisture content which varied from 7.2 to 26.4%. These values are considered lower than the actual moisture contents as

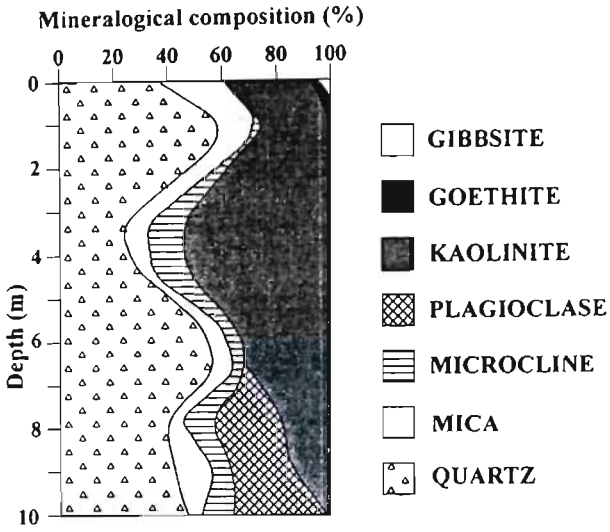

Figure 3. Typical mineralogy of granite saprolite.

some degree of drying out has occurred on the excavation flanks. The moisture content decreased with depth. The degree of saturation determined from the undisturbed samples ranged from 32 to 65%. The soils were of low to intermediate plasticity with plasticity indices ranging from 4 to 13 with a mean of 8. Liquid limits varied from 26 to 40% with a mean of 34 and linear shrinkage fluctuated between 2 to 7% with a mean of 3.5%. The particle size distribution of the saprolite is shown in Figure 4. The two envelopes represent grading carried out with water and sodium hexametaphosphate (dispersion agent), respectively. The discrepancy between the two gradings is indicative of the dispersivity of the material. Water grading indicates that the saprolite is predominantly composed of silt with sand (ML).

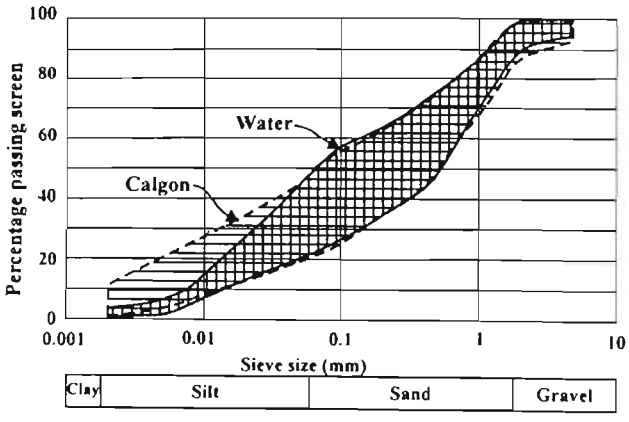

Figure 4. Typical grading envelopes for granite saprolite.

Deeply weathered granites in South Africa have been identified as being especially prone to dispersivity (Elges, 1985). In fact, extensive piping on the excavation flanks at Injaka Dam indicates that the saprolite is dispersive. Cation exchange capacity (CEC in meq/100g clay) and exchangeable sodium percentage (ESP) were quantified for the saprolite to assess its dispersivity. The results of the tests clearly indicate that the material is dispersive (Fig. 5).

The determination of densities from the undisturbed samples proved to be difficult as density differences of up to 15% were observed within the same block. This variability is the result of the observed genetic diversity found within the parent material and a consequence of weathering not acting uniformly due to the anisotropic nature of the rock mass. Comparison of the correlation coeffeicients between the different densities showed that the two field density tests exhibited a higher correlation (r=0.93268) with each other than with the laboratory results (r=0.83979 and r=0.78444 for sand replacement and nuclear methods, respectively). Hence, sand replacement and nuclear density testing were employed as "quick index" tests.

The field dry density values tended to be low, ranging from 1226 kg.m^{-3} to 1855 kg.m^{-3} with a mean of 1475 kg.m^{-3}. Generally, the density increased significantly with depth with an abrupt increase at the saprolite-bedrock contact. The low densities are due to the high void ratio of the saprolite. Laboratory calculated void ratios range from 0.54 to 1.02 with a mean of 0.789, with porosities varying between 35 and 50 %. The porosity can be observed at a macroscopic level by the presence of tubular voids (177 to 2000 μm in diameter) and at a sub- microscopic level by the

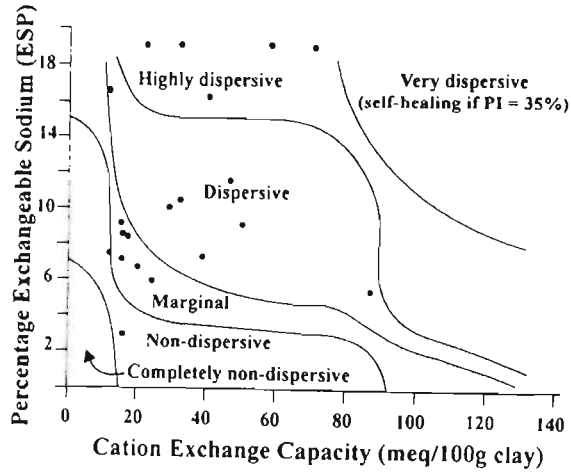

Figure 5. Dispersivity characteristics of the granite saprolite

presence of etch pits, etch trenches and skeletal crystalline frameworks as in Figure 6. The high porosities of the saprolite render them potentially metastable as they can collapse upon saturation and loading.

Collapse potential tests as described by Jennings and Knight (1975), were conducted on the saprolite at 191 kPa and further post saturation loading to 763 kPa . Although the saturation pressure is equivalent to only half the final load (450 kPa) that the embankment will place on the deepest part of the foundation, the testing was expected to provide a general indication of the metastability of the foundation materials. The collapse potential varied substantially laterally but decreased with depth from 6% near the surface to 0 % at 12 m. The collapse potential of the saprolite can be attributed to three components, namely, fabric, permeability and dispersivity. During flooding of the oedometer specimens, saturation occurred almost instantaneously. The high porosity and moderate permeability (1.4 x 10^{-4} to 3.1 x 10^{-5} cm.s^{-1} - calculated from falling head tests) of the sample enabled this to occur. During saturation, it is also thought that the aggressive dispersivity of the soil partially disrupts the interlocking fabric as the clays deflocculate. The disrupted fabric enhances the movement of water through the specimen resulting in accelerated saturation. Typical oedometer curves for the collapse potential tests are given in Figure 7. The initial stiffness of the soil can be attributed to the relict interlocking fabric of the granite and the fact that the skeletal grains do account for some component of strength under partially saturated conditions. Once

Figure 6. Skeletal crystalline framework of plagioclase feldspar against quartz.

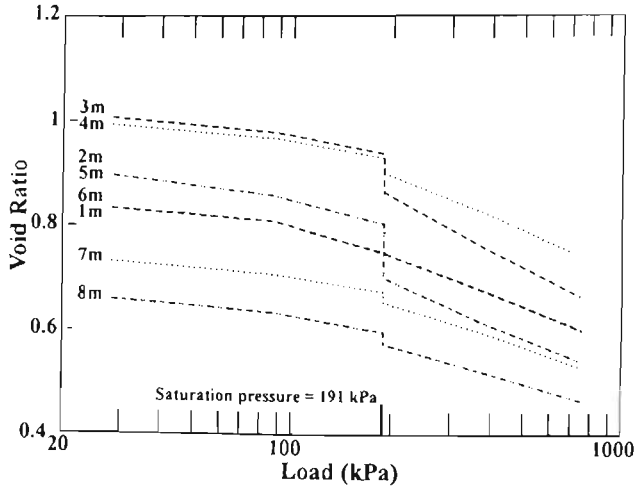

Figure 7. Typical e-log p curves.

saturated, the deflocculation of the clays partially disrupts the relict fabric, simultaneously reducing the strength component of the interlock and effectively increasing the load on the skeletal grains resulting in their collapse. The differences in the amount of collapse between the samples shown in Figure 7 can be related to field dry density and initial void ratio as illustrated in Figure 8. Generally, as dry density increases, the initial void ratio and collapse potential correspondingly decrease.

The high values for the coefficients of consolidation (c_v) for the saprolite suggest that consolidation occurs rapidly. For loading between 381 and 763 kPa, c_v values range from 26.3 to 45.6 m^2/year. The value of

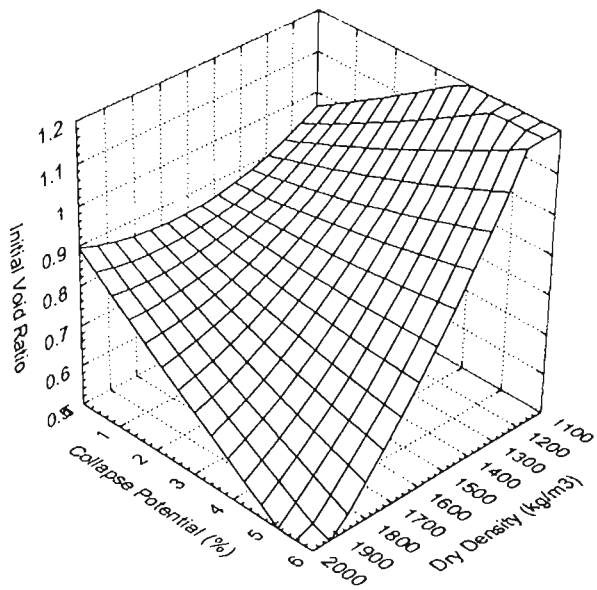

Figure 8. Relationship of dry density, e_0, and collapse potential.

the coefficient of volume compressibility (m_v) generally decreased with increased loading. After saturation, however, there was often an increase in the value of m_v which again decreased at higher loading. According to Northmore *et al.* (1996), this increase suggests a loosening of the soil structure as it becomes more plastic. For a loading between 381 and 763 kPa, m_v ranges from 0.0935 to 0.2813 m^2/MN.

Saturated, consolidated drained triaxial tests were conducted on 38 mm diameter cylindrical samples of saprolite. The values for the effective angle of internal friction (ϕ') ranged from 20.3 to 40.0°, with a mean of 30.9° and a standard deviation of 3.8.Values for the effective cohesion (c') varied from 0.40 to 58.4 kPa, with a mean of 13.7 and a high standard deviation of 13.005. The lack of stiffnesss in the stress-strain curves as observed in Figure 9 can be attributed to the material being saturated and the loss of interlock. Peak shear strength was generally achieved at net strains of 5 to 10% where destructuring of the soil occurs. In some cases where σ_3 was high (500 kPa) peak shear strength was not achieved over a 25% net strain. In these cases it is thought that the high confining stresses prevent the formation of a well defined failure surface only allowing constant readjustment of the microfabric. Nevertheless, it is notable that the values of ϕ' are still relatively high. This strength can probably be attributed to the angular quartz and more resistant K-feldspar grains within the clay matrix. From Figure 9 it can be seen that the effective shear strength of the saturated saprolite is highly variable and is dependent upon the applied normal stress. Generally, however, the shear strength and the angle of internal friction increase with increasing depth as density improves.

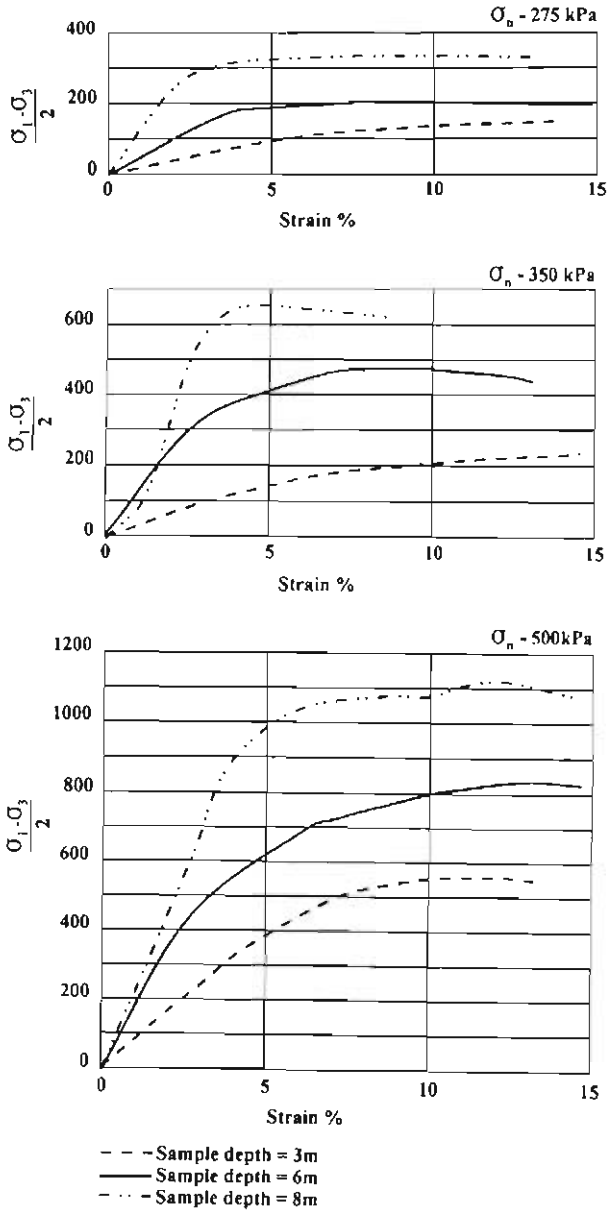

Figure 9. Triaxial test results.

Table 1 below outlines some of the important engineering properties of the saprolite at the specified depth.

Table 1 clearly shows that the engineering properties of the saprolite significantly improve at a depth of 8m. The excavation depth for the footprint was initially considered to be 5m. This investigation has proved that acceptable conditions occur at a depth of 8m.

6 CONCLUSIONS

Intense chemical weathering and leaching at Injaka Dam site has resulted in the formation of a thick saprolite regolith. The granite saprolite is a low to medium plasticity silt with sand. Leaching of the

Table 1 : Basic engineering properties of saprolite with depth

DEPTH (m)	DRY DENSITY ($kg.m^{-3}$)	COLLAPSE POTENTIAL (%)	ϕ'
3	1280-1550	0-6	19-31
4	1280-1550	0-6	21-32
5	1360-1780	0-6	24-35
6	1400-1800	0-6	26-37
7	1460-1900	0-4	28-40
8	1580-2000	0-3	30-42

saprolite has resulted in a low density, high porosity soil with moderate permeability. Density increases with depth towards the bedrock contact where an abrupt change takes place from saprolite to rock. The soil is aggresively dispersive with piping evident on the excavation flanks at the site. The voided nature of the saprolite means that it exhibits a metastable microfabric and is collapsible. The collapse potential was found to decrease from 6% near the surface to 0% at 12m. Triaxial tests on the saprolite showed that the effective angle of internal friction is high, increasing with density towards the bedrock contact.

7 ACKNOWLEDGEMENTS

The authors would like to thank the South African Department of Water Affairs and Forestry for permission to publish this paper. Appreciation is also extended to Mrs W. van der Merwe for drafting of the figures.

8 REFERENCES

Baynes, F.J. & Dearman, W.R. 1978a. The relationship between the microfabric and the engineering properties of weathered granite. *Bull. Int. Assoc. Eng. Geol.*, 18: 191-197.

Elges, H.F. W. K. 1985. Dispersive soils. *Civ. Eng. S. Afr.* 27: No. 7. 347-353.

Irfan, T.Y. (1988). Fabric variability and index testing of a granite saprolite. *Proc. 2nd Int. Conf. Geomechanics in Tropical Soils, Singapore.* 25-35.

Jennings, J.E. & Knight, K. 1975.A guide to Construction on or with materials exhibiting additional settlement due to collapse of grain structure. *Proc. 6th Reg. Conf. Afr. Soil Mech. Found. Eng., Durban.*

Northmore, K.J., Bell, F.G. & Culshaw, M.G 1996. The engineering properties and behaviour of the brickearth of south Essex. *Quart. Journ. Eng. Geol.* 29: 147-161.

Partridge, T.C., & Maud R.R. 1987. Geomorphic evolution of southern Africa since the Mesozoic. *S. Afr. Journ. Geol.*, 90: 179-208.

Schulze, B.R. 1958. The climate of South Africa according to Thornwaite's rational classification. *S. Afr. Geog. Journ.* 40: 31-53.

Stolt, M.H. & Baker, J.C. 1994. Strategies for studying saprolite and saprolite genesis. In: Cremeens, D.L., Brown, R.B. and Huddleston, J.H. (eds.) *Whole Regolith Pedology. Soil Science Society of America Special Publication Number 34.*

Weinert, H.H. 1974. A climatic index of weathering and its application in road construction. *Geotechnique.* 24: No. 4. 475-488.

8th International IAEG Congress/8ème Congrès International de AIGI © 1998 Balkema, Rotterdam, ISBN 90 5410 990 4

The scanning electron microscope: A tool for improving the understanding of the weathering and engineering behaviour of a granite saprolite in South Africa

D.R. Haskins & A. Schall
Environmental, Engineering and Marine Geoscience Division, Council for Geoscience, Pretoria, South Africa

F.G. Bell
Department of Geology and Applied Geology, University of Natal, Durban, South Africa

ABSTRACT: Scanning electron microscope studies have been conducted on an intensely leached granite saprolite to assess the fabric and weathering characteristics. The saprolite is located in one of the wetter regions of South Africa, on an ancient erosion surface. The intensity of chemical weathering has resulted in the formation of very thick saprolitic soils. The contact between the granite saprolite and bedrock is often sharp with no clear corestone formation. Compositionally, the saprolite consists predominantly of quartz and kaolinite, with microcline and plagioclase occurring in varying proportions, depending on the degree of weathering. Mica and occasionally smectite form minor constituents, with gibbsite and goethite present near the surface. Macro- and micro-void formation constitute a distinct component of the fabric exerting a significant effect on the engineering behaviour of the material. The macro-voids tend to be tubular and intergranular, preferentially forming in kaolinite rich zones derived from chemically weathered feldspars. The occurrence of micro-voids within the kaolinite can be so intense that a very porous clay framework can develop. Etch pitting occurs on the surface of some of the less weathered feldspar grains.

RESUME: Les études au microscope électronique à balayage ont été conduites sur une saprolite granitique intensément lessivée afin de déterminer la fabrique et les caractéristiques de l'altération. La saprolite est située dans une des régions les plus humides d'Afrique du Sud, sur une ancienne surface d'érosion. L'intensité de l'altération chimique a provoqué la formation de sols saprolitiques très épais. Le contact entre la saprolite granitique et la roche mère est souvent net, et la zone saprolitique ne contient pas de reliquats clairement granitiques. La saprolite se compose principalement de quartz et kaolinite, et de microcline et plagioclase en proportions variables et dépendantes du degré de l'altération. Le mica et occasionnellement la smectite forment les composants mineurs, avec de l'gibbsite et goethite présents près de la surface. La formation de macro- et microcavités constitue une composante distinctive de la fabrique, affectant de manière significative le comportement mécanique du matériel. Les macrocavités ont tendance à être tubulaires et intergranulaires, se formant préférentiellement dans les zones riches en kaolinite, issues des feldspaths chimiquement altérés. L'occurence de microcavités au sein de la kaolinite peut être si intense qu'une structure argileuse très poreuse peut se développer. Quelques grains de feldspaths les moins altérésprésentent une surface altérée préférentiellement le long des clivages (etch pitting surface).

1 INTRODUCTION

The scanning electron microscope (SEM) has since its introduction been used as a tool to assess the microfabric and weathering characteristics of rocks and soils. As stated by Baynes & Dearman (1978a), the large range of magnification, advantageous depth of field, ease of sample preparation and analytical capabilities of the SEM greatly surpass the ability of the optical microscope to assess fine details of weathering and microfabric. Consequently, a more accurate interpretation and understanding of these processes and features is gained. In the context of granite weathering, the SEM has been applied to the description of feldspar grain-surface textures produced by weathering (Berner & Holdren, 1977); the nature

and origin of some decomposition products (Keller 1978) and to the weathered microfabric (Baynes & Dearman, 1978b).

With regard to geotechnical engineering, limited work has been conducted on the relationship between weathering, microfabric and engineering behaviour. Vargas (1953), Sowers (1963) and Wallace (1973) suggested various microfabric configurations to explain engineering behaviour. Then Collins & McGown (1974) successfully applied their SEM observations to the engineering behaviour of a variety of natural soils highlighting the strength of the SEM in this area of study. They showed that the sensitivity, collapse and expansiveness of these soils could be described in the context of soil microfabric.

The objective of this study is to qualitatively describe the weathering characteristics and microfabric of a granite saprolite at Injaka Dam site, Mpumalanga, South Africa, whilst attempting to correlate these observations with some aspects of the engineering behaviour of the material.

2 GEOCHEMISTRY OF GRANITE

Granite saprolite as described by Haskins et al. (1998) was used for this investigation. The saprolite originates from intensely chemically weathered granite migmatite of the Nelspruit Suite (3 074 Ma). Estimates of the age of weathering are 30 Ma. Table 1 shows typical chemical analyses of the granite saprolite as a function of depth.

Figure 1 shows the typical weathering trend of the granite on a $(CaO^* + Na_2O)$ - Al_2O_3 - K_2O ternary plot, Nesbitt & Young (1984, 1989). CaO^* represents the CaO associated with the silicate fraction of the sample. Compositions are plotted as molar proportions. The initial stages of weathering form a trend parallel to the $(CaO^* + Na_2O)$ and Al_2O_3 axis with the more advanced weathering trend showing a signifcant loss in K_2O. The initial loss of the alkalis and Ca in solution is associated with weathering and leaching of the plagioclase feldspars. The potash feldspars are more resistant to erosion, only becoming significantly affected towards the advanced stages of weathering. These chemical trends are reflected in the microfabrics as seen under the SEM.

3 METHODOLOGY

3.1 *Sample Preparation*

The preparation of samples for SEM analysis is a delicate procedure requiring preservation of the microfabric to prevent the formation of microscopic artifacts. Specimens, 250 cm^3 in size, were cut from undisturbed block samples obtained from the dam site excavation flanks. These specimens were oven dried for 48 hours at 36°C. Although it has been suggested by Tovey & Yan (1973) that freeze drying causes the

Table 1 : Typical XRF major mineral oxide analyses

Major Element Oxide (weight %)	Granite saprolite (2m)	Granite saprolite (4m)	Granite saprolite (6m)	Granite saprolite (8m)	Highly weathered granite bedrock (10m)	Slightly weathered granite bedrock (29m)
SiO_2	69.65	67.27	68.66	70.98	74.42	73.82
TiO_2	0.19	0.34	0.42	0.25	0.10	0.18
Al_2O_3	18.64	18.65	15.63	16.31	14.45	13.73
Fe_2O_3	1.20	2.49	5.92	1.02	0.90	0.28
FeO	0.30	0.15	0.10	0.20	0.10	1.10
MnO	0.01	0.01	0.03	0.03	0.02	0.03
MgO	0.36	0.18	0.48	0.42	0.19	0.38
CaO	0.10	0.10	0.16	0.22	0.34	1.23
Na_2O	0.00	0.00	0.19	2.45	3.58	4.01
K_2O	2.44	4.03	2.27	4.41	4.13	4.02
H_2O^+	6.10	5.85	5.80	2.20	0.86	0.42
H_2O^-	0.28	0.47	0.79	0.27	0.05	0.01
TOTAL	99.13	99.12	99.95	98.54	99.05	99.48

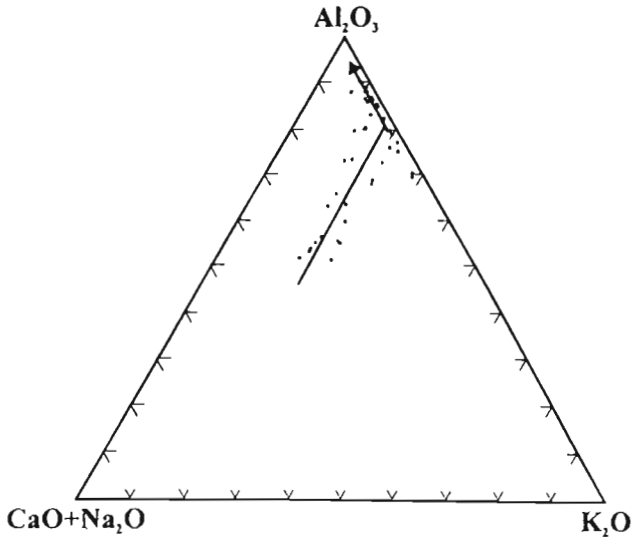

Figure 1. (CaO* + Na_2O) - Al_2O_3 - K_2O ternary plot of the weathering trend for granite at Injaka Dam.

minimum of specimen disturbance, this method was considered technically very difficult by Barden & Sides (1971). Consequently, oven drying was considered the most suitable method for this investigation with successful results being obtained. Smaller specimens, 2 to 4 cm^3 in size were then carefully separated from the larger blocks. Extreme care was taken during this process not to disturb the observational surface by finger contact. In cases where the specimens were notably heterogeneous in nature, two and sometimes three cube samples were taken for observation. Generally, the observational surface was 1 to 2 cm^2 in area. Once the required cube size had been trimmed, a thin layer of *Superglue*® was applied to the sides and bottom faces of the cube to ensure specimen integrity within the SEM. Unlike the peeling methods suggested by Wong & Tovey (1975) it was decided to use air dusting for cleaning the observational surface. This procedure removed any disturbed or loose surface debris and proved successful in preventing the formation of artifacts during cleaning. Once the cube specimen was correctly prepared it was fixed to a glass slide using carbon glue and then coated with a 300Å thick carbon layer.

3.2 *Observational Techniques*

A *Leica Cambridge Stereoscan 440* scanning electron microscope was used for the observational analysis of cube samples. Analytical determinaton of the composition of mineral grains and aggregates was performed using the *Electron Dispersive System Oxford Link ISIS* which was fitted to the SEM. This system allowed the determination of the major and minor elements, and their ratios to be displayed as peaks. The entire system was run off a pentium 100 MHz computer. By observing sequential changes throughout the weathering succession fundamental microfabric changes could be understood.

4 SEM OBSERVATIONS

4.1 *Quartz*

The stable bonding of the silica tetrahedron structure of quartz molecules means that quartz grains are resistant to weathering. Indeed, silica is the major element in water that undergoes the least amount of random variation. Practically then, the weathering effects on quartz can be considered to be almost negligible. However, as observed by Brantley et al. (1986), natural etching of quartz through chemical weathering can occur. Indeed, in several of the upper profile samples collected from Injaka Dam characteristic arcuate etching was observed on the surface of some grains indicating a very high degree of weathering and leaching. Generally, however, the majority of the quartz grains exhibited a smooth or conchoidal fractured surface with common microfracturing.

4.2 *Feldspars*

It is well known that feldspars are susceptible to chemical weathering and tend to undergo incongruent weathering. Observations from this investigation suggest a similar reactivity series for feldspars as that noted by Eggleton (1986), in that Ca-plagiclase is the most reactive phase, followed by Na-plagioclase and then K-feldspar. In fact, such was the intensity of the weathering and severity of leaching of the plagioclase that its absence was conspicuous in the near surface samples. Scanning electron microscope observations of feldspar weathering can also be corroborated with the results of the XRF analyses, where plagioclase was observed to be the most intensely weathered feldspar. The feldspars from this granite saprolite show all the classical SEM textures as described by Berner & Holdren (1977), Baynes & Dearman (1978b) and Anand et al. (1985). The various degrees of etch pitting can be observed from the smallest cupules to the formation of prismatic etch pits (Fig. 2) and prismatic etch trenches (Fig. 3). Intense dissolution can result in the formation of honeycomb-like shells (Fig. 4) located in the upper portions of the profile

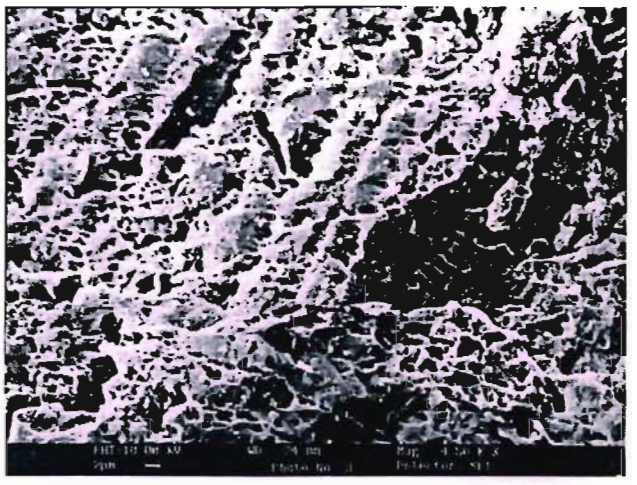

Figure 2. Prismatic etch pits (PEP's) forming on the surface of potash feldspar.

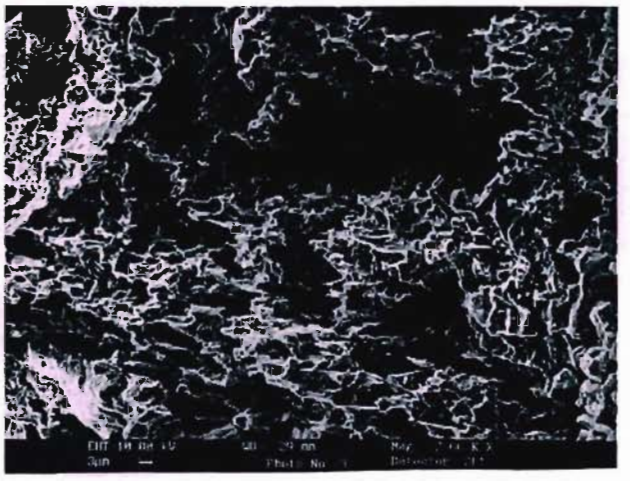

Figure 4. Skeletal framework of a plagioclase feldspar after coalescence of prismatic etch trenches (PET's).

formed by the coalescence of prismatic etch trenches (PET's). The systematic arrangement of etch pits on the feldspar surfaces illustrate that the crystal structure of the feldspar controls the nature and orientation of its weathering features. The formation of the PEP's and PET's starts from the surface of the grains. Montgomery & Brace (1975) have shown by serial sectioning that the shape of these features changes drastically with depth. Generally, with increased weathering etch pit formation extends deeper into the mineral grain.

4.3 *Micas*

Biotite, and to a lesser extent muscovite, are found at various stages of weathering. Muscovite is the more resistant of the two micas,with the absence of biotite in the upper profile sections paying testimony to this. According to Bisdom (1967), and Sawhney & Voigt (1969), mica crystals undergo three changes that may occur simultaneously. These include deformation, opening of cleavage (Fig. 5) and modification of polarizing colours. The opening of mica cleavage involves significant volume increase and can cause disruption of the microfabric.

4.4 *Secondary Minerals*

The major secondary mineral constituent is kaolinite. Interstratified illite and smectite occur on rare occasions. Minor secondary mineral constituents include hematite (found in highly oxidised, near surface samples) and gibbsite (found in highly leached near surface samples).

The kaolinization of feldspar may include the

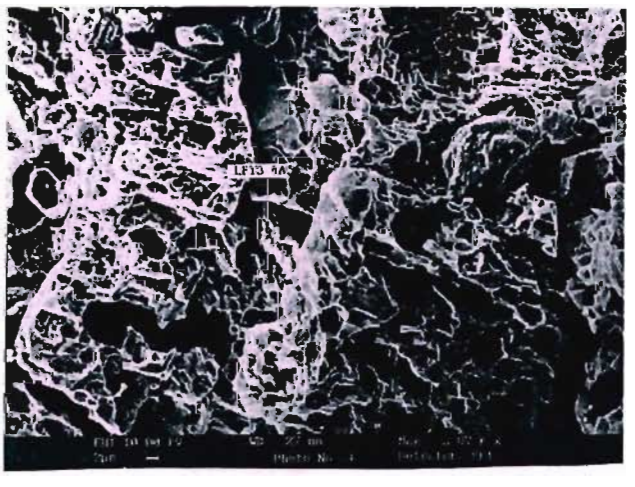

Figure 3. Prismatic etch trenches (PET's) extending through a plagioclase feldspar.

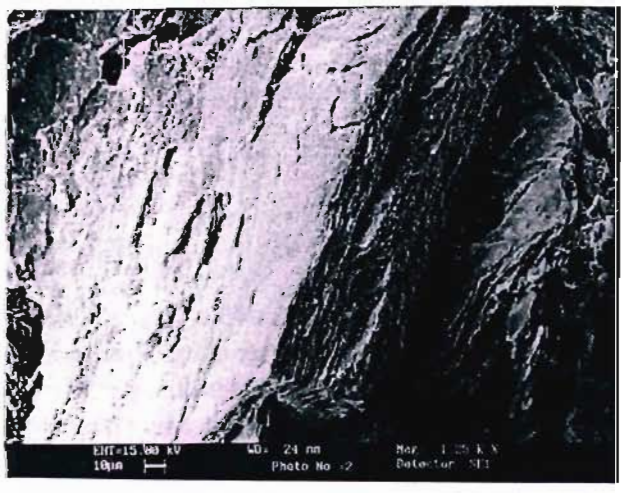

Figure 5. Opening of mica cleavage.

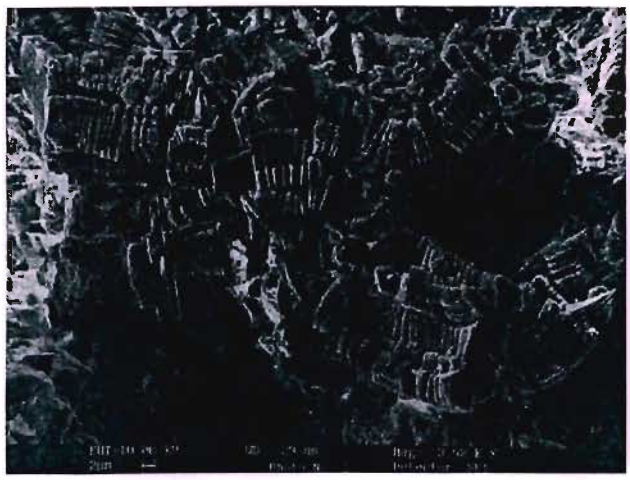

Figure 6. Platy, book-type kaolinite.

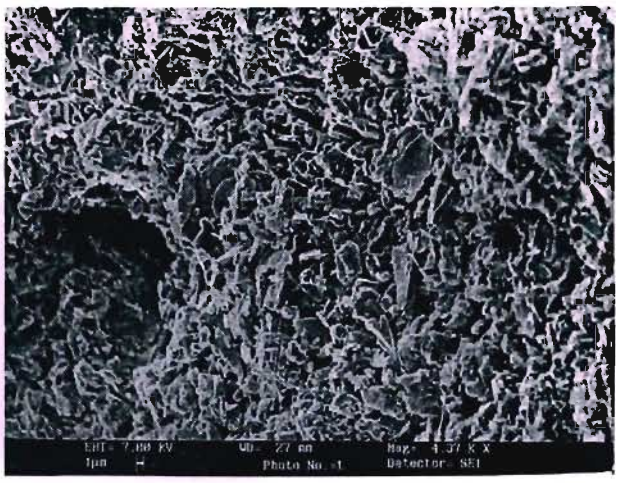

Figure 8. Irregular, angular, loosely packed kaolinite platelets.

formation of a diverse group of kaolin daughter minerals, depending on the weathering environment. These daughter minerals include the platy, book-type kaolinite and the elongate kaolin minerals of halloysite-type. In accordance with Keller's (1978) findings, the most common type of kaolinite observed in this granite saprolite is platy, book-type kaolinite (Fig. 6). This group can be further categorised into sheaves, curved books or straight stack books. The random orientation of these plates in relation to feldspar crystallography suggests that the argillic transition was not a solid-state transition or replacement, but that solution in reaction with the solid phases intervened. Platy, book-type kaolinite is regarded as forming in systems where geochemical equilibrium is maintained between the groundwater solutions and solid phase parent-daughter minerals over a long period of time.

Kaolinite can also be found as a structureless variety consisting of three forms, namely, highly voided, amorphous, fine-grained, clay (Fig. 7); loosely-packed irregular, angular clay platelets (Fig. 8) with edge to face contacts; and more tightly packed aggregates of clay platelets. It is thought that these variations are a result of different weathering microenvironments and degrees of eluviation.

4.5 *Microfractures*

Microfractures can be observed at all levels of weathering. They vary in width from 7 to 800µm and can be open, filled with clay (Fig. 9), or stained with iron oxide. The formation of these microfactures is

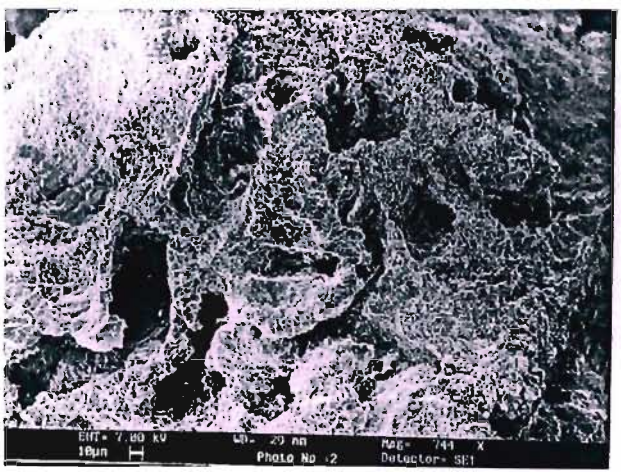

Figure 7. Highly voided, amorphous clay.

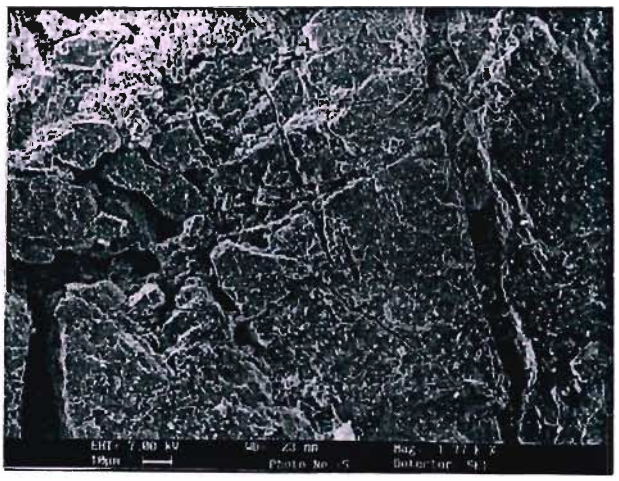

Figure 9. Platy, book-type kaolinite forming within a microfracture of feldspar.

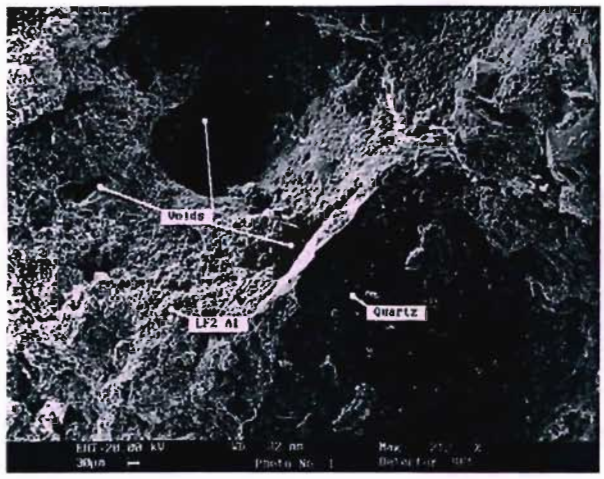

Figure 10. Macro-void situated within amorphous kaolinite.

thought to develop from a number of processes including post-emplacement intrusion by diabase dykes; stress relief due to cooling and exhumation; solution effects, and stress relief due to weathering where the formation of voids facilitates the expansion of the mineral grains towards these zero stress areas.

4.6 *Macrovoids*

A conspicuous component of the saprolite observed in hand specimen is the profusion of circular, tube-shaped voids ranging from 0.3 to 2 mm in diameter (Fig. 10). These voids were also studied under the SEM where it was found that they tend to accumulate in the amorphous kaolinite variety. These voids form from dissolution of the surounding clay and can facilitate further actual eluviation of clay particles.

5 DISCUSSION

The granite saprolite at Injaka Dam exhibits low dry density and is metastable. The low dry density of the material can be attributed to the significant formation of macro- and microvoids. The collapse potential of the granite saprolite has been determined to range from 0% for samples with a dry density greater than 1.9 Mg $.m^{-3}$ to 6% for samples with a dry density less than 1.5 Mg m^{-3}. Scanning electron microscope observations have shown that the degree of leaching, microcracking and void formation decrease with depth as density increases. Typically, the collapse potential of a soil requires two conditions, namely, the soil must be sufficiently porous and the applied load must be sufficiently high to cause structural collapse. Scanning electron microscope observations have proved the existence of a substantially porous microfabric. Figure 11 summarises the proposed collapse mechanism as deduced from scanning electron microscope observations of the microfabric. This model proposes that the aggressive dispersivity of the material accounts for the reduction in strength during saturation as clay deflocculation occurs. Although the clay microfabric is variable, the very porous nature of the clay, feldspars and micas has an effect on the shear strength of the material. The effective angle of internal friction, ϕ', as determined from saturated consolidated drained triaxial tests, can be related to the density of the saprolite as shown in Figure 12.

6 CONCLUSIONS

An SEM study has been conducted on a granite

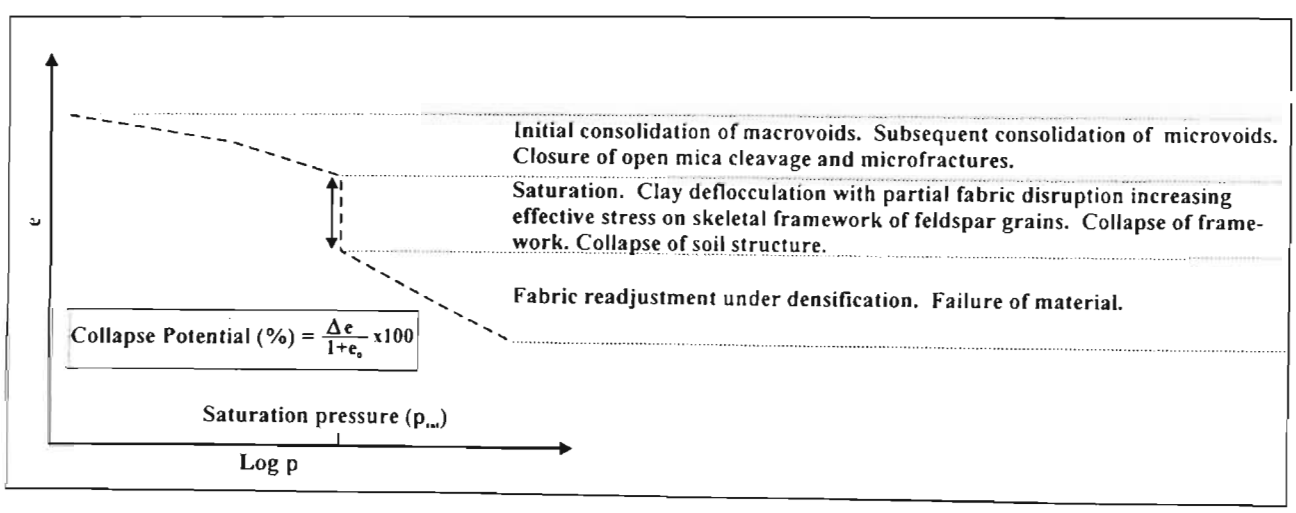

Figure 11. Collapse potential mechanism for granite saprolite.

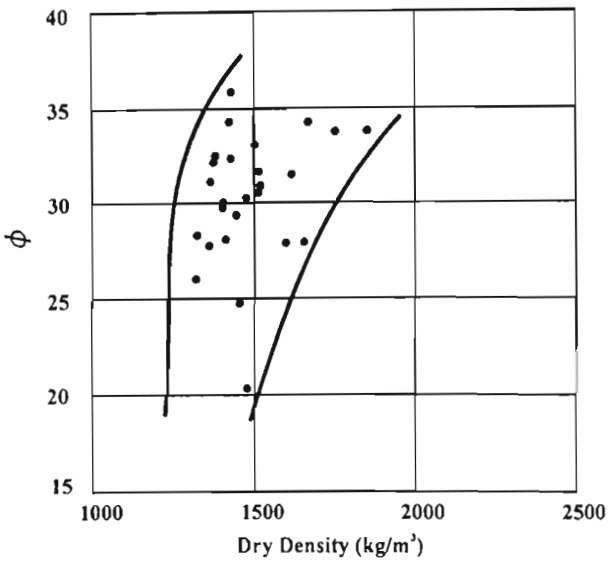

Figure 12. Effective angle of internal friction as a function of density.

saprolite from South Africa. The observations revealed that the saprolite is highly porous accounting for its low dry density and collapse potential. Dissolution of feldspar and clay, opening of mica cleavage and microcracking account for a significant proportion of microvoid formation. Larger diameter macrovoids are also present. The observed microfabric can be related to the collapse potential and shear strength of the saprolite.

7 ACKNOWLEDGEMENTS

The authors would like to thank the South African Department of Water Affairs and Forestry for permission to publish this paper. Special thanks are extended to Mrs W. Van der Merwe and Mrs R. Strydom for production of the drawings and micrographs respectively.

8 REFERENCES

Anand, R.R., Gilkes, R.J., Armitage, T.M. & Hillyer, J.W. 1985. Feldspar weathering in lateritic saprolite. *Clays and Clay Minerals.* 33: No. 1. 31-43.

Barden, L. & Sides, G.R. 1971. Sample disturbance in the investigation of clay structures. *Geotechnique.* 21: 211-222.

Baynes, F.J. & Dearman, W.R. 1978a. Scanning electron microscope studies of weathered rocks: a review of nomenclature and methods. *Bull. Int. Assoc. Eng. Geol.* 18:199-204.

Baynes, F.J & Dearman, W.R. 1978b. The microfabric of a chemically weathered granite. *Bull. Int. Assoc. Eng. Geol.*, 18: 91-100.

Berner, R.A. and Holdren, G.R. 1977. Mechanism of feldspar weathering : some observational evidence. *Geology*, 5:369-372.

Bisdom, E.B.A. 1967. The role of microcrack systems in the spheroidal weathering of an intrusive granite in Galicia (NW Spain). *Geologie en Mynbow.* 46:. 333-340.

.Brantley, S.L., Crane, S.R., Crerar, D.A. Hellman, R. & Stallard, R. 1986. Dissolution at dislocation etch pits in quartz. *Geochimica et Cosmochimica Acta.* 50: 2349-2361.

Collins, K. & McGown, A. 1974. The form and function of microfabric features in a variety of natural soils. *Geotechnique*, 24: No 2. 223-254.

Eggleton, R.A. 1986. The relations between crystal structure and silicate weathering rates. In : *Rates of Chemical Weathering of Rocks and Minerals.* Colman, S.M. & Dethier, D.P. (eds.). Academic Press, 603. London.

Haskins, D.R., Bell, F.G. & Schall, A. 1998.. The evaluation of granite saprolite as a founding medium at Injaka Dam, South Africa. *Proc. 8th IAEG Cong., Vancouver.*

Keller, W.D. 1978. Kaolinization of feldspar as displayed in scanning electron micrographs. *Geology.* 6: 184-188.

Montgomery, C.W. & Brace, W.F. 1975. Micropores in plagioclase. *Contrib. To Min. Petrol.*, 52: 17-28.

Nesbitt, H.W. & Young, G.M. 1984. Prediction of some weathering trends of plutonic and volcanic rocks based upon themodynamic and kinetic considerations. *Geochim. Cosmochim. Acta*, 48: 1523-1534.

Nesbitt, H.W. & Young, G.M. 1989. Formation and diagenesis of weathering profiles. Journ. Geol., 97: 129-147.

Sawhney, B.L. & Voigt, G.K. 1969. Chemical and biological weathering in vermiculite from Transvaal. *Soil. Sci. Soc. Amer. Proc.* 33:625-629.

Sowers, G.F. 1963. Engineering properties of residual soils derived from igneous and metamorphic rocks. *Proc. 2nd. Panam. Cong. Soil Mech. Found. Eng., Brazil.* 1: 39-61.

Tovey, N.K. & Yan, W.K. 1973. The preparation of soils and other geological materials for the S.E.M. *Int. Symp. On Soil. Structur, Gothenburg, Swedish Geotech Soc.* 60-68.

Vargas, M. 1953. Correlation between angle of internal friction and and angle of shearing resistance in consolidated quick triaxial compression tests on

residual clays. *Proc. Int. Conf. Soil Mech. Found. Eng. 3rd., Zurich.* 1: 72-75.

Wallace, K.B. 1973. Strucrural behaviour of the continually wet Highlands of Papua New Guinea. *Geotechnique.* 23: 203-218.

Wong, K.Y. & Tovey, N.K. 1975. A new specimen preparation for the electron microscope. *Geotechnique.* 25: 142-145.

INDEXING THE COLLAPSE BEHAVIOUR OF GRANITE SAPROLITE AT INJAKA DAM, SOUTH AFRICA

David R. Haskins[1] and Fred G. Bell[2]

ABSTRACT: Injaka Dam comprises a 57m high, zoned earthfill embankment with central concrete trough spillway, inlet tower and outlet conduit. The dam is constructed on the Marite River in Mpumalanga Province in the eastern lowveld of South Africa. The 550m long embankment is founded predominantly on granite and granite migmatite intruded by four diabase dykes. The medium-grained quartz-microcline-plagioclase-biotite granite belongs to the 3 075 Ma Nelspruit Suite. An extensive period of intensive chemical weathering from the Cretaceous to the Miocene has produced a thick mantle of granite saprolite overlying the bedrock in this region. The nature of the hydrolysis and dissolution weathering reactions together with severe eluviation of the weathered profile has resulted in the upper portion of the 35m thick saprolite comprising a highly voided structure. This open structure occurs both macroscopically in the form of vermiform tubules up to 2mm in diameter and microscopically in the form of capillaries, and etch pits within mineral grains. Recognising the microfabric as being potentially metastable, an investigation was undertaken to quantify the collapse behaviour of the material. A series of single oedometer collapse potential tests was carried out on samples retrieved from a range of depths within the embankment foundation footprint. The results from these tests showed the granite saprolite to exhibit a collapse potential varying from 0 to 6% at a saturation pressure of 191kPa. By applying a number of pre-formulated collapse indices to the weathered material, with these indices having been derived from the principle properties affecting the collapse of a soil structure, a comparison could be made between the indices and the results derived directly from the laboratory testing. In this way, an indication of the potential metastability of the material could be gauged from the indices without having to undertake expensive and time-consuming oedometer tests. This paper presents these findings and shows the applicability of the various collapse indices to this particular material.

INTRODUCTION

When subjected to vertical pressure with lateral confinement certain differences in terms of the consolidation stress paths have been noted between saprolitic soils formed *in situ* and those soils derived from sedimentary processes. Indeed, it has been shown by Vaughan *et al.* (1988), that the consolidation of residual soils and saprolite is significantly governed by its texture, in particular its void ratio, density and bonding (or "structural interlock") which often impart a characteristic yield stress observed on void ratio-pressure (e-p) curves. It is also well known that saprolitic soils are prone to collapse because of their metastable structure (Dudley, 1970). This mechanism of soil collapse is well understood and according to Schwartz (1985), a collapsible soil may be defined as that which can withstand a relatively large imposed stress with small settlements at low *in situ* moisture content, but which exhibits a decrease in volume and associated notable settlement with no increase in applied stress upon saturation. This decrease in volume is associated with collapse of the soil structure where the changes in compression characteristics are brought about by a decrease in the negative pore pressure (capillary tension) resulting from partial saturation (Jennings and Knight, 1975, Day, 1996 and Dudley, 1970) and collapse or breaking of the respective soil elements.

Injaka Dam comprises a composite earthfill embankment constructed on a thick mantle of weathered granite with the central concrete trough spillway, inlet tower and outlet conduit set on fresh to weathered bedrock. Recognising that the very porous weathered granite would be metastable, the South African Department of Water Affairs and Foresty commissioned an in depth investigation into the collapse behaviour of the weathered granite.

[1] David Haskins. Melis & Du Plessis Consulting Engineers, P.O. Box 1476, Somerset West, 7129, South Africa
[2] Fred Bell, Alwinton, Blyth Hall, Blyth, Nottinhamshire, 881 8HL, United Kingdom

The collapse phenomenum of weathered granites in South Africa was first documented in the 1950's by Jennings and Knight (1956 and 1957). Since this time, engineers have been aware of the settlement problems that can arise due to the collapse of completely weathered granite material. The granite saprolite at Injaka Dam is no exception and exhibits a significant degree of metastability.

The main variables that govern the amount of one dimensional collapse are the soil type, moisture content, dry density and applied vertical pressure. However, a number of criteria are required for a soil to exhibit the collapse phenomenon:

1. The soil must have a high porosity and some degree of strength i.e. a collapsible fabric.
2. The soil must be in a condition of partial saturation as collapse settlement does not occur in soils below the water table. Jennings and Knight (1975) suggested a critical degree of saturation (S_r) above which collapse will not occur. This depends upon the grain size distribution and the following guidelines were presented:

   1-6 mm: S_r = 6-10%
   150-2μ: S_r = 50-60%
   150-0,2μ: S_r = 90-95%

   Errera (1977) also demonstrated that for residual granite this value appears to be 52%. Schwartz (1985), has also shown that a relationship exists between the particle size distribution and the critical degree of saturation.
3. There must be an increase in moisture content which serves as the triggering mechanism for collapse settlement to occur. The rate of collapse is dependant upon the rate of saturation.
4. The soil needs to be subjected to an imposed pressure greater than overburden pressure before collapse will take place.

All of these conditions were met during the construction and impoundment of the dam on the granite saprolite foundation.

THE NATURE OF THE GRANITE SAPROLITE

Macroscopic description

The granite saprolite exhibits a variety of colours and grain sizes which can change over very short distances (0,2 m). This heterogeneity is a product of the heterogeneous parent material fabric and local differences within the weathering microclimate. The saprolite varies from orange with fine yellow and light pink mottles in the upper profile to yellowish white with irregular dark olive patches towards the base of the profile (see Figures 1a and b). The material is equigranular except where localised quartz pegmatite veins occur and is firm in consistency.

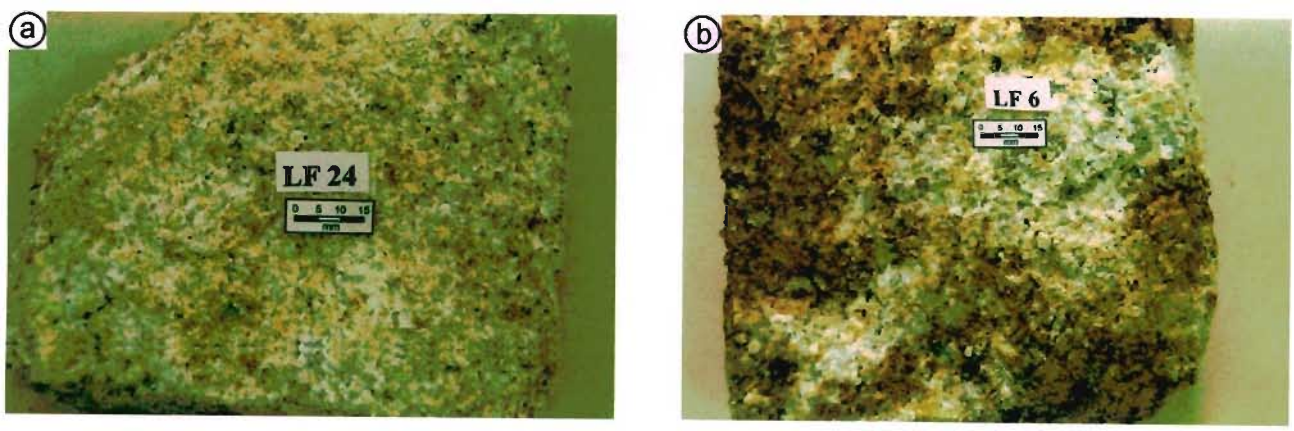

Figures 1a and b. Variation of granite saprolite typical of weathering profile. Note original parent rock fabric still remains intact.

Typical of this material is the presence of numerous vermiform macro-voids (250 to 1000 μm in diameter). These voids tend to preferentially form within feldspar-rich and coarser-grained zones. Micro-voids often manifest themselves as a sponge-like texture within the weathered feldspar pseudomorphs. The quartz grains are often fractured with a slight loss in lustre. Plagioclase feldspar grains are extremely decomposed forming pseudomorphs which break down to soft clay, whilst the less weathered microcline feldspar is moderately to highly decomposed and breaks down to clay and gritty fragments. Biotite may be absent in the upper reaches of the profile, but is highly decomposed lower down, often exhibiting halos of orange staining. The original fabric of the parent material is completely intact even though kaolinite forms a major component of the microfabric. Figure 2 shows the classification system used for the granite saprolite at Injaka Dam.

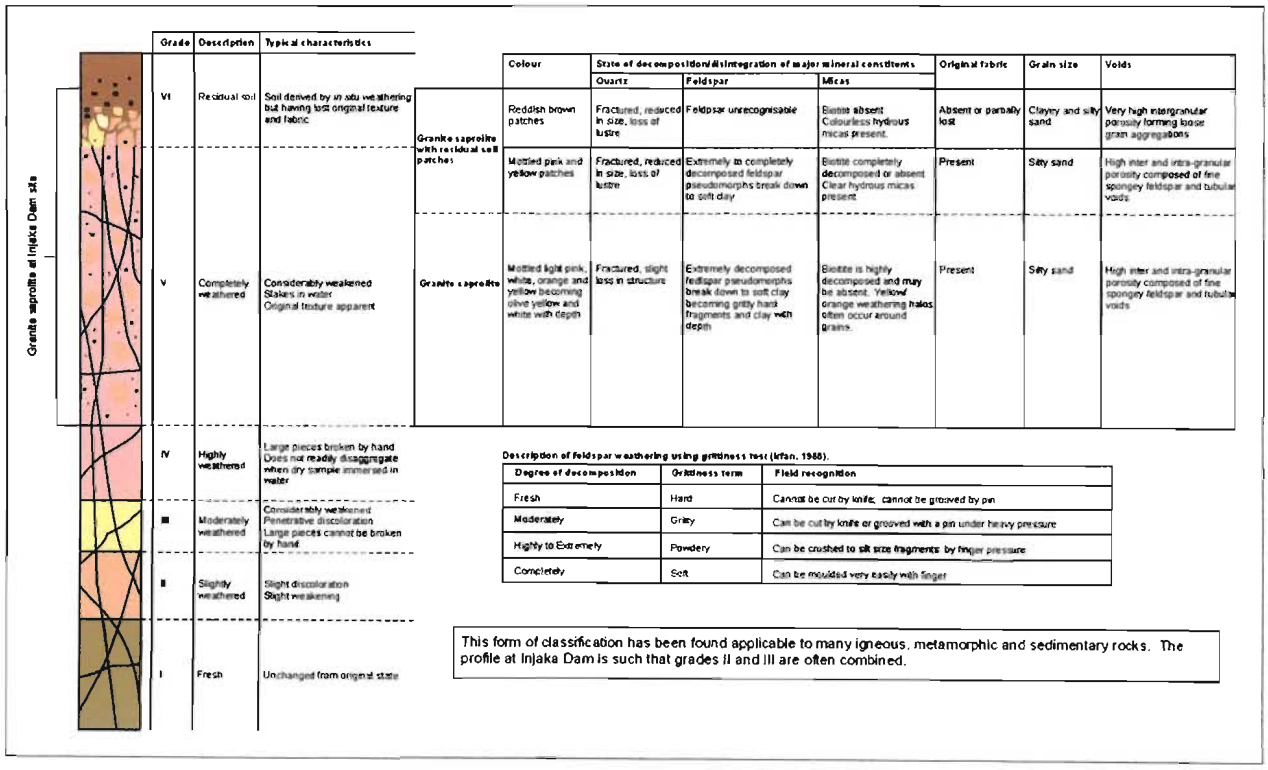

Figure 2. Classification system used for weathering of granite at Injaka Dam site (modified after Anon, 1995 and Irfan, 1988).

Microscopic and sub-microscopic description

Petrographically, a wide range of microfabrics and mineralogy are observable in the saprolite. These fabrics depend upon the degree of alteration and leaching which are affected by the weathering microenvironment. As weathering progresses, microcracking of quartz grains (21%) increases from narrow open microcracks to complete fragmentation of the quartz grains with individual grains separated by clay aggregates or voids with iron oxide staining on the grain boundaries. The intensity of the microcracking reduces the grain size of the quartz. Plagioclase grains (4%) show moderate to often complete alteration. The alteration occurs throughout the grain and along cleavage and twinning planes. Sericitization (2%) is still common within the moderately altered grains whilst the completely altered grains are composed of clay aggregates forming clay pseudomorphs. Microcline (9%) exhibits slight cloudiness with intense microcracking and with scanning electron microscope (SEM) observations showing a porous structure. The microcracks may be tight or open and filled with clay, with partial alteration occurring along microcracks and cleavage. The open microcracking has resulted in disaggregation of the grains effectively reducing grain size. The majority of the biotite (0,5%) has been highly altered, although few remnant grains do exist. Where these occur, the mineral experiences a loss in pleochroism associated with iron loss. Opening of cleavage is visible causing disruption of the biotite structure, whilst grain boundaries become feather-edged. Where alteration is more intense, the biotite alters to a variety of fine-grained secondary micaceous and

kaolin minerals. The occurrence of kaolinite is common in this stage of weathering. It occurs as a platy variety (26%) and as disseminated fine-grained aggregates (17%). A small amount of hematite also occurs with localised dissemination predominantly within microcracks and as coatings on the void walls.

Void formation includes intergranular microcracks, vermiform voids and etch pits in feldspar grains. The microcracks form a reticulate pattern throughout the microfabric. They tend to be open or filled with clay and/or stained with iron oxide. The width of the cracks decreases systematically with a reduction in weathering intensity. The voids tend to be irregular, although maintaining smooth edges typical of solution voids (see Figure 3a). The vermiform voids range in diameter from 0,02 to 2mm and their free surfaces are often clay-lined with iron oxide staining. The voids tend to be preferentially situated within amorphous clay aggregations but, as observed from the SEM investigation, also develop preferentially along the grain boundaries of the more competent grains (see Figure 3b). Etch pitting develops within the feldspar grains and enhanced chemical weathering can result in skeletal shells of feldspar exhibiting a sieve-like texture as shown by Haskins *et al.* (1998). The majority of grain boundaries are open and are responsible for the significant difference in strength and density observed between the granite saprolite and underlying highly weathered granite. The microstructure is generally preserved with the orientation of the grains. From this description it can be seen that the granite saprolite exhibits a porous microstructure susceptible to collapse settlement.

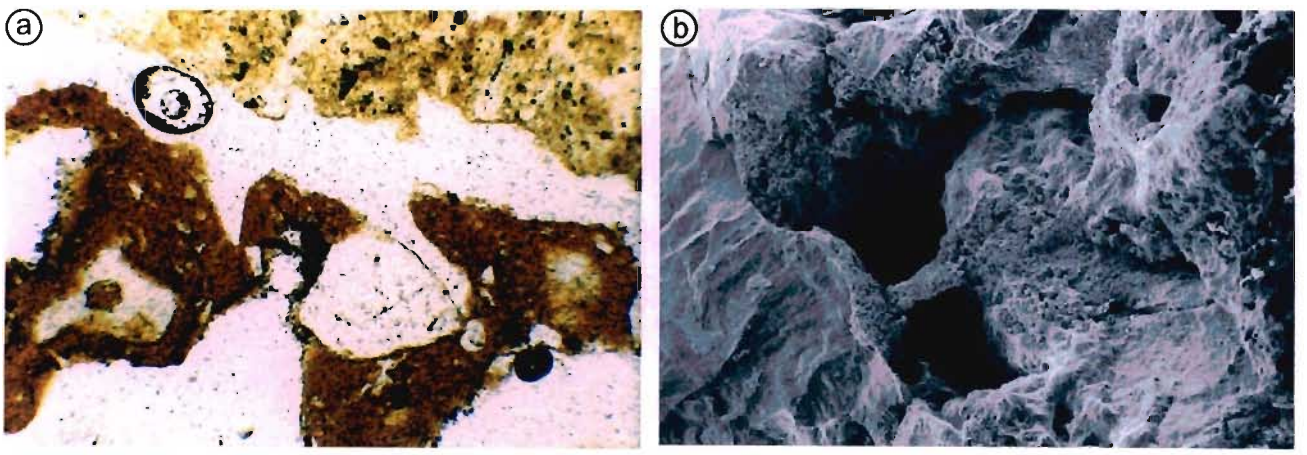

Figures 3a and b. (a) Tubular vermiform void with iron oxide staining on smooth clay-lined surfaces (plane polarised light). (b) Scanning electron microscope view of tubular vermiform void formed adjacent to quartz grain.

OEDOMETER TEST RESULTS

In order to directly quantify the nature of the metastability of the granite saprolite at the dam, a number of single oedometer collapse potential tests (Jennings and Knight, 1957) were carried out on a variety of samples of granite saprolite obtained from various depths within the foundation footprint of the dam. The results from these tests are shown in Table 1 and show the granite saprolite to have a collapse potential at 191 kPa, which can extend up to 6%. Figure 4 shows typical e-log p curves for the granite saprolite. A plot of the effect of dry density on the collapse potential is shown in Figure 5. It can be seen from this figure that for a dry density of greater than 1600kg.m^{-3}, the collapse potential at 191kPa can be expected to be below 1%. The boundary limit for collapsible weathered granite in South Africa, as proposed by Brink (1996), is shown for interest.

In accordance with the findings of Jennings and Knight (1957) relating the degree of saturation (S_r) critical for collapse to occur, a plot of collapse potential against S_r (Figure 6) shows that the granite saprolite undergoes a significant increase in collapse settlement when S_r is less than 50% (shown by the change in slope of the best fit line). This value is very similar to the critical degree of saturation value of 52% proposed by Errera (1977) for residual granite. Figure 7 shows the relationship between the particle size distribution and S_r of various soils in relation to the granite saprolite at Injaka Dam.

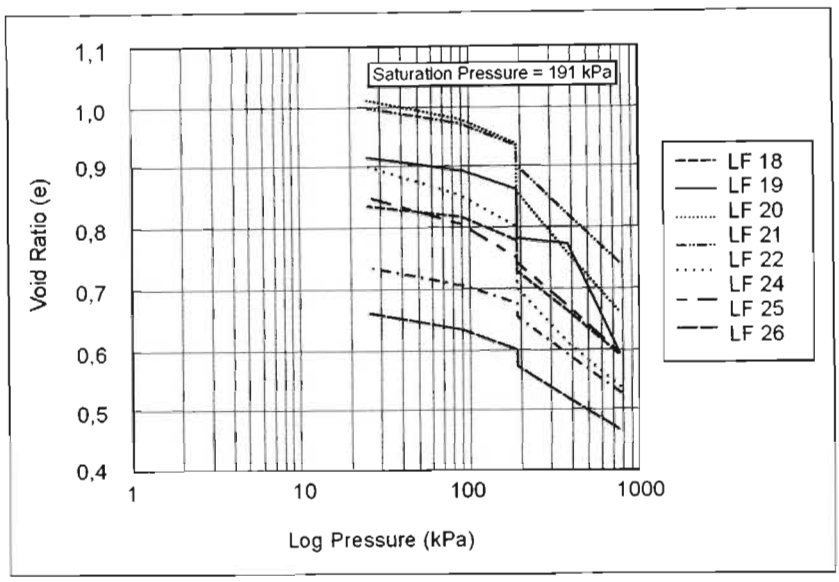

Figure 4. Typical e-log p curves for collapse potential tests carried out at a saturation pressure of 191 kPa.

COLLAPSE INDICES

A considerable amount of work has been conducted on quantifying parameters that qualify settlements associated with collapsibility. These include the oedometer test (Jennings & Knight, 1956), triaxial tests (Grigorian, 1967) and shear tests (Milovic, 1969). The main disadvantage of these tests is that they are specialised and time consuming. Consequently, a number of collapse settlement indices or criteria have been proposed to provide an indication of a materials' metastability. The applicability of these indices has met with varied success depending upon the material type to which they have been applied, with the majority of work having concentrated on loess or loess-like materials.

Table 1. Summary of collapse potential and collapse indices results.

Sample	Depth (m)	Δ_d (kg.m^{-3})	w (%)	S_r (%)	Specific gravity	Collapse potential (%) at 191 kPa	Denisov's value (Denisov, 1951)	Collapse index (I_c) Feda 1988	Absolute collapse index I_{ac} (Feda 1988)	Liquidity Index LI (Gibbs and Bara, 1966 and Handy, 1973)
RF 12	1,0	1463	22,6	71,9	2,71	0,614	1,50	0,29	5,05	-0,22
RF 10	3,5	1369	15,5	44,6	2,61	3,912	1,01	0,80	10,13	-0,73
RF 9	4,9	1349	15,3	42,2	2,64	5,834	0,95	1,37	11,25	-1,18
RF 8	5,7	1715	7,9	38,7	2,64	0,317	1,22	-0,49	-5,17	-1,69
RF 6	2,5	1469	18,1	59,1	2,67	0,859	1,32	0,17	2,12	-0,82
RF 4	6,9	1342	12,5	34,3	2,63	0,140	1,23	0,84	5,59	-2,75
LF 1	0,9	1478	5,6	39,4	2,58	3,381	0,81	2,22	10,20	-2,85
LF 2	2,4	1419	12,9	39,4	2,65	2,888	1,03	0,80	7,04	-1,44
LF 3	3,8	1430	14,9	46,1	2,66	3,110	0,98	0,99	11,44	-0,52
LF 4	4,5	1523	16,9	60,2	2,66	0,823	1,30	-0,48	-5,11	-0,80
LF 5	5,2	1680	15,3	71,2	2,63	0,548	1,21	0,10	0,80	-0,64
LF 6	5,5	1399	22,4	65,8	2,67	0,613	1,24	0,12	0,83	-1,54
LF 7	1,1	1464	12,7	40,5	2,64	5,690	0,83	1,70	12,77	-0,79
LF 8	2,8	1518	13,6	48,3	2,65	3,270	1,13	0,16	1,54	-1,38
LF 9	4,0	1552	10,7	41,3	2,61	2,257	0,95	0,41	2,81	-1,80
LF 10	5,5	1460	21,0	68,9	2,63	1,136	1,25	0,19	2,27	-0,62
LF 11	6,5	1371	20,5	57,5	2,68	1,418	0,99	1,00	6,23	-1,39
LF 12	7,3	1487	19,1	65,0	2,64	2,241	0,98	-0,41	-3,93	-1,48
LF 13	7,7	1927	4,8	34,6	2,63	0,748	1,56	-1,49	-13,73	-2,48
LF 18	1,1	1436	15,3	46,8	2,68	2,447	1,14	1,16	7,29	-1,60
LF 19	2,3	1361	19,5	53,8	2,65	3,788	0,84	1,72	9,28	-1,41
LF 20	3,2	1313	16,9	43,6	2,62	3,615	0,88	1,65	12,06	-1,34
LF 21	4,0	1313	21,2	55,1	2,62	1,661	0,93	2,19	12,68	-0,79
LF 22	5,1	1373	14,2	40,6	2,61	5,14	0,72	3,80	15,58	-1,27
LF 24	5,7	1379	20,2	60,3	2,62	0,043	0,95	1,49	8,96	-0,8
LF 25	6,2	1541	8,7	32,3	2,67	1,442	1,21	0,09	0,64	-2,41
LF 26	7,2	1492	13,2	45,4	2,58	1,218	1,31	-0,11	-0,63	-2,89
RF 17	2,2	1497	15,1	50,9	2,66	0,922	0,99	0,61	7,06	-0,65
RF 18	3,8	1345	15,3	40,7	2,72	4,053	0,87	2,09	12,99	-1,5

Δ_d = dry density
w = moisture content
S_r = degree of saturation

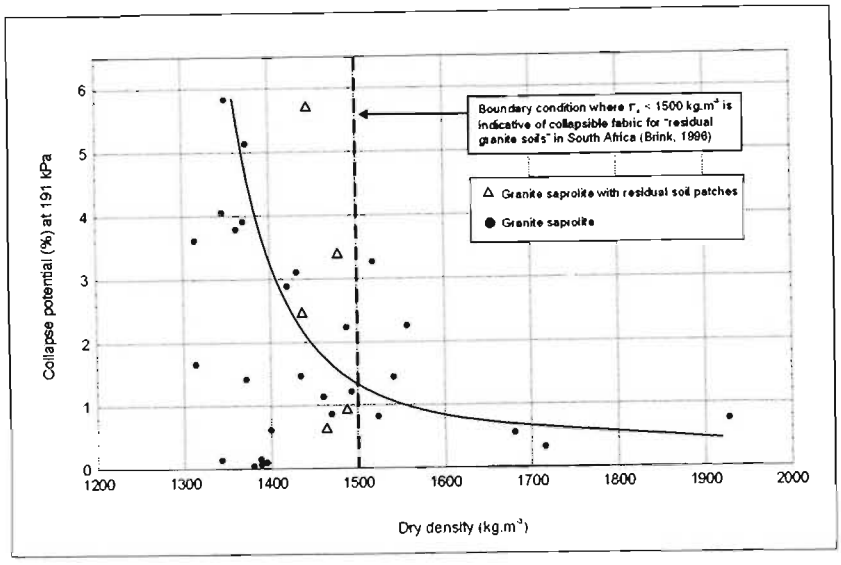

Figure 5. The effect of dry density on the collapse potential of granite saprolite

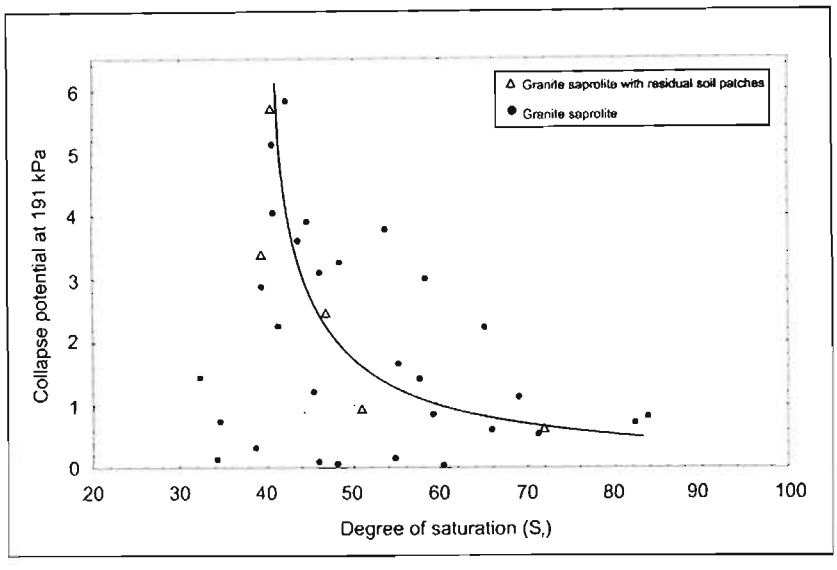

Figure 6. Relationship of collapse potential with degree of saturation (S_r).

Denisov Values

Denisov (1951) was amongst the first to recognise that metastability of soils is determined to some extent by their natural porosity and based his criterion on an evaluation of the voids ratio at the natural moisture content and the liquid limit. He suggested that a soil may be metastable if :

$$\frac{e_L}{e_0} < 1 \qquad (1)$$

where:

e_L= void ratio at liquid limit

e_o = void ratio at natural moisture content

Table 1 presents a summary of the results for the various collapse settlement indices including the values obtained from Denisov's equation. A plot of these values against collapse potential suggests that granite saprolite with a Denisov value of less than 1,3 generally exhibits more than 1% collapse potential (see Figure 8). This is in accordance with Denisov's suggestion of metastability shown in equation (1) where a value less than 1 is indicative of potentially collapsible conditions.

Gibbs and Bara Graphical Method

Gibbs & Bara (1962) presented Denisov's criterion in a graphical form (see Figure 9), stating that a soil with a high enough void space to retain its liquid limit moisture content at saturation is susceptible to collapse on wetting. Their method only applies if the soil is uncemented and the liquid limit is above 20%. The granite saprolite at Injaka Dam complies with both of these requirements. Their chart is divided into two regions by lines drawn at 100% degree of saturation for soils with specific densities of 2,60 and 2,70. Soils which plot above the line of saturation are potentially metastable, whilst those which plot below the line behave as stable or heaving soils. This graphical criterion has been successfully applied to predict subsidence at a number of dam and canal sites in the past (Clemence & Finbarr, 1981).

The metastability as determined by the collapse potential values of the granite saprolite was analysed using this chart and a good relationship was obtained (see Table 2) whereby 83% of samples with a collapse potential between than 3 and 4% plotted in the metastable region on the chart. The method was more

definitive for samples exhibiting more than 4% collapse potential as in this range, all samples plotted as metastable.

Table 2. Summary of collapse potential and graphical collapse index results.

	% samples classified as potentially metastable according to graphical collapse index					
Collapse potential (%) at 191 kPa	0-1	1-2	2-3	3-4	4-5	5-6
Gibbs and Bara's (1962) method	15	40	50	83	100	100
Darwell *et al.*'s (1976) method	42	40	100	100	100	100

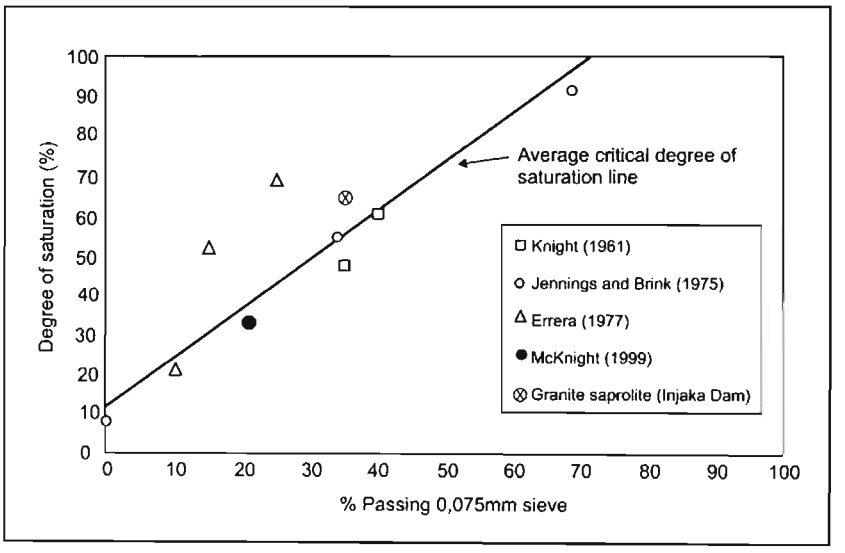

Figure 7. Average critical degree of saturation line as a function of grain size.

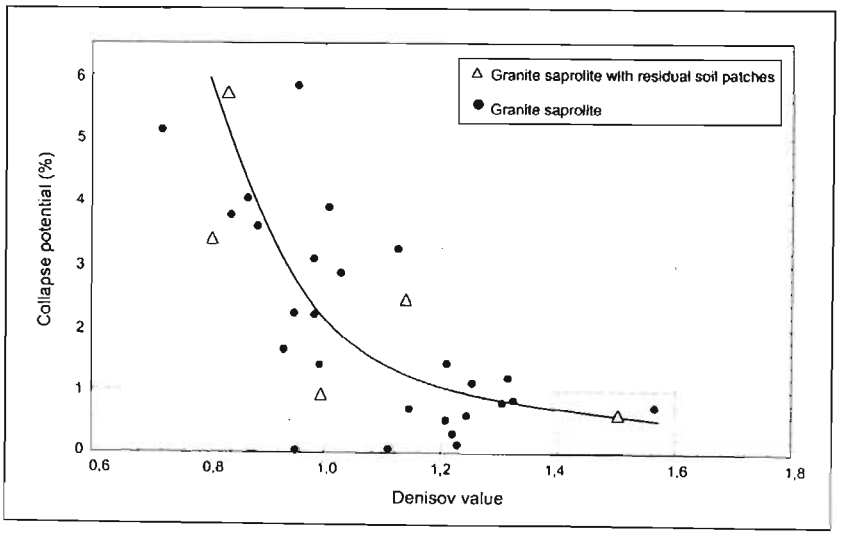

Figure 8. Comparison of Denisov values with collapse potential at 191 kPa.

Feda's Collapse Indices

Feda (1988) has produced the most comprehensive work on collapse indices from his studies of loess. He proposed the collapse index, i_c:

$$i_c = \frac{\frac{m}{S_r} - PL}{PI} \qquad (2)$$

where:
m = natural moisture content
S_r = degree of saturation
PL = plastic limit
PI = plasticity index,

In order to use this index the soil must have a critical porosity greater than or equal to 40%. This requirement is satisfied by the granite saprolite. Feda also proposed that the absolute collapse index, i_{ac}, could be used for collapse prediction where:

$$i_{ac} = \frac{m}{S_r} - PL \qquad (3)$$

Collapse index (I_c) and absolute collapse index (I_{ac}) values for all of the samples are shown in Table 1. Feda suggested that if I_c was greater than 0,85, this was indicative of a metastable soil. A plot of I_c against collapse potential shows a reasonable relationship (see Figure 10) suggesting that when I_c is greater than 0,2 a collapse potential greater than 1% can be assumed. If Feda's criterion of 0,85 is used, a collapse potential greater than 2% can be expected for this material. Figure 11 shows the relationship of I_{ac} with collapse potential and suggests that where I_{ac} is greater than 0 a collapse potential larger than 1% can be expected for the granite saprolite.

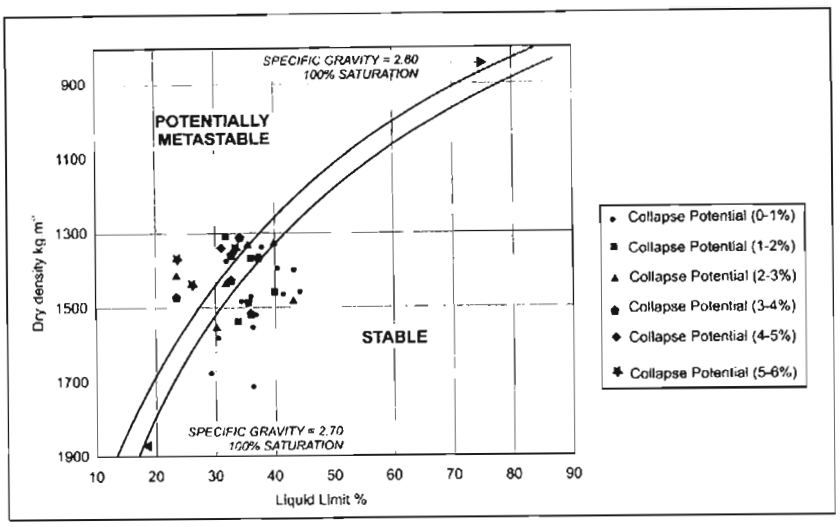

Figure 9. Metastability diagram of Gibbs and Bara (1962) showing data for granite saprolite.

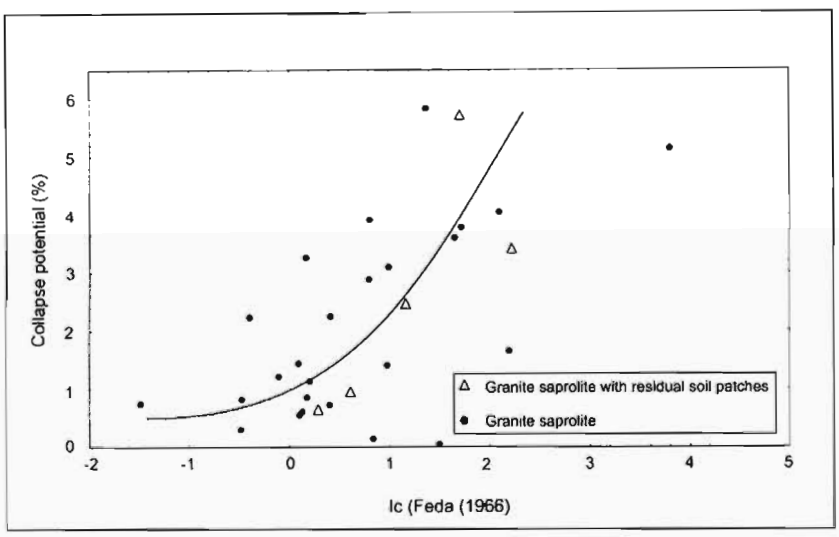

Figure 10. Relationship of Feda's collapse index (i_c) with collapse potential at 191 kPa.

Gibbs and Bara (1962) and Handy (1973) Liquidity Index Method

Gibbs and Bara (1962), and Handy (1973) have shown in loess that when the saturation moisture content exceeds the liquid limit, collapse of the soil structure from an increase in load is possible. They expressed this instability criterion in terms of the liquidity index (LI) defined as:

$$LI = \frac{w - PL}{LL - PL} \qquad (4)$$

where:
LI = liquidity index
w = natural moisture content
PL = plastic limit
LL = liquid limit

When the liquidity index approaches or exceeds a value of unity, experience has shown that collapse may occur. However, the liquidity index values for the granite saprolite correlate poorly with the actual values of collapse potential (see Table 1) and consequently, it is considered a poor criterion for indexing the collapse settlement of this material.

Darwell *et al.* (1976) graphical method

Darwell *et al.* (1976) have developed a relationship between plastic limit, liquid limit and dry density which can be used to assess metastability. They adapted Feda's collapse index (I_c) and rearranged the equation (2) to include values for natural dry density and specific gravity to give equation (5). This was important in that the density of the material was taken into account in the formulation of the index.

$$LL + \frac{3}{17}PL < \frac{1}{0{,}85}\left[\frac{\rho_w}{\rho_d} - \frac{1}{G_s}\right] \qquad (5)$$

Where:
LL = liquid limit
PL = plastic limit
ρ_w = density of water
ρ_d = dry density of soil
G_s = specific gravity

This expression can be written as a series of parallel lines of liquid limit against plastic limit with each line being given a unique combination of natural dry density. One particular line is shown in Figure 12a.

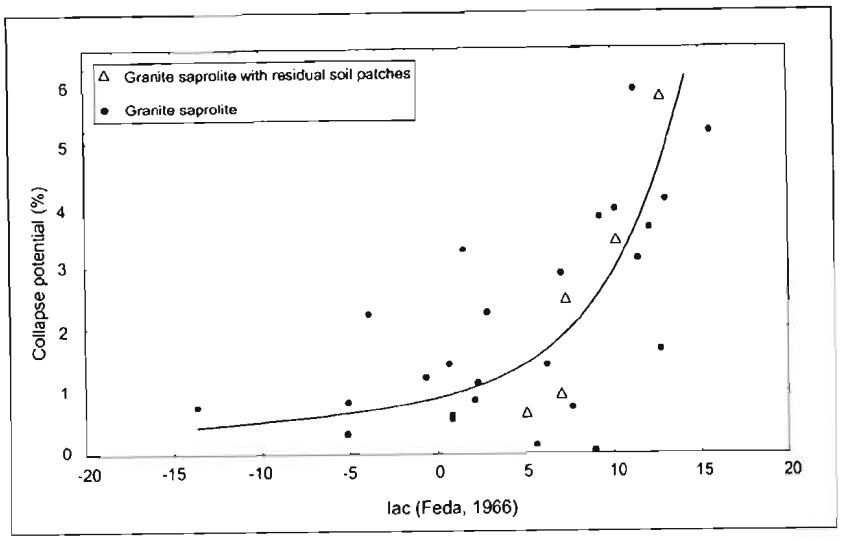

Figure 11. Relationship of absolute collapse index (i_{ac}) with collapse potential at 191 kPa.

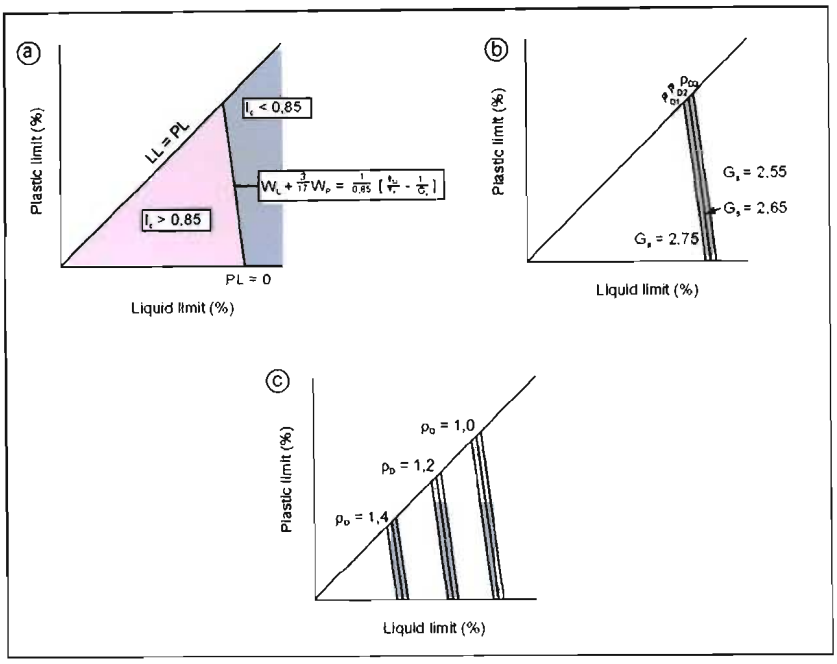

Figure 12a, b and c. Construction of the graphical chart method by Darwell *et al.* (1976).

This line runs from the upper boundary line where LL=PL to the liquid limit axis where PL=0. The areas shaded in Figure 12a between the three lines represent the inequality presented above. Consequently all points shaded in this region represent cases where the liquid and plastic limits are such that the collapse index is greater than 0.85 for given values of dry density and specific gravity and thus any soil with indices located in this region should be metastable. To allow for the prediction of soils with a range of dry density and specific gravity values, a series of lines is drawn for these different values. Examples of these lines are shown in Figure 12b. The central line is the case in which G_s=2.65 whilst the outer two lines represent G_s=2.55 and Gs=2.75 for the same dry density. Any specific gravity can be interpolated between these three lines or extrapolating outside of them if necessary. By varying the dry density, a series of these lines can be created as shown in Figure 12c.

In Figure 13, values for the granite saprolite are plotted as points. If a point given by the liquid and plastic limits of the soil lies to the left of the line corresponding to its dry density, then metastability is likely as the criterion of I_c being greater than 0.85 is met. A good relationship between Darwell's chart and actual collapse potential values was obtained (see Table 2). It can be seen from this table that Darwell *et al.'s* method shows the granite to be potentially metastable when exhibiting a collapse potential greater than 2% and thus this index serves as useful method of identifying metastability.

CONCLUSIONS

The collapse potential of granite saprolite at Injaka Dam has been quantified using single oedometer testing. In order to predict the collapse behaviour of this material, a number of pre-formulated collapse indices were applied to the saprolite. By comparing the performance of these indices in determining the collapsible nature of the saprolite to the actual measurement of collapse potential in the single oedometer test, the usefulness of these indices could be defined for this material.

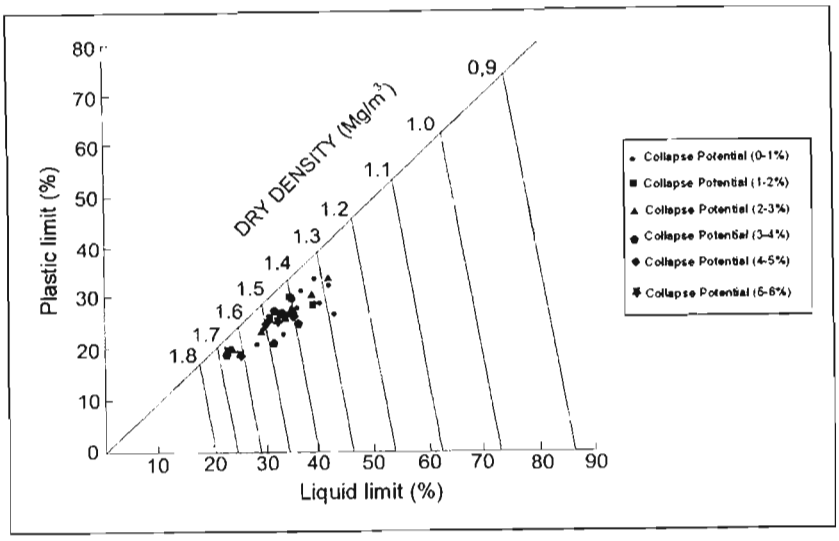

Figure 13. Stability chart of granite saprolite using Darwell *et al.'s* method.

It was found that the Denisov criteria (1951), Gibbs and Bara's graphical method (1962), Feda's collapse index (1988), Feda's absolute collapse index (1988) and Darwell *et al.'s* graphical method (1976) could adequately define the collapse behaviour of the granite saprolite. The liquidity index proposed by Gibbs and Bara (1962) and Handy (1973) was not successful in indexing the collapse behaviour of the granite saprolite.

REFERENCES

Anon (1995). The description and classification of weathered rocks for engineering purposes. Geological Society Working Party Report. *Quarterly Journal of Engineering Geology,* **23**, 207-242.

Brink, A.B.A. (1996). *Engineering Geology of Southern Africa.* Fontein Publishing Company, South Africa. 319pp.

Clemence, S.P. and Finbarr, A.O. (1981). Design considerations for collapsing soils. *Journal of the Geotechnical Engineering Division, ASCE,* **107**, 305-317.

Darwell, J.L.,Denness, B. and Conway, B.W. (1976). Prediction of metastable soil collapse. *International Association of Hydrological Sciences., Proceedings of Anaheim Symposium.* Publication No. 121, 544-552.

Day, R. (1996). Compression and collapse behaviour of fill. *Environmental & Engineering Geoscience,* **II**, No. 3. Technical notes, 407-414.

Denisov, N. Ya. (1951). *The Engineering Properties of Loess and Loess Like Soils* (in Russian). Gosstroiizdat. 133p.

Dudley, J.H. (1970). Review of collapsing soils. *Journal of the Soil Mechanics and Foundations Division, ASCE,* **96**, No. SM3, 925-947.

Errera, L.A. (1977). Stress paths and collapsing soils. Unpublished M.Sc. Thesis. Department of Civil Engineering, University of Cape Town.

Feda, J. (1988). Collapse of loess upon wetting. *Engineering Geology,* **25**, 263-269.

Gibbs, H.J. and Bara, J.P. (1962). Predicting surface subsidence from basic soils tests. American Society for Testing and Materials Special Technical Publication, 231-246.

Grigorian, A.A. (1967). Prediction of deformation of loess soils under building and structure foundations. *Proceedings of the 3rd Asian Regional Conference on Soil Mechanics and Foundation Engineering,* **1/3**, 9-12.

Handy, L. (1973). Collapsible loess in Iowa. *Soil Science Society of America Proceedings,* **37**, 281-284.

Haskins, D.R., Schall, A. and Bell, F.G. (1998). The scanning electron microscope: A tool for improving the understanding of the weathering and engineering behaviour of a granite saprolite in South Africa. *8th International Association of Engineering Geology and the Environment Congress, Vancouver, Canada,* 3035-3041.

Irfan, T.Y. (1988). Fabric variability and index testing of a granite saprolite. *Proceedings of the 2nd International Conference on Geomechanics in Tropical Soils, Singapore.* A.A. Balkema, Rotterdam, 25-35.

Jennings, J.E. and Knight, K. (1956). Recent experiences with the consolidation test as a means of identifying conditions of heaving or collapse of foundations on partially saturated soils. *Transactions of the South African Institute of Civil Engineers,* **6**, No. 8, 255-256.

Jennings, J.E. and Knight, K. (1957). The additional settlement of foundations due to collapse structure of sandy subsoils on wetting. *Proceedings of the 4th International Conference on Soils Mechanics and Foundation Engineering,* London, **1**, 316-319.

Jennings, J.E. and Knight, K. (1975). A guide to construction on or with materials exhibiting additional settlement due to Acollapse@ of grain structure. *5th Regional Conference for Africa on Soil Mechanics & Foundation Engineering, Durban, South Africa,* 99-105.

Knight, K. (1961). The collapse structure of sandy sub-soils on wetting. PhD Thesis, Department of Civil Engineering, University of Witwatersrand.

Schwartz, K. (1985). Collapsible soils. *The Civil Engineer in South Africa*, **27**, no. 7, 379-393.

McKnight, C. (1995). The stratigraphy and engineering geological characteristics of collapsible residual soils on the Southern Mozambique coastal plain. *Geotechnics for Developing Africa.* Wardle, Blight & Fourie (eds.). Balkema, Rotterdam. 633-646.

Milovic, D.M. (1967). On some comparative studies of land loess and swamp loess. *Proceedings of the 3rd Asian Conference on Soil Mechanics and Foundation Engineering, Haifi,* **2**, 25-28.

Vaughan, P.R., Maccarini, M and Mokhtar, S.M. (1988). Indexing the engineering properties of residual soil. *Quarterly Journal of Engineering Geology,* **21**, 69-84.

INJAKA DAM: MITIGATIVE MEASURES FOR DIFFICULT FOUNDATION CONDITIONS

David R. Haskins[1] and Johannes P. Van Zyl[2]

ABSTRACT: The 57 m high Injaka dam built on the Marite River in the Mpumalanga Province, South Africa has a complex geological foundation comprising the 3 075 Ma Nelspruit Suite granite intruded by a number of younger, faulted diabase dykes. Intensive chemical weathering at the site has resulted in the formation of a thick mantle (up to 35m) of weathered saprolitic material overlying the bedrock. The significantly different weathering products of the granite and the diabase dykes and their respective disparate engineering behaviour has meant that extra precautionary measures were necessary during construction of the dam.

The intense leaching of the granite saprolite has resulted in a material of low density exhibiting significant metastability, particularly in the upper portion of the weathered profile. Design estimates of the excavation level for the clay core trench and foundation footprint of the embankment had to be re-evaluated and deepened during construction to prevent excessive collapse settlement of the foundation material. The porous nature of the granite saprolite responsible for marginal permeability conditions in the foundation, as well as the dispersive characteristics of the material required precautionary measures to be undertaken to reduce seepage through the foundation. These included the alignment of the clay core with the lower permeability diabase dykes and the installation of a jet grout curtain on the left flank to act as an engineered cut-off in the granite saprolite. A series of pressure relief wells were also installed along the toe of the dam to control seepage through the foundation. This required large diameter augering under difficult ground conditions and was only successfully achieved using a specialised organic drilling mud.

A locally developed, high water table on the left flank had to be drained to reduce high pore water pressures from developing during placement of the embankment in this area. A grid of large diameter drainage holes in the foundation footprint was constructed for this purpose. This paper outlines the implementation of these construction measures carried out under challenging site conditions.

INTRODUCTION

Injaka Dam site is situated 10 km south of Bushbuckridge, located in Mpumalanga Province, South Africa (see Figure 1). The dam is constructed on the eastward-flowing, perennial Marite River, which is a major tributary of the Sabie River. The dam comprises a zoned earthfill embankment 550m long and 57m high with a central concrete uncontrolled trough spillway, free-standing inlet tower and outlet conduit housing the outlet pipes (see Figure 2).

The dam site is located in a sub-tropical region with rain falling primarily during the summer period. Thornwaite's moisture index of the area is almost zero, suggesting that sub-humid conditions prevail (Schulze, 1958). Using Weinert's (1974) climatic N-value, which has been calculated as N=2, it can be seen that the main, current weathering mechanism at Injaka Dam site is chemical decomposition.

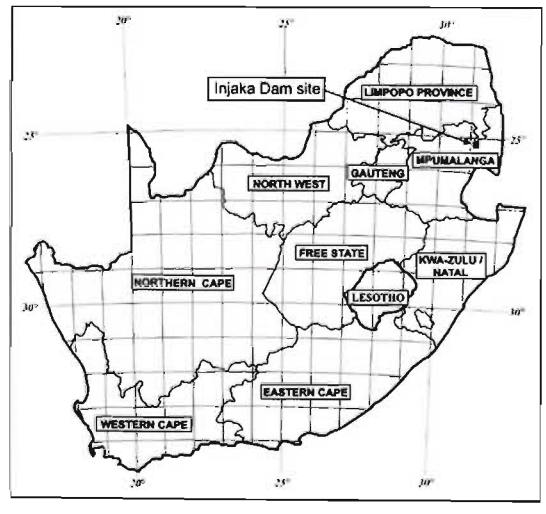

Figure 1. Locality of Injaka Dam site in the north-eastern portion of South Africa.

[1] David Haskins. Melis & Du Plessis Consulting Engineers, P.O. Box 1476, Somerset West, 7129, South Africa.
[2] Johannes Van Zyl, Civil Design Directorate, Department of Water Affairs and Forestry, Private Bag X313, Pretoria, 0001, South Africa.

GEOLOGY OF THE DAM SITE

The dam site is underlain by pink, grey or yellow, medium-grained quartz-microcline-plagioclase-biotite migmatite, granite and gneiss belonging to the 3 075 Ma Nelspruit Suite. Mafic and ultramafic xenoliths occur locally, but do not appear to be very common. Four post-Transvaal age diabase dykes (younger than 2 300 Ma) intrude the area. The diabase is generally dark grey, fine-grained and massive. The dykes vary from 10 m to 20 m in thickness and are generally steeply dipping (>70). A major fault with associated shear zone strikes approximately north-south at the location of the dam site. This feature is composed of pegmatite and mylonitic breccia. Detailed geological mapping of the dam site has revealed a complex temporal relationship between the faulting and the intrusion of the dykes (see Figures 3 and 4).

Figure 2. View of the completed dam showing inlet tower, trough spillway and outlet conduit with main embankment.

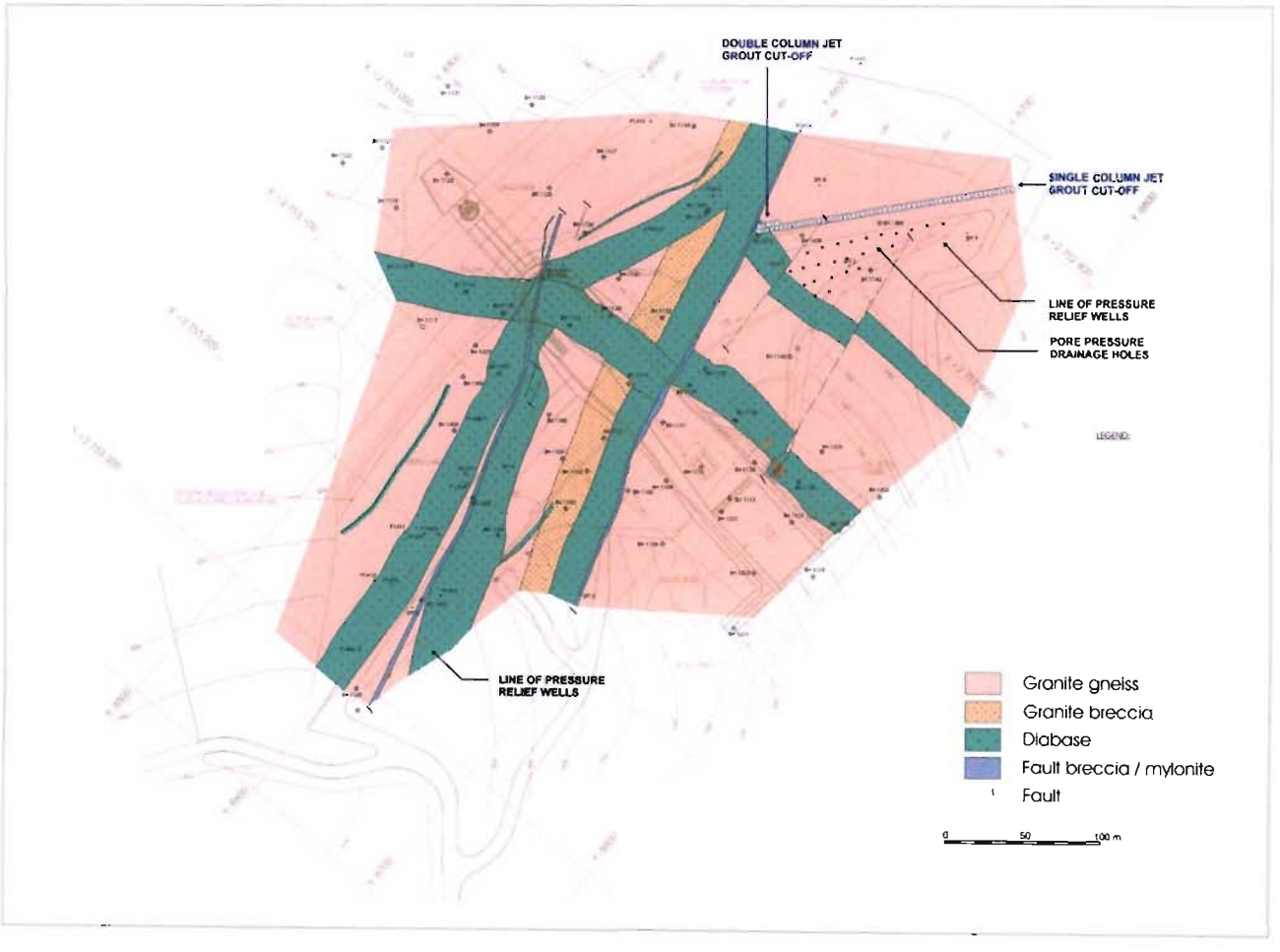

Figure 3. Detailed geology of the dam site showing the positions of the single and double column jet grout cut-off, line of pressure relief wells and pore pressure drainage holes (modified after Council for Geoscience, 2002).

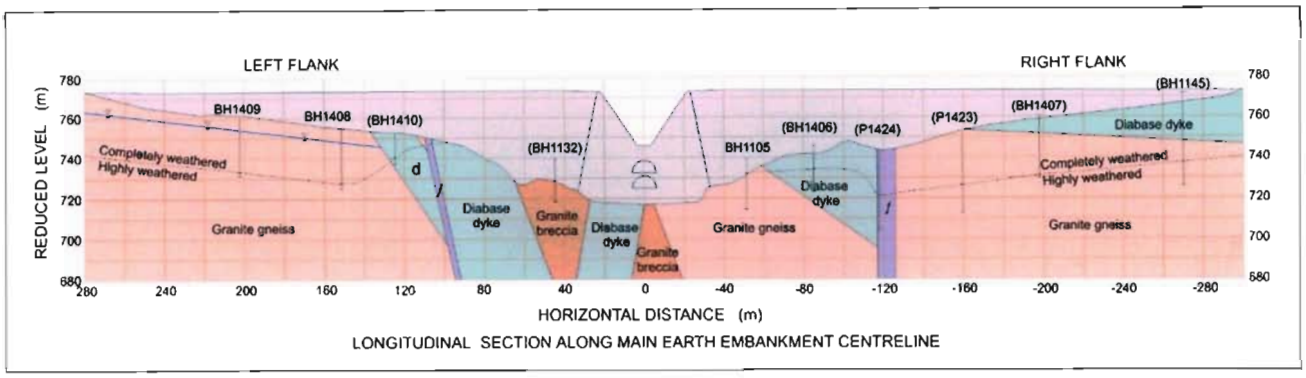

Figure 4. Longitudinal geological section along dam centreline showing the shallow water table on the left flank (modified after Council for Geoscience, 2002).

According to the description of the geomorphic evolution of southern Africa by Partridge and Maud (1987), Injaka Dam site is located below the former position of the African erosion surface - a geomorphic surface formed by multi-cyclic erosion that started in the Cretaceous and ended in the Miocene, lasting some 140 million years. The extreme intensity of the weathering during this period has resulted in the formation of saprolitic soils up to 35m thick on the granite and 15m thick on the diabase, with the current sub-tropical climate also imprinting the effects of chemical weathering. Haskins *et al.* (1998a and b), have provided a synopsis of the weathering and engineering properties of the granite saprolite at the dam.

FOUNDATION MATERIAL: GEOTECHNICAL PROBLEMS AND MITIGATIVE MEASURES

A number of geotechnical problems regarding the highly weathered, intensely leached foundation materials were identified during the feasibility and design phases of the geotechnical investigations undertaken for the dam. These were later confirmed by detailed investigations during construction of the dam.

Metastability of granite saprolite

The intensely leached nature of the granite saprolite with its open soil micro-structure means that the material is susceptible to collapse settlement when saturated. The effect of this on the settlement of the dam foundation and embankment during construction and impoundment was cause for concern. The initial design calculations suggested that by removing the upper 5m of the saprolite, a significant reduction in the collapse settlement could be achieved as the density of the granite saprolite was thought to improve considerably beyond this depth. During construction of the dam and opening of the foundation footprint, a detailed study was undertaken to quantify the collapse behaviour of the granite saprolite and results from part of this study have been presented by Haskins and Bell (2002). The results showed the granite saprolite to exhibit a maximum collapse potential of 6% at 191kPa saturation pressure (extending to 8% at 381kPa saturation) and also proved that the initial assumption for the final excavation level of the foundation

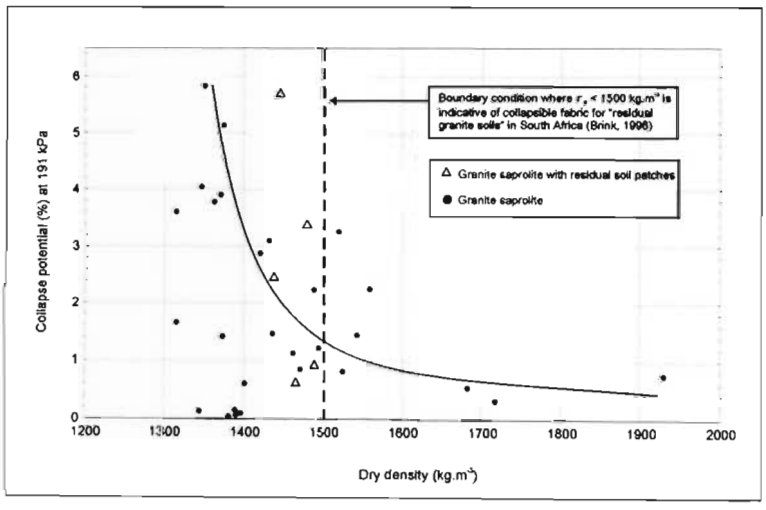

Figure 5. Relationship of dry density and collapse potential for granite saprolite at Injaka Dam.

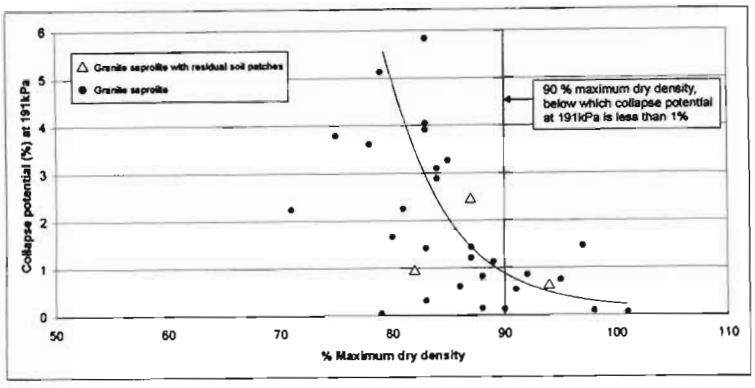

Figure 6. Relationship of collapse settlement with % maximum dry density for granite saprolite at Injaka Dam.

footprint was inadequate. This was determined by assessing the relationship of the dry density with the collapse potential. This relationship is shown in Figure 5 and illustrates the remarkable reduction in collapse potential beyond a dry density of 1600kg.m^{-3}. Brink's (1996) boundary condition indicative of a collapsible soil is shown for weathered granites in South Africa for comparative purposes. When a comparison of the collapse potential with the ratio of dry density to maximum dry density (as determined by Standard Proctor compaction) is carried out, a similar result is seen whereby at 90% maximum dry density, the collapse potential is generally below 1% (see Figure 6). The final design measures required an excavation level for the foundation footprint that met either of these two requirements. This translated to a maximum excavation depth of 13m below original ground level at the deepest point, becoming shallower towards the edges of the embankment. On average, an 8m excavation depth was achieved over the foundation footprint.

Permeability and dispersivity of foundation materials

In light of the very deeply weathered and intensely leached foundation material, it was realised during the design phase of the dam that seepage would occur beneath the dam wall through the weathered granite saprolite. This together with the highly dispersive and erodible nature of the granite saprolite (see Figure 7) was cause for concern. An extensive testing programme was thus undertaken to quantify the permeability of the weathered materials. The results from this testing programme are shown in Table 1.

Table 1. Permeability of granite and diabase saprolite from various methods.

Test type	Material	Mean	N
Laboratory falling head test (Head, 1982)	Granite saprolite	$1,6 \times 10^{-4}$	33
	Diabase saprolite	$1,0 \times 10^{-5}$	2
Field falling head test (Lambe and Whitman, 1969)	Granite saprolite	$6,5 \times 10^{-5}$	38
	Diabase saprolite	$5,0 \times 10^{-5}$	4
Field constant head test (Anon, 1968)	Granite saprolite	$1,8 \times 10^{-5}$	2
	Diabase saprolite	$1,5 \times 10^{-5}$	5

Alignment of clay core

Table 1 shows that the granite saprolite exhibits a slightly higher permeability in comparison to the diabase saprolite. This, together with the fact that the weathered diabase is less dispersive than the granite saprolite, means that the diabase provides a superior flow resistance to water moving through the foundation with less chance of piping failure developing through this material. The favourable position of the diabase dykes (generally coincidental with the clay core of the dam – see Figure 3) meant that the majority of the length of the core could be tied into the dykes to provide a natural, extended cut-off.

Jet grout cut-off

Notwithstanding this design option, on the upper left flank of the dam foundation the alignment of the clay core could not coincide with any of the dykes intersecting the foundation (see Figure 3) and no natural cut-off was available to tie into the core. An extensive grout testing programme was undertaken to determine the success of permeation and tube-a-manchette grout techniques using cementitious products and chemical grouts to consolidate the granite saprolite. The results from this programme proved that neither method nor grout type were suitable for successfully grouting up the saprolite. Consequently, in the area beneath the clay core where no dyke was present, a jet grout curtain was installed to minimise seepage through the foundation and thus prevent the possible formation of piping failure beneath the dam wall.

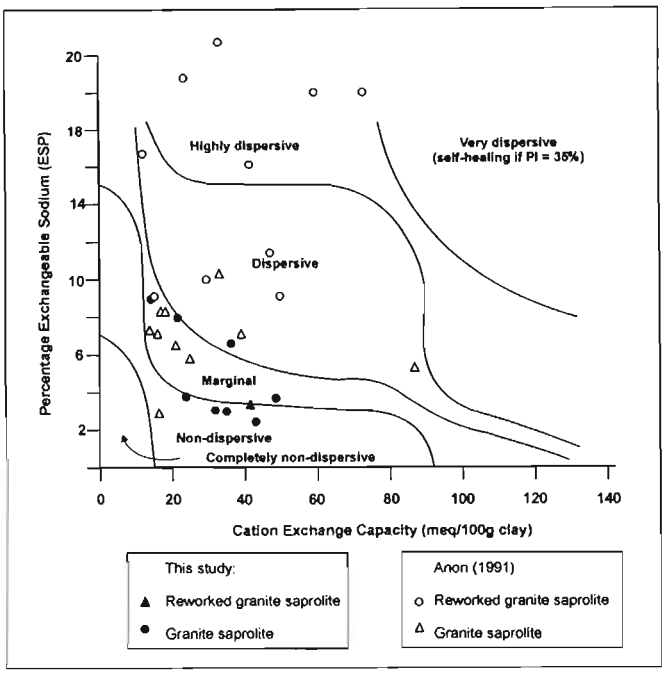

Figure 7. Dispersivity of granite saprolite using ESP-CEC chart.

Jet grouting is essentially a ground improvement technique that increases both the consolidation and cementation of the host material. By doing this, the permeability of the material is also reduced. The basis of the system is the high pressure injection of grout through a rotating drilling rod forming mixed soil and grout columns as the rod is withdrawn from the drilled pilot hole. By interlocking the columns so formed an impervious barrier can be created. Heinz and Segatto (1995), proclaim that the method of jet grouting is extremely effective in consolidating materials in dispersive soil conditions. Figure 3 shows the position of the jet grout curtain whilst Figure 8 illustrates the longitudinal section of the jet grout cut-off.

To test the suitability of the jet grout method in the saprolite materials, a number of test columns were constructed to determine the various factors that affect column diameter and mixing within the columns. The diameter and mixing are critical when creating a cut-off wall as the interlock between columns is determined by the column spacing (dictated by column diameter) whilst the mixing should produce an homogeneous mixture of cementitious product and soil to reduce the permeability of the material within the columns. The factors that affect the diameter and mixing include withdrawal and rotation rate of the cement water jet and the pressure at which the jet is operated. Table 2 shows a summary of the test programme results and the effects that withdrawal rate has on the column diameter and consumption of cement. Figure 9 shows the interlocking test columns, whilst Figure 10 shows the satisfactory mixing achieved within the columns by the jet grout process.

The test grout programme showed that by slightly increasing the withdrawal rate of the jet nozzle from 9 to 6 seconds per 75mm, only 150mm reduction in the column diameter was evident (from 750mm to 600mm). However, a significant reduction in the cement consumption could be gained by increasing this rate, with a saving of approximately 200kg of cement per meter length using the faster withdrawal rate. The actual jet grout columns comprising the cut-off were therefore chosen to be 600mm in diameter with a center-to-center spacing of 450mm, resulting in a 150mm interlock between adjacent columns.

Table 2. Results from test jet grout programme.

Column	Depth of test (m)	Withdrawal rate (seconds/75 mm)	Diameter of column (m)	Cement consumption (kg/m)
1	5-3	9	±750	±500
1	3-1	7	±725	±500
2	5-1	6	±600	±300
3	22-1	6	±600	±300

Although the majority of the 129m long cut-off wall comprised only a single row of interlocking columns, a double row of columns was constructed where the diabase dyke intersects the granite along the line of the cut-off (see Figures 3 and 8). This double row was necessary to provide an effective cut-off over this geological contact that was considered to be a preferential seepage pathway.

The deepest column in the cut-off extended to 26m in the granite saprolite whilst those in the diabase averaged to a depth of 13m. All columns were jetted to 2m below ground level (final excavation level for the foundation footprint), whilst the base of the columns was determined by refusal or near refusal of the tricone bit used to drill the pilot hole.

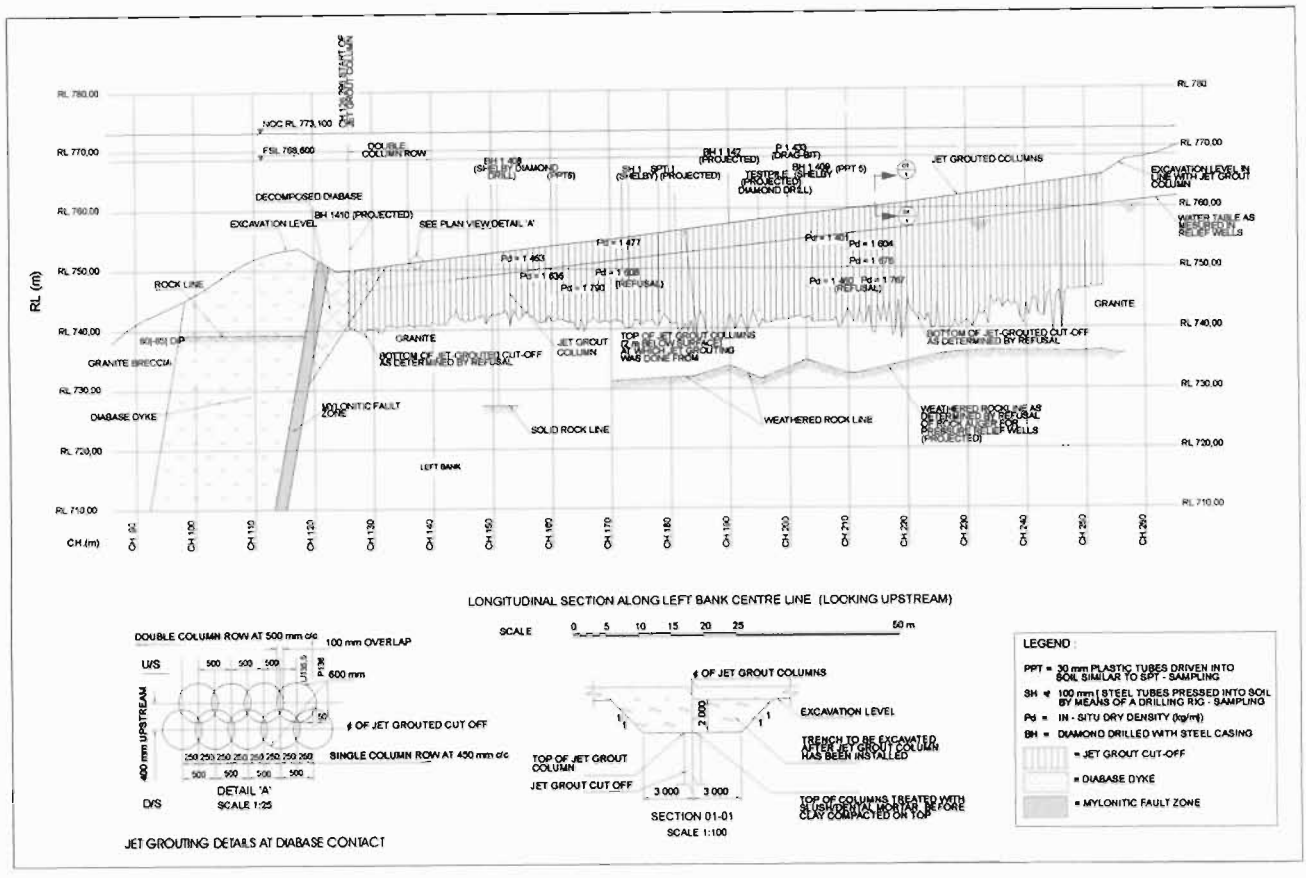

Figure 8. Longitudinal section along center-line of jet grout columns with detail of the double column at the diabase –granite contact and capping details for the column heads.

The grout mix used in the columns consisted of water and cementitous product, with the cementitious product consisting of Pulverised Fly Ash (PFA) and Ordinary Portland Cement (OPC) in an original mass ratio of 50:50 at a water:cementitious product ratio of 1. This was later changed when the PFA and OPC was used in a mass ratio of 67:33 at a water:cementitious product ratio of 0,82. The mix was injected at a pressure of 40 MPa. There were a number of advantages in using the OPC-PFA mix in the jet grout columns and these include:

- PFA as a pozzolan reacts with the by-products of the hydration process of the OPC contributing to the long-term strength increase in the columns.
- The shape of the PFA particles provides higher workability of the grout and the water/cement ratio could therefore be reduced without loss of workability.
- PFA bulking significantly reduced the cost of the columns.
- PFA produces a cementitious product which is less permeable than that which is made up of only OPC.

In order to check the integrity of the jet grout columns a number of core holes were drilled through the columns. These were either drilled vertically to obtain an indication of the mixing within the column or were inclined at 30° to check the condition of the column interlocks. Permeability testing using falling head tests and water pressure testing using packer tests was carried out in these holes. The results from these tests are shown in Table 3 and indicate that an acceptable cut-off was achieved using the jet grout columns.

As a consequence of the expected differential settlement between the jet grout columns and the *in situ* saprolitic material, with the associated risk of cracks developing through the clay core, a 2m thick flexible clay capping (placed wet of optimum moisture content) was constructed over the jet grout columns. The flexible clay capping was designed to allow for plastic deformation around the top of the columns. Figures 8 and 11 show details of the column head clay cap.

Table 3. Results of falling head and water pressure tests on jet grout columns.

Hole No.	Falling head tests			Water pressure tests			
	Time (mins)	Water level drop (mm)	Depth (m)	Pressure (kPa)	Time (mins)	Flow (l)	Depth (m)
C1	5	43	0-18,4	100	5	0	8-18,4
C2	5	20	0-35,5	50	5	0,4	8-35,3
C3	5	25	0-27,34	100			
C4	5	17	0-15,0	100	5	0,9	8-28,5
C5	5	12	0-14,16	100	5	0	8-29,5
C6	5	85	0-23,5	100	5	0	0-23,5

Figure 9. Appearance of excavated jet grout column showing interlock between columns. Column diameter is 600mm nominal.

Pressure relief wells

In order to prevent any uncontrolled seepage through the weathered granite foundation that may lead to piping, a line of 23 pressure relief wells, varying in diameter from 1 200mm to 600mm was constructed along the toe of the dam on both the right and left flanks. The wells were auger drilled to depths varying between 9m and 34m and refused on highly weathered granite or weathered diabase, depending upon their location. Although the drilling of the wells was carried out without incident on the right flank where no water table was measured, the shallow water table conditions encountered on the upper left flank (see Figure 4) proved to be problematic. The shallow water table (between 3,5m and 5,5m below the final excavation level) occurred as a result of the confining nature of the diabase dyke which strikes perpendicular to the slope of the valley (see Figures 3 and 4).

Initial attempts at augering the large diameter holes with casing support proved to be unsuccessful below the water table. The large diameter casing could not be advanced continuously with the auger drill resulting in short sections (0,5m to 1,0m) of the holes being unsupported at times during the drilling operation. Severe caving and collapse of the sidewalls as a result of the softened saprolite material in these areas prevented any further advance of the holes and in fact two of the original pressure relief wells had to be abandoned. With the realisation that conventional auger drill and casing techniques would not be successful for such deep, large diameter drilling in the granite saprolite, a new form of hole support was identified for the drilling operations. This incorporated the use of the organic drilling mud, PAC-R. This product is an organic cellulose gum derived from the linter of cotton. Although other types of cheaper drilling muds could have been chosen, PAC-R was identified because it could also fulfil the requirements necessary for drilling the pressure relief wells. These include the requirement that the drilling mud should not permanently seal the sides of the hole and that the mud must maintain the hole open for a period of 3 to 4 days (thus ensuring support of the hole even in the event of equipment failure).

Despite the fact that the PAC-R temporarily seals the sides of the hole during use, the product is biodegradable after 20 days and washes out. The polymer can also be promptly destroyed by the addition of chlorine should this be required. A further advantage of this product was the fact that it could be recycled and used for multiple holes. During filling of the pressure relief well holes with filter sand, the excess drilling mud was pumped back into the mixing hopper for use in the following hole.

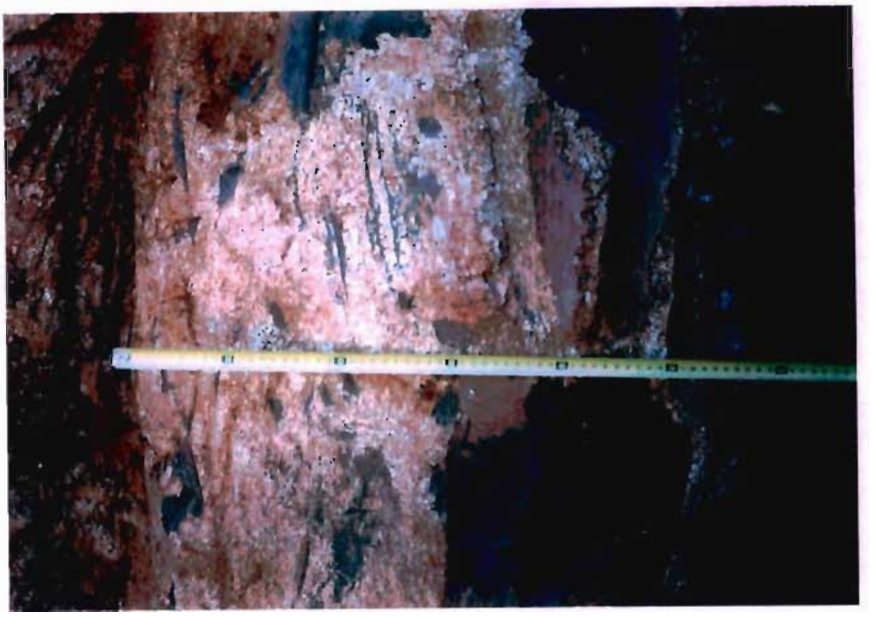

Figure 10. Detail showing mixed cement and saprolite product in 600mm diameter test column.

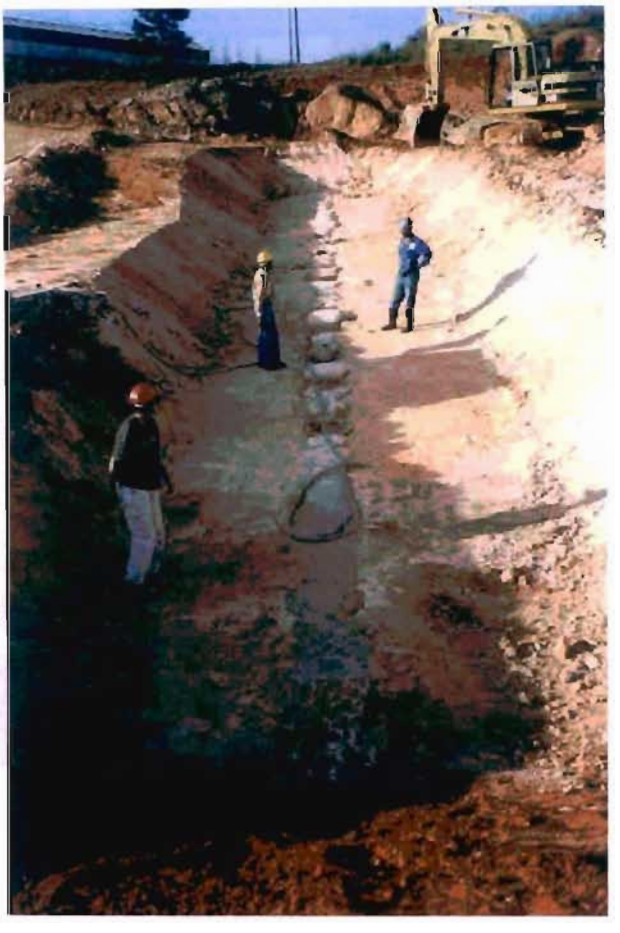

Figure 12. View of part of the completed, single-column, jet grout cut-off with foundation preparation detail for clay capping.

Drainage holes

During excavation of the embankment footprint on the upper left flank, concern was raised regarding the development of excessively high pore water pressures forming during placement of the embankment fill. Consequently, twenty-five drainage holes comprising sand drains were installed in the left flank foundation to relieve the build up of excess pore water pressure in this area. The drains connect with the base of the blanket drain to dissipate any excess pore water pressure during placement of the earthfill embankment. The sand drains ranged from 750 to 450mm in diameter (depending upon their method of drilling) and were spaced at 15m centres. The drainage holes varied in depth from 6,2m to 16,8m and were drilled successfully utilising casing down to the required depths. The holes were either auger drilled with casing or forum bored with casing, with the shallow depths of these holes (in comparison to the pressure relief wells) allowing this type advancement to be a success.

CONCLUSIONS

The highly weathered and intensely leached nature of the foundation materials at Injaka Dam have provided a number of challenging difficulties during construction of the dam. Primarily, the greatest concern during design and construction of the dam was the potential for any significant, uncontrolled seepage to develop through the foundation of the dam resulting in piping failure. A further concern was the metastable nature of the thick saprolitic mantle overlying the bedrock. These two problems have been outlined and some of the innovative solutions that were used to mitigate against such difficult foundation conditions have been briefly discussed. These have included extending the excavation depth required for the embankment footprint until material of suitable quality was obtained; the construction of the clay core on the less permeable, less dispersive weathered diabase material; the construction of a jet grout cut-off below the clay core where no diabase could be used as a natural cut-off; the construction of a pressure

relief well system to control any seepage through the foundation and the construction of a series of drainage holes to relieve the development of excessive pore water pressure during placement of the embankment on the upper left flank.

ACKNOWLEDGEMENTS

The authors would like to express their sincere gratitude to the South African Department of Water Affairs and Forestry (DWAF) for permission to publish this paper. Special thanks are also afforded to Dr A. Schall (Council for Geoscience) and Mr F. Druyts (DWAF) for relevant comments and detail.

REFERENCES

Anon (1968). *Earth Manual.* United States Department of the Interior, Bureau of Reclamation. US Government Printing Office. 783pp.

Anon, (1991). *Sabie River Catchment Development: Sabie-sand First Phase Feasibility Study. Report on the Engineering Geological and Geotechnical Investigations of the Injaka Dam Site on the Marite River.* **1**. Unpublished report prepared by Chunnett, Fourie & Partners.

Brink, A.B.A. (1996). *Engineering Geology of Southern Africa.* Fontein Publishing Company, South Africa. 319pp.

Council for Geoscience (2002). Sabie River Government Water Scheme. Injaka Dam Engineering Geological Construction Completion report.

Haskins, D.R and Bell, F.G. (2002). Indexing the collapse behaviour of granite saprolite at Injaka Dam, South Africa. *9th International Association of Engineering Geology and the Environment Congress, Durban, South Africa.*

Haskins, D.R., Schall, A. and Bell, F.G. (1998a). The evaluation of granite saprolite as a founding medium at Injaka Dam, South Africa. *8th International Association of Engineering Geology and the Environment Congress, Vancouver, Canada,* 3035-3041.

Haskins, D.R., Schall, A. and Bell, F.G. (1998b). The scanning electron microscope: A tool for improving the understanding of the weathering and engineering behaviour of a granite saprolite in South Africa. *8th International Association of Engineering Geology and the Environment Congress, Vancouver, Canada,* 3035-3041.

Head, K.H. (1982). *Manual of Soil Laboratory Testing Volume 2 Permeability, Shear Strength and Compressibility Tests.* Pentech Press, London. 449-458.

Heinz, W.F. and Segatto, P.I. Grouting of dispersive dam foundations. *Geotechnics for Developing Africa.* Wardle, Blight and Fourie (eds.). Balkema, Rotterdam. 539-550.

Lambe, T.W. and Whitman, R.V. (1969). *Soil Mechanics.* Wiley, New York. 553pp.

Partridge, T.C. and Maud, R.R. (1987). Geomorphic evolution of southern Africa since the Mesozoic. *South African Journal of Geology,* **90** (2), 179-208.

Schulze, B.R. (1958). The climate of South Africa according to Thornwaite's rational classification. *South African Geographical Journal,* **40**, 31-53.

Weinert, H.H. (1974). A climatic index of weathering and its application in road construction. *Geotechnique*, **24**, No.4. 475-488.